



**Development of analytical workflows for measurement of
metal pollution in freshwater with citizen scientists**

being a thesis submitted in fulfilment of the
requirements for the degree of

Doctor of

Chemistry

in the University of Hull

by

Mila Sari, S.T., B.Eng

June 2023

Dedication

To Jakarta, Indonesia – for equipping me with the basic knowledge and understanding of environmental pollution from day 1.

Acknowledgements

This research would not be initiated, nor would it be completed without the expert guidance and academic support from my supervisors: Prof. Nicole Pamme, Prof. Mark Lorch, and Prof. Will Mayes, in their respective expertise. Additionally, I would like to express my gratitude to The Doctoral College of the University of Hull for the funding and scholarship support for my research period, including for the opportunities provided to advance my research through conferences and seminars. I would also like to thank the University for the technical and academic support throughout my PhD, including the Library Skills Guide, among others.

I would also like to thank my colleagues in the Sensing and Safeguarding the Water Environment project cluster, as well as the academics and supervisors involved in the project – for the knowledge exchange opportunities and support throughout the research. Similarly, I would like to acknowledge the help and support from my colleagues in the microfluidics group; including but not limited to Sam, Por, Pablo, Samira, and Zakia – as well as others that were not mentioned here. In the same vein, I would like to express my utmost appreciation for other colleagues within the university – including Shu-Mei, Wanhe, Xin, and friends in the Association of Indonesian Students in Hull (PPI Hull) for the constant moral support throughout my time in Hull.

Lastly, I would like to thank my friends, family, and loved ones in Indonesia, for the constant support and love from afar – which is arguably the sole reason for me to keep going, even when times are rough. Special shout out to Michael for listening to all my breakdowns and watching my frustration through video calls – thank you for staying around even when I was at my worst.

Publications and Conferences

The data presented and discussed in this thesis had previously been published and presented in the following:

Bongkot Ngamsom, Samantha Richardson, **Mila Sari**, Alexander Iles, Mark Lorch, Will Mayes, and Nicole Pamme. *Pre-concentration with electrospun membranes coupled with paper-based assays towards onsite monitoring of heavy metals in water [abstract]*. In: MicroTAS 2020, 2020 Oct 4-9; USA (online).

Mila Sari, Bongkot Ngamsom, Alexander Iles, Jeanette Rotchell, Will Mayes, Mark Lorch, Nicole Pamme, and Samantha Richardson. *Simple-to-use paper microfluidic devices for monitoring contaminants in fresh water [abstract]*. In: European Geoscience Union General Assembly 2021, 2021 Apr 19-30; Austria (online). DOI: 10.5194/egusphere-egu21-7834

Mila Sari, Samantha Richardson, Will Mayes, Mark Lorch, and Nicole Pamme. *Development of simple method for nickel detection in freshwater system for citizen science approach [abstract]*. In: Royal Society of Chemistry Analytical Research Forum 2021, 2021 Jun 15-16; UK (online).

Mila Sari, Samantha Richardson, Bongkot Ngamsom, Will Mayes, Mark Lorch, and Nicole Pamme. *Cafetiere-based pre-concentration and μ PAD readout for on-site heavy metal analysis [abstract]*. In: MicroTAS 2021, 2021 Oct 4-9; USA (online).

Mila Sari, Samantha Richardson, Will Mayes, Mark Lorch, and Nicole Pamme. *Method development for on-site freshwater analysis with pre-concentration of nickel via ion-exchange resins embedded in a cafetiere system and paper-based analytical devices for readout [abstract]*. In: European Geoscience Union General Assembly 2-22, 2022 May 23-27; Austria (online). DOI: 10.5194/egusphere-egu22-11892.

Mila Sari, Samantha Richardson, Will Mayes, Mark Lorch, and Nicole Pamme. *Development of on-site heavy metal detection kits for water monitoring through citizen science [abstract]*. In: University of Hull Sustainable Development Goals Conference 2022, 2022 July 6-7; UK.

Abstract

The emergence of heavy metals, such as nickel (Ni^{2+}) and zinc (Zn^{2+}), as freshwater contaminant poses an environmental and public health risk. However, the current monitoring process lacks robustness and the spatiotemporal range, impeded by relatively complex and costly analytical processes. The need for a relatively simpler and rapid monitoring workflow for onsite metal monitoring drives this study in developing a two-step workflow detection system. The design of the workflow consisted of a simple, rapid, and onsite preconcentration method, followed by a microfluidic paper-based analytical device (μPAD) as a chemical sensor for target metal species.

Through this study, two μPAD s for the detection of Ni^{2+} and Zn^{2+} , separately, had been developed using a novel colorimetric reagent: 1,2-cyclohexanedione dioxime and 5-Br-PAPs, respectively. Which, the former had shown its potential as an alternative water-soluble colorimetric reagent for Ni^{2+} detection in μPAD , by improving the device fabrication step due to the use of water as a solvent. Both of the μPAD s developed in this research had shown notable improvement in decreasing the reaction time, consequently producing results within 5 minutes after sample introduction. The μPAD s also omitted the need for pipettes for sample introduction, since μPAD can safely be placed into a volume of sample instead. The Ni^{2+} detection using developed μPAD in this study allowed for detection down to 3 mg L^{-1} within 4 minutes, whereas Zn^{2+} detection using a second μPAD developed in this study achieved a 1 mg L^{-1} detection limit within 5 minutes.

A preconcentration workflow involving Lewatit MonoPlus SP 112 ion exchange resin in a cafetiere and 5 M NaCl as eluent, was also developed in this study, as means of simple, rapid, onsite preconcentration method. With the developed system, the resin was able to adsorb up to 60% and 80% of the initial Ni^{2+} and Zn^{2+} mass in the solution, respectively, within 5 minutes of plunging and mixing. This portable preconcentration system was then coupled with the developed μPAD s for Ni^{2+} or Zn^{2+} detection, lowering the limit of detection to 1 mg L^{-1} and 0.5 mg L^{-1} metal concentration, respectively. Through integration, the total duration of the workflow was set at 15 minutes, including preconcentration, elution, and sensing steps.

The developed workflow also emphasised accessibility and usability for citizen scientists as target users, considering simplicity, rapidness, and chemical hazards in its design. Upon initial review by 31 volunteers at the University of Hull, the developed workflow was regarded as simple and rapid by the users, showing the potential of the approach for water monitoring initiatives. However, further improvements in accessibility would be necessary to improve the analytical aspect of the workflow.

Table of Contents

Dedication.....	III
Acknowledgements.....	IV
Publications and Conferences.....	V
Abstract.....	VI
Table of Contents.....	VII
List of Figures	XII
List of Tables	XVI
List of Equations.....	XVII
Chapter 1 Introduction	1
1.1 Background	1
1.2 Metal in the freshwater environment	1
1.2.1 Toxicity of Ni ²⁺ and Zn ²⁺	4
1.2.2 Ni ²⁺ and Zn ²⁺ in the environment.....	8
1.2.3 Ni ²⁺ and Zn ²⁺ detection methods in the environmental sample.....	12
1.3 Microfluidic paper-based analytical device (μPAD) for environmental metal detection	
14	
1.3.1 Microfluidics fundamentals and its role in environmental metal detection	14
1.3.2 Microfluidic Paper-Based Analytical Device (μPAD).....	15
1.3.3 μPAD for metal detection	20
1.3.4 Preconcentration in μPADs	24
1.4 Colorimetric reaction for metal detection.....	25
1.4.1 Colorimetric detection of heavy metals	26
1.4.2 Ni ²⁺ detection reagent	26
1.4.3 Zn ²⁺ detection reagent.....	28
1.5 Electrospun membrane for metal adsorption	30
1.5.1 Electrospinning fundamentals	30
1.5.2 Ni ²⁺ and Zn ²⁺ adsorption with electrospun nanofibers	31
1.5.3 Elution of metals from electrospun nanofibers	33
1.6 Ion exchange resins for metal preconcentration.....	34
1.6.1 Metal preconcentration with ion exchange resins	34
1.6.2 Ni ²⁺ and Zn ²⁺ adsorption with ion exchange resins	34
1.6.3 Ion exchange column for metal preconcentration	35
1.7 Citizen science for environmental monitoring	36
1.7.1 Citizen science in environmental monitoring.....	36
1.7.2 Citizen science in water monitoring.....	38
1.8 Research aim.....	41
Chapter 2 Development of a microfluidic paper-based analytical device (μPAD) for Ni ²⁺ detection	
in the environmental water sample	42

2.1	Chapter introduction	42
2.2	Materials and methods.....	42
2.2.1	Materials.....	42
2.2.2	Solution preparation	43
2.2.3	UV/Vis spectrophotometry	44
2.2.4	Optimisation of paper-based analytical device for Ni ²⁺ detection	46
2.2.5	Statistical analysis.....	54
2.3	UV/Vis spectrophotometric detection of Ni ²⁺ with nioxime.....	54
2.3.1	Reaction time	54
2.3.2	Effect of nioxime volume	55
2.3.3	Effect of nioxime concentration	56
2.3.4	Effect of initial sample solution pH	57
2.3.5	Calibration curve	58
2.4	Development of nioxime μ PAD.....	59
2.4.1	Design of nioxime μ PAD	60
2.4.2	Optimization of nioxime μ PAD	63
2.4.3	Interference study.....	71
2.4.4	Calibration curve of nioxime μ PAD	79
2.4.5	Stability of nioxime μ PAD.....	82
2.5	Development of alternative μ PAD for Ni ²⁺ detection	85
2.5.1	XO/PDADMAC as a colorimetric reagent for μ PAD.....	85
2.5.2	Distance-based approach with nioxime dPAD.....	86
2.6	Conclusions	88
Chapter 3 Development of rapid preconcentration workflow for nickel ion detection in freshwater samples..... 89		
3.1	Chapter introduction	89
3.2	Materials and Methods.....	90
3.2.1	Chemicals.....	90
3.2.2	Solution preparation	91
3.2.3	PCL/chitosan/PEO electrospun nanomat for Ni ²⁺ adsorption	93
3.2.4	Ion exchange resins for Ni ²⁺ adsorption and preconcentration.....	94
3.2.5	Statistical analysis.....	97
3.3	Results - PCL/chitosan/PEO electrospun nanomats	97
3.3.2	Nickel elution properties by electrospun PCL/chitosan/PEO nanomat	98
3.3.3	Challenges with electrospun nanomat for Ni ²⁺ preconcentration.....	100
3.4	Results – preconcentration with ion exchange resins	102
3.4.1	Nickel adsorption properties of ion exchange resins in cafetière system	104
3.4.2	Nickel elution properties of ion exchange resins.....	114
3.4.3	Effect of other metal ions to Ni ²⁺ adsorption and elution with Lewatit SP in cafetière 118	
3.5	Incorporation of cafetière-based nickel preconcentration workflow into paper-based analytical device system	121
3.5.1	Developed workflow	122
3.6	Conclusion.....	124

Chapter 4 Development of zinc detection kit with cafetière-based preconcentration and paper-based analytical device	126
4.1 Chapter introduction	126
4.2 Materials and Methods.....	127
4.2.1 Materials.....	127
4.2.2 Solution preparations	128
4.2.3 UV/Vis spectrophotometry for Zn ²⁺ detection.....	129
4.2.4 Microfluidics paper-based analytical device (μPAD) development for Zn ²⁺ detection in the water sample	130
4.2.5 Development of onsite preconcentration workflow for Zn ²⁺ preconcentration ..	133
4.2.6 Statistical analysis.....	134
4.3 Result: μPAD for Zn ²⁺ detection with zincon as a colorimetric reagent	134
4.4 μPAD for Zn ²⁺ detection with 5-Br-PAPs as colorimetric reagent.....	135
4.4.1 Observation on 5-Br-PAPs as a colorimetric reagent for Zn ²⁺ detection using UV/Vis spectrophotometry	135
4.4.2 Design and optimisation of μPAD for Zn ²⁺ detection using 5-Br-PAPs as colorimetric reagent.....	140
4.5 Preconcentration of Zn ²⁺ with cafetière and Lewatit SP.....	146
4.5.1 Lewatit SP for Zn ²⁺ adsorption in various initial pH conditions	146
4.5.2 Lewatit SP for Zn ²⁺ adsorption in various initial Zn ²⁺ concentration.....	147
4.5.3 Elution of Zn ²⁺ from Lewatit SP resin in the modified cafetiere system	149
4.5.4 Elution of Zn ²⁺ from 5 M NaCl	150
4.6 Integration of cafetière-based preconcentration with Zn ²⁺ μPAD for Zn ²⁺ detection	
152	
4.6.1 Zn ²⁺ preconcentration and detection with μPAD – workflow.....	152
4.6.2 Testing with environmental water samples	153
4.7 Conclusion.....	155
Chapter 5 User experience evaluation.....	156
5.1 Chapter introduction	156
5.2 Materials and Methods.....	157
5.2.1 Materials.....	157
5.2.2 Workflow development.....	157
5.2.3 Ethics.....	157
5.2.4 Questionnaire	157
5.2.5 Recruitment	158
5.2.6 Obtaining water samples.....	158
5.2.7 μPAD for Zn ²⁺ detection	159
5.2.8 Analysis of questionnaire data	159
5.2.9 Statistical analysis.....	160
5.3 Control – μPAD measurements conducted by the researcher	160
5.4 Volunteer demography.....	161
5.5 Workflow and observational data	164
5.5.1 Materials and equipment for volunteer work	164
5.5.2 Workflow completed by the volunteers	167
5.5.3 Observations	168

5.6	Analytical evaluation of volunteers' data	171
5.6.1	Preconcentration step	173
5.6.2	μ PAD step	174
5.6.3	Picture-taking step.....	178477
5.6.4	Evaluation of volunteers' data	181480
5.6.5	Errors in volunteers' data	184482
5.7	Volunteers' feedbacks.....	185483
5.7.1	Workflow duration.....	185483
5.7.2	Workflow simplicity	185483
5.7.3	Applicability in environmental settings	187485
5.7.4	Input on preconcentration step – open-ended	188486
5.7.5	Input on μ PAD step – open-ended.....	189487
5.7.6	Input on picture-taking step – open-ended	190488
5.8	Conclusion.....	191489
Chapter 6 Conclusion		192490
6.1	Conclusion.....	192490
6.2	Future research.....	195493
References		i
Appendix 1 μ PAD for Ni ²⁺ detection.....		xii
Development of XO/PDADMAC μ PAD		xii
Optimization of XO/PDADMAC μ PAD		xiii
Calibration curve of XO/PDADMAC μ PAD		xvii
Development of nioxime distance-based μ PAD		xix
Optimization of nioxime dPAD.....		xx
Standardised effect		xx
Main effects plot		xxi
Calibration curve.....		xxiii
Drawbacks of dPAD for Ni ²⁺ detection in water sample		xxv
Reaction time		xxv
Robust and repeatable measurement.....		xxvi
Measurement with image processing software.....		xxvi
Reagent introduction process		xxviii
Appendix 2 Cafetiere-based preconcentration.....		xxix
Methods for PCL/chitosan/PEO nanomat fabrication optimisation and adsorption characterisation.....		xxix
Methods for ion exchange resins for Ni ²⁺ adsorption and preconcentration.....		xxx
Ni ²⁺ calibration curve for UV/Vis spectrophotometry		xxxii
Results – PCL/chitosan/PEO nanomat for Ni ²⁺ adsorption		xxxii
Fabrication and optimisation of electrospun PCL/chitosan/PEO nanomat		xxxii
Adsorption performance of electrospun PCL/chitosan/PEO nanomat.....		xxxiii
Results – ion exchange resins for Ni ²⁺ preconcentration.....		xli

Preliminary observation.....	xli
Adsorption kinetics	xlili
Adsorption isotherm	xlili
Effect of pH to Ni ²⁺ adsorption by ion exchange resins	xlvii
Incorporation of cafetiere-based Ni ²⁺ preconcentration workflow into paper-based analytical system	xlix
Alternative workflow: 10 mL 5 M NaCl as elution solution, for laboratory-based experiment	xlix
Appendix 3 Zn ²⁺ detection kit.....	i
μPAD for Zn ²⁺ detection with Zincon monosodium salt as colorimetric reagent	i
Observation on Zincon monosodium salt as colorimetric reagent in Zn ²⁺ detection using UV/Vis spectrophotometry	i
Optimisation of μPAD for Zn ²⁺ detection with Zincon monosodium salt as colorimetric reagent	iii
μPAD for Zn ²⁺ detection with 5-Br-PAPs as colorimetric reagent.....	xi
Optimisation of μPAD for Zn ²⁺ detection using 5-Br-PAPs as colorimetric reagent	xi
Appendix 4 User experience evaluation	xv
Zn ²⁺ calibration curve for μPAD measurement.....	xv
Volunteer’s technical specification	xvi
Letter of ethics approval for the research	xvii
Ethics application as submitted to the committee	xviii
PART G: CONFLICTS OF INTEREST	xlii
PART I: DECLARATIONS	44
Appendix 2: Data Management Plan	20
Volunteer consent form.....	liv
Online questionnaire filled by the participants	lv
Participant information sheet.....	ii
Heavy metal detection in freshwater environment – Participant Information Sheet	ii

List of Figures

Figure 1 The flow of heavy metal contamination from anthropological sources.....	2
Figure 2 A schematic of an electrochemical sensor for water monitoring that	3
Figure 3 Average Ni ²⁺ concentration measured across UK rivers between 2000-2022,.....	10
Figure 4 Average Zn ²⁺ concentration measured across UK rivers between 2000-2021,	12
Figure 5 Example of microfluidics devices for detection of metal in water sample	15
Figure 6 Examples of μ PADs made with different fabrication methods and paper matrix;	16
Figure 7 Illustration of wax printing fabrication method, which was adapted with	16
Figure 8 Illustration of reagent deposition and sample introduction to a colorimetric-based ..	19
Figure 9 Example of paper-based microfluidics with electrochemical sensing reaction.....	20
Figure 10 Example of a Ni ²⁺ detection μ PAD fabricated with wax printing	21
Figure 11 Example of the fabrication and use of μ PAD for multiplex analysis.....	22
Figure 12 (A) Top to bottom: endpoint colour of Zn ²⁺ detection μ PAD with zincon	23
Figure 13 Example of a preconcentration system with solid phase extraction.....	24
Figure 14 A schematic of the device fabrication protocol and its working mechanism.....	25
Figure 15 Dimethylglyoxime complexation reaction with Ni ²⁺ , forming 2:1 ligand.....	27
Figure 16 Metal-ligand complex formation reaction between 1,2-cyclohexanedione dioxime.	28
Figure 17 (A) Outline of reaction process and characteristics of the colour	30
Figure 18 Fundamentals of electrospinning process, as illustrated in [106].	31
Figure 19 SEM imaging of PEO/chitosan fibre for metal adsorption study [109].....	32
Figure 20 Sampling sites as reported by citizen science volunteers in a microplastics	37
Figure 21 Monitored location in a 20 years study on agricultural contaminants in.....	39
Figure 22 (a) Design of a 2-layered device with 31 mm diameter, consisting of 6 sample	46
Figure 23 Illustration of a 3-layered μ PAD design with lamination. Folding and lamination	47
Figure 24 Illustration of the design of intensity-based device made in Autodesk AutoCAD	48
Figure 25 (a) Illustration of wax melting from one side of the paper where solid wax ink	49
Figure 26 Design of (a) two colour-intensity-based devices, which was the main device used.	49
Figure 27 Paper device was placed ontop of two Petri dishes without allowing any sample....	50
Figure 28 Device can be dipped into a sample solution containing the target ion for.....	51
Figure 29 “Black box” image acquisition method with black cardboard placed to cover	51
Figure 30 (a) Absorbance measured with UV/Vis spectrophotometer at 530 nm for	55
Figure 31 (a) Absorbance measured with UV/Vis spectrophotometer at 530 nm for	56
Figure 32 (a) Absorbance measured with UV/Vis spectrophotometer at 530 nm for reaction .	57
Figure 33 (a) Absorbance measured with UV/Vis spectrophotometer at 530 nm for reaction .	58
Figure 34 (a) Calibration curve of 100 μ L 400 mg L ⁻¹ nioxime reacted with 1 mL Ni ²⁺ ion	59
Figure 35 Effect of different device background colours on the naked-eye visibility	62

Figure 36 (a) Nioxime (1400 mg L ⁻¹) μPAD at the endpoint of reaction with 10 mg L ⁻¹	64
Figure 37 Chemical structure of (a) dimethylglyoxime and (b) 1,2-cyclohexanedione dioxime.	65
Figure 38 Coffee-ring effect observed on sample wells of nioxime μPAD upon addition.....	68
Figure 39 Standardised effects plot illustrating the result of reagent concentration	69
Figure 40 Main effects plot illustrating the result of reagent concentration optimization.....	70
Figure 41 (a) 3D- and (b) 2D-contour plots illustrating the result of the reagent concentration	71
Figure 42 (Top) Measured colour intensity at the green channel of 2-layered devices dipped.	72
Figure 43 (Top) Measured colour intensity upon dipping a 2-layered device into a 10 mL	73
Figure 44 Measured colour intensity for 3-layered nioxime μPAD containing respective	75
Figure 45 (Left) Measured colour intensity of nioxime μPAD with and without masking	76
Figure 46 (Top) Measured colour intensity of a 3-layered device containing 1 M NaF and.....	77
Figure 47 Measured colour intensity of nioxime μPAD upon dipping into spiked	78
Figure 48 Colour intensity measurement in RGB colour space of optimised nioxime μPAD	80
Figure 49 (a) Colour intensity measurement in RGB colour space of optimised.....	82
Figure 50 Measured colour intensity of nioxime μPAD reacted with 10 mL 10 mg L ⁻¹ Ni ²⁺ after	84
Figure 51 Colour intensity measured of optimised nioxime device dipped into a 10 mL	85
Figure 52 Calibration curve of optimised XO/PDADMAC μPAD containing 10 μL mixture of	86
Figure 53 Result as seen on the optimised dPAD 30 min after the addition of a gradient	87
Figure 54 Distance-based Ni ²⁺ device calibration curve containing 0.01 M PBS buffer pH 7.4, .	87
Figure 55 (a) Modified cafetière, a basket filled with 2.6 g Lewatit SP; (b) Closer view of	94
Figure 56 Performance of electrospun nanomat in the pH range of 5-8 after dipping into	98
Figure 57 Preliminary test of Ni ²⁺ elution from the electrospun PCL/chitosan/PEO.....	100
Figure 58 Cafetière setup for Ni ²⁺ adsorption from water sample with electrospun.....	103
Figure 59 (a) Design of modified PMMA basket for ion exchange resin housing in the.....	104
Figure 60 Effect of 2.6 g Lewatit SP in basket plunging speed of the modified basket in a	106
Figure 61 Two different resin placements tested in this observation, with.....	107
Figure 62 Effect of resin placement inside or outside the modified basket in a 300 mL	108
Figure 63 Effect of resin mass to Ni ²⁺ adsorption performance of Lewatit SP, Lewatit TP,.....	111
Figure 64 Effect of initial Ni ²⁺ concentration between 0.2-0.8 mg L ⁻¹ , tested with Lewatit SP,	113
Figure 65 (a) Elution of Ni ²⁺ from Lewatit SP in various concentrations (3-5 M) of HCl, NaCl,	115
Figure 66 Amount of eluted Ni ²⁺ upon elution with 5 mL and 10 mL 5 M NaCl after 1 min of	116
Figure 67 Amount of Ni ²⁺ eluted with 10 mL 5 M NaCl solution after mixing with 2.6 g	117
Figure 68 Amount of Ni ²⁺ extracted out of the Lewatit SP resin after 5 min of mixing in	118
Figure 69 Amount of adsorbed Ca ²⁺ , Mn ²⁺ , Fe ²⁺ , Co ²⁺ , Ni ²⁺ , Cu ²⁺ , and Zn ²⁺ in 2.6 g Lewatit SP	120
Figure 70 Amount of eluted Ca ²⁺ , Mn ²⁺ , Fe ²⁺ , Co ²⁺ , Ni ²⁺ , Cu ²⁺ , and Zn ²⁺ from elution of	121
Figure 71 UV/Vis absorbance measured at 530 nm for 0-10 mg L ⁻¹ Ni ²⁺ with and without	123

Figure 72 (a) Colour intensity measured in nioxime μ PAD with and without Ni^{2+}	124
Figure 73 Measured colour intensity on the sample wells of the device containing	135
Figure 74 Reaction time of 100 μL 1, 3, and 5 mg L^{-1} 5-Br-PAPs upon addition to 1000 μL	137
Figure 75 Observation, through absorbance at 552 nm and pictures of the endpoint.....	140
Figure 76 Reaction time of the 5-Br-PAPs μ PAD loaded with the colorimetric.....	141
Figure 77 Linear correlation, with error bars illustrating the standard deviation	142
Figure 78 (a) Performance of 5-Br-PAPs in the presence of interfering metal.....	143
Figure 79 Performance of 5-Br-PAPs μ PAD for Zn detection in the presence of	144
Figure 80 Measured colour intensity of the 5-Br-PAPs μ PAD after storage in a	146
Figure 81 Adsorption of Zn^{2+} from 50 mL sample solution containing 3 mg L^{-1} Zn^{2+}	147
Figure 82 Adsorption performance of Lewatit SP resin in cafetiere system for Zn^{2+}	148 149
Figure 83 Calibration curve of 5-Br-PAPs for Zn^{2+} detection in (blue) 5 M NaCl and	149 150
Figure 84 Amount of Zn^{2+} eluted with 30 mL 5 M NaCl from 2.6 g Lewatit SP resins	150 151
Figure 85 Measured (blue) initial and (orange) final concentration of Zn^{2+} solution.....	151 152
Figure 86 Performance of 5-Br-PAPs μ PAD upon dipping into 10 mL 0-2.5 mg L^{-1} Zn^{2+}	152 153
Figure 87 Measured colour intensity of 5-Br-PAPs μ PAD sample wells after dipping.....	153 154
Figure 88 E-mail sent to the University of Hull postgraduate students.....	158 159
Figure 89 Data acquisition graph, orange was done by the volunteers, and the blue	160 161
Figure 90 Volunteers' level of study at the time of recruitment.	162 163
Figure 91 Volunteers' previous chemistry laboratory experience demography.	163 164
Figure 92 Volunteers' awareness of the terms (a) 'microfluidics' and	164 165
Figure 93 Variation in basket mounting thread in the modified plunger	165 166
Figure 94 Workflow as depicted in the instruction sheet given to the volunteers.	167 168
Figure 95 Metallic band indicating the limit of water sample volume	168 169
Figure 96 Distribution of cafetiere sample accuracy by the 31 volunteers,	169 170
Figure 97 Sampling workflow relative to the volunteer testing activity.....	172 173
Figure 98 Assessment of the volunteer's preconcentration accuracy was done through .	173 174
Figure 99 Preconcentration data produced by volunteers, as measured with a μ PAD.....	174 175
Figure 100 Assessment of volunteer's μ PAD accuracy was done through comparison.....	175 176
Figure 101 μ PADs data produced by volunteers, as measured with a picture taken by....	178 179
Figure 102 Assessment of volunteer's picture-taking accuracy was done through	179 180
Figure 103 Visual comparison for samples 101 and 102 for Zn^{2+} detection between control	180 181
Figure 104 μ PADs pictures produced by volunteers, as measured with a picture	184 185
Figure 105 Volunteers' satisfaction in regard to the duration of the developed Zn^{2+}	185 186

Figure 106 Evaluation of the workflow simplicity divided into four parts: preconcentration,	187 188
Figure 107 Volunteers' feedback on completing the developed workflow in the riverbank.	188 189
Figure 108 Word cloud of thirty most frequent words used in feedback on	189 190
Figure 109 Word cloud of thirty most frequent words used in feedback on the μ PAD step.	190 191
Figure 110 Word cloud of thirty most frequent words used in feedback on the	191 192
Figure 111 Illustration of simple and rapid preconcentration workflow developed for onsite	193 194
Figure 112 User feedback on the usability of the device in riverbank settings.....	194 195

List of Tables

Table 1 Global reports on Ni ²⁺ concentrations in river water.....	9
Table 2 Global reports on Zn ²⁺ concentrations in river water.	11
Table 3 Comparison of commonly used μ PAD fabrication methods [11, 69].....	17
Table 4 Previous research on μ PAD for Ni ²⁺ colorimetric detection in environmental.....	20
Table 5 Previous research on μ PAD for Zn ²⁺ colorimetric detection in environmental	23
Table 6 Colorimetric reagents for nickel detection, its mechanism of the reaction,	27
Table 7 Colorimetric reagents for zinc detection, its mechanism of the reaction,	29
Table 8 Electrospun membranes for Ni ²⁺ or Zn ²⁺ adsorption or removal in the literature.	32
Table 9 Elution of metals from- or regeneration of- electrospun nanomat in the literature.....	34
Table 10 Previous studies on utilisation of commercially available ion exchange	35
Table 11 Study on citizen science data collection utilisation for environmental	40
Table 12 List of chemicals and suppliers used in the development of paper-based analytical..	43
Table 13 Typical trace element levels in Whatman grade 1 qualitative filter	60
Table 14 μ PAD specification comparison between previous studies and this research	66
Table 15 List of chemicals used in this study for Ni ²⁺ preconcentration experiments.	90
Table 16 Mass variations of resins tested in observation on the effect of resin mass on.....	95
Table 17 Chemicals used in the development of Zn ²⁺ -detection μ PAD.....	127
Table 18 Preconcentration workflow integrated with 5-Br-PAPs μ PAD result compared	154
Table 19 Materials used in user experience evaluation with volunteers.	157
Table 20 Observation data on the leak incidence and volunteers' behaviour throughout.....	171
Table 21 Comparison between Zn ²⁺ concentration measured from the elution solution .	177 176
Table 22 Comparison between Zn ²⁺ concentration measured by volunteers in	183 181
Table 23 Key comparison of several parameters between developed Ni ²⁺ detection	192 190
Table 24 Key comparison of several parameters between developed Zn ²⁺ detection.....	194 192
Table 25 Research gap to be addressed in future research and suggested strategy.	196 194

List of Equations

Eq 1	52
Eq 2	52
Eq 3	53
Eq 4	53
Eq 5	93
Eq 6	118

Chapter 1 Introduction

1.1 Background

Since the 1970s, the level of metals has been increasing in freshwater systems around the world [1]. In some cases, the amount of metal exceeded limits set by various health or environmental agencies, such as in the case of Ni^{2+} and Zn^{2+} [2-4]. The global average of Ni^{2+} concentration in freshwater systems had increased from $1.43 \mu\text{g L}^{-1}$ to $80.99 \mu\text{g L}^{-1}$, exceeding the limits set by the EU for freshwater systems of $34 \mu\text{g L}^{-1}$ and World Health Organization drinking water safety limit of $20 \mu\text{g L}^{-1}$ [1, 4]. Through this data alone, it is clear that the issue of environmental monitoring and remediation is of high interest in today's world. However, current technology in freshwater monitoring still lacks the simplicity to support real-time measurement across a wide spatiotemporal cover.

Current methods for metal detection focus on achieving a low detection limit, sacrificing simplicity, affordability, and rapidness. In the face of rising environmental concerns, however, there is a push for quicker, simpler, and more affordable sensing methods, allowing access to similar processes in resource-limited environments. Therefore, in this research, a simple and rapid metal detection method based on a paper-based microfluidic analytical device (μPAD) for citizen-led river monitoring activity was developed.

1.2 Metal in the freshwater environment

The monitoring of the chemical composition of the freshwater environment, especially streams, and rivers, is of high importance due to its critical part in the particle-transfer system in the environment [5]. Streams and rivers played an important role in carrying various chemicals across a wide spatial coverage – touching various ecosystems along the way [5]. This is a particular concern in the context of water pollution, including heavy metal contamination processes in water bodies.

Most metals are naturally occurring in the environment. Geological activities such as rock weathering or volcanic eruption can release metals deposited in minerals, inducing their entry into the freshwater system – among others [6]. Other source of contamination, however, is anthropological activities, which had notably affected the level of metals entering the rivers. For example, the main anthropological sources of Ni^{2+} include the production and processing of Ni^{2+} ores into products, such as jewellery or batteries, as well as the recycling and waste disposal of said products [7]. The danger of anthropological source, however, relies mainly on its increasing trend in metal releases, which may increase with time and the advancement of modern technology requiring electrical devices containing said metal. Despite this, its relatively low

concentration in the environment compared to other elements in the water, grants it the name “trace element”.

Despite being often referred to as a “trace element” due to their low concentration ($< 10 \text{ mg L}^{-1}$) in the water system, these substances – for the most part – are still available over the needs of organisms [3, 5]. The main concern with metal availability in the environment is its bioaccumulating property, and its bio-concentration up the food chains [6, 8]. This means that the danger of metal contamination in the environment does not mainly lie in immediate exposure at low concentrations, but rather in continuous exposure through various means. Metals can accumulate in aquatic flora and fauna, which would transfer through the food chain, and ultimately accumulating in the human body over a relatively long period before showing its toxic symptoms. Therefore, metals do not need to be at high concentrations in the waterways to pose a serious threat to environmental and public health. This underlines the importance of constant monitoring of heavy metal levels, even at low concentrations; which makes it a challenge.

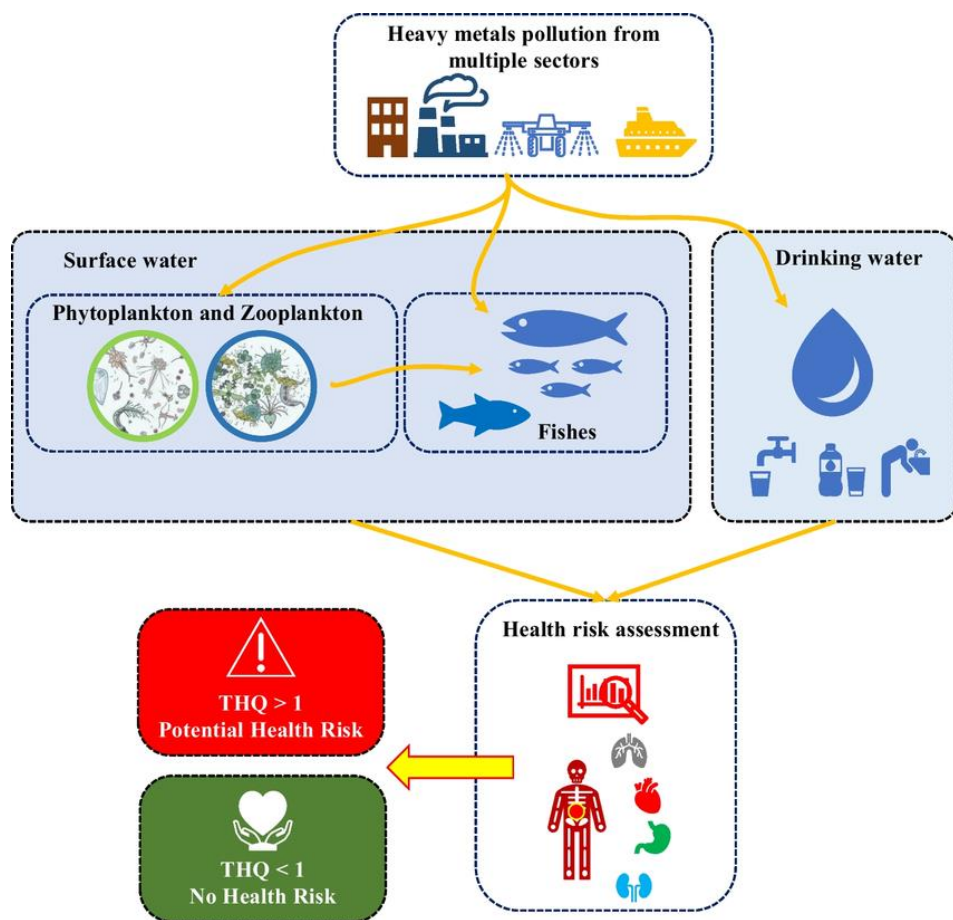


Figure 1 The flow of heavy metal contamination from anthropological sources to the environment, showing exposure channel to human body [9].

Aside from their low concentration, another issue in metal monitoring in the freshwater environment is the possibility that the monitoring device itself – often constructed of metal – could create a contamination problem [5]. Remote monitoring devices may need electrical components for detection method or to power and send the monitored data to the data collector; often, this also means that a certain degree of metals and plastic would be used for housing and structure of the device, as shown in Figure 2 [10]. In the short term, this is a solution for the remote sensing problem, however, due to the nature of the materials, especially metals, a percentage of metal from the component may leach to the water body instead. Therefore, the devices deployed under these criteria may instead end up as a source of contamination in the water body. While conventional methods involving sample collection for further laboratory-based measurement with advanced analytical methods, such as an Inductively Coupled Plasma system combined with Mass Spectrophotometry (ICP-MS) pose another challenge. The latter method would not be able to provide real-time results on the metal level in the environment [11]. Additionally, laboratory-based detection would require a specialised operator and can be relatively costly if an increase in monitoring frequency is to be employed [11-13].

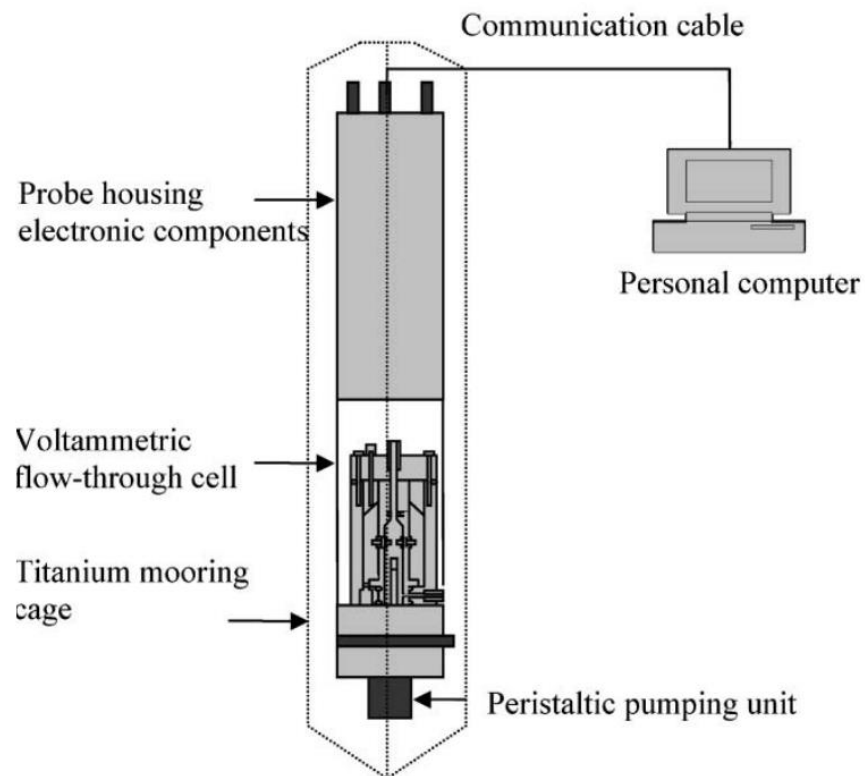


Figure 2 A schematic of an electrochemical sensor for water monitoring that has been developed in previous study, showing its electrical and mechanical components [10].

1.2.1 Toxicity of Ni²⁺ and Zn²⁺

1.2.1.1 The role of nickel in plants and animals

Essential for plant growth, nickel is believed to play a notable role in seedling growth and development. Under optimum supply, the presence of nickel would stimulate plant growth, enhancing its morphological, physiological, and biochemical attributes. However, nickel is only required in very small amounts (0.05-10 mg kg⁻¹) [14]. Nickel is a vital component for the urease enzyme in plants, with deficiency of the metal leading to disturbance in nitrogen metabolism and further accumulation of toxic levels of urea. In leguminous crops, nickel deficiency leads to leaf injury and reduces root growth. Nickel deficiency may also cause a reduction in the activity of the hydrogenase enzyme, among other enzymatic disturbances which are critical for plant growth [15].

Excessive amounts of nickel can induce nickel toxicity in plants, leading to reduced plant growth. A high concentration of nickel could affect the concentration of other essential nutrients, including magnesium. Magnesium deficiency leads to the deterioration of chlorophyll and further leaf chlorosis and necrosis. Nickel toxicity would also affect the water movement from the root to the upper part of the plant, such as leaves and branches. High nickel concentration in a growing medium would result in the formation of reactive oxygen species (ROS) which produce oxidative damage against plant membrane proteins and lipids [14, 15]. Aside from the concern of potential inhibition in plant growth due to nickel toxicity, which would affect the yield of produce and the plant's sustenance, there is also the concern of plants' ability to hyper-accumulate nickel. Hyper-accumulator species can be seen as useful since they would help in the remediation of nickel-contaminated soil. However, it also poses a concern since some of the species are commonly consumed plants, such as spinach, water lettuce, and radish. In this case, their ability to store a considerable amount of nickel in their plant organ could potentially be the gateway for nickel entry into the food chain [14].

Free nickel ion (Ni²⁺) is considered to be a highly toxic nickel chemical species due to its bioavailability. This is also true in the freshwater environment, such as rivers, where nickel is mainly transported as a precipitated coating on particles, and is associated with organic matter [16]. Nickel could gain access to aquatic animals through transporters on epithelial surfaces (fish gills). This can occur via three different routes: ionic mimicry, metal-specific carriers such as the divalent metal transporter, and paracellular diffusion [17]. Risk assessment done on the freshwater ecosystem in Lake Taihu, China, using both quotient and probabilistic methods, has shown nickel to be one of the metals posing the greatest risk along with copper and zinc [18]. Nickel is also believed to be more toxic for freshwater aquatic ecosystems compared to marine ecosystems, this might be due to the effect of salinity [17].

1.2.1.2 The role of nickel in the human body

Nickel is recognized as an essential nutrient, especially for some microorganisms, plants, and animal species, however, its nutritional value in humans is not clear. Studies have suggested that the ion may play a role in enzymatic reactions in the human body, as its deficiency can affect the activities of enzymes involved in carbohydrate and amino acid metabolism [7]. Excessive nickel exposure may, however, instead result in toxic effects. Potential nickel toxicity in humans is dependent on the physicochemical properties of the nickel species, along with the amount, route of exposure, and contact duration. In the United Kingdom, the long-term exposure limit (LTEL) for water-soluble nickel compounds is 0.1 mg m^{-3} or equal to $10^{-4} \text{ mg L}^{-1}$ (8-hour time-weighted exposure average reference period), whereas the short-term exposure limit is 0.24 mg m^{-3} , which is equal to $2.4 \times 10^{-4} \text{ mg L}^{-1}$ with 15 minutes reference period (based on nickel carbonyl) [19]. On average, with samples obtained from European countries, the amount of nickel in drinking water ranges from $2\text{-}13 \text{ }\mu\text{g L}^{-1}$ and can go as high as $200 \text{ }\mu\text{g L}^{-1}$ in a mining area. From this data, the average daily intake of nickel from drinking water only, assuming a normal intake of 2 L of water, can range from $4 \text{ }\mu\text{g L}^{-1}$ up to $400 \text{ }\mu\text{g L}^{-1}$, with the highest intake in areas with nickel mining [20].

Human exposure to nickel is common, since it is used in various industries, and therefore exists in various industrial products. Another route of exposure is in the occupational context for workers in said industries. This is especially in the case of nickel exposure through inhalation which is regarded as one of the riskier routes of nickel exposure. Inhalation of nickel in daily life could happen in nickel-contaminated air due to the combustion of fossil fuels. Exposure can also happen through ingestion of drinking water or food products. Notable food products that potentially have higher nickel prevalence include fruits, grains, seafood, and vegetables and other products such as soya, peanuts, cocoa, and baking powder [8]. Cacao products and peanuts may contain up to 10 and 3 mg kg^{-1} nickel, respectively [20]. In daily life, humans are also potentially exposed to nickel through alloyed metal products such as nickel-containing pieces of jewellery, keys, cell phones, eyeglass frames, paper clips, medical prostheses, orthodontic braces, electrical equipment, and clothing fasteners, or other objects such as cosmetics, cigarettes (tobacco), pigments, and catalysts. Nickel can be dermally absorbed, with nickel ions and nickel particles penetrating the skin at sweat ducts and hair follicles [8]. Inappropriate production and disposal processes of aforementioned industrial products are often to be blamed as anthropogenic sources of high nickel concentration in the environment.

Around 15-50% of total nickel that enters the body through drinking water is absorbed, however, this amount can be lower (up to 1%) in the presence of food in the gastrointestinal tract and it is also dependent on the nickel species [19, 20]. Nickel can be carried through blood, mainly by

albumin. In normal conditions, the amount of nickel in blood plasma is $0.2 \mu\text{g L}^{-1}$, or $1\text{-}2 \mu\text{g L}^{-1}$ in urine and $0.34\text{-}1.4 \mu\text{g L}^{-1}$ in whole blood samples [20]. The main excretion route for nickel is through urine and faeces, however, excretion through sweat glands, saliva, milk, or deposition in hair (0.39 mg L^{-1}) has also been reported. The estimated urinary excretion time of absorbed nickel is 28 ± 9 hours [20-22].

One of the widely known health effects of nickel is skin allergic reaction (nickel dermatitis), which could produce erythema, eczema, and lichenification of skin areas. Hypersensitivity could also cause asthma, conjunctivitis, inflammatory reactions, and systemic reactions. The latter two were usually iatrogenic [16]. Nickel could also cause genotoxicity, developmental toxicity, haematotoxicity, immunotoxicity, neurotoxicity, reproductive toxicity, and carcinogenicity across acute, sub-chronic, and chronic exposure. It also may cause toxic effects mainly on the liver, lungs, and kidneys' peripheral tissues. Nickel ions (Ni^{2+}) is also believed to be able to induce oxidative stress on the human body, generating free radicals, and irreversibly damaging important protein for human DNA [21].

1.2.1.3 The role of zinc in plants and animals

Zinc is an essential nutrient for plant growth, however, it is also the most common metal deficiency found in plants [23]. Zinc is important for enzyme activation in plants, which would affect carbohydrate metabolism, the integrity of the cellular membrane, and protein synthesis, among other processes [24]. Severe zinc deficiency may cause root necrosis, impeding the growth of the plant [23]. Whilst sub-lethal deficiency may be linked to bronzing, goblet leaf, and reduce in leaf size, as well as displaying similar symptoms to auxin-deficiency [23, 24]. Zinc also potentially affects the plant's water uptake, making it an essential micronutrient for the plant [24].

While zinc deficiency is more common in plants, excessive amounts of zinc can be toxic to plants. Toxicity symptoms are usually shown at Zn^{2+} leaf concentrations higher than 300 mg kg^{-1} , however, it can be extremely varied even within the same species [23]. Toxicity symptoms may include reduced yield and stunted growth, depending on the plant's sensitivity to the toxic effects of the metal [23, 24]. Zinc toxicity had also been observed to affect photosynthesis, with a critical concentration at 500 mg kg^{-1} [24].

Zinc is typically the second most abundant heavy metal in organisms, including mammals and other animals, and commonly only exceeded iron [23]. However, zinc cannot be stored by the body, making routine intake necessary, especially in the context of farm animals [25]. Known effects of zinc deficiency varied within a wide range of bodily systems, highlighting its importance in physiological systems. Similar to its effects in humans and plants, zinc plays an

important role in enzymatic reactions and immune responses [23-25]. A deficiency would therefore cause animals to be more prone to various disease and conditions related to the immune system, except in ruminants, which is more resistant to the marginal difference in zinc levels [25].

1.2.1.4 The role of zinc in the human body

Zinc is a heavy metal of group 12 in the periodic table, grouped with cadmium and mercury. It is commonly considered less toxic compared to some other heavy metals such as cadmium, mercury, copper, or nickel. This does not make its presence in the environment less dangerous, however, especially in higher concentrations. Zinc is not involved in the cellular-level redox cycle and is therefore often regarded as non-toxic. The human body normally contains 2-3 g zinc, mostly in muscles and bones, among other organs including the human heart and brain (600-800 ng L⁻¹). Its presence in the human body is useful for various bodily functions within the immune system and neurosensory system including cognition and vision. It is regarded as an essential component for various proteins and enzymes in the human body including DNA and RNA polymerase. In enzymes, it plays an important role in the catalytic and structural roles of the molecules. Zinc also plays a role in cell proliferation and differentiation, protein synthesis, DNA metabolism and repair, insulin storage and release, sequestration of free radicals, and protection against lipid peroxidation [26]. Zinc deficiency leads to decrease nerve conduction, lethargy, decreased wound healing, infertility, immune dysfunction, and infection.

The major routes of entry for zinc into the human body can be divided into three different ways: inhalation, skin contact, and ingestion [27]. In the water system, zinc solubility is dependent on the pH and total inorganic carbon concentration of the water matrix [4]. In the UK, between 2000-2021, the average concentration of zinc in river water was 11.3 µg L⁻¹, with the most commonly occurring concentration of 5 µg L⁻¹ [28, 29]. Zinc-containing smoke generated from industrial processes such as galvanization or military smoke bombs could lead to adult respiratory distress syndrome causing death upon acute high-level exposure. However, the most widely known effect of zinc inhalation would be metal fume fever, which usually occurs due to inadequate protection in occupational settings involving welding or smelting. A few hours after acute exposure, symptoms would occur including fever, muscle soreness, nausea, fatigue, and respiratory effects. Dermal and oral exposure could also occur, with skin-contact causing non-toxic irritation while excessive oral exposure causes abdominal pain, nausea, and vomiting. Excessive exposure to zinc would cause lethargy, respiratory disorder upon inhalation, nausea, diarrhoea, and copper deficiency [27]. One of the bodily systems affected by excessive zinc exposure is gastrointestinal effects. Zinc-induced copper deficiency could also happen due to

the competitive absorption relation between zinc and copper. However, unlike other heavy metal ions, zinc is less likely considered carcinogenic [27].

1.2.2 Ni²⁺ and Zn²⁺ in the environment

1.2.2.1 Limit of Ni²⁺ in the freshwater environment

Nickel is an essential heavy metal that is available in the environment in trace amounts from both natural and anthropogenic sources. Naturally, nickel is present in the Earth's crust in 0.15-0.2 mg kg⁻¹ concentration as oxides and sulphides [8, 30, 31]. Other natural sources of nickel in the environment are from dust in volcanic emissions, meteors, and weathering rocks and soils [8, 30]. The average natural amount of nickel in the soil is 100 mg kg⁻¹, whereas in surface water such as rivers, it is ranging from 0.001-0.005 mg L⁻¹ [14, 31].

Due to its physical and chemical properties, nickel is commonly used in metallurgical processes such as electroplating and alloy production, especially for stainless steel. Nickel is also present as a component in nickel-cadmium battery production and as a catalyst in the chemical and food industries [8, 14, 30]. Inorganic phosphate fertilizers and pesticides can also contain various levels of nickel [30, 31]. Due to its common utilization in various industrial processes, worldwide nickel production from mining reached around 2.7 million tonnes in 2019, with Indonesia, the Philippines, New Caledonia, and Russia as the main producers [32]. Extensive anthropogenic activities involving nickel, such as mining, smelters emission, coal and oil burning, or the use of phosphate fertilizers and pesticides, affect the environment by polluting the soil and surface water, including rivers [31]. In polluted surface water, nickel concentration can reach up to 0.2-2 mg L⁻¹, which is more than 40 times higher compared to its normal amount [14, 17].

The limit of Ni²⁺ levels in a water sample may vary between different types of water (freshwater or saline water) and regional regulations. In the EU, for example, the limit of Ni²⁺ concentration in the freshwater system is set to an annual average of 0.004 mg L⁻¹ and 0.034 mg L⁻¹ as the maximum allowable concentration [33]. This differs from the United States Environmental Protection Agency recommendation, which sets a chronic level of 0.052 mg L⁻¹ and an acute level of 0.47 mg L⁻¹ Ni²⁺ for aquatic life preservation [34]. Another regulatory body that has a set limit of Ni²⁺ in water samples is the World Health Organization (WHO), which regulates the Ni²⁺ limit for drinkable water at 0.02 mg L⁻¹ [4]. These findings, among other subsequent studies in various parts of the world, illustrate the level of Ni²⁺ found in surface water in recent decades; which is at a level far above the natural concentration of the metal – posing risks and potentially hazardous conditions for the environment and public health alike [14, 31].

1.2.2.2 Ni²⁺ contamination trend in the freshwater environment

The global average of Ni²⁺ in the freshwater system had been increasing from 0.001 ± 0.0001 mg L⁻¹ in the 1970s to 0.081 ± 0.027 mg L⁻¹ in the 2010s [1]. This number had passed the allowable amount of Ni²⁺ in drinking water set by World Health Organization (WHO), which was 0.020 mg L⁻¹ [4]. Within the tested decades, Europe ranked the highest in average Ni²⁺ concentration with 0.138 ± 0.05 mg L⁻¹ [1].

In a study focusing on heavy metal measurements in the Nile river of Egypt, Ni²⁺ concentration was found to be ranging between 0.001-0.03 mg L⁻¹ in 2017, exceeding the annual average value of Ni²⁺ according to the EU and drinkable water limit set by the WHO [4, 33, 35]. While a study in Bangladesh found a maximum amount of 0.03 mg L⁻¹ Ni²⁺ in winter [36]. A separate study in Turkey reported Ni²⁺ levels within the range of 0-0.14 mg L⁻¹ in a 2016 observation of the Coruh river basin [37].

Table 1 Global reports on Ni²⁺ concentrations in river water

Ref	Location	Year	Reported amount of Ni ²⁺ (mg L ⁻¹)
[1]	Global average	1970s	0.00143 ± 0.00016
		1980s	0.00573 ± 0.00416
		1990s	0.159 ± 0.117
		2000s	0.059 ± 0.027
		2010s	0.081 ± 0.027
[38]	Canada (industrial area)	1995	0.05-2
[39]	China	2013	0.0-0.008
[35]	Egypt	2017	0.001-0.003
[37]	Turkey	2016	0.0-0.14
[36]	Bangladesh	2017	0.03
[40]	Indonesia	2017	0.001-0.0368

In the UK, Ni²⁺ monitoring data from rivers can be obtained from the Environment Agency database. In recent years, the average Ni²⁺ concentration in river water across the UK had been steadily decreasing from the 22.62 µg L⁻¹ in 2020 to 5.38 µg L⁻¹ in 2022. In most measurement instances between 2000-2022, Ni²⁺ concentration was < 5 µg L⁻¹ across all rivers in the UK. However, as seen in Figure 3, there had been incidents of a significant spike in average Ni²⁺ concentration, notably in the years 2000, 2001, 2007, and 2018. These, according to the database, were often attributed to high levels of Ni²⁺ in proximity to mining sites or other industrial sources of Ni²⁺ [28]. In these areas, rivers can contain up to 0.05 mg L⁻¹ (2000), 4.17mg

L⁻¹ (2001), 0.01 mg L⁻¹ (2007), or 0.04 mg L⁻¹ (2018) Ni²⁺ in respective years [28]. These areas, with their dangerously high Ni²⁺ concentrations, are areas of high concern that would ideally require rapid mitigation and response.

In 2019 and the first quarter of 2020, the detection of nickel across river samples in the UK showed mostly less than 1 µg L⁻¹ nickel concentration [28, 29]. The maximum recorded nickel concentration obtained from the 2019 dataset was 6.5 mg L⁻¹, whereas from the 2020 dataset was 8.6 mg L⁻¹, both measured in Holmewood.

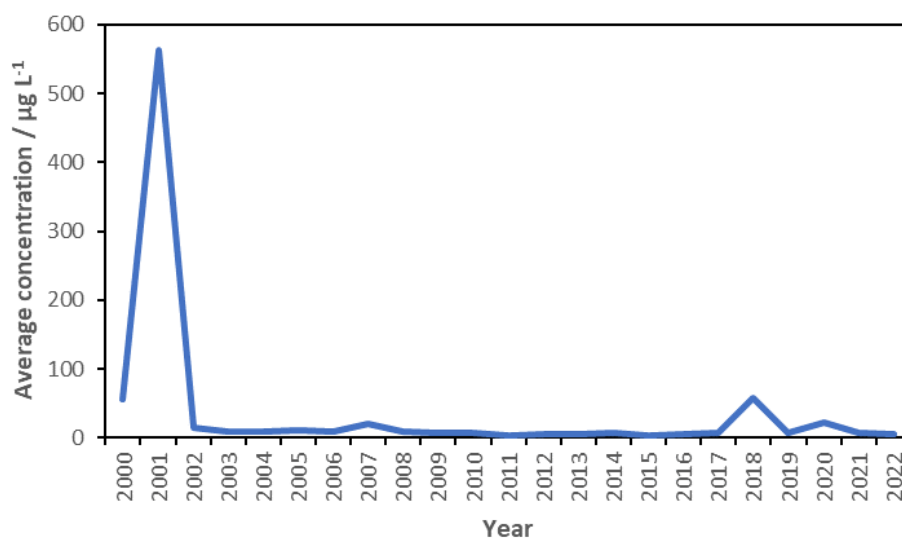


Figure 3 Average Ni²⁺ concentration measured across UK rivers between 2000-2022, according to the Environment Agency database, showing a peak in 2001 and a smaller peak in 2018 [28].

1.2.2.3 Limit of Zn²⁺ in the freshwater environment

Zinc is the 23rd most abundant element on the planet [23]. Naturally, zinc enters the environment through rock and mineral weathering, which contains the element [23, 41]. However, human activity had also significantly impacted the release of zinc into the environment, especially through the mining of precious metals, peaking at 3.4 Mega tonnes per year in the early 1980s [23]. Despite the seemingly higher amount of release, the element is perceived to be less toxic to humans and the environment. The fact that it plays essential roles and is found in relatively higher amounts than other heavy metals may also contribute to less-stringent regulation of the metal. In WHO drinking water guidelines, for example, the limit of Zn²⁺ in the water had not yet been proposed [4]. However, in freshwater systems, the EU guideline sets a limit of annual average at 0.011 mg L⁻¹ [33]. While the US EPA sets the chronic and acute limit of Zn²⁺ in freshwater environments at 0.12 mg L⁻¹ [34].

1.2.2.4 Zn²⁺ contamination trend in the freshwater environment

The lower toxicity of Zn²⁺ means relatively few studies have focussed on monitoring its presence in waterways. At the time of this writing, no accumulated data of Zn²⁺ monitoring across the globe had been published. Instead, individual studies may observe Zn²⁺ concentration along with other metals in a certain area of a river or a certain region of the world. In a study conducted at various points through the Nile river in 2017, the concentration of Zn²⁺ was measured within 0.010-0.115 mg L⁻¹ [35]. While a separate study in Bangladesh recorded an average Zn²⁺ value of 0.04 mg L⁻¹ across the year [36]. In the Coruh river basin in Turkey, the level of Zn²⁺ was recorded within the range of 0-0.08 mg L⁻¹ in 2016 [37].

Table 2 Global reports on Zn²⁺ concentrations in river water.

Ref	Location	Year	Reported amount of Zn ²⁺ / mg L ⁻¹
[42]	Indonesia	2010	165.83-487.69
[39]	China	2013	0.0-0.049
[37]	Turkey	2016	0.0-0.08
[35]	Egypt	2017	0.010-0.115
[36]	Bangladesh	2017	0.04
[40]	Indonesia	2017	0.010-0.041

Similar to Ni²⁺ data, the Zn²⁺ monitoring data for the UK was also obtained from the Environment Agency database. Figure 4 shows the rise and decline in annual average Zn²⁺ concentration measured across the UK within a given year, between 2000 and 2021. In the illustrated average, the average measured concentration of Zn²⁺ in freshwater systems across the UK started at 0.043 ± 0.374 mg L⁻¹ with a mode of 0.005 mg L⁻¹ [28]. Before a significant increase was observed in 2010, increasing the annual average to 0.071 ± 3.942 mg L⁻¹ while maintaining the mode at 0.005 mg L⁻¹ [28]. However, a further annual average increase was recorded at the year of 2012, with an annual average of 0.174 ± 6.455 mg L⁻¹ maintaining the same mode of 0.005 mg L⁻¹ [28]. The next few years showed fluctuating trends before a further increase was recorded in 2018, averaging at 0.183 ± 1.268 mg L⁻¹ while still maintaining the mode of 0.005 mg L⁻¹ [28]. The last increase, which was also the last recorded dataset available at the point of writing, was an increase in the first half of 2021, showing an average of 0.196 ± 0.318 mg L⁻¹ Zn²⁺ with the same mode of 0.005 mg L⁻¹ [28].

Through this dataset, it can therefore be concluded that despite the fluctuation and increasing trend of the annual average of Zn²⁺ in a freshwater environment, most testing sites were still below the limit of detection of the analytical system (<0.005 mg L⁻¹), which is also below the

hazardous limit of Zn^{2+} in the freshwater environment [33, 34]. However, it is interesting to note that the highest recorded Zn^{2+} concentration in the dataset was in the year 2012 when an ad hoc sample reached $628 \text{ mg L}^{-1} Zn^{2+}$ concentration, followed by a sample in River Trent in 2010, where the measured Zn^{2+} concentration reached 436 mg L^{-1} [28, 29].

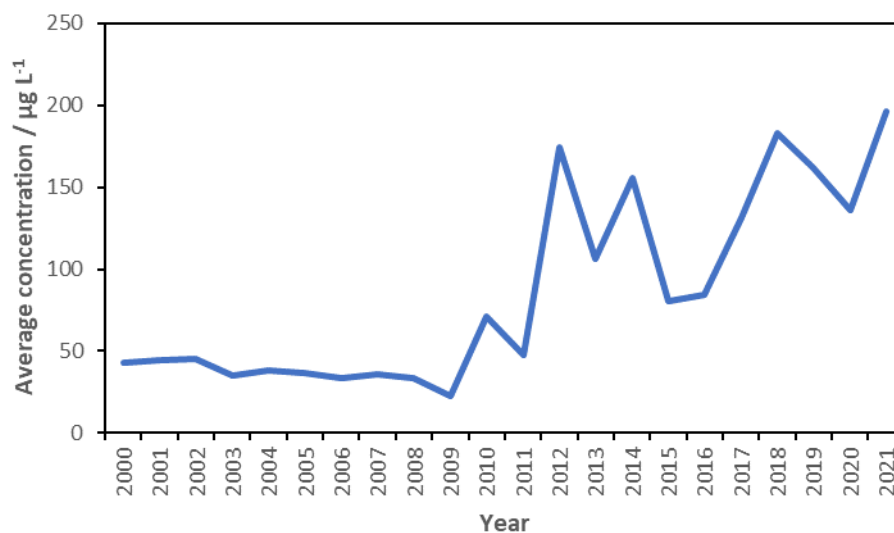


Figure 4 Average Zn^{2+} concentration measured across UK rivers between 2000-2021, according to the Environment Agency database, showing increase in Zn^{2+} concentration measured with fluctuation between 2010-2021 [28].

1.2.3 Ni^{2+} and Zn^{2+} detection methods in the environmental sample

Metal monitoring in water samples occurred as early as the 1960s with the development of atomic absorption spectrometry (AAS) as well as cleaner laboratory workflow to minimise potential contamination[43]. With further advancements in technologies, precise and sensitive analytical equipment has made metal monitoring straightforward. At the time of this writing, the instruments of choice for metal analysis in water samples are Inductively Coupled Plasma – Mass Spectrometry (ICP-MS) or Atomic Absorption Spectroscopy (AAS).

1.2.3.1 Inductively Coupled Plasma – Mass Spectrometry (ICP-MS)

Inductively coupled plasma-mass spectrometry (ICP-MS) is an analytical technique developed utilising initially ionised argon gas through a quartz torch inside the copper coil, which is connected to a radio frequency generator. The ions are then extracted from the nebulised plasma and separated by the mass-to-charge (m/z) ratio [44, 45]. It is a highly sensitive analytical system, capable of detection down to $\mu\text{g L}^{-1}$ level, making it highly beneficial for metal analysis in environmental samples. This method had been used as one of the metal measurement methods in water samples by the United States Environmental Protection Agency (US EPA) [45].

ICP-MS for metal detection may require a preconcentration system, which can be obtained through the integration of offline or online preconcentration systems. For instance, the integration of anion-exchanger column chromatography can complete metal speciation from the environmental complex through concentration and matrix removal steps [46]. Another study utilised a solid-phase extraction (SPE) column with chelating materials packed in it, allowing the sample to be pumped through the column and eluted before metal concentration was measured with ICP-MS [47]. Further discussion on the preconcentration step will be elaborated in section 1.6.3. In other cases, however, the preconcentration step can be omitted depending on the sensitivity required for the data. In these studies, the method validation step was first completed before metal detection in the environmental samples was done [48, 49].

1.2.3.2 Flame Atomic Absorption Spectrometry (FAAS)

Flame atomic absorption spectrometry depends on the atomization of the target element using a direct flame, where the intensity and wavelength of light emitted by the flame is a direct correlation with the concentration of the target element [50]. This method had also been previously used as the standard method for metal measurement in environmental water samples by the US EPA [50]. Select studies still utilised this analytical method, as it has a low enough detection limit ($\mu\text{g L}^{-1}$) for the detection of metal pollution while having the advantage of simplicity and relatively lower capital cost compared to ICP [51].

Similar to ICP-MS, this method is often used in tandem with a preconcentration step to detect lower concentrations. Solid phase extraction (SPE) had been used for the preconcentration of water samples before using reactive polymer matrixes for adsorption with subsequent acidic elution and then feeding the sample into the FAAS system [52, 53]. Other studies utilised coprecipitation methods for preconcentration, depending on the target metal in the water samples [54-56]. More descriptions of preconcentration methods can be found in section 1.6.3.

1.2.3.3 Other methods

1.2.3.3.1 Other laboratory-based detection

As ICP is in itself a separate system of sample ionisation, different analytical methods can be coupled with it instead of mass spectrometry. Other known assemblies include ICP-OES and ICP-AES, the latter of which was also a standard method in US EPA metal in water measurement [57, 58]. Additionally, ICP-MS itself can be varied with its preceding preconcentration method, as had been briefly discussed in the previous section. Similarly, there is another variation for the atomic absorption spectroscopy technique (AAS), where instead of direct flame, a furnace is used for the atomisation process [59]. The method can also vary depending on the preceding preconcentration step. All these similar alternative analytical methods can be used for metal

detection in the environment, depending on the intended sensitivity and the required data. However, the two discussed in the previous section are now the most commonly used methods.

1.2.3.3.2 Deployable sensors

Recent advances in technology have allowed continuous detection of heavy metals in the environment, such as freshwater or streams, through a deployable sensor. The term deployable sensor, in this case, refers to a specially made device that can be placed in a certain area in the environment for monitoring and detection purposes. For metal detection in the environment, these sensors can be electrochemical, bio-electronical, or bio-electrochemical, among other types. In most cases, bio-electrochemical sensors had the highest sensitivity [60].

1.2.3.4 Sample preconcentration methods: solvent evaporation

As has been stated in previous sections, metal detection in environmental samples often requires a preconcentration step due to its trace nature. One popular approach discussed further in section 1.6, is ion exchange column chromatography. Another popular approach involves solvent evaporation. This approach to preconcentration can be achieved through rotary evaporation, automated evaporative concentration systems (EVACS), and gas blow-down [51]. These approaches often require an external device as a heat source to induce the rapid evaporation process.

1.3 Microfluidic paper-based analytical device (μ PAD) for environmental metal detection

1.3.1 Microfluidics fundamentals and its role in environmental metal detection

Microfluidics is a sub-branch of fluid mechanics, dealing with the microscopic (10^{-9} to 10^{-18} litres) scale of fluid flows [61, 62]. At this scale, the properties and flow of fluids differ from macroscopic flows. For instance, in microfluidic systems laminar flow is more commonly found than turbulence. Another stark difference is that the effects of surface tension and gravity are reversed in this smaller-scale system[61]. In the context of this research, the term microfluidic is often used to refer to microfluidic-based devices. These devices manipulate and control the flow of small amounts of liquid for various purposes, such as mixing and separating [63, 64]. Due to the broad definition, fundamentally, microfluidics can be used to describe a wide range of devices involving micro-scale liquid-handling. However, for this research, the only branch of microfluidic to focus on is its potential for the development of novel analytical systems, especially for heavy metal detection. Detection of heavy metals with the aid of microfluidic technology can be achieved through integration with microwave, electrochemical, and optical sensing [65, 66]. Aside from the type of sensing technique, microfluidics can also be

differentiated based on the matrix, such as chip (Figure 5) or paper; the latter of which has sparked interest due to its potential for use in cheap, simple, and disposable sensors [64, 67].

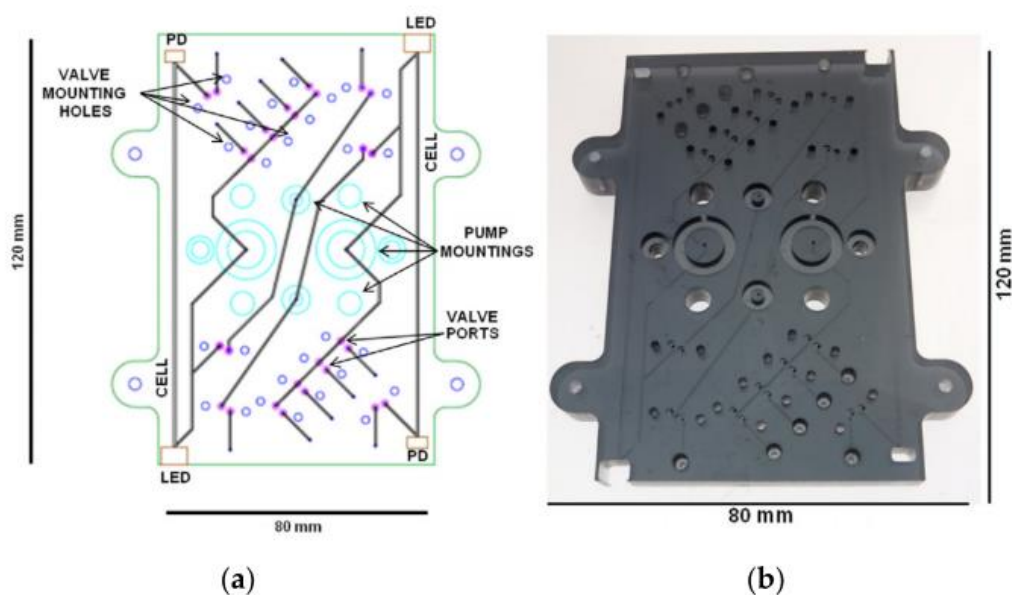


Figure 5 Example of microfluidics devices for detection of metal in water sample as developed in previous studies (a) Diagram of polymethyl methacrylate (PMMA) chip and (b) photograph of a tinted chip [68].

1.3.2 Microfluidic Paper-Based Analytical Device (μ PAD)

1.3.2.1 Fundamentals

Microfluidic paper-based analytical devices, abbreviated as μ PADs in this research, are a branch of microfluidics technology, which utilizes paper or paper-like substrate as a matrix. These are then patterned to create hydrophobic and hydrophilic areas [67]. The increasing interest in rapid and low-cost sensor technology has generated interest in utilising paper-based devices. Paper is an ideal matrix due to its naturally woven structures capable of sample filtration. This leads to capillary action eliminating the need for external pumping actions, and an absorbent nature that helps in the reagent storage system [64, 69]. In addition to these properties, μ PADs also pose advantages in disposability, chemical and biological inertness, portability, and biodegradability [69]. Illustrations of various μ PADs made using different fabrication techniques are shown in Figure 6.

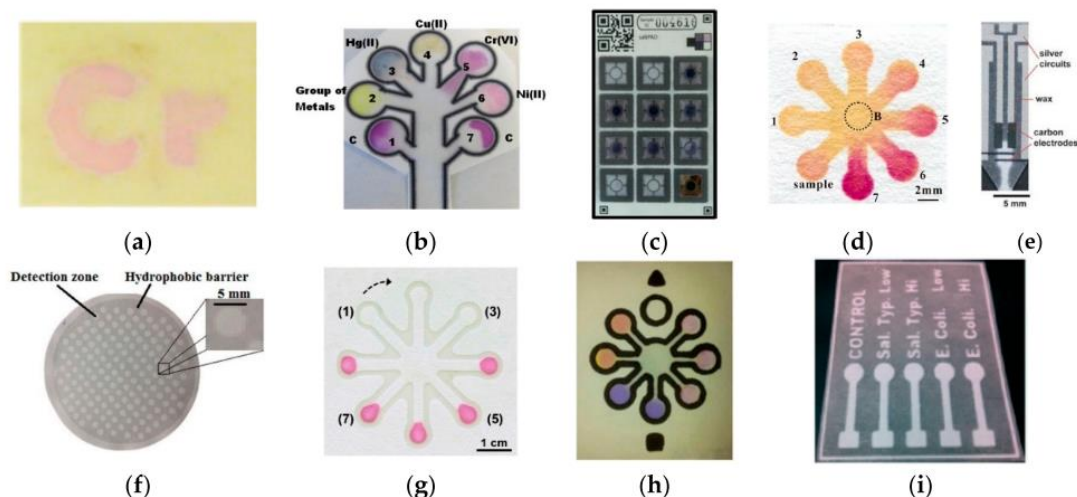


Figure 6 Examples of μ PADs made with different fabrication methods and paper matrix; (a) wax patterning on WCP1, (b) wax printing on WP1, (c) wax printing on AP319, (d) UV/ozone-patterning on WFP1, (e) wax printing with screen-printed electrode on WCP1, (f) polymer screen printing on WFP4, (g) contact stamping on JPP40, (h) contact stamping on WFP1, and (i) photolithography on CP. Where WFP1= Whatman no 1 filter paper, WCP1= Whatman no 1 chromatography paper, WP1= Whatman no 1 paper, AP310= Ahlstrom 319 paper, WFP4= Whatman no 4 filter paper, JPP40= JProLab JP 40 filter paper, and CP= chromatography paper, as illustrated in [70].

1.3.2.2 Classification of μ PAD – Fabrication technique

The main concept of μ PADs is to create hydrophobic barriers as well as hydrophilic channels for an operation on the matrix by patterning the paper with hydrophobic materials. In order to achieve this, various fabrication processes have been developed and are continuously being expanded [11, 69]. These fabrication processes are highly flexible and can be adjusted depending on the device design and operational objectives.

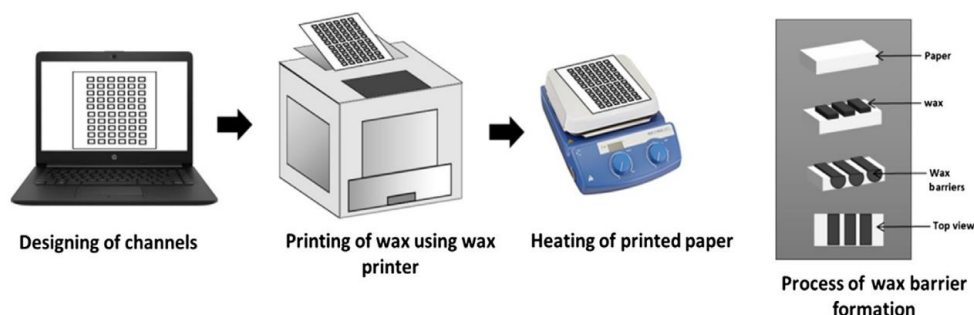


Figure 7 Illustration of wax printing fabrication method, which was adapted with modification in this study [11].

Table 3 lists some of the commonly used μ PAD fabrication methods along with each of their advantages and disadvantages relative to one another. Some techniques, like inkjet etching,

screen printing, wax dipping, and PDMS printing are not readily suitable for mass production – a major drawback in the context of this study, as we are aiming to develop a device for public uses. Whereas others have technical drawbacks, such as low mechanical stability during the cutting of devices, complex preparation steps in photolithography, or inconsistencies in wax stamping processes. Amongst the listed fabrication techniques, the only technique used in this research will be wax printing (Figure 7). This is due to its advantage in simple fabrication and ability to produce the design in high capacity – all with relatively low cost [11, 69].

Table 3 Comparison of commonly used μ PAD fabrication methods [11, 69].

Method	Advantages	Disadvantages
Cutting	<ul style="list-style-type: none"> • Defined features 	<ul style="list-style-type: none"> • Waste of raw material • Low mechanical stability
Photolithography	<ul style="list-style-type: none"> • Sharp barriers • High channel resolution 	<ul style="list-style-type: none"> • Expensive equipment • Complex steps • Expensive reagents
Polydimethylsiloxane printing	<ul style="list-style-type: none"> • Cheap patterning agent (PDMS) • Flexible device 	<ul style="list-style-type: none"> • Inconsistent control of barrier formation • Low resolution • Requires curing • Cannot be readily scaled up
Inkjet etching	<ul style="list-style-type: none"> • Low cost 	<ul style="list-style-type: none"> • Complex steps • Requires customisation of equipment • Not suitable for mass fabrication
Wax dipping	<ul style="list-style-type: none"> • Low cost • Simple fabrication 	<ul style="list-style-type: none"> • Inconsistent between batches • Not suitable for mass fabrication
Flexography printing	<ul style="list-style-type: none"> • Avoids heat treatment 	<ul style="list-style-type: none"> • Expensive process • Complex reagents • High maintenance
Screen printing	<ul style="list-style-type: none"> • Low cost • Simple fabrication 	<ul style="list-style-type: none"> • Low channel resolution • Rough barriers • Not suitable for mass production
Wax printing	<ul style="list-style-type: none"> • High production capacity • Simple fabrication 	<ul style="list-style-type: none"> • Low resolution • Requires extra heating step
Stamping	<ul style="list-style-type: none"> • Low cost • Simple fabrication 	<ul style="list-style-type: none"> • Inconsistent process • Low resolution • Requires preheating of stamp and paper oxidation
Inkjet printing	<ul style="list-style-type: none"> • High resolution 	<ul style="list-style-type: none"> • Requires equipment modification

		<ul style="list-style-type: none"> • Different ink compositions for each printing • Requires extra heating step
Plasma treatment	<ul style="list-style-type: none"> • Cheap patterning agent (alkenyl ketene dimer or fluorocarbon) 	<ul style="list-style-type: none"> • High cost • Complex steps
Vapour phase deposition	<ul style="list-style-type: none"> • Simple fabrication • Can achieve complex patterns 	<ul style="list-style-type: none"> • High equipment cost
Wet etching	<ul style="list-style-type: none"> • Simple fabrication 	<ul style="list-style-type: none"> • High cost
Hand-held corona treatment	<ul style="list-style-type: none"> • Low cost • Simple fabrication 	<ul style="list-style-type: none"> • Requires extra heating process

1.3.2.3 Classification of μ PAD - Reaction type

μ PADs also offer flexibility in the type of reaction and readout that can be integrated into the system. In heavy metal detection, colorimetric readouts are common, and fluorescence, electrochemical, and chemiluminescence detect methods have all been utilised [71]. These reactions also have their advantages and disadvantages, from a chemical perspective (e.g. sensitivity, selectivity) as well as from a commercialization perspective (e.g. complexity, cost). In some cases, fluorescence sensing can achieve very low limits of detection [72, 73]. However, commercialization of such devices would depend on the miniaturization of fluorescence readers, as well as cost reductions [69]. An example of a fluorescence reaction for metal detection is seen in a device developed for Cu^{2+} detection on ion-imprinted polymer grafted paper [74]. The developed device was able to detect down to $0.012 \text{ mg L}^{-1} \text{ Cu}^{2+}$ within 15 min, with data acquisition involving a fluorescence reader. Colorimetric sensing offers relative simplicity in the signal readout, with little to no requirements for the development of additional readout devices. An example of a colorimetric μ PAD is illustrated in Figure 8.

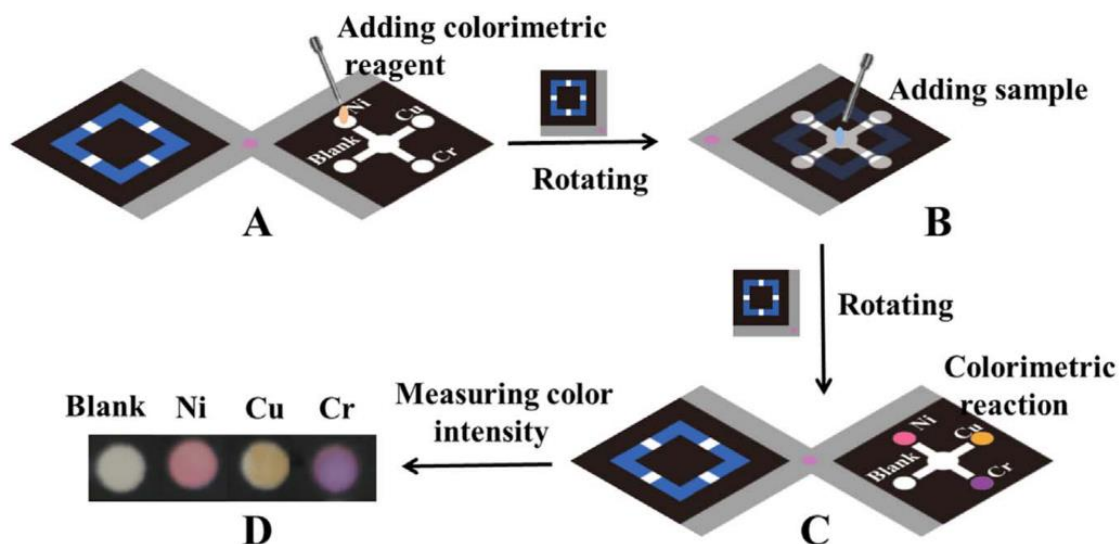


Figure 8 Illustration of reagent deposition and sample introduction to a colorimetric-based μ PAD for metal detection as published in [75].

Electrochemical sensing (Figure 9) is another interesting method, offering relatively rapid readout and high sensitivity [76, 77], despite its operational complexity and higher cost of production [69]. An example of μ PADs for electrochemical sensing of Ni^{2+} utilised a Cu^{2+} enhancer to amplify the electrochemical signal detected on the screen-printed carbon electrode, is shown in Figure 9 [78]. This process required deposition of 50 μL of pre-treated sample on the hydrophilic channel of the device; where the pre-treatment steps consist of filtration, mixing with HNO_3 , and evaporation of HNO_3 , followed by repeated rinsing and drying before sonication [78]. Despite its ability to detect down to 0.5 mg L^{-1} , the device still requires a laboratory setting to operate as reported. Whereas chemiluminescence, although used less frequently, allows for rapid detection and low detection limits [79]. However, this type of sensing requires specialised equipment for readout, which can be relatively costly.

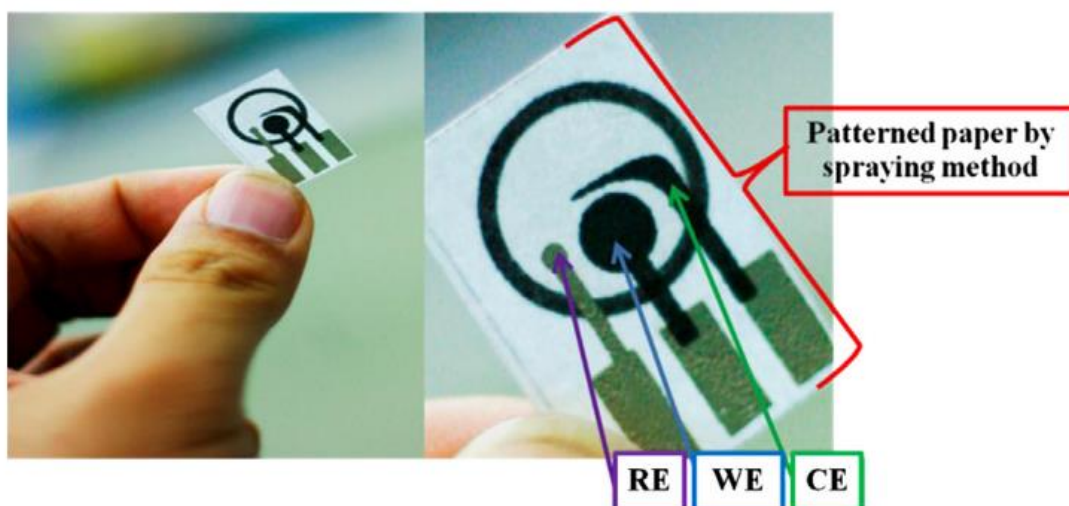


Figure 9 Example of paper-based microfluidics with electrochemical sensing reaction for Ni^{2+} detection, with RE= reference electrode, WE= working electrode, and CE= counter electrode, as published by Nurak, *et.al.* [78].

1.3.3 μ PAD for metal detection

1.3.3.1 Ni^{2+} detection

As mentioned in previous sections, nickel is one of the heavy metals which presents a significant health and environmental hazard. Therefore, nickel monitoring in the environment, including in surface water systems such as rivers, is of great interest and importance. Previous researchers had developed μ PADs for nickel detection in river water systems with colorimetric methods (Table 4).

Table 4 Previous research on μ PAD for Ni^{2+} colorimetric detection in environmental water samples.

Ref	Reagent	Additives	Reaction time (min)	LOD (mg L^{-1})	Linear range (mg L^{-1})
[80]	3 μL 60 mM dimethylglyoxime	8 μL 0.5 mg L^{-1} hydroxylamine hydrochloride; 4 μL 0.03 M ammonium hydroxide; 5 μL 0.5 M NaF; and 5 μL 6.3 M acetic acid	120	5.9	5.87-352.16
[81]	100 mM dimethylglyoxime	50 mM tris base; 1 M NaF; 6 M ammonium acetate		100	100-1100
[77]	Dimethylglyoxime	NaF, acetic acid		15	30-300
[75]	10 μL 0.1 M dimethylglyoxime	4 μL 1 M NaF; 4 μL 1 M sodium thiosulfate; 4 μL ammonium hydroxide buffer	10	4.8	15-60

[13]	30 μ L 0.15 mol L ⁻¹ dimethylglyoxime	3 μ L 1 mol L ⁻¹ NaF; 3 μ L 1 mol L ⁻¹ sodium thiosulfate; 3 μ L 1 mg mL ⁻¹ chitosan in acetic acid; 3 μ L 6.3 mol L ⁻¹ acetate buffer; 3 μ L 3 mg mL ⁻¹ Tween 20	20	0.3	0.4-23
[82]	Dimethylglyoxime	APTES functionalized paper	5	0.24	

Kamnoet, *et al.* [80] have developed a multiplex heavy metal detection μ PAD, with one of the channels dedicated to nickel colorimetric detection with dimethylglyoxime (Figure 10). The μ PAD contained two pre-treatment steps with hydroxylamine hydrochloride, ammonium hydroxide, and sodium fluoride (NaF), along with acetic acid for pH adjustment. The reaction time for overall detection was 120 minutes, with a 5.9 mg L⁻¹ detection limit and linear range between 5.87-352.16 mg L⁻¹ nickel concentration. This is an improvement on Cate, *et al.* [80, 81], who developed a multiplexed distance-based colorimetric nickel detection with dimethylglyoxime as the colorimetric reagent. The device also contained a tris base for pH adjustment, along with ammonium acetate and sodium fluoride as masking agents. The distance-based device showed linearity in the range of 100-1100 mg L⁻¹, with a limit of detection of 100 mg L⁻¹ [80]. Whereas Rattanarat, *et al.* [77] developed a hybrid device combining colorimetric and electrochemical detection, where nickel detection was done through a colorimetric reaction with dimethylglyoxime. This device had a linear range of 30-300 mg L⁻¹ nickel concentration with a detection limit of 15 mg L⁻¹.

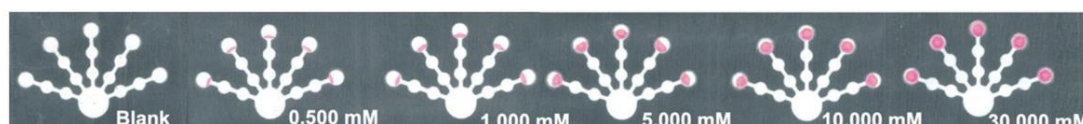


Figure 10 Example of a Ni²⁺ detection μ PAD fabricated with wax printing technique on Whatman grade 1 qualitative filter paper with dimethylglyoxime as the colorimetric reagent, as illustrated in [80].

Sun, *et al.* [75], developed a multiplex heavy metal detection μ PAD with a rotational valve, where nickel detection was achieved through a colorimetric reaction with dimethylglyoxime (Figure 8). This device showed linear colour intensity responses between 15-60 mg L⁻¹, with a limit of detection of 4.8 mg L⁻¹. Li, *et al.* [13], also developed a multiplex heavy metal detection μ PAD, where nickel was detected with a colorimetric method through a reaction with dimethylglyoxime, in the presence of masking agents: sodium fluoride and sodium thiosulfate. The device also contained chitosan as a means of preconcentration as well as acetate buffer for

pH adjustment. It can detect nickel down to 0.3 mg L^{-1} concentration in 20 minutes, with a linear working range of $0.4\text{-}23 \text{ mg L}^{-1}$ nickel concentration. Lastly, Devadhasan, *et al.* [82], also developed colorimetric nickel detection μ PADs by paper functionalization and using dimethylglyoxime as a colorimetric reagent. For nickel, the detection area was functionalized with APTES. This device required 5 minutes of reaction time but was able to detect nickel down to 0.24 mg L^{-1} .

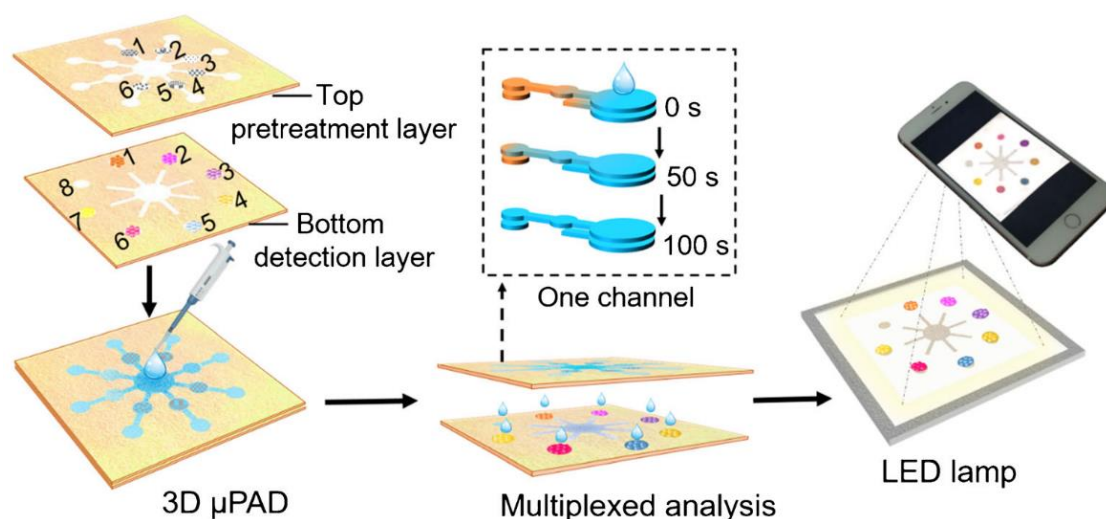


Figure 11 Example of the fabrication and use of μ PAD for multiplex analysis of various metals, published in [13].

Most of the μ PADs developed for nickel detection rely on colour intensity measurements of a dimethylglyoxime-nickel complex formed on the paper matrix. Due to the limited selectivity of the colorimetric reagent, masking agents are often integrated into the μ PADs (sodium fluoride/NaF and sodium thiosulfate/ $\text{Na}_2\text{S}_2\text{O}_3$) [13, 75, 77, 80, 81]. However, as can also be seen in Table 4, the developed devices were not able to detect nickel to an environmentally-relevant level, based on the Environment Agency data of common occurrence of nickel in a freshwater environment, which is in $5 \text{ } \mu\text{g L}^{-1}$ level [28, 29]. In addition to this problem, the reaction time of most of the devices was not favourable for rapid on-site nickel level monitoring, especially with the citizen science approach.

1.3.3.2 Zn²⁺ detection

Compared to nickel, the detection of zinc using μ PADs has not received as much attention. Therefore, it is an interesting heavy metal to focus on in this research. Most μ PADs that have been developed for zinc detection using colorimetric reaction utilized zincon monosodium salt as a colorimetric reagent [12, 83]. Muhammad-Aree, *et al.* [12], had developed a zinc detection

strip with cyanide and cyclohexanone masking that produced results within 1 minute. The limit of detection of this device was 0.04 mg L^{-1} with a linear range between $2\text{-}6 \text{ mg L}^{-1}$.

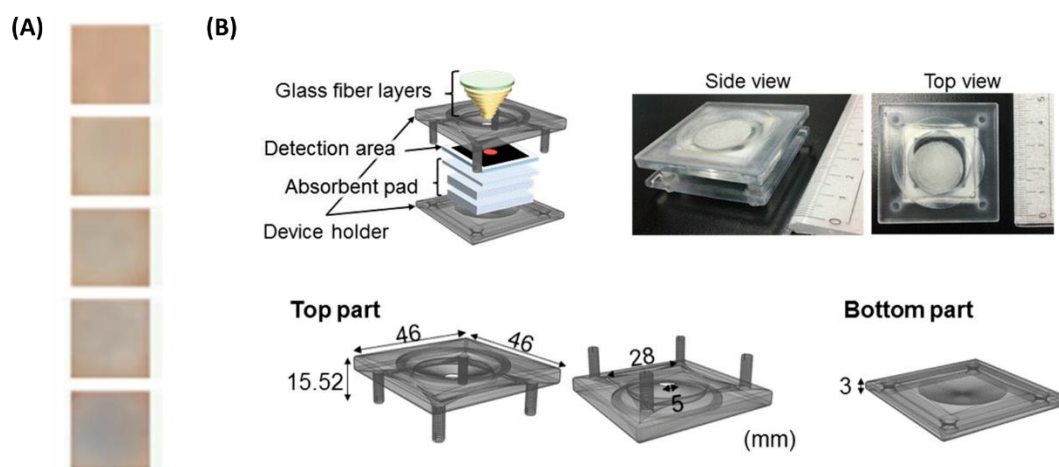


Figure 12 (A) Top to bottom: endpoint colour of Zn^{2+} detection μPAD with zincon colorimetric reagent introduced into Zn^{2+} assay within $0\text{-}10 \text{ mg L}^{-1}$ concentration range [12]; (B) Design of 3D- μPAD for Zn^{2+} detection with zincon as colorimetric reagent, as illustrated in [83].

Kudo, *et al.* [83], had previously developed a μPAD with glass fibre integration, PDADMAC, and salicylaldoxime masking for zinc detection down to 8 mg L^{-1} . In contrast, Li, *et al.* [13] developed their zinc detection zone in a multiplex heavy metal detection μPAD with dithizone as a colorimetric reagent. This was coupled with sodium thiosulfate for masking and acetate buffer to regulate the pH and was able to detect zinc within a $0.05\text{-}24 \text{ mg L}^{-1}$ linear range with a 0.04 mg L^{-1} detection limit within 15 minutes. For zinc detection, one of the previously developed μPAD s had a fast reaction time, requiring only 1 minute of detection time. However, none of the developed devices were able to detect zinc at environmentally-relevant levels, based on the Environment Agency data on the commonly occurring amount of zinc in freshwater systems, which is $5 \mu\text{g L}^{-1}$ [28, 29]. The research on zinc detection using μPAD s is summarised in Table 5.

Table 5 Previous research on μPAD for Zn^{2+} colorimetric detection in environmental water samples.

Ref	Reagent	Additives	Reaction time (min)	LOD (mg L^{-1})	Linear range (mg L^{-1})
[13]	$2 \mu\text{L}$ 0.5 mg mL^{-1} dithizone	$3 \mu\text{L}$ 1.5 mol L^{-1} sodium thiosulfate; $3 \mu\text{L}$ 6.3 mol L^{-1} acetate buffer	15	0.04	0.05-24
[12]	$3 \mu\text{L}$ 0.4 mM zincon monosodium salt	Cyanide; cyclohexanone	1	0.63	2-6

[83]	1.6 mM zincon monosodium salt	14.3 mM salicylaldehyde in 400 mM TAPS/TMAOH; PDADMAC;	15	8	
------	-------------------------------	--	----	---	--

1.3.4 Preconcentration in μ PADs

Where analytes are present at concentrations below the μ PAD level of detection preconcentration may be required. This process can be through the direct incorporation of a preconcentration system in the μ PAD itself or through an additional external device which is then coupled with the μ PAD workflow. Quinn, *et al.* (2018), described an external device (offline system) to be integrated with a μ PAD for trace Cu^{2+} detection (Figure 13) [84]. In this work, a preconcentration system utilising solid-phase-extraction (SPE) principles within a syringe was developed for Cu^{2+} preconcentration from drinking water samples [84]. The study claimed that the developed workflow was able to detect Cu^{2+} within the 0.002 mg L^{-1} to 500 mg L^{-1} range [84]. Despite its attractive potential for Cu^{2+} detection, the study did not check the effect of the presence of other ions in the sample. The integrated μ PAD in the research required 30 min to reach an endpoint of the reaction – which may be too long of a reaction duration for onsite detection. Additionally, the elution step of the workflow required the introduction of corrosive acid through a syringe. The risks involved in handling the acid will restrict the pool of target users who can safely operate the developed workflow.

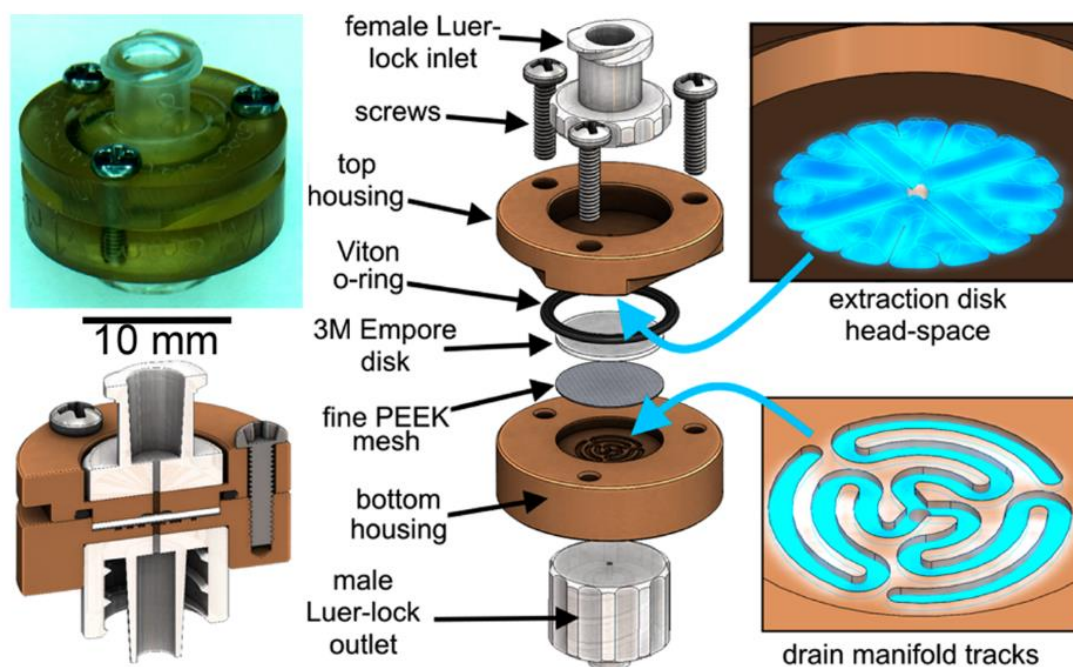


Figure 13 Example of a preconcentration system with solid phase extraction method with 3M Empore Chelation disk [84].

Another preconcentration method that is often integrated directly into μ PADs is known as ion concentration polarization (ICP). This method has been utilised on various devices developed for different enrichment processes on various substrates [85]. However, in the case of heavy metals, as per the time of writing, only one publication had discussed and developed the system; for As^{3+} allowing for the detection of the ion as low as 0.001 mg L^{-1} with only $40 \mu\text{L}$ of the sample [65, 86]. Rather than using filter paper, this technique utilised a patterned Nafion membrane as a means of preconcentration [86]. The preconcentration system itself requires a DC power source to induce the ion-based separation – therefore it may require additional equipment to operate [86]. The study revealed detection of As^{3+} required 10 min of processing, with increasing duration affecting the sensitivity of the device, with 30 V introduced to the system [86]. For onsite analysis, the need for a battery or electricity source can be seen as a challenge. However, this had not been addressed in the study.

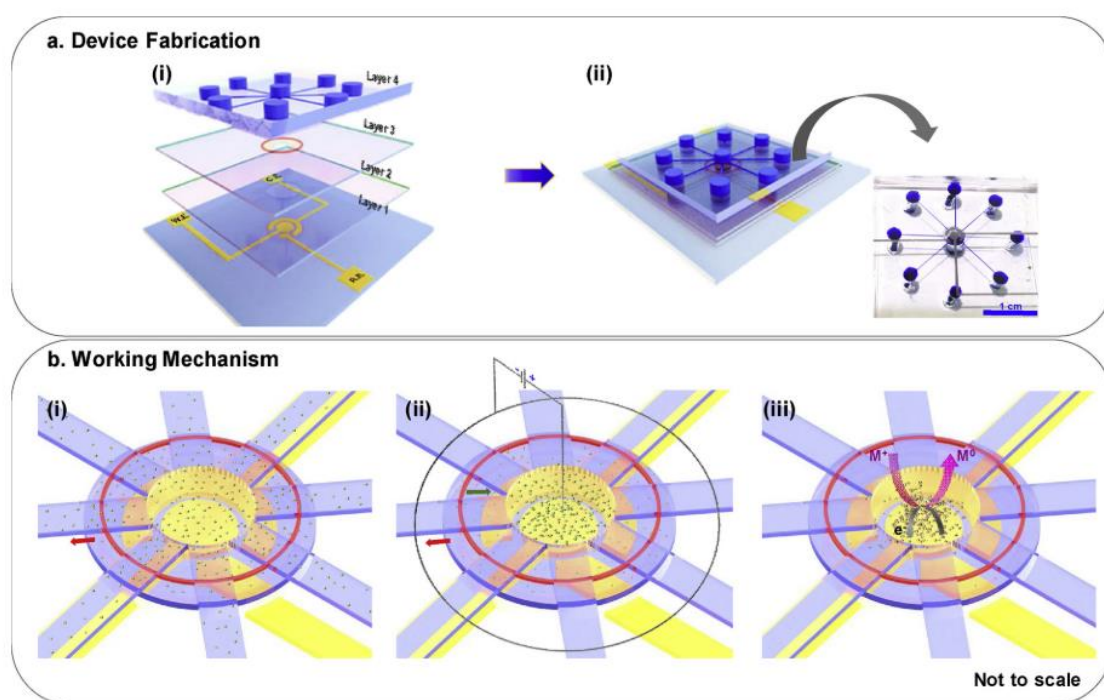


Figure 14 A schematic of the device fabrication protocol and its working mechanism. (a) shows the device fabrication, (i) representation of the various layers of the device, (ii) shows the fully fabricated device, inset shows an optical image of the fabricated device (bottom view); (b) shows the working mechanism of the device. (i) schematic showing the device is filled with the analyte, (ii) represents the application of external to induce ion concentration, and (iii) depicts the reduction of concentrated ions after ICP [86].

1.4 Colorimetric reaction for metal detection

Colorimetric sensing is the most common technique used for the detection of heavy metals. This is typically based on absorbance-based detection using UV/Vis spectrophotometry, which is

commonly used due to its sensitivity and relatively simple setup [87]. Colorimetric sensing on μ PADs shifts the measured parameter from light absorbance following Beer-Lambert Law to measurement of colour intensity produced by a reaction occurring within the paper. Measurement of colour intensity has the advantage of equipment independence compared to absorbance-based measurement, which would require a light source. With increasingly easy access to high-quality smartphone cameras and sophisticated smartphone applications, colorimetric sensing becomes an interesting and accessible option, especially for low-cost remote sensing of various substrates. However, the method itself is not free from drawbacks, especially in real-world applications. Since colorimetric μ PADs often require colour intensity measurement of the complex formed on the matrix, it is highly dependent on the smartphone camera – which is often the preferred method of image acquisition. However, to achieve repeatable and reliable results, there is a need for either method standardization or technological improvement to achieve similar images with equal colour intensity or lighting conditions upon repeats [69].

1.4.1 Colorimetric detection of heavy metals

1.4.2 Ni^{2+} detection reagent

Numerous methods for the detection of Ni^{2+} in the environment using solution-based colorimetric means have been described. Some of the chemical compounds that have been researched for colorimetric nickel detection are listed in Table 6. However, there is a notable lack of alternative colorimetric reagents used in the colorimetric analysis for nickel detection in μ PAD settings (see Table 4 in section 1.3.3.1). This is despite extensive alternatives in reagents producing coloured complexes.

Dimethylglyoxime, often abbreviated as DMG, is a ligand widely known for its selectivity to Ni^{2+} . The chemical's ability in Ni^{2+} complexation has been recorded since 1945; however, the study also shows possible interferences in the presence of other ions, such as Cd^{2+} , Ca^{2+} , or Zn^{2+} [88]. The colorimetric reaction between Ni^{2+} and the colourless ligand forms a 2:1 ligand-to-metal magenta-coloured complex formation, as shown in Figure 15

Previous studies had utilised the chemical for Ni^{2+} detection in μ PAD settings, as well as other settings, such as Ni^{2+} removal workflow and electrochemical-based monitoring systems [89], Ni^{2+} detection with solid phase extraction technique [90], as well as Ni^{2+} sensing in electrospun fibres [91].

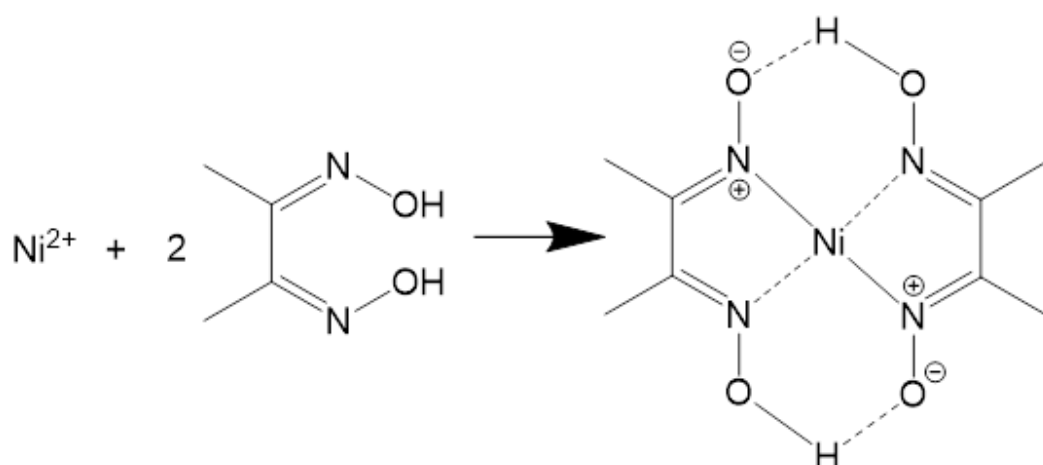
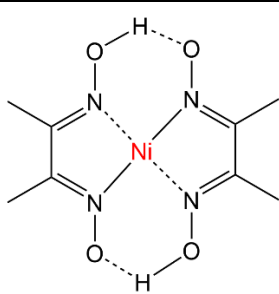
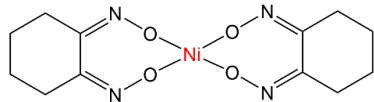


Figure 15 Dimethylglyoxime complexation reaction with Ni^{2+} , forming 2:1 ligand to metal complex.

As shown in Table 6 colorimetric detection of Ni^{2+} often requires separation, due to possible interference by other metals. This also includes reaction with dimethylglyoxime, which is used in most μPAD for Ni^{2+} colorimetric detection [13, 75, 77, 80-82]. The avenue of exploring other colorimetric reagents, therefore, is interesting due to the lack of research in the area, as well as to possibly improve the disadvantageous points of dimethylglyoxime; especially the requirement of organic-based solvent [75].

Table 6 Colorimetric reagents for nickel detection, its mechanism of the reaction, limit of detection or linear range, and interferences by other ions.

Ref	Compound name	Mechanism	LOD or (Linear range) (mg L^{-1})	Interference
[88]	Dimethylglyoxime	 2:1 ligand-to-metal ratio	(0.1-5)	Au, Co, Cr_2O_7 , Cd, Ca, Zn
[92]	1,2-cyclohexanedione dioxime	 2:1 ligand-to-metal ratio	0.2	Cu, Fe, Co
[93]	Xylenol orange/PDADMAC	In the presence of PDADMAC, a 2:1 ligand-to-metal ratio	4.3×10^{-3}	Al, Cd, Co, Cu, Hg, Zn
[94]	1-nitroso-2-naphthol		3.9×10^{-5}	Fe, Cr, Co

[95]	Alizarin complexone/PDAD MAC		2.2×10^{-2}	Al, Ca, Cd, Co, Cu, Cr, Fe, Hg, Mg, Mn, Pb, Zn
------	------------------------------	--	----------------------	--

1.4.2.1 1,2-cyclohexanedione dioxime or nioxime

1,2-cyclohexanedione dioxime, commercially known as nioxime, was first prepared by Wallach in 1924, as a more sensitive reagent for Ni^{2+} detection compared to dimethylglyoxime (DMG). Its solubility in water is reported to be 8500 g L^{-1} at 20°C , with possibly higher solubility in alcohol [92]. The detection limit of the compound for Ni^{2+} colorimetric reaction was initially reported to be 0.5 mg L^{-1} , however, further research has reported the detection of Ni^{2+} in lower concentrations, down to 0.2 mg L^{-1} [92]. The mechanism of the reaction between the ligand and Ni^{2+} ion is illustrated in Figure 16, where a complexation reaction occurs at a 2:1 ligand-to-metal ratio. The use of nioxime as a colorimetric reagent for Ni^{2+} detection in UV/Vis spectrophotometric analysis would show colour gradient from colourless to magenta, which can be quantified by measuring the absorbance of the solution at 530 nm wavelength [96, 97].

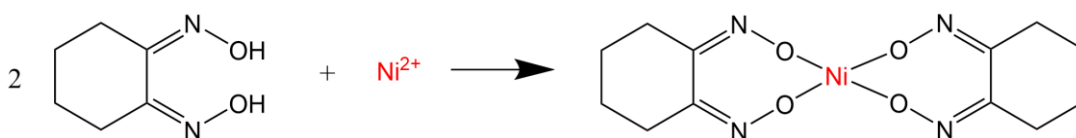


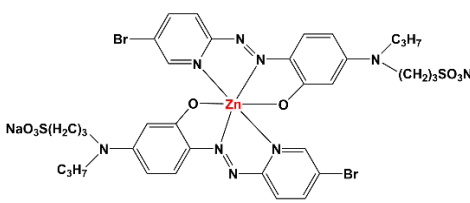
Figure 16 Metal-ligand complex formation reaction between 1,2-cyclohexanedione dioxime (nioxime) with Ni^{2+} ion (a 2:1 ligand-to-metal ratio).

1.4.3 Zn^{2+} detection reagent

Zn^{2+} can also be detected through colorimetric means. Common Zn^{2+} colorimetric detection utilises Zincon [83, 98]. Zincon is a market name for 2-carboxy-2'-hydroxy-5'-sulfoformazylbenzene monosodium salt and was first used in 1952 for Zn^{2+} , as well as Cu^{2+} measurement [99]. It is a versatile ligand, with the ability to form a colorimetric complex with several species of metal ions, such as Cu^{2+} , Co^{2+} , Ni^{2+} , Pb^{2+} , Hg^{2+} , and Cd^{2+} , as well as Zn^{2+} [99]. While its versatility may be useful in some contexts of analytical measurements, in the analysis of specific metals in an environmental sample, it also indicates low selectivity. Therefore, while its mechanism of the reaction is well researched and the reagent can detect low levels of Zn^{2+} , utilisation of Zincon would require the need of extensive masking processes to suppress the impact of competing ions. Other colorimetric reagents may provide similar or satisfactory sensitivity without the need for such extensive masking, as listed in

Table 7 Table 7.

Table 7 Colorimetric reagents for zinc detection, its mechanism of the reaction, limit of detection or linear range, and interferences by other ions.

Ref	Compound name	Mechanism	LOD (mg L ⁻¹)	Interference
[98, 99]	2-carboxy-20-hydroxy-50-sulfoformazylbenzene (Zincon)	1:1 ligand-to-metal ratio	0.014	Cu ²⁺ , Co ²⁺ , Ni ²⁺ , Pb ²⁺ , Hg ²⁺ , Cd ²⁺
[100]	5-Br-PAPs	 <p>2:1 ligand-to-metal ratio</p>	0.038	Cu ²⁺ , Fe ²⁺ , Mg ²⁺ , Mn ²⁺
[101]	Pyrogallol red/PDADMAC	In the presence of PDADMAC, a 1:1 ligand-to-metal molecular ratio	0.654	Al ³⁺ , Cr ³⁺ , Fe ²⁺
[102]	Titanium oxide nanoparticle + dithizone	Preconcentration with TiO ₂ -NP followed by spectrophotometry with dithizone	0.33 x 10 ⁻³	Cd ²⁺ , Cu ²⁺ , Co ²⁺ , Fe ²⁺

1.4.3.1 5-Br-PAPs

5-Br-PAPs is an abbreviation for a chemical known as 2-(5-Bromo-2-pyridylazo)-5-[N-propyl-N-(3-sulfopropyl)amino]phenol, which had been used in previous studies for Zn²⁺ colorimetric reaction [100]. However, compared to Zincon, its uses in Zn²⁺ detection have been scarcely reported in recent years. The description of the proposed colorimetric reaction is illustrated in Figure 17.

Previous studies have used the compound and compared it to 2-(5-bromo-2-pyridylazo)-5-diethylaminophenol (Br-PADAP) for determination of Zn²⁺ in serum [103]. The study concluded that 5-Br-PAPs was a more suitable reagent compared to the latter due to its solubility in water as well as high molar absorptivity [103]. Another study observed the usability of the reagent in the spectrophotometric method, with measurement done at 554 nm [104]. The same study also underlines the sensitivity of the reagent and its long-term stability, however, also shows possible interference in the presence of iron and copper [104]. The reagent had also been used in the development of a kit for Zn²⁺ determination in human seminal plasma, by Wako Pure Chemical Industries, as published in 1987 [105].

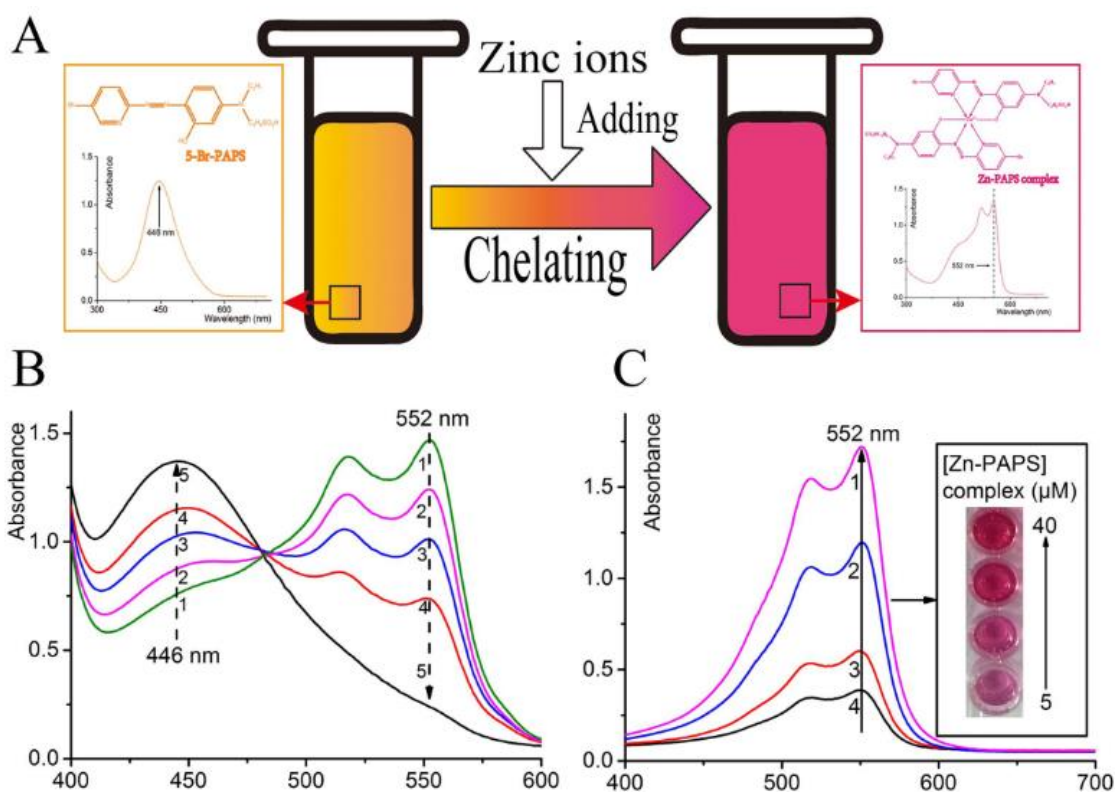


Figure 17 (A) Outline of reaction process and characteristics of the colour change of 5-Br-PAPs for Zn^{2+} detection; (B) Wavelength scanning of 5-Br-PAPs and Zn-PAPs complex with decreasing Zn^{2+} concentration in the mixture of 20, 15, 10, and 5 μM from 1 to 4, respectively ($n=2$); (C) Wavelength scanning of the concentrations and illustration of the observed colour with naked eyes observation, as illustrated in [100].

1.5 Electrospun membrane for metal adsorption

1.5.1 Electrospinning fundamentals

Electrospinning has been described as a straightforward, highly customizable, and relatively inexpensive sub-micron-/nano-fibre-production method [106]. It is a technology promising facile and versatile production of nanofibers from a wide variety of polymers with a suitable solvent [106, 107]. It, therefore, has the potential to be used as a substrate for μ PAD devices.

The setup consists of three main modules: a direct current power source, a syringe pump with a syringe, and a grounded collector, often made of aluminium [106, 108]. This setup is illustrated in Figure 18.

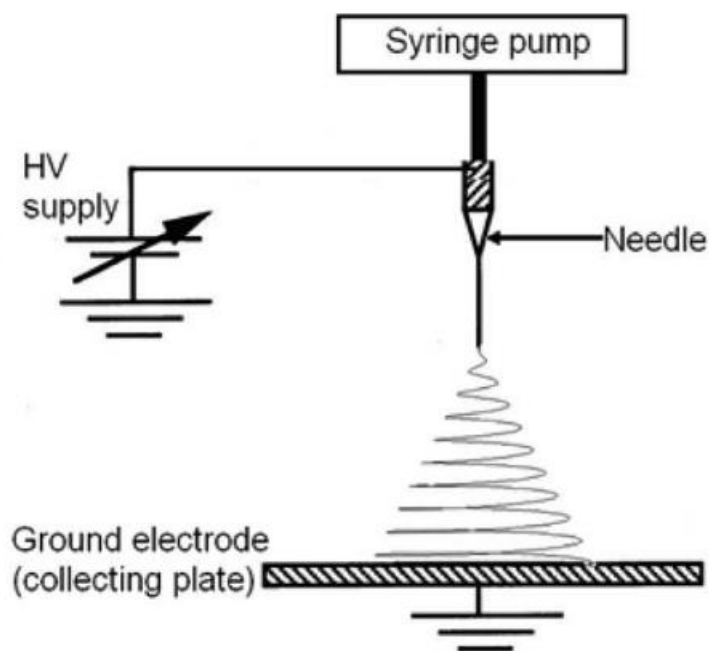


Figure 18 Fundamentals of electrospinning process, as illustrated in [106].

1.5.2 Ni²⁺ and Zn²⁺ adsorption with electrospun nanofibers

Electrospun fibres have also been used in Ni²⁺ or Zn²⁺ adsorption from water samples. [Table 8](#) lists previous studies utilising various electrospun polymers for Ni²⁺ or Zn²⁺ adsorption. In the case of adsorption study, often the maximum adsorption capacity was calculated based on a fitting adsorption model at a certain temperature. This is listed in the table along with the average fibre diameter. Average fibre diameter becomes an interesting measurement in adsorption due to the correlation between the increasing surface area with the decrease of average fibre diameter – theoretically promoting better adsorption.

Previous studies on chitosan/PEO electrospun nanomat with 98 nm average fibre diameter had shown Ni²⁺ adsorption capability, with 175.1 mg g⁻¹ experimental-based adsorption capacity after contact with 1000 mg L⁻¹ Ni²⁺ at 25°C [109]. Further, the maximum adsorption capacity of the produced fibres was modelled, resulting in 357.1 mg g⁻¹ Ni²⁺ adsorption at 45°C based on the Langmuir adsorption isotherm model [109]. In the same study, at lower temperatures, the maximum adsorption capacity of Ni²⁺ was calculated to be 338.6 and 350.2 mg g⁻¹ for 25°C and 35°C, respectively [109].

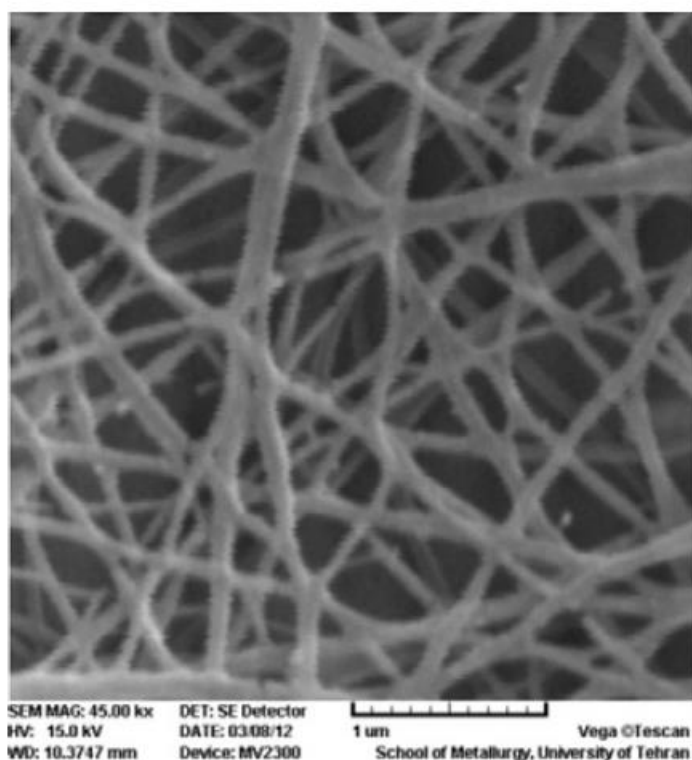


Figure 19 SEM imaging of PEO/chitosan fibre for metal adsorption study [109].

Whereas for Zn^{2+} adsorption, previous studies using chitosan/PEO/activated-carbon nanomat had shown potential for $>80\%$ Zn^{2+} adsorption within 11 min [110]. In the same study, the performance of chitosan/PEO fibres was compared to chitosan/PEO/activated carbon; while the latter was able to adsorb up to 85.1% Zn^{2+} , the absence of activated carbon lowers the adsorption performance down to 60.2% [110]. The maximum adsorption capacity was then calculated based on the Langmuir adsorption isotherm model, resulting in 186.2 mg g^{-1} maximum Zn^{2+} adsorption for chitosan/PEO/activated carbon, while chitosan/PEO nanomat was able to adsorb up to 117.2 mg g^{-1} Zn^{2+} in the same condition [110].

Table 8 Electrospun membranes for Ni^{2+} or Zn^{2+} adsorption or removal in the literature.

Ref	Polymer type	Target ion	Avg. ϕ / nm	Ads. cap. / mg g^{-1}	Details
[111]	Chitosan/hydroxyapatite	Ni^{2+}	198	180.2	At 30 min, 45°C
[109]	Chitosan/PEO	Ni^{2+}	98	357.1	At 45°C
[112]	PVA/nano-zeolites	Ni^{2+}	170	342.8	At 60 min, 45°C
[110]	Chitosan/PEO/activated carbon	Zn^{2+}	83 ± 12.5	186.2	

1.5.3 Elution of metals from electrospun nanofibers

As previously mentioned, metal elution from electrospun nanofibers in the context of preconcentration had not been recorded in the literature up to the time of this writing. However, processes involving the 'detachment' of metal ions from electrospun nanomats after prior adsorption had been studied in the context of nanomat regeneration. This is an important factor in membrane development, since it extends the lifetime of the produced membrane, through a fairly simple process.

One of the studies on this matter is the regeneration of chitosan/PEO nanofibers following the adsorption of Ni^{2+} , Cu^{2+} , Cd^{2+} , and Pb^{2+} , separately [109]. In this study, regeneration was done through washing with 1 M HNO_3 , followed by washing with deionised water and vacuum drying at 80°C [109]. As part of the study was focused on the reusability of the membrane, no discussion on the amount of metal eluted was recorded. However, a degree of elution might have been achieved as the nanomat can be used at least two more times with a regeneration process. After this, a decline in adsorption performance can be notably observed for the Ni^{2+} adsorption process [109].

Another record on elution or regeneration process was in electrospun chitosan/PEO/activated carbon fibres, for Cr^{6+} , Fe^{2+} , Cu^{2+} , Zn^{2+} , and Pb^{2+} adsorption [110]. In this study, the regeneration process involved agitating the fibres in 200 mL distilled water for 10 min, followed by oven drying at 60°C for 3 hours [110]. Similarly, five cycles of regeneration were observed against the adsorption performance, showing the reusability of the electrospun mat at least 3 more times with the regeneration method for all metals tested [110]. The loss of adsorption efficiency, in this study, was attributed to the loss of active sites due to the acid wash of the fibres, which was not elaborated further in the study [110].

Table 9 Elution of metals from- or regeneration of- electrospun nanomat in the literature.

Ref	Polymer type	Target ion	Eluent	Details
[109]	Chitosan/PEO	Ni ²⁺	1 M HNO ₃	<u>Regeneration process:</u> washing with HNO ₃ , washing with deionised water, and drying in a vacuum oven at 80°C <u>Regeneration result:</u> five cycles of regeneration were performed, and adsorption performance was maintained for at least 2 cycles for all metals tested
		Cu ²⁺		
		Cd ²⁺		
		Pb ²⁺		
[110]	Chitosan/PEO/activated carbon	Cr ⁶⁺	Distilled water	<u>Regeneration process:</u> washing with distilled water for 10 min, followed by drying at 60°C for 3 h <u>Regeneration result:</u> five cycles of regeneration were performed, and adsorption performance was maintained for at least 3 cycles for all metals tested
		Fe ²⁺		
		Cu ²⁺		
		Zn ²⁺		
		Pb ²⁺		

1.6 Ion exchange resins for metal preconcentration

1.6.1 Metal preconcentration with ion exchange resins

Metal preconcentration involving ion exchange principles had been used as a preceding step in various analytical techniques. Different processes may use or require different resins, depending on the inherent characteristics of the resin. A strongly acidic cation exchange resin with a sulfonic functional group reacts easily with metals in the solution, however, may not have a certain affinity to a metal ion. Some other resins had a better-known theoretical affinity to certain metals than others. Lewatit TP 207, for example, with an iminodiacetic acid functional group had been recorded to have bigger theoretical selectivity in the following order: Fe³⁺ > Cu²⁺ > Ni²⁺ > Zn²⁺ > Fe²⁺ > Mn²⁺ > Mg²⁺ [113]. While Lewatit TP 220, with a bis-picolylamine functional group, has the theoretical selectivity in the following order: Cu²⁺ >> Ni²⁺ > Fe³⁺ > Co²⁺ > Mn²⁺ > K⁺ > Ca²⁺ > Na⁺ > Mg²⁺ > Al³⁺ [113]. This selectivity data can be used as a point of reference in the resin selection process for adsorption or preconcentration.

1.6.2 Ni²⁺ and Zn²⁺ adsorption with ion exchange resins

Different ion exchange resins had been used for Ni²⁺ and Zn²⁺ adsorption processes. Continuous exploration of the variety in ion exchange resins follows the increase in resin capacity or selectivity, depending on its utilisation. Listed in Table 10 are previous studies on different ion exchange resins used for Ni²⁺ and Zn²⁺ adsorption in different water samples. An interesting point to be observed through the previous studies was the difference in calculated maximum adsorption capacity even when targeting the same metal or utilising similar resin with the same

functional groups. The highest adsorption capacity was reported for Amberlite IR 120 for resins with a sulfonic functional group, with the calculated maximum adsorption capacity reaching 235.3 mg g⁻¹ Ni²⁺ [114]. Similarly, for Zn²⁺, the highest reported maximum adsorption capacity was Amberlite IR 120 with 765.1 mg g⁻¹ Zn²⁺ [114]. Whereas for the iminodiacetic acid functional group, Lewatit TP 207 was reported to be able to adsorb as much as 77.3 mg g⁻¹ Ni²⁺ and D401 adsorbing up to 176.5 mg g⁻¹ Zn²⁺ [115, 116]. Another type of functional group used was bis-picolylamine and carboxylic acid, which were able to adsorb up to 6.24 mg g⁻¹ from 100 mg L⁻¹ 50 mL solution agitated at 180 rpm, while carboxylic acid adsorbs up to 275.9 mg g⁻¹ Ni²⁺ [114, 117]. These maximum adsorption capacities were calculated using the best-fit models through the adsorption isotherm experiment.

Table 10 Previous studies on utilisation of commercially available ion exchange resins for Ni²⁺ and Zn²⁺ adsorption, along with its functional group and maximum adsorption capacity.

Ref	Resin name	Functional group	Target metal	Adsorption capacity / mg g ⁻¹
[118]	Lewatit SP MonoPlus 112	Sulfonic	Ni ²⁺	171.0
[114]	Lewatit CNP 80	Carboxylic acid	Ni ²⁺	275.9
			Zn ²⁺	307.3
	Amberlite IR 120	Sulfonic	Ni ²⁺	235.3
			Zn ²⁺	765.1
[117]	Lewatit MonoPlus TP 220	Bis-picolylamine	Ni ²⁺	6.24 [†]
			Zn ²⁺	9.09 [†]
[119]	Amberlite IRN-77	Sulfonic	Ni ²⁺	62.1
[115]	Lewatit TP 207	Iminodiacetic	Ni ²⁺	77.3
[120]	Dowex HCR S/H	Sulfonic	Ni ²⁺	87.8
[121]	Dowex IR 120H	Sulfonic	Ni ²⁺	27.9
[122]	Dowex HCR S/S	Sulfonic	Ni ²⁺	156.3
			Zn ²⁺	222.2
[116]	D401	Iminodiacetic	Zn ²⁺	176.5

[†]: adsorption capacity at equilibrium (>240 min) from the initial concentration of 100 mg L⁻¹ at ambient temperature, 50 mL solution, agitation speed of 180 rpm

1.6.3 Ion exchange column for metal preconcentration

Previous studies have employed ion exchange columns as a means of preconcentration for laboratory-based analytical systems. This process often involves the introduction of a sample stream through a packed column, where target ions would attach to the packing active sites, followed by a selective elution to separate and preconcentrate the target ions.

Ammann, *et.al.* (2002), for instance, utilized an anionic hydrophilic column for the preconcentration process before subsequent analysis was completed with ICP-MS [46]. The developed preconcentration step involved a column packed with quaternary alkanol aluminium anion exchange sites followed by elution with ammonium nitrate as elution solution [46]. While other studies may use completely different types of resin and elution solutions. For instance, one study utilized a cation exchange resin (referred to as type 732) placed in a flow injection-microwave plasma torch-AES (FI-MPT-AES) system as part of an online preconcentration process, with HCl as an eluent [123]. This method allows detection of Co^{2+} and Ni^{2+} down to $1.28 \mu\text{g L}^{-1}$ and $1.80 \mu\text{g L}^{-1}$, respectively; with a relative standard deviation of 3.73% and 4.23% respectively [123]. While another study utilized chelating ion exchange resin Lewatit TP 207 with iminodiacetic acid functional group for batch preconcentration process of Zn^{2+} , Cd^{2+} , and Ni^{2+} ; further, the study claimed elution can be achieved through washing with double distilled water before metal detection can be performed with AAS [124].

Through the given examples, it can be concluded that metal preconcentration can be a highly customized process, varying in resin type and elution solution, amongst other parameters. These previous studies are interesting background knowledge for the preconcentration studies to be conducted in this research, which would require accessibility to the target users – the citizen scientists.

1.7 Citizen science for environmental monitoring

1.7.1 Citizen science in environmental monitoring

Citizen science can be defined as the involvement of volunteers, usually members of the public, in scientific processes [125]. The application of this data collection technique can vary depending on the purpose of the research, even in the field of environmental science itself. One of the most well-known citizen science projects, based in the Cornell Lab of Ornithology (CLO), focused on utilizing the help of citizen scientists in collecting pictures and data of bird populations across time and geographies [126]. In this type of citizen science project, volunteers were asked to submit pictures or information depending on their observation of the target species in nature. While in other projects, citizen science can require more involvement from the volunteers, such as asking the volunteers to take multiple water samples and sending them back to the researchers (Figure 20) [127]. These different approaches and degrees of volunteer involvement would then lead to different degrees of success and challenges to obtain the required data.

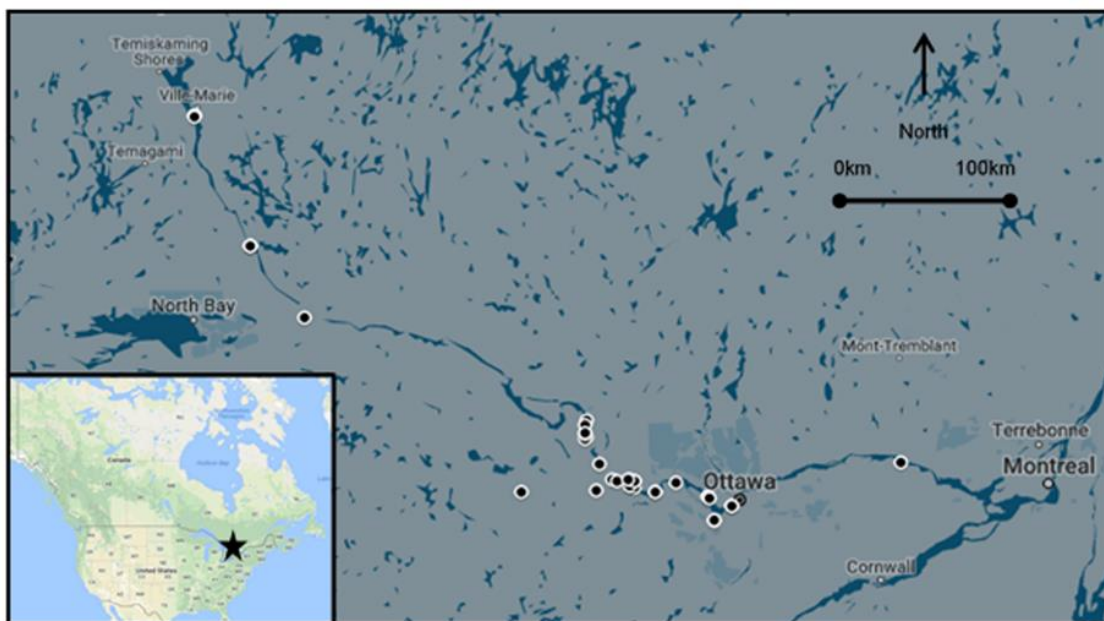


Figure 20 Sampling sites as reported by citizen science volunteers in a microplastics monitoring study [127].

1.7.1.1 Benefits

The benefits of citizen science as a data collection technique in environmental research are largely the sheer number of potential participants involved. Engaging with citizen scientists allows researchers to conduct a wider spatial analysis, which sometimes can also include sampling private or restricted land that may not be normally easily accessible to researchers [127]. This additional mobility also subsequently allows for more efficient data collection in terms of financial and time expenditure – delegating a task that would normally be done by a limited number of scientists across a longer period of time to volunteers, which may already reside in the area of interest [127]. Additionally, working with citizen scientists increase public engagement and public awareness on the topic of the research – an essential and in most cases of environmental research, a helpful step to the main goal addressed in the research [127]. Another interesting potential of citizen science is a two-way communication between the researchers' rising environmental awareness and the local community and their perspectives on the local knowledge and problems [128].

1.7.1.2 Challenges

Citizen science can be seen as an interesting data collection technique, especially for environmental monitoring research. However, despite its potential benefits, it still faces many challenges and criticisms as a valid method of scientific investigation. This is mainly due to the issues related to [127]: (1) potential error, (2) bias, (3) reliability of data collection, (4) lack of

appropriate protocols, (5) training or oversight, and (6) concerns related to replicability, comparability, and completeness.

1.7.2 Citizen science in water monitoring

Examples of citizen science in water monitoring studies can be found in the literature. Citizen science data collection for monitoring microplastics in the Ottawa River has been done, obtaining 48 samples from 28 sample points (Figure 20) [127]. In this research, volunteers were asked to collect three field samples at a certain location and a tap water sample as a control and send all collected samples and control back to the researchers for laboratory analysis [127]. Unfortunately, it was found that volunteers were often unable to follow the instructions given by the researchers, be it by omitting control or by sampling from different locations – making triplicate measurement impossible [127]. This shows the challenge in training or oversight, or lack of accessible sampling protocol – resulting in discrepancies between the activities designed by the researcher and the activities done by the volunteers.

Another interesting report on citizen science was on a project in Vancouver, where citizen scientists were asked to sample watersheds for TSS (total suspended solid), NO_3^- , and DOC (dissolved oxygen content) analysis [128]. An interesting aspect of this research is the qualitative analysis of the ‘stories’ behind groups of volunteers participating in the research. Through descriptive accounts of each group, a picture of each group’s motivations and potential bias to the data can be illustrated clearly, resulting in the following identified challenges that may skew or create errors in data collected and interpreted by the citizen scientists [128]: (1) Criteria for what an outlier is can be difficult to determine, due to the possible error in citizen science data; (2) Aberrations that are within normal distribution can be interpreted as more meaningful due to collection context, therefore scientist needs to be able to communicate complex data or concepts; (3) Citizens and citizen-led groups may bias data collection as a result of their particular interests; (4) The interests of the scientists and citizens may not coincide, and; (5) Data might be primary for scientists, but secondary to citizen scientists.

Despite the possible challenges faced during the initiation of citizen science participation, persistent and continuous projects are possible. For example, Ecoflux in Brittany, France, was able to utilize the technique for water monitoring over almost two decades (Figure 21) [129]. Rather than reporting the challenges faced during the early initiation of the project, this study reflects on the strong potential of citizen science to not only complement environmental data but also to engage the public and boost morale for continuous environmental improvements [129]. Despite the availability or development of more vogue cutting-edge sensors, deployable for continuous monitoring, the study argues for the importance of low-cost, engaging projects

such as Ecoflux, which can help the local communities to be involved in the environmental monitoring process [129].

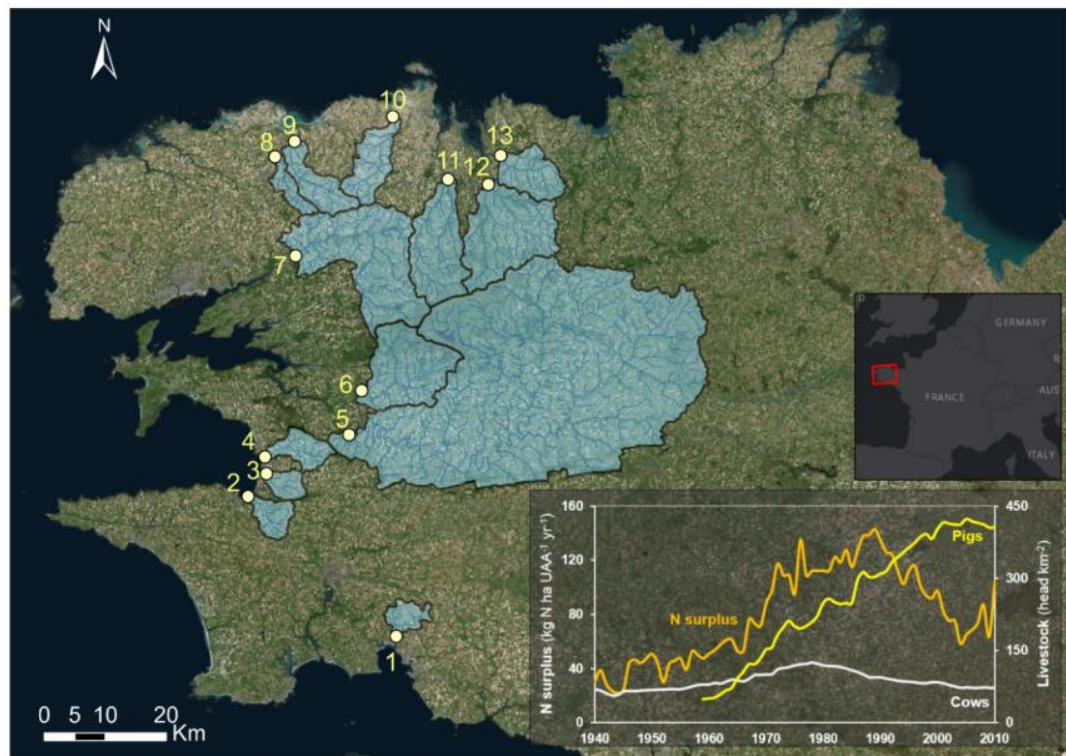


Figure 21 Monitored location in a 20 years study on agricultural contaminants in catchments of Brittany, France [129].

Another approach to engage and boost participation by citizen scientists is through remuneration. This approach had been used in a study on rain gauging and measurements in Nepal [130]. A simple rain gauge was installed for volunteers to read and report back to the scientists [130]. The researchers then approached different groups of participants through different communication channels: (1) leveraging personal relationships (n=53), (2) social media posts (n=11), (3) outreach programs (n=61), (4) random sites visit (n=29) [130]. Amongst the participants, further, follow-up on the motivations of the participants was enquired about and categorized into: (a) personal follow-up, (b) bulk SMS messages, (c) outreach and workshops, (d) data dissemination, (e) lucky draws for routine samplers, (f) certificate of involvements, and (g) monetary payment [130]. Through this study, it was observed that citizen scientists that receive monetary reimbursement took more measurements compared to the volunteers [130]. It was also observed that not all volunteers required monetary compensation for their participation, as students involved in the project became more engaged in the research; the drawback of student participation in this research, however, was the concentrated region of reporting – especially in urban areas where the students live [130].

Other studies on the utilization of citizen science data collection process for environmental water monitoring is as listed in Table 11, describing the region of research, type of activity, number of volunteers, and details based on the details provided.

Table 11 Study on citizen science data collection utilisation for environmental water monitoring in various regions of the world.

Ref	Region	Type	Number of volunteers	Details
[127]	Ottawa River, Canada	Sampling	48 samples from 28 sample points, collected by 17 groups	-Volunteers were asked to collect three samples + tap water (as control, with label) -Only six follow the instruction exactly (often omitting control) -Suspicion of labelling errors
[128]	Vancouver (watershed), Canada	Sampling and observation (river environment)	145 of 221 samples returned	-Volunteers were asked to take one sample and take observations on the environment (GPS tag, brief description of the location) -Some data does not correspond to the control data obtained by scientists
[129]	Brittany, France	Sampling	Approximately: 18 researchers, 10 graduate students, 21 adult volunteers, and 5000 high-school students from 6 educational institutions	-Project spans 18 years -Volunteers were asked to collect sample, filter, and store it in cold storage
[130]	Nepal	Observation (rainwater)	53 through personal relations, 11 from social media, 61 through outreach programs, and 29 from a random visit	-More than 30 data were submitted throughout the research duration for each observed condition (resulting in more than 100 data) -Volunteer motivation was observed and categorized
[131]	Eshito, Ethiopia	Observation (groundwater, well)	Volunteers selected through recommendation by the community	-Volunteers were asked to measure, observe, and report the height of the water in the designated well at a certain time of the day
[132]	New Hampshire, US	Sampling	147 of 800 distributed package was received back	-Return in this project was merely 18%, however, data coverage reached 140.4 km ² -Monetary compensation played a minor role in participation

1.8 Research aim

In this research, a simple, rapid, and onsite detection workflow was developed for Ni^{2+} and Zn^{2+} detection in the freshwater sample, separately. The workflow development started with the construction of an improved μPAD for Ni^{2+} and Zn^{2+} detection in freshwater samples. In prior studies, as described in previous sections, μPAD development for Ni^{2+} detection often utilises dimethylglyoxime as a colorimetric reagent – despite its drawback in the reagent deposition process. Whereas μPAD for Zn^{2+} detection was scarcely researched. Therefore, in this research, a focus was drawn into the simplicity of μPAD usage for the detection process, the use of the water-soluble colorimetric process for ease of manufacture, rapid colour formation (below 5 min), as well as selectivity for all developed μPADs . The developed μPAD was then combined with a simple and rapid ion-exchange-based preconcentration process using cafetiere as a stirring vessel. The developed workflow was then tested with environmental water samples collected by a small number of volunteers for user experience feedback.

Chapter 2 Development of a microfluidic paper-based analytical device (μ PAD) for Ni^{2+} detection in the environmental water sample

2.1 Chapter introduction

Paper-based microfluidic device (μ PAD), in this research, has been offered as a solution to the need in simple, rapid, and onsite metal detection method in the environment, specifically, in river water. In μ PAD, a paper-matrix is patterned, creating hydrophobic and hydrophilic areas; where detection agent can be placed in the hydrophilic area, and aqueous sample can then be introduced and reacted with it. The idea to develop such device, however, is not novel – and several attempts had been made in previous study. These devices claimed to be able to detect metal such as Ni^{2+} with varying detection limit and varying reaction time, despite using the same colorimetric reagent (as discussed in Section 1.3.3.1). In this research, instead, a different colorimetric reagent would be used for Ni^{2+} detection, which create a novel approach to the μ PAD development. Instead of dimethylglyoxime (DMG), 1,2-cyclohexanedione dioxime (nioxime) would be used as colorimetric reagent, owing to its previously studied potential in Ni^{2+} detection, as well as its solubility in water – creating an advantage in μ PAD fabrication process compared to DMG.

This chapter starts by listing the materials and discussing the methods used throughout the experimental processes related to μ PAD development for Ni^{2+} detection (section 2.2). Followed by the observation on reaction between Ni^{2+} and nioxime with UV/Vis absorbance spectrometry method (section 2.3). The reaction was then transferred onto a μ PAD with colour intensity readout and tested with some environmental samples (section 2.4). Additionally, a variation of the device with similar detection reagents was made; creating a distance-based μ PAD (dPAD), where the colour produced through the colorimetric reaction through a hydrophobic channel can be corresponded to the concentration of Ni^{2+} in the sample (section 2.5). In the same section, a variation of μ PAD with different reagent (XO/PDADMAC) was also developed and discussed. Lastly, a conclusion was drawn from the experiments and development of Ni^{2+} -detection μ PAD in section 2.6.

2.2 Materials and methods

2.2.1 Materials

The materials used for the development of the paper-based analytical device for Ni^{2+} detection in water samples is listed in

[Table 12](#)Table 12.

Table 12 List of chemicals and suppliers used in the development of paper-based analytical device for Ni²⁺ detection in water samples.

Chemical	Supplier
Nickel (II) chloride hexahydrate, 99.9% trace metal basis	Sigma Aldrich
1,2-cyclohexanedione dioxime, 96%	Sigma Aldrich
Xylenol orange disodium salt, for spectrophotometric determination of metal ions	Sigma Aldrich
Phosphate-buffered saline tablets	Sigma Aldrich
Poly(diallyldimethylammonium chloride) 20 wt% solution in H ₂ O	Sigma Aldrich
Sodium fluoride, Puriss., meets analytical specification of BP, Ph.Eur., USP, 98.5-100.5%	Honeywell
Sodium thiosulfate, ReagentPlus [®] , 99%	Sigma Aldrich
Zinc (II) sulfate heptahydrate, ACS reagent, 99%	Sigma Aldrich
Sodium carbonate, powder, ≥99.5%, ACS reagent	Sigma Aldrich
Sodium bicarbonate, ACS reagent, ≥99.7%	Sigma Aldrich
Iron (II) chloride tetrahydrate, ReagentPlus [®] , 98%	Acros Organics
Sodium chloride, ACS Reagent, ≥99.0%	Sigma Aldrich
Potassium chloride, ACS reagent, 99.0-100.5%	Sigma Aldrich
Sodium phosphate dibasic, ACS reagent, ≥99.0%	Sigma Aldrich
Potassium nitrate, ACS reagent, ≥99.0%	Fisher Scientific
Iron (III) chloride hexahydrate, ACS reagent, 97%	Sigma Aldrich
Cobalt (II) chloride hexahydrate, ACS reagent, 98%	Sigma Aldrich
Copper (II) sulphate pentahydrate, ACS reagent, ≥98%	Sigma Aldrich
Calcium sulphate dihydrate, ReagentPlus [®] , ≥99%	Sigma Aldrich

2.2.2 Solution preparation

2.2.2.1 Preparation of nickel stock solution

4.0 mg of Nickel (II) chloride hexahydrate ($M_w = 237.69 \text{ g mol}^{-1}$) was weighed and made up to volume within a 100 mL volumetric flask with Milli-Q water. This was mixed thoroughly to yield a colourless and clear solution, with $10 \text{ mg L}^{-1} \text{ Ni}^{2+}$ concentration. Operations involving this solution were carried out in the fume hood.

2.2.2.2 Preparation of nioxime solution

146 mg of 1,2-cyclohexanedione dioxime (nioxime) was weighed and made up to volume with 10 mL of Milli-Q water within a volumetric flask. This yield in a solution with 1400 mg L^{-1} nioxime concentration.

2.2.2.3 Preparation of 4 wt% PDADMAC solution

10 mL 20 wt% Poly(diallyldimethylammonium chloride) in H₂O (PDADMAC) was pipetted and made up to 50 mL with Milli-Q water within a volumetric flask. This was mixed thoroughly, producing a clear solution with a slight yellow tint, with 4 wt% PDADMAC concentration.

2.2.2.4 Preparation of 0.001 M phosphate buffered saline solution

One tablet of phosphate-buffered saline was diluted with Milli-Q water and made up to 200 mL. This was mixed thoroughly and vortexed if necessary. By the end of the mixing process, the solution would be clear and colourless.

2.2.2.5 Preparation of 0.1 M sodium fluoride solution

41.9 mg of sodium fluoride ($M_w = 41.98 \text{ g mol}^{-1}$) was weighed and diluted with Milli-Q water to make a 10 mL solution. This was mixed thoroughly, producing a clear colourless solution. A change of temperature may occur temporarily, during the mixing process.

2.2.2.6 Preparation of 0.1 M sodium thiosulfate solution

250.0 mg sodium thiosulfate ($M_w = 158.11 \text{ g mol}^{-1}$) was weighed and made up to 10 mL with Milli-Q water. The solution was mixed thoroughly, producing a clear colourless liquid. A change of temperature may occur temporarily, during the mixing process.

2.2.2.7 Preparation of 100 mg L⁻¹ interference ion stock solution

An appropriate amount of interference ion salt (1.8 mg sodium carbonate ($M_w = 105.99 \text{ g mol}^{-1}$), 1.4 mg sodium bicarbonate ($M_w = 84.01 \text{ g mol}^{-1}$), 3.6 mg iron (II) chloride tetrahydrate ($M_w = 198.81 \text{ g mol}^{-1}$), 1.9 mg potassium chloride ($M_w = 74.55 \text{ g mol}^{-1}$), 1.5 mg sodium phosphate dibasic ($M_w = 141.96 \text{ g mol}^{-1}$), 1.6 mg potassium nitrate ($M_w = 101.10 \text{ g mol}^{-1}$), 4.9 mg iron (III) chloride hexahydrate ($M_w = 270.30 \text{ g mol}^{-1}$), 4.0 cobalt chloride hexahydrate ($M_w = 237.93 \text{ g mol}^{-1}$), 3.9 mg copper sulphate pentahydrate ($M_w = 249.69 \text{ g mol}^{-1}$), 4.3 mg calcium sulphate dihydrate ($M_w = 172.17 \text{ g mol}^{-1}$)) was weighed and diluted with Milli-Q water to form a 10 mL solution. The concentrations of these solutions were 100 mg L⁻¹, upon usage, further dilution from this stock solution might be necessary. The solutions were mixed thoroughly, producing a clear solution. It is stored in safe storage or under the fume hood.

2.2.3 UV/Vis spectrophotometry

2.2.3.1 UV/Vis spectrometer

Unless otherwise specified, the UV/Vis spectrophotometer data in this research was obtained with Perkin Elmer portable single beam spectrophotometer and 1.6 mL Sarstedt polystyrene 10 x 4mm, 10mm optical pathway, 45mm length disposable semi-micro cuvette.

2.2.3.2 Absorbance measurement

The wavelength for the Nickel-nioxime complex was set at 530 nm. The measured absorbance was recorded and measurements were taken in triplicate.

2.2.3.3 Reaction time

In order to determine the reaction time, the absorbance of the sample solution was observed between 0 min and 20 min following the addition of the nioxime into the Ni^{2+} solution. This was done with 100 μL of 100, 200, or 400 mg L^{-1} nioxime being added to the 1 mL of 1 mg L^{-1} Ni^{2+} solution. Reaction time would be determined as the first data point at which the measurement stabilised across the different nioxime concentrations tested.

2.2.3.4 Effect of nioxime volume

In order to study the effect of nioxime volume on the measured absorbance, reactions between 1 mL of 1 mg L^{-1} Ni^{2+} ion solution with a variety of 400 mg L^{-1} nioxime solution volumes ranging from 100 to 500 μL were observed. The mixture was left to incubate for 20 min. Each data point was repeated three times. The optimum nioxime volume would be determined as the volume which produced the highest measured absorbance at the set condition.

2.2.3.5 Effect of nioxime concentration

The effect of nioxime concentration was studied by reacting 1 mL of 1 mg L^{-1} Ni^{2+} solution with a volume of 100 μL nioxime solution within the 50-1000 mg L^{-1} concentration range. The mixture was left to incubate for 20 min. The absorbance was measured with UV/Vis spectrophotometry at 530 nm. Each data point was repeated three times.

2.2.3.6 Effect of initial sample solution pH

The effect of the pH of the initial sample solution was investigated by reacting 1 mL of 1 mg L^{-1} Ni^{2+} solutions with their pH adjusted within 4-8, with 100 μL of 400 mg L^{-1} nioxime. The mixture was left to incubate for 20 min. The absorbance at the endpoint was measured at 530 nm and each data point was repeated three times.

2.2.3.7 Construction of calibration curve

A calibration curve for the nickel/nioxime reaction was constructed in the Ni^{2+} concentration of 0.0 mg L^{-1} to 0.9 mg L^{-1} . This was achieved by adding 100 μL of nioxime solution (400 mg L^{-1}) to 1000 μL of Ni^{2+} solutions within the 0 to 0.9 mg L^{-1} concentration range. The mixtures were left to incubate for 20 min before absorbance measurement at 530 nm. 10 different concentrations were investigated in 0.1 mg L^{-1} increment, and each data point was measured in triplicate.

2.2.4 Optimisation of paper-based analytical device for Ni²⁺ detection

2.2.4.1 Design of paper-based analytical device

The design of the paper-based analytical device with nioxime as detection agent for Ni²⁺ detection was created with Autodesk AutoCAD 2021¹⁹ Student version. The final design of nioxime μ PAD used in this research is a \varnothing 31 mm circular device consisting of 3 layers with the same patterns across all layers. For each layer, 1 magenta-coloured reference circle (\varnothing 7 mm) is printed in the middle of the circle, circled with 6 sample wells (\varnothing 7 mm). Between the 6 sample wells, only 5 will be loaded with reagents, while the other one well serves as a 'blank well', as shown in [Figure 22](#)~~Figure 33~~ below. Through the development of the device, layering became an important part in optimizing the fabrication process of the μ PAD.

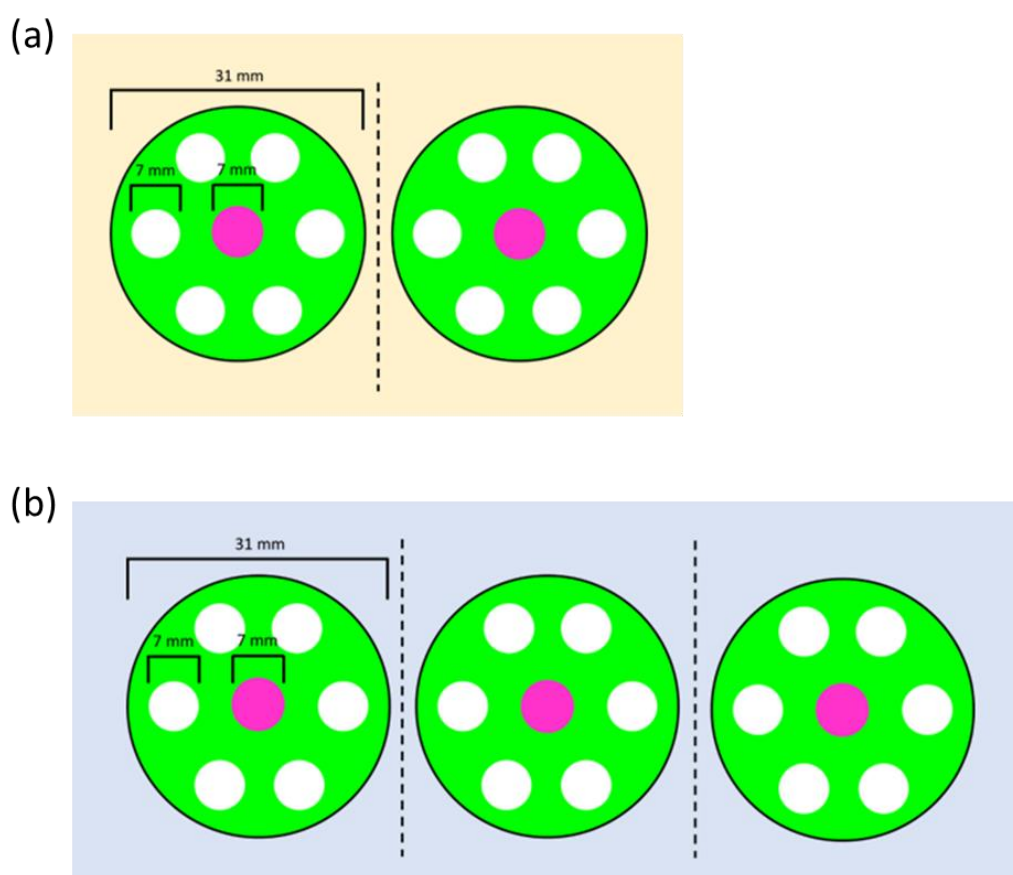


Figure 22 (a) Design of a 2-layered device with 31 mm diameter, consisting of 6 sample wells and 1 reference circle with 7 mm diameter. (b) Design of a 3-layered device with the same dimensions.

In layered design of the μ PAD, the μ PAD circles would be printed in close group of threes, indicating that the μ PAD should be cut in the groups of threes. To ease the folding process, which is illustrated in Figure 23, the cutting of the three circles would be done in such manner that a guiding handle is left in. This cutting process is similar to the process of cutting an origami paper chain or decoration, in which multiple copies of the same design is held together by not cutting the designs completely off of each other.

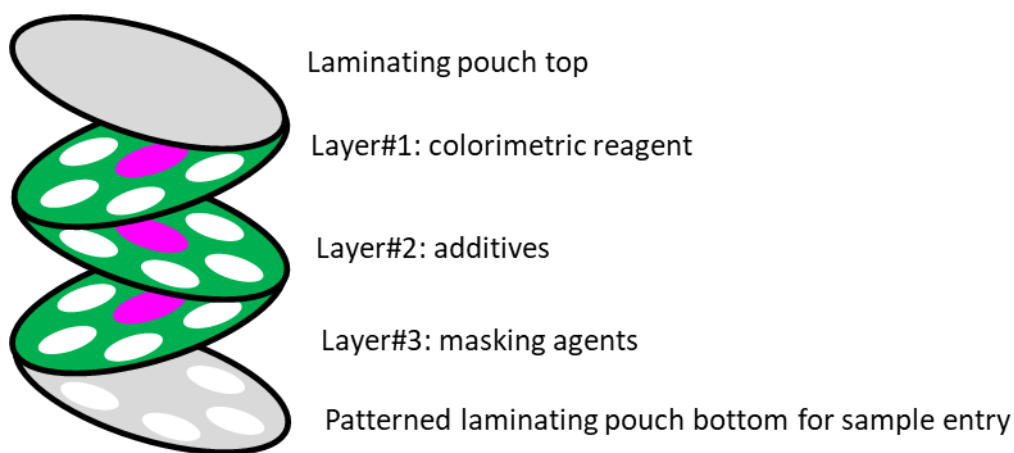


Figure 23 Illustration of a 3-layered μ PAD design with lamination. Folding and lamination would be done after reagent deposition into the sample wells. Stacking was done in such a way that all sample wells would be on top of each other, this can be helped by cutting the μ PAD design in folded position and leaving a guiding handle to re-fold the μ PAD afterwards.

2.2.4.2 Fabrication of paper-based analytical device

The fabrication of a paper-based analytical device (μ PAD) started with the digital design of the device, made in Autodesk AutoCAD 2021 Student version. For *intensity-based* measurements ([Figure 24](#)~~Figure-22~~), the devices featured multiple layers on circular pieces of paper with a total diameter of 31 mm. Devices were printed with green, pink and black wax. There were six paper circular wells arranged symmetrically around one central pink wax-printed circle acting as an internal standard. All circles inside the device had a diameter of 7 mm. A *distance-based device* was also used at times instead of an intensity-based device (design schematic available in Appendix 1). This design was single-layered and featured a circular sample well of 10 mm diameter merging with a 40 mm long channel with 3 mm width printed with 0.5 mm thick lines of black wax.

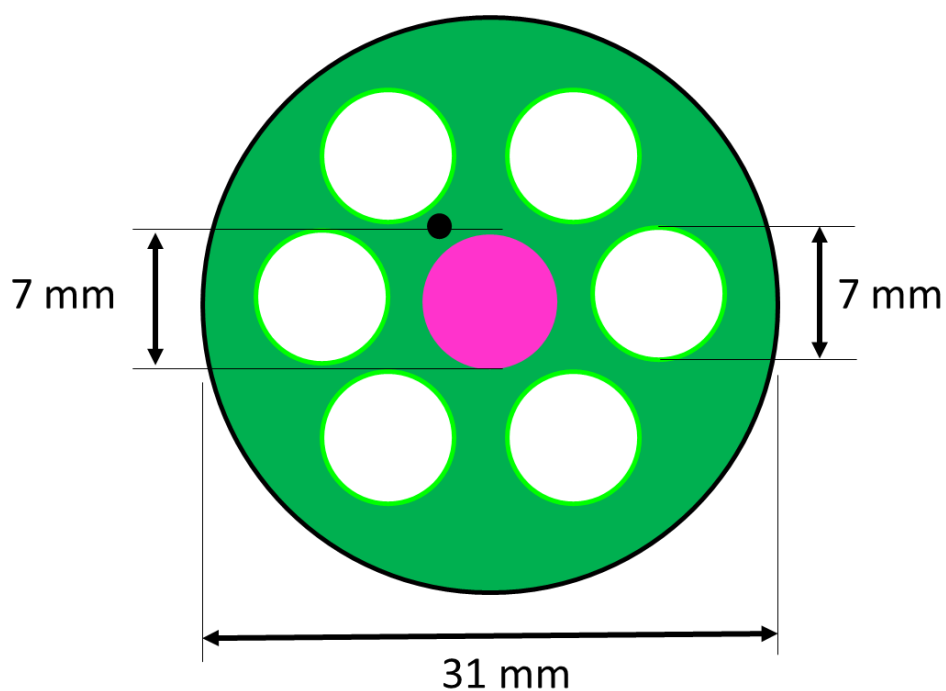


Figure 24 Illustration of the design of intensity-based device made in Autodesk AutoCAD 2021 Student version. The device was green and 30 mm in diameter, with six circles placed as sample wells around a magenta-coloured reference circle. All circles placed inside the device were designed with a 7 mm diameter.

This design was then printed on a Whatman® qualitative filter paper no 1, with Xerox ColorQube 8570DN solid ink printer and corresponding solid CMYK wax ink. However, this printer was only able to print the wax ink on one side of the paper, as shown in [Figure 25](#)[Figure 23b](#) (i) and (ii). In this condition, the printed wax would not work as a barrier as liquids would seep through the capillary layers of the paper and flow through the back side, where no solid ink was deposited. Therefore, a wax melting process was necessary, in order to ensure the deposited solid wax would create a barrier on both sides of the paper, as shown in [Figure 25](#)[Figure 23a](#).

Printed devices were then melted by placing them into a Saturn 3i95 A4 office laminator at a 125 gsm setting. The setting was the highest available in the laminator. This process was repeated three times until the printed wax melted through the filter paper and became vivid on both sides, as shown in [Figure 25](#)[Figure 23b](#) (iii) and (iv).

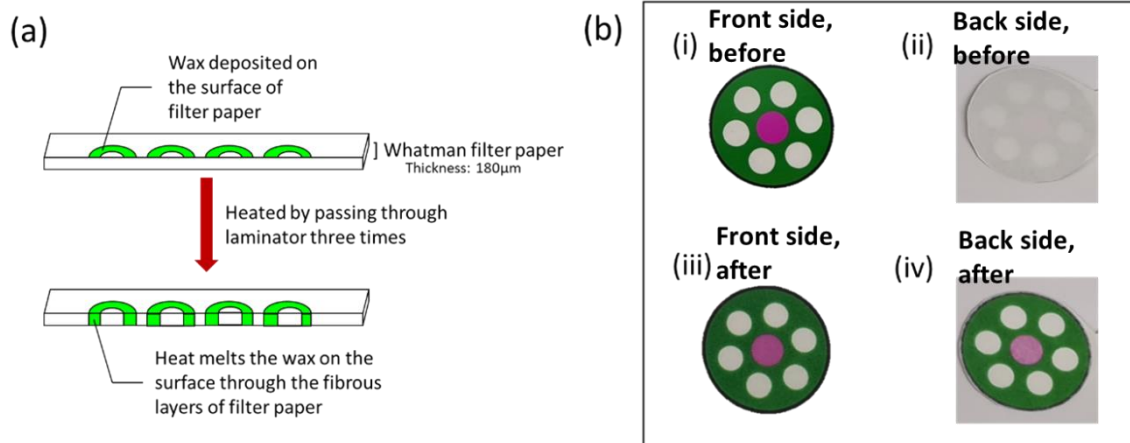


Figure 25 (a) Illustration of wax melting from one side of the paper where solid wax ink was deposited into the other side of the paper, to create a wax barrier; (b) Visual comparison between (i) μ PAD printed with solid ink, before heat treatment, printing side, (ii) μ PAD printed with solid ink, before heat treatment, backside, (iii) μ PAD printed with solid ink, after heat treatment, printing side, and (iv) μ PAD printed with solid ink, after heat treatment, backside.

Throughout the entire process up to this point, the device was still on an A4-sized printing paper, where multiple copies of the design had been printed. The end step, after ensuring that the solid wax ink had been melted through the paper, was to cut the device to shape. The design of the intensity-based Ni^{2+} detection μ PAD was circular, therefore, the device was cut following the outer lines of the design, creating a singular μ PAD at approximately 30 mm diameter to be loaded with reagents for experimental uses. In distance-based μ PAD, the device was not cut to the shape of the design, rather was cut into rectangular shapes with the measuring lines. This was done to ensure that in its application, the user would have an approximation of the distance travelled by the liquid through the available channel.

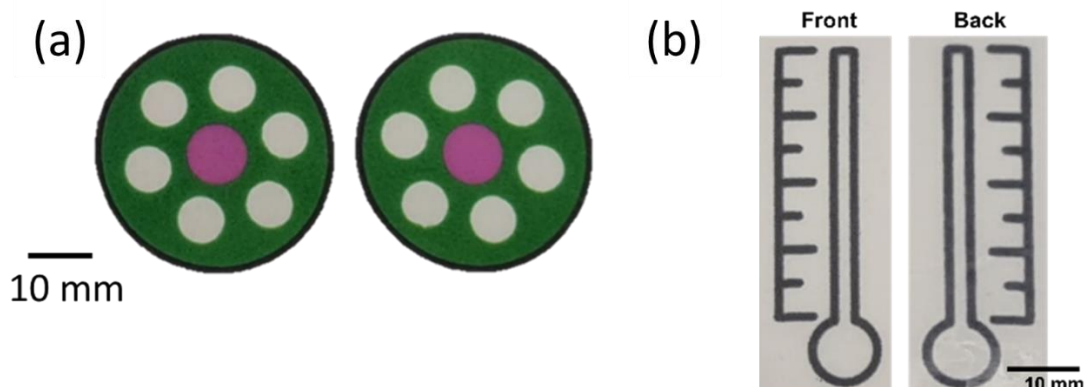


Figure 26 Design of (a) two colour-intensity-based devices, which was the main device used in this research for Ni^{2+} detection μ PAD, after heat treatment and being cut to shape (b) distance-based device.

2.2.4.3 Reagent loading and lamination

The reagent loading process was initiated by placing the device on top of two Petri dishes, not allowing any sample well to touch any solid or liquid surface ([Figure 27](#)[Figure-25](#)). This step was required to ensure uniformity by reducing the possibility of reagent loss through wicking or flowing through another surface. By elevating all sample wells, all reagents pipetted would be deposited in the targeted sample well and deviation would only be possible through evaporation. The reagents were then pipetted onto five of six sample wells on the device, leaving one well unloaded to act as blank. All reagents were left to dry before another reagent was added, if necessary, or before any further steps. The device containing dried reagents was folded to shape and laminated with a modified Lyreco 150 microns A4 laminating pouch (PET, 216 x 303 mm), which has been patterned with holes according to the pattern of the sample wells; these holes would serve as the sample entry point. Lamination was achieved by passing the device-containing pouch through the Fellowes Saturn 3i95 A4 office laminator at 80°C for one time. After the device was laminated, it was ready for further use.

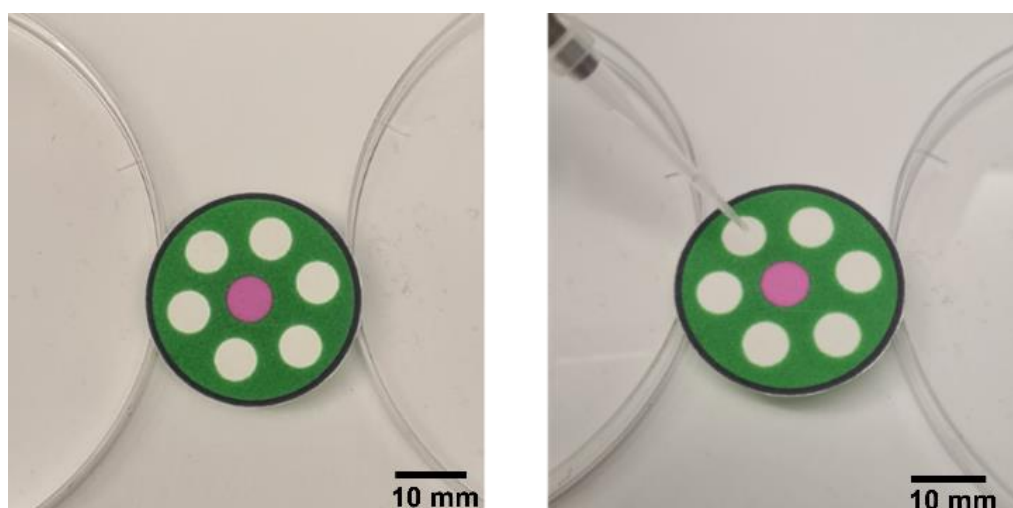


Figure 27 Paper device was placed on top of two Petri dishes without allowing any sample well to touch any solid surfaces. The reagent was loaded into the wells of the device with a 10 μ L micropipette.

2.2.4.4 Data acquisition

The prepared device can be used for Ni^{2+} detection by dipping it into at least 10 mL of aqueous sample. Upon contact with water, the sample wells would be visibly wet. As soon as the sample well is wet, the reaction would proceed up to the endpoint. The submersion time of the device is a minimum of 10 s complete submersion. The illustration of the dipping process is depicted in [Figure 28](#)[Figure-26](#). In the illustration, the sample solution was placed in a petri dish.

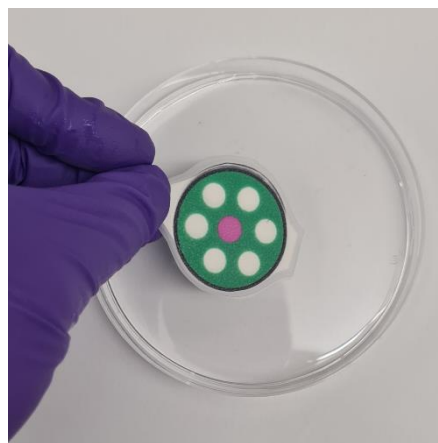


Figure 28 Device can be dipped into a sample solution containing the target ion for detection purposes.

In this research, the data collection process in the form of an image of the device was achieved using either Nokia 6.1 Pro rear camera with 16 MP resolution and F2.0 physical aperture or Samsung Galaxy S20 rear triple camera with 12.0, 64.0, and 12.0 MP resolutions, and F1.8, F2.0, and F2.2 physical aperture. The camera was used in auto-focus mode and placed on the slit on top of a black cardboard box (Figure 29Figure-27). The device was placed inside the black cardboard box, which serve as a controlled environment, where the image of the device would be taken with a smartphone camera flash on.

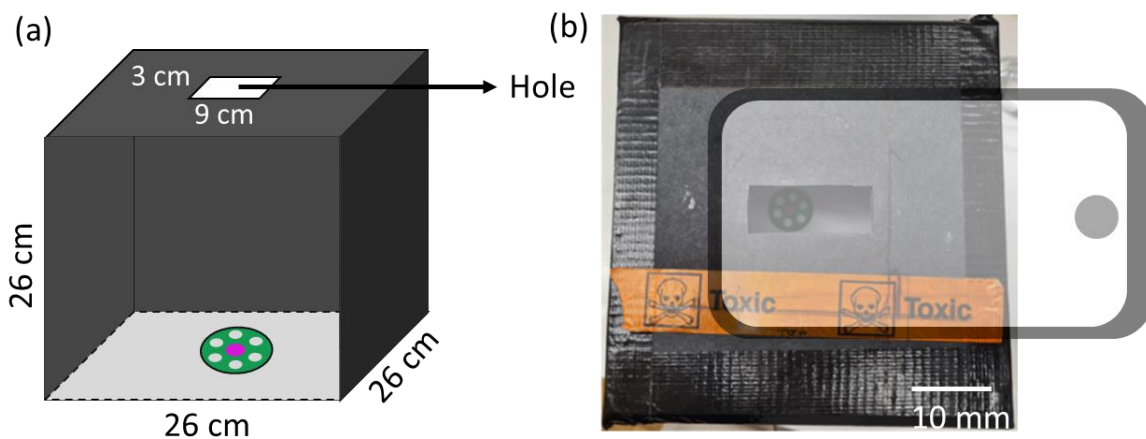


Figure 29 “Black box” image acquisition method with black cardboard placed to cover the paper-based analytical device, minimizing possible light interference caused by the presence of multiple light sources. The picture was taken through a slit on top of the box with flash settings on. (a) Illustration on the black box method usage and positioning, and (b) camera position over the slit, taking picture into the box with flash on, unless stated otherwise.

Whereas the image colour intensity was measured using ImageJ, a digital image analysis open-sourced software developed by the National Institute of Health and Laboratory for Optical and Computational Instrumentation, University of Wisconsin. Unless otherwise specified, the image would be cropped to shape, and inverted to produce a 'negative' image, where the colour channels would be separated (stacked) into red, green, and blue channels. The average colour intensity of pixels in a certain area can then be measured. Through this method, the colour intensity of the internal standard, blank, and sample wells in the device was measured. The colour intensity of the reaction was calculated with [Eq 1](#) or [Eq 2](#).

$$c = \frac{\text{measured intensity of sample well}}{\text{measured intensity of internal standard}} \quad \text{Eq 1}$$

$$c_0 = \frac{\text{measured intensity of sample well} - \text{measured intensity of blank}}{\text{measured intensity of internal standard}} \quad \text{Eq 2}$$

2.2.4.5 Reaction time

The prepared device was used in various experiments as a part of the optimization of the device. Firstly, the reaction time would be observed by dipping the prepared device into 25 mL 10 mg L⁻¹ nickel ion solution. The device would contain three different concentrations of nioxime: 400, 900, and 1400 mg L⁻¹. Data were acquired every minute for 10 minutes and colour intensity would consequentially be measured every minute. Each experiment with different nioxime concentrations was repeated three times. Reaction time would be defined as the time at which colour intensity measured peaked and stabilized for the next 5 minutes.

2.2.4.6 Box-Behnken design of experiment for optimisation

Upon knowing the reaction time for the device, the optimization experiment was designed following the Box-Behnken method in Origin 2020b OriginLab software with the design of experiment (DOE) plug-in. The variables were the concentration of nioxime, PDADMAC, and buffer solution at 10 µL volume. The concentration of nioxime was varied between 400-1400 mg L⁻¹ concentration range, PDADMAC between 0-6 wt%, and PBS buffer pH 7 between 0-0.01 M concentration range. Measured colour intensity was then recorded and the standardized effect, main effect, response surface, and contour plots were generated in the Origin 2020b OriginLab software with DOE plug-in. Calculation of optimization was also achieved through the software. The optimum condition for the intensity-based device was calculated through maximization, which means that the objective of the optimization is to increase the obtained response as high as possible. This would serve as baseline data for optimum conditions for the intensity-based device.

2.2.4.7 Construction of calibration curve

Further, the device sensitivity was observed by dipping the optimized device into a 25 mL nickel ion solution with various concentrations. For a nickel, this was done twice with the same device, which contains 1400 mg L⁻¹ nioxime, 4 wt% PDADMAC, and 0.01 M PBS buffer. Each data point measured in this study was repeated three times.

The first calibration curve was obtained between 0-1000 mg L⁻¹ nickel ion solution and the second calibration curve, narrowing the concentration range to between 0-10 mg L⁻¹. The sensitivity of the device was equal to the slope of the calibration curve, whereas the limit of detection (LOD) and limit of quantification (LOQ) were calculated with the equations below, where $\sigma_{\text{at lowest concentration}}$ is the standard deviation at nickel ion concentration of 0 mg L⁻¹.

$$LOD = \frac{3 \times \sigma_{\text{at lowest concentration}}}{\text{slope of calibration curve}} \quad \text{Eq 3}$$

$$LOQ = \frac{10 \times \sigma_{\text{at lowest concentration}}}{\text{slope of calibration curve}} \quad \text{Eq 4}$$

2.2.4.8 Selectivity

In the observation of interference by the presence of other ions, the device was dipped into 25 mL 10 mg L⁻¹ target heavy metal solution that simultaneously contain interfering ions at the same concentration. The interfering ions observed in this research were: zinc, copper, cobalt, iron, calcium, potassium, sodium, chloride, phosphate, nitrate, bicarbonate, and sulphate. Should masking be required due to interference, the experiment was repeated after the addition of the masking layer. The masking reagents used in this research were 1 M sodium fluoride and 1 M sodium thiosulfate at 10 μ L each. The measurement after masking was compared to the control solution (Ni²⁺ solution without added ions) to evaluate masking effectiveness. Each data point measured in this study was repeated three times.

2.2.4.9 Stability

The device stability was also observed, by placing the fabricated and laminated device in a closed petri dish and placed at room temperature for a set duration. On designated days, the device was tested for performance repeated at the same reagent and sample conditions. The measured data after storage was compared to the control data, which was the data obtained on day-0, where the device was immediately used after fabrication. Each data point measured in this study was repeated three times.

2.2.5 Statistical analysis

Within the scope of this research, several methods of statistical analysis had been employed to analyse various obtained data. For each μ PAD measurements, mean and standard deviation of the colour intensity was calculated, resulting in the colour intensity of the device, as shown in [Eq 2Eq-2](#). Further, when three repetitions of the μ PAD was indicated, mean and standard deviation between the result each device would also be calculated and often illustrated in a graph. Should a mean of a data be calculated in any other data and repeats collected throughout this research, a standard deviation of the data would also be calculated. These calculations were obtained through Microsoft Excel formula or Origin Lab Pro student version.

Another type of statistical analysis done throughout this research was hypothesis testing, this was done with student t-test or ANOVA. These calculations and testing were obtained through Origin Lab Pro student version. In case of comparing a group of data to observe whether measurements differ significantly from control, such as in the stability study, the ANOVA test would be used. In case ANOVA was used, the significance level would be set at 0.05, with assumption of normal data distribution. While a paired student t-test would be used in instances where a group of data was to be compared with its 'previous' state, such as in metal masking observation. In this case, the significance level would also be set at 0.05, with assumption of approximately normal data distribution. Should result of the calculation be considered significant, in the illustrated graph, an asterisk (*) would be placed between the tested data sets. Should the result show non-significant difference, an abbreviation of 'n.s.' would be placed between the tested data sets.

2.3 UV/Vis spectrophotometric detection of Ni^{2+} with nioxime

2.3.1 Reaction time

The reaction time observation, with the method described in section 2.2 is illustrated in [Figure 30Figure-28](#). The nioxime concentration tested in this study was based on a preliminary study, where 400 mg L^{-1} nioxime was used in UV/Vis spectrophotometry in an attempt to develop nioxime-based μ PAD [133]. Based on this data, a lower concentration of nioxime was also tested to further optimize the reaction. It can be observed that the increase in absorbance occurs immediately and can be observed within 1 min of reaction. With the naked eye, the increase in absorbance would correspond to a visible colour change to magenta. This colour development continued to occur and increase in intensity, as measured in [Figure 30Figure-28a](#), to 10 min after the addition of the colorimetric reagent, for 400 mg L^{-1} nioxime solution. In lower nioxime concentrations, the colour development was slower, requiring up to 20 min of reaction time to produce stable colour intensity – or stable absorbance measurement.

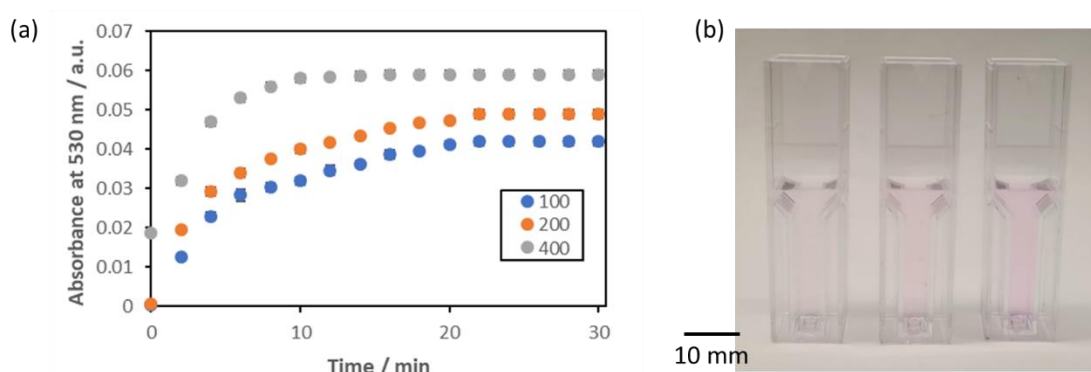


Figure 30 (a) Absorbance measured with UV/Vis spectrophotometer at 530 nm for the reaction between 1 mL 1 mg L⁻¹ Ni²⁺ ion solution with 100 μ L 100, 200, and 400 mg L⁻¹ nioxime between 0-20 minutes; (b) Left to right: endpoint of reaction, after 20 minutes, between 1 mL 1 mg L⁻¹ Ni²⁺ ion solution with 100 μ L 100, 200, and 400 mg L⁻¹ nioxime.

2.3.2 Effect of nioxime volume

In UV/Vis spectrophotometry method, the volume of nioxime used for the reaction with 1 mL Ni²⁺ ion sample was determined to be 100 μ L. [Figure 31](#)~~Figure 29~~ shows the result of the observation on the effect of nioxime volume with the method described in section 2.2.3.4. The tested volume was kept within 100-500 μ L for 1000 μ L of the sample since this is the range of volume that would produce enough change in absorption in a preliminary study. As can be seen in [Figure 31](#)~~Figure 29~~a, the measured absorbance was stable between 100-300 μ L nioxime volume but decreased upon the addition of 400-500 μ L volume. This drop in measured absorbance may be counterintuitive at first since increasing the volume of nioxime would correspond to the increase of nioxime availability in the reaction. However, there is a certain limit to this correlation, with excessive nioxime addition reducing the measured absorbance instead since most Ni²⁺ has reacted, and the rest of the nioxime would just dilute the solution.

The main idea of optimisation was to find the lowest nioxime amount possible that would produce the highest signal possible – in this case, producing high measured absorbance at 530 nm. Exceeding this point or peak will usually lower the signal perceived instead. In the case of the volume of 400 mg L⁻¹ nioxime to completely react and produce the highest colour intensity possible with 1 mL 1 mg L⁻¹ Ni²⁺ ion solution, the optimum 400 mg L⁻¹ nioxime volume was 100 μ L. Exceeding this amount to 200-300 μ L would produce similar signal intensity, which already shows the ‘peak’ intensity, this is further proven by the fact that upon exceeding the nioxime amount to 400-500 μ L, the measured absorbance declined instead. Therefore, in Ni²⁺-nioxime reactions measured using a UV/Vis spectrophotometer at 530 nm throughout this experiment, 100 μ L 400 mg L⁻¹ nioxime would be added to the 1 mL Ni²⁺ solution.

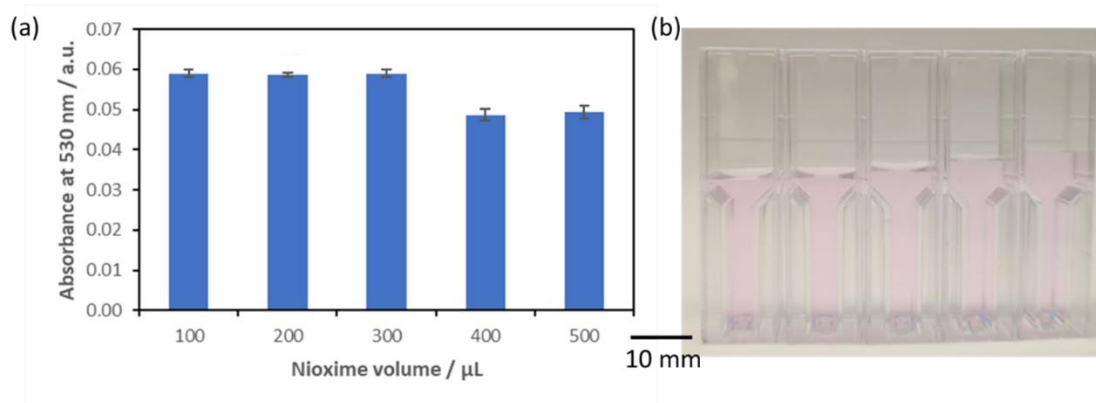


Figure 31 (a) Absorbance measured with UV/Vis spectrophotometer at 530 nm for reaction between 1 mL 1 mg L⁻¹ Ni²⁺ ion solution with 100, 200, 300, 400, and 500 μL 400 mg L⁻¹ nioxime after 20 minutes; (b) Left to right: endpoint of reaction between 1 mL 1 mg L⁻¹ Ni²⁺ ion solution with 100, 200, 300, 400, and 500 μL of 400 mg L⁻¹ nioxime.

2.3.3 Effect of nioxime concentration

Whereas the nioxime concentration for the UV/Vis measurement in this research was 400 mg L⁻¹ nioxime for reaction with 1 mL Ni²⁺ ion solution. The determination of nioxime concentration used for the reaction was done through a similar process as the determination of nioxime volume, as can be seen in [Figure 32](#)~~Figure 30~~. This follows the method described in section 2.2.3.5. However, it was not as straightforward to draw this conclusion. In [Figure 32](#)~~Figure 30a~~, the reaction between 1 mL 1 mg L⁻¹ Ni²⁺ ion solution with 100 μL nioxime with a varying concentration between 50-1000 mg L⁻¹ shows constantly increasing measured absorbance throughout tested nioxime concentrations. A sharp increase can be observed from 50 to 100 mg L⁻¹ nioxime concentration, which is to be expected. Further, the increase of nioxime concentration was relatively steady up to 800 mg L⁻¹ nioxime concentration. At 1000 mg L⁻¹ nioxime concentration, the measured absorbance does not have a significant difference from the measured absorbance at 800 mg L⁻¹. Looking at this data alone, one might conclude that the optimum nioxime concentration for this reaction between 100 μL nioxime and 1 mL 1 mg L⁻¹ Ni²⁺ ion solution was 800 mg L⁻¹.

However, another important aspect of this experiment was the observational data. In this case, in addition to a nioxime concentration higher than 400 mg L⁻¹ precipitation of the Ni²⁺-nioxime complex occurred. Precipitation has been reported for Ni²⁺-nioxime reaction in previous research and is one of the important properties of the reaction for gravimetric analysis [92, 96]. Through observation in this experiment, it can be concluded that precipitation may occur at different times, possibly correlated to the concentration of the nioxime added to the solution. However, for this experiment, precipitation is an unwanted and non-ideal condition. This is

because the analytical method used for Ni^{2+} analysis in this research is UV/Vis spectrophotometry. In UV/Vis spectrophotometry, absorbance was measured through Beer-Lambert's law at which the value of absorbance was obtained by comparing the intensity of light emitted from the light source to the intensity of light transmitted after it passes through the solution. The presence of precipitate would then create a light-scattering effect, which influences the measured absorbance. Therefore, in this research, for UV/Vis spectrophotometric measurement of absorbance at 530 nm wavelength between 1 mL Ni^{2+} ion solution with 100 μL nioxime, 400 mg L^{-1} nioxime concentration would be used.

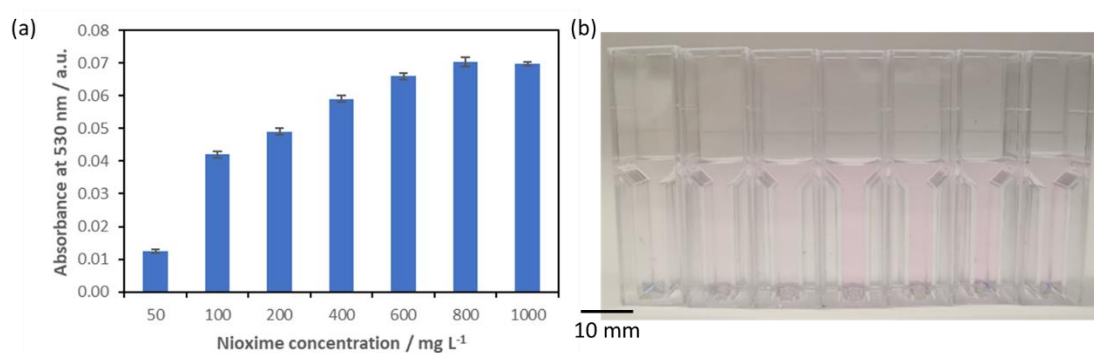


Figure 32 (a) Absorbance measured with UV/Vis spectrophotometer at 530 nm for reaction between 1 mL 1 mg L^{-1} Ni^{2+} ion solution with 100 μL 50, 100, 200, 400, 600, 800, and 1000 mg L^{-1} nioxime after 20 minutes; (b) Left to right: endpoint of reaction between 1 mL 1 mg L^{-1} Ni^{2+} ion solution with 100 μL 50, 100, 200, 400, 600, 800, and 1000 mg L^{-1} nioxime.

2.3.4 Effect of initial sample solution pH

Another important reaction characteristic to look at, especially in working with environmental samples, is the effect of different sample pH conditions on the measured absorbance with a UV/Vis spectrophotometer. This is because in working with environmental water samples, the pH of the sample would be an uncontrollable variable. Usually, 'fixing' the pH to a desired value would be achieved by the addition of diluted acid (hydrochloric acid) or base (sodium hydroxide). However, this desired pH value will have to be determined beforehand, through this observation process, in order to ensure the reaction happened in an optimum condition, producing the highest absorbance possible.

Nioxime, the ligand used in this experiment, showed the highest absorbance upon reaction with Ni^{2+} ion solution between pH 7-8, within the tested pH range based on the method described in section 2.2.3.6 Effect of initial sample solution pH. [Figure 33](#) shows the measured absorbance at 530 nm after a reaction between 100 μL 400 mg L^{-1} nioxime with 1 mL 1 mg L^{-1} Ni^{2+} ion solution at an adjusted pH value between 4-8. As can be seen, the measured absorbance

showed a significant difference between the tested pH values, with pH 7 and 8 showing the highest absorbance measured. Therefore, to produce the highest possible measured absorbance – or highest colour intensity, the pH value of the reaction must be adjusted to a neutral level. In order to achieve this condition, the addition of a buffer solution might be required in developing the paper-based device. Buffer solution would help in maintaining the pH condition of the reaction to the desired level, especially in the event of the addition of samples with more acidic or basic pH values. In the UK, the measured pH range for river water samples between 2019-2021 was commonly between 7-9, although a pH value in the 5-6 range was not uncommon.

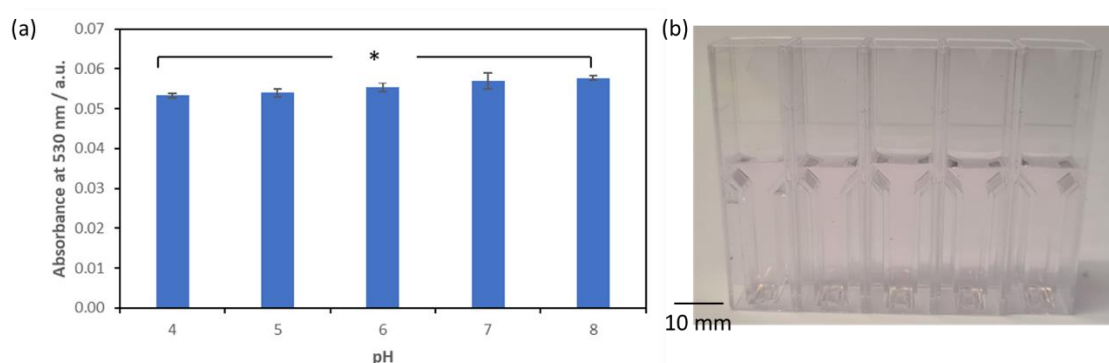


Figure 33 (a) Absorbance measured with UV/Vis spectrophotometer at 530 nm for reaction between 1 mL 1 mg L⁻¹ Ni²⁺ ion solution with pH adjusted between 4-8, with 100 µL 400 mg L⁻¹ nioxime after 20 minutes. The measured absorbance showed significant ($F_{(4,20)} = 11.12, p = 0.0001$); (b) Left to right: endpoint of reaction between 1 mL 1 mg L⁻¹ Ni²⁺ ion solution with pH adjusted between 4-8, with 100 µL 50, 100, 200, 400, 600, 800, and 1000 mg L⁻¹ nioxime.

2.3.5 Calibration curve

After optimizing the concentration and volume of reagent for the Ni²⁺-nioxime reaction in a liquid medium for detection via UV/Vis spectrophotometry, a calibration curve was constructed with the method described in section 2.2.3.7 Construction of calibration curve. [Figure 34](#) [Figure 32a](#) shows the linearity for the Ni²⁺-nioxime reaction after 20 min reaction time. The experiment was repeated three times for each Ni²⁺ concentration. Based on this linear correlation, the limit of detection was calculated (3σ) to be 0.06 mg L⁻¹ (0.06 ppm, or 60 ppb). This detection limit is higher than the Scottish Environment Protection Agency (SEPA) for the annual average and maximum allowable concentration of Ni²⁺ in the freshwater environment [33]. However, it would comply with the United States Environmental Protection Agency's (US EPA) acute Ni²⁺ limit in a freshwater environment of 0.47 mg L⁻¹ [34]. Whereas the limit of quantification (LOQ) was 0.18 mg L⁻¹ and limit of blank (LOB) was 0.02 mg L⁻¹.

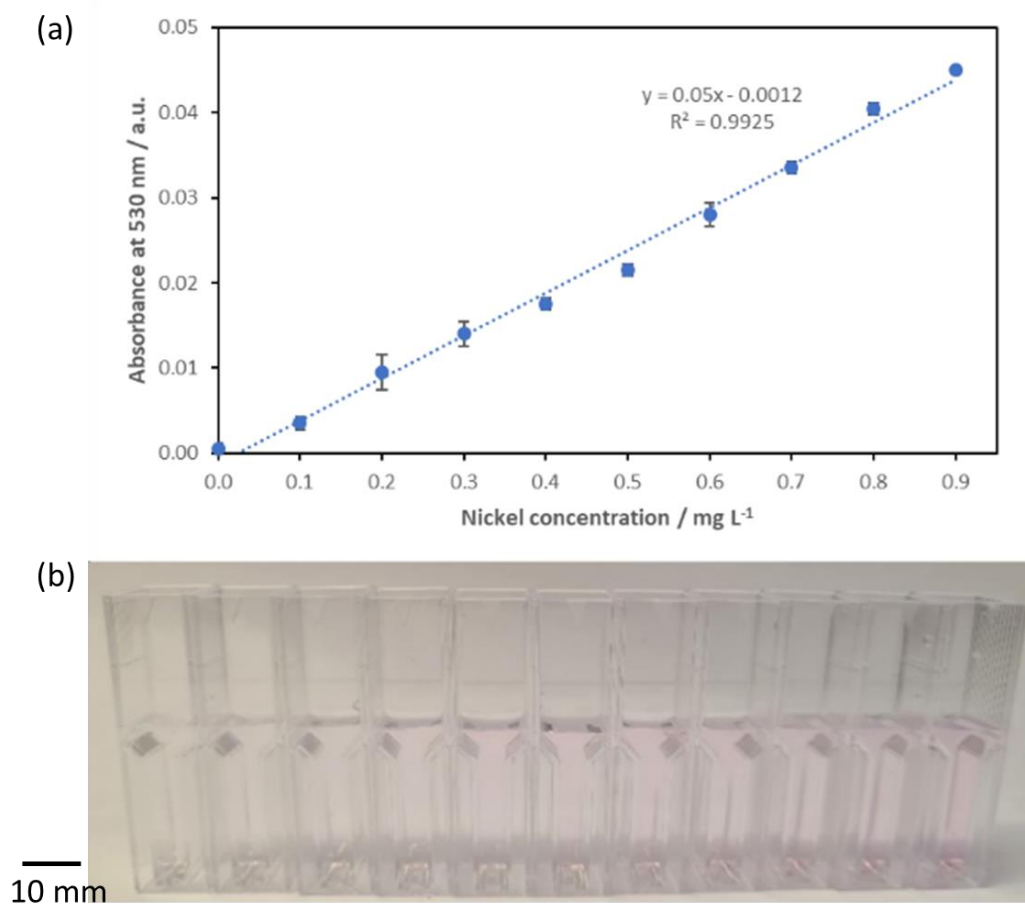


Figure 34 (a) Calibration curve of 100 μL 400 mg L^{-1} nioxime reacted with 1 mL Ni^{2+} ion the solution between 0-0.9 mg L^{-1} concentration; (b) Left to right: endpoint of reaction between 100 μL 400 mg L^{-1} nioxime reacted with 1 mL 0-0.9 mg L^{-1} Ni^{2+} ion solution ($n=3$)

2.4 Development of nioxime μPAD

The microfluidic paper-based analytical device is an emerging technology for the detection of various substances involving small volumes of samples. In the context of this research, this device is developed for cheap and rapid heavy metal detection in environmental water samples, with citizen scientists as target users. The use of a microfluidics paper-based analytical device for Ni^{2+} detection itself, as has been discussed in the previous chapter is not a completely new idea. However, most μPADs developed for Ni^{2+} detection using colorimetric sensing depended on dimethylglyoxime (DMG) as a colorimetric reagent, despite the availability of other Ni^{2+} colorimetric reagents on the market. Compounding this problem of lack of colorimetric reagent variety for Ni^{2+} detection on μPAD is the low solubility of DMG in an aqueous solvent, requiring organic solvent instead [75]. In wax-printed μPADs , the use of organic solvent as a reagent matrix is non-ideal due to the potential reaction between the solvent and the wax barrier. Previous research handled this problem by the incremental introduction of the reagent on the

sample well, essentially depending on the relatively rapid evaporation of organic reagent to dry on the well before the solvent meets the barrier. In this research, however, we are attempting to use 1,2-cyclohexanedione dioxime (nioxime) as a colorimetric reagent instead of dimethylglyoxime. This would be a novel attempt in exploring alternative colorimetric reagents for Ni²⁺ detection with μ PAD. Nioxime was chosen due to its solubility in an aqueous solvent and reported a similar stable Ni²⁺-ligand complex reaction to DMG.

In developing μ PAD for Ni²⁺ detection using nioxime as a colorimetric reagent (further referred to as nioxime μ PAD), we started by exploring the highly customizable design of the paper-based device itself (section 2.4.1), followed by the reagent optimization process using Box-Behnken design of experiment (section 2.4.2). The optimized device was then further tested for interference by other commonly occurring ions and used to produce a calibration curve for Ni²⁺ detection between 0-10 mg L⁻¹ (section 2.4.3 and section 2.4.4), where its stability was further assessed for the purpose of this study (section 2.4.5).

2.4.1 Design of nioxime μ PAD

It was decided early in the research that wax printing will be used as a device fabrication method. Compared to other μ PAD fabrication processes, wax printing allows simple fabrication with high production capacity. The process requires a digital design of the μ PAD, a wax printer containing solid wax inks, and a paper matrix. In this research, Xerox ColorQube 8570DN solid ink printer was used as the wax printer, capable of printing the design on one side of the paper. The ink used to print out the design was Xerox Solid Ink Black, Cyan, Yellow, and Magenta for ColorQube 8570. According to the material safety data sheet (MSDS) provided, the ink contains 50-60% paraffin wax, 10-20% resin, and 0-10% of the respective dye colour [134]. Whereas the paper matrix used in this research for μ PAD is the Whatman grade 1 qualitative filter paper by Cytiva. This filter cellulose filter paper is 180 μ m in thickness, with 0.06% nominal ash content. The typical water flow rate through this paper is documented to be 57 mL min⁻¹ for a 9 cm diameter (0.89 mL min⁻¹ cm⁻²). The typical trace element levels of the paper are listed in [Table 13](#) [135].

Table 13 Typical trace element levels in Whatman grade 1 qualitative filter paper standard grade

Trace element	Amount (μ g g ⁻¹)	Trace element	Amount (μ g g ⁻¹)
Aluminium	3.6	Iron	13.7
Antimony	<0.5	Lead	<0.5
Arsenic	<0.5	Magnesium	21
Barium	<0.5	Manganese	<0.5

Boron	<1	Mercury	<0.5
Calcium	27.5	Potassium	6.2
Chromium	1	Silicon	8.8
Copper	0.9	Zinc	58.3

The final design of nioxime μ PAD used in this research is a \varnothing 31 mm circular device consisting of 3 layers with the same patterns across all layers. For each layer, 1 magenta-coloured reference circle (\varnothing 7 mm) is printed in the middle of the circle, circled with 6 sample wells (\varnothing 7 mm). Between the 6 sample wells, only 5 will be loaded with reagents, while the other one well serves as a 'blank well'. The 5 loaded sample wells will allow 5 repeats of the reaction per use, which is especially useful during the development phase. The blank well, on the other hand, functions as a control to observe possible colour interference in the environmental sample matrix. Illustration of this design can be seen in [Figure 22](#)[Figure-33](#).

In designing the device, a large part of the decisions was made to ensure the user-friendliness of the device. For instance, the device was designed for sample introduction through dipping instead of pipetting. Therefore, the sample well will serve as a reagent deposit as well as the sample entry point. This allows the elimination of the 'channel' structure that is often incorporated in μ PAD designs. Consequently, the designed device can be smaller in size, due to less area requirement for the reaction. This influenced the small size of the designed device, increasing its portability to be used by citizen scientists in the field. The device was designed and printed with a 31 mm diameter, consisting of 6 sample wells and 1 reference circle with a 7 mm diameter.

2.4.1.1 Colour of the μ PAD

Another aspect of the design process was the colour of the device. In nioxime μ PAD, the main colour of the device is green, designed with RGB (0, 255, 0) in AutoCAD. Green was chosen since it is the complementary colour of magenta – which is the colour observed at the endpoint of the Ni^{2+} -nioxime reaction. Being a complementary colour, the high contrast of a magenta circle forming on a green background eases naked-eye observation (illustrated in [Figure 35](#)[Figure-34](#)). Accordingly, with magenta being the expected colour at the endpoint of the reaction, the reference circle was coloured magenta, designed with RGB (255, 0, 255) in AutoCAD.

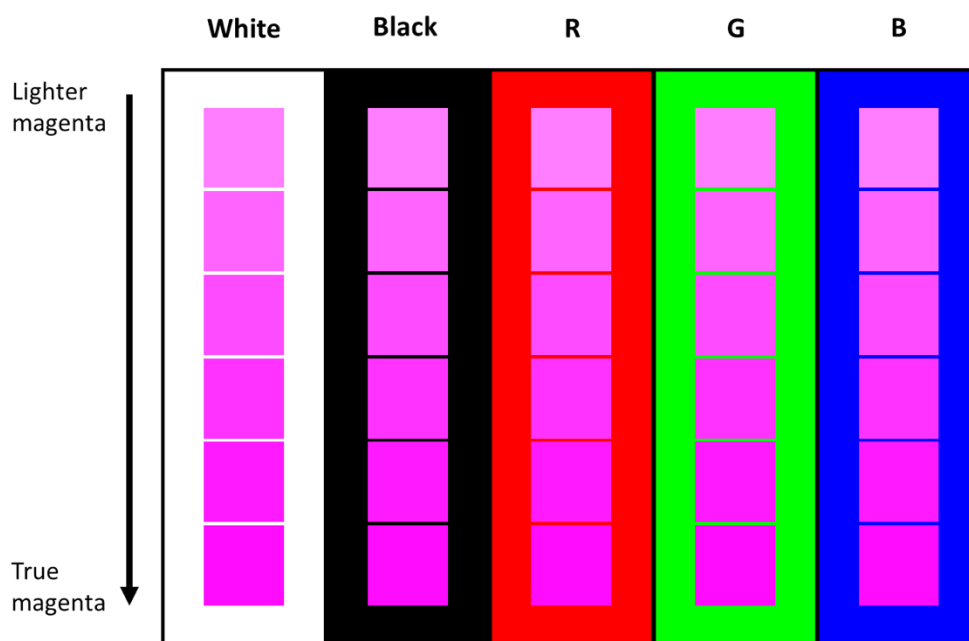


Figure 35 Effect of different device background colours on the naked-eye visibility of a gradient of magenta (endpoint of Ni^{2+} -nioxime reaction) colour.

It is important to note, however, that the printed colour is slightly different than the designed colour. The wax printer ink, as many other printers in recent years, consist of a CMYK (cyan, magenta, yellow, and black) palette instead of RGB (red, green, and blue). Therefore, in printing the device, there might be some adjustments necessary to compensate for the difference between the design and ink availability. A study on the effect of wax ink colour or a combination of colours printed on a paper-based device has been done in the literature [136]. According to this study, CY (cyan-yellow) combination, which will create green colour, is one of the colour combinations with the lowest barrier failure, corresponding to better resistance to leaking. The study suggested this is related to the high mass of ink deposited on the paper upon printing (1.86 mg cm^{-2}), even after heat treatment (1.55 mg cm^{-2}). This further strengthens the decision to use green as the main colour of the device, which will also serve as a barrier colour for the wells.

2.4.1.2 The effect of wax-melting on the μ PAD design

In this research, the wax-melting step was accomplished by placing the printed paper in an aluminium foil pouch and running it through a laminator. The laminator was Fellowes Laminator Saturn 3i set at 125 gsm setting. Different settings in the laminator correspond to the different thicknesses of the document to be laminated, which correlates to the ideal temperature range for smooth and clear lamination. Through observation, it was determined that the printed paper needs to be placed through the laminator 3 times to achieve adequate melting. This melting

process increased the device diameter from 31 mm to 32 mm, and decrease the sample well diameter from 7 mm to 6 mm, while the reference circle diameter is maintained at 7 mm. After the wax melting step, the device is ready for reagent loading. In the case of a layered device, however, in this research, the device will be placed under the laminator again for lamination with Fellowes 80 gsm lamination pouch at 80 gsm setting. In this step, the device will only be heated one time to minimise possible damage from heating.

2.4.2 Optimization of nioxime μ PAD

The device developed in this research has a reaction time of 4 minutes. This implies that after dipping, the device needed 4 min to develop stable colour on the sample well. The reaction duration was obtained through observation, by dipping a device loaded with 400, 900, and 1400 mg L^{-1} nioxime into a 10 mL 10 mg L^{-1} Ni^{2+} solution. A picture of the device was then taken every minute with a smartphone. Through this experiment, the change of colour intensity on the sample well every minute can be observed. The reaction time, in this case, is defined as the shortest time required by the device to reach stable colour intensity.

[Figure 36](#)~~Figure 35~~b shows the measured colour intensity on respective devices against time. Evidently, after minute 1, the difference in colour intensity between devices loaded with 900 and 1400 mg L^{-1} sharply increased, compared to the device loaded with 400 mg L^{-1} . In all concentrations, the result then showed stable colour intensity after minute 4 up to minute 10. The stark difference in colour intensity measured between 400 mg L^{-1} and 900-1400 mg L^{-1} , in this case, can be attributed to the amount of nioxime deposited on the sample well. Since the volume of nioxime was maintained throughout the devices, the device with the highest concentration would have the biggest amount of nioxime deposited on its sample well. A bigger amount of nioxime can then be correlated to the bigger number of active ligand sites for the colorimetric reaction to occur. Thus, a higher concentration of nioxime gave a more vivid colour complex formed within the sample well – consequently, a higher value of measured colour intensity.

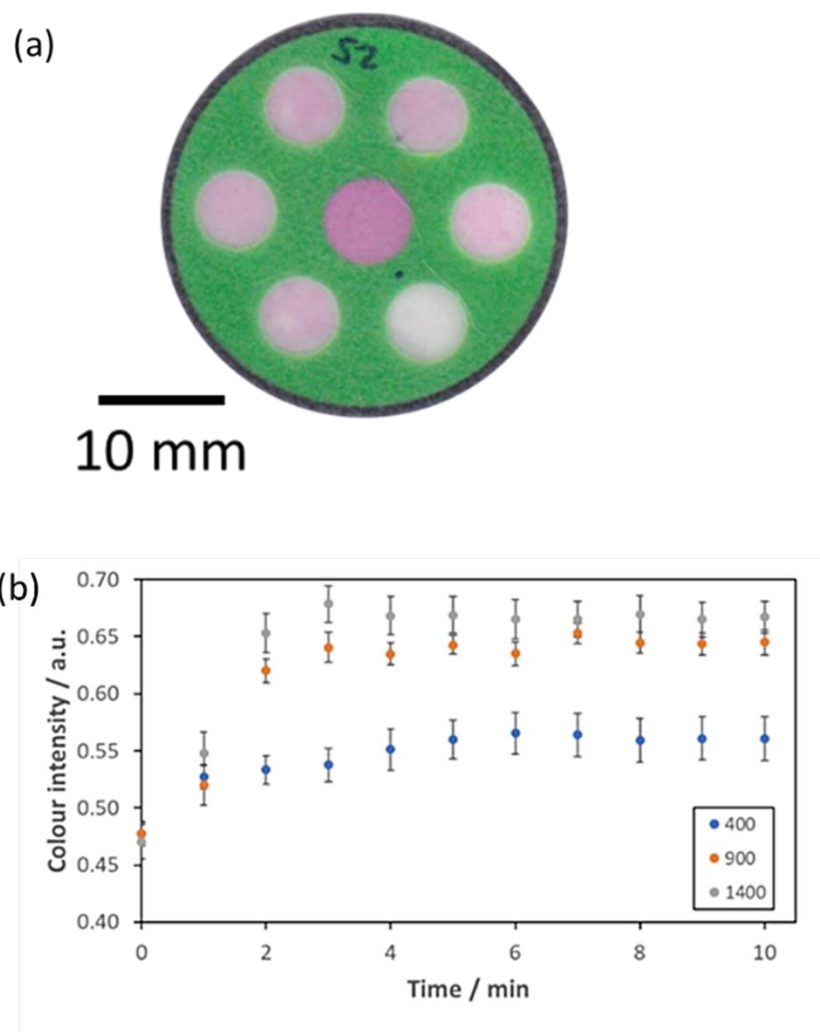


Figure 36 (a) Nioxime (1400 mg L^{-1}) μ PAD at the endpoint of reaction with 10 mg L^{-1} Ni^{2+} solution, (b) colour intensity measured on $400\text{-}1400 \text{ mg L}^{-1}$ nioxime μ PAD sample wells after dipping into $10 \text{ mL } 10 \text{ mg L}^{-1} \text{Ni}^{2+}$ solution ($n=3$).

Compared to previous research developing μ PAD for Ni^{2+} detection, the reaction time of this nioxime device is notably shorter. The shortest device reaction time in previous research was in the multiplex device by [75], with 10 min reaction time using DMG as a colorimetric reagent. Other research required longer duration, ranging from 15 to 120 min [13, 80]. The common denominator with these studies was the use of DMG as a colorimetric reagent, the sample introduction method, and the device design used in the workflow.

Chemically, the performance of DMG and nioxime for Ni^{2+} complexation, reaction, or detection is comparable. The chemical structure (2D) of the two colorimetric reagents is illustrated in [Figure 37](#)~~Figure 36~~. Both ligands are *vic*-dioximes, forming a chelate complex with Ni^{2+} ion in a 2:1 ligand-to-metal ratio [92]. The stability constant of the complexes in water is also comparable, with $\log K_2$ of 17.00 and 17.34 for DMG and nioxime, respectively [137]. Due to

high similarity in its properties and reaction mechanism, there is no strong evidence on how the difference in colorimetric reagent used contributes to the difference in reaction time on μ PAD.

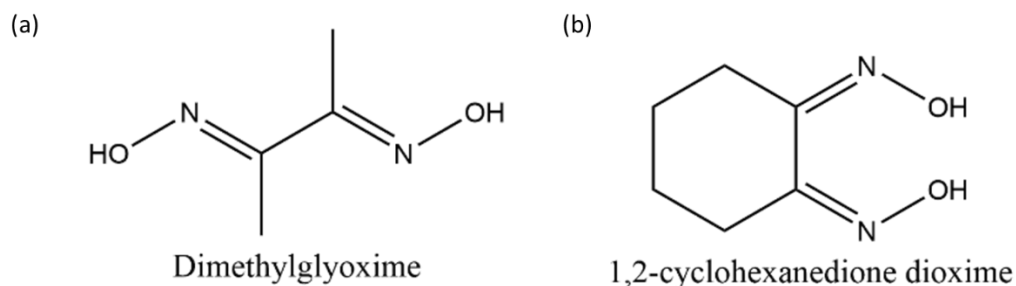


Figure 37 Chemical structure of (a) dimethylglyoxime and (b) 1,2-cyclohexanedione dioxime.

However, the rate of a chemical reaction is a correlation of concentrations between each chemical involved in the reaction. Generally, in the developed μ PADs, the colour-forming reaction was between the colorimetric reagent and the Ni^{2+} existing in the water sample. Therefore, the amount of reagent stored or loaded in the device became one interesting factor in determining the stark difference in reaction time. In previous devices, DMG was typically used in high concentrations, ranging from 60 mM to 0.1 M, which translates to within the 6900-11600 mg L^{-1} range [13, 75, 80]. Not only is variety in DMG concentration used the volume of DMG loaded onto the sample well also differs. This is possibly due to a difference in sample well size design. From this information, the mol (n) and mass of the reagent loaded on the sample well can be calculated and compared to the nioxime μ PAD developed in this research. However, upon calculation, the amount of reagent stored in the sample wells in this research was not higher compared to previous studies, as shown in [Table 14](#). The highest amount of nioxime stored in the μ PAD developed in this research is comparable to [13, 75] and only 0.04 μmol higher than [80]. Despite this, the reaction rate of nioxime μ PAD is faster than preceding devices.

Another factor that could influence the rate of reaction is sample concentration, or in this instance, the amount of sample involved in the reaction. In this aspect, then, it becomes important to note the big difference between the sample introduction method in this research compared to prior research. In previous studies, samples were usually introduced by pipetting a specific volume of sample to a special well, known as a "sample zone". The sample would then travel through capillary forces to a different well for pre-treatment or directly to a detection well, where the colorimetric reagent is stored. Further, the device is usually designed for multiplex detection. This implies that there are multiple channels for the sample to travel to. In this case, the amount of sample actually entering the detection zone might be much smaller than the amount of sample introduced.

In this research, however, the sample was introduced by dipping the device into a relatively bigger volume of sample. A bigger volume of sample is a drive for vertical capillary movement through layers of the μ PAD and it also essentially ‘floods’ the detection area to its maximum capacity. Assuming that the sample is always aqueous with a relatively non-significant change in solution viscosity, maintaining the immersion duration would aid in ensuring the μ PAD repeatability. Additionally, the design of μ PAD in this research removes the horizontal capillary movement of the sample. Instead, through dipping, the sample is directly introduced into a well with either pre-treatment reagents or detection reagents stored. This cuts down the waiting time from uncontrollable capillary diffusion. Therefore, the biggest factor in the decrease of reaction time for the μ PAD in this research is the elimination of capillary movement from separate sample zone and a bigger volume of sample.

Table 14 μ PAD specification comparison between previous studies and this research

Name	Reagent				Sample introduction method	Sample volume / μ L	Reaction time /min	Ref
	Total volume stored / μ L	Conc. /mg L ⁻¹	Mol stored / μ mol	Mass stored /mg				
DMG	10	11,612	0.10	0.12	Pipetted	50	10	[75]
DMG	30	17,418	0.15	0.52	Pipetted	130	15	[13]
DMG	3	6,967	0.06	0.02	Pipetted	300	120	[80]
Nioxime	10	1,400	0.10	0.02	Dipped	10,000	4	This work

Careful observation of [Figure 36](#)[Figure 35a](#), however, would show unevenness of colour formed on the sample well. This is due to nioxime and nioxime-Ni²⁺ complex solubility in water. Upon contact with the water sample through the dipping process, nioxime and nioxime-Ni²⁺ complex risk being released out of the sample well. This solubility issue also occurs in the Ni²⁺-DMG complex at a slightly higher degree. The solubility of the Ni²⁺-DMG complex in water is 2.1 x 10⁶ mol L⁻¹, which is 1.3 times higher than the Ni²⁺-nioxime complex solubility of 1.6 x 10⁶ mol L⁻¹ [138]. Consequently, the release of nioxime out of the device results in colour unevenness on the sample well, as well as higher standard deviation upon colour intensity measurement. Further, this release is not controllable and might be affected by the water sample properties. Therefore, it was decided that an additive is required to bind the nioxime or the coloured complex formed onto the sample well of the μ PAD.

2.4.2.1 Box-Behnken design of experiment

In this research, the developed nioxime μ PAD requires 1400 mg L⁻¹ nioxime, 4 wt% PDADMAC, and 0.01 M PBS buffer in order to reliably perform Ni²⁺ detection, each at 10 μ L volume upon addition. The concentration values were not obtained separately, but rather through an optimization process accounting for the effect of individual reagents as well as the interaction between the reagents, through the Box-Behnken design of the experiment. This approach was chosen over factorial design due to the fewer experiments required for the response surface methodology for device optimization. Box-Behnken design of experiment also allow avoidance of extreme points in testing – meaning that it would eliminate the need to test extreme conditions such as 0 concentration of all tested reagents. In the case of nioxime μ PAD, an optimum condition is defined as the smallest reagent concentration possible to achieve the highest signal or colour intensity with a repeatable result for various water matrices. Therefore, the parameters to be observed and varied were the reagent concentrations required for the μ PAD. The reagents of interest were nioxime as a colorimetric reagent, PDADMAC as a binding polymer, and PBS as a buffer solution. The volume of the reagent was not optimized in this research and instead was fixed at 10 μ L. Since the use of nioxime for Ni²⁺ detection in the μ PAD system is a novel approach, there have been no prior reports on the optimization process for this combination of reagents.

Nioxime concentration was varied between 400-1400 mg L⁻¹ in this experiment and for ease of data processing, the concentration was coded between -1 to 1. A similar approach was employed for the concentration variation of other reagents. PDADMAC concentration was varied between 0-4 wt% and PBS concentration was varied between 0-0.01 M. Addition of PDADMAC in the nioxime μ PAD was necessary to prevent coloured complex leaking out of the sample well. PDADMAC is a cationic polymer that has been previously used for metal-ligand complex binding polymer in μ PADs [83]. Ni²⁺ in its free ion form in the water is a cation, however, upon complex formation reaction with nioxime, it produces an anionic complex. Therefore, as the device is dipped into the water sample and an anionic metal-ligand complex is formed, the presence of PDADMAC on the device layer would help to bind the coloured complex through ionic interaction.

While the concentration range of nioxime in this optimization process was determined by the increment of 500 mg L⁻¹ from the working concentration for UV/Vis spectroscopy analysis, the range of concentration for PDADMAC and PBS buffer has not yet been investigated in UV/Vis analysis. Further, the two reagents could be considered an additive, since it is not directly involved in the Ni²⁺-nioxime reaction itself, rather ensuring the reaction is in a suitable environment in the μ PAD. Therefore, in optimisation, the absence of these additives was

included as the lowest concentration. For PBS buffer, the highest concentration was determined to be 0.01 M. This concentration is equal to the molarity of 1X working PBS buffer concentration. This is the concentration at which it is commonly used and widely available commercially. Whereas for PDADMAC, 4 wt% PDADMAC concentration was chosen. As a point of reference, the highest PDADMAC solution in water available in the market is 35 wt% [139]. Upon loading the polymer at 6 wt%, however, it was observed that a coffee-ring stain was formed on the edges of the sample well. This effect persisted with the increase in PDADMAC concentration.

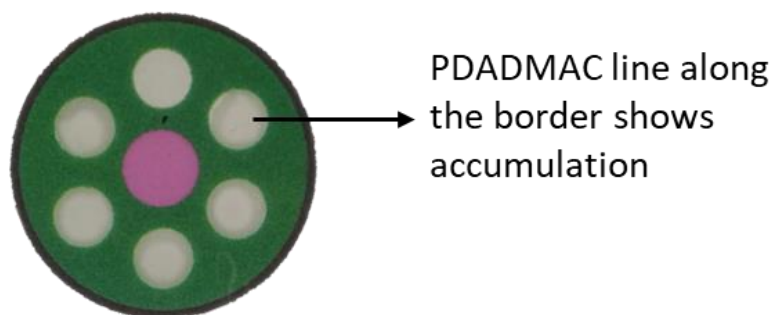


Figure 38 Coffee-ring effect observed on sample wells of nioxime μ PAD upon addition of ≥ 6 wt% PDADMAC solution onto the wax-printed device.

The coffee-ring effect is a ring pattern originating from capillary flow induced by droplet evaporation, where liquid evaporating from the edges of the droplet is replenished by liquid from the interior of the droplet. This constant flow may push the substances dispersed in the liquid to deposit and concentrate at the edges of the droplet, creating a concentrated ring at the edges of the droplet. This is especially true for liquids with weak Marangoni flow. In μ PAD, this coffee-ring effect may lead to uneven colour formation upon colorimetric complexation reaction. Uneven colour formation on a sample well would lead to unrepeatable or unreliable colour intensity measurement since the image would have 'patches' of colour that will affect the average intensity of the well area. This may lead to unrepeatable results or result with high standard deviation since the coffee-ring formation is uncontrollable and may differ in thickness for every well. Therefore, the coffee-ring effect is undesirable in this design of μ PAD.

2.4.2.2 Standardised effect

[Figure 39](#) ~~Figure 38~~ shows the result of the optimization experiments carried out with response surface methodology through Box-Behnken. [Figure 39](#) ~~Figure 38~~ shows the standardized effects of varying the reagent concentrations and interaction between the reagents to the measured colour intensity of the μ PAD after dipping into $10 \text{ mg L}^{-1} \text{ Ni}^{2+}$ ion solution. In this chart, it is shown that the standardized effect of all factors accounted for is beyond the threshold line of 3.182,

and therefore all factors had significant effects on the measured colour intensity. However, the extent to which these factors affect the colour intensity is different and correlated to the value of the standardized effects. Therefore, for nioxime μ PAD, both buffer concentration and interaction between buffer and PDADMAC are two of the most influential factors affecting the colour intensity measured on the μ PAD after the reaction.

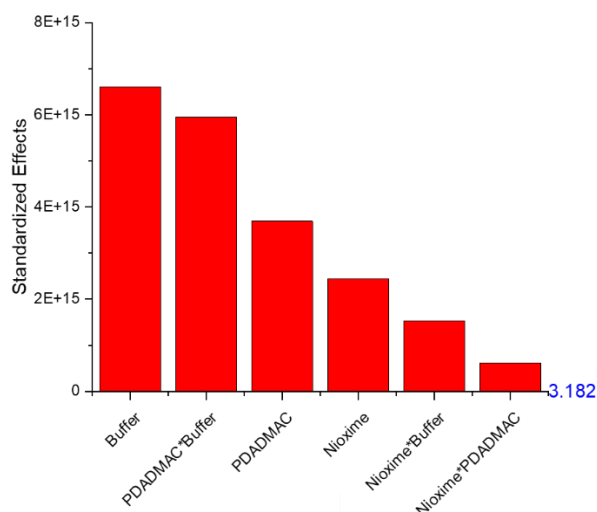


Figure 39 Standardised effects plot illustrating the result of reagent concentration optimization process for nioxime μ PAD using Box-Behnken design. The optimum condition for nioxime μ PAD was defined as the highest signal obtained in the lowest reagent concentration possible. Reagents involved in this optimization were: 400-1400 mg L⁻¹ nioxime, 0-4 wt% PDADMAC, and 0-0.01 M PBS. Colour intensity was measured after 3 minutes of reaction at the green channel.

2.4.2.3 Main effects plot

Further, through the main effects plot in [Figure 40](#)[Figure 39](#), the direction of this influence can be determined. There are three main conclusions to be taken out of the main effects plot, which are whether the increase of each reagent concentration increases or decreases the colour intensity measured. The increase of nioxime concentration within the tested range, for example, is shown to increase the colour intensity measured on the μ PAD. This is a correlation between the amount of nioxime available for complex-formation reaction on the sample well with the intensity of colour observed. The higher the nioxime concentration, the more ligand interaction sites available for complex formation, and the higher signal measured on the well. Whereas the increase of concentration of the additives – PDADMAC and buffer, are shown to have a negative effect on the measured colour intensity. Through naked-eyes observation, PDADMAC, which was introduced to the μ PAD as a polymeric binding agent, had an obvious impact on the homogeneity of the colour on the well. The absence of PDADMAC would result in Ni²⁺-nioxime complex being released to the water over time, which can be seen by the change of water sample colour at high enough Ni²⁺ or nioxime concentration. Whereas PBS buffer was added to

maintain the pH value during the reaction. This additive is critical for reaction with the environmental water sample matrix, which might vary in acidity. Incorporating a buffer into the reaction will help to minimize the water pH variation variable and consequently increase the robustness of the developed μ PAD.

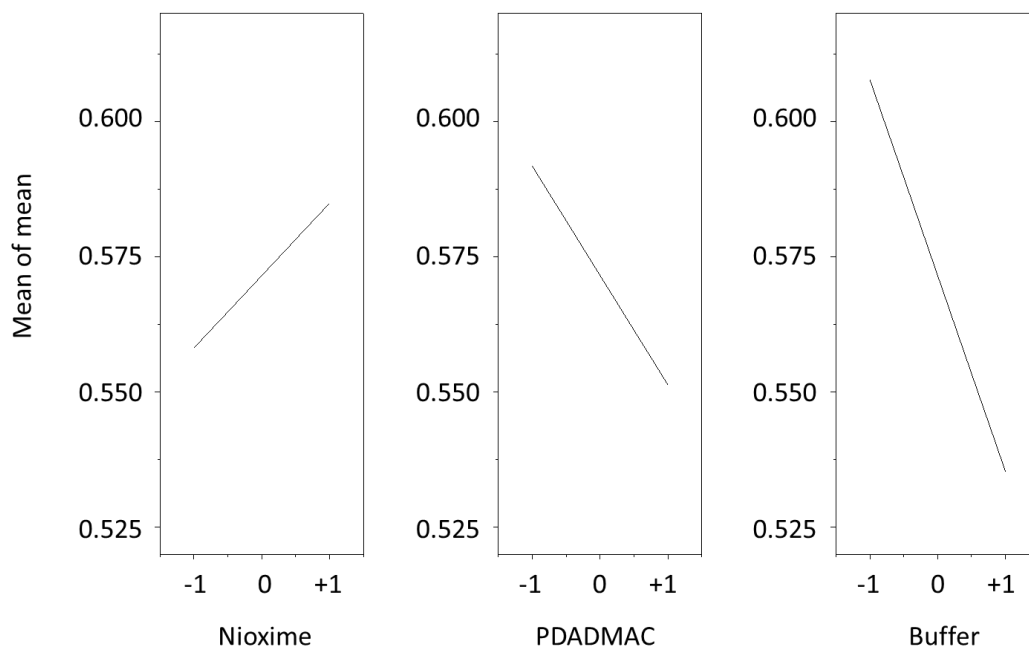


Figure 40 Main effects plot illustrating the result of reagent concentration optimization process for nioxime μ PAD using Box-Behnken design. The optimum condition for nioxime μ PAD was defined as the highest signal obtained in the lowest reagent concentration possible. Reagents involved in this optimization were: 400-1400 mg L⁻¹ nioxime, 0-4 wt% PDADMAC, and 0-0.01 M PBS. Colour intensity was measured after 3 minutes of reaction at the green channel.

2.4.2.4 3D- and contour-plot (response surface methodology)

Through these first two graphs, the effects of individual reagents and interactions between reagents were observed. However, no direct conclusion can be made on the optimum concentration for each reagent to obtain the highest colour intensity (signal). In order to obtain the optimum concentration of the reagents, a plot illustrating the relationship between different reagents in a gradient of concentration against the colour intensity produced upon reaction is required. This is presented in [Figure 41](#) through the 3D contour and 2D contour plots.

In plotting the contour plot, one 'value' must be held – meaning only two interacting reagents can be plotted, whereas one of the reagents will be treated as constant. In this research, due to its importance for Ni²⁺ detection in the environmental sample matrix, the concentration of PBS buffer was held constant at its highest. Therefore, in further discussions, the concentration of PBS will be held at 0.01 M (10 mM), unless stated otherwise.

Both [Figure 41](#) [Figure 40a](#) and b show that at the highest buffer concentration (0.01 M PBS), the highest signal can be obtained with the highest concentration of PDADMAC and nioxime tested. In the 3D contour plot ([Figure 41](#) [Figure 40a](#)), this area is shown to be the peak of the parallelogram, whereas, in the 2D contour plot ([Figure 41](#) [Figure 40b](#)), this area is in red colouration – both indicating that the highest colour intensity signal was obtained. This is an interesting result, since, at a glance, it seems to contradict the main effects plot ([Figure 40](#) [Figure 39](#)). While the main effects plot shows that overall, the increase of PDADMAC concentration has a negative impact on the signal, the contour plots show that at a certain condition (buffer= 0.01 M), the increase of PDADMAC concentration seems to correlate to a higher signal instead. This highlights the importance to consider the interaction between two different reagents in the reaction, instead of observing the effects individually. As supported by the standardized effects ([Figure 39](#) [Figure 38](#)) plot, the interaction between PDADMAC and buffer would have a notably high effect on the signal intensity.

Referring to the optimization results and plots through the Box-Behnken design of the experiment, especially the model based on the observations in the optimisation process ([Figure 41](#) [Figure 40](#)), the optimum reagent concentrations to obtain the highest signal possible is therefore as follows: 1400 mg L⁻¹ nioxime, 4 wt% PDADMAC, and 10 mM PBS buffer.

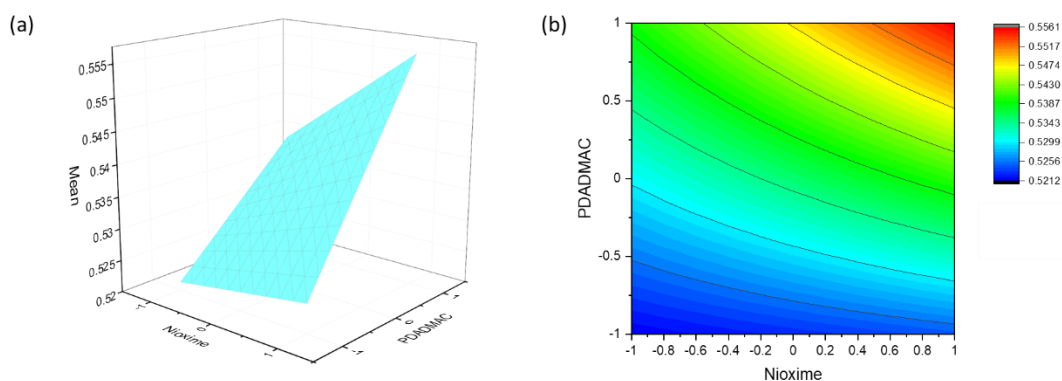


Figure 41 (a) 3D- and (b) 2D-contour plots illustrating the result of the reagent concentration optimization process for nioxime μ PAD using Box-Behnken design. The optimum condition for nioxime μ PAD was defined as the highest signal obtained in the lowest reagent concentration possible. Reagents involved in this optimization were: 400-1400 mg L⁻¹ nioxime, 0-4 wt% PDADMAC, and 0-0.01 M PBS. Colour intensity was measured after 3 minutes of reaction at the green channel.

2.4.3 Interference study

An observation on the effect of the presence of other commonly occurring ions in the sample was made by the addition of other ions at an equal concentration as Ni²⁺ in the sample solution. The ions tested include various commonly co-existing metals (Fe²⁺, Fe³⁺, Co²⁺, Cu²⁺, Zn²⁺) and ions

that may be naturally available in water bodies such as Cl^- , K^+ , Ca^{2+} , Na^+ , HCO_3^- , PO_4^{3-} , NO_3^- , and SO_4^{2-} . However, the initial focus was on the effect of the presence of other similar metal cations, as interference by these metal species has been reported in the literature for Ni^{2+} -nioxime reaction [92, 96].

Dipping the 2-layered device into a 10 mg L^{-1} of Fe^{3+} , Cu^{2+} , or Co^{2+} showed a weaker colorimetric reaction occurring in the sample well. In this experiment, a 2-layered device containing 10 mM PBS, 4 wt% PDADMAC, and 1400 mg L^{-1} nioxime at $10 \mu\text{L}$ each was laminated and dipped into 10 mL solution containing 10 mg L^{-1} of Ni^{2+} , Fe^{3+} , Cu^{2+} , or Co^{2+} solution. The device was then left to react for 4 min before pictures of the respective devices were taken. Each experiment was repeated 3 times. The colour of the inverted image was measured with ImageJ software in the G (green) channel of the RGB colour stack. This is the exact same procedure used to measure the colour intensity upon dipping into Ni^{2+} solution in this research. [Figure 42](#) shows the result of this experiment, where devices dipped into Ni^{2+} solution show the highest measured colour intensity. However, the colour intensity measured in other devices also cannot be disregarded. Compared to the blank sample well (colour intensity average= 0.55 a.u.), the colour intensity measured upon dipping the device into Fe^{3+} , Cu^{2+} , and Co^{2+} showed notable differences. However, a more important observation for the purpose of this device would be its performance in the presence of both target analyte (Ni^{2+}) and interfering ions.

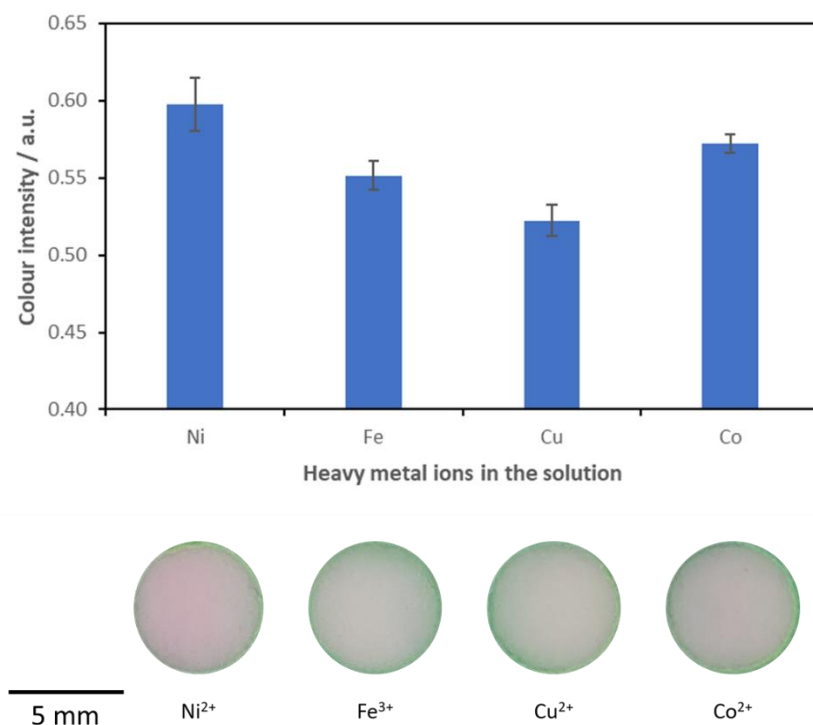


Figure 42 (Top) Measured colour intensity at the green channel of 2-layered devices dipped into 10 mL solution of 10 mg L^{-1} Ni^{2+} , Fe^{3+} , Cu^{2+} , or Co^{2+} , respectively. (Bottom) The sample well of 2-layered devices after dipping into 10 mL solution of 10 mg L^{-1} Ni^{2+} , Fe^{3+} , Cu^{2+} , or Co^{2+} , respectively.

In the presence of these potentially interfering metal ions, it was observed that the colour intensity measured on the sample well decreased significantly, correlating the presence of the other metal ion species to interference in the coloured-complex formation. Dipping the 2-layered device containing a layer of PBS-PDADMAC and a layer of nioxime to a 10 mL solution containing $10 \text{ mg L}^{-1} \text{ Ni}^{2+}$ and 10 mg L^{-1} other metal ion species showed interference by Fe^{3+} , Co^{2+} , and Cu^{2+} ions, as can be seen in [Figure 43](#)~~Figure 42~~. This is in line with previous studies on the reagent [92]. In studies involving nioxime- Ni^{2+} reaction in a liquid medium (gravimetric or spectrophotometric), the addition of excess nioxime in ammoniacal was used to obtain Ni^{2+} measurements [92]. The problem of interference with Cu^{2+} and Fe^{3+} was further underlined in [96], with no masking reagent introduced to solve the interference problem.

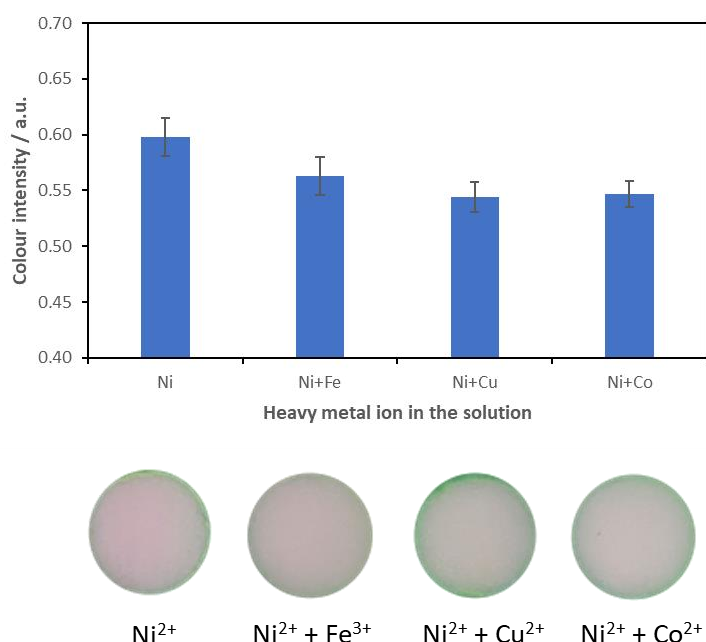


Figure 43 (Top) Measured colour intensity upon dipping a 2-layered device into a 10 mL solution containing 10 mg L^{-1} of Ni^{2+} , $10 \text{ mg L}^{-1} \text{ Ni}^{2+}$ and $10 \text{ mg L}^{-1} \text{ Fe}^{3+}$, $10 \text{ mg L}^{-1} \text{ Ni}^{2+}$ and $10 \text{ mg L}^{-1} \text{ Cu}^{2+}$, or $10 \text{ mg L}^{-1} \text{ Ni}^{2+}$ and $10 \text{ mg L}^{-1} \text{ Co}^{2+}$ showing decreasing intensity in the presence of tested interfering metal ions. (Bottom) The sample well of devices after dipping into 10 mL of respective solutions.

However, this problem with Cu^{2+} , Fe^{3+} , and Co^{2+} is not exclusively to the nioxime- Ni^{2+} reaction. Paper devices created with DMG as a colorimetric reagent also faced interference problems with these ions. The key considerations in selecting a suitable masking reagent for this type of device focus on (1) the specificity of the reagent and (2) the colour at the endpoint of the masking reaction. The specificity of the masking reagent is important since it ideally should react with most or all interfering ions, while not reacting with the target analyte (in this case, Ni^{2+}).

Additionally, the colour at the endpoint of the reaction between the masking reagents and the interfering ions should ideally be colourless. Since the device is dependent on colour intensity reading on the sample well, coloured complex formation at the masking layer would interfere with the colour measurement. Consequently, creating an error in the measurement process. In previous devices, sodium fluoride has been added to mask Fe^{3+} and Co^{2+} ions, and sodium thiosulfate has been added for masking Cu^{2+} ions [13, 75, 80, 140]. Although the mechanisms of masking were not explained for these devices, the chosen masking reagents are well-known masking reagents for these target ions, due to the formation of rapid and strong colourless complexes [141]. Fluoride is also a well-known masking agent for various metals, including Cu^{2+} , Fe^{3+} , and Co^{2+} [141]. Whereas thiosulfate is usually utilised as a less toxic alternative to cyanide in metal extraction processes from natural ores, proving its ability for the rapid formation of complexes with different metal ions.

A new layer was therefore added to the device, creating a 3-layered paper-based device. This layer was placed nearest to the sample entry point. Theoretically, through this placement, the interfering ions will react with the masking reagents deposited in this layer before it is able to react with nioxime. The masking reagents added into this layer were: 1 M sodium fluoride and 1 M sodium thiosulfate, both at 10 μL volume. The addition of these masking reagents was first evaluated separately. In order to evaluate each of the masking reagents, a 3-layered device was made with one of the masking reagents in the masking layer, 4 wt% PDADMAC and 10 mM PBS in the second layer, and 1400 mg L^{-1} nioxime in the detection layer, each at 10 μL volume. These devices were then dipped into a 10 mL solution containing 10 mg L^{-1} Ni^{2+} and 10 mg L^{-1} of one species of the interfering ions. Each experiment was repeated three times. Tolerable error, in this case, was determined to be 3 times the standard deviation of the control.

With the determined criteria, both of the masking reagents tested showed to be suitable for Co^{2+} , while thiosulfate was able to overcome the interference of Fe^{3+} . [Figure 44](#)~~Figure 43~~ showed the result of this experiment, where the interfering ion species evaluated were expanded to commonly available ions in water samples. This include Ca^{2+} , K^+ , Na^+ , Cl^- , PO_4^{3-} , NO_3^- , HCO_3^- , and SO_4^{2-} . It was evident that the addition of the individual masking agents did not further cause interference with the tested ions, rather improving the performance of the device in the presence of Co^{2+} and Fe^{3+} . The individual masking agents also did not produce notable colorimetric products with the interfering ion species, target analyte (Ni^{2+}), nor with the reagents suspended in the μPAD . All of the measured colour intensity was, therefore, still within the set criteria (3σ). However, the addition of individual masking agents did not seem to notably improve the performance of nioxime μPAD in the presence of an equal level of Cu^{2+} (10 mg L^{-1}).

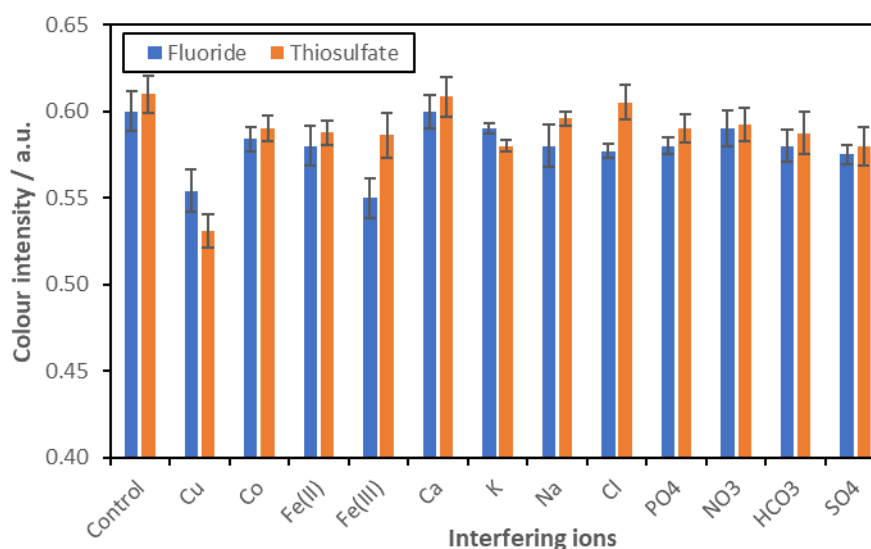


Figure 44 Measured colour intensity for 3-layered nioxime μ PAD containing respective masking agent (1 M sodium fluoride or 1 M sodium thiosulfate), dipped into a 10 mL solution containing a mixture of $10 \text{ mg L}^{-1} \text{ Ni}^{2+}$ and 10 mg L^{-1} respective interfering ion ($n=3 \mu\text{PADs}$ with 5 sample wells each).

Upon addition of the masking layer, a significant improvement in the device performance in the presence of identified interfering metal ions (Fe^{3+} , Co^{2+} , Cu^{2+}) was observed. In [Figure 45Figure 44a](#), the positive effect of the addition of the masking layer to the colour intensity observed on the μ PAD is illustrated. In devices without masking agents, a significant decrease in the colour intensity can be observed upon dipping into a 10 mL solution containing equal concentration (10 mg L^{-1}) of Ni^{2+} and respective interfering ions (*paired t-test*, $p \leq 0.05$). However, in devices containing masking agents (3-layered), no significant difference was observed upon dipping into a solution containing interfering ions. This change may not be easily observed with the naked eye ([Figure 45Figure 44b](#)); however, it is observable through measurement with digital image processing software.

Contrary to the result obtained by testing individual masking agents ([Figure 44Figure 43](#)), the μ PAD containing both masking agents showed successful and notable masking of Cu^{2+} ion. In the previous figure, where the 3-layered μ PAD only contain either 1 M NaF or 1 M $\text{Na}_2\text{S}_2\text{O}_3$ ([Figure 44Figure 43](#)), the device performance did not improve or reached a satisfactory level according to the set parameter (3σ). Through the experiment, it can easily be concluded that neither of the masking agents was able to mask the Cu^{2+} ion in the solution. However, through this follow-up experiment where the device masking layer contained both 1 M NaF and 1 M $\text{Na}_2\text{S}_2\text{O}_3$, it was proven that Cu^{2+} ions can be masked in the tested concentration. This shows the potential of a synergistic effect on Cu^{2+} masking.

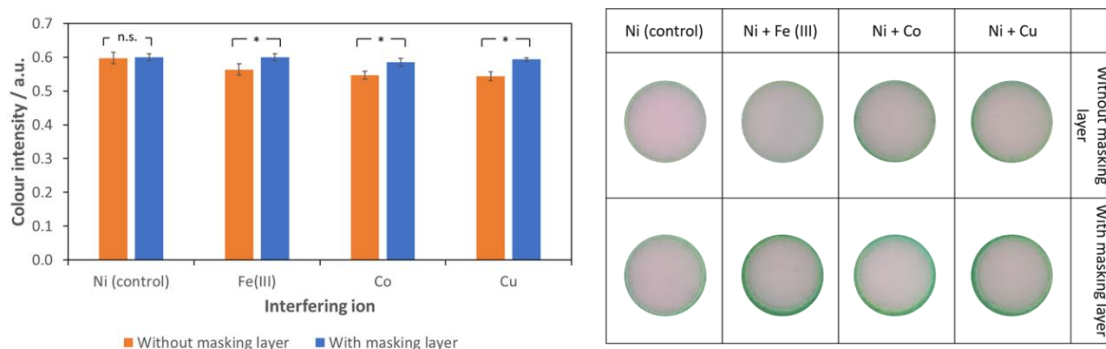


Figure 45 (Left) Measured colour intensity of nioxime μ PAD with and without masking agents (1 M NaF and 1 M Na₂S₂O₃) dipped into 10 mL solution containing 10 mg L⁻¹ Ni²⁺ and 10 mg L⁻¹ of respective interfering ion: Fe³⁺ ($t_{(2)}=4.65$, $p=0.043$), Co²⁺ ($t_{(2)}=6.95$, $p=0.021$), or Cu²⁺ ($t_{(2)}=5.31$, $p=0.033$), showing significant difference in all metal masking results, and no significant difference in pure Ni²⁺ detection process ($t_{(2)}=2.147$, $p=0.165$); (Right) Observed colour on the devices' sample wells with or without masking agents, 4 minutes after dipping into 10 mL solution containing 10 mg L⁻¹ Ni²⁺ and 10 mg L⁻¹ of respective interfering metal ions ($n=3$ μ PADs, each consisting of 5 sample wells).

The addition of this masking layer did not significantly affect the colour intensity produced on the device. As can be seen in [Figure 46](#)[Figure 45](#), upon dipping the 3-layered device containing a masking layer with 1 M NaF and 1 M Na₂S₂O₃, the additive layer containing 4 wt% PDADMAC and 10 mM PBS buffer, and a detection layer containing 1400 mg L⁻¹ with 10 μ L volume each, into 10 mL solution containing 10 mg L⁻¹ Ni²⁺ and 10 mg L⁻¹ interfering ions, no significant ($p=0.3418$, $F_{(13,28)}=1.18$) colour intensity difference was observed compared to control. This shows that both masking solutions were colourless and did not form any coloured product with other reagents involved on the device, nor with the metal species being masked. Through this experiment, it can be concluded that the addition of the masking layer is an effective way to reduce interference from coexisting metal ions as well as other commonly occurring ions in a water sample up to 10 mg L⁻¹ concentration, or at equal Ni²⁺ and interfering ion concentration (10 mg L⁻¹).

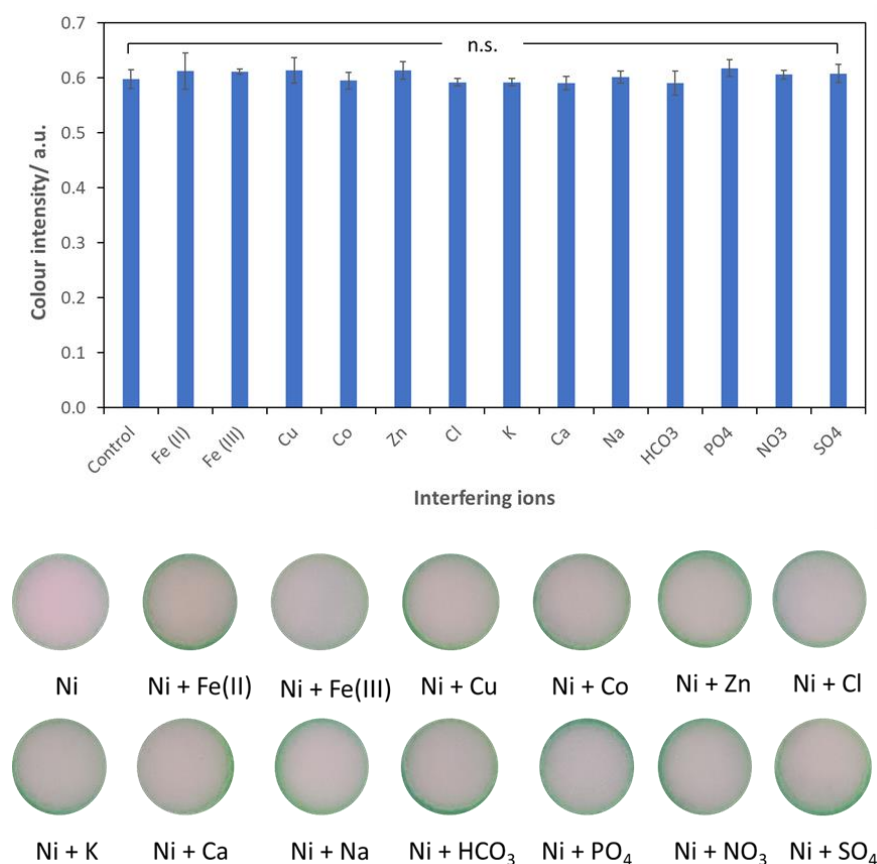


Figure 46 (Top) Measured colour intensity of a 3-layered device containing 1 M NaF and 1 M Na₂S₂O₃ in the masking layer at 10 μ L each, dipped into 10 mL solution containing 10 mg L⁻¹ Ni²⁺ and 10 mg L⁻¹ of respective interfering ion, showing no significant difference ($p=0.3418$, $F_{(13,28)}=1.18$); (Bottom) The observed sample well of the 3-layered device containing 1 M NaF and 1 M Na₂S₂O₃, 4 minutes after dipping into 10 mL solution of 10 mg L⁻¹ Ni²⁺ and 10 mg L⁻¹ of respective interfering ion ($n= 3 \mu$ PADs consisting of 5 sample wells each).

However, in the target water sample, it may be unrealistic to assume 10 mg L⁻¹ concentration as the commonly found concentration of the interfering ion. Depending on the ion species and geographical area, ion concentration may far exceed or be far below this tested concentration. Heavy metal ions such as Fe³⁺, Cu²⁺, or Co²⁺, for example, may present in a far lower range compared to 10 mg L⁻¹. Such ions commonly amount to ppb or parts per billion (μ g L⁻¹) level before it is considered as pollution – consequently rendering the water sample hazardous and toxic. Whereas ions such as Cl⁻, HCO₃⁻, or Ca²⁺ may be more common and exist in higher levels than tested in previous experiments, as it is naturally occurring in high levels and is relatively non-toxic. Therefore, in order to ensure the developed device is suitable for use in realistic environmental samples, further testing was done on the nioxime μ PAD.

In order to ensure the device's performance in the environmental water matrix, the device was dipped into an environmental water sample spiked with 10 mg L⁻¹ Ni²⁺. In this condition, the

performance of the device in more realistic noise can be observed. The water samples were obtained from various areas along the Humber, around Hull, United Kingdom, with a variation in water contents. Welton Springs is a freshwater source located to the west of the city of Hull, in the Brough area (53°44'16.62"N, 0°32'35.17"E). Whereas another water sample was collected from the outer Humber estuary (53°38'29.29"N 0° 4'12.35"E), where the sample was expected to be more brackish, due to the geographical location. The Ni²⁺-spiked solution from these two samples was compared to a control solution, made using Milli-Q water in the laboratory.

Figure 47 shows no significant difference ($p=0.149$, $F_{(3,6)}=2.581$) was observed when comparing the device performance in spiked water samples to control. Upon dipping the 3-layered device with masking layer to spiked samples with expected environmental noise and comparing to the control, where the water matrix is relatively of higher purity. This indicates that in detectable Ni²⁺ concentrations, the presence of co-existing ions in various concentrations did not significantly affect the measured colour intensity of the formed complex. It also further ascertains the suitability of the device for use in the target environmental water matrix, which is a freshwater environment. Despite the uncontrolled variation in the tested sample matrix, the device was able to detect Ni²⁺ accurately.

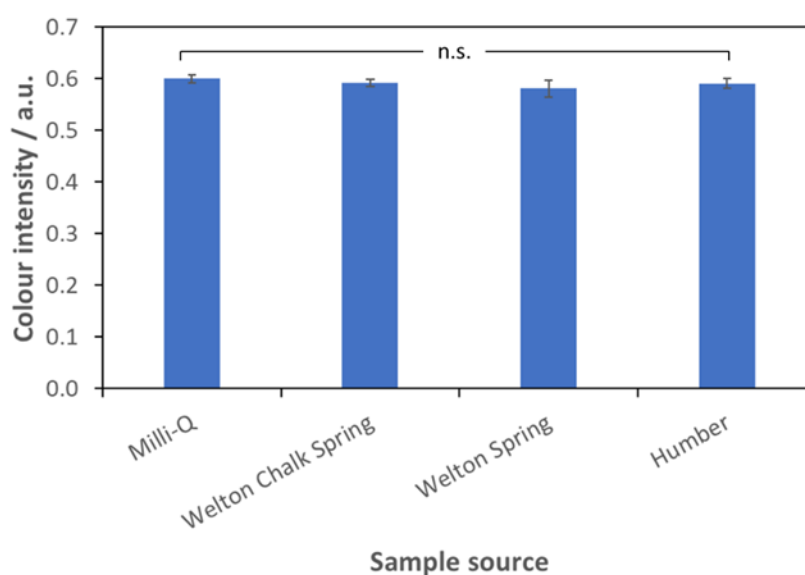


Figure 47 Measured colour intensity of nioxime μ PAD upon dipping into spiked (10 mg L⁻¹) control and environmental water matrix from Welton Spring and Humber area show device robustness to be used in the target environmental water sample with no significant difference in different water matrix ($p=0.149$, $F_{(3,6)}=2.581$; $n=3$ μ PADs consisting of 5 sample wells each).

2.4.4 Calibration curve of nioxime μ PAD

The Ni^{2+} detection calibration curve was then constructed with the optimized μ PAD by dipping it into a gradient of Ni^{2+} concentration. The μ PAD used for this process was a 3-layered device with masking agents loaded in the first layer, additives in the second layer, and detection agent in the third layer – with the first layer being the closest to the sample entry. The masking agent was: 10 μL 1 M NaF and 10 μL 1 M $\text{Na}_2\text{S}_2\text{O}_3$, the additives were: 10 μL 4 wt% PDADMAC and 10 μL 0.01 M PBS buffer, and the detection agent was 10 μL 1400 mg L^{-1} nioxime. The μ PAD was dipped into 10 mL Ni^{2+} ion solution until all sample wells were in contact with the sample solution before μ PAD was removed and placed on a clean, sterile plastic petri dish. After 4 minutes, the device was placed under the black box for picture-taking with a smartphone through a slit on the topside of the box.

Firstly, the μ PAD performance was tested within 0-1000 mg L^{-1} Ni^{2+} ion solution. This concentration range is the concentration range of commercially available Ni^{2+} semi-quantitative test strips Quantofix[®] by Macherey-Nagel GmbH & Co., KG. The colour intensity at this range was measured using ImageJ, by inverting the colour of the picture file and separating the colour channels into RGB stacks. Measurement was only done in the green channel (G) since the coloured complex formed was magenta. Upon inversion, magenta will be converted into its complementary colour, which is green. Therefore, the increase in Ni^{2+} concentration, which through naked eye observation was linear with the increase of magenta colour intensity, would also correlate linearly upon the measurement in the G channel.

[Figure 48](#)~~Figure 47~~a shows the correlation between the measured colour intensity with the increase of Ni^{2+} concentration in the range of 0-1000 mg L^{-1} . Evidently, the correlation at this concentration range is non-linear. The measured colour intensity increased sharply between 0-100 mg L^{-1} Ni^{2+} ion concentration, followed by a gentler increase between 100-500 mg L^{-1} Ni^{2+} ion concentration and stable intensity from 500-1000 mg L^{-1} . Linearisation of this plot, as shown in [Figure 48](#)~~Figure 47~~b, was made by taking the log of Ni^{2+} concentration (10-1000 mg L^{-1}) showing a linear correlation ($R^2=0.988$) with the colour intensity measured. This non-linear correlation between the colour intensity and the Ni^{2+} concentration signifies linear relation at a narrower concentration range.

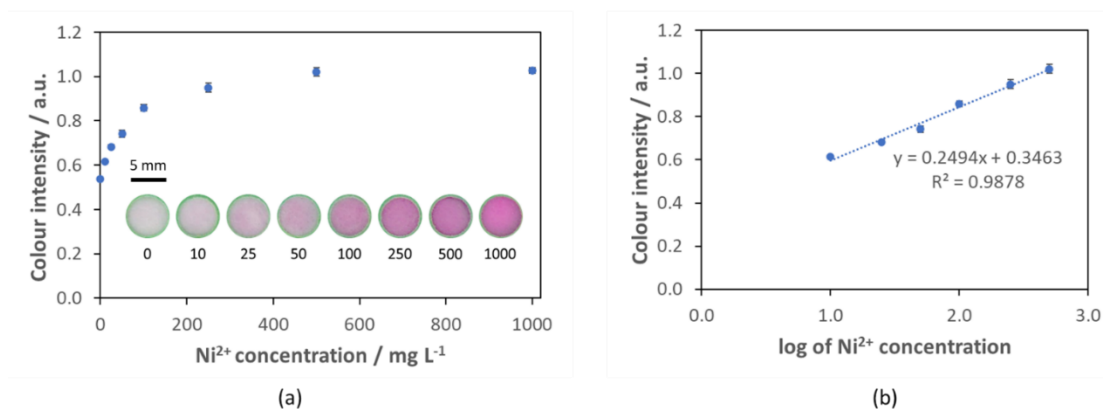


Figure 48 Colour intensity measurement in RGB colour space of optimised nioxime μ PAD dipped into 10 mL Ni^{2+} solution within the 0-1000 mg L^{-1} concentration range. Colour intensity was plotted against (a) Ni^{2+} concentration and (b) log of Ni^{2+} concentration ($n=3$ μ PADs consisting of 5 sample wells each).

Further, the tested concentration range in [Figure 48](#) is far higher than the Ni^{2+} concentration commonly found in environmental freshwater samples. According to the UK Environment Agency data from 2000-2020, Ni^{2+} was commonly found in river water at 0.008 mg L^{-1} or 8 parts per billion [28]. This amount is lower than the Scottish Environment Protection Agency's (SEPA) maximum allowable concentration of Ni^{2+} in the river water is 0.034 mg L^{-1} and the United States Environmental Protection Agency (US EPA) chronic and acute Ni^{2+} concentrations of 0.052 and 0.470 mg L^{-1} , respectively [33, 34].

Therefore, the concentration range of interest for Ni^{2+} detection is at the lower range of concentration tested in [Figure 48](#). The performance of the optimised nioxime μ PAD was then further tested at a narrower concentration range within 0-10 mg L^{-1} with a 2 mg L^{-1} increment. The experimental procedure followed the previous calibration curve, where colour was measured in RGB colour space. The measured colour intensity was then plotted against the Ni^{2+} concentration.

[Figure 49](#) shows the plot between the measured colour intensity of the green channel of the sample well in the nioxime μ PAD against the Ni^{2+} concentration tested. The plot shows a linear correlation between the measured intensity and Ni^{2+} concentration ($R^2=0.987$). Through three repeats ($n=3$), the detection limit of the nioxime μ PAD was determined to be 3 mg L^{-1} . This is 100 times higher than the SEPA maximum allowable concentration of Ni^{2+} of 0.034 mg L^{-1} and approximately 6.5 times higher than the US EPA limit of acute Ni^{2+} concentration of 0.470 mg L^{-1} [33, 34]. The calculated limit of detection is also 50 times higher compared to the UV/Vis experiment conducted earlier in this research for the same ligand-metal reaction, where the limit of detection reached 0.06 mg L^{-1} .

However, compared to the DMG-based devices developed in the literature, the nioxime μ PAD developed in this research had a shorter reaction time and a lower working concentration range. In previous attempts to develop Ni^{2+} detection μ PADs, DMG was mainly used as the ligand for colorimetric complex formation. These devices had been reported to have a limit of detection in the 4.8-15 mg L^{-1} Ni^{2+} concentration range, with reaction time ranging from 10-120 minutes [75, 77, 80]. Compared to these reports, the nioxime μ PAD developed in this research can reliably detect Ni^{2+} down to 3 mg L^{-1} within 4 min reaction time. This result was also obtained by measuring pictures taken with a smartphone rather than an ideal condition such as a desktop scanner [77, 80]. The image acquisition workflow and its reliability for the colour intensity measurement increase the portability of the device, allowing for possible onsite measurement.

Repeatability test of nioxime μ PAD on different days with the same operator result in [Figure 49](#)[Figure 48b](#), showing statistically insignificant ($p>0.05$) difference between the linear fits of the repeats. This experiment was done by repeating the calibration curve experiment through three different days, fabricating new devices each day and dipping them into fresh solutions each day. Throughout these different repeats, the significance of the difference in the measured colour intensity was statistically calculated and showed no significant difference through the three repeats. This shows that the device developed can reliably produce repeatable results throughout the different device production or fabrication days. Additionally, it also shows the reliability of the picture-taking step with the black box method.

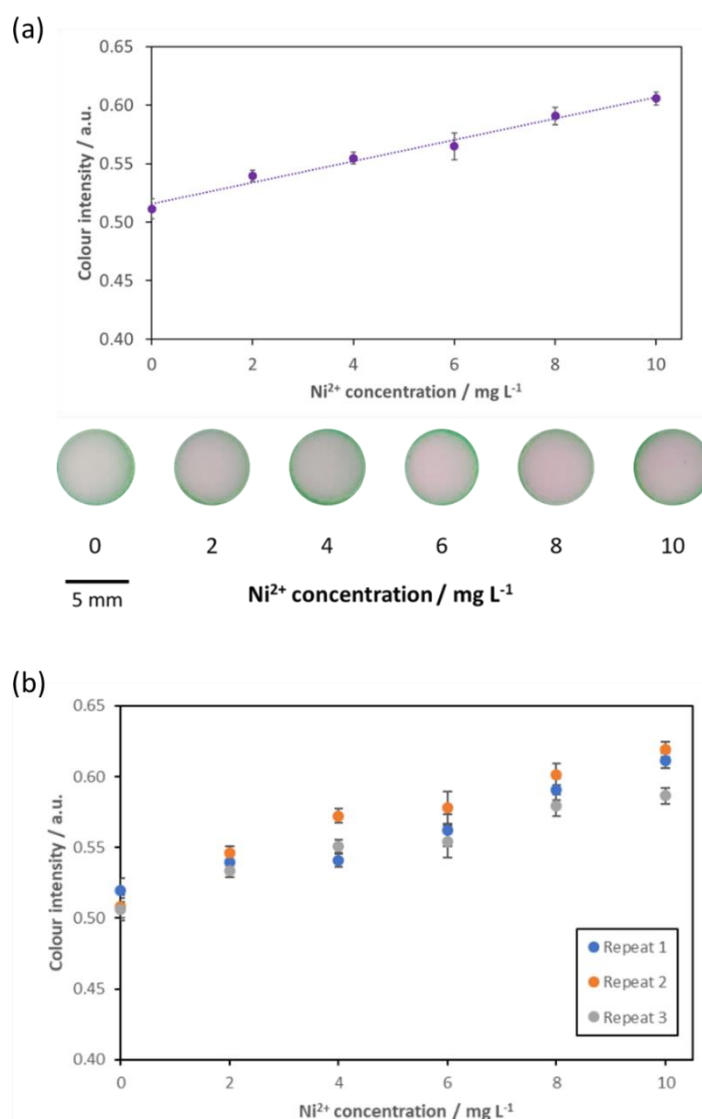


Figure 49 (a) Colour intensity measurement in RGB colour space of optimised nioxime μ PAD dipped into 10 mL Ni²⁺ solution within 0-10 mg L⁻¹ concentration range ($n=5$); (b) Repeated colour intensity measurement of the calibration curve across three different days ($n=3$ μ PADs consisting of 5 sample wells each).

2.4.5 Stability of nioxime μ PAD

The stability of the developed μ PAD is an important factor to ensure how long can the device be stored from the fabrication day to usage day. The stability of the device, in this research, is defined as a measure at which the device can still produce reliable results within pre-determined limits after adequate storage. The stability experiment can also be used to determine the suitable storage condition for the device. Although filter paper is generally a resilient matrix that can be stored at room temperature for a prolonged period of time, given no contamination occurred, the chemicals stored in the μ PAD may degrade with time or environmental conditions.

Among the chemicals stored in the developed μ PAD, none are known to have particular unstable nature or special storage requirements. Therefore, it was safe to assume that individually, these chemicals will not degrade in a way that will interfere with the colorimetric reaction. However, it is important to consider the possibility of interaction upon prolonged storage. Additionally, due to the design of the μ PAD, one side of the sample well is exposed to the environment (entry hole) that may accelerate or cause instability of the reagents stored in the sample wells.

In order to observe the appropriate storage conditions and the duration of storing before the device can no longer produce reliable results, a stability test was commenced by dipping the pre-fabricated 3-layered device into a fresh 10 mL solution containing $10 \text{ mg L}^{-1} \text{ Ni}^{2+}$ after a certain duration of storage. The storage condition for nioxime μ PAD was by placing it in a cool, dry, and dark area without any temperature control or modification. Practically, the μ PAD was laminated and placed in a closed petri dish, which was stored in a drawer in the laboratory. The temperature of this storage area was $18 \pm 2^\circ\text{C}$ with relative humidity up to $60 \pm 10\%$. The measured colour intensity results were then compared to the control, which is the measured colour intensity upon dipping the device into the sample solution on the same day the device is fabricated. Stability is defined as the condition at which the colour intensity produced by the stored device is not significantly different ($p > 0.05$) compared to the control. Upon significant increase or reduction of the measured colour intensity, the device will no longer be regarded stable and the last measurement at which it was still stable would be regarded as the maximum storage time before the device is deemed unstable.

[Figure 50](#)~~Figure 49~~ shows the result of the stability experiment, which showed the stability of the device was maintained up to 28 days after device fabrication, backed by the fact that on day-35 the measured value was significantly different to the control ($p=0.247$, $F_{(4,10)}=1.606$). This data showed that the device was able to reliably produce similar results to control up to 1 month after device fabrication. After 28 days, the measured colour intensity decreased significantly but was maintained at the same level up to 7 weeks (49 days) after device fabrication. This indicates that the device was still able to detect Ni^{2+} after 28 days, however, the concentration of Ni^{2+} detected would not be as accurate when calculated with the calibration curve made at day -0. In this sense, the device is no longer able to accurately quantify the concentration of Ni^{2+} but is still usable to a certain extent. However, for the purpose of this research, for nioxime μ PAD stored in a closed petri dish and dark area at $18 \pm 2^\circ\text{C}$ with a relative humidity of $60 \pm 10\%$, the device stability is up to 28 days after device fabrication day.

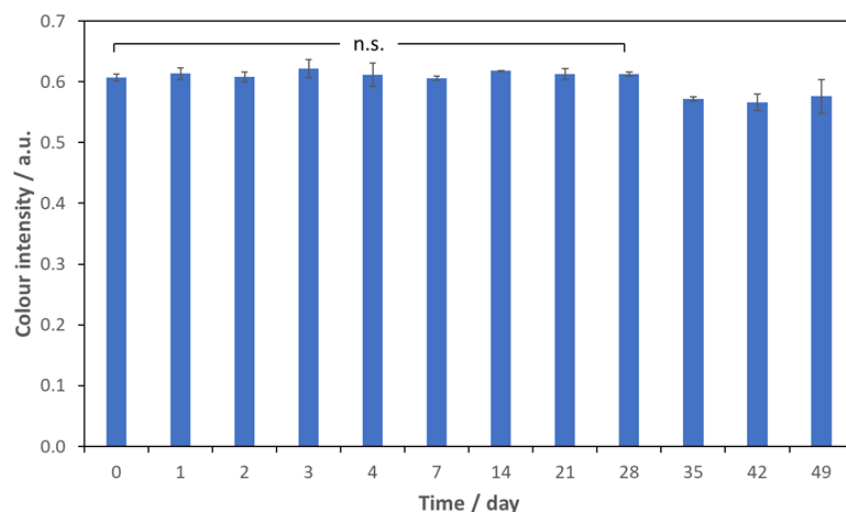


Figure 50 Measured colour intensity of nioxime μ PAD reacted with 10 mL 10 mg L⁻¹ Ni²⁺ after storage in a closed petri dish stored in a dark area at 18 ± 2°C with relative humidity up to 60 ± 10%, showed stability up to 28 days after device fabrication ($p=0.247$, $F_{(4,10)}=1.606$; $n=3$ μ PADs with 5 sample wells each).

Supporting this stability experiment is the data in [Figure 51](#)~~Figure 50~~, where the nioxime μ PAD was tested at a gradient of concentration between 0-10 mg L⁻¹ after pre-determined storage periods, showing results with no significant difference ($p>0.05$) compared to the calibration curve made on the day of fabrication (day-0). This data implies that the device can still reliably produce statistically similar results after 7, 14, 21, and 28 days of storage at room temperature (18 ± 2°C) as if it is used immediately after fabrication. Therefore, showing further the stability of the device was maintained throughout this storage period. This is especially important for the objective of this research, where devices are designed to be used outside laboratory settings. With 28 days of stability, the device shows potential to be used on-site and for distribution to local areas for remote uses.

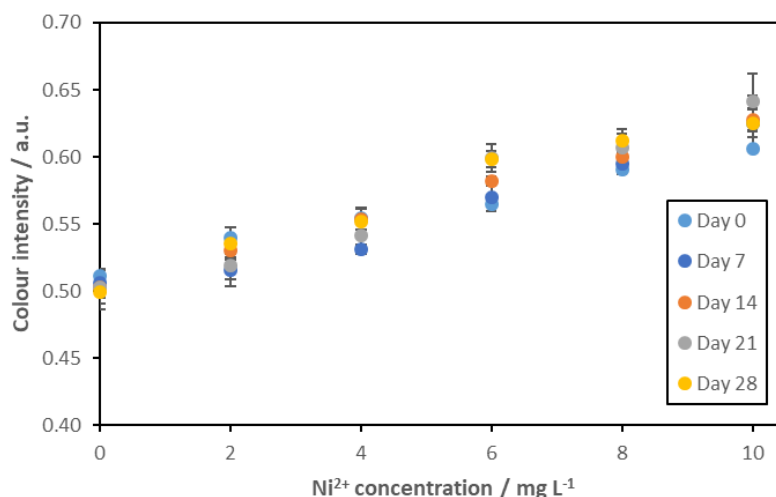


Figure 51 Colour intensity measured of optimised nioxime device dipped into a 10 mL Ni²⁺ solution within 0-10 mg L⁻¹ concentration range on the day of fabrication and 7, 14, 21, and 28 days after storage at room temperature ($n=5$).

2.5 Development of alternative μ PAD for Ni²⁺ detection

2.5.1 XO/PDADMAC as a colorimetric reagent for μ PAD

An alternative reagent was tested for the designed μ PAD: xylenol orange mixture with PDADMAC. This selection of reagent was based on previous research, which shows the potential of the mixture for sensitive detection of Ni²⁺ in an aqueous solution [93]. The optimization process of this device is available in Appendix 1. The device contained a 10 μ L mixture containing 200 mg L⁻¹ XO and 1 wt% PDADMAC in 1:1.

[Figure 52](#) ~~Figure 51~~ shows that a linear correlation can be made between the Ni²⁺ concentration and the colour intensity measured on the developed XO/PDADMAC μ PAD. From this linear regression, the LOD for the device was calculated and resulted in 0.56 mg L⁻¹ LOD. This is a lower detection limit compared to the nioxime μ PAD. The picture attached in the same figure shows the colour gradient observed from 0-1 mg L⁻¹ concentration of Ni²⁺, shifting from yellow to bluish-purple.

However, this coloured complex formed in the sample well of the device was not as even as the ones observed in nioxime μ PAD. In the 1 mg L⁻¹ result, slightly yellow patches can still be seen in the middle section of the well. Uneven colour formation across the sample well can contribute to a high standard deviation of the μ PAD since these uneven patches would appear uncontrollably throughout the well, and the dispersion of the patches would affect the average intensity measured upon measuring the intensity of the well. Due to this problem with the unevenness of the well, the development of the device was halted.

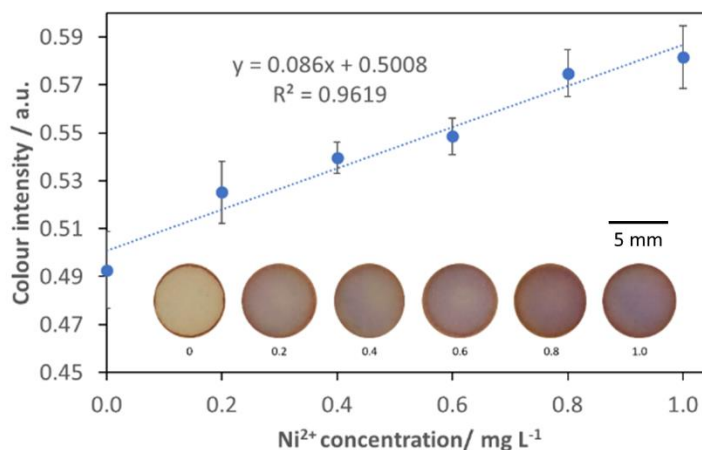


Figure 52 Calibration curve of optimised XO/PDADMAC μ PAD containing 10 μ L mixture of 200 mg L^{-1} XO and 1 wt% PDADMAC, reacted with 10 mL Ni^{2+} solution in 0-1 mg L^{-1} concentration gradient ($n=3$).

2.5.2 Distance-based approach with nioxime dPAD

Another approach to the device was by developing a device which correlates distance measurement to Ni^{2+} concentration. Further discussion on the optimisation and working principles of the device is available in Appendix 1. This device was optimised at 0.01 M PBS buffer, 2 wt% PDADMAC, and 1400 mg L^{-1} nioxime.

The optimised dPAD was then tested in a gradient of Ni^{2+} concentration, by pipetting 40 μ L of sample solution onto the sample well and leaving the sample to wick through the channel. For dPAD, the measurement of the distance was taken as soon as the sample dried up from the device. This usually requires up to 30 min, for the entire wicking process through the 40 mm channel length followed by evaporative drying at room temperature ($18 \pm 2^\circ\text{C}$). The tested Ni^{2+} concentration was between 0 to 2000 mg L^{-1} . However, as shown in [Figure 54](#)[Figure 53a](#), the increase in measured distance is only linear before the 500 mg L^{-1} point. By 100 mg L^{-1} Ni^{2+} , the colorimetric complex was forming almost throughout the entire channel length – which is 40 mm. Increasing the channel length by design, in this case, might help in increasing the detectable range of Ni^{2+} . However, that is beyond the objective of current research. An illustration of the endpoint of the dPAD reaction is shown in [Figure 53](#)[Figure 52](#).

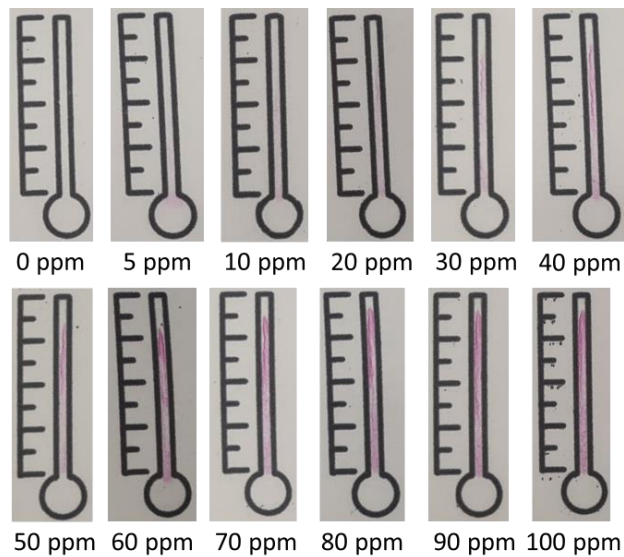


Figure 53 Result as seen on the optimised dPAD 30 min after the addition of a gradient of sample concentration within 0-100 mg L⁻¹ Ni²⁺ range. The magenta length of the magenta line at the endpoint of the reaction was recorded as a measurement.

Figure 54a shows the linearization of the otherwise non-linear correlation between the Ni²⁺ concentration and the measured distance between 0-100 mg L⁻¹. The linearized graph may serve as a calibration curve to predict – taking into account possible inaccuracies due to linearization – the concentration of Ni²⁺ based on distance measurement on the dPAD. The limit of detection of dPAD, calculated (3σ) by only accounting for the linear section of Figure 54a, resulting in 0.3 mg L⁻¹ Ni²⁺ concentration. Compared to the intensity-based device, this limit of detection is 10 times lower, making it a possible alternative design of the paper-based analytical device for citizen science Ni²⁺ detection. Further discussion on the drawbacks of the device is available in Appendix 1.

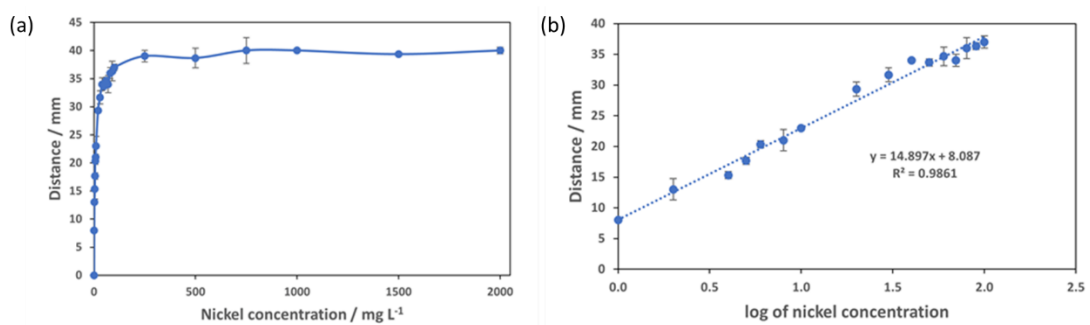


Figure 54 Distance-based Ni²⁺ device calibration curve containing 0.01 M PBS buffer pH 7.4, 2 wt% PDADMAC, and 1400 mg L⁻¹ nioxime at 10 μL each. The Ni²⁺ concentration range tested was between (a) 0-2000 mg L⁻¹ and (b) 0.5-100 mg L⁻¹ (*n*=3 dPADs).

2.6 Conclusions

Paper-based devices for colorimetric Ni^{2+} detection had shown potential in utilising an alternative reagent: 1,2-cyclohexanedione dioxime, also known as nioxime. An optimised 3-layered paper device consisting of 5 sample wells, 1 blank well, and a reference circle had been developed. In this device, each layer serves separate, interconnected functions – where the first layer that comes into contact with the sample acts as the masking layer, followed by additives in the second layer, and detection at the third layer. The masking layer contains 10 μL 0.1 M NaF and 10 μL 0.1 $\text{Na}_2\text{S}_2\text{O}_3$ to react with other metal species, including Cu^{2+} , Fe^{3+} , and Co^{2+} - which would form a colorimetric complex with the reagent. The additive layer contained 10 μL 4 wt% PDADMAC and 10 μL 0.01 M PBS at pH 7.4, which aid in optimising the coloured-complex formation. While the detection layer contained 10 μL 1400 mg L^{-1} nioxime – the reagent that would form magenta coloured complex upon interaction with Ni^{2+} , increasing in intensity with the increase of Ni^{2+} concentration in the sample. This device was able to detect down to 3 mg L^{-1} Ni^{2+} after 4 min of reaction. The device can also be stored before use for 28 days before a significant ($p>0.05$) intensity decline was observed. Despite the stability of the device, the relatively higher concentration range detectable by the developed device means that an additional preconcentration step would be required; ideally, without sacrificing the device's portability and simplicity.

Chapter 3 Development of rapid preconcentration workflow for nickel ion detection in freshwater samples

3.1 Chapter introduction

In previous chapter, a simple and rapid Ni²⁺ detection μ PAD was successfully developed with 3 mg L⁻¹ limit of detection within 4 min reaction time. Despite the advantage in reaction time and relatively low detection limit demonstrated by the device, its detection limit is still far above chronic or acute level of Ni²⁺ allowable in freshwater environment set by various environmental agencies (Chapter 1). In this chapter, therefore, a supplementary method was developed to aid in improving the detection limit of the μ PAD. The aim of this chapter is to discuss the development of a simple and rapid (~10 min) Ni²⁺ preconcentration step using a cafetièrre as a method for onsite preconcentration of Ni²⁺ from environmental water samples. This method was specifically designed to be combined with the nioxime μ PAD for environmental Ni²⁺ detection, as discussed in Chapter 2. In order to achieve this objective, two different materials were tested as preconcentration alternatives: fabricated electrospun nanomat and commercially available ion exchange resins. For each material, Ni²⁺ adsorption was evaluated followed by elution with non-hazardous solution. The emphasis on non-hazardous elution is important to ensure workflow usability by untrained, non-specialist users. The materials would also be incorporated into a cafetièrre system as a preconcentration vessel.

The difference between the two types of materials discussed in this chapter can immediately be drawn by looking at their commercial availability. Electrospun nanomats are a novel membrane-production technology; taking advantage of polymer solubility in volatile solvents and high applied voltage to produce the thin, fibrous strands which can provide a high specific surface area for sorption of aqueous metals, as discussed in Chapter 1. For Ni²⁺ entrapment purposes, chitosan – a naturally available polymer derived from chitin – had been studied with the electrospinning method for membrane production [142-144]. However, previous studies indicate difficulty in using pure chitosan for the process. This is often attributed to the low mechanical stability and low solubility of the polymer [109], as well as pH sensitivity and susceptibility to swelling [145]. Therefore, the addition of other polymers was suggested and had been tested to enhance the properties of chitosan, making it easier to process with the electrospinning setup [146, 147].

Following the observation on the performance of electrospun nanomat in both Ni²⁺ adsorption and elution – the two steps involved in preconcentration in this research – studies on the use of commercially available ion exchange resins were conducted. The main reasoning for this approach is to benchmark the electrospun nanomats against well-established commercial media

that could be used for preconcentration or separation of Ni²⁺ from a water matrix [148, 149]. Its commercial availability would also provide the possibility of a more cost-effective approach, compared to the extensive work required to produce the electrospun nanomat.

This chapter is therefore divided into three sections, which reflect the development of the workflow chronologically. It starts with section 3.3, evaluating the development of electrospun nanomat, subsequently followed by its performance in preconcentration workflow development. Followed by section 3.4, where commercially available ion exchange resins (IE resins) were observed as an alternative to the electrospun nanofiber in this process. Lastly, section 3.5, summarised the developed workflow using IE resins in a cafetière setting, integrated into the developed μ PADs.

3.2 Materials and Methods

This section started with a list of materials used in this study, as well as the supplier for each of the materials, and continued with the solution preparation for each solution used in this study. It was then followed with a general description of the methods used throughout the study related to the development of rapid Ni²⁺ preconcentration workflow.

3.2.1 Chemicals

The chemicals used in this research for the development of rapid Ni²⁺ preconcentration workflow are listed in Table 15.

Table 15 List of chemicals used in this study for Ni²⁺ preconcentration experiments.

Description	Supplier
Diaion [®] HP-20 (effective size 0.34 mm)	Sigma Aldrich
Lewatit [®] MonoPlus SP-112 Na ⁺ form	Sigma Aldrich
Lewatit [®] TP 207	Sigma Aldrich
Ambersep [®] M4195 chelating anion resin	Sigma Aldrich
Methanol, USP Reference Standard	Sigma Aldrich
Polycaprolactone, M _n = 80,000	Sigma Aldrich
Poly(ethylene oxide), M _w =900,000	Sigma Aldrich
Chitosan, medium molecular weight, M _w =190,000-310,000 Da	Sigma Aldrich
Acetic acid glacial, 95%	VWR Scientific
Hydrochloric acid 37%	Honeywell Fluka
Sodium hydroxide, 10.0 N in aqueous solution	VWR Scientific

Sodium chloride, ReagentPlus® ≥99%	Sigma Aldrich
Ethylenediaminetetraacetic acid disodium salt dihydrate, ≥97%	Sigma Aldrich
Ammonium hydroxide ~14.8 M	Sigma Aldrich
Nickel (II) chloride hexahydrate, 99.9% trace metal basis	Sigma Aldrich
Iron (II) chloride tetrahydrate, ReagentPlus®, 98%	Acros Organics
Potassium chloride, ACS reagent, 99.0-100.5%	Sigma Aldrich
Sodium phosphate dibasic, ACS reagent, ≥99.0%	Sigma Aldrich
Potassium nitrate, ACS reagent, ≥99.0%	Fisher Scientific
Iron (III) chloride hexahydrate, ACS reagent, 97%	Sigma Aldrich
Cobalt (II) chloride hexahydrate, ACS reagent, 98%	Sigma Aldrich
Copper (II) sulphate pentahydrate, ACS reagent, ≥98%	Sigma Aldrich
Calcium sulphate dihydrate, ReagentPlus®, ≥99%	Sigma Aldrich
Sodium bicarbonate, ACS reagent, ≥99.7%	Sigma Aldrich
Zinc (II) sulphate heptahydrate, ACS reagent, 99%	Sigma Aldrich

3.2.2 Solution preparation

The solution preparation methods for each solution used in this study are described in this section.

3.2.2.1 Preparation of 20 wt% PCL solution

2000 mg polycaprolactone (PCL) ($M_w = 14,000 \text{ g mol}^{-1}$) was weighed and made up to 10 g with glacial acetic acid ($M_w = 60.05 \text{ g mol}^{-1}$). The solution was then stirred in an enclosed vessel with a magnetic stirrer on top of a heating plate at 40 °C for 24 h. By the end of the mixing process, the 20 wt% PCL solution would be clear and colourless, without any pieces of pellets visible.

3.2.2.2 Preparation of dilute acetic acid solution

90 g of glacial acetic acid was weighed ($M_w = 60.05 \text{ g mol}^{-1}$) and made up to 100 g solution with Milli-Q water. The solution was labelled as 9 :1 AA/Water solution and stored after thorough mixing.

3.2.2.3 Preparation of 3 wt% chitosan solution

0.3 g chitosan, medium molecular weight ($M_w = 190\text{-}310 \text{ kDa}$), the powder was weighed and made up to 10 g of solution with dilute acetic acid. The solution was then stirred in an enclosed vessel on top of a heating plate at 30 °C for 24 h. By the end of the mixing process, the 3 wt% chitosan solution would be clear with a yellow tint, without any clumps of chitosan powder.

3.2.2.4 Preparation of chitosan/PEO mixture

2.5 g of polyethylene oxide (PEO) powder ($M_w = 900,000 \text{ g mol}^{-1}$) was weighed and mixed into the prepared 10 g chitosan solution. The solution was then continued to be stirred on top of 30 °C for a further 24 h. By the end of the mixing process, the solution would be clear with a yellow tint and labelled with a 4 :1 chitosan/PEO mixture.

3.2.2.5 Preparation of Ni²⁺ stock solution

4.0 mg of Nickel (II) chloride hexahydrate ($M_w = 237.69 \text{ g mol}^{-1}$) was weighed and made up to volume within a 100 mL volumetric flask with Milli-Q water. This was mixed thoroughly to yield a colourless and clear solution, with $10 \text{ mg L}^{-1} \text{ Ni}^{2+}$ concentration. Operations involving this solution were carried out in the fume hood.

3.2.2.6 Preparation of 3 M HCl solution

25 mL of concentrated hydrochloric acid (HCl) ($M_w = 36.46 \text{ g mol}^{-1}$) was pipetted and made up into a 100 mL solution with Milli-Q water. The solution was prepared under the fume hood. The solution was mixed thoroughly and would produce a colourless and clear 3 M HCl solution by the end of the mixing process.

3.2.2.7 Preparation of 3 M NaOH solution

15.8 mL of concentrated sodium hydroxide (NaOH) ($M_w = 40.0 \text{ g mol}^{-1}$) was pipetted and made up to 100 mL solution with Milli-Q water. The solution was prepared under the fume hood. The solution was mixed thoroughly and would produce a colourless and clear 3 M NaOH solution by the end of the mixing process.

3.2.2.8 Preparation of 5 M NaCl solution

29.2 g of sodium chloride (NaCl) powder ($M_w = 58.44 \text{ g mol}^{-1}$) was weighed and made up to 100 mL solution with Milli-Q water. The mixture was placed in an enclosed vessel on top of a heating plate at 80 °C, and stirred for 3 h, if necessary. By the end of the mixing process, all NaCl powder would dilute completely and produce a clear and colourless 5 M NaCl solution.

3.2.2.9 Preparation of 0.5 M EDTA pH 8 solution

18.6 g ethylenediaminetetraacetic acid disodium salt dihydrate powder ($M_w = 372.24 \text{ g mol}^{-1}$) was weighed and made up to 100 mL solution with Milli-Q water. The solution was mixed thoroughly and the pH of the 0.5 M EDTA solution was adjusted through the addition of NaOH, if necessary.

3.2.2.10 Preparation of 3 M ammonium hydroxide solution

20.3 mL concentrated ammonium hydroxide solution ($M_w = 35.04 \text{ g mol}^{-1}$) was pipetted and made up to 100 mL solution with Milli-Q water. The 3 M ammonium hydroxide solution was mixed thoroughly.

3.2.3 PCL/chitosan/PEO electrospun nanomat for Ni^{2+} adsorption

The PCL/chitosan/PEO electrospinning optimisation and adsorption characterisation methods are available in Appendix 2. The following sections focused on the Ni^{2+} adsorption and elution performance of the electrospun nanomat

3.2.3.1 Effect of initial Ni^{2+} concentration on Ni^{2+} adsorption with nanomat

The spun nanomat was weighed to 0.002 g and placed in 50 mL Ni^{2+} solution with adjusted Ni^{2+} concentration within 0.2-0.8 mg L^{-1} , and mixed with a magnetic stirrer at 100 rpm for 20 min. The experiment was done at room temperature, which was approximately $20 \pm 2 \text{ }^\circ\text{C}$. The solution was sampled at the beginning of the experiment (initial) and at minutes 1, 2, 3, 4, 5, 10, 15, and 20. The Ni^{2+} concentration in the sampled solution was measured by UV/Vis spectrophotometry with nioxime as a colorimetric reagent. The experiment was repeated three times for each pH condition.

3.2.3.2 Effect of pH on Ni^{2+} adsorption with nanomat

The spun nanomat was weighed to 0.002 g and placed in 50 mL Ni^{2+} solution with adjusted pH, and mixed with a magnetic stirrer at 100 rpm for 20 min. The experiment was done at room temperature, which was approximately $20 \pm 2 \text{ }^\circ\text{C}$. The solution was sampled at the beginning of the experiment (initial) and at minutes 1, 2, 3, 4, 5, 10, 15, and 20. The Ni^{2+} concentration in the sampled solution was measured by UV/Vis spectrophotometry with nioxime as a colorimetric reagent. The experiment was repeated three times for each pH condition.

3.2.3.3 Ni^{2+} elution from nanomat

Elution from the nanomat was observed by placing the Ni^{2+} -loaded nanomat from the adsorption process into a 25 mL solution of chosen eluent : 3 M HCl, 3 M NaOH, 50% glacial acetic acid, 3 M NaCl, or 0.5 M EDTA. The nanomat was shaken in the solution for 5 min, with sampling immediately, at minute-1, 2, 3, 4, and 5. The concentration of the sampled solution was then measured with UV/Vis spectrophotometry with 400 mg L^{-1} nioxime at 530 nm. The mass percentage of eluted Ni^{2+} was then calculated with the following formula (Eq 5):

$$\%m = \frac{C_{eluted} \times V_{eluted}}{m_{adsorbed}} \quad \text{Eq 5}$$

3.2.4 Ion exchange resins for Ni²⁺ adsorption and preconcentration

Preliminary observation and adsorption characterisation of the different ion exchange resins used in this research is available in Appendix 2. The sections below focused on the utilisation of the ion exchange resins in cafetiere for Ni²⁺ adsorption.

3.2.4.1 Cafetiere for Ni²⁺ adsorption

The cafetière used in this experiment was Nerthus FIH 319 cafetière with 350 mL capacity. This cafetière came with assembled filter system consisting of a patterned plate and metal mesh for coffee filtration. However, in this research, this pre-assembled system was modified. In place of the filter, a circular PMMA basket made through CNC milling and laser cutting was placed. This basket consisted of two circular \varnothing 63 mm PMMA discs, patterned with more than 1000 100 μ m holes across its surface and \varnothing 5 mm centre hole for the metal rod. One of the two PMMA discs was attached with a \varnothing 63 mm PMMA ring with 1 mm thickness to create depth for the basket. The assembly of the basket require placing a metal nut on the metal rod of the cafetière, and a detachable metal nut to secure the basket on the metal rod of the cafetière.

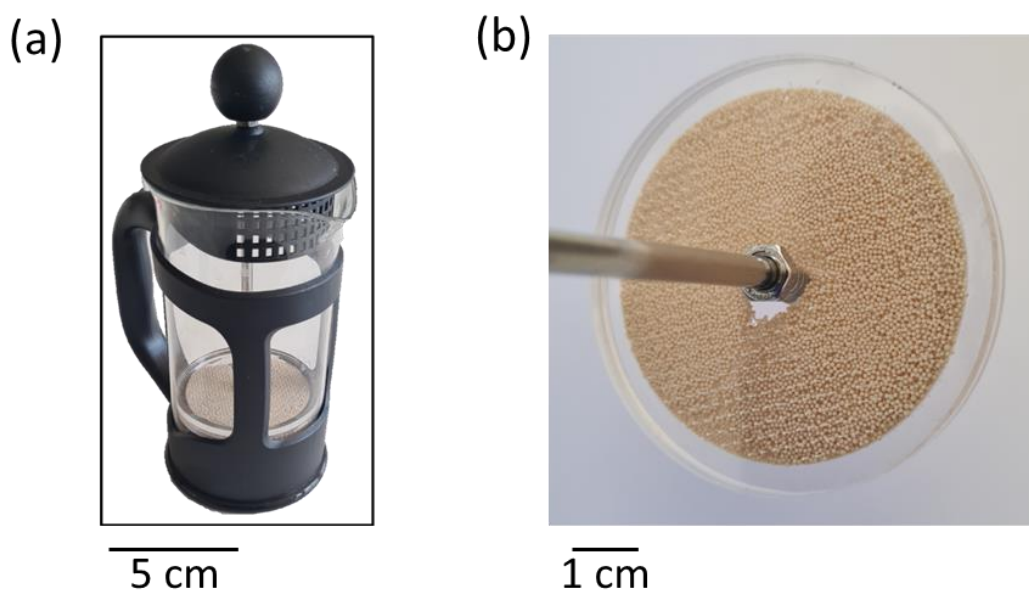


Figure 55 (a) Modified cafetière, a basket filled with 2.6 g Lewatit SP; (b) Closer view of the modified basket was filled with 2.6 g Lewatit SP resins.

3.2.4.2 Effect of dipping speed on Ni²⁺ adsorption in cafetiere

The effect of dipping speed was observed by plunging 2.6 g Lewatit SP resin in a modified cafetière basket into a 300 mL 3 mg L⁻¹ Ni²⁺ solution. Within the 5 minutes of plunging, the solution was sampled before the experiment and every minute to test Ni²⁺ concentration by UV/Vis spectroscopy with 400 mg L⁻¹ nioxime as a colorimetric reagent. The dipping speed varied from no plunging at all, 1 plunge every 30 seconds, 1 plunge every 5 seconds, and 1 plunge every

2 seconds. A plunge, in this experiment, is defined as one upward motion of the basket followed by 1 downward motion (1 cycle). The variation in plunging speed was based on certain intervals, which would be easy to monitor by target users. The variation spans between no plunging at all, 2 plunges in a minute, 12 plunges in a minute, and 30 plunges in a minute.

3.2.4.3 Effect of resin placement on Ni²⁺ adsorption in cafetiere

The effect of resin containment in the modified basket was observed using 300 mL 3 mg L⁻¹ Ni²⁺ solution in cafetière as a sample solution, and 2.6 g of Lewatit SP resin. In one set of experiments, the resin was placed inside the modified basket as in most experiments in this cafetière system in this research. In the other set of experiments, the resin was instead poured directly into the cafetière without placing it in the modified basket. In both cases, the plunging motion was still performed for 5 min and the solution was sampled before contact with resin, and minutes 1, 2, 3, 4, and 5 after plunging started.

3.2.4.4 Effect of resin mass on Ni²⁺ adsorption in cafetiere

The cafetière, with a basket filled with different amounts of resin (see Table 16), was plunged constantly for 20 min, and sampled for Ni²⁺ concentration measurement before the process, and at minutes 1, 2, 3, 4, 5, 10, 15, and 20 of the plunging. This mimicked the observational data at the resin characterisation step, which was done in a stirred vessel at 100 rpm. The measurement of Ni²⁺ concentration in this experiment was done by UV/Vis spectroscopy, using 400 mg L⁻¹ nioxime as a colorimetric reagent. 1000 µL sample was reacted with 100 µL of the colorimetric reagent and incubated for 20 min before measurement of absorbance at 530 nm. The concentration of Ni²⁺ was then calculated with a calibration curve, available in Appendix 2.

Table 16 Mass variations of resins tested in observation on the effect of resin mass on Ni²⁺ adsorption in cafetiere

	Mass variation #1 / g	Mass variation #2 / g
Lewatit SP	1.8	2.6
Lewatit TP	0.6	1.1
Ambersep	1.2	1.7

3.2.4.5 Effect of initial Ni²⁺ concentration on Ni²⁺ adsorption in cafetiere

In this experiment, 300 mL Ni²⁺ solution with various Ni²⁺ concentrations within 0.2-0.8 mg L⁻¹ was used as the sample. Resins were then placed in the modified basket and plunged repeatedly for 5 min. At the beginning of the experiment and every 1 minute, the solution was sampled for Ni²⁺ concentration measurement, where 1000 µL Ni²⁺ sample was reacted with 100 µL 400 mg

L⁻¹ nioxime and incubated for 20 minutes. After incubation, the absorbance of the mixture was measured at 530 nm in a UV/Vis spectrophotometer.

3.2.4.6 Ni²⁺ elution evaluation/screening

The elution solution tested for this study was: HCl, NaOH, and NaCl. Each of the elution solutions was prepared at the concentration range of 3-5 M in 1 M increments. The 3 M solution would further be referred to as low concentration, 4 M solution as mid concentration, and 5 M as high concentration. The experiment started with loading the resins with Ni²⁺ through 5 min plunging in 300 mL 3 mg L⁻¹ Ni²⁺ solution. The resins – still in the basket – were then dipped and swirled in 30 mL elution solution with varying concentrations and types. The amount of eluted Ni²⁺ was calculated by comparing the amount of Ni²⁺ in the elution solution after 5 min swirling to the amount of Ni²⁺ adsorbed by the resins. Further, the elution process with NaCl was observed through 5 elution cycles. One cycle is defined in this research as the addition of 10 mL fresh elution solution shaken for 1 min, followed by the removal of the elution solution.

3.2.4.7 Effect of elution volume

In this experiment, two different elution volume was observed, which were 5 and 10 mL. This was observed by pouring the Ni²⁺-loaded resins into a centrifuge containing the elution solution and shaking it for 1 min. The amount of expected elution was calculated based on the mass of Ni²⁺ in the resin and the amount of eluted Ni²⁺ was calculated by measuring the concentration of Ni²⁺ at the endpoint of the elution using UV/Vis spectroscopy with nioxime as a colorimetric reagent. The experiment was repeated three times.

3.2.4.8 Effect of elution mixing time

The effect of elution mixing time was observed by mixing Ni²⁺-loaded Lewatit SP resin in a 10 mL 5 M NaCl in a centrifuge tube for 1, 3, or 5 minutes. The solution was then sampled at the end of the mixing period, and the concentration of Ni²⁺ in the solution was measured by UV/Vis spectrophotometry. Each data point was repeated three times.

3.2.4.9 Effect of NaCl concentration

The effect of NaCl concentration was also observed within the range of 3-5 M for elution with 10 mL eluent within 5 min mixing time. The observation was done by placing the 2.6 g Ni²⁺-loaded Lewatit SP resin in 10 mL of NaCl solution with respective concentrations. The mixture was then shaken for 5 min before being measured with UV/Vis spectrophotometry with nioxime as a colorimetric reagent. The amount of Ni²⁺ extracted from the resin was calculated in comparison to the amount of Ni²⁺ trapped in the resin.

3.2.4.10 Effect of other metal ions on Ni²⁺ adsorption and elution

Adsorption of Ni²⁺ in the presence of other metal ions in this experiment was observed by placing 2.6 g Lewatit SP resin in a modified basket into a 300 mL mixed-ion solution. The mixed-ion solution was made by the addition of 0.1 mg L⁻¹ of each of the following ions: Ca²⁺, Mn²⁺, Fe²⁺, Co²⁺, Cu²⁺, Ni²⁺, and Zn²⁺. The adsorption step was done by plunging for 5 min in the cafetière followed by elution with 10 mL 5 M NaCl through shaking in a centrifuge tube for 1 min. Samples were taken of the 300 mL solution post-adsorption and of the elution solution after 1 min of mixing. The concentration of the ions in the samples was measured with Thermo Scientific iCAP Qc ICP-MS.

3.2.5 Statistical analysis

Methods of statistical analysis employed within this chapter follows the previously described method in section 2.2.5.

3.3 Results - PCL/chitosan/PEO electrospun nanomats

3.3.1.1 Effect of pH on Ni²⁺ adsorption by PCL/chitosan/PEO composite

The nickel adsorption performance of PCL/chitosan/PEO nanomat after crosslinking with glutaraldehyde for 24 hours was observed [150, 151]. The observation started with varying the initial pH of the Ni²⁺ solution within the 5-8 pH range. This pH range was chosen to cover the commonly occurring pH range in a river water sample in the UK [28]. The method for this experiment is described in section 3.2.3.2 [Effect of pH on Ni²⁺ adsorption with nanomat](#)~~Effect of pH on Ni²⁺ adsorption with nanomat.~~

Error! Reference source not found. Figure 55 shows the Ni²⁺ adsorption performance of the spun nanomat at the tested pH range, within the first 20 min of 100 rpm mixing with a magnetic stirrer. In all tested pH values, the adsorption performance was particularly unstable in the first five minutes. On average, the Ni²⁺ adsorption is more effective at a higher pH range than 5, with 6 showing the highest amount of Ni²⁺ adsorbed compared to the initial Ni²⁺ concentration. By minute 20, the adsorption of Ni²⁺ was shown to be more effective at pH of 6, before decreasing at pH 7 and 8.

Previous studies show different optimum pH conditions for effective chitosan-metal chelating reactions. One study would argue that a higher pH value or increase in alkalinity is more favourable due to less competition between the metal ions and protons available in the solution [152]. Conversely, other studies would show an increase in the adsorption of metal up to a certain point, followed by either stability or a decrease after the optimum point [153, 154]. The result of this experiment for the electrospun nanomat is closely resembling the latter. Where

the adsorption of Ni^{2+} generally increases with the increase of pH value up to a certain point, in this case, pH of 6.

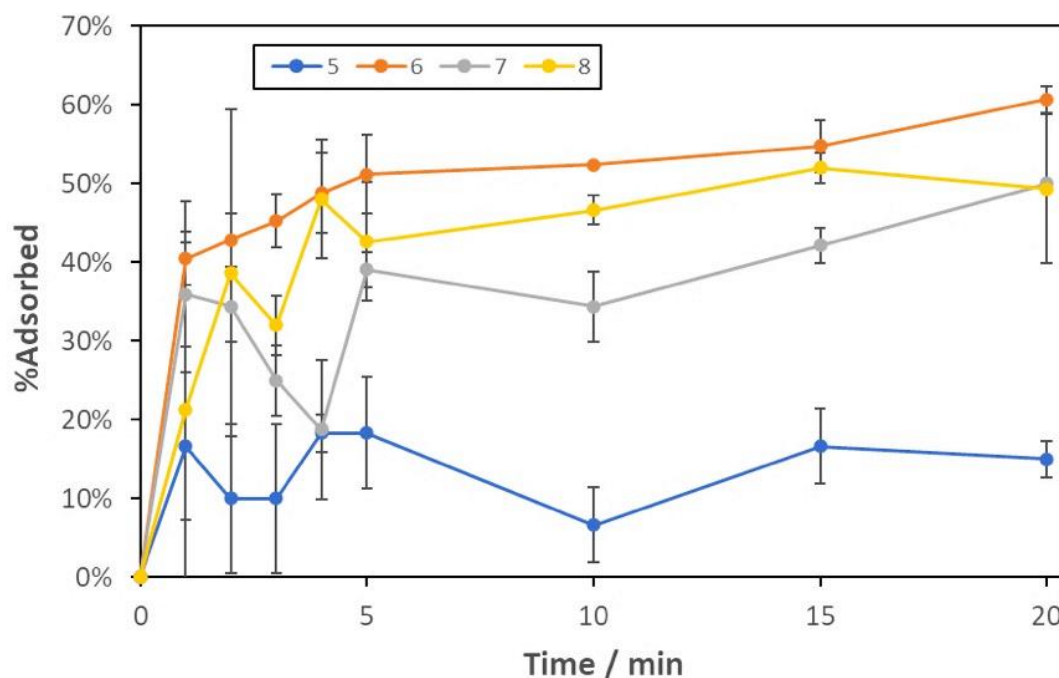


Figure 56 Performance of electrospun nanomat in the pH range of 5-8 after dipping into 300 mL 3 mg L⁻¹ nickel ion solution for 20 minutes. Error bars illustrate the standard deviation between the result of the three repeats (n=3).

3.3.2 Nickel elution properties by electrospun PCL/chitosan/PEO nanomat

3.3.2.1 Elution strategies

Unlike in most previous studies, in this research, Ni^{2+} recovery from the nanomat, with a low volume of eluent is an important aspect. Additionally, the elution process ideally should not involve hazardous substances and require short elution time given the potential for citizen scientists to operate the workflow. In membrane operation settings, running a solution to remove the trapped ions is referred to as membrane regeneration. However, optimisation of a regeneration process often focuses on the reusability of the membrane and therefore the trapped ions are not necessarily obtained in a more concentrated state. Up to the point of this writing, no prior studies had observed the use of electrospun nanomat for the preconcentration of heavy metal.

Eluents used for detaching the trapped ions from an adsorbent can either (1) have a higher affinity to the trapped ions than the adsorption site or (2) have a higher affinity to the adsorption site than the trapped ions. This mechanism usually also correlates to the pH of the elution

solution (eluent). Therefore, in preliminary tests, the elution of trapped Ni^{2+} from nanomat was observed with solutions in various pH values – acidic, neutral, or alkaline. In this research, three different acidic solutions were tested for Ni^{2+} elution: 3 M hydrochloric acid (HCl), 3 M nitric acid (HNO_3), and 50% glacial acetic acid (GAA), all within $\text{pH} \leq 2$. Additionally, 3 M NaCl was also tested as a neutral eluent (pH 7) and 0.5 M EDTA (pH 8). The choice of acids was based on previous literature. Both concentrated HCl and HNO_3 had previously been used in preconcentration studies involving divalent metal ions elution with or without chitosan as chelating agents [155-157]. Whereas the use of diluted glacial acetic acid was to dissolve the chitosan nanofibers [158]. Further, in the use of chitosan as a metal adsorption agent, adsorption is usually favoured in more alkaline environments due to possible competition with H^+ in acids [159]. Whereas the choice of using NaCl and EDTA was based on its possible complexation reaction with Ni^{2+} , therefore detaching the complexed Ni^{2+} from the Ni^{2+} -chitosan chelate complex [160, 161].

3.3.2.2 Ni^{2+} elution screening with various eluents

Error! Reference source not found. Figure 56 shows the result of preliminary observation on Ni^{2+} elution from electrospun nanomat with various eluents. Of the five tested eluents, NaCl was the one not showing any measurable Ni^{2+} recovery after 5 minutes of submersion in 25 mL of the eluent solution in the Petri dish. Whereas the amount of Ni^{2+} eluted in the same condition increases from 0.23% for 3 M HNO_3 , 1% for 0.5 M EDTA, 2.26% for 3 M HCl, and 26% for 50% GAA. Increasing the concentration of HCl, HNO_3 , and GAA might aid in increasing the elution effectiveness of the system, however, especially for HCl and HNO_3 , this would incur a higher risk for the operator. While GAA is relatively not hazardous compared to the other two acids tested, it is still a corrosive, flammable substance, capable of causing severe health problems upon unmitigated exposure. EDTA, while being the safer option in the list, would not be suitable for subsequent colorimetric measurement of the preconcentrated Ni^{2+} with μPADs , since it forms a strong metal-ligand complex with the Ni^{2+} ions. Therefore, the most suitable option would be 5 min submersion in 25 mL 50% GAA for up to 26% Ni^{2+} elution from the electrospun nanomat.

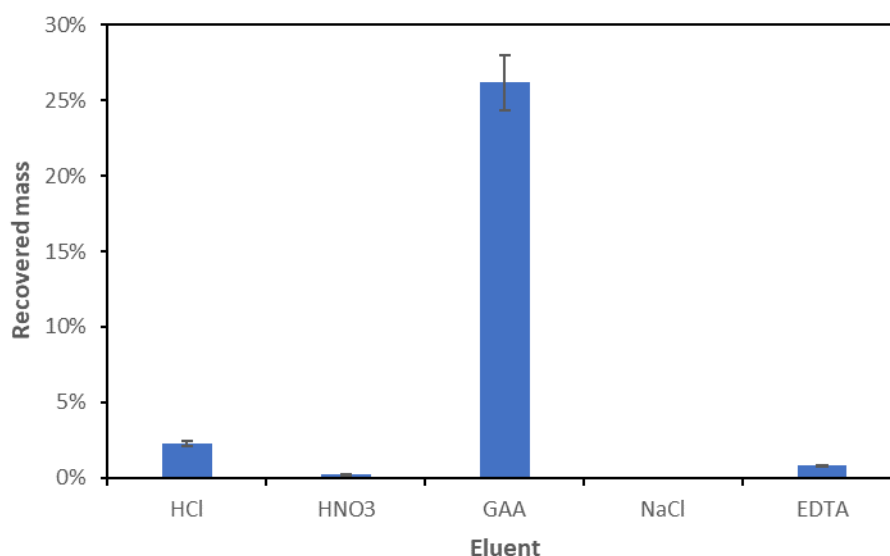


Figure 57 Preliminary test of Ni²⁺ elution from the electrospun PCL/chitosan/PEO nanomat by 5 min submersion into 25 mL solution of the following eluent solution: 3 M HCl, 3 M HNO₃, 50% GAA, 3 M NaCl, or 0.5 M EDTA. Error bars illustrate the standard deviation between the result of the three repeats (n=3).

3.3.3 Challenges with electrospun nanomat for Ni²⁺ preconcentration

Despite the demonstrated potential of electrospun nanomat for Ni²⁺ preconcentration, there are several problems attributed to the various steps involved in the process. These challenges restrict the scope for using the electrospun nanomats in a citizen science freshwater monitoring application. However, the demonstrated potential might still be useful in other contexts. The problems associated with electrospun nanomat developed in this research started with the nanomat fabrication step itself, namely: uncontrollable variables, time, and repeatability. Due to problems in the fabrication step, the adsorption of Ni²⁺ out of the sample solution would subsequently be affected, as well as the elution step.

One of the biggest challenges in the electrospinning step in this research is the effect of uncontrollable variables. The electrospinning setup used in this research was not equipped with a temperature and humidity controller. While some studies might oversee the effect of these uncontrollable parameters, it is clear in this experiment that these variables affect the electrospinning process, especially humidity [162]. Adding to this problem is the observation of increasing humidity in longer electrospinning duration due to evaporative build-up of the solvent. Since the setup was encased in a plastic box without a vent, this build-up would affect the humidity of the process, creating a non-steady state process condition. In other studies, the

effect of humidity had been correlated with fibre breakages, depending on the polymer hydrophobicity and solvent properties [163].

It is important to note that the problem with humidity in this electrospinning process was not whether it is too high or too low, but rather the uncontrollability of it. According to the varied results of previous studies, it seems possible to optimise a process for low or high relative humidity, or to a certain humidity range [164]. However, fluctuating humidity is a problem since it affects the optimum parameters of the process. As a rule of thumb, the electrospinning setup used in this research has its best performance at a relative humidity below 30%. In order to counteract the problem with humidity in this research, a dehumidifier was introduced to the laboratory area to maintain the desired value. However, even with this aid, it can be hard to achieve the required low humidity since it would depend on the laboratory heating and ventilation system, as well as activities in the area on the day. In winter months, which is when most of the optimisation process for the electrospinning was done in this research, the relative humidity of the electrospinning setup area can reach below 10%. However, in warmer seasons, the humidity can reach up to 60%, changing the performance of the previously optimised process.

Due to these uncontrolled variables, time and repeatability of the process became a challenge. The fabrication process itself, without the additional challenge, already requires 4 days. The first day would be PCL electrospinning followed by a 24 h drying process, the second day was chitosan/PEO electrospinning followed by 24 h drying. The third day was 24 h crosslinking with GA, and the fourth day is washing the crosslinked nanomat followed by 24 h drying. Therefore, the electrospun mat would be ready to use by day-5. This can be considered time-consuming, especially if the humidity of the electrospinning setup increases after some time, limiting the amount of electrospinning that can be achieved during the day. Additionally, since humidity might have an effect on the electrospinning process, it is also hard to determine how repeatable the process is. Low repeatability of the electrospinning process may result in a high variation of nanomat properties and morphology. Subsequently, this would affect the Ni²⁺ adsorption process of the nanomat.

Considering the explained factors, there were no further studies on the use of electrospun nanomat for Ni²⁺ adsorption in this research. However, it is still important to note that the produced nanomat has shown potential for high Ni²⁺ adsorption capacity. The preliminary study on the elution step also show potential for nanomat regeneration, although this was limited. Therefore, this electrospun nanomat may be able to be used as an alternative for Ni²⁺ adsorption membrane in other contexts and settings.

3.4 Results – preconcentration with ion exchange resins

Further experiments for preconcentration in this research focused on the utilisation of commercially available ion exchange resins. Ion exchange resins had previously been studied for inline preconcentration steps for various analytical methods such as flame atomic absorption spectrometry (FAAS) [124] and atomic emission spectrometry (AES) [123]. Further, some ion exchange resins had also been studied quite extensively for Ni²⁺ adsorption, making it an interesting option for this research [114, 117, 118, 165, 166]. Extensive discussion on ion exchange resin in metal adsorption and preconcentration is seen in Chapter 1.

However, in this research, the preconcentration process is to be conducted in a cafetière system. This is mainly to ensure accessibility upon usage by citizen scientists – which is the target user in this research, as discussed in Chapter 1. Therefore, the challenge in incorporating ion exchange resins into a cafetière system, as proposed in this research is: (1) to modify the cafetière part, as well as (2) to observe its adsorption properties in a much shorter duration with the modified cafetière system.

In experiments involving electrospun nanomat as an adsorbent, the cafetière plunger is shown in [Error! Reference source not found. Figure 57](#). At the end of the plunger, where the nanomat is placed, are two poly(methyl methacrylate) (PMMA) discs with 12 holes. The discs were 63 mm in diameter with 12 circular ø10 mm holes spread across the area of the circle. For electrospun nanomat, this type of adsorbent housing is sufficient. It provides several inlets for the sample solution to come into contact with the nanomat, is relatively simple to fabricate, and is mechanically strong. However, this type of housing would not be suitable for commercial ion exchange resins. Therefore, in this research, a modified resin container was designed – further referred to as a basket.



Figure 58 Cafetière setup for Ni²⁺ adsorption from water sample with electrospun PCL/chitosan/PEO nanomat.

The basket for ion exchange resins was fabricated through laser cutting and CNC milling of PMMA discs, following the design illustrated in [Figure 59](#)[Figure 58a](#). It is constructed by placing a 1 mm ϕ 63 mm circular ring on top of a PMMA disc. The base PMMA disc was patterned with more than 500 hundred ϕ 0.1 mm holes. This hole diameter would allow the containment of the smallest resin to be tested in this research, which is Diaion[®] HP with the smallest particle size of 250 μ m. The disc diameter in this design would leave \pm 1 mm space between the disc and cafetière wall upon dipping, since the cafetière used had a diameter of 65 mm.

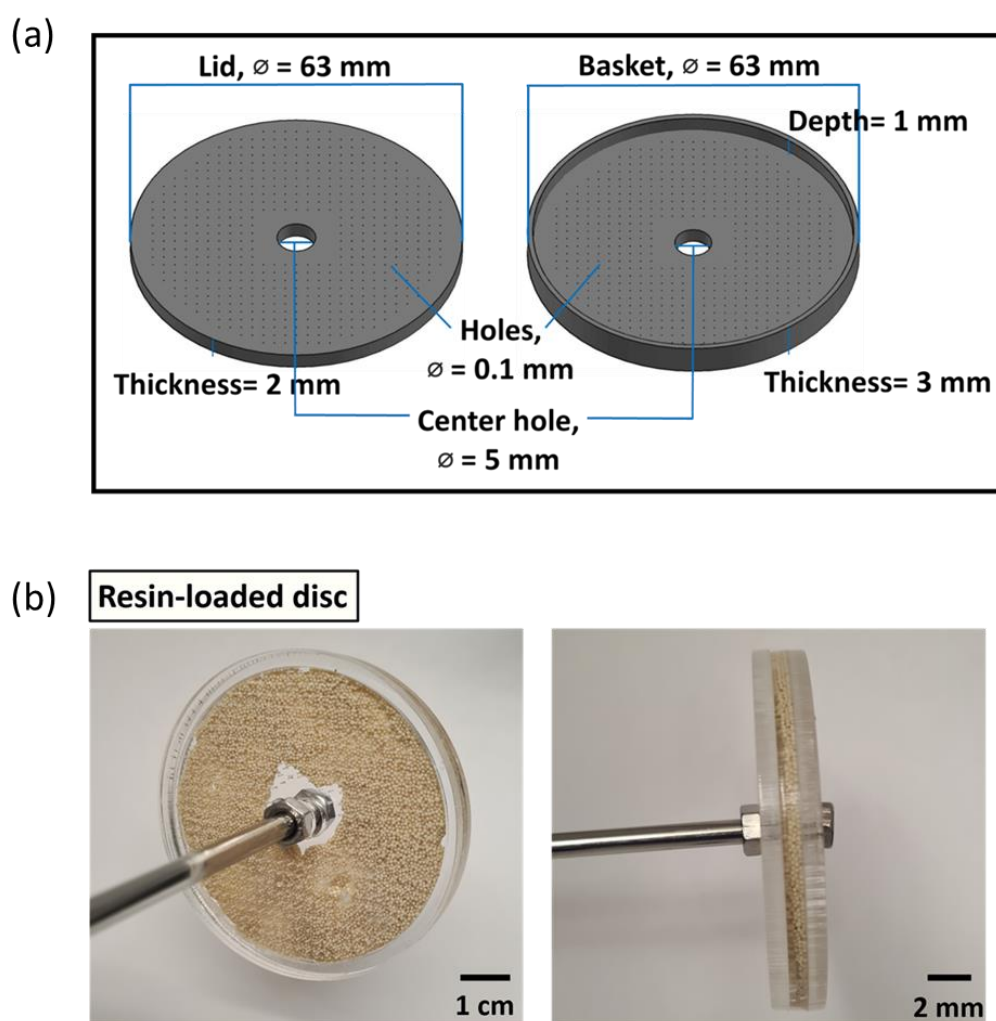


Figure 59 (a) Design of modified PMMA basket for ion exchange resin housing in the cafetière, (b) basket loaded with Lewatit® MonoPlus SP 112 resin.

3.4.1 Nickel adsorption properties of ion exchange resins in cafetière system

Given the simpler and more repeatable performance of ion exchange resins, further observations were made using the material for the onsite preconcentration step using the cafetière system. In this section, the Ni^{2+} adsorption properties of the ion exchange resins were observed by placing them into the modified cafetière system. Effect of dipping speed on Ni^{2+} adsorption in cafetière system

3.4.1.1 Effect of dipping speed on Ni^{2+} adsorption in cafetiére

Before further optimisation, the effect of dipping speed was observed with the method described in section 3.2.4.2 [Effect of dipping speed on \$\text{Ni}^{2+}\$ adsorption in cafetiére](#)~~Effect of dipping speed on Ni^{2+} adsorption in cafetiére~~. The volume of 300 mL was chosen based on the maximum working capacity of the cafetière. The cafetière itself can contain up to 350 mL of

solution as storage, however, upon plunging, this volume would produce the risk of spilling. In cafetière-based adsorption, a bigger volume would theoretically lead to a higher amount of Ni^{2+} adsorbed from the solution. However, spillage, which can be uncontrollable would introduce a random effect, possibly leading to a non-repeatable process. Therefore, the maximum working volume of 300 mL was chosen for cafetière-based processes in this research, unless stated otherwise. Whereas the Ni^{2+} concentration of 3 mg L^{-1} was chosen as the target concentration to be preconcentrated based on the calculated detection limit of the nioxime μPAD , which this preconcentration process was designed to be integrated with. The mass of Lewatit SP resin tested in this study was the maximum amount of Lewatit SP resin that can be contained in the modified basket.

The observation of the effect of plunging speed on the adsorption of Ni^{2+} is important since the design of the system depends on the turbulence of the sample solution to create as much contact opportunity between the target analyte and the adsorption site. It is hypothesized that faster plunging, which would create more turbulence of the water passing through the holes in the basket, would correspond to better adsorption performance. Whereas without plunging – consequently less movement of the solution – the adsorption performance will significantly decline due to lack of contact incidence between the target analyte and the adsorption site. Furthermore, since the method is developed for citizen scientists, variability in plunging from person to person should be mitigated and observed.

[Figure 60](#)~~[Figure 59](#)~~ shows the result of the dipping speed experiment with 2.6 g Lewatit SP in the modified basket, placed in 300 mL 3 mg L^{-1} Ni^{2+} solution without plunging, with 1 plunge per 30 s, per 5 s, and per 2 s. Confirming the hypothesis, faster dipping correlates with a higher amount of Ni^{2+} adsorbed to the resin. This difference is especially distinctive in minute 5, where two of the fastest plunging speed showed similar amounts of Ni^{2+} adsorbed, at $\geq 50\%$. Whereas the slower plunging and non-plunged resin showed a notably lower amount of Ni^{2+} adsorbed, at $\leq 30\%$. Therefore, it can also be concluded that the optimum plunging speed for this method would be at least 1 plunger per 5 seconds. Nevertheless, controlling the plunging speed in a human-operated method is more difficult, and through this experiment, it can be confirmed that the plunging speed can affect the Ni^{2+} adsorption performance of the resins. It is important to take this factor into account as a possible source of error, especially during the volunteer-testing phase.

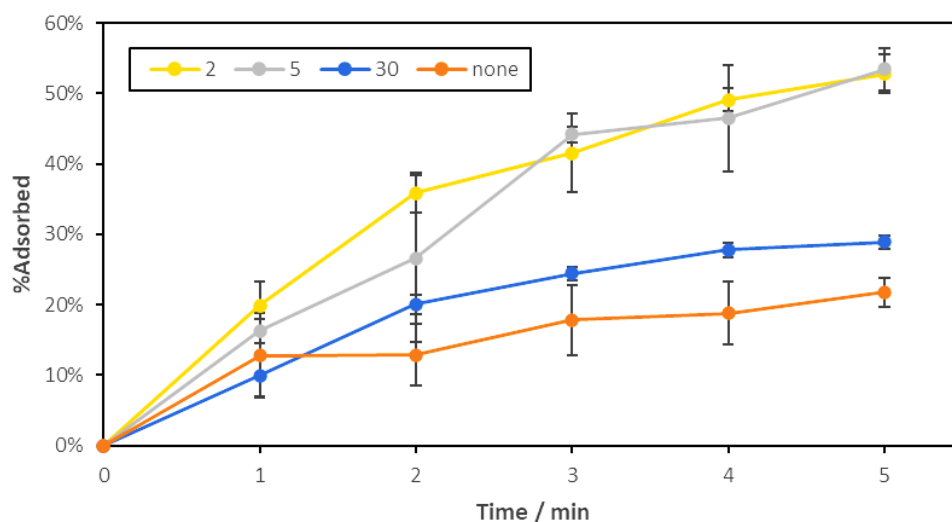


Figure 60 Effect of 2.6 g Lewatit SP in basket plunging speed of the modified basket in a cafetière filled with 300 mL 3 mg L⁻¹ Ni²⁺ solution for 5 min at the following variations: 1 plunge per 2, 5, and 30 seconds, and no plunging. Error bars illustrate the standard deviation between the result of the three repeats (n=3).

3.4.1.2 Effect of resin placement on Ni²⁺ adsorption in cafetière system

Another experiment related to the use of cafetière as a vessel for Ni²⁺ adsorption from environmental water samples was the effect of resin placement. As has been briefly discussed, the basic principle of Ni²⁺ adsorption in this system is related to the contact incidence between the target analyte with the adsorption sites. By placing the resins in the modified basket, the movement of the resin upon plunging is very restricted and contact with the solution happens mainly from the holes or other gaps in the basket. Therefore, the volume of the solution that would come into contact with the resins is also more restricted compared to if the resins were placed directly in the cafetière, without containing it in the modified basket. However, placing the resins outside the basket would not be practical for the objective of this research, where citizen scientists should be able to operate the workflow on site, i.e. riverbanks. Additionally, it is also important to observe the effect of basket containment to predict the performance of the workflow in resin-leak incidence. Since the current system was assembled manually by the researcher, there was the possibility of basket failure due to excessive plunging or other factors, causing the securing-nut to loosen and resulting in the release of the resin out of the basket.

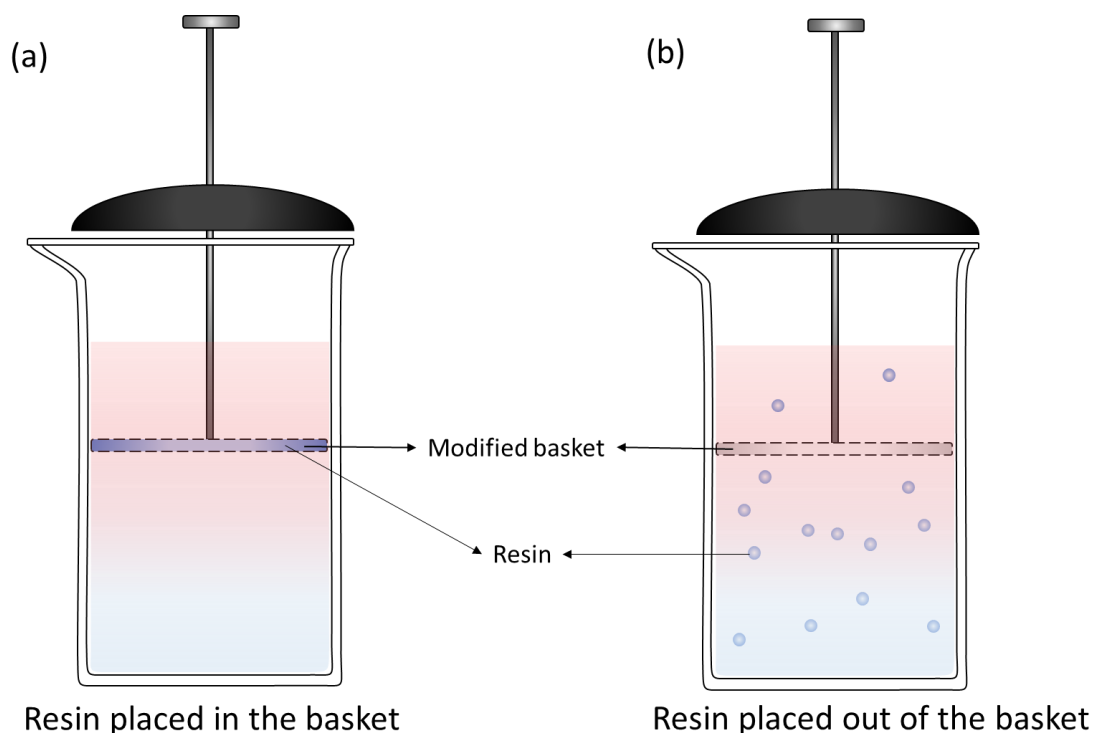


Figure 61 Two different resin placements tested in this observation, with (a) being placement of resin inside the modified basket, while (b) being placement of resin outside of the modified basket.

The effect of resin placement was observed through the method described in section 3.2.4.3 [Effect of resin placement on Ni²⁺ adsorption in cafetière](#)~~Effect of resin placement on Ni²⁺ adsorption in cafetière~~. The parameters for volume, Ni²⁺ concentration, and resin mass were chosen as discussed in the previous section. In the later set of experiments, where the resin was not contained in the basket, the plunging motion was used as means to mix the resin throughout the cafetière, allowing unrestrained movement of the resin beads throughout the volume of the solution. This condition was hypothesized to allow better Ni²⁺ adsorption due to direct contact with a larger surface area of the resin. However, it would not be practical to use this approach on the field – which would require mechanical separation between the solid resins and the sample solution, in order to further process the resin.

In Figure 62, the effect of resin containment is plotted against the time of sampling for both conditions – resin containment and resin outside the modified basket. In the early stage of plunging, up to minute 3, there was no significant difference observed between the two conditions. This may be attributed to the early stage of mixing, at which the resin outside the basket was not mixed throughout the solution evenly and therefore the effect of the freedom of movement can be neglected. However, at minute 4, the difference in the adsorption performance became apparent. In this case, the resins outside the modified basket would have

considerably more incidence of contact with the volume of the water sample. This experiment shows that in order to maintain repeatability of the result, resin-leak incidence should be minimised and avoided since it might affect the Ni²⁺ adsorption.

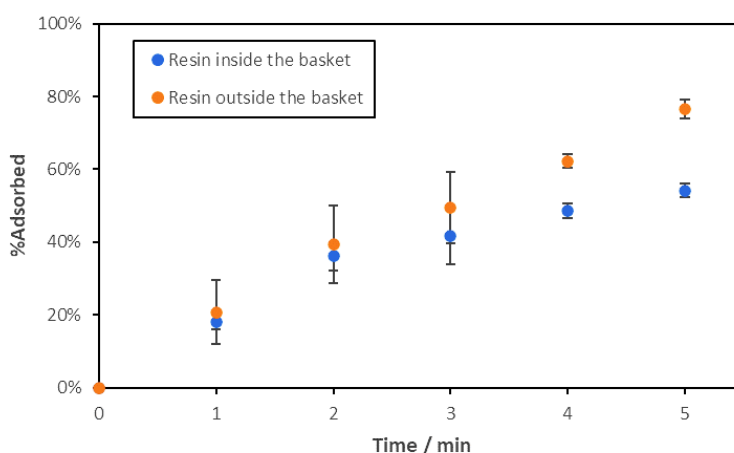


Figure 62 Effect of resin placement inside or outside the modified basket in a 300 mL 3 mg L⁻¹ Ni²⁺ solution in a cafetière, tested with 2.6 g Lewatit SP, with a plunging speed of 1 plunge per 2 seconds. Error bars illustrate the standard deviation between the result of the three repeats (n=3).

3.4.1.3 Effect of resin mass on Ni²⁺ adsorption in cafetière system

One of the limitations of the cafetière method compared to other possible uses of ion exchange resins in this process is the capacity of the PMMA basket. Therefore, it is important to study the effect of the different masses of resins on the Ni²⁺ adsorption from a designated sample volume (methods described in section 3.2.4.4 [Effect of resin mass on Ni²⁺ adsorption in cafetiere](#)[Effect of resin mass on Ni²⁺ adsorption in cafetiere](#)). In this case, a 300 mL 3 mg L⁻¹ Ni²⁺ water sample was used for each experiment, varying the mass of resins based on a preliminary study of the resin-to-solution ratio. For Lewatit SP, for instance, the tested mass variations were 1.8 g and 2.6 g of resins against the 300 mL Ni²⁺ sample. This value differs between resins, where Lewatit TP was tested with 0.6 g and 1.1 g, while Ambersep was tested with 1.2 g and 1.7 g. These differences are based on preliminary observation of the resin adsorption capability in stirred vessels, available in Appendix 2. In the section, it was observed that Lewatit TP and Ambersep were able to adsorb more than 90% of Ni²⁺ from the 50 mL solution within 5 min of stirring at 0.1 g and 0.2 g resin mass, respectively. Therefore, assuming the cafetière can replicate the mixing characteristics of the magnetic stirrer, for 300 mL of solution, the amount of resin required to achieve the same result would be 0.6 g and 1.2 g for Lewatit TP and Ambersep, respectively (1:500 resin to solution ratio). In order to compensate for the difference between the mixing characteristics of the stirrer with cafetière, adsorption was also observed in the increased mass of resin by the addition of 0.5 g of resin for each condition. For Lewatit SP, the

observation at 1.8 g follows a similar proportional increase, since the best adsorption of Ni^{2+} was observed at 0.3 g. However, since the adsorption at preliminary observation only reach more than 90% after 20 min of stirring – unlike the other two resins observed, a decision was made to observe its adsorption behaviour at 2.6 g. This is the maximum amount of Lewatit SP resin that can be contained in the modified basket, and 0.3 g higher than the pattern of increase in the other resins.

In Figure 63, the effect of resin mass variation was observed in the Ni^{2+} adsorption experiment from a 300 mL 3 mg L^{-1} solution in a cafetière system. For Lewatit SP and Ambersep, it is evident that the higher mass of resin would correlate to the Ni^{2+} adsorption performance of the system. However, for Lewatit SP, the Ni^{2+} adsorption, even at the highest mass of resin tested, peaked at 60%. Though increasing the amount of resin might result in better adsorption performance, the basket was not designed to hold a higher amount of Lewatit SP resin. Therefore, the addition of resin mass would need to be preceded by a change of basket design. On the other hand, for Lewatit TP and Ambersep, nearly the maximum amount of Ni^{2+} can be observed with the current basket design, shown by $\geq 90\%$ of Ni^{2+} adsorption at minute 15 and 3 for 0.6 g of Lewatit TP and 1.7 g of Ambersep, respectively. Due to this experiment, the mass of resins used in further experiments involving these resins in cafetière was set to 2.6 g for Lewatit SP, 1.1 g for Lewatit TP, and 1.7 g for Ambersep.

An interesting point to be observed in this experiment is that although in some cases almost 100% of the ions were trapped in the resin, the capacity of the resin at that point is still far below its maximum adsorption capacity. Lewatit SP, for example, has a maximum adsorption capacity of up to 86.89 mg g^{-1} resin. This number was obtained through the adsorption isotherm model, available in Appendix 2. In this experiment with 300 mL 3 mg L^{-1} Ni^{2+} , however, the maximum available mass of Ni^{2+} was 0.9 mg in the 300 mL solution. Further, only 60% of this mass was adsorbed to the resin even after 20 min of plunging 2.6 g Lewatit SP. Therefore, at this point, the adsorption capacity of the resin was much lower, down to 0.207 mg g^{-1} resin. This indicates that only 0.23% of the capacity of the resin was utilised at this point. This low capacity is true for all resins used in this experiment with the cafetière, with a higher mass of resin resulting in a lower percentage of capacity utilised.

However, it is important to remember that the aim of this experiment, ultimately, was not to completely fill the adsorption sites of the resin. Rather, the increase in the amount of resin was necessary to reduce the time required for this component of the workflow. Increasing the amount of resin correlates with the increase of adsorption sites available for the reaction. Therefore, for this research, rather than focusing on the efficiency and maximising the resin

adsorption capacity, the focus was more on whether the process would be able to adsorb most of the target ions within 5 min plunging time.

The biggest drawback of this approach, however, is due to the number of empty sites still available throughout the process, the selectivity of the adsorption process would be very low. The plunged resin essentially acts as a sponge, adsorbing all interactable ions in the solution. Adding to this problem is the fact that ion exchange resins can have very low selectivity in the first place, rather, relying on affinity to classify their uses. The problem with selectivity, however, will not be addressed in the adsorption step in this research.

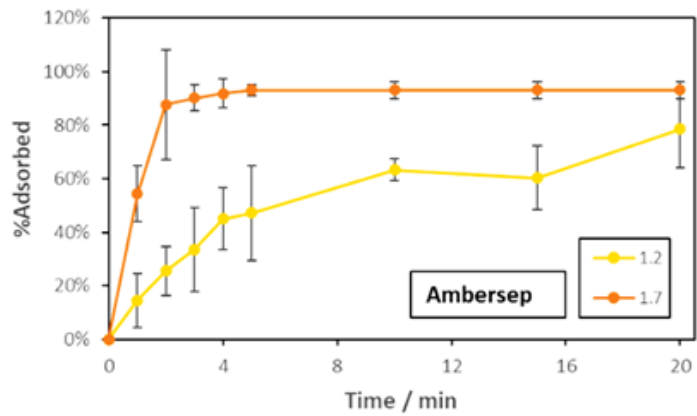
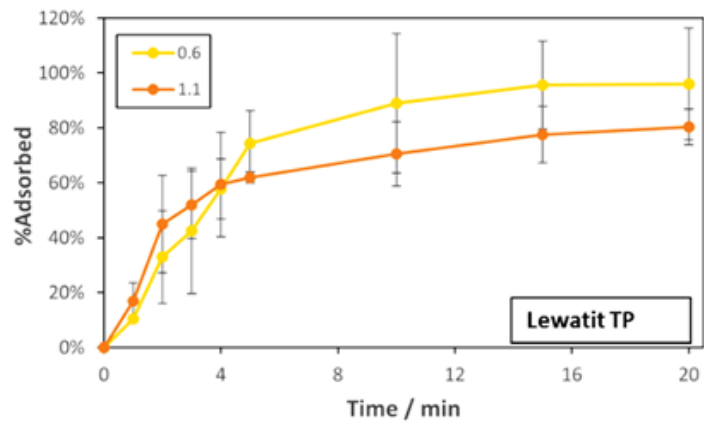
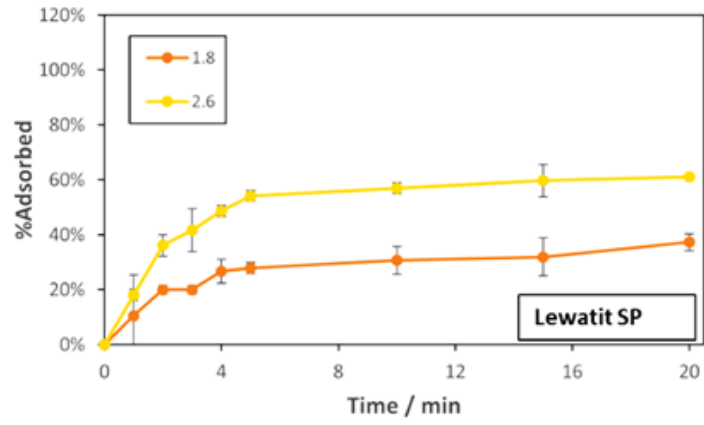


Figure 63 Effect of resin mass to Ni²⁺ adsorption performance of Lewatit SP, Lewatit TP, and Ambersep resin in 300 mL 3 mg L⁻¹ Ni²⁺ sample solution in a cafetière. Error bars illustrate the standard deviation between the result of the three repeats (n=3).

3.4.1.4 Effect of initial Ni²⁺ concentration on Ni²⁺ adsorption in cafetière system

Other properties to be observed in the cafetière system for all of the resins tested was its adsorption performance in different initial Ni²⁺ concentrations. Ideally, the adsorption performance (%adsorption) of the resins should be similar in their effective working concentration. This way, the amount of Ni²⁺ adsorbed would be predictable and proportional across the concentrations. Therefore, the preconcentration would also be predictable and the initial level of Ni²⁺ before the adsorption step can easily be calculated to a degree of precision. For Ni²⁺ in this research, the preconcentration was initially designed to be used in 0.2-0.8 mg L⁻¹ Ni²⁺ concentration. These values are one factor lower than the effective working concentration of the previously designed Ni²⁺ detection μ PAD, made with nioxime as a colorimetric reagent. The method for this experiment is described in section 3.2.4.5 [Effect of initial Ni²⁺ concentration on Ni²⁺ adsorption in cafetièr](#)~~Effect of initial Ni²⁺ concentration on Ni²⁺ adsorption in cafetièr~~.

As shown in Figure 64, Lewatit SP showed similar adsorption performance across the tested concentration range. This means that at this tested concentration range, at minutes 4-5, the amount of Ni²⁺ adsorbed by the Lewatit SP resin upon plunging in the cafetière was reliably around 60%. The other two resins showed interesting adsorption performance at different concentrations. Lewatit TP showed a slower adsorption rate at the first two minutes of the plunging for lower concentration (0.2-0.4 mg L⁻¹). However, by minute 5, the difference in the amount of Ni²⁺ adsorbed was no longer significant ($p>0.05$). Whereas in the process using Ambersep resin, the adsorption was slower for higher initial Ni²⁺ concentration (0.4-0.8 mg L⁻¹) during the first minute. However, this difference was no longer considered as soon as the process reached minute 3. The result of this experiment underlines an interesting contrast between Lewatit TP and Ambersep adsorption performance in a gradient of concentration. This difference may be attributed to the difference in the adsorption mechanism between the two chelating resins.

While the concentration range may not reflect the concentration range of Ni²⁺ in the environment, this level of Ni²⁺ in the sample solution should be easily detectable by the developed nioxime μ PAD. Since the main focus of this research was to develop an integrated simple preconcentration step for the μ PAD, the focus of the initial concentration of the solution involved in the preconcentration development relies on the effective working concentration range of the developed μ PAD.

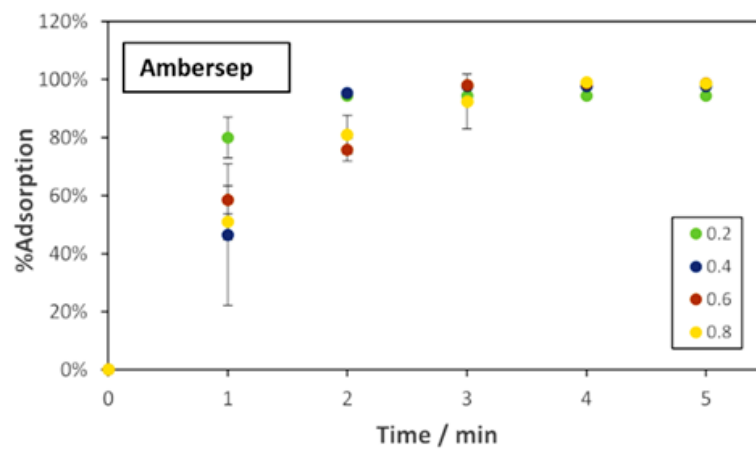
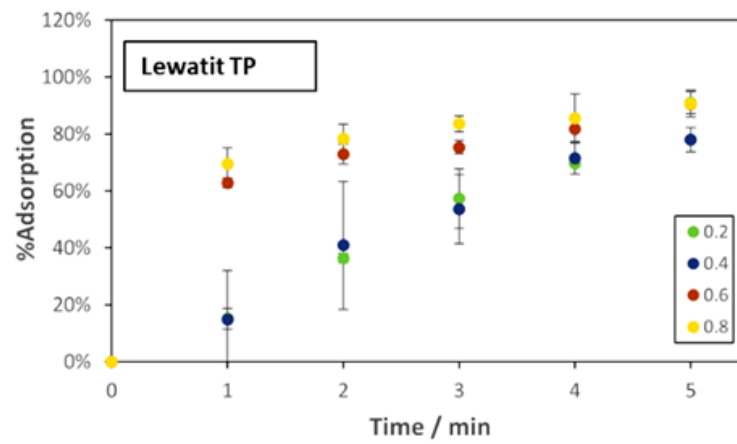
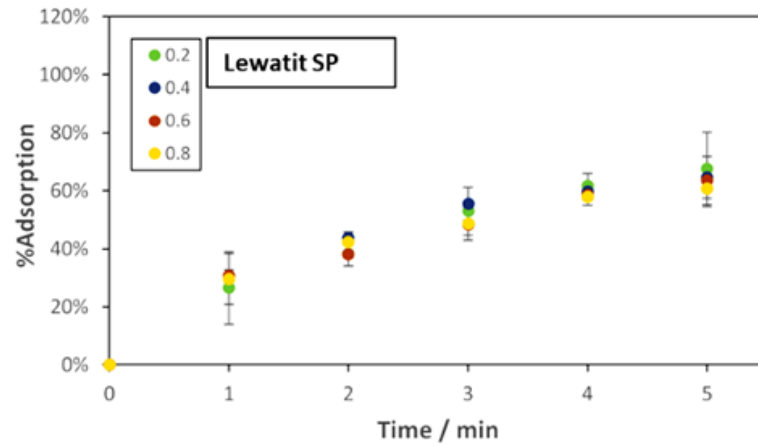


Figure 64 Effect of initial Ni²⁺ concentration between 0.2-0.8 mg L⁻¹, tested with Lewatit SP, Lewatit TP and Ambersep were plunged repeatedly for 5 min in 300 mL Ni²⁺ concentration in a cafetière. Error bars illustrate the standard deviation between the result of the three repeats (n=3).

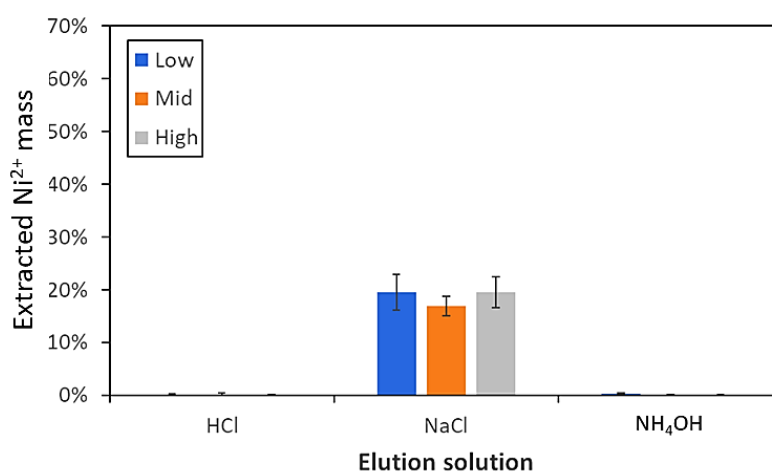
3.4.2 Nickel elution properties of ion exchange resins

The other aspect of the development of a preconcentration process is the release of trapped or adsorbed analyte back to a solution. This process, in this research, is referred to as the elution process. In ion exchange processes, the elution of adsorbed ions would be similar to the recovery process, where the trapped ions – separated from their original mixture – can be ‘detached’ from the resins to a certain degree. This process is usually accomplished by the introduction of a solvent containing either 1) an ion with a bigger affinity to the trapped analyte compared to the trapping site, therefore essentially ‘pulling’ the analytes away from the trapping sites; or 2) an ion with a bigger affinity to the counterion compared to the trapped analyte, therefore essentially ‘evicting’ the trapped ions and replacing it with itself. In the ion exchange process, the elution process usually involves the introduction of an acidic (or alkaline) solution in various concentrations. Some commonly used acids include HCl and H₂SO₄, which are strong acids. Although in high molarity these acids may be able to be used in the elution process for the preconcentration method developed in this research, its uses would increase risk upon onsite implementation.

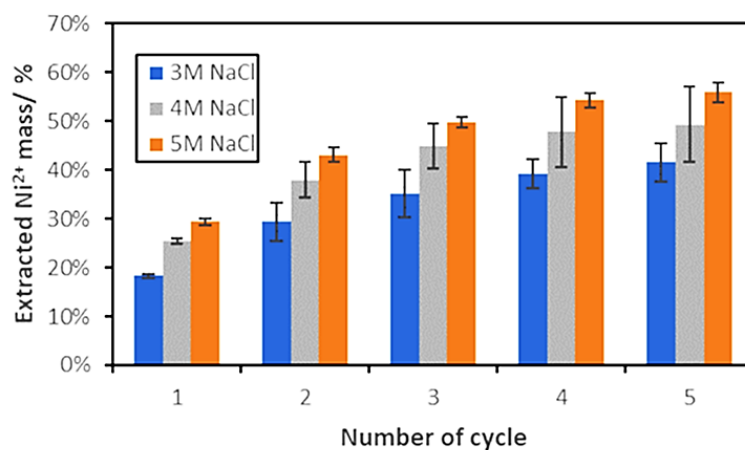
Therefore, one of the challenges faced in this research is to find a safer alternative elution solution that can rapidly elute the trapped Ni²⁺ ion out of the resin. In the preliminary stage, however, the use of three different solutions was used to observe the ideal pH for elution. The chosen solutions were HCl as the acidic solution, NaCl as the neutral solution, and NH₄OH as the alkaline solution. The choice of HCl and NH₄OH solution was based on literature, which had used these solutions for metal elution from various ion exchange resins [113, 167, 168]. However, the choice of NaCl was not only based on its neutral pH but also based on the ion exchange mechanism; where some resins may have higher affinity to Na⁺, especially with the concentration gradient, compared to the already adsorbed metal ion [169, 170].

With the method described in section 3.2.4.6 [Ni²⁺ elution evaluation](#)~~Ni²⁺ elution evaluation~~, the elution of Ni²⁺ from ion exchange resin was observed. Figure 65a show the elution of Ni²⁺ from loaded resins swirled in a 30 mL elution solution of various concentration of HCl, NaCl, or NH₄OH. In this figure, it is evident that in the 5 min of swirling, elution solution with acidic or alkaline pH did not effectively elute the target analyte. Whereas the elution process with NaCl as an elution solution shows potential for Ni²⁺ elution out of the Lewatit SP resin. Preliminary elution experiments for the other resins – Lewatit TP and Ambersep with this elution method also did not produce a detectable amount of Ni²⁺ in the elution solution. Due to this preliminary study, further observation in the use of NaCl for Ni²⁺ elution from Lewatit SP was done.

In Figure 65b, the elution of Ni^{2+} from Lewatit SP in 3-5 M NaCl concentration at multiple cycles. The cycle was defined as the addition of 10 mL of respective solution, swirling for 1 min, and draining the elution solution from the mixture. The amount of extracted Ni^{2+} calculated in the figure was a cumulative number. From this plot, it can be seen that the increase in NaCl concentration correlated to an increase in the effectiveness of the elution process. Additionally, multiple cycles of elution would be able to remove the trapped ion from the resin and after 5 cycles with 5 M NaCl, approximately 50% of Ni^{2+} was eluted from the resin. This shows the possibility of resin regeneration using concentrated NaCl solution in the application process.



(a)



(b)

Figure 65 (a) Elution of Ni^{2+} from Lewatit SP in various concentrations (3-5 M) of HCl, NaCl, or NH_4OH after swirling the loaded resin in a 30 mL elution solution. (b) Elution of Ni^{2+} from Lewatit SP in 3-5 M NaCl repeated for 5 1 min cycles, each cycle is the addition of fresh 10 mL elution solution after discarding the previous elution solution. Error bars illustrate the standard deviation between the result of the three repeats ($n=3$).

3.4.2.1 Effect of elution volume on Ni²⁺ elution from ion exchange resin

One of the factors needed to be observed in the elution process is the volume of the elution solution used. Ideally, for the purpose of this research, the elution solution should be enough for μ PAD measurement – which can detect at 5 mL solution in a petri dish, but not so much that it would not result in preconcentration. The observation was then done with the method described in section 3.2.4.7 Effect of elution volume.

Figure 66 shows the result of the experiment, comparing the amount of extracted or eluted Ni²⁺ out of the Lewatit SP resin mixed for 1 min in a centrifuge tube containing the respective amount of 5 M NaCl. Through this observation, it is clear that the variation in elution volume within the tested range did not significantly affect the Ni²⁺ elution process. This might be attributed to the small range of volume variation tested in this experiment. Rather than concluding that volume would not affect the elution process, it is more accurate to conclude that the 5 mL difference between the tested eluent volume did not significantly affect the extraction process. Another parameter to be noted is the short mixing time, which might render the volume difference insignificant in this process.

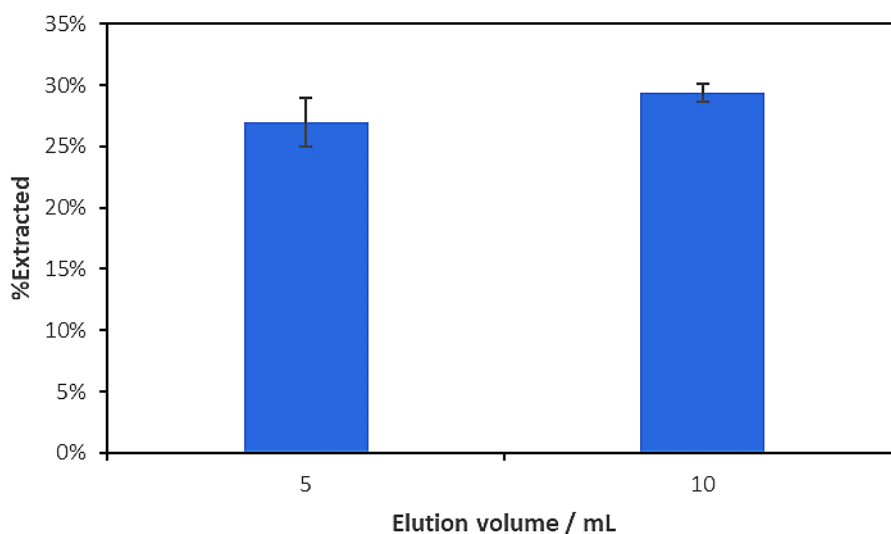


Figure 66 Amount of eluted Ni²⁺ upon elution with 5 mL and 10 mL 5 M NaCl after 1 min of mixing with 2.6 g Lewatit SP loaded with Ni²⁺. Error bars illustrate the standard deviation between the result of the three repeats (n=3).

3.4.2.2 Effect of elution mixing time on Ni²⁺ elution from ion exchange resin

Another factor in the elution process is the mixing time, which was observed by mixing Ni²⁺-loaded Lewatit SP resin in a 10 mL 5 M NaCl in a centrifuge tube for 1, 3, or 5 minutes (following the method in 3.2.4.8 Effect of elution mixing time). The choice to limit the elution time to 5

minutes in this experiment is due to the realistic duration of an onsite rapid preconcentration for citizen scientists. In this research, 5 minutes was taken as the maximum allowable time for the elution step of the preconcentration to keep the total process duration short enough for citizen science purposes. This is considering that the adsorption and μ PAD processes each require approximately 5 min on their own.

Hypothetically, prolonging the contact duration between the resin and the elution solution would aid the elution process, since the kinetics of the reaction might not be as instantaneous. Therefore, allowing the resin to come in contact with the solution longer would allow more exchange between the Na^+ in the solution with the Ni^{2+} attached to the resin. However, since the difference between the observed time variance is small, there is also a chance that the difference in elution effectivity would not be apparent. In Figure 67, the effect of mixing time during the elution process with 10 mL 5 M NaCl was observed. It is evident from the given figure that there is no significant difference between the variation in mixing time within the tested range.

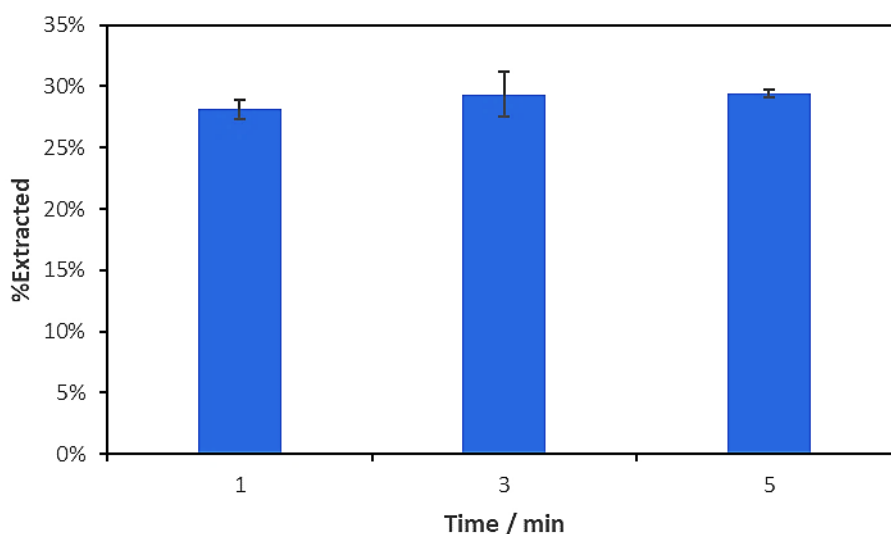


Figure 67 Amount of Ni^{2+} eluted with 10 mL 5 M NaCl solution after mixing with 2.6 g Lewatit SP loaded with Ni^{2+} for 1, 3, and 5 minutes. Error bars illustrate the standard deviation between the result of the three repeats ($n=3$).

3.4.2.3 Effect of NaCl concentration on Ni^{2+} elution from ion exchange resin

The effect of NaCl concentration was observed with the method described in section 3.2.4.9 Effect of NaCl concentration. In Figure 68, it can be seen that an increase in the amount of Ni^{2+} extracted from the resin is observed upon mixing with a higher concentration of NaCl. After 5 min of mixing, up to 40% of Ni^{2+} trapped in the resin was released back into the 3 M NaCl solution.

This amount increased up to 47% in 4 M NaCl and up to 50% in 5 M NaCl. This is consistent with the hypothesis since increasing the concentration of NaCl would push the ion exchange reaction to the left direction in the following equation:



Therefore, the amount of Ni^{2+} released from the resin would increase. Consequently, at the same eluent volume, the concentration of Ni^{2+} in the solution would increase at a higher NaCl concentration, giving a higher preconcentration factor and a more effective preconcentration process. Therefore, in future experiments, 5 M NaCl would be used as preconcentration eluent, unless stated otherwise.

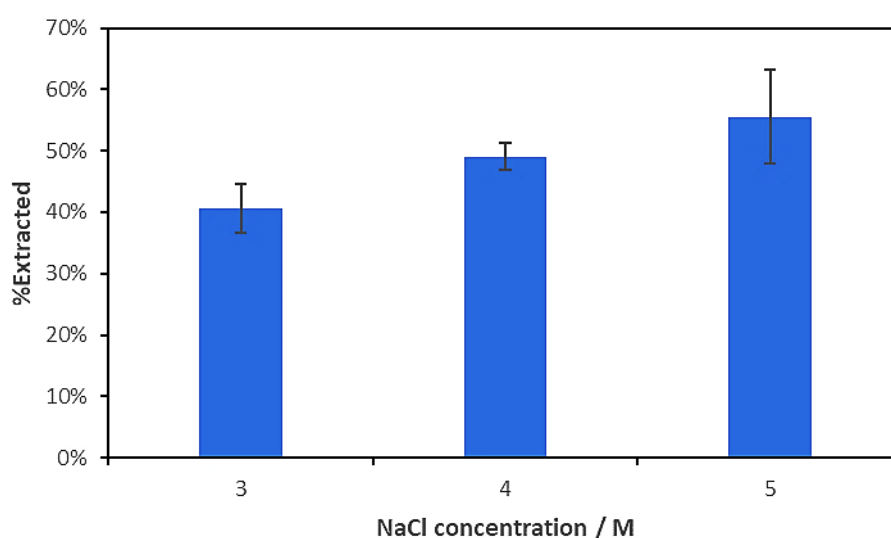


Figure 68 Amount of Ni^{2+} extracted out of the Lewatit SP resin after 5 min of mixing in 10 mL 3-5 M NaCl as elution solution. Error bars illustrate the standard deviation between the result of the three repeats (n=3).

3.4.3 Effect of other metal ions to Ni^{2+} adsorption and elution with Lewatit SP in cafetière

Unlike in the experiments done in this research, an environmental water sample would contain a certain level of other metal ions. Therefore, the performance of the adsorption process in the presence of other competing metal ions was first observed by spiking Milli-Q water with 0.1 mg L^{-1} of various metal ions, which were: Mn^{2+} , Fe^{2+} , Co^{2+} , Cu^{2+} , and Zn^{2+} . The level of metal ions tested in this experiment was chosen to mimic the concentration of interest in a real sample. Along with these metal ions, Ca^{2+} ion at the same level was also added since it is one of the most common divalent ions found in environmental water samples. This observation was done using

the method described in section 3.2.4.10 [Effect of other metal ions on Ni²⁺ adsorption and elution](#)~~Effect of other metal ions on Ni²⁺ adsorption and elution~~.

From the previous discussion (see 3.4.1 Nickel adsorption properties of ion exchange resins in cafetière system), it was already inferred that the low efficiency of the ion exchange resin used in this adsorption method would give a chance for adsorption of other ions. In 3.4.1.3 [Effect of resin mass on Ni²⁺ adsorption in cafetière system](#)~~Effect of resin mass on Ni²⁺ adsorption in cafetière system~~, the cafetière method maximum adsorption capacity was merely 0.23% of the resin maximum capacity in ideal working condition. Therefore, there is still a vast number of adsorption sites available for the adsorption of other ions in the solution, including divalent ions tested in this experiment. Figure 69 shows the adsorbed amount of each ion measured in the solution. In the figure, it is evident that the developed adsorption process for Ni²⁺ was able to adsorb most of the Ni²⁺ available in the solution in the presence of other ions. This is an interesting result since it exceeds the adsorption performance of the process in a single Ni²⁺ ion solution. Therefore, rather than competing with other ions in the solution, it seemingly implies that certain ions in the mixture might instead reinforce the Ni²⁺ adsorption process. This interaction is chemically unlikely and had never been observed before. Now, it is important to remember that the adsorption performance in this experiment was obtained through calculation, not necessarily direct measurement. The adsorption performance was a comparison between the amount of Ni²⁺ measured at the endpoint of the process to its initial amount in the solution. Therefore, the low amount of Ni²⁺ observed at the endpoint – although mostly might have been adsorbed to the resin, since it is eluted in a later step – might be due to interaction with other chemicals in the mixture.

Another notable observation from the data illustrated in Figure 69 is the other ions adsorbed to the resin. Following the high adsorption of Ni²⁺, Mn²⁺ was the metal with the second highest adsorption to the resin, with nearly 90% of the ion adsorbed from the sample solution. The next metal ion with high adsorption effectiveness is Zn²⁺ with more than 80% adsorption, which was on par with the adsorption of Ca²⁺. Whereas Co²⁺, Cu²⁺, and Fe²⁺ were not adsorbed as effectively compared to the other ions, with less than 60% of the spiked ions adsorbed by minute 5. Therefore, through this experiment, the selectivity of the resin amongst the tested metal species follows the following: Ni²⁺ > Mn²⁺ > Zn²⁺ > Ca²⁺ > Co²⁺ > Cu²⁺ > Fe²⁺. This is an interesting result since it differs from typical affinity series for strongly acidic cation exchange resins, which typically are: Ca²⁺ > Ni²⁺ > Cu²⁺ > Co²⁺ > Zn²⁺ > Fe²⁺ [171]. Unfortunately, there is no data for Mn²⁺ adsorption for this type of resin. This difference may be attributed to the properties of the mixed ion solution that may easily change the affinity of metals for the ion exchange process. An example of this parameter is solution temperature.

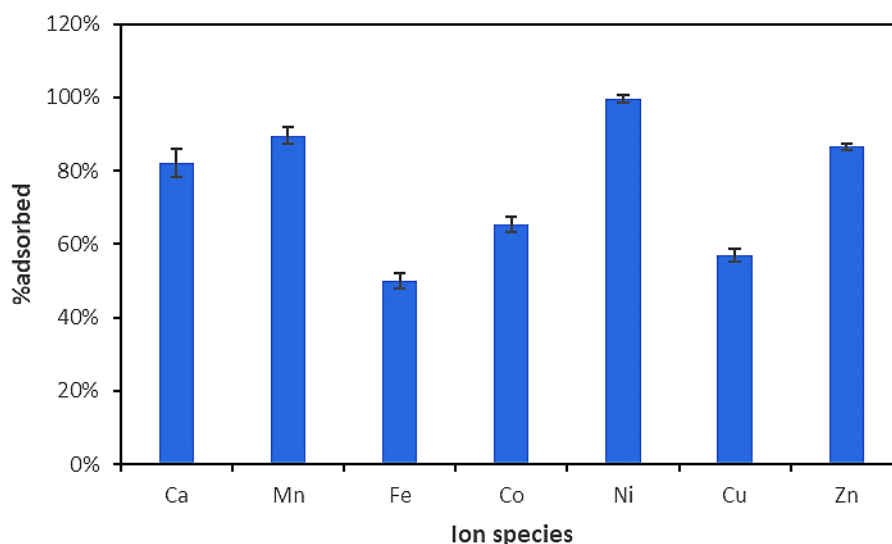


Figure 69 Amount of adsorbed Ca^{2+} , Mn^{2+} , Fe^{2+} , Co^{2+} , Ni^{2+} , Cu^{2+} , and Zn^{2+} in 2.6 g Lewatit SP workflow in a cafetière from a mixed ion sample solution spiked with 0.5 mg L^{-1} of respective ions. Error bars illustrate the standard deviation between the result of the three repeats ($n=3$).

Despite the adsorption performance for various ions, it is equally important to observe the amount and species of ions eluted with the developed elution process. In this experiment, elution was achieved by mixing the Lewatit SP resin loaded with the ions in 10 mL 5 M NaCl for 1 min. The amount of eluted ions was measured with Thermo Scientific iCAP Qc ICP-MS. The saline samples were diluted for the measurement.

Between the tested species of ions, elution with 5 M NaCl within 1 min was only achieved for Zn^{2+} , Ni^{2+} , Cu^{2+} , and Co^{2+} , in varying degrees of effectiveness, as illustrated in Figure 70. Despite the adsorption of Ca^{2+} , Mn^{2+} , and Fe^{2+} , no elution was achievable with the developed method for these ions. Therefore, the elution process was able to create a level of specificity for the preconcentration process, since effectively, no amount of Ca^{2+} , Mn^{2+} , and Fe^{2+} can be released back into the elution solution. However, the effectiveness of the elution process was much higher for Zn^{2+} , which reach up to 55%, compared to Ni^{2+} , which reach up to 30%. This is followed by Cu^{2+} elution (up to 12%) and Co^{2+} elution (up to 10%). Therefore, the preconcentration process might also be usable for Zn^{2+} preconcentration aside from Ni^{2+} preconcentration.

Regardless of the high effectiveness of Zn²⁺ elution, the level of Ni²⁺ elution was not affected, showing the possibility of simultaneous Zn²⁺ and Ni²⁺ elution.

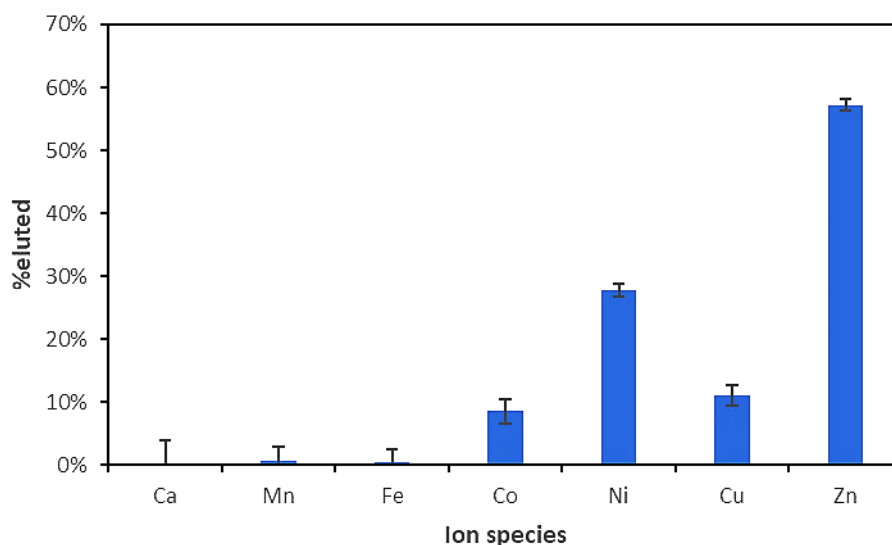


Figure 70 Amount of eluted Ca²⁺, Mn²⁺, Fe²⁺, Co²⁺, Ni²⁺, Cu²⁺, and Zn²⁺ from elution of 2.6 g Lewatit SP in 10 mL 5 M NaCl for 1 min. Error bars illustrate the standard deviation between the result of the three repeats (n=3).

3.5 Incorporation of cafetière-based nickel preconcentration workflow into paper-based analytical device system

The developed workflow which consisted of a preconcentration system with the cafetière paired with the paper-based device, can be optimised further depending on the objective of the process. This is due to the findings throughout the development of the preconcentration process, which show degrees of process effectiveness based on variations in different steps of cafetière preconcentration, e.g. different resin placement might lead to different adsorption performance (see 3.4.1.2 [Effect of resin placement on Ni²⁺ adsorption in cafetière system](#)~~Effect of resin placement on Ni²⁺ adsorption in cafetière system~~). Further, referring back to the objective of this research, the elution step might need further modification to ensure the user-friendliness of the developed workflow – which might be less important in the hands of more expert users.

The aim of this experiment is to test the performance of different elution processes in the preconcentration step of the workflow. Depending on whether the workflow is developed for laboratory settings with more trained users or for onsite settings with less trained users, the elution step can be adjusted, producing different – but reliable results. In the following section, the developed workflow from this study was described to be applied by citizen scientists.

Whereas an alternative workflow developed for low-cost laboratory settings is available in Appendix 2.

3.5.1 Developed workflow

In the workflow developed for citizen scientists, it is important to take into account simplicity and accessibility along with analytical prowess. In order to make the preconcentration workflow easier for less trained users such as this, it is imperative that the resins should stay in the basket and no pouring process should be done. This is due to simplicity since onsite measurement of the sample would be very complex if users are required to pour out the resins from the basket to a smaller container, also to prevent variation due to improper transfer of the resin from the basket to the elution solution. Additionally, the resin-transfer process such was done in another workflow (discussed in Appendix 2), may pose increased risks for citizen scientists. As a consequence of this design decision, the volume of the eluent solution cannot remain at 10 mL in a petri dish. This is because this volume simply would not suffice for thorough contact between the resins stored in the basket and the elution solution.

Therefore, in this workflow, 30 mL 5 M NaCl elution solution was used instead of the 10 mL in the previous workflow. This is the minimum volume of 5 M NaCl placed in a crystallising dish at which the modified basket would be submerged thoroughly upon placement. This 30 mL solution was placed in a crystallising dish, where the basket – still containing resins and still attached to the plunger, can be dipped and swirled for 5 min for the elution process. Based on preliminary studies, the process cannot replicate a similar level of preconcentration as the previous elution process (discussed in Appendix 2), which can be accomplished within 1 min. Therefore, 5 min was chosen and determined as the maximum duration of elution in this developed process to still ensure its rapid accessibility for onsite environmental detection. This increase in elution duration already increased the preconcentration time from 6 min in the previous workflow, to 10 min. After 5 min, the basket can be removed from the crystallising dish and the nioxime μ PAD can be dipped into the solution for 4 min for the colour change. A picture of the device can then be obtained and analysed.

Before incorporating the workflow into the μ PAD system, the preconcentration performance of this adjusted workflow was evaluated with UV/Vis spectrophotometry with nioxime as a colorimetric reagent. In Figure 71, it can be seen that there is an increase in absorbance compared to the initial absorbance of Ni^{2+} at the same concentration and sample solvent matrix. This indicates that the preconcentration was able to increase the level of Ni^{2+} from its original solution. Through calculation, it was obtained that 3 times preconcentration was achieved through this method. This shows that the adjusted method was still able to accomplish the

preconcentration, albeit with lower effectiveness compared to the previously described workflow – where the elution volume is lower.

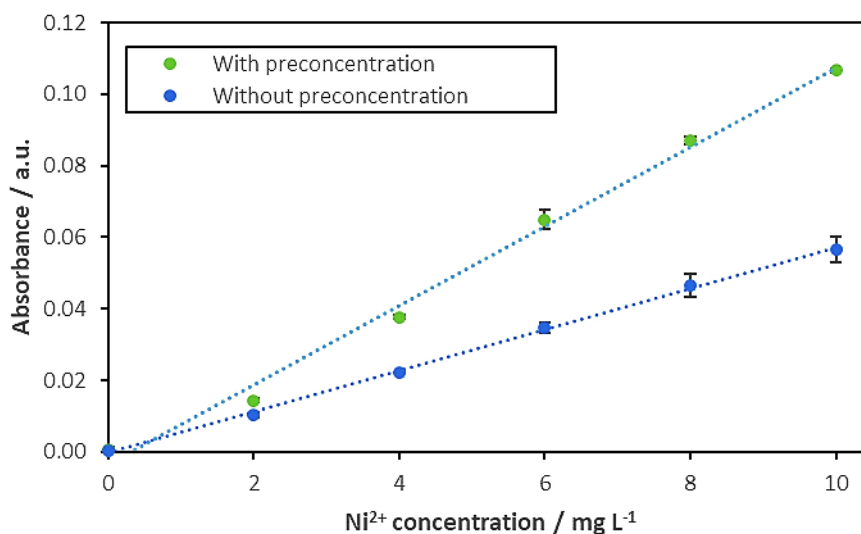
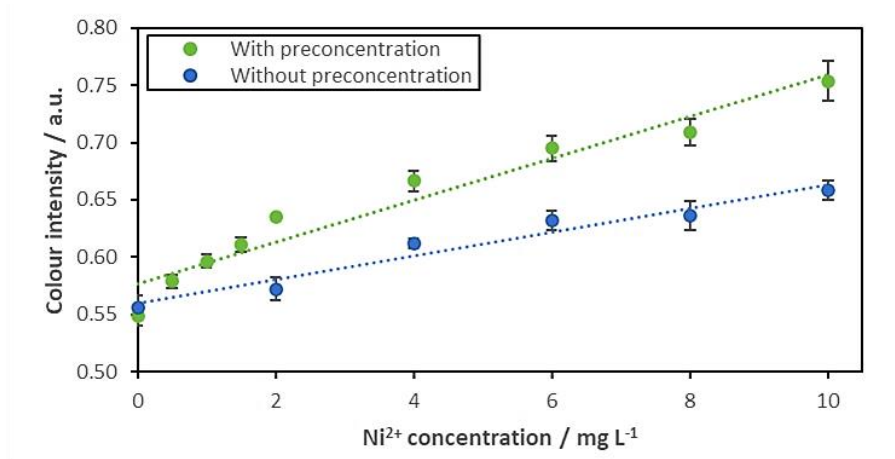
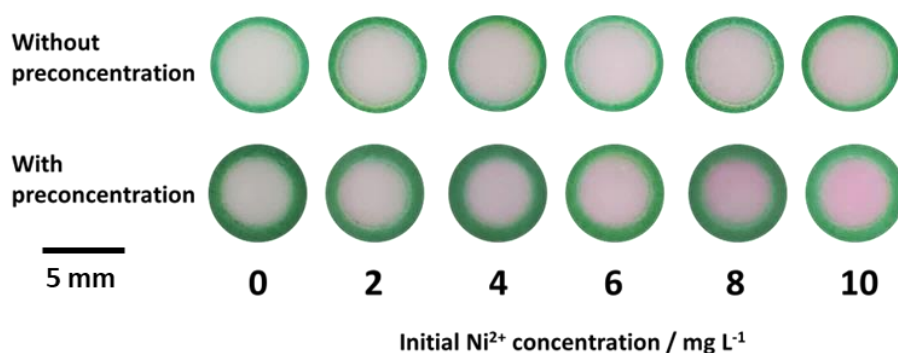


Figure 71 UV/Vis absorbance measured at 530 nm for 0-10 mg L⁻¹ Ni²⁺ with and without preconcentration with 2.6 g Lewatit SP in cafetière and subsequent elution with 30 mL 5 M NaCl. All measurement was done with 5 M NaCl as the sample matrix. Error bars illustrate the standard deviation between the result of the three repeats (n=3).

Integrating the workflow with nioxime μ PAD further showed agreement with the UV/Vis result, where the preconcentration method was able to increase the concentration of Ni²⁺ by 3 times its initial concentration. In the complete workflow with nioxime μ PAD, this would allow the detection of Ni²⁺ with the initial concentration of 1 mg L⁻¹, which is 3 times higher than the previous workflow. However, this higher detection limit is favoured in this workflow, in exchange for the simplicity and accessibility of the workflow for the citizen science approach. The lower preconcentration factor obtained in this workflow may be caused by the higher volume of elution solution used despite longer mixing time, and the use of a basket as resin containment, limiting the contact between the resin and elution solution.



(a)



(b)

Figure 72 (a) Colour intensity measured in nioxime μ PAD with and without Ni^{2+} preconcentration with 2.6 g Lewatit SP in cafetière with subsequent 30 mL 5 M NaCl elution for 5 min. All sample matrix was 5 M NaCl. Error bars illustrating standard deviation between the result of the three repeats ($n=3$); (b) Colour intensity of the sample wells without and with Ni^{2+} preconcentration at the same level of Ni^{2+} within 0-10 mg L^{-1} concentration range with nioxime μ PAD.

3.6 Conclusion

In this research, a preconcentration step to enhance Ni^{2+} detection with μ PADs was developed using a cafetière design for rapid, riverside preconcentration of environmental samples. Two materials were tested as media to facilitate this preconcentration step: PCL/chitosan/PEO nanomat and commercially available ion exchange resins. However, the development of a cafetière-based preconcentration process with electrospun nanofiber was terminated due to its complex fabrication steps and unsatisfactory elution results (see section 3.3.3).

On the other hand, commercially-available ion exchange resins such as Lewatit[®] MonoPlus SP 112, Lewatit[®] TP 207, and Ambersep[™] M4195 showed promising Ni^{2+} adsorption with the

cafetière system. Further, Lewatit® MonoPlus SP 112 was able to be paired with a non-hazardous elution solution, making it an ideal candidate for the objective of this research to facilitate both effective Ni²⁺ and non-hazardous elution suitable for a workflow that could be operated by a non-specialist citizen scientist. Through adjustments to increase the user-friendliness of the workflow, the preconcentration process was capable of concentrating Ni²⁺ by a factor of three.

The workflow comprised of placing a 300 mL water sample into a cafetière, followed by plunging a modified basket loaded with 2.6 g Lewatit® MonoPlus SP 112 for 5 min. Elution can then be achieved by placing the resin-filled basket into a 30 mL elution solution and mixing it for another 5 min. To integrate the μ PAD workflow, soon after the elution process, a prepared nioxime μ PAD can immediately be placed in the elution solution. Data acquisition can then proceed as designed, as discussed in Chapter 2.

However, as shown in section 3.4.3, this preconcentration step also shows potential for Zn²⁺ preconcentration, which could have useful applications given the ubiquity of Zn²⁺ as a potential pollutant in many urban freshwater systems. Therefore, in the next section of this research, a similar workflow comprising the cafetière-based preconcentration step and Zn²⁺ detection μ PAD was developed for environmental metal detection by citizen scientists.

Chapter 4 Development of zinc detection kit with cafetière-based preconcentration and paper-based analytical device

4.1 Chapter introduction

The need for a rapid, onsite detection method of heavy metal was not only critical for Ni^{2+} but also for other metals, such as Zn^{2+} . Despite often being regarded as less dangerous compared to other divalent metals, excessive and continuous exposure to Zn^{2+} through freshwater contamination can still lead to environmental and public health concerns [2, 4, 27]. Unfortunately, despite the similar danger posed by and the importance of Zn^{2+} monitoring, there have been limited studies utilising paper-based microfluidic devices for Zn^{2+} detection. Kudo, *et.al.*, had previously developed a Zn^{2+} detection μPAD with zincon monosodium salt that required 15 min reaction time and was able to detect down to $8 \text{ mg L}^{-1} \text{ Zn}^{2+}$ [83]. While other studies had developed Zn^{2+} detection μPAD that was able to detect down to 0.04 and $0.63 \text{ mg L}^{-1} \text{ Zn}^{2+}$ with a variety of colorimetric agents and additives [12, 13]. These approaches, despite their promising results, often require either: (1) around 15 min undisturbed reaction time, making it harder to use in onsite settings, or (2) hazardous additives, such as cyanide as a masking agent which would severely restrict field-based applications. Therefore, in this study, an alternative Zn^{2+} μPAD was developed to be paired with a portable preconcentration system for rapid, onsite analysis.

As opposed to the approach in Ni^{2+} preconcentration and detection discussed in Chapters 3 and 4, the development of the workflow for zinc detection was not from the ground up. Rather, the development was based on the workflow for Ni^{2+} preconcentration, coupled with a similar paper-based analytical device (μPAD). This decision was made based on the result of the preconcentration workflow performance in the mixed-ion matrix, as discussed in Chapter 3. The result of the aforementioned experiment showed potential for Zn^{2+} preconcentration using the developed preconcentration workflow involving Lewatit SP in a cafetière. The idea of using the same preconcentration workflow was to allow for parallel onsite preconcentration and detection of Ni^{2+} and Zn^{2+} , and in the future, of other divalent metals as well. Ideally, the developed preconcentration step can adsorb both Ni^{2+} and Zn^{2+} in tandem and elute in tandem without interfering with each other. Other ideal operating conditions would involve different elution solutions for different metal species but with a single adsorption step [172-174]. Therefore, the observation of the potential of the developed workflow for Zn^{2+} preconcentration was an exciting one in this research. However, the developed nioxime μPAD was not suitable for Zn^{2+} detection. Therefore, an alternative μPAD was to be developed in the same working principle as nioxime μPAD but for Zn^{2+} detection.

Therefore, this chapter aims to develop a preconcentration and μ PAD detection workflow for Zn^{2+} . Specific objectives of the chapter are to develop and compare the effectiveness of two different μ PAD for Zn detection (section 4.3 and section 4.4) and evaluate the effectiveness of the best-performing μ PAD with preconcentration steps on Zn^{2+} -spiked environmental samples (section 4.5 and 4.6),

4.2 Materials and Methods

This section started with a list of materials used in this study, as well as the supplier for each of the materials, and continued with the solution preparation for each solution used in this study. It was then followed with a general description of the methods used throughout the study related to the development of Zn^{2+} detection and preconcentration workflow.

4.2.1 Materials

The chemicals used in the development of Zn^{2+} detection and preconcentration workflow are listed in Table 17.

Table 17 Chemicals used in the development of Zn^{2+} -detection μ PAD and Zn^{2+} preconcentration.

Description	Supplier
2-(5-Bromo-2-pyridylazo)-5-[N-propyl-N-(3-sulfopropyl)amino]phenol disodium salt dihydrate (5-Br-PAPs), $\geq 95.0\%$ (HPLC)	Sigma Aldrich
Zincon monosodium salt, for spectrophotometric detection of Cu, Zn	Alfa Aesar
Phosphate-buffered saline tablets	Sigma Aldrich
Poly(diallyldimethylammonium chloride) 20 wt% solution in H_2O	Sigma Aldrich
Sodium fluoride, Puriss., meets analytical specification of BP, Ph.Eur., USP, 98.5-100.5%	Honeywell
Dimercapto-succinic acid, $\sim 98\%$	Sigma Aldrich
Zinc (II) sulphate heptahydrate, ACS reagent, 99%	Sigma Aldrich
Nickel (II) chloride hexahydrate, 99.9% trace metal basis	Sigma Aldrich
Sodium carbonate, powder, $\geq 99.5\%$, ACS reagent	Sigma Aldrich
Sodium bicarbonate, ACS reagent, $\geq 99.7\%$	Sigma Aldrich
Iron (II) chloride tetrahydrate, ReagentPlus [®] , 98%	Acros Organics
Sodium chloride, ACS Reagent, $\geq 99.0\%$	Sigma Aldrich
Potassium chloride, ACS reagent, 99.0-100.5%	Sigma Aldrich

Sodium phosphate dibasic, ACS reagent, ≥99.0%	Sigma Aldrich
Potassium nitrate, ACS reagent, ≥99.0%	Fisher Scientific
Iron (III) chloride hexahydrate, ACS reagent, 97%	Sigma Aldrich
Cobalt (II) chloride hexahydrate, ACS reagent, 98%	Sigma Aldrich
Copper (II) sulphate pentahydrate, ACS reagent, ≥98%	Sigma Aldrich
Calcium sulphate dihydrate, ReagentPlus®, ≥99%	Sigma Aldrich
Lewatit® MonoPlus SP-112 Na ⁺ form	Sigma Aldrich

4.2.2 Solution preparations

The preparation process for each solution used in this research is described in the following sections.

4.2.2.1 Preparation of Zn²⁺ stock solution

43.4 mg Zinc (II) sulphate heptahydrate ($M_w = 287.56 \text{ g mol}^{-1}$) was weighed and made up to 100 mL solution with Milli-Q water. The 100 mg L⁻¹ Zn²⁺ stock solution was then mixed thoroughly and by the end of the mixing process, it would produce a clear and colourless solution.

4.2.2.2 Preparation of Zincon monosodium salt stock solution

10.5 mg zincon monosodium salt ($M_w = 463.42 \text{ g mol}^{-1}$) was weighed and made up to 50 mL solution with Milli-Q water. The 200 mg L⁻¹ zincon solution was then mixed thoroughly to ensure the powder was completely dissolved.

4.2.2.3 Preparation of 5-Br-PAPs stock solution

5 mg 2-(5-Bromo-2-pyridylazo)-5-[N-propyl-N-(3-sulfopropyl)amino]phenol disodium salt dihydrate (5-Br-PAPs) ($M_w = 537.34 \text{ g mol}^{-1}$) was weighed and made up to 50 mL solution with Milli-Q water. The 100 mg L⁻¹ 5-Br-PAPs solution was then mixed thoroughly to ensure complete dissolution. The prepared solution was stored in refrigerated storage.

4.2.2.4 Preparation of 4 wt% PDADMAC solution

10 mL 20 wt% Poly(diallyldimethylammonium chloride) in H₂O (PDADMAC) was pipetted and made up to 50 mL with Milli-Q water within a volumetric flask. This was mixed thoroughly, producing a clear solution with a slight yellow tint, with 4 wt% PDADMAC concentration.

4.2.2.5 Preparation of bicarbonate buffer solution

95.4 mg of sodium carbonate ($M_w = 105.99 \text{ g mol}^{-1}$) and 764.5 mg of sodium bicarbonate ($M_w = 84.01 \text{ g mol}^{-1}$) were weighed and made up to 100 mL solution with Milli-Q water. The pH of the bicarbonate solution was then adjusted with the addition of diluted NaOH or HCl.

4.2.2.6 Preparation of 0.001 M phosphate buffered saline solution

1 tablet of phosphate-buffered saline was diluted into a 200 mL solution with Milli-Q water. It was then mixed thoroughly. By the end of the mixing process, the 0.001 M phosphate buffered saline solution would be clear and colourless.

4.2.2.7 Preparation of 0.1 M sodium fluoride solution

41.9 mg of sodium fluoride ($M_w = 41.98 \text{ g mol}^{-1}$) was weighed and diluted with Milli-Q water to make a 10 mL solution. This was mixed thoroughly, producing a clear colourless solution. A change of temperature may occur temporarily, during the mixing process.

4.2.2.8 Preparation of 300 mg L⁻¹ dimercaptosuccinic acid

3 mg of dimercaptosuccinic acid ($M_w = 182.22 \text{ g mol}^{-1}$) was weighed and diluted to a 10 mL solution with Milli-Q water. The 300 mg L⁻¹ solution was then mixed thoroughly, producing a clear colourless solution. The solution was then stored in refrigerated storage.

4.2.2.9 Preparation of 5 M NaCl solution

29.2 g of sodium chloride (NaCl) powder ($M_w = 58.44 \text{ g mol}^{-1}$) was weighed and made up to 100 mL solution with Milli-Q water. The mixture was placed in an enclosed vessel on top of a heating plate at 80 °C, and stirred for 3 h, if necessary. By the end of the mixing process, all NaCl powder would dilute completely and produce a clear and colourless 5 M NaCl solution.

4.2.2.10 Preparation of 100 mg L⁻¹ interference ion stock solution

An appropriate amount of interference ion salt (1.8 mg sodium carbonate ($M_w = 105.99 \text{ g mol}^{-1}$), 1.4 mg sodium bicarbonate ($M_w = 84.01 \text{ g mol}^{-1}$), 3.6 mg iron (II) chloride tetrahydrate ($M_w = 198.81 \text{ g mol}^{-1}$), 1.9 mg potassium chloride ($M_w = 74.55 \text{ g mol}^{-1}$), 1.5 mg sodium phosphate dibasic ($M_w = 141.96 \text{ g mol}^{-1}$), 1.6 mg potassium nitrate ($M_w = 101.10 \text{ g mol}^{-1}$), 4.9 mg iron (III) chloride hexahydrate ($M_w = 270.30 \text{ g mol}^{-1}$), 4.0 cobalt chloride hexahydrate ($M_w = 237.93 \text{ g mol}^{-1}$), 3.9 mg copper sulphate pentahydrate ($M_w = 249.69 \text{ g mol}^{-1}$), 4.3 mg calcium sulphate dihydrate ($M_w = 172.17 \text{ g mol}^{-1}$)) was weighed and diluted with Milli-Q water to form a 10 mL solution. The concentrations of these solutions were 100 mg L⁻¹, upon usage, further dilution from this stock solution might be necessary. The solutions were mixed thoroughly, producing a clear solution. It is stored in safe storage or under the fume hood.

4.2.3 UV/Vis spectrophotometry for Zn²⁺ detection

4.2.3.1 Reaction time

The UV/Vis measurement was undertaken using a Perkin Elmer portable single beam spectrophotometer with 1.5 mL polystyrene disposable cuvette with Zincon monosodium salt

as a colorimetric reagent for zinc detection can be done at the wavelength of 615 nm. For observation of the reaction time, the 1000 μL sample was reacted with 100 μL of Zincon monosodium salt in respective concentration within the 10-1000 mg L^{-1} range and left to react for 10 min, before the spectroscopic measurement was done. Each data point was repeated three times.

4.2.3.2 Effect of zincon concentration

The effect of zincon concentration was observed and measured at 615 nm. In the observation of the effect of Zincon concentration, 100 μL Zincon with concentration ranging from 10-200 mg L^{-1} was added to a 1000 μL 1 mg L^{-1} Zn^{2+} solution. The reaction was left for 5 min before the spectrophotometric measurement was done. Each data point was repeated three times.

4.2.3.3 Effect of zincon volume

The effect of zincon volume on the measured absorbance at 615 nm was observed by varying the volume of 100 mg L^{-1} Zincon solution within the 20-120 μL volume range. After the addition of the colorimetric reagent to the 1000 μL 1 mg L^{-1} Zn^{2+} sample followed by a 5 min incubation period, the spectrophotometric measurement was done. Each data point was repeated three times.

4.2.3.4 Effect of Zn^{2+} concentration

The effect of Zn^{2+} concentration on the measured absorbance upon reaction with 100 μL 100 mg L^{-1} Zincon monosodium salt was observed, creating a calibration curve for this optimised reaction. A stock solution of Zn^{2+} was diluted to produce 1000 μL Zn^{2+} solutions within the 0-1 mg L^{-1} concentration range. The sample solution was then reacted with 100 μL 100 mg L^{-1} each and incubated for 5 min before absorbance measurement at 615 nm. Each data point was repeated three times.

4.2.4 Microfluidics paper-based analytical device (μPAD) development for Zn^{2+} detection in the water sample

4.2.4.1 μPAD design

The design of μPAD in this study followed the design for Ni^{2+} -detection μPAD (Circular μPAD M04 and M05) discussed in Chapter 2. This design was demonstrated to be optimal for reagent contact and colour development in Chapter 3.

4.2.4.2 μPAD fabrication

The μPAD fabrication process in this study followed the fabrication step for the Ni^{2+} -detection μPAD discussed in Chapter 2. The fabrication step involved wax printing the design on a

Whatman® filter paper grade 1 with Xerox ColorQube 8570 solid ink printer, followed by wax-melting by passing the printed paper through the office laminator. The reagents were then introduced to the paper and left to dry. The dried μ PAD was then laminated and stored or ready for use. The complete step-by-step method of fabrication is provided in Chapter 2.

4.2.4.3 μ PAD data collection

The data collection step for the prepared Zn^{2+} detection μ PAD followed the data collection step of Ni^{2+} -detection μ PAD in Chapter 2. Prepared μ PAD can be submerged in the sample solution for 5 min before a picture of the μ PAD would be taken with a smartphone camera. In this study, the smartphone used was Samsung Galaxy S20, unless otherwise stated. The picture-taking step was aided by a cardboard black box, acting as a photography light box to ensure the picture quality for further analysis. The colour intensity of the sample wells was then compared to the colour intensity of the reference circle to obtain the average colour intensity of the μ PAD. Zn^{2+} concentration can then be interpolated by comparing the average colour intensity measured on the μ PAD with the previously-constructed calibration curve.

4.2.4.4 μ PAD optimisation

4.2.4.4.1 Reaction time

4.2.4.4.1.1 Zincon μ PAD

In order to obtain the reaction time for zincon μ PAD, the sample wells were loaded with 10 μL 10-200 mg L^{-1} Zincon monosodium salt and left to dry. It was then dipped into a 10 mL 10 mg L^{-1} Zn^{2+} solution. A picture of the device was taken before contact with the sample solution and every 2 minutes after, up to 10 minutes after the reaction. The colour intensity of the sample wells was then measured using ImageJ, by measuring the red channel of RGB after inversion of the image. The intensity was compared to the intensity of the reference circle in the middle of the μ PAD.

4.2.4.4.1.2 5-Br-PAPs μ PAD

The reaction time of the 5-Br-PAPs upon incorporation into μ PAD was observed within the 3-20 mg L^{-1} concentration range. The prepared device was dipped into 10 mL 10 mg L^{-1} Zn^{2+} solution and pictures of the device were taken every 2 min for 10 min. Image analysis was then done on the pictures obtained. Each data point was repeated three times.

4.2.4.4.2 Optimisation of reagent concentration

4.2.4.4.2.1 Zincon μ PAD

Similar to nioxime μ PAD optimization Chapter 2, the Zincon μ PAD optimization process would also be achieved using the Box-Behnken design of the experiment followed by an analysis of the

standardized effect, main effects, response surface, and contour plot. The design of this experiment involved three reagents: zincon monosodium salt, poly(diallyldimethylammonium chloride), and bicarbonate buffer. The concentration of each of the reagents was coded with -1 being the minimum concentration and +1 being the maximum concentration loaded into the μ PAD. For the optimization process, the range of concentration used was between 50-150 mg L⁻¹ Zincon monosodium salt, 2-6 wt% PDADMAC, and 0-0.1 M bicarbonate buffer.

4.2.4.4.2.2 5-Br-PAPs μ PAD

Following the steps in previous studies on the development of μ PAD for metal detection in this research, an optimisation step was employed through the Box-Behnken design of the experiment. This optimisation process involved analysis of standardised effects, main effects, response surface, and contour plot. The concentration of the reagents observed in this study was coded with -1 being the minimum concentration and +1 as the maximum concentration. For 5-Br-PAPs, the concentration tested were between 10-100 mg L⁻¹. Whereas for PDADMAC, the concentration range was within 0-4 wt%; and for PBS buffer was within the 0-0.01 M concentration range.

4.2.4.4.3 Calibration curve or effect of Zn²⁺ concentration

The calibration curve for Zn²⁺ detection was constructed through the same methods as one used in the construction of the calibration curve for Ni²⁺ detection in Chapter 2. For zincon μ PAD, the μ PAD deposited with 100 mg L⁻¹ zincon monosodium salt, 4 wt% PDADMAC, and 0.1 M bicarbonate buffer at pH 9 was dipped into different sample solutions containing Zn²⁺ in the concentration range of 0-10 mg L⁻¹. The colour intensity measurement was done on the picture of the μ PAD after 5 min of reaction time. Each data point was repeated three times.

Whereas for 5-Br-PAPs μ PAD, the optimised 5-Br-PAPs μ PAD containing 10 μ L 100 mg L⁻¹ 5-Br-PAPs, 10 μ L 4 wt% PDADMAC, and 10 μ L 0.01 M PBS buffer in the two-layered device was used for the test. This developed μ PAD was then dipped into 10 mL Zn²⁺ sample solution within the 0-2.5 mg L⁻¹ concentration range. Each data point was repeated three times.

4.2.4.5 μ PAD selectivity test

The selectivity test for Zn²⁺ detection μ PAD was tested by dipping the prepared μ PAD into a sample solution containing Zn²⁺ at 10 mg L⁻¹ concentration, with or without the addition of one interfering ion solution. The interfering ions tested for Zn²⁺ detection were : Fe²⁺, Fe³⁺, Ni²⁺, Cu²⁺, Co²⁺, Na⁺, K⁺, Cl⁻, Ca²⁺, NO₃⁻, HCO₃⁻, SO₄²⁻, and PO₄³⁻. The prepared device was dipped and left to react for 5 min before a picture of the device was taken for the image analysis process. Interference was defined as the measured colour intensity of more than 10% of the control data. Each data point was repeated three times.

4.2.4.6 μPAD stability test

The stability test was conducted by preparing the Zn²⁺ detection μPAD for 4 weeks of testing. The device would be stored in a cool, dry storage space before use. The stability was defined as the change of measured colour intensity after a certain duration of storage. At the time of testing, the stored device was dipped into 10 mL 2 mg L⁻¹ Zn²⁺ solution. The colour measurement was obtained on the day of fabrication, day-1 after fabrication, day 2, day 3, day 4, day 7, day 14, day 21, and day 28. On each day of measurement, the measurement was repeated three times.

4.2.5 Development of onsite preconcentration workflow for Zn²⁺ preconcentration

4.2.5.1 Observation on the effect of pH in Zn²⁺ preconcentration with Lewatit SP resin

The effect of pH in the Zn²⁺ preconcentration process with 0.1 g Lewatit SP was observed following the method described in the previous chapter for Ni²⁺ preconcentration (Chapter 3). The resin was placed in a beaker filled with 50 mL solution of 3 mg L⁻¹ Zn²⁺ with adjusted pH within the range of 4-8. The solution was then stirred at 100 rpm for 20 min and the solution was sampled (100 μL x 3) immediately, at minute-1, 2, 3, 4, 5, 10, 15, and 20. The concentration of Zn²⁺ was measured with UV/Vis spectrophotometry.

4.2.5.2 Observation on the effect of initial Zn²⁺ concentration

The effect of initial Zn²⁺ concentration to the preconcentration process with Lewatit SP in cafetière settings followed the previous experiment in this study, described in Chapter 3. 300 mL Zn²⁺ solution at 0.2-0.8 mg L⁻¹ Zn²⁺ concentration range was placed in a cafetière, where the plunger had been replaced by a modified basket, as discussed in Chapter 3, filled with 2.6 g Lewatit SP. The solution was then plunged for 5 min, and sampled (100 μL x 3) immediately, at minute-1, 2, 3, 4, and 5. The concentration of Zn²⁺ was measured with UV/Vis spectrophotometry.

4.2.5.3 Elution of Zn²⁺ from Lewatit SP resin

Elution of Zn²⁺ from Lewatit SP resin was following the developed workflow in Chapter 4. The elution process was done by placing the basket in a 30 mL 5 M NaCl solution for 5 min. At the end of the elution process, the solution was sampled (100 μL x 3) for Zn²⁺ concentration measurement using UV/Vis spectrophotometry.

4.2.5.4 Water sampling

The water samples used in this research were obtained from various sources. Milli-Q water sample also referred to as laboratory (lab) water, was obtained from the Milli-Q filtration machine in the Biology Department of the University of Hull. The tap water sample was obtained from the water tap at the sink of the chemistry laboratory C208 in the Chemistry building of the

University of Hull and provides a carbonate-rich matrix to test the devices given the water is sourced from the East Yorkshire chalk aquifer (of Cretaceous age). Unless otherwise stated, the tap water sample was obtained immediately prior to use.

The last water sample was obtained from a sampling point of a Sustainable Drainage System (SuDS) available at the University of Hull. Unless otherwise stated, the sample would be taken from the sampling point near the car parking building inside the University grounds. This water was sampled from a swale (small linear treatment wetland) receiving runoff from a multi-story car park using a sampling pole. This sample provides a useful real-world environmental sample that is potentially enriched in Zn (e.g. from wear and tear of galvanised brake discs). The sampled water would then be stored in a plastic sample bottle and left to settle overnight. The next day, the water sample would be filtered with 0.45 μm filter paper, unless otherwise stated.

4.2.6 Statistical analysis

Methods of statistical analysis employed within this chapter follows the previously described method in section 2.2.5.

4.3 Result: μPAD for Zn^{2+} detection with zincon as a colorimetric reagent

Zn^{2+} detection μPAD with zincon monosodium salt as a colorimetric reagent had been developed through the course of this research, full results and discussions on this device are provided in Appendix 3. This μPAD was optimised as a two-layered device with 10 μL 4 wt% PDADMAC and 10 μL 0.1 M bicarbonate buffer at pH 9 on one layer, and 10 μL 100 mg L^{-1} zincon monosodium salt. Upon testing against Zn^{2+} solution within 0-10 mg L^{-1} Zn^{2+} concentration, the device showed a linear correlation with a limit of detection of 2 mg L^{-1} (Figure 73). However, further testing on the device performance in the presence of interfering ions (available in Appendix 3), and the colorimetric reagent showed interference in most of the tested ions, including ones that may abundantly be available in freshwater systems, such as Ca^{2+} or K^{+} . This interference meant that numerous masking processes may be required to ensure the robustness of the device. Therefore, the development of this device was halted in favour of more potential colorimetric reagents.

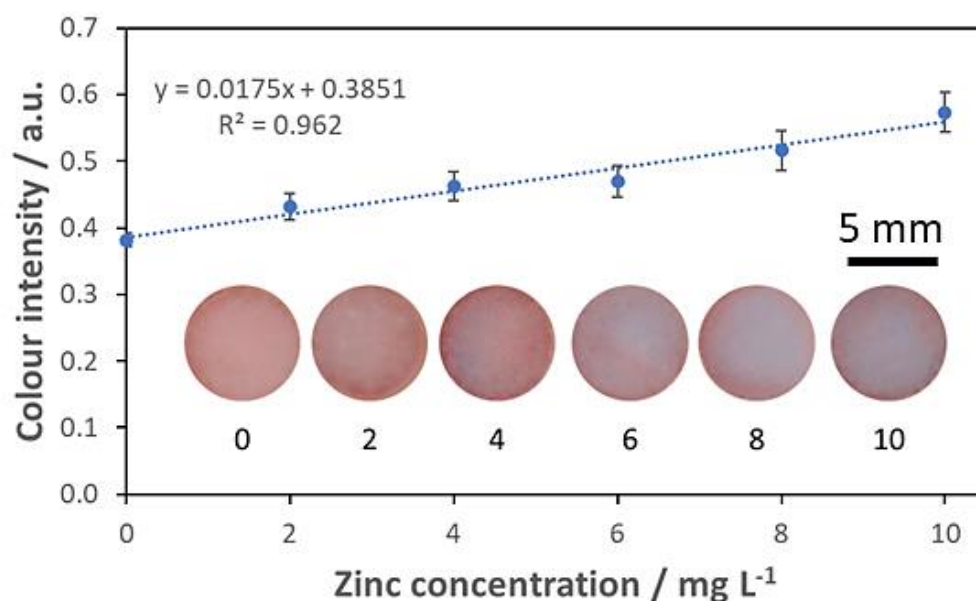


Figure 73 Measured colour intensity on the sample wells of the device containing 10 μL Zincon monosodium salt as colorimetric reagent (100 mg L^{-1} zincon monosodium salt, 4 wt% PDADMAC, and 0.1 M bicarbonate buffer pH 9).

4.4 μPAD for Zn^{2+} detection with 5-Br-PAPs as colorimetric reagent

5-Br-PAPs is an abbreviation for a commercially available dye known as 2-(5-Bromo-2-pyridylazo)-5-[N-propyl-N-(3-sulfopropyl)amino]phenol. It is available in the form of disodium salt and is known to be used as a reagent for metals such as copper and iron in the flow injection-catalytic photometric method [175]. It has also been used in Zn^{2+} detection in different sample matrices, such as drinking water and animal feed [100]. In this research, 5-Br-PAPs were chosen as an alternative reagent for Zn^{2+} detection with a colorimetric approach. However, due to the lack of research on this colorimetric reagent for μPAD colorimetric-based detection, observation of the 5-Br-PAPs through UV/Vis spectrophotometry was done and discussed in section 4.4.1. The observation on the use of 5-Br-PAPs as a colorimetric reagent in μPAD format is discussed in section 4.4.2.

4.4.1 Observation on 5-Br-PAPs as a colorimetric reagent for Zn^{2+} detection using UV/Vis spectrophotometry

The observation of the performance of 5-Br-PAPs was done through UV/Vis spectrophotometry measurement at 552 nm wavelength [99]. This was done to identify and characterise the performance of the colorimetric reagent with the conventional analytical method, before applying the reaction to a relatively novel analytical method, μPAD . In section 4.4.1.1, the reaction time was observed, whilst, in section 4.4.1.2, further observations were undertaken to

investigate the performance of the colorimetric reagent in Zn^{2+} detection with UV/Vis spectrophotometry method.

4.4.1.1 Reaction time

As shown in Figure 74, the performance of 5-Br-PAPs was observed in three different concentrations: 1, 3, and 5 $mg\ L^{-1}$ against 10 $mg\ L^{-1}\ Zn^{2+}$. In the illustrated figure, it is evident that the highest measured absorbance was observed upon reaction with the highest concentration of 5-Br-PAPs. At 5 $mg\ L^{-1}$ 5-Br-PAPs, within the first minute of reagent introduction, the absorbance spiked up to 0.250. However, this is followed by a slight decrease in the absorbance down to around 0.240 by minute 4. This spike in absorbance may be due to the reagent introduction step employed in this experiment. For the purpose of this experiment, 1000 μL of the Zn^{2+} sample was placed in the cuvette, whereupon 100 μL 5-Br-PAPs were introduced. Due to this step, the reagent reacted slowly from the top down in the vessel, creating instability in the absorbance. This would also explain further instability in the absorbance up to minute 10 of the observation.

A similar pattern was observed in other 5-Br-PAPs concentrations. Upon introduction of 3 $mg\ L^{-1}$ 5-Br-PAPs, the absorbance also spiked up to 0.150. Interestingly, this reaction showed more fluctuation compared to the 5 $mg\ L^{-1}$ 5-Br-PAPs. However, it also stabilised after 10 minutes of reaction and observation. Conversely, upon the addition of 1 $mg\ L^{-1}$ 5-Br-PAPs, the absorbance was comparatively more stable. The absorbance measured, however, was notably lower than the other two 5-Br-PAPs concentrations. Through this observation, the reaction time for the 5-Br-PAPs reaction with Zn^{2+} solution was concluded to be 10 min. Therefore, all UV/Vis spectrophotometry measurements done for detection of Zn^{2+} with 5-Br-PAPs would be done after 10 min of the incubation period.

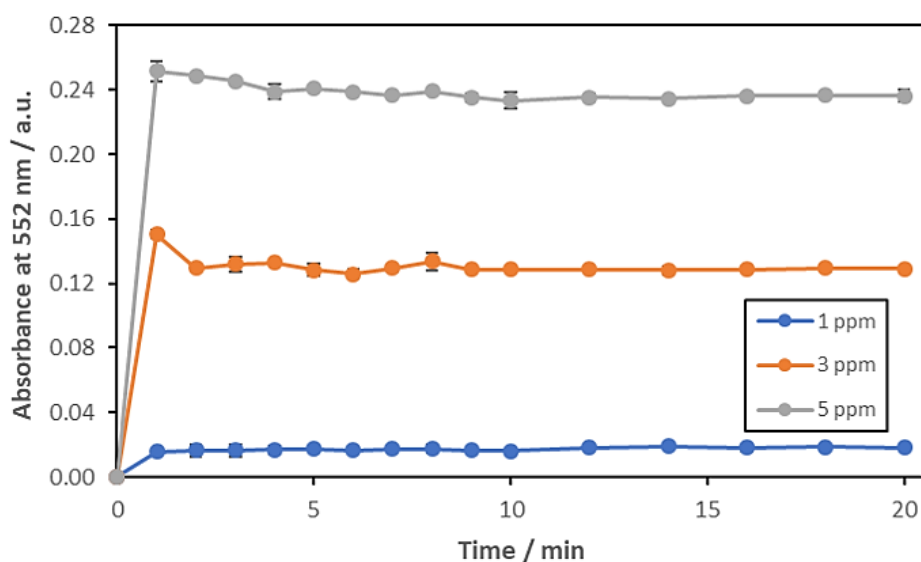


Figure 74 Reaction time of 100 μL 1, 3, and 5 mg L^{-1} 5-Br-PAPs upon addition to 1000 μL sample solution containing 10 mg L^{-1} Zn^{2+} , absorbance was measured at 552 nm, error bars illustrating standard deviation ($n=3$).

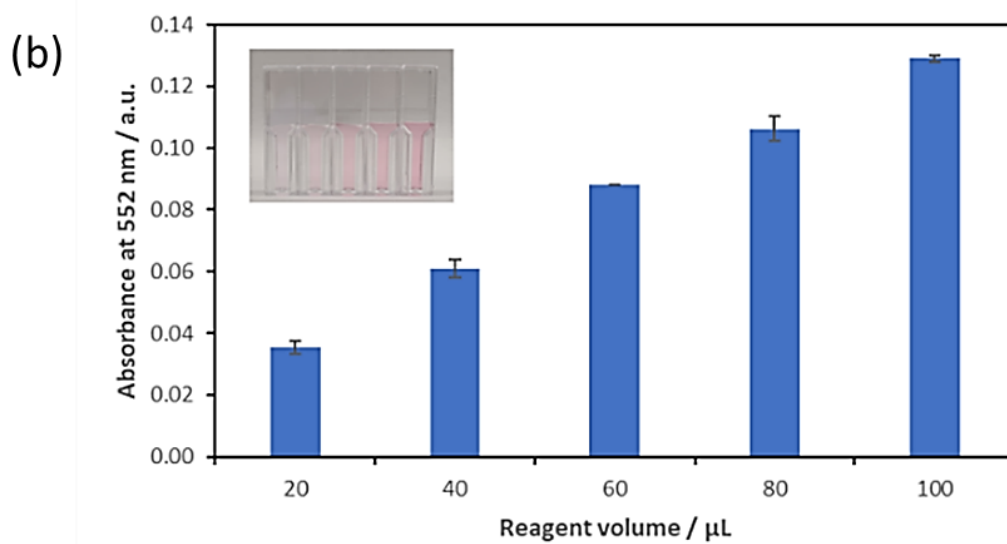
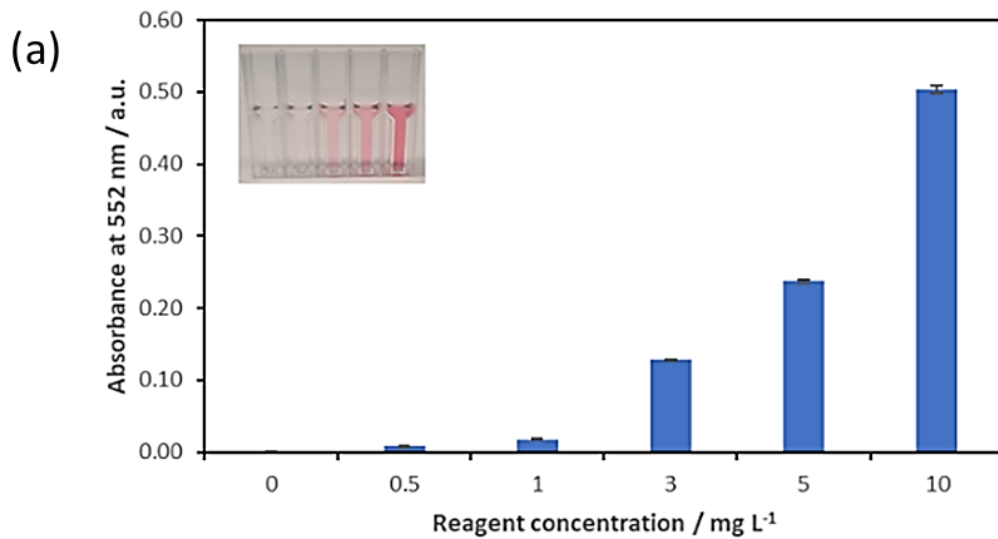
4.4.1.2 Observation on the effects of 5-Br-PAPs concentration, 5-Br-PAPs volume, sample pH range, and calibration curve for Zn^{2+} detection

A further observation was made on the effect of 5-Br-PAPs concentration upon reaction with Zn^{2+} solution. In Figure 75a, the effect of the colorimetric reagent was vividly shown through absorbance measurement and provided illustration. With the increase of 5-Br-PAPs concentration, the colour at the endpoint of the reaction changed from visibly colourless to magenta. It is evident that the increase in 5-Br-PAPs within the tested range of 0.5-10 mg L^{-1} can be correlated to the increase in absorbance measured at the wavelength of 552 nm. Further, in Figure 75b, the effect of reagent volume is presented within 20-100 μL . Through this experiment, it was evident that the increase in the reagent volume introduced to the sample can also be correlated to the increase in the measured absorbance at 552 nm. This gradient in absorbance can also be seen visibly through the intensity of the colour at the endpoint of the reaction in the cuvette.

Figure 75c shows the effect of the initial sample pH value on the absorbance measured at the endpoint of the reaction. This observation was done to investigate the requirement for a buffer to ensure the robustness of the reaction upon detection of Zn^{2+} in environmental samples. The effect of pH was observed within the range of 4-8, covering both slightly acidic and alkaline environments typical of surface waters. It is evident that the reaction was able to produce the highest absorbance and most vivid colour change at a more neutral pH, rather than the extremes.

The absorbance measured increased between the pH value of 4 to 5, followed by a slight increase between 5 to 6. The absorbance then peaked at 7, which is the neutral pH and dropped notably at the initial pH of 8, the most alkaline value tested. Therefore, in this research, buffering at near neutral pH value may be beneficial to ensure an optimum reaction can be reached. This information would be used in the μ PAD development step, in choosing the buffer that would be added to the device.

Figure 75d shows the calibration curve constructed through the reaction between 100 μ L 5 mg L⁻¹ 5-Br-PAPs with 1000 μ L Zn²⁺ sample solution within the concentration range of 0-8 mg L⁻¹. In this illustration, it is evident that the colour of the endpoint of the reaction transitioned from light yellow to magenta, as provided in the figure. With the visible transition of colour, the measured absorbance at the endpoint by minute 10, after the reaction with a gradient concentration of the sample, also changed. The measured absorbance can be seen to correlate non-linearly with the change of Zn²⁺ concentration tested (Figure 75d). Taking the linear correlation within the 0-1 mg L⁻¹ range allowed for the calculation of the detection limit at 0.01 mg L⁻¹. This is lower than the US EPA National Recommended Water Quality for acute and chronic Zn²⁺ levels in the water, which is set at 0.12 mg L⁻¹ [34].



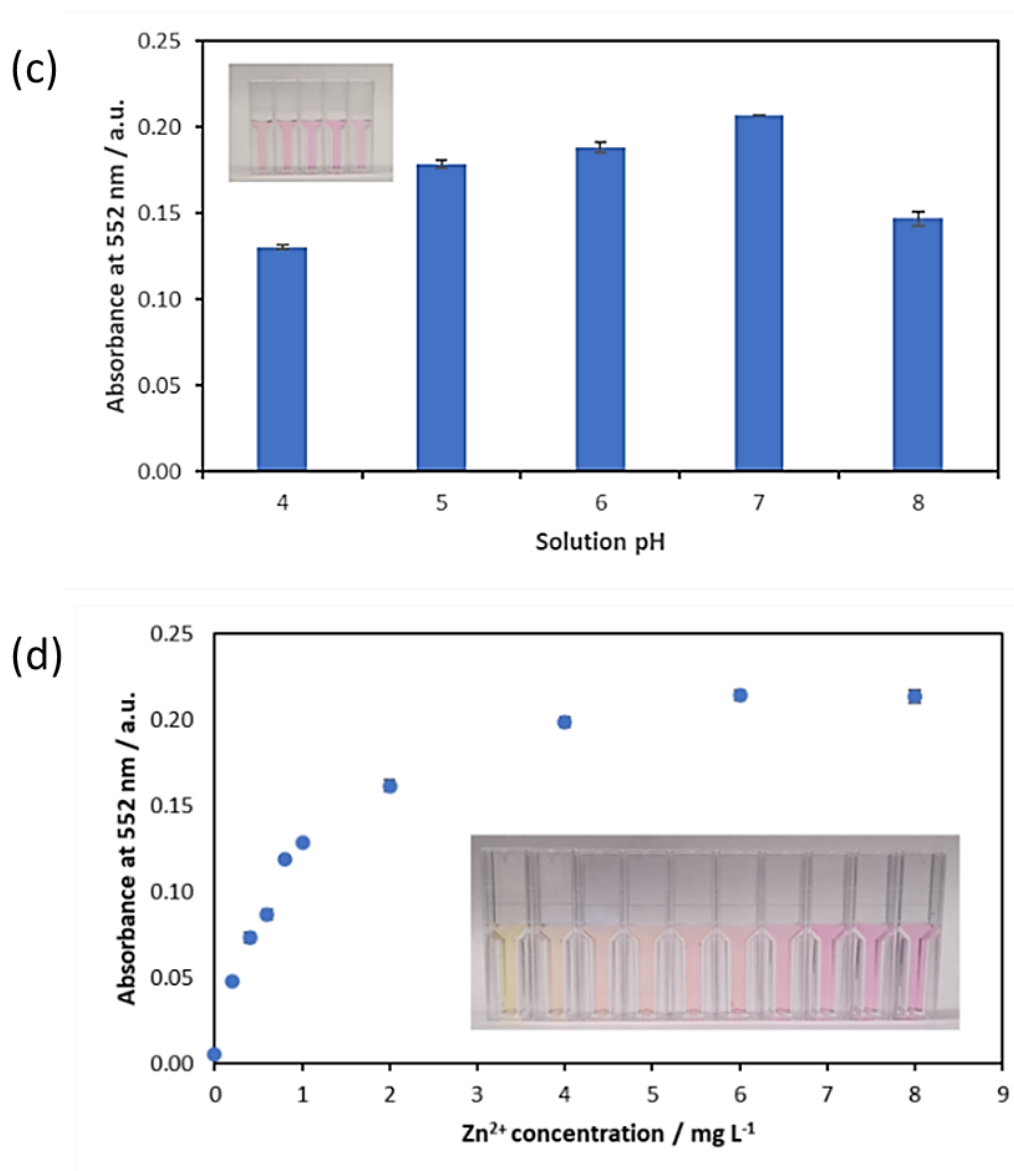


Figure 75 Observation, through absorbance at 552 nm and pictures of the endpoint of the experiment, on the effect of (a) 5-Br-PAPs concentration within 0-10 mg L⁻¹, (b) 5-Br-PAPs volume within 20-100 μ L, and (c) initial sample pH value upon reaction with 1000 μ L 10 mg L⁻¹ Zn²⁺ solution ($n=3$). While (d) calibration curve was constructed with 5 mg L⁻¹ 5-Br-PAPs reacted with 0-8 mg L⁻¹ Zn²⁺ solution ($n=3$).

4.4.2 Design and optimisation of μ PAD for Zn²⁺ detection using 5-Br-PAPs as colorimetric reagent

The performance of the colorimetric reagent for Zn²⁺ detection, observed through the UV/Vis spectrophotometry analytical method showed satisfactory results. 5-Br-PAPs allowed for the detection of Zn²⁺ at a lower concentration than the value set for Zn²⁺ in the US EPA National Recommended Water Quality for aquatic life, which was 0.12 mg L⁻¹ [34]. The colorimetric reagent was able to detect down to 0.01 mg L⁻¹, which was ten times lower than the limit.

Therefore, the development of μ PAD with 5-Br-PAPs as a colorimetric reagent proceeded. In this section of the chapter, various steps of optimisation and observation of its performance were made. In section 4.4.2.1, the reaction time of μ PAD loaded with 5-Br-PAPs was observed as a baseline to ensure the incubation time required to obtain stable results. In section 4.4.2.2, the performance of the optimised 5-Br-PAPs μ PAD was observed through a gradient of Zn^{2+} concentration. While section 4.4.2.3 describes the performance of the μ PAD in the presence of various potentially interfering ions. Lastly, in section 4.4.2.4, the stability of the developed μ PAD was observed to ensure the storage condition and period that would preserve the performance of the μ PAD.

4.4.2.1 Reaction time

Reaction time for 5-Br-PAPs μ PAD was tested with the procedure described in section 4.2.4.4.1.2 5-Br-PAPs μ PAD. Figure 76 shows the differences in measured colour intensity in the sample wells of the μ PAD from the moment of dipping into the sample solution to 20 minutes after the sample introduction. For 3 and 5 $mg\ L^{-1}$ 5-Br-PAPs concentration, the measured colour intensity did not differ notably between each other for the entirety of the observed time period. Within these concentrations, the measured colour intensity peaked and stabilised after 2 minutes. Similar patterns can be seen in different concentrations, which were 10 and 20 $mg\ L^{-1}$ 5-Br-PAPs concentrations. However, the measured colour intensity was notably higher for these two concentrations; with a higher concentration of 5-Br-PAPs producing higher colour intensity.

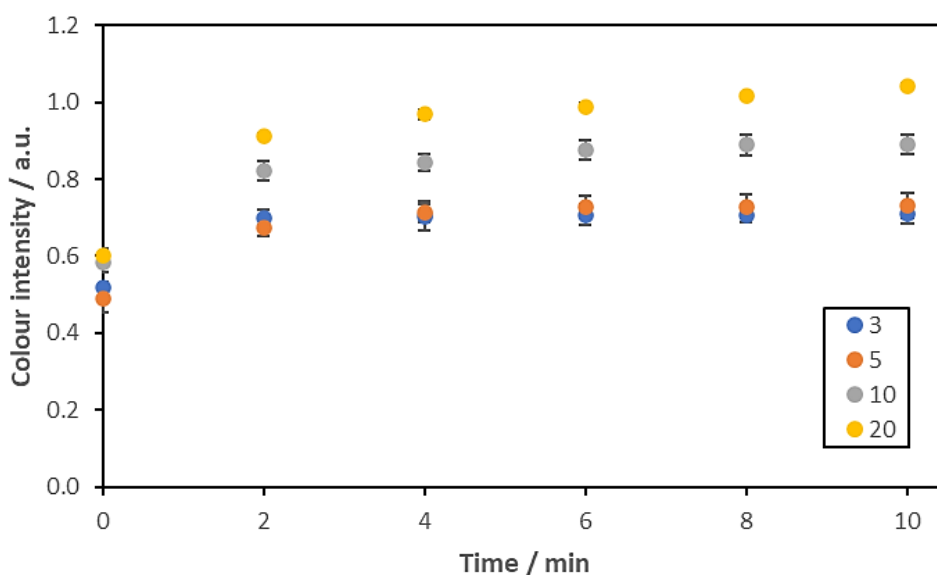


Figure 76 Reaction time of the 5-Br-PAPs μ PAD loaded with the colorimetric reagent within the 3-10 $mg\ L^{-1}$ concentration range, observed up to minute 10, after dipping into 10 $mg\ L^{-1}$ Zn^{2+} solution ($n=3$).

4.4.2.2 Linearity of 5-Br-PAPs μ PAD for Zn^{2+} detection between 0-2.5 $mg L^{-1}$

Calibration curve for 5-Br-PAPs μ PAD was tested within the 0-2.5 $mg L^{-1}$ Zn^{2+} concentration range following the method described in section 4.2.4.4.3. This concentration range was chosen based on a preliminary study where the μ PAD was tested in a wider concentration range of 0-10 $mg L^{-1}$. This resulted in a non-linear correlation between the measured colour intensity to the increase in Zn^{2+} concentration. Therefore, the concentration range was reduced to the linear range, which was 0-2.5 $mg L^{-1}$.

Figure 77 shows the linear correlation between the increase of Zn^{2+} concentration with the measured colour intensity. The colour on the sample well can be seen to transition from yellow to magenta within the tested concentration range. The detection limit calculated from this data resulted in a LOD of 0.5 $mg L^{-1}$, just five times higher than the US EPA National Recommended Water Quality acute and chronic Zn^{2+} concentration, which was 0.12 $mg L^{-1}$ [34]. Therefore, the integration of a preconcentration step would notably improve the detection performance of the developed μ PAD.

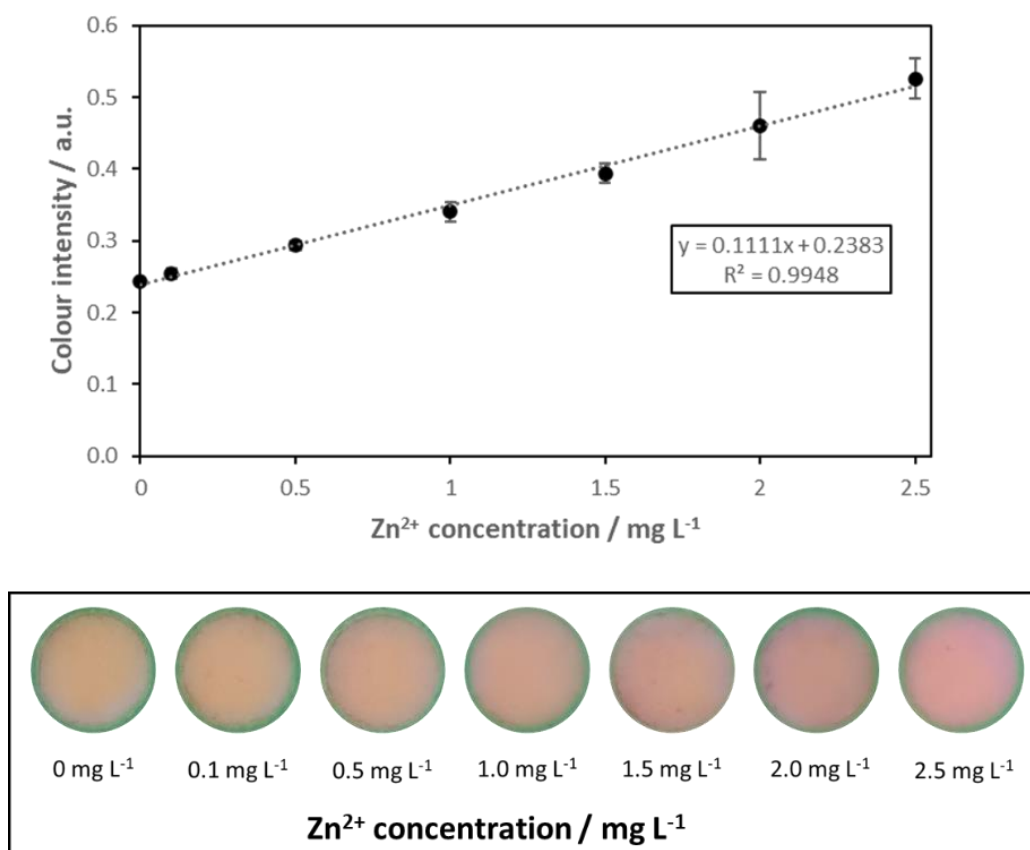


Figure 77 Linear correlation, with error bars illustrating the standard deviation of the data points, between the increase in Zn^{2+} concentration between 0-2.5 $mg L^{-1}$ range to the measured colour intensity on the developed 5-Br-PAPs μ PAD ($n=3$).

4.4.2.3 Performance of 5-Br-PAPs μ PAD in the presence of other ions

The developed 5-Br-PAPs μ PAD performance was then tested in the presence of other commonly found ions in environmental water samples. Firstly, the 5-Br-PAPs μ PAD was tested in the presence of other metal ions: Ni^{2+} , Cu^{2+} , Co^{2+} , Fe^{2+} , and Fe^{3+} . Figure 78a shows the result of this observation, where a notable decrease in colour intensity was observed in the sample containing Cu^{2+} . This decrease in colour intensity is not visible to the naked eye's observation, similar to the decrease in intensity in the presence of Fe^{3+} . While samples containing Ni^{2+} and Fe^{2+} did not show a notable change in measured colour intensity. Interestingly, in the sample containing Co^{2+} , the measured colour intensity did not seem to decrease compared to the control (less than 5% difference). However, evidently, in Figure 78b, the colour at the endpoint of the reaction was vividly different – showing the colour purple instead of magenta. Therefore, aside from Cu^{2+} and Fe^{3+} , Co^{2+} was also added as a target masking agent in this μ PAD.

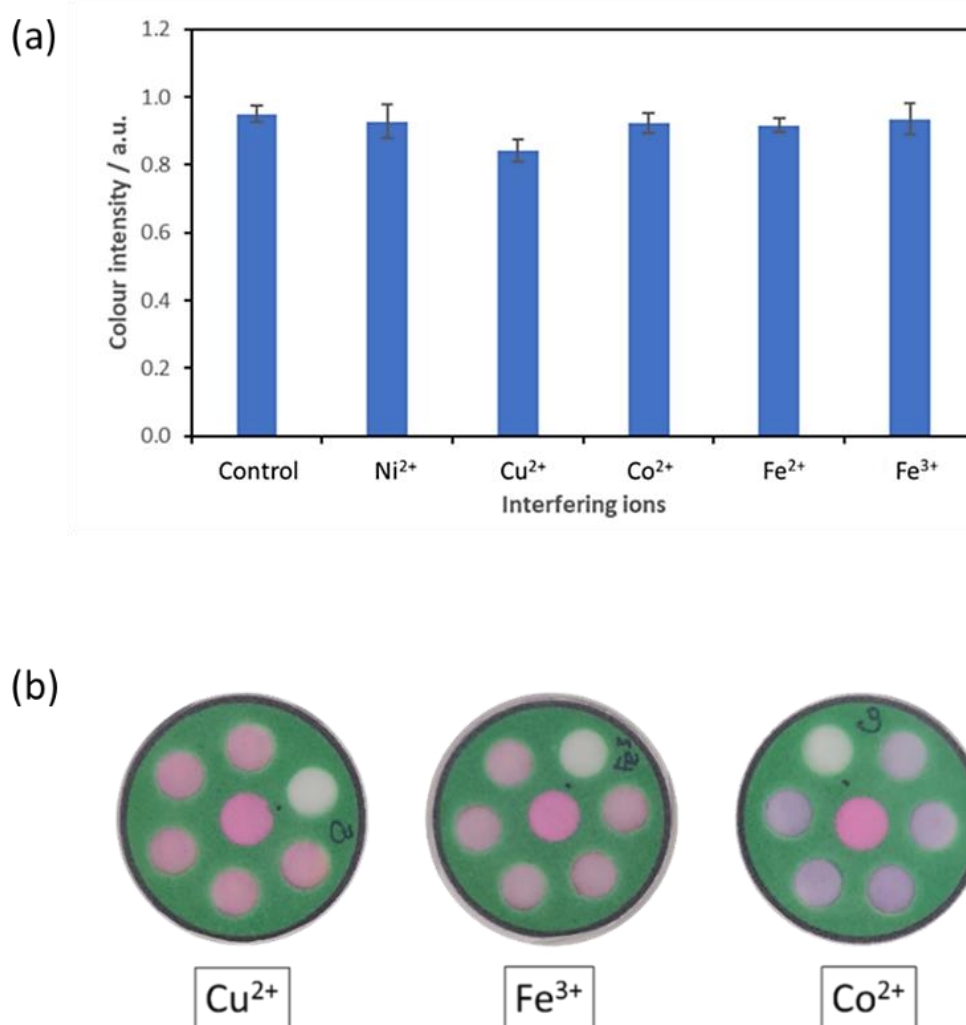


Figure 78 (a) Performance of 5-Br-PAPs in the presence of interfering metal ions: Ni^{2+} , Cu^{2+} , Co^{2+} , Fe^{2+} , and Fe^{3+} ($n=3$); (b) illustration of developed 5-Br-PAPs μ PAD after dipping into Cu^{2+} , Fe^{3+} , and Co^{2+} without masking layer.

In order to mask these target ions, 0.1 M NaF was used as a masking agent, as well as 300 mg L⁻¹ dimercaptosuccinic acid (DMSA), which has been known for metal chelation reaction producing relatively colourless complex [176, 177]. These masking agents were added in a third layer, for the sole purpose of stopping the interfering ions from reacting with the colorimetric reagent. The now three-layered device was then tested in the presence of various ions commonly found in environmental water samples. [Figure 79](#) shows the measured colour intensity on the sample well of the 5-Br-PAPs μ PAD after dipping into a sample solution containing other ion species. Evidently, the addition of a masking layer aided in the performance of the μ PAD in the presence of these ions. All measured colour intensities after the addition of masking agents were within a 5% difference with the control, which was deemed acceptable in comparison to the internal error and standard deviation of the μ PAD itself (RSD <5%).

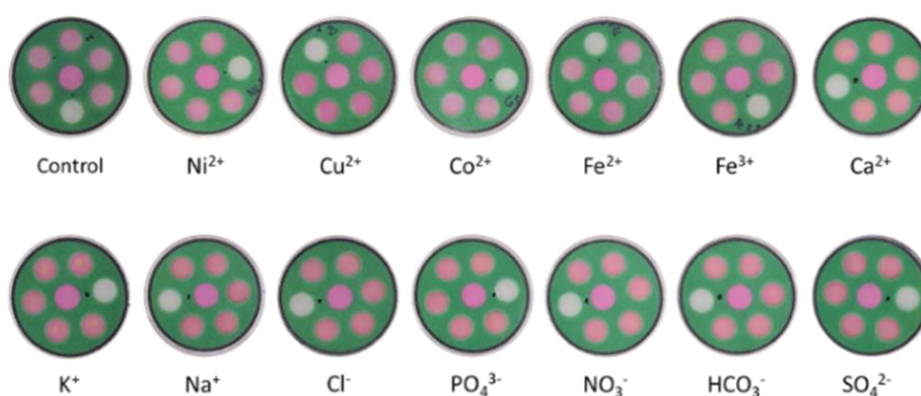
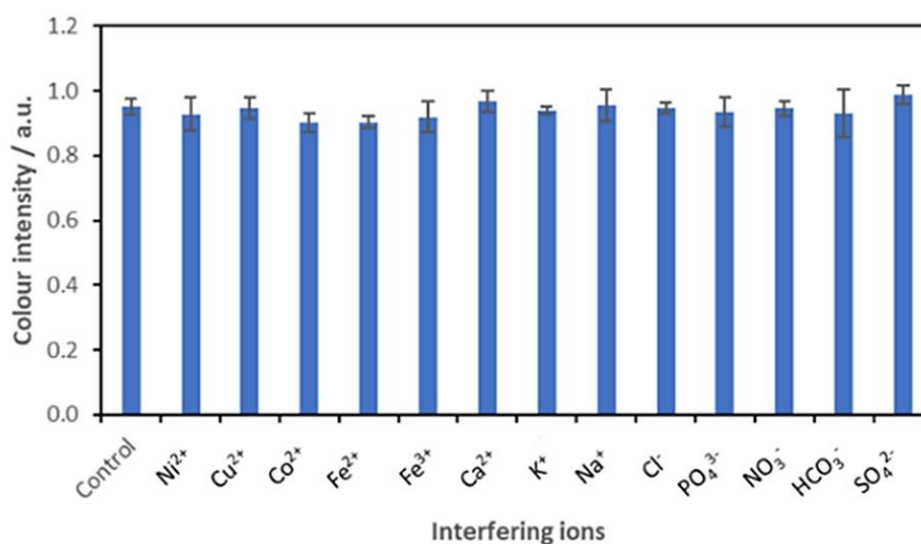


Figure 79 Performance of 5-Br-PAPs μ PAD for Zn detection in the presence of interfering ions commonly found along the target contaminant in the water sample through measured colour intensity and visible colour on μ PAD ($n=3$).

4.4.2.4 Stability of 5-Br-PAPs μ PAD

The last step in the development of 5-Br-PAPs μ PAD was to observe the stability of the μ PAD after a certain storage treatment and time. This was done to ensure the μ PAD would be able to be used and reliably produce detection results after a storage process. This observation was done following the methods described in section 4.2.4.6. Through preliminary observation, the colorimetric reagent 5-Br-PAPs may be affected by storage in non-refrigerated areas. Refrigeration of the reagent was able to extend the stability of the reagent for 2-3 days. Therefore, for the stability test of the μ PAD, these two different storage approaches were observed immediately to mitigate the potential instability of the colorimetric reagent.

Figure 80 shows the measured colour intensity measured on the sample well of the 5-Br-PAPs μ PAD after dipping into $2 \text{ mg L}^{-1} \text{ Zn}^{2+}$ solution. At day 0, which would be treated as control, the μ PAD was used within hours of fabrication. This allowed the μ PAD to be refrigerated, observing the initial effect of refrigeration on the colour intensity of the μ PAD. Evidently, the colour intensity already differed at this stage, with refrigerated μ PAD showing lower measured colour intensity. However, immediately the next day, the measured colour intensity for non-refrigerated μ PAD immediately dropped. While the refrigerated μ PAD also dropped in intensity, however in less notable magnitude than the non-refrigerated μ PAD. The colour intensity was stable around the dropped value in both cases up to day-3 for non-refrigerated μ PAD, while it stayed for up to day-7 in the refrigerated case. The conclusion drawn from this experiment was the limited stability of the μ PAD, in agreement with preliminary observation on the limited stability of the colorimetric reagent: 5-Br-PAPs. Therefore, for the purpose of this research, μ PADs would be made on immediate use basis – meaning that in further experiments involving this μ PAD, the μ PAD was made on the same day of use, eliminating possible errors due to storage. However, in further uses, the developed μ PAD can still be used after 7 days of refrigeration for semi-quantitative estimation of Zn^{2+} concentration in the water sample or after 3 days of non-refrigerated storage. In future research, the stability of the developed μ PAD may be improved through the addition of inert preservatives or better packaging and storage technology.

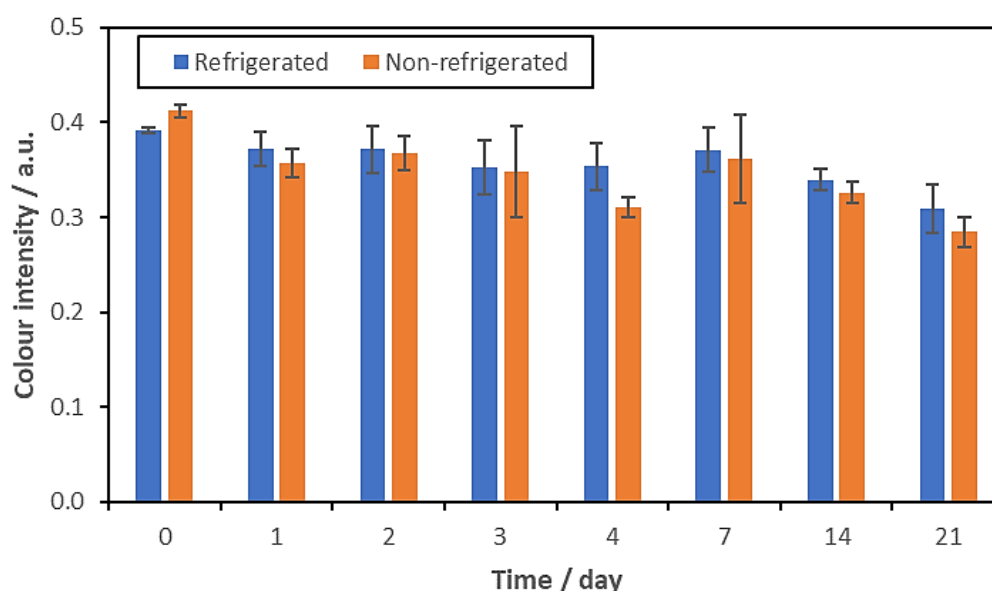


Figure 80 Measured colour intensity of the 5-Br-PAPs μ PAD after storage in a refrigerated (0-5 °C) and non-refrigerated (cool, dark storage at 20 ± 3 °C) area, after dipping into 10 mL $2 \text{ mg L}^{-1} \text{ Zn}^{2+}$ solution ($n=3$).

4.5 Preconcentration of Zn^{2+} with cafetière and Lewatit SP

As mentioned previously, for Zn^{2+} preconcentration, instead of working ground-up, the developed workflow involves Lewatit SP and cafetiere. Therefore, the adsorption performance of Zn^{2+} by the selected resin (Lewatit SP) was first observed in various sample pH conditions to ensure similar robustness can be achieved as Ni^{2+} adsorption (section 4.5.1). Subsequent testing then characterised Zn^{2+} adsorption performance at various initial Zn^{2+} concentrations (section 4.5.2). And lastly, the elution of Zn^{2+} out of the Lewatit SP resin, using the same workflow as Ni^{2+} elution (section 4.5.3).

4.5.1 Lewatit SP for Zn^{2+} adsorption in various initial pH conditions

The performance of Lewatit SP for Zn^{2+} adsorption in various initial sample pH conditions was observed to ensure the robustness of the resin for its utilisation in untreated environmental samples. As the workflow was developed for onsite preconcentration, ideally, the gathered environmental sample could not be treated to adjust the initial pH value; as this is an additional step that would increase the complexity of the workflow. Therefore, the adsorption performance in the initial sample pH value became important to observe whether the resin can produce similar results in the commonly found pH range for environmental samples – in this case, river water.

As shown in Figure 81, the adsorption of Zn^{2+} from provided sample solution (50 mL) initially proceeds in a similar manner within the first minute of stirring. Between the tested pH, slightly higher adsorption can be observed, even at the early stage, at the pH value of 6, followed by 5 and 7, and then 4 and 8 – which are the extremes. Throughout the duration, these differences between the adsorption performance became more evident, especially once it crossed the 5-minute stirring point.

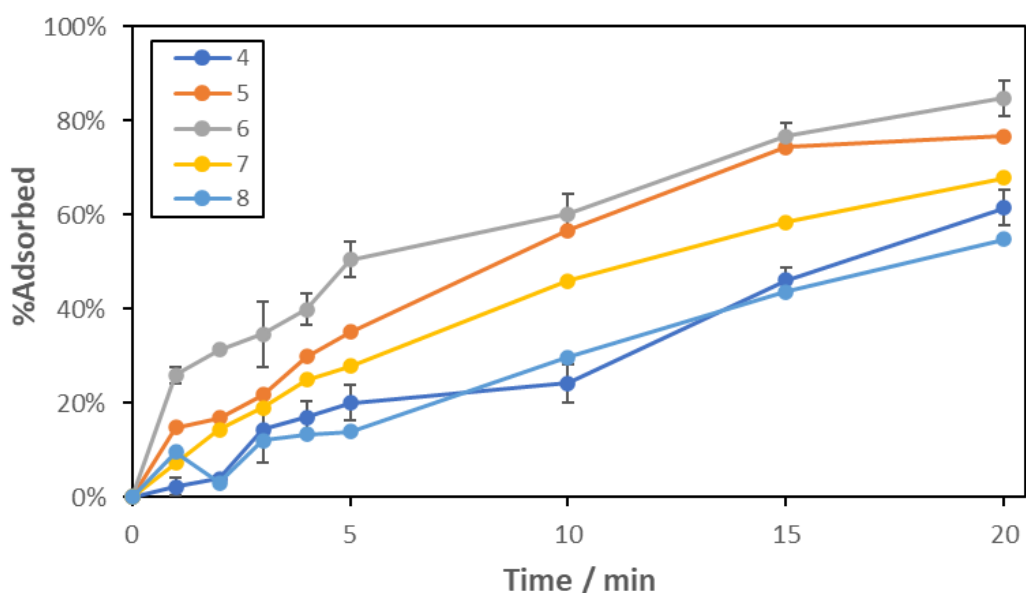


Figure 81 Adsorption of Zn^{2+} from 50 mL sample solution containing $3 \text{ mg L}^{-1} Zn^{2+}$ concentration and 0.1 g Lewatit® MonoPlus SP 112, stirred at 100 rpm with a magnetic stirrer for 20 min (n=3).

4.5.2 Lewatit SP for Zn^{2+} adsorption in various initial Zn^{2+} concentration

The performance of Lewatit SP resin was further observed for Zn^{2+} adsorption in various initial concentrations. This was done similarly for Ni^{2+} adsorption observation in Chapter 3. Despite having observed the adsorption performance in Ni^{2+} , Zn^{2+} adsorption may differ due to the resin's selectivity. Although not specified in the technical specification sheet for Lewatit SP, it is not uncommon for ion exchange resins to have levels of affinity to different ions. Lewatit TP, for example, has a bigger affinity towards divalent cations in the following order: copper > vanadium > uranium > lead > nickel > zinc > cadmium > iron > beryllium > manganese > calcium > magnesium > strontium > barium >>> sodium [178]. Lewatit SP may not follow similar order of affinity due to the difference in the active site – Lewatit TP with iminodiacetic acid and Lewatit SP with sulfonic acid. This difference would also affect the type of bond formed upon exchange; while Lewatit TP would function as a chelate and create a complex, Lewatit SP with the strong

acid on the site would not. Therefore, it is important to observe the performance separately rather than assuming a similar performance to Ni^{2+} adsorption.

Additionally, similar to the observation in Ni^{2+} adsorption, the experiment on the adsorption performance at different initial concentrations was important for the end goal of the workflow development. The preconcentration workflow developed in this study was meant to be used for onsite heavy metal preconcentration from an environmental water sample. Therefore, the developed workflow, at its adsorption step, should be robust and constant across a certain range of concentration. This makes an observation of the adsorption performance at different initial concentrations of Zn^{2+} .

In Figure 82, within the tested initial concentration range of $0.2\text{-}0.8\text{ mg L}^{-1}$, the adsorption performance was recorded across a 5-minute time range. Within the tested concentration range, the adsorption performance of the Lewatit SP resin was similar throughout the range. In the first minute, less than 20% of Zn^{2+} was adsorbed through the range of concentration. However, upon longer plunging duration, it can be seen that more Zn^{2+} was adsorbed, reaching up to 50% by minute 5. Comparing this to the Ni^{2+} adsorption process, it is evident that the resin was able to more effectively adsorb Ni^{2+} , as discussed in Chapter 2, than Zn^{2+} , possibly indicating a bigger affinity to Ni^{2+} than Zn^{2+} . However, the weaker affinity may also mean better elution, since it might be easier for the resin to replace Zn^{2+} with other ions. Therefore, further observation was made on the elution aspect before concluding the suitability of the developed workflow for the onsite Zn^{2+} preconcentration step.

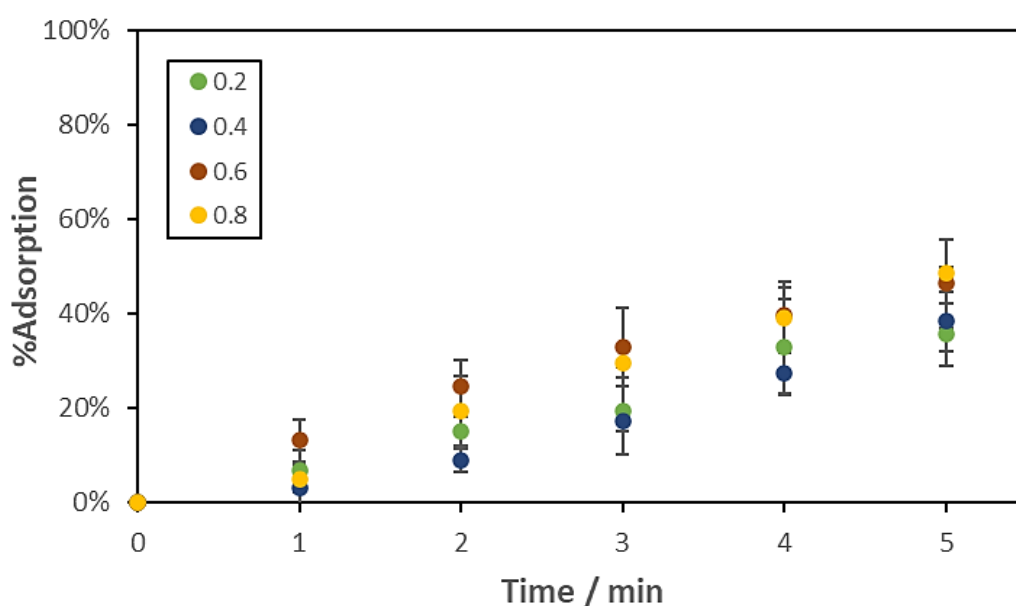


Figure 82 Adsorption performance of Lewatit SP resin in cafetiere system for Zn^{2+} adsorption within the initial concentration range of $0.2\text{-}0.8\text{ mg L}^{-1}$ after 5 min of plunging ($n=3$).

4.5.3 Elution of Zn^{2+} from Lewatit SP resin in the modified cafetiere system

Initial observation on the elution of Zn^{2+} from Lewatit SP resin was observed in Chapter 3. However, the experiment only observed the elution process in a mixed ion solution, rather than isolated Zn^{2+} incidence. Therefore, in this section, elution was observed after adsorption from the Zn^{2+} sample solution containing no other added interfering ions. Preliminary observation showed, however, unlike nioxime, 5-Br-PAPs are affected by the change of solution matrix from aqueous to saline (5 M NaCl). This complicated the elution process as a different calibration curve would be needed in the colorimetric measurement of Zn^{2+} concentration before and after the preconcentration process. Figure 83 shows the difference in absorbance (at 552 nm) of 5-Br-PAPs colorimetric reagent with Zn^{2+} diluted in Milli-Q water or 5 M NaCl. Therefore, for the purpose of this experiment, the data interpolation to calculate the concentration of Zn^{2+} was made using the corresponding curve depending on the sample matrix.

Despite the difference in the absorbance values, both curves can still detect below the US EPA recommendation for water quality criteria for aquatic life, which sets acute and chronic limits of Zn^{2+} contamination at 0.12 mg L^{-1} [34]. In water, 5-Br-PAPs can detect down to 0.01 mg L^{-1} Zn^{2+} concentration, while in 5 M NaCl, it can detect down to 0.04 mg L^{-1} .

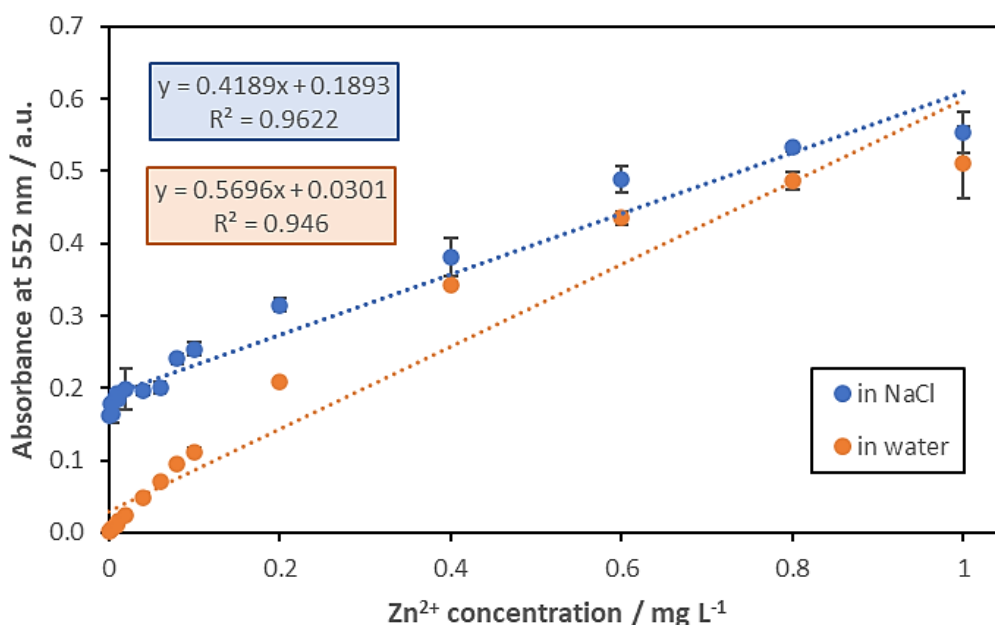


Figure 83 Calibration curve of 5-Br-PAPs for Zn^{2+} detection in (blue) 5 M NaCl and (orange) Milli-Q water within $0\text{-}1 \text{ mg L}^{-1}$ concentration range ($n=3$).

4.5.4 Elution of Zn²⁺ from 5 M NaCl

The elution of Zn²⁺ from a Zn²⁺-loaded 2.6 g Lewatit SP resin with 30 mL 5 M NaCl was observed and shown in Figure 84. This figure illustrates the correlation between the amount of Zn²⁺ loaded in the resin, measured through the concentration of Zn²⁺ loss through the adsorption process, to the performance of elution using the concentrated NaCl solution. As shown in the figure, the amount of loaded Zn²⁺ in the resin varied throughout the different processes, however, generally, it was between 0.01-0.07 mg Zn²⁺. The variation of the amount of Zn²⁺ adsorbed was made by varying the initial concentration of the sample solution. The experiment showed an indication of a non-linear correlation between the amount of Zn²⁺ in the resin to the amount of Zn²⁺ eluted, where more Zn²⁺ can be eluted from resin loaded with less Zn²⁺. The elution performance showed a potential decrease with the increase of the Zn²⁺ in the resin. This correlation shows a possible limitation of the elution solution, 30 mL 5 M NaCl, in eluting Zn²⁺ out of the resin.

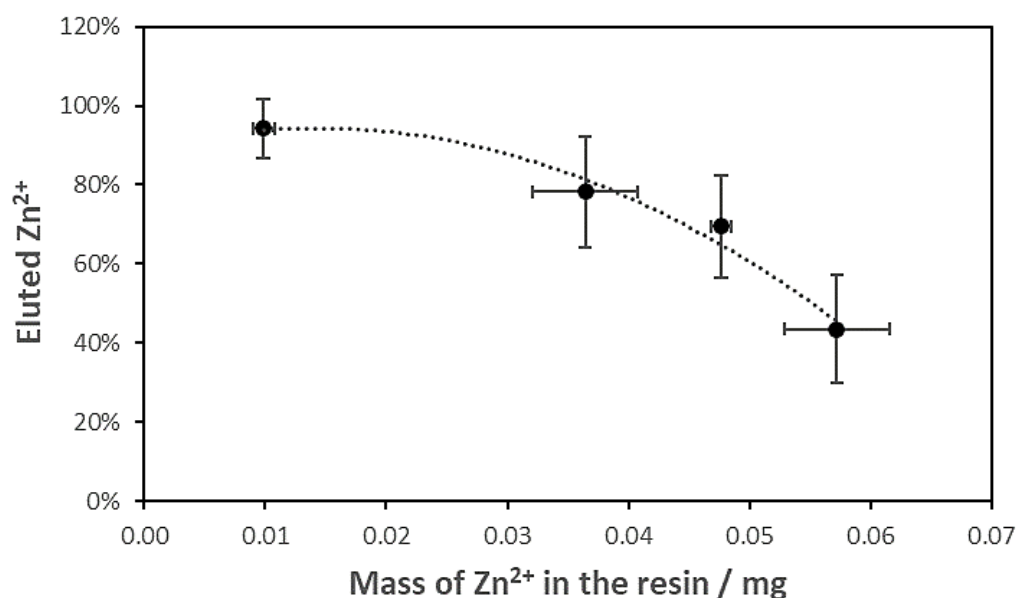


Figure 84 Amount of Zn²⁺ eluted with 30 mL 5 M NaCl from 2.6 g Lewatit SP resins loaded with varying amounts of Zn²⁺ within 0.01-0.07 mg Zn²⁺ range (n=3).

Further, the elution step was combined with the adsorption process, creating a preconcentration workflow. The preconcentration workflow was tested within a range of initial Zn²⁺ concentrations between 0.05-0.9 mg L⁻¹. In Figure 85, the initial concentration of Zn²⁺ was shown as 'without preconcentration', showing the corresponding concentration measured with UV/Vis spectrophotometry at 552 nm. After preconcentration, an increase in measured concentration can be observed across the tested range. The concentration measured after the preconcentration still follows the increasing pattern of the initial concentration, especially

within the 0.1-0.9 mg L⁻¹ range. While the preconcentration result of 0.05 mg L⁻¹ and 0.1 mg L⁻¹ were nearly indistinguishable, resulting in 1.40 ± 0.04 mg L⁻¹ and 1.51 ± 0.01 mg L⁻¹ solution, respectively. While preconcentration from 0.3, 0.5, 0.7, and 0.9 mg L⁻¹ initial concentration resulted in 2.38 ± 0.01, 3.29 ± 0.11, 3.85 ± 0.02, and 4.16 ± 0.01 mg L⁻¹ solution, respectively. Lower initial concentration had been correlated to the low amount of Zn²⁺ trapped by the resin, which through the elution process had also been correlated to lower elution performance. Following this pattern, the preconcentration factor also lowers with the increase of initial concentration. At the lowest tested concentration of 0.05 mg L⁻¹, the preconcentration factor reached 23 times the original value. Meaning that the concentration measured at the endpoint of the preconcentration workflow can reach up to 23 times the initial concentration of the sample. Whereas at the highest tested concentration of 0.9 mg L⁻¹ Zn²⁺, the preconcentration factor was as low as 4.4 times higher than the original value. This shows that the preconcentration factor of the developed workflow is dependent on the initial concentration of the sample. Therefore, for its use in predicting the level of Zn²⁺ in environmental samples, a calibration curve can be constructed to immediately correlate the measurement to its initial concentration. This approach can be seen in the following section on the integration of the preconcentration method with the developed 5-Br-PAPs μPAD for Zn²⁺ detection.

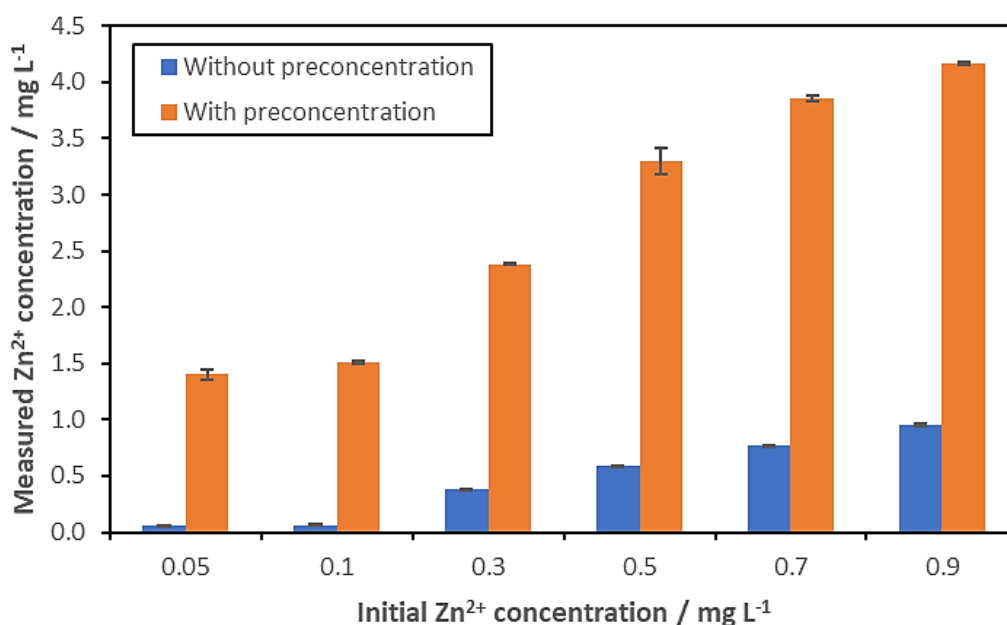


Figure 85 Measured (blue) initial and (orange) final concentration of Zn²⁺ solution after reaction with 100 μL 5-Br-PAPs, at 552 nm wavelength, before and after preconcentration with Lewatit SP followed by elution with 30 mL 5 M NaCl solution (n=3).

4.6 Integration of cafetière-based preconcentration with Zn^{2+} μPAD for Zn^{2+} detection

4.6.1 Zn^{2+} preconcentration and detection with μPAD – workflow

The developed and tested preconcentration method was then integrated with 5-Br-PAPs μPAD for the detection of Zn^{2+} . The complete workflow started with filling the cafetière with a 300 mL water sample and plunging 2.6 g Lewatit SP resin in a modified basket for 5 min. After the plunging period, the basket was taken out of the cafetière and swirled in 30 mL 5 M NaCl placed in a crystallising dish for another 5 min, completing the elution step. The developed 5-Br-PAPs μPAD was then dipped into the elution solution and left to react for 5 min. A picture of the device was taken at minute 5, using the black box method with a back-side camera of a smartphone, using the flash option on (Chapter 2). The picture would then be used for digital colour analysis with ImageJ, to estimate the Zn^{2+} concentration through interpolation with a pre-constructed calibration curve (Figure 86).

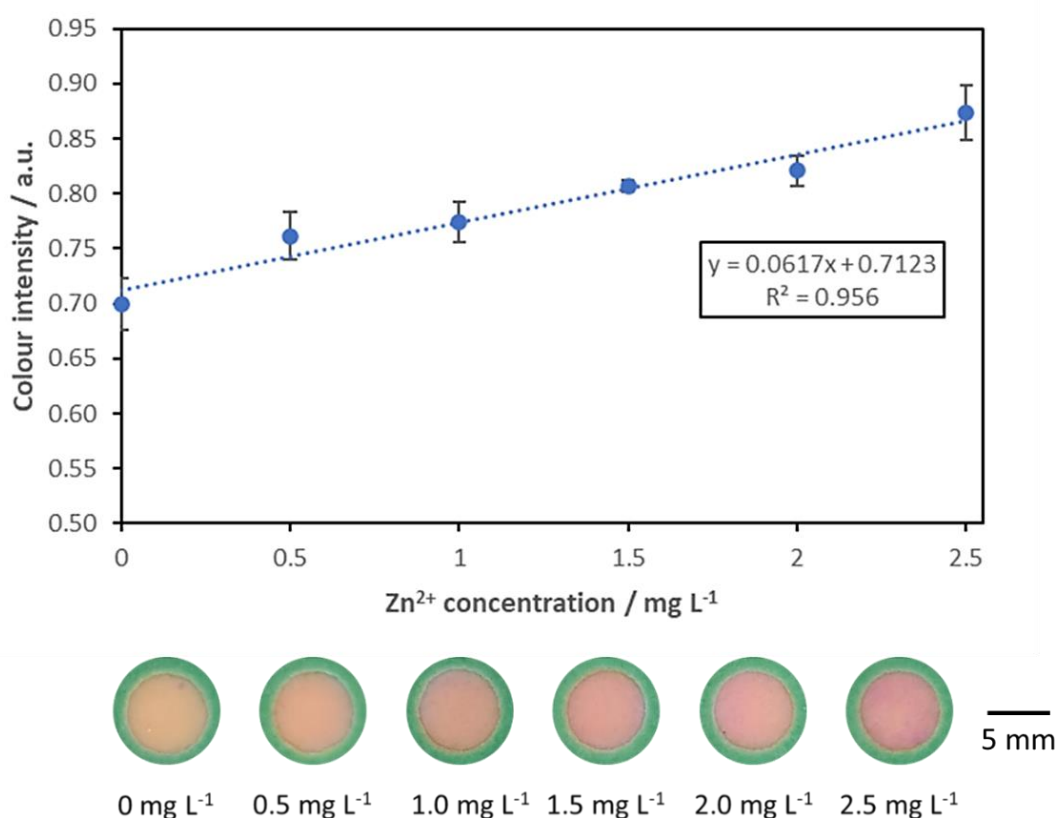


Figure 86 Performance of 5-Br-PAPs μPAD upon dipping into 10 mL 0-2.5 mg L^{-1} Zn^{2+} diluted in 5 M NaCl ($n=3$). This can be used for the estimation of Zn^{2+} concentration in the elution solution after the preconcentration workflow.

Shown in Figure 87 is the measured colour intensity of the 5-Br-PAPs μ PAD after dipping into 30 mL elution solution of Zn^{2+} within 0.05-0.9 mg L^{-1} initial concentration range. Evidently, the increase in initial Zn^{2+} concentration corresponds to a relatively linear increase of measured colour intensity, as shown in the figure. Due to the linear correlation, this data can immediately be used to estimate the initial concentration of the Zn^{2+} sample without the need for back-calculation. The detection limit of the developed workflow can therefore be calculated through $3\sigma/m$, resulting in the LOD of 0.1 mg L^{-1} and LOQ of 0.3 mg L^{-1} . This calculated detection limit is just below the chronic and acute limit of Zn^{2+} in the freshwater environment as regulated by the US EPA, which had a limit of 0.12 mg L^{-1} [34].

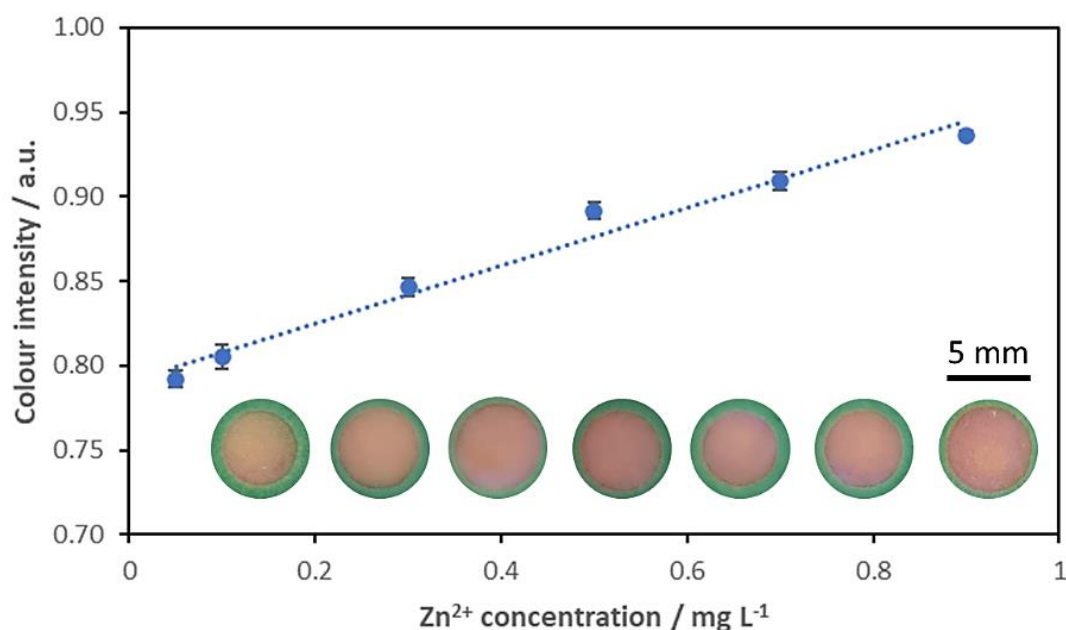


Figure 87 Measured colour intensity of 5-Br-PAPs μ PAD sample wells after dipping into elution solution after pre-concentration step of 0.05-0.9 mg L^{-1} Zn^{2+} solution ($n=3$).

4.6.2 Testing with environmental water samples

Furthermore, the developed workflow was tested with environmental water samples, spiked and non-spiked, and a comparison was drawn between the pre-concentration workflow paired with μ PAD to the conventional analytical measurement done with ICP-MS. The result of this experiment is summarised in Table 18, listing three different water samples used in this research: Milli-Q, tap water, and a sample from the University of Hull sustainable drainage system (SuDS). The procedure for procuring the water samples was described in section 4.2.5.4. In a spiked water sample, Zn^{2+} was added to increase the concentration by 0.5 mg L^{-1} . For non-spiked Milli-Q water, which was obtained from the equipment in the University of Hull biology department

laboratory, both μ PAD and ICP workflow showed a concentration of Zn^{2+} of 0.00 mg L^{-1} . Quantitatively, the percentage recovery of Zn^{2+} cannot be determined in this case, however, it shows matching results between the two analytical approaches. Similar satisfactory and matching results can be seen in the measurement of Zn^{2+} in the non-spiked SuDS sample, where the estimated Zn^{2+} concentration was $0.00 \pm 0.16 \text{ mg L}^{-1}$ and $0.03 \pm 0.01 \text{ mg L}^{-1}$ for μ PAD and ICP analysis, respectively. Additionally, in the spiked tap water sample, the two analytical approaches also agreed. The measured concentration (after three repeats) for this sample was $0.56 \pm 0.22 \text{ mg L}^{-1}$ and $0.56 \pm 0.01 \text{ mg L}^{-1}$ for μ PAD and ICP analysis, respectively.

While in the spiked Milli-Q water sample, the μ PAD estimated Zn^{2+} concentration of $0.44 \pm 0.09 \text{ mg L}^{-1}$, while the ICP-MS showed a concentration of $0.50 \pm 0.02 \text{ mg L}^{-1}$. This is a difference of 12% between the two analytical approaches, or 88% of Zn^{2+} recovery in the μ PAD system in comparison with the ICP result. A bigger difference can be seen in the measurement of Zn^{2+} in the spiked SuDS sample, where the μ PAD measurement resulted in $0.61 \pm 0.06 \text{ mg L}^{-1} \text{ Zn}^{2+}$, which is 30% higher than the ICP result of $0.47 \pm 0.02 \text{ mg L}^{-1}$. However, the highest difference between the μ PAD and ICP was shown in the measurement of the tap water sample, where a gap of up to 52% was recorded between the two analytical methods. Here, the μ PAD measurement resulted in $0.05 \pm 0.17 \text{ mg L}^{-1} \text{ Zn}^{2+}$, while the ICP result was $0.11 \pm 0.01 \text{ mg L}^{-1}$. Despite the seemingly large difference in measurements, the difference between measured concentrations with the μ PAD approach compared to the ICP result was within $0\text{-}0.14 \text{ mg L}^{-1}$. Therefore, in the application of the μ PAD workflow for environmental monitoring, an increase in the limit of concentration of concern can be increased to mitigate possible deviation from Zn^{2+} concentration as measured through more conventional means.

Table 18 Preconcentration workflow integrated with 5-Br-PAPs μ PAD result compared to ICP-MS result of three different water samples, spiked and non-spiked. The water samples tested were: Milli-Q, tap water, and a sustainable drainage system. †: calculated by comparison between concentration measured by μ PAD to ICP-MS result (%recovery= concentration measured by μ PAD/result of ICP-MS).

Sample	μ PAD / mg L^{-1}	ICP / mg L^{-1}	%recovery [†]
Milli-Q	0.00 ± 0.06	0.00 ± 0.01	<i>n.d.</i>
Spiked Milli-Q	0.44 ± 0.09	0.50 ± 0.02	88%
Tap water	0.05 ± 0.17	0.11 ± 0.01	48%
Spiked tap water	0.56 ± 0.22	0.56 ± 0.01	100%
SuDS	0.00 ± 0.16	0.03 ± 0.01	<i>n.d.</i>
Spiked SuDS	0.61 ± 0.06	0.47 ± 0.02	130%

4.7 Conclusion

The preconcentration workflow previously developed for onsite Ni^{2+} preconcentration was employed for Zn^{2+} preconcentration. This workflow, involving Lewatit SP cation exchange resin deposited in a modified cafetière basket plunged into a 300 mL sample in cafetière was kept as is. Further elution process requiring 30 mL 5 M NaCl was also employed in a similar manner as Ni^{2+} , and proven effective for Zn^{2+} preconcentration. However, a new μPAD needed to be developed for Zn^{2+} detection. In order to achieve this, two different colorimetric reagents were tested: zincon monosodium salt and 5-Br-PAPs. The former showed potential for Zn^{2+} detection, however, it is relatively reactive to commonly found ions in environmental water samples that cause potential interference in the signal. The latter showed a more specific complex formation, only to be disrupted in the presence of metal ions. The addition of masking agents was able to solve this problem, resulting in a more robust μPAD with a 0.5 mg L^{-1} detection limit. Upon integration of preconcentration workflow, this detection limit fell to 0.1 mg L^{-1} , which is just below the chronic and acute limit of Zn^{2+} in freshwater environments regulated by the US EPA (0.12 mg L^{-1}) [34]. This shows potential for the developed workflow for onsite Zn^{2+} analysis or at least estimation of Zn^{2+} concentration within the range of interest.

Chapter 5 User experience evaluation

5.1 Chapter introduction

The citizen science approach for environmental monitoring is an interesting and important method for a cost-effective monitoring process through wide spatiotemporal coverage [179-181]. Aside from its advantages in the research data collection perspective, citizen science also aids in enhancing the community's ability to monitor the environment, subsequently increasing public awareness of an environmental issue [182-184]. Long-running citizen science campaigns had been used in at least three studies for water monitoring purposes and proved useful for observing trends and changes in the environment [129, 185, 186].

Previous publications had discussed the involvement of citizen scientists in environmental monitoring [125, 126, 129, 181, 187-197], however, they rarely include reports of user evaluations of the workflow from the perspective of the citizen scientist. This is a critical step, as the development of an easy-to-flow method is crucial for accurate and reproducible measurements. This evaluation can be done through user experience testing, by giving the developed workflow to a group of volunteers, allowing further quantitative or qualitative data collection. However, studies that have tested the workflows with user groups tend to be heavily focused on comparing the data obtained by the volunteers to a conventional analytical technique [198-200]. While this is an important factor in the development of a paper-based analytical device such as in this research, user feedback from the pool of volunteers itself might also produce inputs that would increase the feasibility and usability of the developed workflow. In this research, the qualitative aspect of the study would not only be obtained through observation by the researchers, but also through a questionnaire completed by the volunteers at the end of the testing process.

This chapter starts with an explanation of the methods in section 5.2. Followed by a discussion on the volunteers' demography in section 5.4, followed by an in-depth description of the workflow tested by the volunteers and the observation methods in section 5.5. Section 5.3 shows the experiments conducted by the researchers to obtain control data for the μ PAD measurements in the volunteers' activity. Section 5.6 elaborates on the analytical evaluation obtained through the volunteers' activity as quantifiable data. Followed by section 5.7, where the volunteers' feedback on the tested workflow is discussed and possible causes for any problems were addressed.

5.2 Materials and Methods

5.2.1 Materials

This section lists the materials used in the observation of the user experience evaluation. Further discussion on the materials listed in Table 19 is deliberated in section 5.5.1 Materials and equipment for volunteer work.

Table 19 Materials used in user experience evaluation with volunteers.

Description	Supplier
Milli-Q water	Merck Millipore
Tap water	University of Hull
Sustainable Drainage System (SuDS) water	University of Hull
Sodium chloride, ACS Reagent, ≥99.0%	Sigma Aldrich
Zinc μPAD	
Modified cafetiere	Nerthus
Lewatit® MonoPlus SP 112	Sigma Aldrich

5.2.2 Workflow development

The workflow completed by participants in this research was developed throughout this study, as discussed in Chapter 4 and further discussed in section 5.5.2 Workflow completed by the volunteers. Whereas control data for Zn²⁺ and the metal content of water samples were obtained through ICP-MS, and analysed by a third party.

5.2.3 Ethics

Ethics clearance was obtained for this study involving non-specialist participants through the Ethics Committee of the Faculty of Science and Engineering at the University of Hull. The ethics document was labelled FEC_2022_38. Complete ethics-related documentation is provided in Appendix 4 for the letter of ethics clearance and for the ethics form submitted.

5.2.4 Questionnaire

The questionnaire for the volunteers was developed in Microsoft Forms, through access provided by the University of Hull. This allowed anonymous form submission by the university students and staff members. The questionnaire consisted of three sections: privacy statements, workflow evaluation, and demographic questions. Participants would also upload the picture they obtain from the workflow to the questionnaire. The completed questionnaires as filled out by the participants are provided in Appendix 4.

5.2.5 Recruitment

Volunteers were recruited through emails distributed through various student channels within the university, e.g., the postgraduate students' mailing list (Figure 88). In the email, students were invited to participate in the study by replying to the provided email address to book a place according to their availability. Students were given the participant information sheet (Appendix 4) as an initial brief of the work expected and encouraged to inquire further, should there be any questions. In the information sheet, it was made clear that by participating, students would not be compensated either through financial or academic means. They were also free to resign from participation at any point before questionnaire submission – at which point the data would be anonymised.

Volunteers needed! (for citizen science project)

MILA SARI <M.Sari-2019@hull.ac.uk>

Thu 5/12/2022 10:59 PM

To: postgrads

1 attachments (100 KB)

Participant Information Sheet - Heavy metal in Freshwater.pdf

Hi everyone!

I'm in need of **volunteers** for a citizen-science-related project. You will be asked to test a kit we've developed for testing contaminants in the water and give some feedback. See attached document for more information. The activity (*approx. 45 min*) will be held on campus, in Ferens building. **All students from any department are welcome!**

If you are interested or have any further questions, please don't hesitate to contact me: @MILA SARI (m.sari-2019@hull.ac.uk)

Thank you in advance!

Best regards,
Mila

Figure 88 E-mail sent to the University of Hull postgraduate students mailing list for volunteer recruitment in this study.

5.2.6 Obtaining water samples

The water sample for Milli-Q and tap water was obtained from the biology and chemistry laboratories at the University of Hull, respectively. These water samples were taken approximately one week before volunteer activities started. For each water type, more than 4 L of water was sampled and stored in refrigerated storage in the chemistry laboratory.

Whereas the water sample from the Sustainable Drainage System (SuDS) was obtained from one of the measurement points in the University of Hull SuDS, on the same day of sampling. The sample was obtained from the accessible parking building SuDS measurement point at the University of Hull, using a sampling bucket and appropriate safety measures. The water sample was then filtered with the 0.45 µm filter before storage in refrigerated storage.

5.2.7 μ PAD for Zn^{2+} detection

The μ PAD used by participants in this study was based on the μ PAD developed for Zn^{2+} detection in Chapter 4. This μ PAD was made with wax printed and cut filter paper, where 5-Br-PAPs were deposited as a colorimetric reagent, allowing a colour-changing reaction from yellow to magenta. Other additives were also added to enhance the reaction and ensure the selectivity of the μ PAD. Semi-quantitative detection with this μ PAD would be based on the picture-taking process of the μ PAD after 5 min of reaction. In this study, the picture-taking process was done with the aid of a black box, as explained in the previous chapter.

5.2.8 Analysis of questionnaire data

5.2.8.1 Quantitative

The quantitative data obtained from the volunteer activity ranged from simple volume measurement to ICP-MS. In the volume measurement data-taking, the volume of the sample placed in the cafetiere by the volunteers was measured with a graduated cylinder. This data was recorded to be compared with other volunteers' data.

The elution solution produced by the volunteer (30 mL 3 M NaCl) was stored in a 50 mL centrifuge tube for further testing. 10 mL of the solution was sent for ICP-MS measurement, and the 20 mL was stored in a 5°C fridge in the laboratory to be tested by the researcher with the developed μ PAD. At the end of the volunteer activity period (+/- 2 weeks) the samples were tested simultaneously with freshly fabricated μ PAD for Zn^{2+} and Ni^{2+} . The testing was done by placing laminated μ PAD into the 20 mL elution solution for 3 min before taking a picture of the device. The picture was then measured for colour intensity and the result of the measurement was compared to the control data.

In order to test the accuracy of the μ PAD used by the volunteers, a picture of the μ PAD dipped into the elution solution by the volunteers was taken immediately after the volunteer activity. The image was taken with the black box method with Samsung Galaxy S20+ back camera. The image was then analysed for Zn^{2+} concentration by interpolation with the calibration curve (Appendix 4). The Zn^{2+} concentration measured through the picture taken by the researcher was then compared to the Zn^{2+} concentration measured from the elution solution using freshly made μ PAD. The former was also compared to control μ PAD.

Testing the picture-taking step was done by comparing the Zn^{2+} concentration measured on the picture submitted by μ PAD with the picture taken of the same μ PAD by the researcher. It was also compared to control μ PAD. The figure to illustrate the data obtained and the comparisons are depicted in Figure 89.

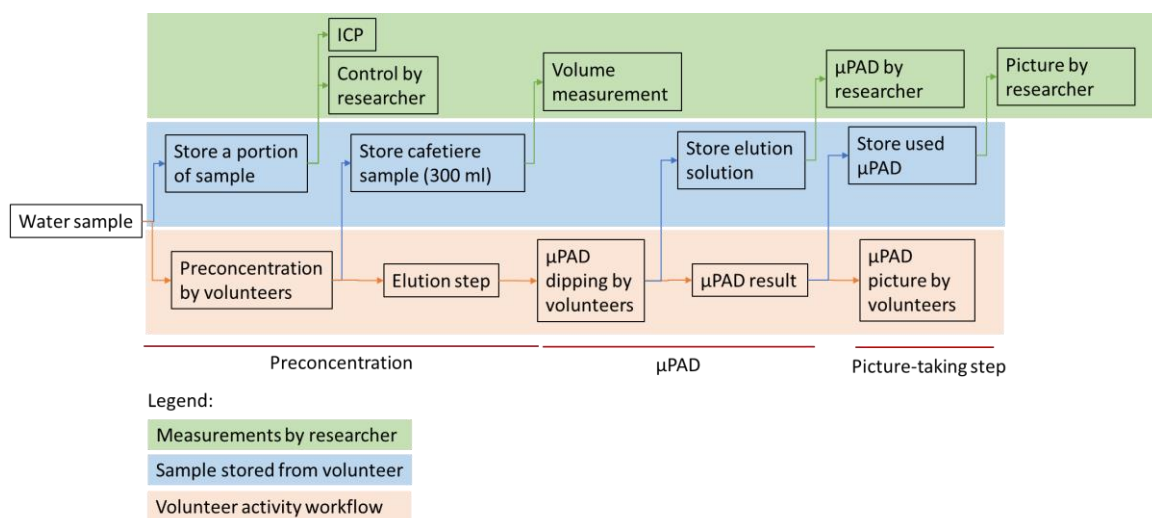


Figure 89 Data acquisition graph, orange was done by the volunteers, and the blue and green area was done by researcher. Comparison between two different data was also drawn for preconcentration, μ PAD, and the picture-taking test discussed.

5.2.8.2 Qualitative

Qualitative data was obtained through observation while volunteers were testing the developed workflow, as well as through the questionnaire result. The questionnaire contained both open questions and questions answered using Likert scales, yes/no options and multiple choice options.

For open-ended questions, all response was analysed with NVivo (by QSR International). All responses were then coded as necessary and compiled into word clouds separately. For the purpose of analysis at this step, the top 30 most frequently used words in each answer were compiled into 3 different word clouds: preconcentration, μ PADs, and overall workflow. Deliberated answers were further discussed as necessary in the given section.

5.2.9 Statistical analysis

Methods of statistical analysis employed within this chapter follows the previously described method in section 2.2.5.

5.3 Control – μ PAD measurements conducted by the researcher

As part of the evaluation process, the results obtained by the volunteers were compared to control measurements carried out by trained researchers using both ICP and μ PADs. The results of these control measurements are shown in Table 18 Preconcentration workflow integrated with 5-Br-PAPs μ PAD result compared, comparing the data obtained by the researcher for each sample to the ICP-MS result of the sample.

In the hands of researchers and when the amount of Zn^{2+} was within the working range of the workflow, the μPAD system was able to measure the concentration relatively accurately. In non-spiked tap water containing $0.11 \text{ mg L}^{-1} \text{ Zn}^{2+}$, the workflow reported slightly lower concentrations, of 0.05 mg L^{-1} . More accurate results were displayed in the spiked SuDS sample, where the workflow overestimated the Zn^{2+} concentration by 0.14 mg L^{-1} , followed by measurement at spiked Milli-Q sample where the workflow detected 0.44 mg L^{-1} instead of the true value of 0.50 mg L^{-1} , and lastly at spiked tap water sample where the workflow was able to detect exactly the concentration measured by ICP-MS.

These results showed that despite the much simpler and low-cost approach of the developed method compared to the ICP-MS method, the μPAD and associated workflow is able to produce a comparable result and showed potential for environmental screening purposes. Considering the simplicity and usability of the developed workflow for non-specialist users, the developed workflow may serve as an alternative method in environmental monitoring.

5.4 Volunteer demography

During the recruitment process, the volunteer population was restricted to the students at the University of Hull. This restriction was made in consideration of the aim of the evaluation – which was to get an early picture of how non-specialist users would interact with the workflow. However, no restrictions were made on the level of study nor on the field of study. This also means that students from laboratory-based studies, e.g., postgraduate researchers in chemistry or biology, could take part. However, students from the same research group as this project were not recruited. Data on volunteer demography and background were collected to assist with the evaluation.

From 31 volunteers recruited for the user evaluation, 45% were studying at the undergraduate level, 23% were postgraduate research students and 22% were postgraduate taught students. The last 10% of the volunteers describe their current study level as 'others'. This group included postdoctoral researchers and exchange or visiting students who were at the University at the time of the study. A pie chart of the volunteers' study levels is illustrated in Figure 90. This information on the volunteer demographic underlines the spread of the level of education tested among the participant. Aside from having a reasonable spread of participants, with nearly half from undergraduate students, and another half from postgraduate degrees, due to the restriction in volunteer recruitments, no participants without tertiary education were represented. For this stage of observation, this was regarded as acceptable. However, further, down the line, more inclusive participation can be encouraged to ensure a sample pool that would more closely reflect the possible target user.

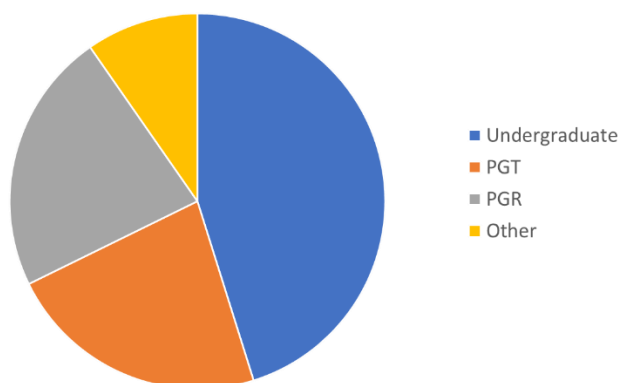


Figure 90 Volunteers' level of study at the time of recruitment.

Another important consideration was the volunteers' previous experience in chemistry laboratories. This measure was preferred over documenting volunteers' current study field since it would provide better background information on the volunteer's potential knowledge of Good Laboratory Practices (GLP).

Volunteers' prior chemistry laboratory experience was classified into three different groups based on their responses: no prior experience, limited chemistry laboratory experience through studies (e.g. supervised undergraduate labs), and actively working in a chemistry laboratory at the time of the recruitment. An open-ended answer was also provided under 'others', where volunteers were given the opportunity to elaborate further if their experience cannot be classified by the provided options.

Figure 91 shows the demographic data of the volunteers based on their prior laboratory experiences. Out of the 31 volunteers, 29% had no prior experience working in a chemistry laboratory. 42% of the volunteers had some level of experience working in a chemistry laboratory during their studies. Opting for this option implies that the volunteers were not working in a chemistry laboratory on a daily basis at the time of participation. Therefore, this can be categorised as limited working experience in laboratory settings. 19% of volunteers recruited were actively working in a chemistry laboratory at the time of participation. While the last 10% opted to self-describe their previous laboratory experience. One described a high school-level laboratory experience, another described experience as a laboratory assistant, and the last one disclosed a PhD research experience in ion exchange processes. It is worth noting that the latter is closely related to the preconcentration workflow developed in this research.

This shows quite a spread of experience within the volunteer pool. While the majority of the volunteers had experience working in the laboratory throughout their study, there is still around a quarter of the participants who did not have any prior experience in laboratory work. This shows the variation in volunteers' backgrounds related to working with accuracy and with potentially hazardous substances. Therefore, a diverse point of view in completing the process and the questionnaire could be expected.

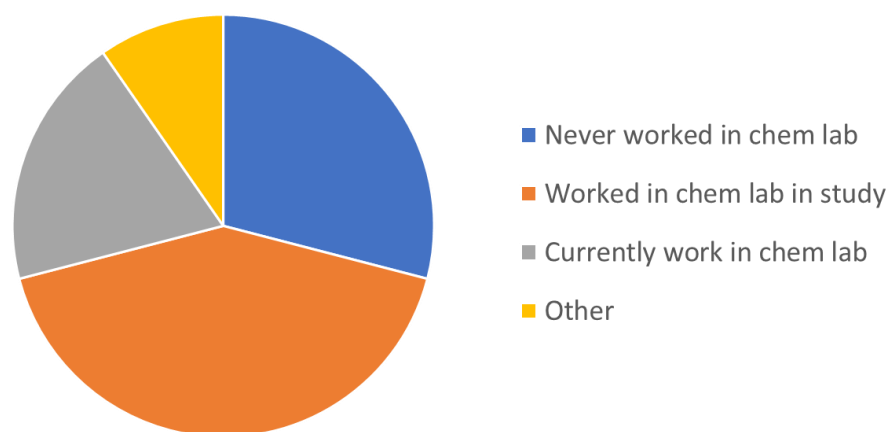


Figure 91 Volunteers' previous chemistry laboratory experience demography.

Volunteers were also asked about their prior knowledge and/or experience related to microfluidics devices. This question was included to ascertain whether volunteers might have an understanding of the use of the device even in the lack of complete instructions. The question was a branched question starting with whether volunteers had prior knowledge of microfluidics technology. As seen in Figure 92, 77% of participants had never heard about microfluidics prior to the testing session. Within the 23% of participants who had prior knowledge of microfluidics, 71% claimed to only be familiar with the term 'microfluidics', without further related experience. While 14% of participants who had prior knowledge of microfluidics had learnt about the technology in their taught courses and another 14% were researchers working on projects that involved microfluidics technology. Therefore it can be safely concluded that most participants would not know how to use the provided microfluidic devices without complete instructions.

The term 'citizen science' was much more familiar to the participants; 42% had heard about it prior to the study. Upon further questioning, 19% of the 31 participants had previously participated in a citizen science project. Another 19% had known of 'citizen science' but never participated in any projects prior to this study. 3% of the total participants were researching a

topic related to citizen science. This variety in the understanding of citizen science was important information since the diversity of participants allowed a comprehensive view of the performance of the evaluated workflow. It would also offer an interesting spread in the open-ended feedback, gathering perspectives from people who had never been exposed to the concept before and people who already had some experience in the field. It is expected that people who had prior experience related to citizen science activities would reflect on their experience while evaluating the developed workflow.

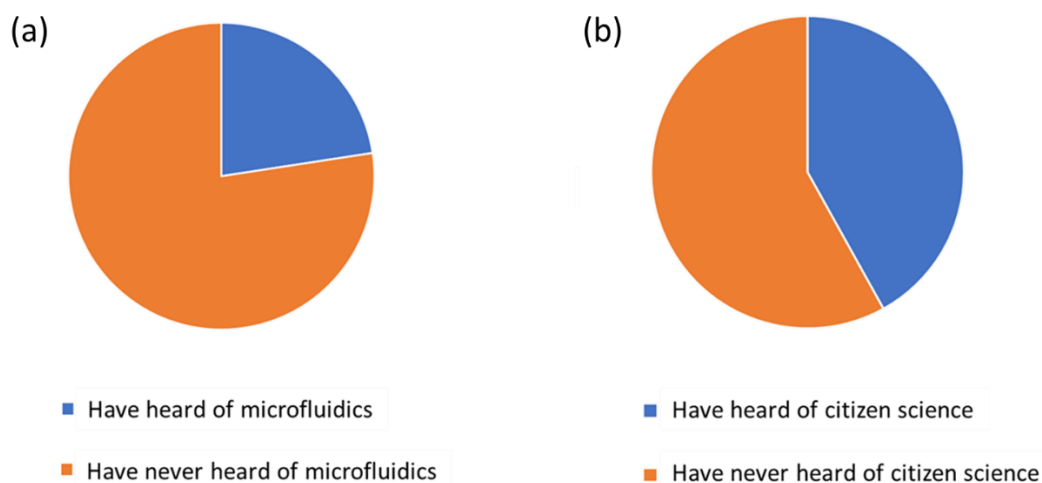


Figure 92 Volunteers' awareness of the terms (a) 'microfluidics' and (b) 'citizen science'.

5.5 Workflow and observational data

The workflow tested by the volunteers was very similar to the workflow used in the development and optimisation steps (Chapter 4). Minor changes or differences in the workflow and equipment used by the volunteers will be explained and justified in this section. Further, some observational data will also be discussed. This observational data was obtained by the researcher's observation while volunteers were completing the testing process. The observational data can be critical in evaluating aspects of the process that was not or cannot be reflected in the questionnaire or through analytical means, e.g., plunging behaviour during the use of the cafetiere-based preconcentration.

5.5.1 Materials and equipment for volunteer work

5.5.1.1 Cafetiere modifications

Throughout the optimisation process, two different cafetieres of similar specifications (Nerthus FIH 319 French press cafetiere 350 mL) were used. The minor difference was mainly in the design

of the cafetiere which was not critical to the performance of the cafetiere itself, e.g. colour and other aesthetics.

However, rather than using the plunger as is, a minor modification was required to fix a hex nut on the plunger rod. This hex nut was readily available in the cafetiere used throughout the optimisation process; however, it was not included in the design of the new cafetiere. In order to create a pinch to fix the resin-filled basket at the end of the plunger, the hex nut was welded on the base of the thread at the end of the rod. This process secured the placement of the modified basket throughout the plunging step in the preconcentration workflow. This is crucial since the basket would act as the container of the ion exchange resins in this research and should be tightly secured to prevent leaks due to the movement of the basket parts while plunging.

The two cafétieres used in the optimisation process were adapted as follows. A hex nut was placed right at the base of the thread, allowing a basket to be placed securely on the thread and allowing enough thread for a detachable nut to securely fix the basket in place. Unfortunately, during further modifications of the cafetiere, not all were welded correctly. The hex nut was placed at the base of the thread, but the thread used for placing the basket was varying in length (Figure 93). This variation causes differences in the strength and security of the basket-mounting system between the cafetieres.



Figure 93 Variation in basket mounting thread in the modified plunger causing different basket mounting strength – shorter thread often led to resin leakage.

During the evaluation process, volunteers were instructed not to dispose of the water sample inside the cafetiere. By leaving the water sample in the cafetiere, the researcher was able to measure volunteers' accuracy in estimating the sample volume. Throughout this evaluation, volunteers were asked to estimate the volume of water using the line available on the outside

of the cafetiere. The ability to do this would ensure simplicity during onsite application. However, in this study, this accuracy was to be observed and therefore the water sample was not removed from the cafetiere as volunteers proceed through the preconcentration steps. In practical application, this water sample would no longer be needed and can safely be disposed of back to the environment.

5.5.1.2 Blackbox

A previous, closely related, study [201] described problems with the quality of volunteers' photographs of microfluidic devices. In an attempt to combat this issue, we designed a black box to support a uniform picture-taking process.

A black box of approximately 26 x 26 x 26 cm in size was constructed out of black cardboard material. One of the sides of the box was open, which would be referred to as the down-side of the box, while the opposite of this side was slitted with a 9 x 3 cm rectangle. The inside of the box was lined with white 80 gsm copy paper. The box was put together with black tape on each edge, ensuring all edges of the box were sealed to prevent light from coming in. This method has previously been explained in Chapter 2, [Figure 29](#).

This black box was to be used as a picture-taking aid, as it provides constant angle and distance between the camera and the subject, while also ensuring a controlled environment to reduce interference from ambient light. Fixing the angle of the picture ensures that the size of the sections in the picture would be of constant shape. For example, a picture of a circle taken from an angle may appear more oval. Fixing the distance also aid in ensuring picture quality by giving a point of reference on the scale of the picture expected, as opposed to not using the box, where participants would use personal judgement to capture the device. It was assumed that controlling for variables, such as lighting and angles would aid in controlling the quality of the picture taken.

5.5.1.3 Paper-based analytical device

A paper-based analytical device (μ PAD) for Zn^{2+} detection was provided to the volunteers along with other equipment. The development of the μ PAD is described in Chapter 4. The device was a 30 mm circular paper sensor, equipped with a magenta reference circle, a blank well, and 5 sample wells in each of the 3 layers: masking, binding, and detection. These devices are designed to be placed in a water sample containing Zn^{2+} . Within 10 min of dipping, the sample wells of the device reach stable colours and a picture of the device can be taken for further analysis.

5.5.1.4 Water samples

There were six different water samples tested in this research, consisting of two varieties for each: (1) non-spiked and (2) spiked to $0.5 \text{ mg L}^{-1} \text{ Zn}^{2+}$. The source of the water sample was divided

into three: (a) laboratory-grade Milli-Q water, (b) tap water, and (c) a sample from the sustainable drainage system at the University of Hull. All six samples were tested for Zn^{2+} by researchers using the μ PAD workflow and also ICP-MS. Each volunteer was given only one of the samples at random, ensuring at least five repeats of each sample by five different volunteers. The designation of the sample was based on the volunteer code, which was assigned at random.

5.5.2 Workflow completed by the volunteers

Volunteers were given a set of equipment consisting of an 800 mL unlabelled water sample, a black box (as described in Chapter 2 and 5.5.1.2 Blackbox), a 350 mL Nerthus FIH 319 French press cafetiere loaded with 2.6 g Lewatit SP resin in a modified basket, one crystallising dish, one centrifuge tube containing 30 mL 5 M NaCl, one non-sharp pair of tweezers, and one 5-Br-PAPs μ PAD. This set of equipment was placed on a workbench covered with absorbent material, mitigating potential spillage. The volunteers were briefed on laboratory safety as well as the workflow and the samples they would be working on. They were then asked to read through and complete the provided information sheet and consent form (Appendix 4). They were encouraged to ask questions if anything was unclear throughout the process. Volunteers were also encouraged to write down these questions as input in the questionnaire at the end of the testing. Volunteers were asked to, if possible, use their own mobile devices for timekeeping and picture-taking throughout the workflow testing. A smartphone and timers were also provided when necessary.

With provided adjustment clarified in the previous section, the workflow tested by volunteers was as pictured in Figure 94.

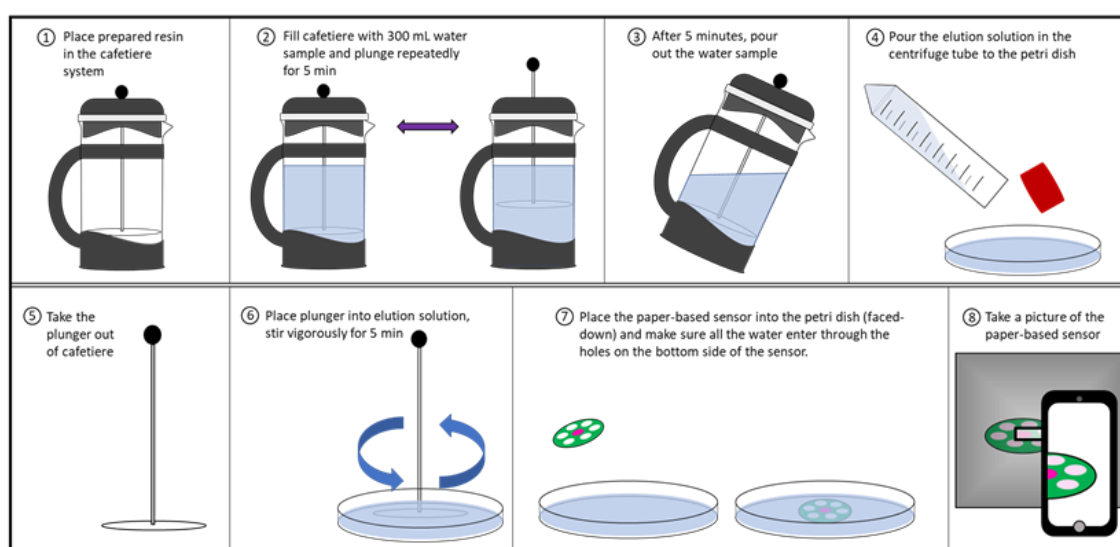


Figure 94 Workflow as depicted in the instruction sheet given to the volunteers. The workflow utilises the cafetiere system and modified basket as described in the previous chapter (see Chapter 2). Volunteers were verbally asked to omit step 3 of the depicted workflow.

In this workflow, volunteers were asked to pour 300 mL of water sample into the provided cafetiere. They were asked to use the indicator line on the cafetiere to approximate the target volume. Volunteers would then place the plunger into the sample solution, plunging it in the vertical direction for 5 min. Afterwards, volunteers were asked to pour the elution solution provided into the petri dish and transfer the plunger from the cafetiere to the dish. They then mixed the resin by swirling the basket in a random angular direction for 5 min, with the hex nut as the swirling axis. The plunger was then removed from the dish and μ PAD was dipped into the elution solution. Volunteers were asked to wait for 5 min before taking a picture of the μ PAD. As soon as the picture was taken, volunteers were asked to fill feedback form via an online questionnaire. In both picture-taking and questionnaire-filling steps, volunteers were encouraged to use their personal devices but were provided with the option to use a prepared smartphone.

5.5.3 Observations

The first observation made in the volunteer workflow was the accuracy of the volume of the sample. By giving the volunteers approximately 800 mL of the water sample, they would have to estimate the required water sample on their own. Volunteers were also purposefully not given any aid in making an analytically accurate measurement, rather relying on visual cues on the cafetiere, which was a plastic or metallic band on the cafetiere (Figure 95). This margin of error had been accounted for in the design of the workflow.

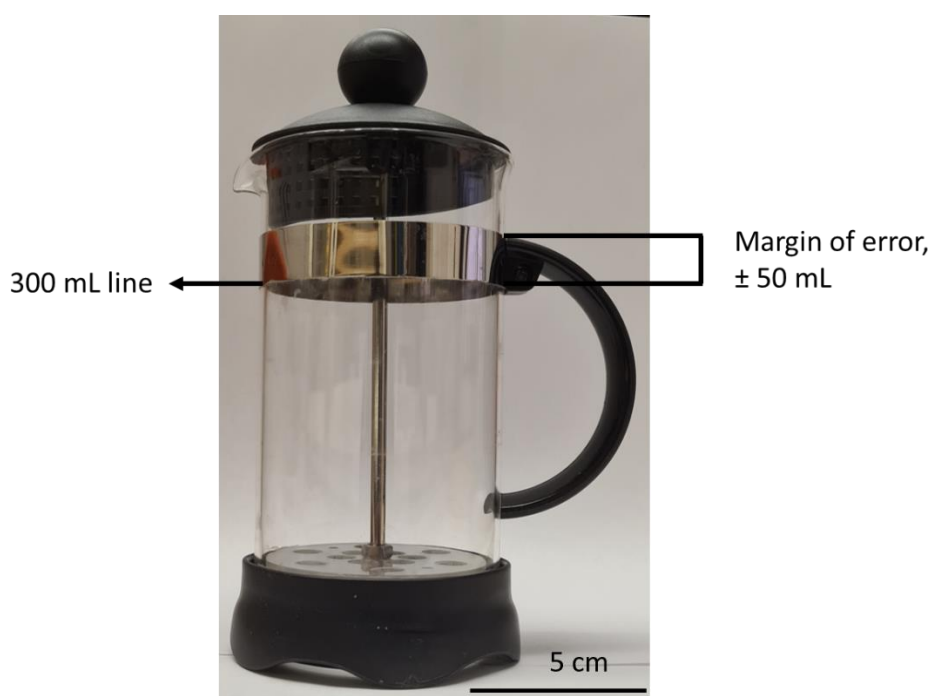


Figure 95 Metallic band indicating the limit of water sample volume

corresponding to 300-350 mL volume of sample.

Upon being asked to pour 300 mL from the provided solution, volunteers were able to pour the required volume with notable accuracy. The average volume used by the volunteers in this research was 299 ± 22 mL, with variation as illustrated in the box plot in Figure 96. As can be seen, out of 31 volunteers, there was only one significant outlier at approximately 350 mL. The rest of the cases were within the range of 250-340 mL, close to the target volume. In Figure 96, the spread of the data points can be observed by looking at the dots on the plot.

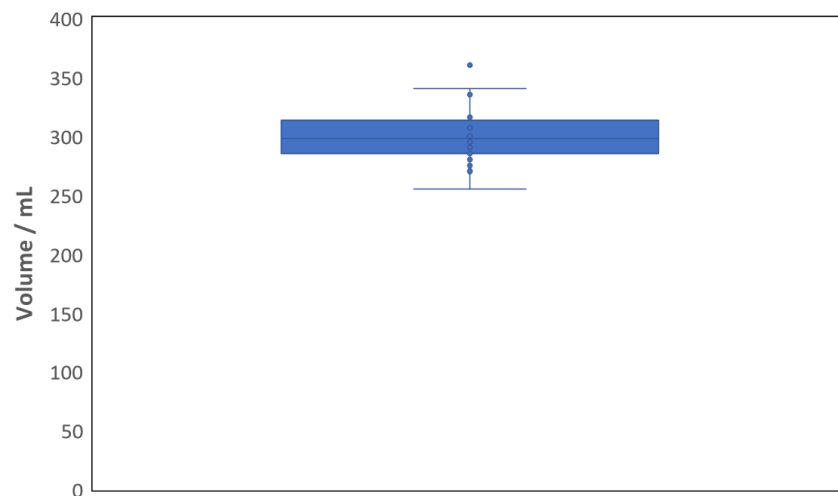


Figure 96 Distribution of cafetiere sample accuracy by the 31 volunteers, averaging 299 mL. Coloured lines indicate the maximum, median, and minimum values of the dataset. Dots indicate data points.

Further, observation of the volunteer's behaviour during the testing process was made to note possible causes of deviation or error. It was also a useful observation for the further optimisation process, noting how non-specialist users would approach the workflow.

The leak was the term used to describe the incidence at which any amount of resin can be found outside the modified basket. This can occur if the basket breaks or the fixing became loose during the plunging process. From the 31 volunteers, there was a 48% leak incidence for various reasons, as seen in Table 20.

Some notable observations made throughout the process were aggressive plunging, minimal swirling, and problems taking useable pictures. In the preconcentration process, the amount of force used by the volunteers through the plunging process exceeded our expectations. In some cases, the aggressive plunging process led to the spillage of the solution out of the cafetiere

container. In another, it led to the breaking of the fixed modified basket, releasing the resins into the solution. Aggressive plunging might also be motivated by maximising mixing since faster plunging movement would lead to more turbulence in the cafetiere. However, excessive force in plunging motion was not accounted for in the design. Researchers often use maximum plunging force up to once every 2 s (0.5 plunging per second). Slower plunging can still allow turbulence of the solution – whilst maintaining safe speed to minimise spilling or forces applied to the fixed modified basket.

Another point in the observation was the design flaw of the black box used for picture taking, which did not take into account the possibility of different smartphone camera designs. In one case, a volunteer was not able to use their own device due to the unaccounted design of their smartphone camera. Had the slit on top of the box been longer, the smartphone might be able to be used for the process. This problem could only be discovered through observation, which again highlights the importance of the volunteer-testing for the developed workflow.

Table 20 Observation data on the leak incidence and volunteers' behaviour throughout the testing process by 31 volunteers. Further details on volunteers' smartphone camera specifications are in Appendix 4.

Volunteer number	Leak	Vol sample / mL	Measured concentration / mg L ⁻¹			Observation ‡
			Preconc. †	PAD	Picture	
Sample #1			0.001			
1	No	316	0.00	0.00	0.00	Minimal swirling (elution)
2	Yes	300	0.00	0.00	0.00	Basket breaks completely, aggressive plunging
3	Yes	285	0.00	0.00	0.00	Workflow completed, resin leak
4	No	270	0.00	0.00	0.00	Workflow completed
5	No	270	0.00	0.00	0.28	Spill
6	No	340	0.0	0.05	0.00	Workflow completed
Sample #2			0.44			
7	No	320	0.0	0.00	0.57	Minimal swirling (elution)
8	No	307	0.3	0.11	2.00	Workflow completed
9	No	300	0.4	0.37	0.00	Workflow completed
10	Yes	296	0.0	0.33	0.00	Workflow completed, min resin leak
11	Yes	310	0.5	0.12	2.69	Leak at elution, spill
Sample #3			0.05			
12	No	285	0.00	0.00	0.00	Workflow completed
13	No	285	0.00	0.00	0.00	Workflow completed
14	Yes	303	0.00	0.00	0.00	Workflow completed, resin leak
15	Yes	360	0.00	0.00	0.00	Resin leak, device break in swirling, phone cannot take picture as intended
16	Yes	317	0.00	0.00	0.00	Resin leak, spill
Sample #4			0.56			
17	Yes	307	0.00	0.00	0.45	Minimal plunging, resin leak
18	Yes	277	0.00	0.64	0.00	Workflow completed, resin leak
19	Yes	295	0.23	0.00	0.31	Workflow completed, resin leak
20	No	285	0.00	0.00	0.00	Workflow completed
21	No	290	0.00	0.00	0.00	Leak at elution, spill
Sample #5			0.00			
22	Yes	255	0.00	0.23	0.00	Aggressive plunging, resin leak
23	Yes	275	0.00	0.34	0.00	Aggressive plunging, resin leak
24	No	294	0.00	0.00	0.00	Workflow completed
25	No	320	0.00	0.00	0.67	Workflow completed
26	No	280	0.00	0.00	0.45	Spill
Sample #6			0.61			
27	Yes	298	0.57	0.75	0.00	Aggressive plunging, resin leak
28	Yes	318	1.44	1.02	0.81	Workflow completed, resin leak
29	No	280	0.69	0.82	0.90	Workflow completed
30	No	335	2.22	1.44	2.77	Workflow completed
31	Yes	300	1.01	0.91	0.54	Leak

†: preconc. in this context refers to the concentration of Zn²⁺ measured in the final elution solution produced by the volunteers. Further explanation on this will be discussed in section 5.6.

‡: 'Workflow completed' in the observation note refers to a situation where volunteers were able to complete the workflow without any observed difficulties.

5.6 Analytical evaluation of volunteers' data

Analytical evaluation of the measurement data obtained by volunteers was done in three different steps; preconcentration, use of μ PADs, and picture-taking. This separation was necessary to identify which (if any) steps may result in errors. However, it is also important to keep in mind that since the steps were sequential, errors from the previous step would be compounding to the next step.

The workflow used for the water sampling process is illustrated in Figure 97. Here, the workflow is divided into two: researchers and volunteers. The researcher workflow outlines the steps taken by researchers upon obtaining the water sample and throughout the volunteer activity. First, the water sample's metal content was analysed with ICP, it is also subsequently tested for Zn^{2+} and Ni^{2+} with a developed preconcentration workflow – creating control data for the developed μ PAD workflow.

Upon the start of the volunteer testing process, 300 mL of the water sample was poured into the cafetiere by the volunteer and used for the first part of the preconcentration step, involving repeated plunging of the resin into the water. After this adsorption process, the resin basket would be removed from the cafetiere. The water sample left in the cafetiere was stored for further volume measurement, while volunteers proceed to complete the elution step. In the elution step, the resin basket was swirled for 5 min, and a μ PAD was then dipped into the elution solution. This workflow was developed more in the details in Chapter 4. The μ PAD was then removed for the picture-taking step by the volunteer. While the volunteer proceeded to fill out the questionnaire, researchers stored the elution solution produced by the volunteers, as well as took pictures of the μ PADs used by the volunteer with the black box method.

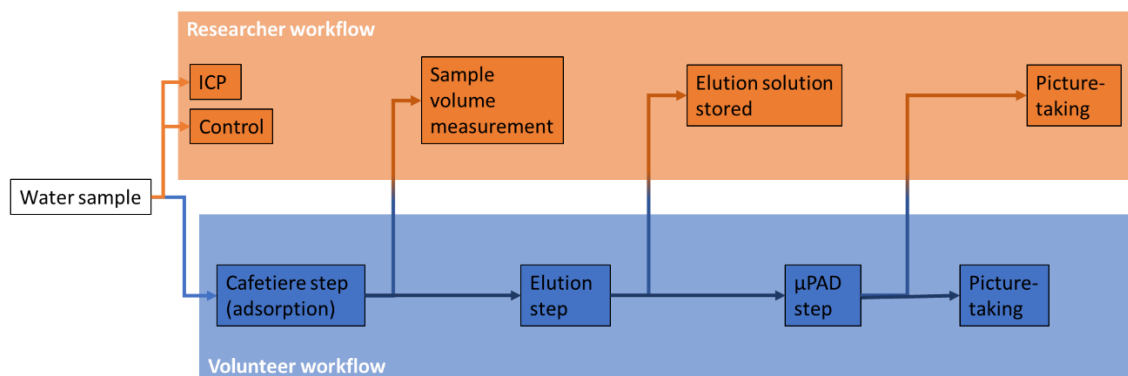


Figure 97 Sampling workflow relative to the volunteer testing activity

In evaluating the preconcentration step, the elution solution produced by the volunteers was gathered and analysed with the developed μ PAD by the researcher. The result was then compared to the control data obtained by the researcher (see section 0, or Figure 98) and to the ICP measurement of the same water sample. Through this process, it can be determined whether the volunteers were able to complete the preconcentration step and produce accurate results – affirming the suitability of the developed preconcentration step for citizen-led monitoring efforts.

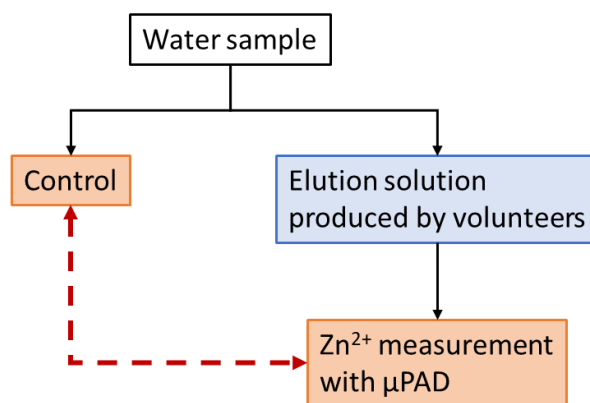


Figure 98 Assessment of the volunteer’s preconcentration accuracy was done through comparison between the Zn^{2+} measured in the volunteer’s elution solution to control data (red dashed line).

5.6.1 Preconcentration step

Figure 99 shows a box plot of the Zn^{2+} concentration measured in the elution solution produced by the volunteers, compared to the control measurement made by researchers (shown as a black line marked with X). Through this comparison, it is obvious that in non-spiked water samples, the volunteers’ results agreed relatively well with the control data. Except in the non-spiked tap water sample where the volunteer data was notably lower than the control data. However, in the spiked water sample, the preconcentration result by the volunteers spread across quite a wide variance. In spiked Milli-Q sample. Conversely, in the spiked SuDS water sample, some of the volunteers’ data range was n close to the control data, whilst others were nearly four times the control data. While the preconcentration process in spiked tap water samples showed a lower measured concentration of Zn^{2+} compared to the control.

Each of the errors in this preconcentration data can be correlated to the observational data during the volunteer testing activity, as detailed in Table 20. For example, in the SuDS water sample, it was observed that out of the five volunteers working with the sample, four experienced some form of resin leakage through the preconcentration step. This was an interesting observation which would need further investigation on whether it was an error in the equipment used by the volunteers (coincidental) or whether there is a correlation between the sample type and the difficulty in the preconcentration step. Either way, the leakage could lead to an increase in adsorption and subsequently elution, provided that the leaked resins were transferred into the elution solution. Leakage during elution – which was observed in a number of cases during volunteer work – could exacerbate this effect, since it allowed bigger and less controlled surface area of the resins to be in contact with the elution solution. This condition may be the main cause of the positive increase (higher than the target concentration) of the Zn^{2+}

amount detected in the elution solution, seemingly creating a higher elution performance than the design.

Similarly, but resulting a reverse effect is leakage during the plunging process without being followed with a complete transfer of the released resin to the elution solution. In some cases, it was observed that by the point of elution, the amount of resin available in the modified basket swirled by the volunteers was significantly lower than initially provided. The consequence of this event is: despite similar elution performance, the amount of Zn^{2+} available for elution was low, to begin with. Therefore, the concentration of Zn^{2+} detected with the μ PAD was lower than the control. This fact just highlights the importance of further design improvement to mitigate aggressive plunging by users and reduce leakage incidence. It also highlights the importance of multiple measurements with this type of device, since the average value in each group of samples resulted in closer results to the control – with both extreme cases of measurement results eliminating each other's effect.

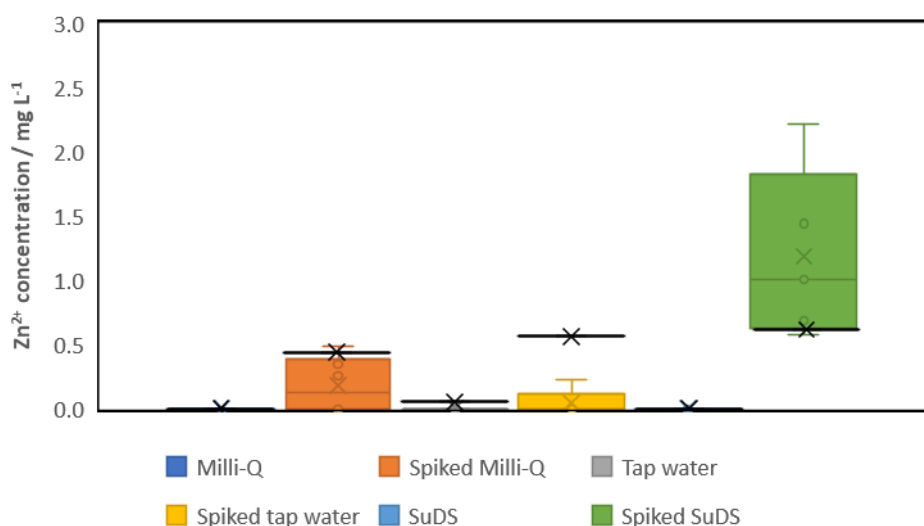


Figure 99 Preconcentration data produced by volunteers, as measured with a μ PAD by the researcher, in comparison to the control data produced by the researcher. Coloured lines indicate the maximum, median, and minimum values of the dataset, while coloured x symbolizes the mean of the dataset and circles indicate data points within the dataset. The black line with x indicates the value obtained in control.

5.6.2 μ PAD step

The accuracy of the μ PADs step as operated by the volunteers was evaluated by taking a picture of the μ PAD dipped into the elution solution by the volunteers after the appropriate incubation time (Figure 100). The key to this evaluation is to observe whether the μ PAD detection step done by the volunteers was comparable to the result obtained by the researcher upon dipping into

the same elution solution. This isolates the μ PAD from the entirety of the workflow and allows for analysis of only the μ PAD accuracy by volunteers.

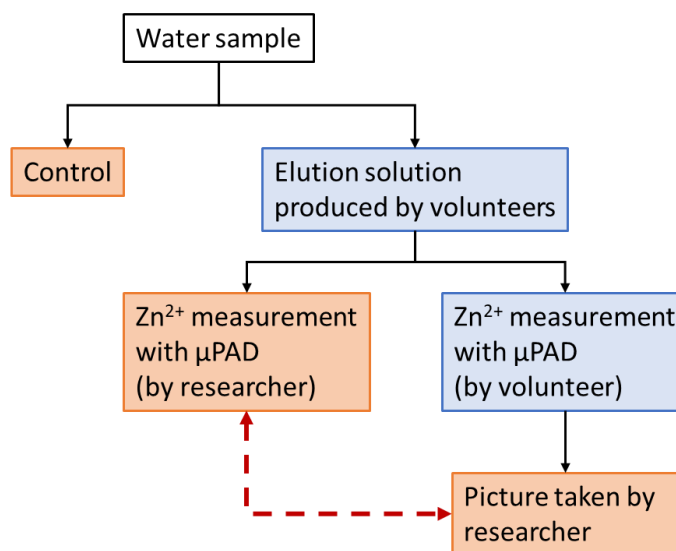


Figure 100 Assessment of volunteer's μ PAD accuracy was done through comparison between the Zn^{2+} measured in the volunteer's elution solution done by the volunteer and researcher (red line); in both cases, pictures of the μ PADs were taken by the researcher using the black box method.

As seen in

[Table 21](#)

[Table 21](#), in most of the non-spiked water samples, the μ PAD by volunteers agreed with the result obtained by the researcher, with the exception of two data in the SuDS sample where the volunteers seemingly were able to detect Zn^{2+} while the researcher's μ PAD did not return quantifiable result. However, even in the spiked water sample, the volunteer's μ PAD was able to produce relatively reliable results compared to the researcher's result. The biggest discrepancy found was at 0.78 mg L^{-1} difference, where volunteers' μ PAD produced a lower value than researchers in an elution solution of spiked SuDS sample code R4.

Table 21 Comparison between Zn²⁺ concentration measured from the elution solution – which was produced by the volunteers – by researchers and volunteers.

	Researcher	Volunteer
Milli-Q		
R1	0.00	0.00
R2	0.00	0.00
R3	0.00	0.00
R4	0.00	0.00
R5	0.00	0.00
Spiked Milli-Q		
R1	0.00	0.00
R2	0.25	0.11
R3	0.35	0.37
R4	0.00	0.33
R5	0.49	0.12
R6	0.00	0.05
Tap water		
R1	0.00	0.00
R2	0.00	0.00
R3	0.00	0.00
R4	0.00	0.00
R5	0.00	0.00
Spiked tap water		
R1	0.00	0.00
R2	0.00	0.64
R3	0.23	0.00
R4	0.00	0.00
R5	0.00	0.00
SuDS		
R1	0.00	0.23
R2	0.00	0.34
R3	0.00	0.00
R4	0.00	0.00
R5	0.00	0.00
Spiked SuDS		
R1	0.57	0.75
R2	1.44	1.02
R3	0.69	0.82
R4	2.22	1.44
R5	1.01	0.91

Comparing the volunteer μ PAD result to the control was also done to observe the compounding effect from the errors in the preconcentration step and μ PAD step. In this comparison, as seen in Figure 101, the compounding effect of errors from the previous step of the process can be seen to affect the result. Control values of spiked samples were all outside the range of variance of the results produced by the volunteers.

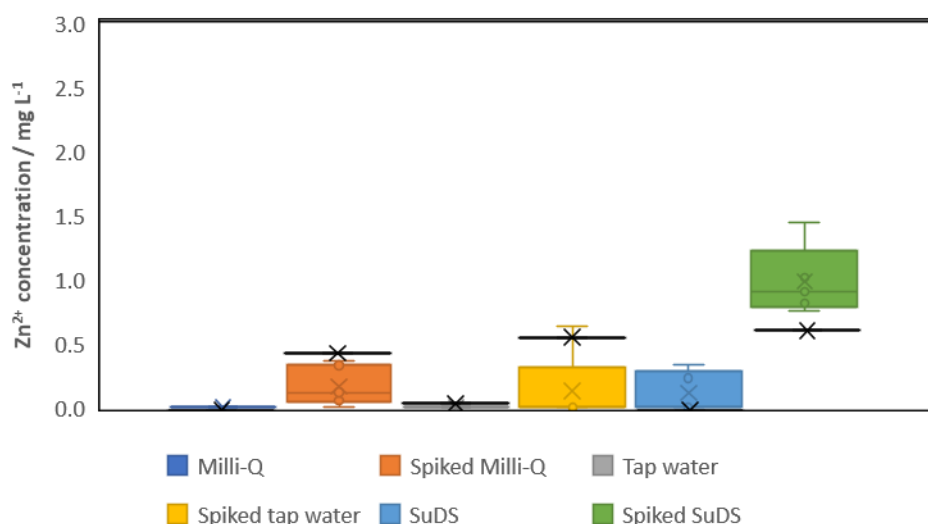


Figure 101 μ PADs data produced by volunteers, as measured with a picture taken by the researcher, in comparison to the control data produced by the researcher. Coloured lines indicate the maximum, median, and minimum values of the dataset, while coloured x symbolizes the mean of the dataset and circles indicate data points within the dataset. The black line with x indicates the value obtained in control.

5.6.3 Picture-taking step

The picture-taking step, utilising the black box provided, was the main reason this analytical evaluation was divided into different steps. The approach was developed to ensure a constant quality of the image of the device taken by the volunteers. Image quality, in this context, is crucial for the image analysis process. This would subsequently affect the quantification of the colour developed on the device, therefore affecting the measured concentration.

This black-box approach had never been tested with untrained users. Throughout the picture-taking step, volunteers were unguided and asked to submit a picture with as good quality as they could. This gave nearly full control of the process to the volunteers – but was done to observe whether the designed black-box process could help to improve the quality of pictures nonetheless. Volunteers were asked to submit the picture through the questionnaire in anonymity.

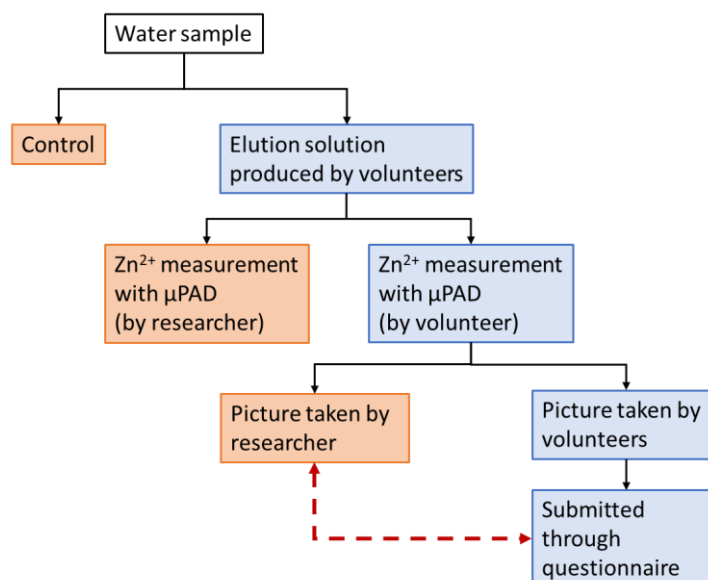


Figure 102 Assessment of volunteer’s picture-taking accuracy was done through comparison between the μ PAD produced by the volunteer, where the volunteer or researcher took the picture of the device (red line).

5.6.3.1 Problem with black-box

The picture-taking step developed in this research, utilising the black box to control the light of the environment was similar to a published article by Zheng, *et.al.* (2022) [202]. In the published study, however, rather than a microfluidic device, the researchers directly utilised a reaction between the sample and colorimetric reagent in a bottle, in a similar manner as a cuvette for UV/Vis spectrophotometry. Claiming to be developed for citizen scientists, the study did not provide any citizen science data or non-researcher data. Therefore, it is possible that this study was the first testing of such a picture-taking method and can be used as an initial indication that the method would not be as intuitive as it seemed for the researcher.

When volunteers were given a black box and asked to place the device underneath and take a picture of the device through the slit, their interpretation of the instructions was varied. Some volunteers decided to place the smartphone vertically, as long as the camera went through the slit. This approach of taking the picture with the black box method instead renders the equipment and method useless. Since the slit was not fully covered, light from the environment would go through and create interferences in the picture. This approach to picture-taking was not considered by the researcher before.

Some tried to zoom in to take a picture with the device filling as much of the frame as possible. As volunteers zoomed in with their smartphones, the pixels of the image grew larger, which could reduce the quality of the picture. Zooming also defeated one purpose of the box, which

was to fix the picture-taking distance. Some also tried to take an image through the slit but did not place their phone on the box, which defeated one of the main purposes of the box to fix the angle and distance between the camera and the μ PAD.

The use of flash during picture-taking also created problems for users, even trained ones. Due to the lamination of the device, triggering a flash while taking a picture might produce reflections, obscuring detail on the μ PAD. However, this can easily be mitigated if the device was not placed directly beneath the flash, but rather slightly to the side of it.

5.6.3.2 The future of black box

This study proved that the black box method, or a picture-taking approach where the volunteers were given an isolated chamber to guarantee picture quality by minimizing light interference may not be as intuitive as had been thought of before. The addition of this equipment did not minimize the need for prior volunteer training. Instead, it potentially complicates the training process since volunteers would be introduced to a new concept. Should an approach with this equipment would be done in the future, this observation had shown that improvements were still needed on the instruction sheet and that the design of black-box was not as intuitive as expected. Therefore, in future, more careful instructions and training will be required. The visual comparison between the difference between trained and untrained picture-taking results with the same black box method is shown in Figure 103. However, accounting for its added complication to an otherwise quite simple process, a simpler alternative without additional equipment may be the best approach for future experiments and workflow development involving volunteers and μ PAD picture taking for analysis.

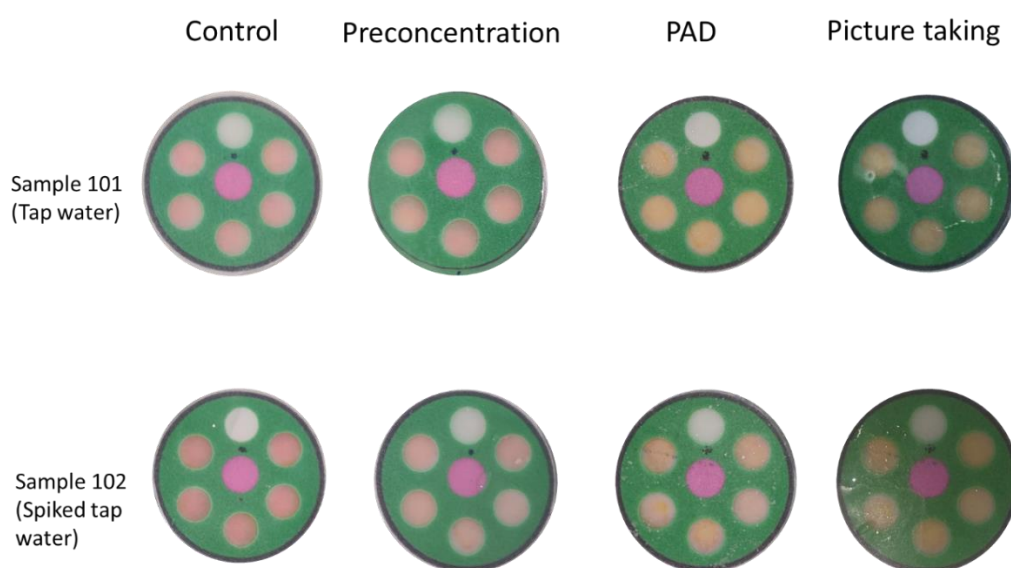


Figure 103 Visual comparison for samples 101 and 102 for Zn^{2+} detection between control

μ PAD by the researcher, evaluation of the volunteer's preconcentration step with the researcher's μ PAD, evaluation of the volunteer's μ PAD with the picture taken by the researcher, and evaluation of the picture submitted by the volunteers.

[5.6.4](#) Evaluation of volunteers' data

5.6.4 [Table 22](#)

[Table 22](#) serves as a complete comparison between the three steps done by the volunteers, which shows how different the results measured from the volunteers' image submission to the data partly collected by the researcher. For this step, however, the discrepancy can directly be seen just by visually comparing the image obtained from the volunteers to the image gathered by the researcher. It is duly noted, at this point, that the workflow was able to produce relatively reliable results up to the point when the μ PAD were used. However, the picture-taking process still needs a lot of work and possibly extensive training. This is of extreme importance since the monitoring process through the citizen science method would depend on an unsupervised monitoring activity by citizen scientists. And the picture submitted by these volunteers would be the sole basis of concentration estimation.

Table 22 Comparison between Zn²⁺ concentration measured by volunteers in the produced preconcentration's elution solution used μ PAD and picture of the μ PAD submitted.

	Preconcentration	PAD	Picture-taking
Milli-Q			
R1	0.00	0.00	0.00
R2	0.00	0.00	0.00
R3	0.00	0.00	0.00
R4	0.00	0.00	0.00
R5	0.00	0.00	0.28
Spiked Milli-Q			
R1	0.00	0.00	0.57
R2	0.25	0.11	2.00
R3	0.35	0.37	0.00
R4	0.00	0.33	0.00
R5	0.49	0.12	2.69
R6	0.00	0.05	0.00
Tap water			
R1	0.00	0.00	0.00
R2	0.00	0.00	0.00
R3	0.00	0.00	0.00
R4	0.00	0.00	0.00
R5	0.00	0.00	0.00
Spiked tap water			
R1	0.00	0.00	0.45
R2	0.00	0.64	0.00
R3	0.23	0.00	0.31
R4	0.00	0.00	0.00
R5	0.00	0.00	0.00
SuDS			
R1	0.00	0.23	0.00
R2	0.00	0.34	0.00
R3	0.00	0.00	0.00
R4	0.00	0.00	0.67
R5	0.00	0.00	0.45
Spiked SuDS			
R1	0.57	0.75	0.00
R2	1.44	1.02	0.81
R3	0.69	0.82	0.90
R4	2.22	1.44	2.77
R5	1.01	0.91	0.54

The high variance of the overall Zn²⁺ detection workflow performed fully by the volunteers – up to the picture-taking step, is shown in Figure 104. Here, the highest variance was observed in spiked Milli-Q and spiked SuDS samples. The variance observed in this step, however, is a mixture of compounding errors from previous steps, as well as personal familiarity with photography concepts and skillsets.

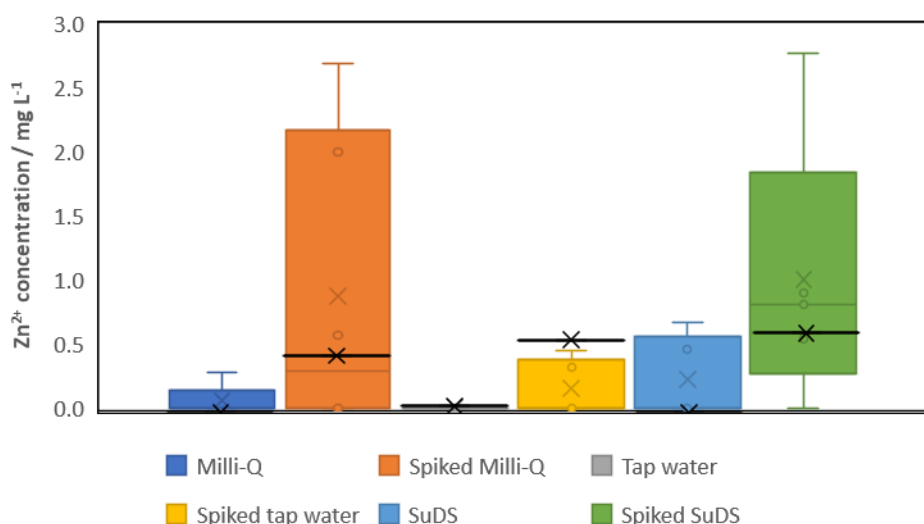


Figure 104 μ PADs pictures produced by volunteers, as measured with a picture taken by the volunteers, in comparison to the control data produced by the researcher. Coloured lines indicate the maximum, median, and minimum values of the dataset, while coloured x symbolizes the mean of the dataset and circles indicate data points within the dataset. The black line with x indicates the value obtained in control.

5.6.5 Errors in volunteers' data

Paper-based devices are a relatively novel approach for the detection of heavy metals in water samples for volunteers. For most, this study was their first contact with the technology; and often, in previous studies, paper-based devices were not necessarily tested by volunteers. This lack of exposure to the technology may translate to error due to unfamiliarity with the device in this research, especially since the volunteers were not trained extensively beforehand. Rather, they were only given access to instruction mere minutes before they had to do the experiment, although it was accompanied by the researcher's explanation. Therefore, there might not be enough explanation and time for trial-and-error for the volunteers, resulting in compounding, bigger-and-bigger errors with each step.

However, it is important to note that this case, of the accuracy of volunteers or citizen science data compared to 'professional' or control data, had long been discussed in the field. Cases comparing long-running citizen science activities with long and well-developed methods still find errors compared to professional datasets, such as documented in Albus, *et.al.* (2020) [188]. This further underlines the importance of training and clear instruction for the volunteers in order to improve their accuracy – two aspects which were lacking in this research. In Richardson, *et.al.* and Ho, *et.al.*, for example, citizen scientists were required to attend a full-day training before conducting any individual sampling procedures [198, 201].

5.7 Volunteers' feedbacks

After the testing step, volunteers were asked to provide feedback on the developed workflow. The questions posed in this survey was focusing on the volunteers' opinions and perceptions of the developed workflow, with an emphasis on its duration and simplicity. Regarding the duration of the workflow, volunteers were asked to rate the two separate steps, as well as the overall workflow. The options given were between 'too short', 'just right', or 'too long'.

5.7.1 Workflow duration

As shown in Figure 105, the majority of the volunteers agreed that the process duration, as it is currently (± 13 min) was just right. This sentiment was shared between the different steps of the workflow. In both preconcentration and μ PAD steps, 94% of 31 volunteers agreed that the duration currently is just right, while another 3% thought it is too short, and the other 3% thought it was too long. The overall workflow, on the other hand, showed that 97% agreed that the overall workflow was just the right duration, while 3% stated that it is too short.

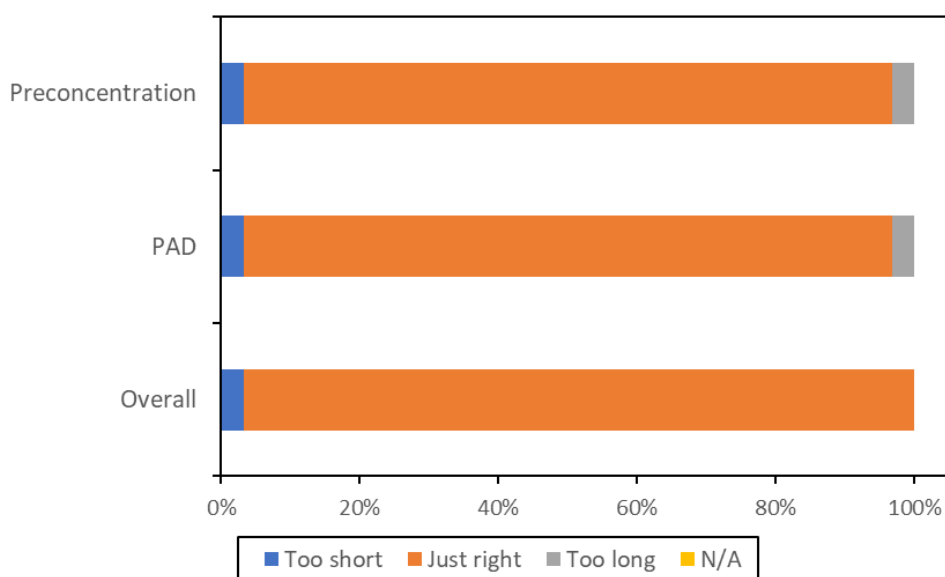


Figure 105 Volunteers' satisfaction in regard to the duration of the developed Zn^{2+} detection workflow is divided into three categories: preconcentration step only, μ PAD step only, and overall workflow.

5.7.2 Workflow simplicity

The simplicity of the developed workflow is another important user experience parameter to be observed in this study. Similar to the duration question, the simplicity of the workflow was also divided into the preconcentration step, μ PAD step, or overall, with the addition of the picture-

taking step. The measure of simplicity is extremely qualitative, and therefore can only be obtained through gathering information from a target user – such as done in this study.

In Figure 106, the simplicity of four different parts of the developed workflow was evaluated by the volunteers. For the preconcentration step, 84% of volunteers stated that the complexity of the process was just right – while another 16% thought it was too easy. This is an interesting insight since it provides the researcher with a baseline of what is perceived as simple by non-specialist users. Further, in evaluating the μ PAD workflow, 81% of volunteers agreed that it is not too complex or too simple, while 19% stated that it was too easy. Therefore, it can be concluded that the μ PAD workflow was only slightly simpler than the preconcentration workflow.

Interestingly, when asked about the simplicity of the picture-taking step, an even higher percentage of volunteers (29%) thought that was too easy. But as had been seen in the analytical data, the picture-taking step was the part where most volunteers were not able to produce replicable data. In this question, only 3% of the volunteers stated that the step was too hard or too complicated – an expected answer in relation to the submitted pictures. Therefore, through this one question, it is interesting to see how the perceived simplicity of the workflow did not translate to accuracy. It is also interesting since through observation, the picture-taking step was the step where most volunteers would ask a question or seek validation on whether they were doing the step correctly, yet upon being asked whether the step was simple enough, most agreed that it was simple enough.

Upon the question on the simplicity of the overall developed workflow, all volunteers agree that the developed workflow was simple enough. This is reflected by the 10% answering that the overall process was too easy, and 90% stating it was just right. However, it is important, at this point, to remember that the volunteers might evaluate this with laboratory settings in mind. In the absence of environmental effects in the field, the developed workflow can sound extremely easy to accomplish. Especially in the laboratory, where most risks are mitigated and the area is relatively controlled.

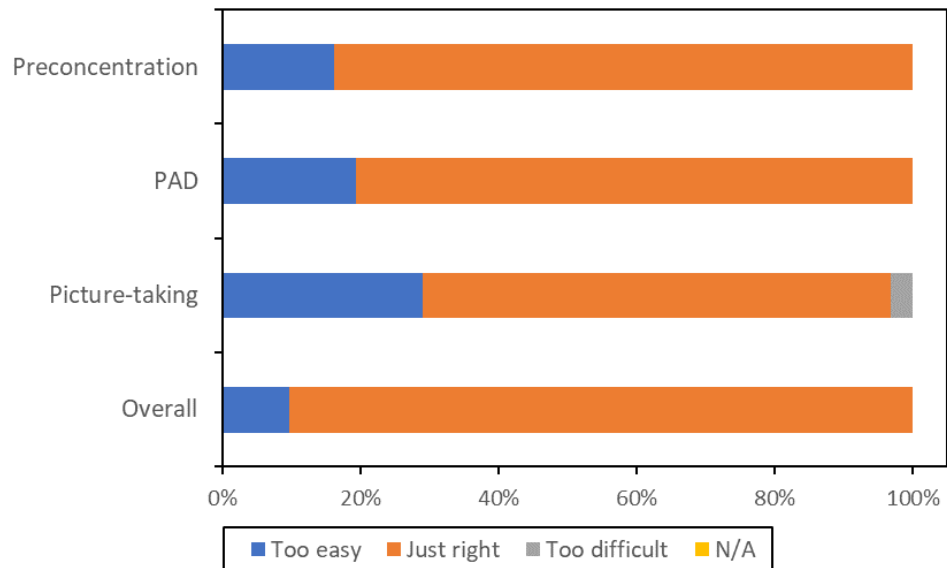


Figure 106 Evaluation of the workflow simplicity divided into four parts: preconcentration, μ PAD, picture-taking, and overall workflow. Volunteers were asked to rate whether each step of the workflow was 'too easy', 'just right', or 'too difficult'.

5.7.3 Applicability in environmental settings

In the following question, an element of imagination was introduced. Volunteers were asked their thoughts on completing the developed workflow in riverbanks settings. This question asked the volunteers to imagine the addition of environmental elements, and whether in this situation, they would be confident enough to test out the workflow. The answer to this question was more diverse, as shown in Figure 107. Most of the volunteers still agreed that it would be easy enough to complete the workflow, even on the field. However, through this question, some started to doubt the simplicity of the workflow for field uses. Here, 13% of the volunteers answered neutral, within the five options. And another 13% stated that it would be somewhat difficult to complete the workflow in riverbank settings. This question was added to remind volunteers that the workflow they were evaluating was intended for field use. Therefore, they were asked to critically think about how to make the workflow even simpler and more accessible for them. In the end, this is the type of feedback that would be most valuable in the further development of this device. This is why directly after this question, volunteers were faced with three open-ended questions, each allowing them to input their ideas to improve the different steps in the workflow: preconcentration, μ PAD, and overall workflow.

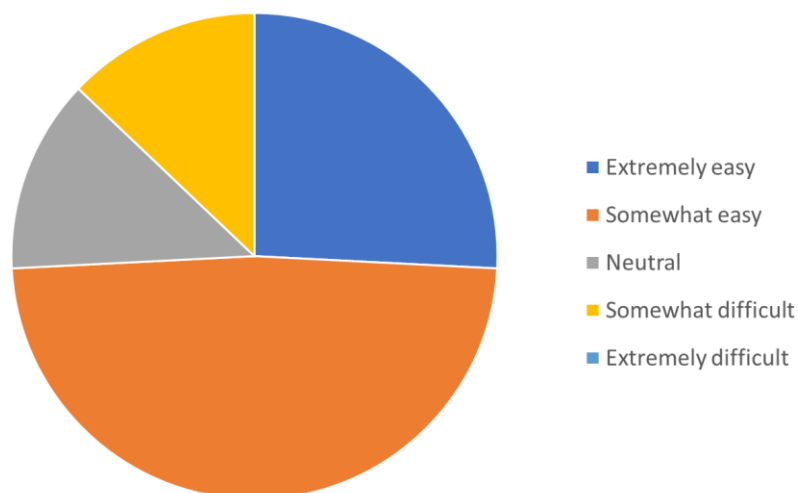


Figure 107 Volunteers' feedback on completing the developed workflow in the riverbank.

5.7.4 Input on preconcentration step – open-ended

The first open-ended question to be analysed was on preconcentration. As a note, however, some feedbacks were a mix between the questions and other steps of the workflow. In Figure 108, the thirty most frequently used words in the feedback on the preconcentration step are presented as a word cloud. One of the most frequent feedback items was on the resin leakage. It was mainly concerned about whether the resins should be released from the basket or should have stayed in the basket. Another interesting input is the inclusion of a timer in the setup. While another addressed the possibility of the effect of bubble formation on the overall workflow and the oxidation-reduction potential (ORP).

One of the most notable feedback items was on the accessibility aspect of the workflow. The repetitiveness of the workflow, despite being vital to its simplicity, can pose a challenge to neurodivergent individuals. It has to be acknowledged, that at this stage of the development, the workflow had not been developed with much accessibility in mind – rather focusing merely on the chemistry (accuracy) and the onsite monitoring aspect (simplicity and duration).



Figure 108 Word cloud of thirty most frequent words used in feedback on the preconcentration step.

5.7.5 Input on μ PAD step – open-ended

Further, the volunteers were asked to provide their input, if any, on the μ PAD step of the workflow. In Figure 109, the thirty most frequent words used in the feedback are presented as a word cloud. Here, the feedback is mainly focused on the design of the μ PAD. Requests to mark the top and bottom side of the μ PAD were the most raised issue, since volunteers seem to have difficulty in determining which side of the μ PAD was the sample entry side – despite the presence of the patterned holes of the laminating paper in the said side. This feedback accentuated the blind spot in the researcher’s design – in thinking that the holes would be enough of a sign on which side should the μ PAD be dipped in. Or that the yellow-coloured detection side would be enough of an indication that that would be where the colour change can be observed.

In observing this problem with the first few volunteers, the researcher tried to give a clearer brief at the beginning of later tests, on which side should be facing up. This was done with multiple different trial and error approaches. Firstly, the researcher was explaining which side was the ‘top side’ at the beginning of the test, however, soon observed that volunteers still needed help in determining the sides upon testing. Next, the researcher added a sign of which side is up with a marker and included this detail in the brief. However still, observed that volunteers needed further confirmation upon testing. Therefore, it can be concluded that this might require an even more fundamental design modification. An even starker difference on which side should be facing the sample upon dipping.

Clearly, this issue would not be as much of a problem if the device was submerged in the sample. Or if volunteers were able to identify whether the water sample had successfully entered the sample well. This brings the next feedback related to whether the device should float or submerge in the solution. This was an interesting point to be brought up because otherwise, it would completely be overlooked by the researcher. Volunteers cannot differentiate whether the sample well is wetted or not – which makes these two feedbacks a bigger issue than expected. The easiest solution, at this point, might be a volunteer training session rather than drastically changing the design of the μ PAD. Because in both cases, changing the design of the μ PAD would not guarantee sample entry to the well – this is a problem that can simply be solved if the observer can identify and confirm sample entry.

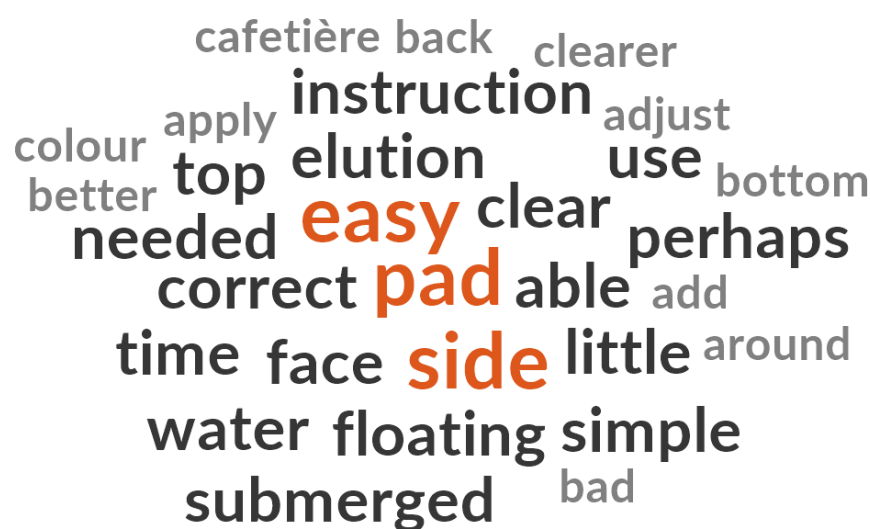


Figure 109 Word cloud of thirty most frequent words used in feedback on the μ PAD step.

5.7.6 Input on picture-taking step – open-ended

In the last feedback section for the overall workflow, volunteers were free to put any input that was not covered in the previous open-ended questions. Similarly, Figure 110 shows the thirty most frequently used words in the question. Here, the last brought-up point in the feedback was on the instruction sheet. Interestingly, in the questionnaire, upon being asked whether the instruction sheet provided was clear, 100% of the volunteers answered yes. However, it is clear from this feedback section, that further improvement was necessary to make it even clearer. The items missing from the instruction sheet included: time, picture-taking procedure, and troubleshooting in case of resin leakage.

Chapter 6 Conclusion

This chapter will summarise the findings of this research in section 6.1. In section 6.2 are suggestions and ideas for future research developing from the contents of this thesis.

6.1 Conclusion

In this research, a workflow has been developed for Ni²⁺ and Zn²⁺ detection in freshwater environments for the use of citizen scientists. This study began with the development of microfluidics paper-based analytical devices (μ PAD) for Ni²⁺ and Zn²⁺ detection. It described designs and optimisation of the device and the workflows, with the target user in mind. We have successfully developed Ni²⁺-detection μ PAD with nioxime as a colorimetric reagent, with a detection limit of 3 mg L⁻¹ Ni²⁺. Key to the μ PADs developed in this research is their ability to produce a rapid result, within 4 minutes. This is a significant improvement in the description of previously described devices. Additionally, the use of nioxime for Ni²⁺ detection in μ PAD is novel in this research, giving the advantage of easier reagent introduction to the μ PAD. Therefore, in comparison with previous devices, the μ PAD developed for Ni²⁺ detection in this research has the advantages of (1) an easier manufacturing process, (2) faster production of colorimetric signal and detection result, as well as (3) simpler sample introduction through dipping mechanism. Table 23 listed several key parameters, including colorimetric reagent, reaction time, detection limit, and sample introduction method, comparing the μ PAD developed in this research to previous studies.

Table 23 Key comparison of several parameters between developed Ni²⁺ detection μ PAD to previous studies.

Ref	Reagent	Reaction time /min	LOD / mg L ⁻¹	Sample introduction method
[80]	3 μ L 60 mM dimethylglyoxime	120	5.9	Pipetted to a sample zone
[81]	100 mM dimethylglyoxime		100	Pipetted to a sample zone
[77]	Dimethylglyoxime		15	Pipetted to a sample zone
[75]	10 μ L 0.1 M dimethylglyoxime	10	4.8	Pipetted to a sample zone
[13]	30 μ L 0.15 mol L ⁻¹ dimethylglyoxime	20	0.3	Pipetted to a sample zone
[82]	Dimethylglyoxime	5	0.24	Pipetted to a sample zone
This study	1400 mg L ⁻¹ nioxime	4	3 1 [†]	Device dipped into the sample

†: with integrated preconcentration workflow

Next, further integration of ion-exchange-based preconcentration process – simplified through the use of cafetiere as preconcentration vessel, with Lewatit® MonoPlus SP 112 as resins were done. In achieving this, a slight modification process was done in the cafetiere design, in order to allow resin placement in the cafetiere itself. This was done by swapping the metallic mesh of the cafetiere with a PMMA basket with >500 holes, where resin can be deposited safely. The integration of preconcentration workflow was able to improve the performance of the μ PAD, allowing it to detect down to $1 \text{ mg L}^{-1} \text{ Ni}^{2+}$ concentration. This simple and rapid workflow was a novel, simpler alternative, with the potential for an onsite preconcentration method for Ni^{2+} and Zn^{2+} in freshwater systems.

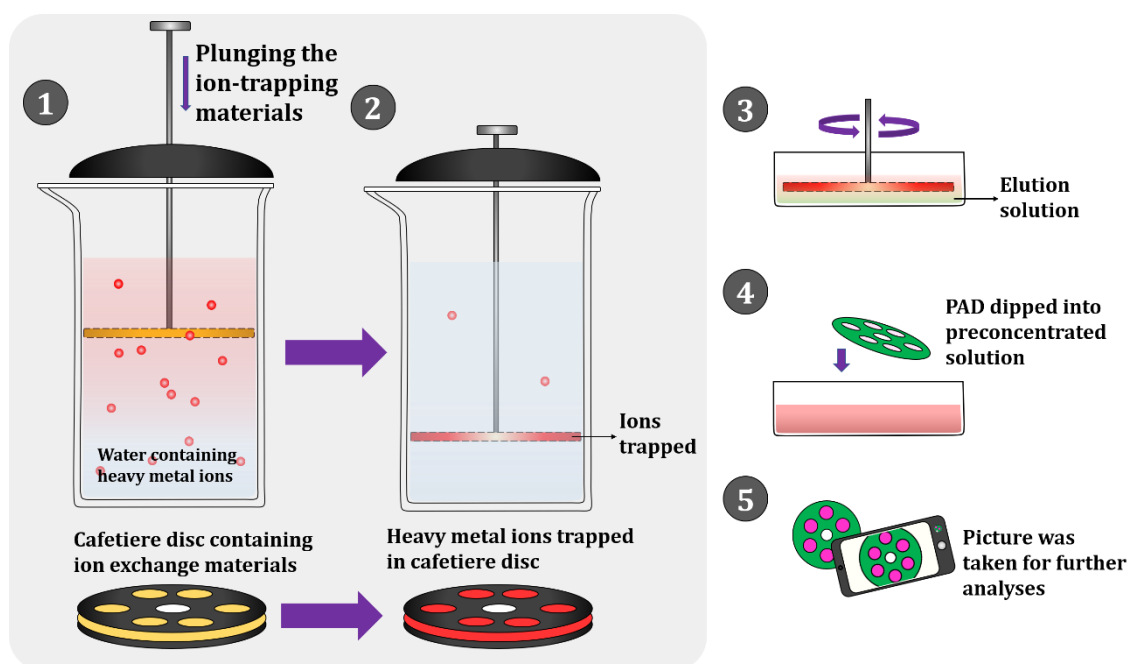


Figure 111 Illustration of simple and rapid preconcentration workflow developed for onsite preconcentration of Ni^{2+} and Zn^{2+} using cafetiere and ion-exchange resin Lewatit SP 112.

A similar workflow was also developed for Zn^{2+} detection. μ PAD with 5-Br-PAPs as colorimetric reagent was developed and integrated with a preconcentration process with cafetiere and Lewatit® MonoPlus SP 112 as cation exchange resin. The integration of preconcentration workflow in this process was able to improve the performance of the developed μ PAD from a limit of detection of 0.5 mg L^{-1} to $0.1 \text{ mg L}^{-1} \text{ Zn}^{2+}$ concentration. This further underlines the potential of the developed preconcentration workflow in enhancing the performance of μ PADs for metal detection in freshwater samples. Table 24 listed several key parameters, including colorimetric reagent, reaction time, detection limit, and sample introduction method, comparing the μ PAD developed in this research to previous studies.

Table 24 Key comparison of several parameters between developed Zn²⁺ detection μ PAD to previous studies.

Ref	Reagent	Reaction time / min	LOD / mg L ⁻¹	Sample introduction method
[13]	2 μ L 0.5 mg mL ⁻¹ dithizone	15	0.04	Pipetted to a sample zone
[12]	3 μ L 0.4 mM zincon monosodium salt	1	0.63	Pipetted to a sample zone
[83]	1.6 mM zincon monosodium salt	15	8	Pipetted to a sample zone
This study	100 mg L ⁻¹ 5-Br-PAPs	5	0.5 0.1 [†]	Device dipped into the sample

†: with integrated preconcentration workflow

Lastly, a user-experience observation was done to observe the usability of the developed workflow with its targeted user. 31 student volunteers participated in the study, testing the workflow for Zn²⁺ detection in water samples. The overall reception of the workflow was positive from the users, with more than 50% agreeing that the developed workflow would be simple enough to use in riverbank settings (Figure 112). However, further improvements would be necessary to enhance the data quality required for reliable Zn²⁺ measurements.

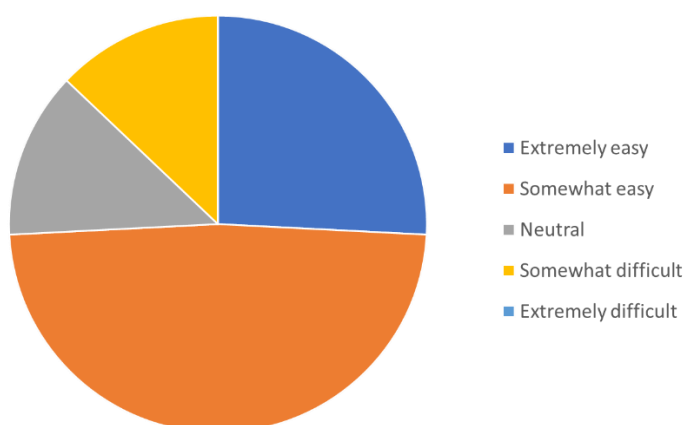


Figure 112 User feedback on the usability of the device in riverbank settings.

6.2 Future research

Despite the findings in this study, the metal detection workflow development for the citizen science approach can still benefit from further research. Due to constraints as well as the established scope of this research, not all gaps were identified and observed in the study and therefore can be addressed in future studies, as discussed below and summarized in Table 25.

Several approaches for future research identified in this section were: (1) research on alternative colorimetric reagents, adsorption materials, and elution solutions; (2) development of a mobile app as a companion for citizen-science-based detection; and (3) user experience evaluation with wider demographic coverage.

Further research into alternative colorimetric reagents for the μ PAD can aid in exploring other viable options for metal detection, especially Ni^{2+} and Zn^{2+} . Other reagents may provide higher selectivity and sensitivity, or detection at $\mu\text{g L}^{-1}$ level. Higher selectivity of reagent can also open the possibility of simultaneous multiplex detection of several different metal species, therefore, further improving the device. In similar veins, research into alternative adsorption materials and elution solutions could also enhance workflow performance by improving the preconcentration step. In order to improve the process, alternative adsorption material and elution solutions should maintain (1) rapid adsorption and elution capabilities, (2) low environmental and health risks, and (3) cost-effectiveness, while further improve on the adsorption and elution capacities.

Aside from improvements that can be made as stated above, a mobile app can be developed to improve the volunteer's workflow. A mobile app with camera access that is tailored for picture taking of the device would aid the volunteers greatly. The mobile app should be able to automatically aid with picture correction, namely by (1) controlling the shadow on the image and (2) correcting the angle of the device upon picture taking process. Ideally, the mobile app should also be able to (3) automatically measure the colour intensity of the sample wells and reference circle, followed by (4) automated calculation and interpolation of the analyte concentration based on an updateable calibration curve database. Despite all these features, the mobile app should still be able to (5) save and upload the raw image taken by the volunteers to a database that would allow the researcher to verify the concentration of analyte detected. By adding an automated step to the workflow, the image and data quality obtained by the volunteers would notably improve, consequently improving the data gathered by the researchers.

Another improvement that can be made was to conduct a user experience study on a larger scale. This study would require a bigger number of volunteers, preferably with more diverse

backgrounds. This might be achieved by working with citizen science groups or communities living near the rivers, as well as opening a public call for volunteers. A bigger scale of user experience study would allow a better assessment of the required improvement to ensure that the developed device would be suitable for use by target users – the public.

Table 25 Research gap to be addressed in future research and suggested strategy.

Research gap	Research strategy
Increase in workflow detection sensitivity	<ul style="list-style-type: none"> - Alternative water-soluble reagent for Ni²⁺ and Zn²⁺ detection - Alternative adsorption material for the preconcentration process - Alternative elution step for the preconcentration process
Simultaneous detection of multiple metal species	<ul style="list-style-type: none"> - Alternative reagents with high selectivity - Further investigation of the masking reagent. - μPAD design alternation to aid selectivity
Simplification in the data acquisition process	<ul style="list-style-type: none"> - Mobile app for citizen scientists
User experience evaluation	<ul style="list-style-type: none"> - A larger scale of evaluation, involving wider demography

References

1. Zhou, Q., et al., *Total concentrations and sources of heavy metal pollution in global river and lake water bodies from 1972 to 2017*. Global Ecology and Conservation, 2020. **22**.
2. World Health Organization, *Environmental Health Criteria for Zinc*. 2001.
3. Tchounwou, P.B., et al., *Heavy metal toxicity and the environment*. Exp Suppl, 2012. **101**: p. 133-64.
4. World Health Organization, *Guidelines for Drinking-water Quality*. 2008.
5. Moss, B., *Ecology of Freshwaters: a view for the twenty-first century*. 4th edition ed. 2010: Blackwell Publishing.
6. Dodds, W. and M. Whiles, *Freshwater Ecology*. 2nd edition ed. Aquatic ecology series, ed. J.H. Thorp. 2010: Elsevier.
7. Denkhaus, E. and K. Salnikow, *Nickel essentiality, toxicity, and carcinogenicity*. Crit Rev Oncol Hematol, 2002. **42**(1): p. 35-56.
8. Genchi, G., et al., *Nickel: Human Health and Environmental Toxicology*. Int J Environ Res Public Health, 2020. **17**(3).
9. Ajala, O.A., et al., *Concentrations, bioaccumulation, and health risk assessments of heavy metals in fishes from Nigeria's freshwater: a general overview*. Environ Sci Pollut Res Int, 2022. **29**(55): p. 82660-82680.
10. Hanrahan, G., D.G. Patil, and J. Wang, *Electrochemical sensors for environmental monitoring: design, development and applications*. J Environ Monit, 2004. **6**(8): p. 657-64.
11. Bansiwali, A., K. Ram, and R. Dahake, *Paper-based microfluidic sensor devices for inorganic pollutants monitoring in water*, in *Inorganic Pollutants in Water*. 2020. p. 399-413.
12. Muhammad-Aree, S. and S. Teepoo, *On-site detection of heavy metals in wastewater using a single paper strip integrated with a smartphone*. Anal Bioanal Chem, 2020. **412**(6): p. 1395-1405.
13. Li, F., et al., *Three-dimensional microfluidic paper-based device for multiplexed colorimetric detection of six metal ions combined with use of a smartphone*. Anal Bioanal Chem, 2019. **411**(24): p. 6497-6508.
14. Shahzad, B., et al., *Nickel; whether toxic or essential for plants and environment - A review*. Plant Physiol Biochem, 2018. **132**: p. 641-651.
15. Hassan, M.U., et al., *Nickel toxicity in plants: reasons, toxic effects, tolerance mechanisms, and remediation possibilities-a review*. Environ Sci Pollut Res Int, 2019. **26**(13): p. 12673-12688.
16. Cempel, M. and G. Nikel, *Nickel: A Review of Its Sources and Environmental Toxicology*. Polish Journal of Environmental Study, 2006. **15**(3): p. 375-382.
17. Blewett, T.A. and E.M. Leonard, *Mechanisms of nickel toxicity to fish and invertebrates in marine and estuarine waters*. Environ Pollut, 2017. **223**: p. 311-322.
18. Wang, Q., et al., *Ranking Ecological Risk of Metals to Freshwater Organisms in Lake Taihu, China*. Journal of Chemistry, 2020. **2020**: p. 1-6.
19. Public Health England, *Nickel Toxicological Overview*. 2009, Public Health England.
20. World Health Organization, *Nickel*, in *WHO air quality guidelines for Europe*. 2000, World Health Organization.
21. Das, K.K., S.N. Das, and S.A. Dhundasi, *Nickel, its adverse health effects & oxidative stress*. Indian Journal of Medical Research, 2008. **128**: p. 412-425.
22. Agency for Toxic Substance and Disease Registry, *Public Health Statement: Nickel*. 2005, Agency for Toxic Substance and Disease Registry.
23. Broadley, M.R., et al., *Zinc in plants*. New Phytol, 2007. **173**(4): p. 677-702.
24. Hafeez, B., Y.M. Khanif, and M. Saleem, *Role of Zinc in Plant Nutrition- A Review*. American Journal of Experimental Agriculture, 2013. **3**(2): p. 374-391.

25. Swain, P.S., et al., *Nano zinc, an alternative to conventional zinc as animal feed supplement: A review*. Anim Nutr, 2016. **2**(3): p. 134-141.
26. Nriagu, J., *Zinc Toxicity in Humans*. School of Public Health, University of Michigan, 2007: p. 1-7.
27. Plum, L.M., L. Rink, and H. Haase, *The essential toxin: impact of zinc on human health*. Int J Environ Res Public Health, 2010. **7**(4): p. 1342-65.
28. Environment Agency, *Water quality archive dataset*, Environment Agency, Editor. 2020, Environment Agency.
29. Environment Agency, *Water quality archive dataset*, E. Agency, Editor. 2019.
30. Al-Fartusie, F.S. and S.N. Mohssan, *Essential Trace Elements and Their Vital Roles in Human Body*. Indian Journal of Advances in Chemical Science 2017. **5**(3): p. 127-136.
31. Hussain, J., et al., *Studies on heavy metal contamination in Godavari river basin*. Applied Water Science, 2017. **7**(8): p. 4539-4548.
32. McRae, M.E., *Nickel Data Sheet*, in *Mineral Commodity Summaries*. 2020.
33. Scottish Environment Protection Agency, *Supporting Guidance (WAT-SG-53): Environmental Quality Standards and Standards for Discharges to Surface Water*. 2020, Scottish Environment Protection Agency.
34. United States Environmental Protection Agency. *National Recommended Water Quality Criteria - Aquatic Life Criteria Table*. 2021 [05/12/2021]; Available from: <https://www.epa.gov/wqc/national-recommended-water-quality-criteria-aquatic-life-criteria-table>.
35. Abdel-Satar, A.M., M.H. Ali, and M.E. Goher, *Indices of water quality and metal pollution of Nile River, Egypt*. The Egyptian Journal of Aquatic Research, 2017. **43**(1): p. 21-29.
36. Bhuyan, M.S., et al., *Heavy metal contamination in surface water and sediment of the Meghna River, Bangladesh*. Environmental Nanotechnology, Monitoring & Management, 2017. **8**: p. 273-279.
37. Bilgin, A. and M.U. Konanç, *Evaluation of surface water quality and heavy metal pollution of Coruh River Basin (Turkey) by multivariate statistical methods*. Environmental Earth Sciences, 2016. **75**(12).
38. Chau, Y.K. and O.T.R. Kulikovskiy-Cordeiro, *Occurrence of nickel in the Canadian environment*. Environ. Rev., 1995. **3**.
39. Wen, Y., Z. Yang, and X. Xia, *Dissolved and particulate zinc and nickel in the Yangtze River (China): Distribution, sources and fluxes*. Applied Geochemistry, 2013. **31**: p. 199-208.
40. Hartono, D.M., E. Suganda, and M. Nurdin, *Metal Distribution at River Water of Mining and Nickel Industrial Area in Pomalaa Southeast Sulawesi Province, Indonesia*. Oriental Journal of Chemistry, 2017. **33**(5): p. 2599-2607.
41. Bodar, C.W.M., M.E.J. Pronk, and D.T.H.M. Sijm, *The european union risk assessment on zinc and zinc compounds: The process and the facts*. Integrated Environmental Assessment and Management, 2005. **1**(4): p. 301-319.
42. Takarina, N.D., *GEOCHEMICAL FRACTIONATION OF TOXIC TRACE HEAVY METALS (CR, CU, PB, AND ZN) FROM THE ESTUARINE SEDIMENTS OF 5 RIVER MOUTHS AT JAKARTA BAY, INDONESIA*. Journal of Coastal Development, 2010. **13**(2).
43. Meybeck, M., *Heavy metal contamination in rivers across the globe: an indicator of complex interactions between societies and catchments*, in *Understanding Freshwater Quality Problems in a Changing World*. 2013, IAHS Press: Gothenburg, Sweden.
44. Sparks, D.L., et al., *Inductively Coupled Plasma Emission Spectrometry and Inductively Coupled Plasma-Mass Spectrometry*, in *Methods of Soil Analysis Part 3—Chemical Methods*. 1996, Soil Science Society of America and American Society of Agronomy.
45. United States Environmental Protection Agency, *METHOD 1640: DETERMINATION OF TRACE ELEMENTS IN WATER BY PRECONCENTRATION AND INDUCTIVELY COUPLED PLASMA-MASS SPECTROMETRY*. 1997: Washington.
46. Ammann, A.A., *Speciation of heavy metals in environmental water by ion chromatography coupled to ICP-MS*. Anal Bioanal Chem, 2002. **372**(3): p. 448-52.

47. Dai, B., et al., *Schiff base-chitosan grafted multiwalled carbon nanotubes as a novel solid-phase extraction adsorbent for determination of heavy metal by ICP-MS*. J Hazard Mater, 2012. **219-220**: p. 103-10.
48. Cengiz, M.F., et al., *Evaluation of heavy metal risk potential in Bogacayi River water (Antalya, Turkey)*. Environ Monit Assess, 2017. **189**(6): p. 248.
49. Juliasih, N.L.G.R., et al., *Verification of the Determination Method of Dissolved Metal Content using ICP-OES and Its Application for River Water in Bandar Lampung City*. Journal of Scientific and Applied Chemistry, 2021. **24**(1): p. 29-36.
50. United States Environmental Protection Agency, *Method 7000A: Atomic absorption methods*. 1990, United States Environmental Protection Agency.
51. Dean, J.R., *Methods for Environmental Trace Analysis*. Analytical techniques in the sciences. 2003: Wiley. 259.
52. Daşbaşı, T., et al., *SPE and determination by FAAS of heavy metals using a new synthesized polymer resin in various water and dried vegetables samples*. Journal of Macromolecular Science, Part A, 2018. **55**(3): p. 288-295.
53. Ghaedi, M., et al., *Flame atomic absorption spectrometric determination of trace amounts of heavy metal ions after solid phase extraction using modified sodium dodecyl sulfate coated on alumina*. J Hazard Mater, 2008. **155**(1-2): p. 121-7.
54. Tuzen, M. and M. Soylak, *Multi-element coprecipitation for separation and enrichment of heavy metal ions for their flame atomic absorption spectrometric determinations*. J Hazard Mater, 2009. **162**(2-3): p. 724-9.
55. Soylak, M. and A. Aydin, *Determination of some heavy metals in food and environmental samples by flame atomic absorption spectrometry after coprecipitation*. Food Chem Toxicol, 2011. **49**(6): p. 1242-8.
56. Ipeaiyeda, A.R. and A.R. Ayoade, *Flame atomic absorption spectrometric determination of heavy metals in aqueous solution and surface water preceded by co-precipitation procedure with copper(II) 8-hydroxyquinoline*. Applied Water Science, 2017. **7**(8): p. 4449-4459.
57. United States Environmental Protection Agency, *Method 200.7, Revision 4.4: Determination of Metals and Trace Elements in Water and Wastes by Inductively Coupled Plasma-Atomic Emission Spectrometry*. 1994.
58. Perkin Elmer, *Analysis of Wastewater for Metals using ICP-OES*. 2020.
59. Thermo Elemental, *AAS, GFAAS, ICP or ICP-MS? Which technique should I use*. 2015.
60. Xiang, H., et al., *Sensors Applied for the Detection of Pesticides and Heavy Metals in Freshwaters*. Journal of Sensors, 2020. **2020**: p. 1-22.
61. Rapp, B.E., *Microfluidics: modeling, mechanics, and mathematics*. Second edition ed. 2023: Elsevier.
62. Whitesides, G.M., *The origins and the future of microfluidics*. Nature, 2006. **442**(7101): p. 368-73.
63. Manz, A., et al., *Microfluidics and Lab-on-a-chip*. 2021: Royal Society of Chemistry.
64. Wang, R. and X. Wang, *Sensing of inorganic ions in microfluidic devices*. Sensors and Actuators B: Chemical, 2021. **329**.
65. Cui, W., et al., *Development and potential for point-of-care heavy metal sensing using microfluidic systems: A brief review*. Sensors and Actuators A: Physical, 2022. **344**.
66. Frau, I., et al., *Detection of Zn in water using novel functionalised planar microwave sensors*. Materials Science and Engineering: B, 2019. **247**.
67. Lin, Y., et al., *Detection of heavy metal by paper-based microfluidics*. Biosens Bioelectron, 2016. **83**: p. 256-66.
68. Milani, A., et al., *Development and application of a microfluidic in-situ analyzer for dissolved Fe and Mn in natural waters*. Talanta, 2015. **136**: p. 15-22.
69. Akyazi, T., L. Basabe-Desmonts, and F. Benito-Lopez, *Review on microfluidic paper-based analytical devices towards commercialisation*. Anal Chim Acta, 2018. **1001**: p. 1-17.
70. Busa, L.S.A., et al., *Advances in Microfluidic Paper-Based Analytical Devices for Food and Water Analysis*. Micromachines (Basel), 2016. **7**(5).

71. Almeida, M., et al., *Developments of microfluidic paper-based analytical devices (muPADs) for water analysis: A review*. Talanta, 2018. **177**: p. 176-190.
72. Salins, L.L., et al., *A fluorescence-based sensing system for the environmental monitoring of nickel using the nickel binding protein from Escherichia coli*. Anal Bioanal Chem, 2002. **372**(1): p. 174-80.
73. Qi, J., et al., *Three-dimensional paper-based microfluidic chip device for multiplexed fluorescence detection of Cu²⁺ and Hg²⁺ ions based on ion imprinting technology*. Sensors and Actuators B: Chemical, 2017. **251**: p. 224-233.
74. Wang, X.-R., et al., *An Ion Imprinted Polymers Grafted Paper-based Fluorescent Sensor Based on Quantum Dots for Detection of Cu²⁺ Ions*. Chinese Journal of Analytical Chemistry, 2015. **43**(10): p. 1499-1504.
75. Sun, X., et al., *Improved assessment of accuracy and performance using a rotational paper-based device for multiplexed detection of heavy metals*. Talanta, 2018. **178**: p. 426-431.
76. Medina-Sanchez, M., et al., *Eco-friendly electrochemical lab-on-paper for heavy metal detection*. Anal Bioanal Chem, 2015. **407**(28): p. 8445-9.
77. Rattanarat, P., et al., *Multilayer paper-based device for colorimetric and electrochemical quantification of metals*. Anal Chem, 2014. **86**(7): p. 3555-62.
78. Nurak, T., N. Praphairaksit, and O. Chailapakul, *Fabrication of paper-based devices by lacquer spraying method for the determination of nickel (II) ion in waste water*. Talanta, 2013. **114**: p. 291-6.
79. Alahmad, W., et al., *A miniaturized chemiluminescence detection system for a microfluidic paper-based analytical device and its application to the determination of chromium(iii)*. Analytical Methods, 2016. **8**(27): p. 5414-5420.
80. Kamnoet, P., et al., *Highly selective simultaneous determination of Cu(ii), Co(ii), Ni(ii), Hg(ii), and Mn(ii) in water samples using microfluidic paper-based analytical devices*. Analyst, 2021. **146**(7): p. 2229-2239.
81. Cate, D.M., et al., *Multiplexed paper analytical device for quantification of metals using distance-based detection*. Lab Chip, 2015. **15**(13): p. 2808-18.
82. Devadhasan, J.P. and J. Kim, *A chemically functionalized paper-based microfluidic platform for multiplex heavy metal detection*. Sensors and Actuators B: Chemical, 2018. **273**: p. 18-24.
83. Kudo, H., et al., *Paper-Based Analytical Device for Zinc Ion Quantification in Water Samples with Power-Free Analyte Concentration*. Micromachines, 2017. **8**(4).
84. Quinn, C.W., et al., *Solid-Phase Extraction Coupled to a Paper-Based Technique for Trace Copper Detection in Drinking Water*. Environ Sci Technol, 2018. **52**(6): p. 3567-3573.
85. Liang, S.-J., et al., *Research and Application Progress of Paper-based Microfluidic Sample Preconcentration*. Chinese Journal of Analytical Chemistry, 2019. **47**(12): p. 1878-1886.
86. Subramanian, V., et al., *Enhancing the sensitivity of point-of-use electrochemical microfluidic sensors by ion concentration polarisation – A case study on arsenic*. Sensors and Actuators B: Chemical, 2020. **304**.
87. Lace, A. and J. Cleary, *A Review of Microfluidic Detection Strategies for Heavy Metals in Water*. Chemosensors, 2021. **9**(4).
88. Mitchell, A.M. and M.G. Mellon, *Colorimetric Determination of Nickel with Dimethylglyoxime*. Industrial & Engineering Chemistry Analytical Edition, 1945. **17**(6): p. 380-382.
89. Ferancová, A., et al., *Complexation of Ni(II) by Dimethylglyoxime for Rapid Removal and Monitoring of Ni(II) in Water*. Mine Water and the Environment, 2016. **36**(2): p. 273-282.
90. Gazda, D.B., J.S. Fritz, and M.D. Porter, *Determination of nickel(II) as the nickel dimethylglyoxime complex using colorimetric solid phase extraction*. Analytica Chimica Acta, 2004. **508**(1): p. 53-59.
91. Poltue, T., et al., *Nickel (II) ions sensing properties of dimethylglyoxime/poly(caprolactone) electrospun fibers*. Materials Letters, 2011. **65**(14): p. 2231-2234.

92. Johnson, W.C. and M. Simmons, *1 : 2 Cyclohexanedionedioxime ("Nioxime") as a Reagent for Nickel*. *Analyst*, 1946. **71**: p. 554-556.
93. Fukushima, Y. and S. Aikawa, *Colorimetric detection of Ni²⁺ based on an anionic triphenylmethane dye and a cationic polyelectrolyte in aqueous solution*. *Tetrahedron Letters*, 2019. **60**(9): p. 675-680.
94. Yun, J. and H. Choi, *Micellar colorimetric determination of iron, cobalt, nickel and copper using 1-nitroso-2-naphthol*. *Talanta*, 2000. **52**: p. 893-902.
95. Inoue, K., S. Aikawa, and Y. Fukushima, *Colorimetric chemosensor for Ni²⁺ based on alizarin complexone and a cationic polyelectrolyte in aqueous solution*. *Journal of Applied Polymer Science*, 2019. **136**(19).
96. Feng, L., et al., *Colorimetric filtrations of metal chelate precipitations for the quantitative determination of nickel(II) and lead(II)*. *Analyst*, 2011. **136**(20): p. 4197-203.
97. Voter, R.C. and C.V. Banks. *Water-Soluble 1,2-Dioximes as Analytical Reagents*. in *2nd Annual Summer Symposium — Organic Reagents*. 1949.
98. Sabel, C.E., J.M. Neureuther, and S. Siemann, *A spectrophotometric method for the determination of zinc, copper, and cobalt ions in metalloproteins using Zincon*. *Anal Biochem*, 2010. **397**(2): p. 218-26.
99. Kocyla, A., A. Pomorski, and A. Krezel, *Molar absorption coefficients and stability constants of Zincon metal complexes for determination of metal ions and bioinorganic applications*. *J Inorg Biochem*, 2017. **176**: p. 53-65.
100. Wang, J., et al., *A micro-plate colorimetric assay for rapid determination of trace zinc in animal feed, pet food and drinking water by ion masking and statistical partitioning correction*. *Food Chem*, 2018. **245**: p. 337-345.
101. Sakamaki, M., S. Aikawa, and Y. Fukushima, *Colorimetric chemosensor for Zn²⁺ based on pyrogallol red and poly(diallyldimethylammonium chloride) in aqueous solution*. *Polymer Bulletin*, 2017. **75**(4): p. 1667-1680.
102. Pourreza, N. and T. Naghdi, *Combined cloud point-solid phase extraction by dispersion of TiO₂ nanoparticles in micellar media followed by semi-microvolume UV-vis spectrophotometric detection of zinc*. *Talanta*, 2014. **128**: p. 164-9.
103. Homsher, R. and B. Zak, *Spectrophotometric Investigation of Sensitive Complexing Agents for the Determination of Zinc in Serum*. *Clin. Chem*, 1985. **31**(8): p. 1310-1313.
104. Makino, T., et al., *A highly sensitive calorimetric determination of serum zinc using water-soluble pyridylazo dye*. *Clinica Chimica Acta*, 1982. **120**: p. 127-135.
105. Johnsen, O. and R. Eliasson, *Evaluation of a commercially available kit for the colorimetric determination of zinc in human seminal plasma*. *Int J Androl*, 1987. **10**(2): p. 435-40.
106. Angamma, C.J. and S.H. Jayaram, *Fundamentals of electrospinning and processing technologies*. *Particulate Science and Technology*, 2015. **34**(1): p. 72-82.
107. Ahmed, F.E., B.S. Lalia, and R. Hashaikeh, *A review on electrospinning for membrane fabrication: Challenges and applications*. *Desalination*, 2015. **356**: p. 15-30.
108. Huang, Y., Y.-E. Miao, and T. Liu, *Electrospun fibrous membranes for efficient heavy metal removal*. *Journal of Applied Polymer Science*, 2014. **131**(19): p. n/a-n/a.
109. Aliabadi, M., et al., *Electrospun nanofiber membrane of PEO/Chitosan for the adsorption of nickel, cadmium, lead and copper ions from aqueous solution*. *Chemical Engineering Journal*, 2013. **220**: p. 237-243.
110. Shariful, M.I., et al., *Adsorption capability of heavy metals by chitosan/poly(ethylene oxide)/activated carbon electrospun nanofibrous membrane*. *Journal of Applied Polymer Science*, 2018. **135**(7).
111. Aliabadi, M., et al., *Design and evaluation of chitosan/hydroxyapatite composite nanofiber membrane for the removal of heavy metal ions from aqueous solution*. *Journal of the Taiwan Institute of Chemical Engineers*, 2014. **45**(2): p. 518-526.
112. Rad, L.R., et al., *Removal of Ni²⁺ and Cd²⁺ ions from aqueous solutions using electrospun PVA/zeolite nanofibrous adsorbent*. *Chemical Engineering Journal*, 2014. **256**: p. 119-127.

113. Botelho, A.B., et al., *EFFECT OF pH TO RECOVER Cu(II), Ni(II) AND Co(II) FROM NICKEL LATERITE LEACH USING CHELATING RESINS*. *Tecnologia em Metalurgia Materiais e Mineração*, 2019. **16**(1): p. 135-140.
114. Pehlivan, E. and T. Altun, *Ion-exchange of Pb²⁺, Cu²⁺, Zn²⁺, Cd²⁺, and Ni²⁺ ions from aqueous solution by Lewatit CNP 80*. *J Hazard Mater*, 2007. **140**(1-2): p. 299-307.
115. Seggiani, M., S. Vitolo, and S. D'Antone, *Recovery of nickel from Orimulsion fly ash by iminodiacetic acid chelating resin*. *Hydrometallurgy*, 2006. **81**(1): p. 9-14.
116. Shek, T., et al., *Kinetics of zinc ions removal from effluents using ion exchange resin*. *Chemical Engineering Journal*, 2009. **146**(1): p. 63-70.
117. Wołowicz, A. and Z. Hubicki, *The use of the chelating resin of a new generation Lewatit MonoPlus TP-220 with the bis-picolyamine functional groups in the removal of selected metal ions from acidic solutions*. *Chemical Engineering Journal*, 2012. **197**: p. 493-508.
118. Dizge, N., B. Keskinler, and H. Barlas, *Sorption of Ni(II) ions from aqueous solution by Lewatit cation-exchange resin*. *J Hazard Mater*, 2009. **167**(1-3): p. 915-26.
119. Kang, S.Y., et al., *Competitive adsorption characteristics of Co²⁺, Ni²⁺, and Cr³⁺ by IRN-77 cation exchange resin in synthesized wastewater*. *Chemosphere*, 2004. **56**(2): p. 141-7.
120. Fil, B.A., et al., *Adsorption of Ni(II) on ion exchange resin: Kinetics, equilibrium and thermodynamic studies*. *Korean Journal of Chemical Engineering*, 2012. **29**(9): p. 1232-1238.
121. Yousef, N.S., R. Farouq, and R. Hazzaa, *Adsorption kinetics and isotherms for the removal of nickel ions from aqueous solutions by an ion-exchange resin: application of two and three parameter isotherm models*. *Desalination and Water Treatment*, 2016. **57**(46): p. 21925-21938.
122. Alyuz, B. and S. Veli, *Kinetics and equilibrium studies for the removal of nickel and zinc from aqueous solutions by ion exchange resins*. *J Hazard Mater*, 2009. **167**(1-3): p. 482-8.
123. Kong, X., Q. Jia, and W. Zhou, *Coupling on-line preconcentration by ion-exchange with microwave plasma torch-atomic emission spectrometry for the determination of cobalt and nickel*. *Microchemical Journal*, 2007. **87**(2): p. 132-138.
124. Akcin, N., I. Koyuncu, and G. Akcin, *Determination of zinc, nickel and cadmium in natural water samples by flame atomic absorption spectrometry after preconcentration with ion exchange and flotation techniques*. *Reviews in Analytical Chemistry*, 2011. **30**(2).
125. Blaney, R.J.P., et al., *Citizen Science and Environmental Monitoring: Towards a Methodology for Evaluating Opportunities, Costs and Benefits*. 2016, UK Environmental Observation Framework.
126. Bonney, R., et al., *Citizen Science: A Developing Tool for Expanding Science Knowledge and Scientific Literacy*. *BioScience*, 2009. **59**(11): p. 977-984.
127. Forrest, S.A., et al., *Citizen science sampling programs as a technique for monitoring microplastic pollution: results, lessons learned and recommendations for working with volunteers for monitoring plastic pollution in freshwater ecosystems*. *Environ Monit Assess*, 2019. **191**(3): p. 172.
128. Jollymore, A., et al., *Citizen science for water quality monitoring: Data implications of citizen perspectives*. *J Environ Manage*, 2017. **200**: p. 456-467.
129. Abbott, B.W., et al., *Trends and seasonality of river nutrients in agricultural catchments: 18years of weekly citizen science in France*. *Sci Total Environ*, 2018. **624**: p. 845-858.
130. Davids, J.C., et al., *Soda Bottle Science—Citizen Science Monsoon Precipitation Monitoring in Nepal*. *Frontiers in Earth Science*, 2019. **7**.
131. Ferede, M., et al., *Multi-method groundwater recharge estimation at Eshito micro-watershed, Rift Valley Basin in Ethiopia*. *Hydrological Sciences Journal*, 2020. **65**(9): p. 1596-1605.
132. Jakositz, S., et al., *Protection through participation: Crowdsourced tap water quality monitoring for enhanced public health*. *Water Res*, 2020. **169**: p. 115209.

133. Cowley, D., *Citizen Science - Environmental Analysis with Paper Microfluidics*. 2019, University of Hull.
134. Xerox, *Solid Ink - Black, Cyan, Yellow, Magenta*, Xerox, Editor. 2007.
135. General Electric Life Sciences, *Laboratory Filtration Product Guide*. 2007, General Electric.
136. Potter, J., P. Brisk, and W.H. Grover, *Using printer ink color to control the behavior of paper microfluidics*. Lab Chip, 2019. **19**(11): p. 2000-2008.
137. Banks, C.V. and S. Anderson, *Stability Constants and Intrinsic Solubility of Several Nickel (II)-vic-Dioxime Complexes*. Inorganic Chemistry, 1962. **2**(1): p. 112-115.
138. Banks, C.V. and D.W. Barnum, *Intermolecular Metal-Metal Bonds and Solubility of Some Nickel and Palladium Complexes of vic-Dioximes*. Journal of the American Chemical Society, 1958. **80**: p. 3579-3582.
139. Sigma Aldrich, *Poly(diallyldimethylammonium chloride) solution: Product Specification*, S. Aldrich, Editor. 2019.
140. Wang, H., et al., *Paper-based three-dimensional microfluidic device for monitoring of heavy metals with a camera cell phone*. Anal Bioanal Chem, 2014. **406**(12): p. 2799-807.
141. Dean, J.A., *Lange's Handbook of Chemistry*. Fifteenth edition ed. 1999, United States of America: McGraw-Hill, Inc.
142. Antaby, E., K. Klinkhammer, and L. Sabantina, *Electrospinning of Chitosan for Antibacterial Applications—Current Trends*. Applied Sciences, 2021. **11**(24).
143. Cui, C., et al., *Electrospun chitosan nanofibers for wound healing application*. Engineered Regeneration, 2021. **2**: p. 82-90.
144. Ohkawa, K., et al., *Electrospinning of Chitosan*. Macromolecular Rapid Communications, 2004. **25**(18): p. 1600-1605.
145. Habiba, U., et al., *Chitosan/(polyvinyl alcohol)/zeolite electrospun composite nanofibrous membrane for adsorption of Cr(6+), Fe(3+) and Ni(2)*. J Hazard Mater, 2017. **322**(Pt A): p. 182-194.
146. Lemma, S.M., F. Bossard, and M. Rinaudo, *Preparation of Pure and Stable Chitosan Nanofibers by Electrospinning in the Presence of Poly(ethylene oxide)*. Int J Mol Sci, 2016. **17**(11).
147. Pakravan, M., M.-C. Heuzey, and A. Ajji, *A fundamental study of chitosan/PEO electrospinning*. Polymer, 2011. **52**(21): p. 4813-4824.
148. Pohl, P. and B. Prusisz, *Pre-concentration of Cd, Co, Cu, Ni and Zn using different off-line ion exchange procedures followed by the inductively coupled plasma atomic emission spectrometric detection*. Analytica Chimica Acta, 2004. **502**(1): p. 83-90.
149. Wang, J. and E.H. Hansen, *Coupling on-line preconcentration by ion-exchange with ETAAS A novel flow injection approach based on the use of a renewable microcolumn as demonstrated for the determination of nickel in environmental and biological samples*. Analytica Chimica Acta, 2000. **424**: p. 223-232.
150. Singh, Y.P., et al., *Optimization of electrospinning process & parameters for producing defect-free chitosan/polyethylene oxide nanofibers for bone tissue engineering*. J Biomater Sci Polym Ed, 2020. **31**(6): p. 781-803.
151. Shawky, H.A., *Synthesis of ion-imprinting chitosan/PVA crosslinked membrane for selective removal of Ag(I)*. Journal of Applied Polymer Science, 2009. **114**(5): p. 2608-2615.
152. Vold, I.M.N., et al., *Binding of ions to chitosan—selectivity studies*. Carbohydrate Polymers, 2003. **54**(4): p. 471-477.
153. Juang, R.-S. and H.-J. Shao, *Effect of pH on Competitive Adsorption of Cu(II), Ni(II), and Zn(II) from Water onto Chitosan Beads*. Adsorption, 2002. **8**: p. 71-78.
154. Wang, J. and C. Chen, *Chitosan-based biosorbents: modification and application for biosorption of heavy metals and radionuclides*. Bioresour Technol, 2014. **160**: p. 129-41.
155. Ferreira, S.L.C., W.N.L. dos Santos, and V.A. Lemos, *On-line preconcentration system for nickel determination in food samples by flame atomic absorption spectrometry*. Analytica Chimica Acta, 2001. **445**: p. 145-151.

156. Moghimi, A., *Preconcentration of trace Ni (II) using C18 disks modified cyclodextrin-chitosan/nano graphene oxide*. African Journal of Pure and Applied Chemistry, 2013. **7**(7): p. 242-251.
157. Sabarudin, A., et al., *Application of chitosan functionalized with 3,4-dihydroxy benzoic acid moiety for on-line preconcentration and determination of trace elements in water samples*. Microchimica Acta, 2007. **159**(3-4): p. 341-348.
158. Duan, B., et al., *Electrospinning of chitosan solutions in acetic acid with poly(ethylene oxide)*. J Biomater Sci Polym Ed, 2004. **15**(6): p. 797-811.
159. Vakili, M., et al., *Regeneration of chitosan-based adsorbents used in heavy metal adsorption: A review*. Separation and Purification Technology, 2019. **224**: p. 373-387.
160. Muzzarelli, R.A.A., *The determination of copper in sea water by atomic absorption spectrometry with a graphite atomizer after elution from chitosan*. Analytica Chimica Acta, 1974. **69**: p. 35-42.
161. Chui, V., et al., *REMOVAL AND RECOVERY OF COPPER(II), CHROMIUM(III), AND NICKEL(II) FROM SOLUTIONS USING CRUDE SHRIMP CHITIN PACKED IN SMALL COLUMNS*. Environment International, 1996. **22**(4): p. 463-468.
162. Beachley, V. and X. Wen, *Effect of electrospinning parameters on the nanofiber diameter and length*. Mater Sci Eng C Mater Biol Appl, 2009. **29**(3): p. 663-668.
163. Nezarati, R.M., M.B. Eifert, and E. Cosgriff-Hernandez, *Effects of humidity and solution viscosity on electrospun fiber morphology*. Tissue Eng Part C Methods, 2013. **19**(10): p. 810-9.
164. Casper, C., et al., *Controlling Surface Morphology of Electrospun Polystyrene Fibers: Effect of Humidity and Molecular Weight in the Electrospinning Process*. Macromolecules, 2004. **37**: p. 573-578.
165. Kolodynska, D., D. Fila, and Z. Hubicki, *Recovery of Lanthanum(III) and Nickel(II) Ions from Acidic Solutions by the Highly Effective Ion Exchanger*. Molecules, 2020. **25**(16).
166. Ates, N. and A. Basak, *Selective removal of aluminum, nickel and chromium ions by polymeric resins and natural zeolite from anodic plating wastewater*. Int J Environ Health Res, 2019: p. 1-18.
167. Littlejohn, P. and J. Vaughan, *Selective elution of nickel and cobalt from iminodiacetic acid cation exchange resin using ammoniacal solutions*. Hydrometallurgy, 2014. **141**: p. 24-30.
168. Botelho Junior, A.B., D.B. Dreisinger, and D.C.R. Espinosa, *A Review of Nickel, Copper, and Cobalt Recovery by Chelating Ion Exchange Resins from Mining Processes and Mining Tailings*. Mining, Metallurgy & Exploration, 2018. **36**(1): p. 199-213.
169. Beck, M.T. and I. Nagypal, *Chemistry of Complex Equilibria*. Ellis Horwood series in inorganic chemistry. 1990: Ellis Horwood Ltd and Akademiai Kiado.
170. Harland, C.E., *Ion exchange: theory and practice*. 2nd edition ed. 1994: Royal Society of Chemistry.
171. Hubicki, Z. and D. Koodynsk, *Selective Removal of Heavy Metal Ions from Waters and Waste Waters Using Ion Exchange Methods, in Ion Exchange Technologies*. 2012.
172. Challenger, O.J., S.J. Hill, and P. Jones, *Separation and determination of trace metals in concentrated salt solutions using chelation ion chromatography*. Journal of Chromatography, 1993. **639**.
173. Nesterenko, P.N. and P. Jones, *Single-column method of chelation ion chromatography for the analysis of trace metals in complex samples*. Journal of Chromatography A, 1997. **770**.
174. Nesterenko, P.N. and P. Jones, *Recent developments in the high-performance chelation ion chromatography of trace metals*. J Sep Sci, 2007. **30**(11): p. 1773-93.
175. Sigma Aldrich. *2-(5-Bromo-2-pyridylazo)-5-[N-propyl-N-(3-sulfopropyl)amino]phenol disodium salt dihydrate*. 2022; Available from: <https://www.sigmaaldrich.com/GB/en/product/sial/93832>.

176. Aposhian, H.V. and M.M. Aposhian, *MESO-2,3-DIMERCAPTOSUCCINIC ACID: Chemical, Pharmacological and Toxicological Properties of an Orally Effective Metal Chelating Agent*. Annu. Rev. Pharmacol. Toxicol., 1990. **30**: p. 279-306.
177. Lenz, G.R. and A.E. Martell, *Metal Chelates of Mercaptosuccinic and α,α' -Dimercaptosuccinic Acids*. Inorganic Chemistry, 1965. **4**(3): p. 378.
178. Lanxess-Lenntech, *Product information: Lewatit TP 207*. 2011, Lanxess.
179. Vincent, A., et al., *Citizen science datasets reveal drivers of spatial and temporal variation for anthropogenic litter on Great Lakes beaches*. Sci Total Environ, 2017. **577**: p. 105-112.
180. Little, K.E., M. Hayashi, and S. Liang, *Community-Based Groundwater Monitoring Network Using a Citizen-Science Approach*. Ground Water, 2016. **54**(3): p. 317-24.
181. Breuer, L., et al., *HydroCrowd: a citizen science snapshot to assess the spatial control of nitrogen solutes in surface waters*. Sci Rep, 2015. **5**: p. 16503.
182. Bonney, R., et al., *Can citizen science enhance public understanding of science?* Public Underst Sci, 2016. **25**(1): p. 2-16.
183. Land-Zandstra, A.M., et al., *Citizen science on a smartphone: Participants' motivations and learning*. Public Underst Sci, 2016. **25**(1): p. 45-60.
184. Geoghegan, H., et al., *Understanding Motivations for Citizen Science*. 2016, UK Environmental Observation Framework
185. Nelms, S.E., et al., *Marine anthropogenic litter on British beaches: A 10-year nationwide assessment using citizen science data*. Sci Total Environ, 2017. **579**: p. 1399-1409.
186. Walther, B.A., A. Kunz, and C.S. Hu, *Type and quantity of coastal debris pollution in Taiwan: A 12-year nationwide assessment using citizen science data*. Mar Pollut Bull, 2018. **135**: p. 862-872.
187. Abokifa, A.A., L. Katz, and L. Sela, *Spatiotemporal trends of recovery from lead contamination in Flint, MI as revealed by crowdsourced water sampling*. Water Res, 2020. **171**: p. 115442.
188. Albus, K.H., et al., *Accuracy of long-term volunteer water monitoring data: A multiscale analysis from a statewide citizen science program*. PLoS One, 2020. **15**(1): p. e0227540.
189. Anhalt-Depies, C., et al., *Tradeoffs and tools for data quality, privacy, transparency, and trust in citizen science*. Biological Conservation, 2019. **238**.
190. Araujo, G., et al., *Population structure, residency patterns and movements of whale sharks in Southern Leyte, Philippines: results from dedicated photo-ID and citizen science*. Aquatic Conservation: Marine and Freshwater Ecosystems, 2017. **27**(1): p. 237-252.
191. Baalbaki, R., et al., *Citizen science in Lebanon-a case study for groundwater quality monitoring*. R Soc Open Sci, 2019. **6**(2): p. 181871.
192. Baker, E., et al., *Enhancing plant biosecurity with citizen science monitoring: comparing methodologies using reports of acute oak decline*. Journal of Geographical Systems, 2018. **21**(1): p. 111-131.
193. Ballard, H.L., et al., *Contributions to conservation outcomes by natural history museum-led citizen science: Examining evidence and next steps*. Biological Conservation, 2017. **208**: p. 87-97.
194. Barrows, A.P.W., et al., *A watershed-scale, citizen science approach to quantifying microplastic concentration in a mixed land-use river*. Water Res, 2018. **147**: p. 382-392.
195. Bergmann, M., et al., *Citizen scientists reveal: Marine litter pollutes Arctic beaches and affects wild life*. Mar Pollut Bull, 2017. **125**(1-2): p. 535-540.
196. Bos, J.S., et al., *Citizen science for Saskatchewan lakes: a pilot project*. Lake and Reservoir Management, 2019. **35**(1): p. 77-89.
197. Brown, A., et al., *Safecast: successful citizen-science for radiation measurement and communication after Fukushima*. J Radiol Prot, 2016. **36**(2): p. S82-S101.
198. Ho, S.Y., S.J. Xu, and F.W. Lee, *Citizen science: An alternative way for water monitoring in Hong Kong*. PLoS One, 2020. **15**(9): p. e0238349.

199. Thatoe Nwe Win, T., T. Bogaard, and N. van de Giesen, *A Low-Cost Water Quality Monitoring System for the Ayeyarwady River in Myanmar Using a Participatory Approach*. *Water*, 2019. **11**(10).
200. Fehri, R., S. Khelifi, and M. Vanclooster, *Testing a citizen science water monitoring approach in Tunisia*. *Environmental Science & Policy*, 2020. **104**: p. 67-72.
201. Richardson, S., et al., *Citizen-led sampling to monitor phosphate levels in freshwater environments using a simple paper microfluidic device*. *PLoS One*, 2021. **16**(12): p. e0260102.
202. Zheng, S., et al., *Towards citizen science. On-site detection of nitrite and ammonium using a smartphone and social media software*. *Sci Total Environ*, 2022. **815**: p. 152613.
203. Choy, C.M., *INVESTIGATION OF PHYSICAL AND CHEMICAL REACTIONS ON MICROFLUIDIC PAPER-BASED ANALYTICAL DEVICES*. 2016, California State Polytechnic University.
204. Lim, H., A.T. Jafry, and J. Lee, *Fabrication, Flow Control, and Applications of Microfluidic Paper-Based Analytical Devices*. *Molecules*, 2019. **24**(16).
205. Abdolmaleki, A.Y., et al., *Adsorption of tetracycline from water using glutaraldehyde-crosslinked electrospun nanofibers of chitosan/poly(vinyl alcohol)*. *Water Sci Technol*, 2018. **77**(5-6): p. 1324-1335.
206. Dastbaz, A. and A.R. Keshtkar, *Adsorption of Th⁴⁺, U⁶⁺, Cd²⁺, and Ni²⁺ from aqueous solution by a novel modified polyacrylonitrile composite nanofiber adsorbent prepared by electrospinning*. *Applied Surface Science*, 2014. **293**: p. 336-344.
207. Robb, B. and B. Lennox, *The electrospinning process, conditions and control*, in *Electrospinning for Tissue Regeneration*. 2011. p. 51-66.
208. Nayak, U.Y., et al., *Glutaraldehyde cross-linked chitosan microspheres for controlled delivery of zidovudine*. *J Microencapsul*, 2009. **26**(3): p. 214-22.
209. Kajjumba, G.W., et al., *Modelling of Adsorption Kinetic Processes—Errors, Theory and Application*, in *Advanced Sorption Process Applications*. 2019, IntechOpen.
210. Ebelegi, A.N., N. Ayawei, and D. Wankasi, *Interpretation of Adsorption Thermodynamics and Kinetics*. *Open Journal of Physical Chemistry*, 2020. **10**(03): p. 166-182.
211. Zia, Q., et al., *A Review on Chitosan for the Removal of Heavy Metals Ions*. *Journal of Fiber Bioengineering and Informatics*, 2019. **12**(3): p. 103-128.
212. Wang, J. and X. Guo, *Adsorption isotherm models: Classification, physical meaning, application and solving method*. *Chemosphere*, 2020. **258**: p. 127279.
213. Bozorgi, M., et al., *Performance of synthesized cast and electrospun PVA/chitosan/ZnO-NH₂ nano-adsorbents in single and simultaneous adsorption of cadmium and nickel ions from wastewater*. *Environ Sci Pollut Res Int*, 2018. **25**(18): p. 17457-17472.
214. Yang, S.-J., et al., *Research on the modification of PAN hollow fiber membrane with high heavy metal ions adsorption*. *Ferroelectrics*, 2019. **547**(1): p. 121-128.
215. Zhang, X., et al., *Preparation of Chitosan Stacking Membranes for Adsorption of Copper Ions*. *Polymers (Basel)*, 2019. **11**(9).
216. Zahabi, S.R., S.A. Hosseini Ravandi, and A. Allafchian, *Removal of nickel and cadmium heavy metals using nanofiber membranes functionalized with (3-mercaptopropyl)trimethoxysilane (TMPTMS)*. *J Water Health*, 2016. **14**(4): p. 630-9.
217. Yang, D., et al., *Functionalized chitosan electrospun nanofiber membranes for heavy-metal removal*. *Polymer*, 2019. **163**: p. 74-85.
218. Hallaji, H., A.R. Keshtkar, and M.A. Moosavian, *A novel electrospun PVA/ZnO nanofiber adsorbent for U(VI), Cu(II) and Ni(II) removal from aqueous solution*. *Journal of the Taiwan Institute of Chemical Engineers*, 2015. **46**: p. 109-118.
219. Al-Ghouti, M.A. and D.A. Da'ana, *Guidelines for the use and interpretation of adsorption isotherm models: A review*. *J Hazard Mater*, 2020. **393**: p. 122383.
220. Rengaraj, S., et al., *Studies on adsorptive removal of Co(II), Cr(III) and Ni(II) by IRN77 cation-exchange resin*. *Journal of Hazardous Materials*, 2002. **B92**: p. 185-198.
221. Deepatana, A. and M. Valix, *Comparative adsorption isotherms and modeling of nickel and cobalt citrate complexes onto chelating resins*. *Desalination*, 2008. **218**(1-3): p. 334-342.

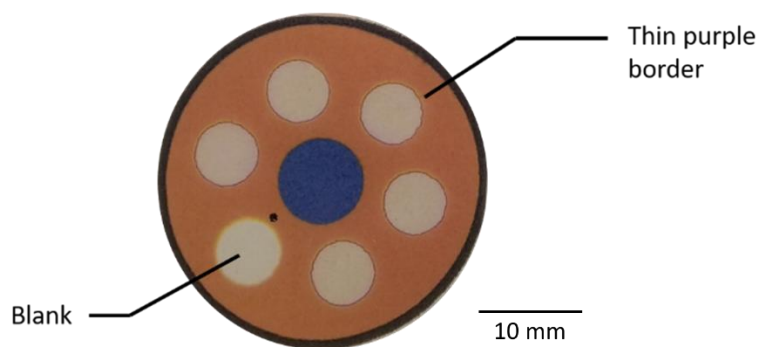
222. Mendes, F.D. and A.H. Martins, *Selective sorption of nickel and cobalt from sulphate solutions using chelating resins*. International Journal of Mineral Processing, 2004. **74**(1-4): p. 359-371.
223. Liebenberg, C.J., et al. *The recovery of nickel and cobalt from a sulphate bioleach solution using Dow M4195*. in *The Southern African Institute of Mining and Metallurgy Base Metals Conference 2013*. 2013. South Africa.
224. Wołowicz, A. and M. Wawrzkievicz, *Screening of Ion Exchange Resins for Hazardous Ni(II) Removal from Aqueous Solutions: Kinetic and Equilibrium Batch Adsorption Method*. Processes, 2021. **9**(2).

Appendix 1 μ PAD for Ni^{2+} detection

Development of XO/PDADMAC μ PAD

Similar to the design of nioxime μ PAD, the design of XO/PDADMAC μ PAD consist of one reference circle located in the middle of the device, circled with 6 sample wells (5 sample wells + 1 blank well) as shown in Appendix-Figure 1. However, as opposed to the green-coloured base for nioxime μ PAD, the XO/PDADMAC μ PAD base colour was printed as red. However, upon wax melting process, the printed red wax ink colour faded into more orange-coloured. This shift in colour would not affect the reaction, and was therefore left as is. The main reason of changing the based colour of the μ PAD was due to the different expected colour at the end point of the reaction. In nioxime reaction, the colour of the end point was expected to be magenta, since the metal-ligand complex formed magenta colour through UV/Vis experiment. Similarly, in XO/PDADMAC utilisation as Ni^{2+} colorimetric reagent, the observed end point of reaction had more bluish-purple colour. In order to contrast the colour of the end point of the reaction, the base colour of the μ PAD was changed to red, which is the exact inverse of blue. Contrasting the base colour to the end point colour would provide ease of observation and make the slightest colour change more visible. In similar vein, the colour of the reference circle was also changed from magenta to blue, since the colour of the end point of the reaction is closer to blue.

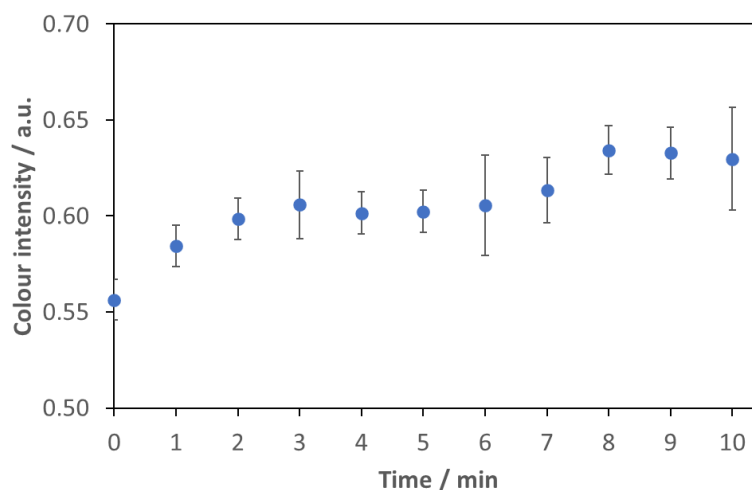
Interestingly, upon addition of XO/PDADMAC mixture, a thin purple border can be observed on the edges of the sample well. At this point, this border formation was ignored since its effect to the reaction was unclear. However, upon further observation, the thin purple border was suspected to be formed due to reaction between the reagent with the wax barrier or accumulation of PDADMAC on the edges of the sample well. Upon further experiment, leakage can at times be seen at sample wells that show notable purple border. Another interesting observation was that despite the reddish-purple colour of the XO/PDADMAC mixture, drying of the solvent on the sample well will produce yellow colour. This further explained the interaction between XO and PDADMAC, which is governed by electrostatic forces in the presence of aqueous solvent. Therefore, upon the loss of aqueous solvent, no electrostatic interaction can be observed, rendering the sample well colour to yellow – the colour of XO indicator.



Appendix-Figure 1 Design of XO/PDADMAC μ PAD is similar to nioxime μ PAD, consisting of red base colour with one blue reference circle, circled by 5 sample wells and 1 blank well. Upon addition of XO/PDADMAC solution, thin purple border can occasionally be observed on the sample well. Further observation indicated possible reaction between the reagents and the wax barrier or deposition of PDADMAC on the edges of the well.

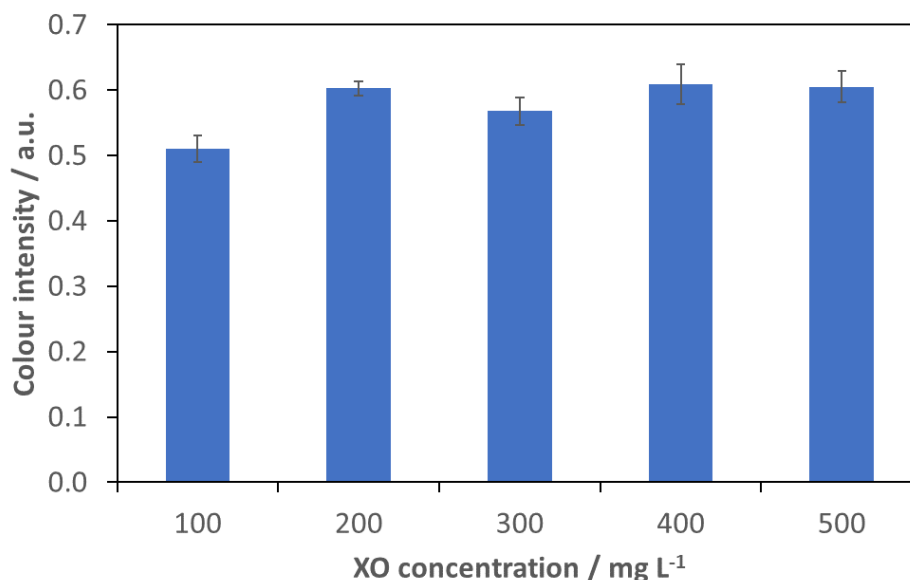
Optimization of XO/PDADMAC μ PAD

The reaction time on the XO/PDADMAC μ PAD was then observed, showing stable colour intensity measurement in R channel of RGB between 3-6 min, before it increased and stabilised again at 8-10 min. This reaction time measurement was done by dipping a device containing 10 μ L of 200 mg L^{-1} XO and 4 wt% PDADMAC mixture with addition of 10 μ L 10 mM PBS buffer. A picture of the device was taken using black box method every minute after dipping the device into 10 mL solution of 10 mg L^{-1} Ni^{2+} . Appendix-Figure 2 shows the measured colour intensity on the sample well against time, where steady increase was observed up to minute 3, before stabilising until minute 6. However, further increase in colour intensity was then observed between minute 7 to minute 8, before stabilising again to minute 10. Due to this two time increase in the measured colour intensity, further experiment would use 10 min as reaction time to ensure peak colour intensity was achieved. An important note to be made related to this reaction is its high standard deviation. This is a problem that hopefully would be solved upon further optimisation of the reagent concentrations.



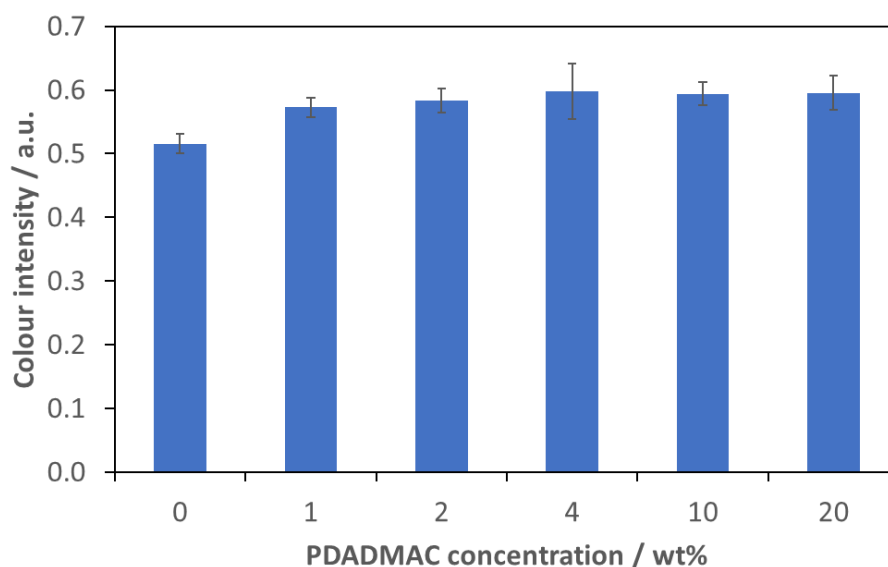
Appendix-Figure 2 Colour intensity of XO/PDADMAC μ PAD containing 10 μ L mixture of 200 mg L^{-1} XO and 4 wt% PDADMAC in 1:1 volumetric ratio was measured at R channel of RGB after dipping into 10 mL 10 mg L^{-1} Ni^{2+} solution. Picture was taken with black box method every minute from 0-10 min ($n=3$).

The effect of XO concentration was subsequently observed by varying the concentration from 100-500 mg L^{-1} , showing no significant difference in observed colour intensity after 200 mg L^{-1} XO concentration. XO/PDADMAC μ PAD was loaded with 10 μ L mixture of varying XO concentration and 4 wt% PDADMAC at 1:1 volumetric ratio, before being dipped into 10 mL solution containing 10 mg L^{-1} Ni^{2+} . After 10 min of reaction, a picture of the device was taken with the black box method. Colour intensity was then measured by inverting the image and measurement in red channel of RGB due to the blue-coloured endpoint of the reaction. Appendix-Figure 3 show that significant difference was only observed at 100 mg L^{-1} XO, where the colour intensity measured was significantly lower than in devices containing higher than 200 mg L^{-1} XO. A slight dip was observed at 300 mg L^{-1} , however, this is not a notable difference. Therefore, 200 mg L^{-1} XO, which is the lowest concentration that produce the stable high intensity was chosen as optimum value of XO concentration for this XO/PDADMAC device.



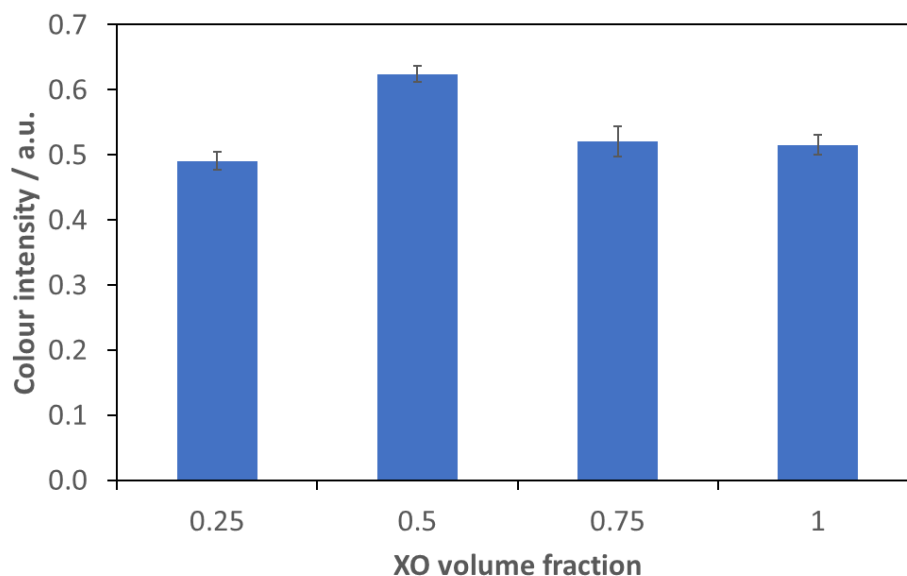
Appendix-Figure 3 Effect of XO concentration was observed by varying the concentration within 100-500 mg L⁻¹ and mixing with 4 wt% PDADMAC at 1:1 ratio. 10 µL of this mixture was loaded into the sample well of the device and dipped into 10 mL 10 mg L⁻¹ Ni²⁺ solution ($n=3$).

Similarly, the effect of PDADMAC concentration was also observed, and showed no significant difference in the tested concentration range. The device was loaded with 10 µL mixture of 200 mg L⁻¹ XO and varying PDADMAC concentration at 1:1 volumetric ratio. It is then dipped into 10 mL 10 mg L⁻¹ Ni²⁺ solution and left to react for 10 min before picture-taking process. Appendix-Figure 4 show that significantly lower colour intensity was only observed in the absence of PDADMAC. Whereas in the presence of PDADMAC between 1-20 wt%, no significant difference ($p>0.05$) of colour intensity was observed. A slightly bigger standard deviation was observed in 4 wt% PDADMAC concentration. Due to the insignificant difference of colour intensity measured in the presence of PDADMAC, the optimum PDADMAC concentration was regarded to be 1 wt%. As this is the lowest concentration that would give the maximum colour intensity measured.



Appendix-Figure 4 Effect of PDADMAC concentration was observed by varying the concentration between 0-20 wt% and mixing with 200 mg L⁻¹ XO at 1:1 volumetric ratio. 10 µL of this mixture was loaded into the sample well of the device and dipped into 10 mL 10 mg L⁻¹ Ni²⁺ solution (*n*=3).

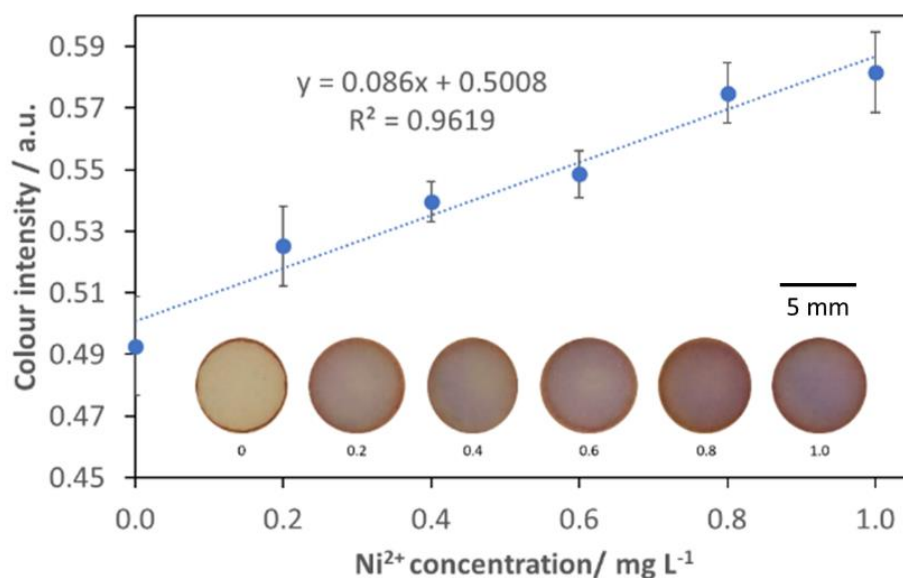
In the case of XO/PDADMAC as colorimetric reagent for Ni²⁺ detection in µPAD, the effect of the volumetric ratio between the two reagents was observed and resulted in optimum ratio of 1:1. This result was obtained by loading the device with 10 µL solution containing 200 mg L⁻¹ XO and 1 wt% PDADMAC in 1:3, 1:1, 3:1, and 1:0 XO to PDADMAC ratio. To simplify the writing of these different ratios, it will be stated as the volumetric fraction of XO from here on. Therefore, the variations are: 0.25, 0.5, 0.75, and 1 XO volume fraction in the solution mixture. The devices were then dipped into 10 mL 10 mg L⁻¹ Ni²⁺ solution and left to react for 10 min before picture-taking step. Appendix-Figure 5 show that no significant difference (*p*>0.05) was observed between 0.25, 0.75, and 1 XO volume fraction, however, a peak was observed at 0.5 XO volume fraction. This showed that the optimum ratio between the XO and PDADMAC for 200 mg L⁻¹ XO and 1 wt% PDADMAC was 1:1 volumetric ratio. This is an important parameter in this experiment, since the addition of the reagents to the device was done in mixture of XO and PDADMAC, since the colorimetric reagent is a mixture of XO/PDADMAC rather than XO alone.



Appendix-Figure 5 Effect of XO and PDADMAC volumetric ratio to the measured colour intensity was observed by loading μ PAD with 10 μ L mixture of 200 mg L^{-1} XO and 1 wt% PDADMAC in varying XO volume fraction. Device was then dipped into 10 mL 10 mg L^{-1} Ni^{2+} solution ($n=3$).

Calibration curve of XO/PDADMAC μ PAD

After the optimisation process of the reagents involved, calibration curve was made for the XO/PDADMAC μ PAD by addition of 10 μ L mixture containing 200 mg L^{-1} XO and 1 wt% PDADMAC in 1:1 volumetric ratio into the μ PAD and dipping it to 10 mL solution of varying Ni^{2+} concentration, ranging from 0 to 1 mg L^{-1} . After 10 min of reaction, picture of the device was taken with the black box method and analysed by measuring the colour intensity of red channel in inverted RGB stack of the picture. [Figure 52](#)~~Figure 51~~ show linear correlation can be made between the Ni^{2+} concentration and the colour intensity measured. From this linear regression, the LOD for the device was calculated and resulted in 0.56 mg L^{-1} LOD. This is a lower detection limit compared to the nioxime μ PAD. Picture attached in the same figure show the colour gradient observed from 0-1 mg L^{-1} concentration of Ni^{2+} , shifting from yellow to bluish-purple. However, this coloured complex formed in the sample well of the device was not as even as the ones observed in nioxime μ PAD. In 1 mg L^{-1} result, slightly yellow patches can still be seen in the middle section of the well. Uneven colour formation across sample well can contribute to high standard deviation of the μ PAD, since these uneven patches would appear uncontrollably throughout the well, and the dispersion of the patches would affect the average intensity measured upon measuring the intensity of the well.



Appendix-Figure 6 Calibration curve of optimised XO/PDADMAC μ PAD containing 10 μ L mixture of 200 mg L^{-1} XO and 1 wt% PDADMAC, reacted with 10 mL Ni^{2+} solution in 0-1 mg L^{-1} concentration gradient ($n=3$).

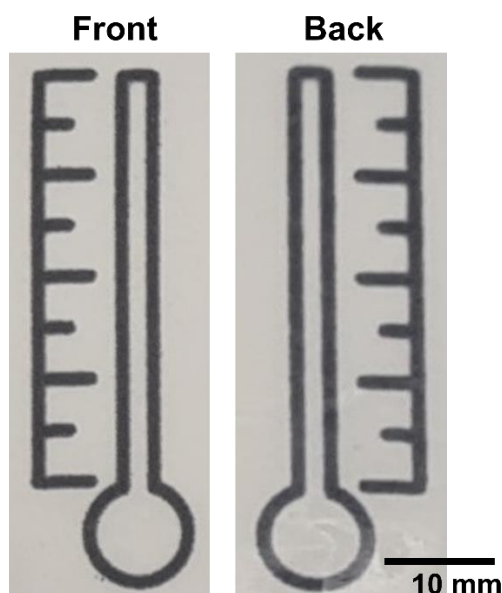
Further, despite the lower limit of detection, there is no discernible advantage of the XO/PDADMAC μ PAD compared to the nioxime μ PAD. One of the problems was occasional leakage that can be observed in the XO/PDADMAC μ PAD. As opposed to nioxime μ PAD, which never shown any leakage through the wax barrier throughout the experiments, the XO/PDADMAC μ PAD showed several instances of leakage through the wax barrier in addition to the formation of purplish ring on the edges of the well. The cause of the leakage through the barrier is unknown, since the solvent used throughout the experiments were strictly Milli-Q water. One possible cause of this leakage is interaction between the XO indicator with the paper matrix or with the paraffin-dominated wax ink. This problem with leakage had been observed in previous study that incorporate XO for Fe^{3+} detection, however, the cause was attributed to barrier thickness [203]. This is not applicable for current design of the μ PAD. Therefore, it is suspected that there is an additional cause, possibly related to interaction between XO and the wax barrier that underlies the leakage problem on the μ PAD.

Since leakage is a significant issue for colour-intensity-based μ PADs, the development of XO/PDADMAC μ PAD was terminated at this stage. Further experiments on Ni^{2+} detection would utilise nioxime μ PAD, which despite its higher detection limit, is a more robust and reliable device compared to the XO/PDADMAC μ PAD. Further investigative work on the leakage problem would otherwise be necessary in future utilisation of XO as colorimetric reagent or indicator in wax-printed paper microfluidic devices.

Development of nioxime distance-based μ PAD

Distance-based μ PAD, with the same colorimetric reagent and reactions was also developed in this research. In this type of μ PAD, instead of relying on colour intensity developed on the sample well of the paper, the length of colour produced through the reaction was measured and correlated with the concentration of the reagent. This is possible since in this type of device, reagents were distributed evenly across a rectangular channel and sample was introduced on one end of the channel and left to wick through the paper matrix. As the sample is wicking, it reacts with the stored reagents, producing colorimetric complex. Eventually, the reaction will reach its end point and further wicking will not change the colour of the channel due to insufficient target analyte amount in the wicking sample. The length of the channel that changes colour was then measured and correlated with the concentration of target analyte in the sample. Through this correlation, quantification of analyte in the sample can be made in the future by comparing the distance to the calibration curve.

In this research, the colorimetric reaction in the developed distance-based μ PAD (further referred to as dPAD) for Ni^{2+} detection was the same as the reaction used in the colour intensity-based device (nioxime μ PAD). However, instead of placing 10 μL of the reagent on a circular sample well bordered by wax, the reagents were pipetted throughout a rectangular channel of 40 mm length and 2 mm width. The back side of the dPAD was taped with a transparent adhesive tape which serve as a barrier to prevent liquid exiting from the back side of the channel. In order to ensure even distribution of the reagent, only the top half, which was furthest away from the sample entry point was pipetted with 10 μL of the reagent, by dragging the pipette tips from the furthest point to the mid-section. The reagent would wick from this half to fill the rest of the channel without entering the sample entry point. Therefore, reagent is stored throughout the channel through wicking and distance can be measured reliably without any leakage to the sample entry point. This is one of the complexities of dPAD, since there is no reliable means of ensuring even distribution of the colourless reagents throughout the channel before the colorimetric reaction with the sample. This wick-loading method was developed after observation of effective reagent loading step with lowest occurrence of errors.



Appendix-Figure 7 The front and back section of designed dPAD, consisting of a ruler with 5 mm increase, with 10 mm diameter sample well attached to 40 mm long channel at 2 mm width. The back part of the dPAD was blocked with transparent tape.

Optimization of nioxime dPAD

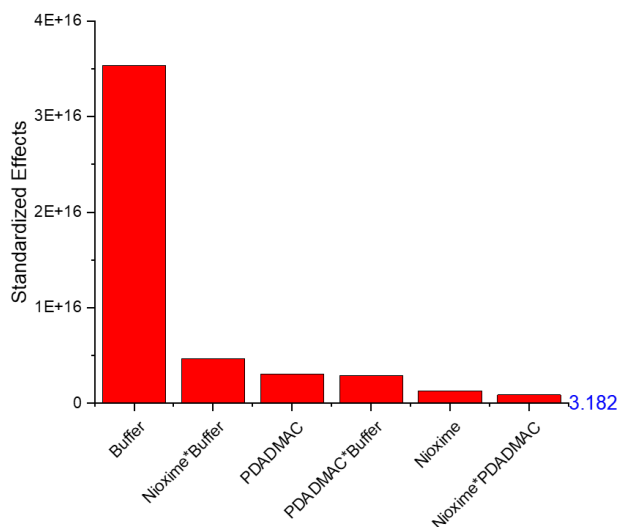
Box-Behnken design of experiment for nioxime dPAD

Despite having the same reaction, the principle at which the reaction is utilised to quantify the concentration is not the same between nioxime μ PAD and dPAD. Therefore, the optimum concentration of the reagent used in the dPAD, or whether a certain reagent is still needed for the dPAD, needed a re-evaluation and re-optimization. The optimization process for the dPAD was similar to that of intensity-based μ PAD, which utilise Box-Behnken design of experiment. In this optimization process, the concentration of nioxime, PDADMAC, and buffer were varied, coded with -1 to 1 where -1 is the lowest concentration tested and 1 is the highest concentration tested. All reagents were introduced layer-by-layer, with buffer introduced first, followed by PDADMAC, and finally nioxime. Each reagent was added as 10 μ L solution with its respective concentration variation, which was between 400-1400 mg L^{-1} for nioxime, 0-6 wt% for PDADMAC, and 0-10 mM for PBS buffer.

Standardised effect

Appendix-Figure 8 show the standardised effect graph where all of the tested parameters and interaction between parameters affect the measured distance on the device. However, among these parameters, buffer concentration stands as the parameter with biggest effect on the distance measured. This indicates that the concentration of buffer stored in the dPAD had the most significant effect to the length of colorimetric complex produced on the device. Buffer

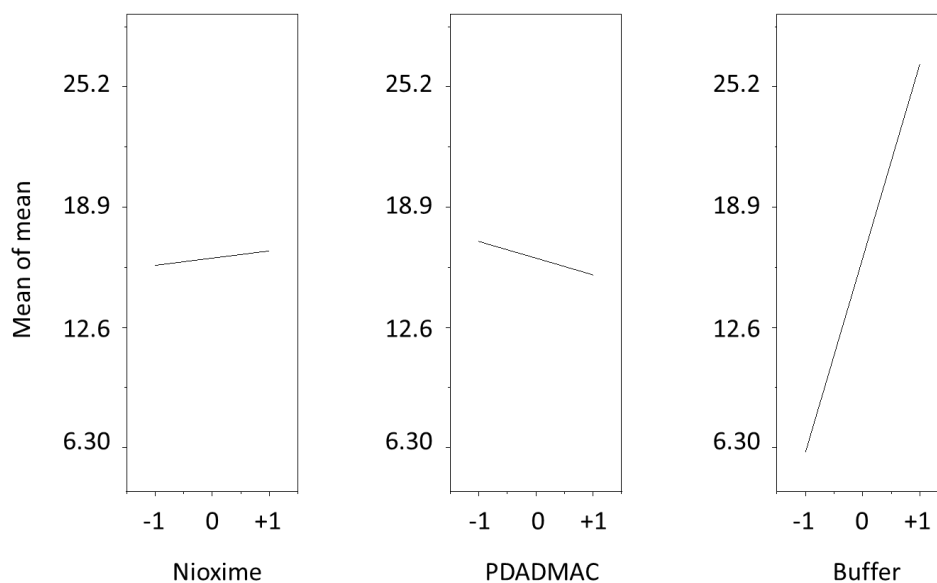
concentration prevails even nioxime-buffer interaction, PDADMAC concentration, and PDADMAC-buffer concentration.



Appendix-Figure 8 Standardized effect graph of variables and interaction between variables to the measured distance ($n=3$ dPADs).

Main effects plot

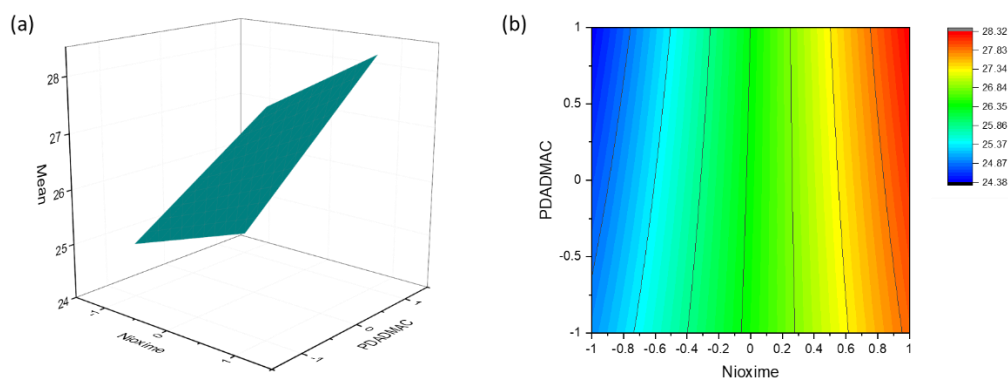
Further, in Appendix-Figure 9, the increase of buffer concentration showed increase in measured distance on the device, proving linear correlation between the two. Similarly, the increase of nioxime concentration also affect linear increase in measured distance, in notably less significant manner. Whereas the increase of PDADMAC concentration had reverse effect on the measured distance on the dPAD. Interestingly, this result is a contrast to the result of optimisation in intensity-based device with the same reagents. In the intensity-based μ PAD, buffer concentration also had the most significant effect on the colour intensity measured, however it affects the colour intensity negatively. This led to a conclusion that the increase of buffer concentration stored on the device had negative effect on the target of optimisation (maximise colour intensity). Whereas in dPAD, the increase of buffer concentration, which is necessary to maintain the reaction pH throughout variation of sample pH, showed indication of positive effect to the target of optimisation (maximised distance measured).



Appendix-Figure 9 Main effects graph of three main variables: nioxime, PDADMAC, and PBS solution concentration in respect to the measured distance ($n=3$ dPADs).

Chapter 7 3D- and contour-plot (response surface methodology)

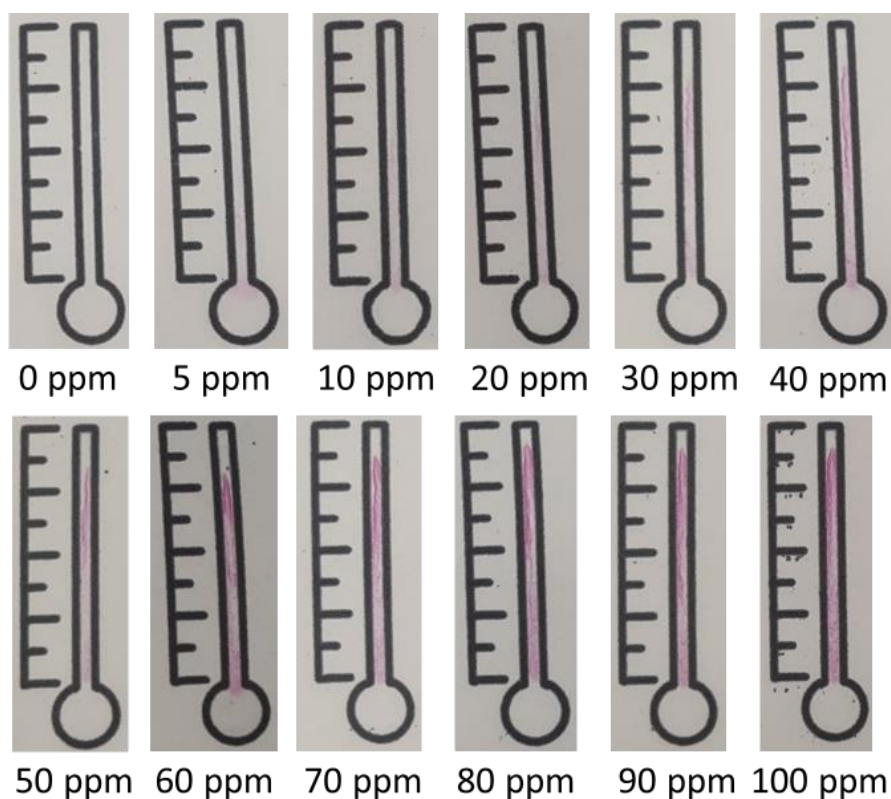
Appendix-Figure 10 show response surface graphs for the optimum concentration of nioxime and PDADMAC at held buffer value. The value of buffer, in these graphs were held at its maximum level since the presence of buffer is of high importance in application of the dPAD with real samples. Additionally, the high concentration of buffer corresponded to the ideal condition of the optimisation process, which is bigger measured distance. From the graph, it can be concluded that the optimum nioxime and PDADMAC concentration in this condition is achieved by maximising both reagent concentrations, in this case, 1400 mg L^{-1} nioxime and 6 wt% PDADMAC. However, upon observation, addition of 6 wt% PDADMAC on the channel created visible colour strip due to its high viscosity. This colour strip is a yellowish waterline created at the last point of PDADMAC wicking, and is visually similar to the coffee-ring formed in the intensity-based device. Upon further observation, similar waterline can still be observed in 4 wt% PDADMAC addition and only disappear in addition of 2 wt% PDADMAC. Therefore, the optimum reagent concentrations for the dPAD were determined to be 1400 mg L^{-1} nioxime, 2 wt% PDADMAC, and 10 mM PBS buffer.



Appendix-Figure 10 (a) 3D- and (b) 2D-contour graph at PBS concentration 0.01 M, observing the effect of nioxime and PDADMAC concentration variation to the measured distance ($n=3$ dPADs)

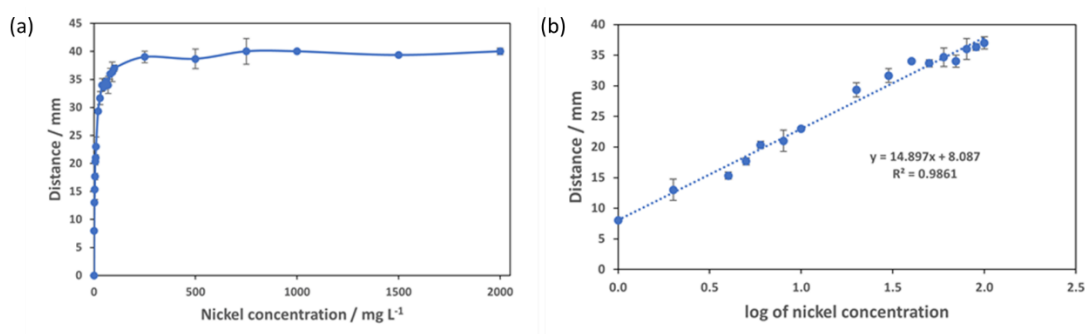
Calibration curve

The optimised dPAD was then tested in a gradient of Ni^{2+} concentration, by pipetting 40 μL of sample solution on to the sample well and leaving the sample to wick through the channel. For dPAD, the measurement of the distance was taken as soon as the sample dried up from the device. This usually require up to 30 min, for the entire wicking process through the 40 mm channel length followed with evaporative drying at room temperature ($18 \pm 2^\circ\text{C}$). The tested Ni^{2+} concentration was between 0 to 2000 mg L^{-1} . However, as shown in [Figure 54](#)[Figure-53a](#), the increase of measured distance is only linear before 500 mg L^{-1} point. By 100 mg L^{-1} Ni^{2+} , the colorimetric complex was forming almost throughout the entire channel length – which is 40 mm. Increasing the channel length by design, in this case, might help in increasing the detectable range of Ni^{2+} . However, that is beyond the objective of current research. Illustration of the endpoint of the dPAD reaction is shown in [Figure 53](#)[Figure-52](#).



Appendix-Figure 11 Result as seen on the optimised dPAD 30 min after addition of a gradient of sample concentration within 0-100 mg L⁻¹ Ni²⁺ range. The magenta length of the magenta line at the endpoint of the reaction was recorded as measurement.

[Figure 54](#)[Figure 53b](#) shows the linearization of the otherwise non-linear correlation between the Ni²⁺ concentration and the measured distance between 0-100 mg L⁻¹. The linearized graph may serve as calibration curve to predict – taking into account possible inaccuracies due to linearization – the concentration of Ni²⁺ based on distance measurement on the dPAD. The limit of detection of dPAD, calculated (3σ) by only accounting the linear section of [Figure 54](#)[Figure 53a](#), resulted in 0.3 mg L⁻¹ Ni²⁺ concentration. Compared to the intensity-based device, this limit of detection is 10 times lower, making it a possible alternative design of paper-based analytical device for citizen science Ni²⁺ detection.



Appendix-Figure 12 Distance-based Ni²⁺ device calibration curve containing 0.01 M PBS buffer pH 7.4, 2 wt% PDADMAC, and 1400 mg L⁻¹ nioxime at 10 μL each. The Ni²⁺ concentration range tested was between (a) 0-2000 mg L⁻¹ and (b) 0.5-100 mg L⁻¹ (*n*=3 dPADs).

Drawbacks of dPAD for Ni²⁺ detection in water sample

Reaction time

However, aside from the lower limit of detection, there are considerable drawbacks of this design compared to intensity-based. The biggest drawback is reaction time. In intensity-based device, the reaction time is mainly controlled by the complexometric reaction between Ni²⁺ and nioxime or other reagents on the sample well. However, in dPADs, the reaction time is hugely dependent on the wicking time of the sample solution from the sample introduction well to the end of the channel. Manipulating the wicking time has proven to be no easy task. Wicking, in paper, can be predicted with Lucas-Washburn equation derived from Hagen-Poiseuille's Law, as Appendix-Eq 1. Further, the presence of wax boundary would result in higher contact angle compared to bulk capillary flow, which require resistance to be considered in the equation (Appendix-Eq 2). These equations were based on Lim, *et.al.* [204].

$$l = \sqrt{\frac{\gamma r \cos\theta t}{2\mu}} \quad \text{Appendix-Eq 1}$$

$$l_{b(t)} = c \sqrt{\left(1 + \beta \frac{d \cos\theta_b}{\phi^{1/3} \omega \cos\theta}\right) \frac{\gamma}{\mu} t} \quad \text{Appendix-Eq 2}$$

where *l* is length travelled, γ is surface tension of the liquid, *r* is effective pore radius, θ is contact angle between fluid and boundary wall, *t* is time, and μ is viscosity, β is length of the advancing contact angle lines which is in contact with the hydrophobic wall and should be determined by experimentation, ω is width of the channel, ϕ is porosity, *b* is thickness of the channel, and *d* is pore diameter.

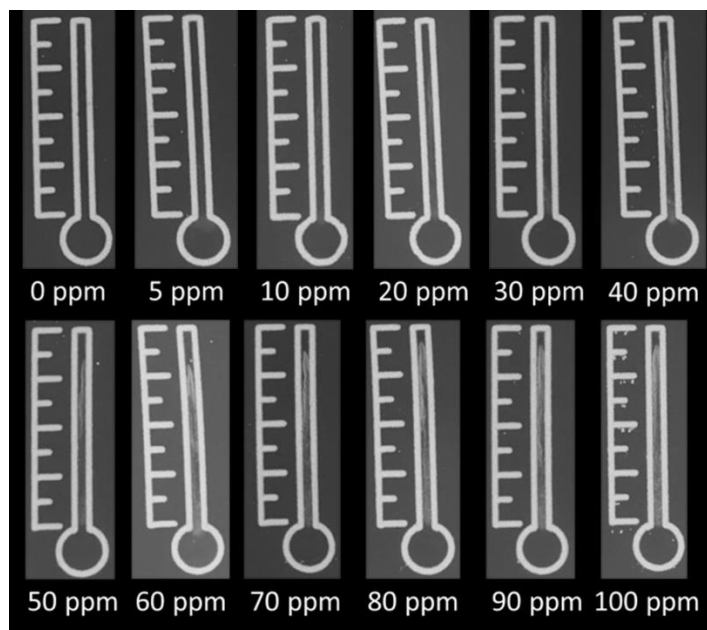
Therefore, as can be seen in Appendix-Eq 1 and Appendix-Eq 2, the length travelled by the reagent through wicking cannot simply be determined through calculation, rather requiring experimental procedures. It is also important to note that the wicking process would depend on the liquid properties, therefore might differ between the reagents and concentrations. Based on the equations, practical alterations that can be done to increase the wicking rate is by using papers with bigger pore diameter or decreasing the width of the channel. However, upon preliminary experiments in design alterations process, these two parameters did not notably enhance the performance of dPAD for this reaction.

Robust and repeatable measurement

The distance measurement with this design of dPAD can be made or approximated with a ruler, which at first glance, is a notable advantage compared to the intensity-based μ PAD. However, further observation would prove that this measurement method might also not be as straightforward. Since the μ PAD rely on the experimenter's perception of colour change, it is not readily accessible for various types of users. Additionally, even in users with the best vision, the reaction commencing on the dPAD is not always even. There are instances at which the sample solution did not wick evenly through the 2 mm wide channel, instead forming a protrusion in the middle part of the channel where liquid did not come in contact with the wax barrier. This is expected, based on the equations presented previously (Appendix-Eq 1 and Appendix-Eq 2). Based on this model, the wicking rate of the sample solution is a gradient across the channel width, with faster gradient at the middle section where liquid does not come in contact with the wax barrier. This is evident in the model which shows that one of the parameters determining rate of wicking is contact angle with the hydrophobic wall. In the case of significantly faster wicking at the mid-section, the distance measurement becomes ambiguous. A question of up to which point should the distance be measured might arise and will possibly lead to errors in the distance measurement.

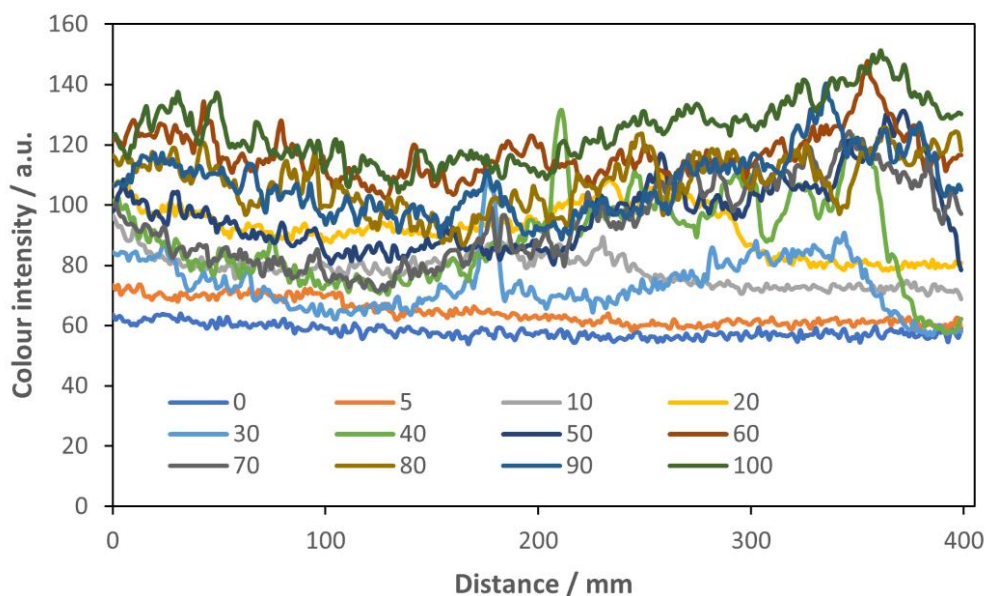
Measurement with image processing software

Additionally, distance measurement with software-based analysis, as was done in intensity-based μ PADs was proven to be difficult. Using the same colour intensity measurement technique as in section 2.4. This colour measurement technique utilises inverted picture of the device combined with RGB stacking, where the colour channel of the image is separated into the primary colour scheme. For magenta-coloured reaction, such as nickel-nioxime complex formation, the measurement would be obtained in the green (G) channel. Illustration of the measured image after processing with inversion and stacking is shown in Appendix-Figure 13.



Appendix-Figure 13 Results of 0-100 mg L⁻¹ Ni²⁺ detection in dPAD after 30 min of reaction, on the inverted green channel (G) of RGB colour stacking in ImageJ.

As shown in Appendix-Figure 14, colour intensity measurement through the channel fluctuates in tested concentrations between 0-100 mg L⁻¹. Without further study to determine cutting off point of where the measurement should end, distance measurement with this method would be challenging. Determining criteria for this measurement would need further extensive research. Previous literatures often have different set of criteria to determine the end point of the distance measurement and up to the point of writing, there has not been a standardised method or commonly used method in determination of distance end-point for dPAD through software-based analysis.



Appendix-Figure 14 Colour intensity measured across the 40 mm channel of the dPAD, 30 min after addition of 0-100 mg L⁻¹ Ni²⁺ sample solution. The colour intensity is measured in G channel of RGB colour space.

Reagent introduction process

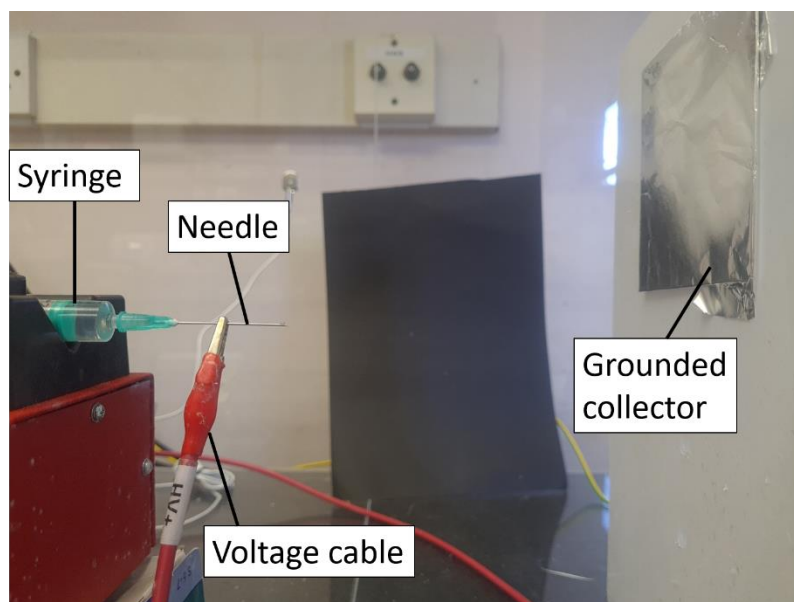
In addition to aforementioned disadvantages of the dPAD, from fabrication perspective, the dPAD also pose notable challenge in reagent deposition process. Unlike the intensity-based μ PAD where reagent can simply be pipetted on to a sample well and left to dry, in dPAD, the reagent had to be introduced in such a way to prevent leaking of the reagent to the sample well. In this research, the reagent was added halfway through the channel instead of pipetting it throughout the channel. This method is proven to decrease the possibility of reagent leakage to the sample well, however, it is still not fool-proof. Additionally, since the reagents used in this dPAD are colourless, the leakage might not be detected until sample is introduced to the device. Realistically, this will be a big problem in bigger or mass production, since there is no way to know whether the device is up to standard (no reagent leakage to sample well) until user is pipetting the sample on to the device. There is also no guarantee that the reagent wicks evenly upon introduction, which might create gradient of reagent concentration stored on the channel. If there is gradient of reagent concentration stored in the channel, it would lead to significant error in the result. Due to these discussed drawbacks, the development of dPAD was terminated at this stage since it did not show bigger advantage compared to the intensity-based μ PAD.

Appendix 2 Cafetiere-based preconcentration

Methods for PCL/chitosan/PEO nanomat fabrication optimisation and adsorption characterisation

Electrospinning optimisation

Electrospinning is a membrane fabrication process, as discussed in Chapter 1. The electrospinning setup used in this research was contained in a colourless, transparent plastic enclosure with detachable window to set up the process (Appendix-Figure 15). However, the enclosure was equipped with a safety circuit system, making the process only possible if the window was closed – connecting the electrical system. This setup was not equipped with humidity or temperature controller, however, due to its closed system, would induce an increase in relative humidity with the duration of electrospinning due to lack of ventilation for the evaporating solvent. Therefore, temperature and relative humidity sensor was placed within the enclosure to observe the uncontrolled parameters.



Appendix-Figure 15 Electrospinning setup involves a 10 mL disposable syringe mounted on a syringe pump, where a power supply was connected to the needle through an alligator clip. A grounded collector was placed in front of the needle, wrapped in an aluminium foil sheet. The entire setup was placed in a secured plastic enclosure, with detachable parts to access the setup.

In this research, the optimisation of electrospinning process was done by solely focusing on some of the controllable process parameters: applied voltage, flow rate, and tip-to-collector distance (TCD). Ambient parameters such as temperature and humidity were not controlled, albeit recorded. Optimum electrospinning process was determined based on observation, which was the one producing the smallest diameter of fibres possible with highest process stability. The process stability in this study was a qualitative measure, based on the observation on the

process stability for a duration of the electrospinning. Stability can be assessed by observing the lack of: (1) spitting, (2) pool formation, (3) beads formation on the fibres, or (4) splitting streams of polymer jet.

Adsorption kinetics

The adsorption kinetics model for the nanomat was observed through mixing of 0.002 g of spun nanomat into 50 mL solution containing $3 \text{ mg L}^{-1} \text{ Ni}^{2+}$ with magnetic stirrer at 100 rpm for 20 minutes at room temperature ($20 \pm 2 \text{ }^\circ\text{C}$). The concentration of Ni^{2+} in the solution was measured before and throughout the mixing process through UV/Vis spectrophotometry with nioxime as colorimetric reagent, with dilution, when necessary. The recorded data was then processed, and best fit was found, comparing the data obtained to the following adsorption kinetics models, based on previous literatures: pseudo-first order (PFO), pseudo-second order (PSO), intraparticle (IP), and Elovich adsorption kinetics model [205].

Adsorption isotherm

The adsorption isotherm process in this research was observed by placing 0.002 g of spun fibre into a 10 mL solution containing 0.5-2000 $\text{mg L}^{-1} \text{ Ni}^{2+}$ and mixing with a magnetic stirrer at 100 rpm for 24 hours at room temperature ($20 \pm 2 \text{ }^\circ\text{C}$). The amount of nanomat was based on the availability of the nanomat. A 0.002 g spun fibre would normally be around the size of 50 mm x 50 mm square. The concentration of Ni^{2+} in the solution was measured before and after the mixing process through UV/Vis spectrophotometry with nioxime as colorimetric reagent, with dilution, when necessary. The recorded data was then processed, and best fit was found, comparing the data obtained to the following linearised isotherm models, chosen based on previous studies on electrospun fibres for metal adsorption: Henry, Langmuir, Freundlich, and Dubinin-Radushkevich (DR) [205, 206].

Methods for ion exchange resins for Ni^{2+} adsorption and preconcentration

Preliminary observation of ion exchange resin

Preliminary observation for ion exchange resins was done by placing 0.1 g of the resin in a 50 mL $3 \text{ mg L}^{-1} \text{ Ni}^{2+}$ solution, stirred at 100 rpm at 20°C . The solution was then sampled ($100 \text{ } \mu\text{L} \times 3$) immediately, at minute-1, 2, 3, 4, 5, 10, 15, and 20. The sample was then diluted and reacted with $100 \text{ } \mu\text{L}$ nioxime for UV/Vis spectrophotometry measurement of the Ni^{2+} concentration at the time of sampling.

Adsorption kinetics

The adsorption kinetics model for the ion exchange resins were observed through mixing of 0.1 g of resin into 50 mL solution containing $3 \text{ mg L}^{-1} \text{ Ni}^{2+}$ with magnetic stirrer at 100 rpm for 20 minutes at room temperature ($20 \pm 2 \text{ }^\circ\text{C}$). The concentration of Ni^{2+} in the solution was measured before and throughout the mixing process through UV/Vis spectrophotometry with nioxime as

colorimetric reagent, with dilution, when necessary. The recorded data was then processed, and best fit was found, comparing the data obtained to the following adsorption kinetics models, based on previous literatures: pseudo-first order (PFO), pseudo-second order (PSO), intraparticle (IP), and Elovich adsorption kinetics model [205].

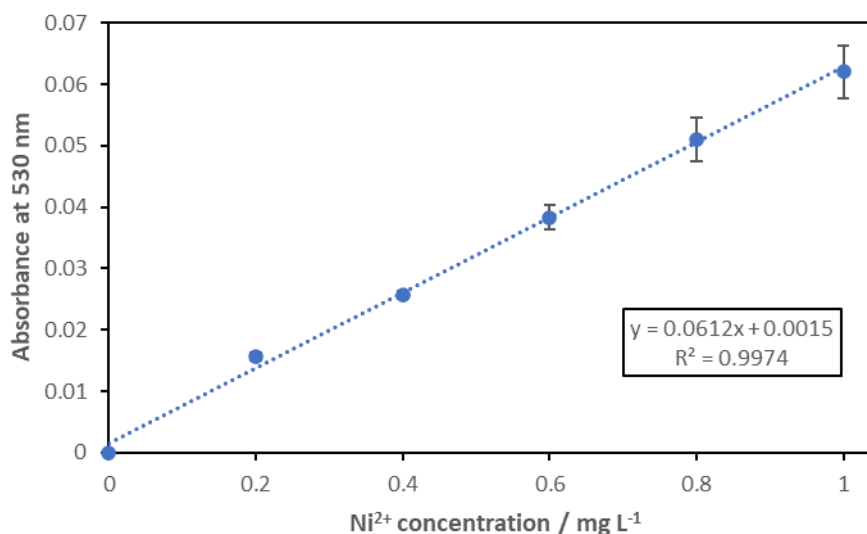
Adsorption isotherm

The adsorption isotherm process in this research was observed by placing 0.1 g of ion exchange resin into a 10 mL solution containing 0.5-2000 mg L⁻¹ Ni²⁺ and mixing with a magnetic stirrer at 100 rpm for 24 hours at room temperature (20 ± 2 °C). The amount of nanomat was based on the availability of the nanomat. The concentration of Ni²⁺ in the solution was measured before and after the mixing process through UV/Vis spectrophotometry with nioxime as colorimetric reagent, with dilution, when necessary. The recorded data was then processed, and best fit was found, comparing the data obtained to the following linearised isotherm models, chosen based on previous studies on electrospun fibres for metal adsorption: Henry, Langmuir, Freundlich, and Dubinin-Radushkevich (DR) [205, 206].

Effect of pH to Ni²⁺ adsorption by ion exchange resin

The effect of pH to the Ni²⁺ adsorption properties of each resin were then observed by stirring 0.1 g of respective resins into 50 mL 3 mg L⁻¹ Ni²⁺ solution at 100 rpm for 20 min. The Ni²⁺ solution pH was adjusted through addition of diluted HCl or NaOH to the desired pH value. The solution was sampled before the procedure (initial), and at minute 1, 2, 3, 4, 5, 10, 15, and 20 after the start of stirring time. The Ni²⁺ measurement was done by UV/Vis spectrophotometry with nioxime as colorimetric reagent. In this Ni²⁺ concentration measurement, 100 µL nioxime was added into a 1000 µL sample solution and left to react for 20 min before absorbance measurement at 530 nm. Each experiment was repeated three times. The mass of adsorbed Ni²⁺ at each time points were then compared to the initial mass of Ni²⁺ in the solution.

Ni²⁺ calibration curve for UV/Vis spectrophotometry



Appendix-Figure 16 Ni²⁺ calibration curve for UV/Vis spectrophotometry measurement at the wavelength of 530 nm.

Results – PCL/chitosan/PEO nanomat for Ni²⁺ adsorption

Fabrication and optimisation of electrospun PCL/chitosan/PEO nanomat

In this research, a composite consisting of two layers of polymers was designed for Ni²⁺ adsorption. The backbone structure would be made of PCL – which is easier to spin, but relatively non-reactive to metal. On top of this backbone structure, chitosan/PEO fibres would be electrospun, forming the adsorptive layer for Ni²⁺ trapping through chitosan-metal complex formation. In order to optimally produce these fibres, optimization of the electrospinning process was done for both PCL and chitosan/PEO electrospinning.

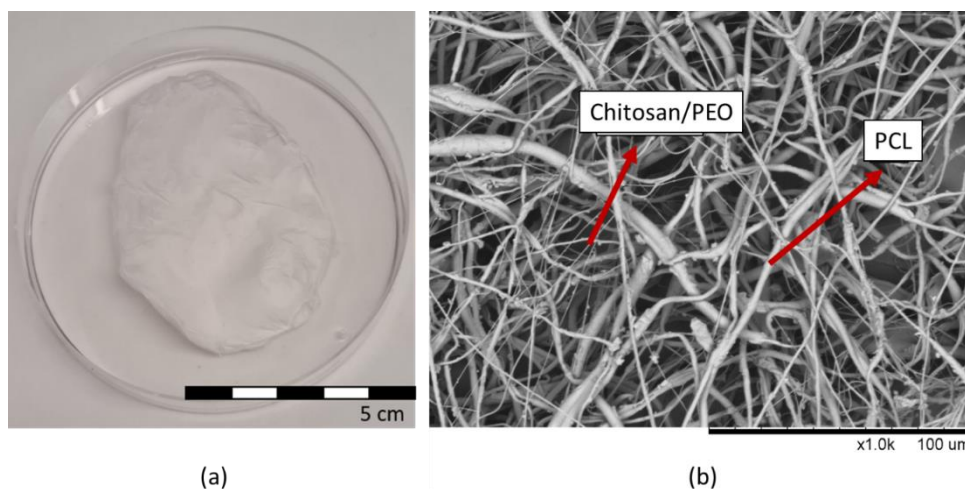
Electrospinning process can be affected by various parameters, both controllable and uncontrollable. Some controllable parameters include polymer type, solvent choice, flow rate, and applied voltage, which was used for optimisation in this study [207]. Whereas less controllable or uncontrollable parameters include relative humidity and temperature of electrospinning process, as discussed in Chapter 1. The type of solvent was restricted glacial acetic acid, water, or a mixture between the two. This restriction complies to a green electrospinning procedure, where relatively less hazardous solvents were used. It also ensures safety of the process in the available electrospinning setup, which was not equipped with exhaust or ventilation system to flow the evaporating solvent out of the setup. The restriction in solvent type subsequently affects the type and concentration of polymers used in the process.

The optimisation was done separately for PCL and for chitosan/PEO fibres, before combining the two processes by electrospinning the chitosan/PEO fibres at its optimum process parameters on

top of a layer of PCL, spun at optimum process parameters. Through the study, it was found that the optimum process parameters for PCL electrospinning was at tip-to-collector distance of 20 cm, with 11 kV applied voltage, and 1 mL h⁻¹ flow rate. While the chitosan/PEO fibres were spun at 20 cm tip-to-collector distance with 17 kV applied voltage and 0.8 mL h⁻¹ flow rate.

Adsorption performance of electrospun PCL/chitosan/PEO nanomat

Through observation with the naked eye, the electrospun nanomat did not seem physically different with other membranes or paper-like matrixes, such as filter-paper. As can be seen in Appendix-Figure 17a, it is white in colour, since both PCL and chitosan/PEO resulted in white-coloured fibres. However, after crosslinking process, the nanomat may turn yellowish, possibly due to crosslinking of a chitosan-rich area [208]. The texture of the nanomat, however, is closer to that of glass-fibre membrane than of filter paper. It is softer and have more cotton-like feel to the touch. Further observation through SEM imaging of the composite, the size difference between the two spun materials can still be seen (Appendix-Figure 17b). This composite consists of PCL nanofibers at the average diameter of 2323 ± 513 nm, and chitosan/PEO nanofibers at the average diameter of 306 ± 33 nm. The use of 20 wt% PCL as the base was necessary to cut down the electrospinning time, while also providing relatively a matrix with small fibre diameter. As a comparison, Whatman no 1 qualitative filter paper, when placed under SEM imaging and measured with the same method as the spun fibres (n=40), has an average fibre diameter of 10,964 ± 5,467 nm. Not only does this show that the commercially available filter paper has approximately 5 times bigger fibre diameter – and consequently a much lower surface area – it also shows higher size variability, with almost 50% relative standard deviation (*RSD*, σ/\bar{x}). Compared to the *RSD* of the electrospun fibres, which were 22% and 11% for PCL and chitosan/PEO, respectively.



Appendix-Figure 17 (a) Electrospun nanomat after crosslinking with 20% glutaraldehyde for 24 hours and dried for another 24 hours; (b) SEM image of chitosan/PEO fibres on PCL matrix.

Adsorption isotherm and kinetics of PCL/chitosan/PEO composite

The adsorption kinetics of the nanomat was observed with the method described in section Adsorption kinetics. The concentration of Ni^{2+} chosen was the target set based on the detection limit of the paper-based microfluidic device for Ni^{2+} detection, as discussed in Chapter 2. Whereas the duration and volume were determined based on a preliminary observation.

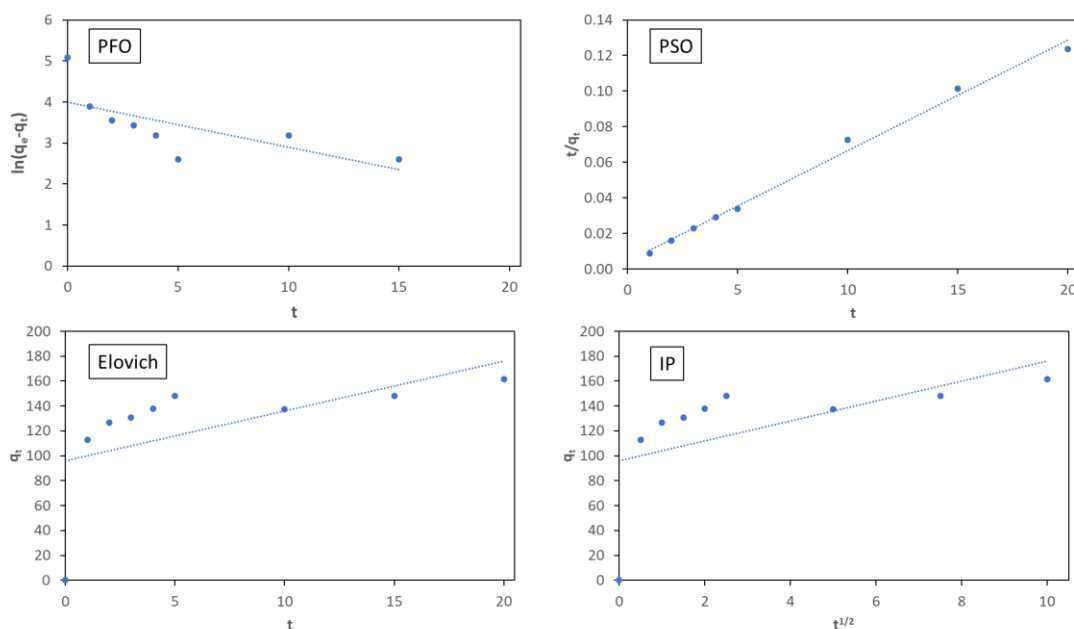
The method of observation for the adsorption isotherm of the nanomat is as described in section Adsorption isotherm. The duration of the reaction was chosen to ensure maximum adsorption capacity to be reached by the mat, at 100 rpm stirring and 10 mL volume.

Adsorption kinetics of electrospun composite

Since Ni^{2+} concentration for each minute in the 20 min was measured and recorded, the adsorption capacity of the nanomat at each given time point can be calculated. For pseudo-first order (PFO) model, the time (t) was plotted against $\ln(q_e - q_t)$ to obtain a linear regression, fitting the model to the data. Similarly, for pseudo-second order (PSO), time was plotted against t/q_t ; Elovich plotted time against q_t ; and for IP was q_t against $t^{1/2}$. These plots are illustrated in Appendix-Figure 18.

[Appendix-Table 1](#)

Appendix-Table 1 (right) shows the result of fitting the obtained kinetics data to the PFO, PSO, IP, and Elovich models. It is evident that in the 20 minutes of mixing, the adsorption kinetics of the spun nanomat follows the PSO model with $r^2 = 0.99$. PSO is the model that assumes that the adsorption rate is dependant, or proportional to the availability of sites on the adsorbent. Therefore, the reaction rate is dependent on the number of active sites available at given time [209]. The interaction between the adsorbate and the adsorbent, in this model, is most often described as based on chemical bonding (chemisorption) [210]. This interpretation can be justified by the known interaction between chitosan and heavy metal, where chelation would happen between 2 chitosan molecules with 1 heavy metal ion (2:1 ligand to metal) [211]. This model also indicates that the adsorption kinetics of the spun fibres will be affected by the pH of the solution and temperature, among other factors [209].



Appendix-Figure 18 Fitting for Ni²⁺ adsorption kinetics models: pseudo-first order, pseudo-second order, Elovich, and intra-particle, by electrospun PCL/chitosan/PEO composite.

Adsorption isotherm of electrospun composite

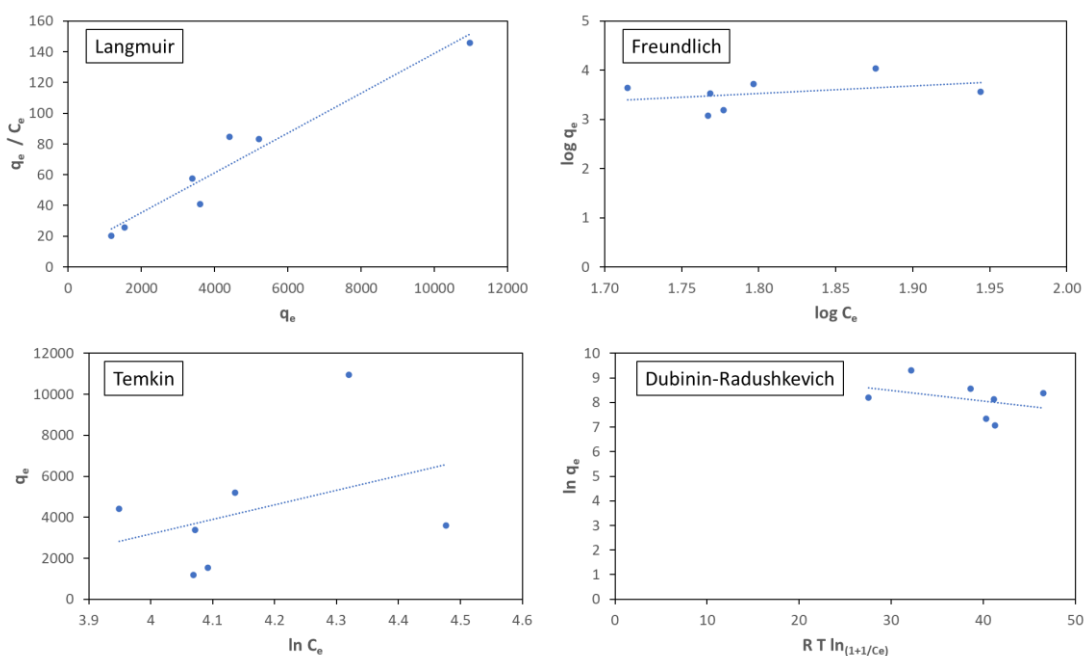
The initial and final concentration of Ni²⁺ solutions were recorded and used in the fitting of the adsorption models. Through this information and the mass of nanomat immersed, the adsorption capacity of the nanomat at the end point of the adsorption can be calculated. For Langmuir model, the adsorption capacity after 24 h of mixing (adsorption capacity at equilibrium or q_e) was plotted against the adsorption capacity divided by end concentration (q_e/C_e). This shows a relatively linear trend, confirming a degree of agreement between the model and the experimental data. Similar approach was done to fit the data to Freundlich, Temkin, and

Dubinin-Radushkevich (DR) linearised models. In Freundlich model, $\log q_e$ was plotted against $\log C_e$; in Temkin the q_e was plotted against $\log C_e$; and in DR the $\ln q_e$ was plotted against $RT \ln(1+1/C_e)$, where R is the ideal gas constant and T is the temperature. These figures were shown in Appendix-Figure 19.

As listed in

[Appendix-Table 1](#)

Appendix-Table 1 (left), the best fit for the spun nanomat was found for Langmuir adsorption model ($r^2= 0.94$). Langmuir isotherm model is categorised as chemical adsorption [212]. It assumes monolayer adsorption with homogenous distribution of adsorption sites and constant adsorption energy [212]. This agrees with the adsorption model fitted for chitosan-based electrospun nanofiber for Ni^{2+} adsorption (see Appendix-Table 2).



Appendix-Figure 19 Fitting for Ni^{2+} adsorption isotherm models: Langmuir, Freundlich, Temkin, and Dubinin-Radushkevich, by electrospun PCL/chitosan/PEO composite.

For both adsorption isotherm and kinetics study, relevant parameters were listed in

[Appendix-Table 1](#)

[Appendix-Table 1](#). These variables may vary between different models. However, the recurring and most important variable to take into account in this step is the fit, which is the r^2 value of the linear regression plotted for each model (see Appendix-Figure 19 and Appendix-Figure 18).

Appendix-Table 1 (left) Adsorption isotherm and (right) adsorption kinetics model-fitting data to Henry and linearized Langmuir, Freundlich, Temkin, and Dubinin-Radushkevich for adsorption isotherm and to pseudo-first order, pseudo-second order, intra-particle, and Elovich for adsorption kinetics.

Model		
Henry	K	75.8
	D	1124.2
	fit	0.34
Langmuir	qm	722.73
	K	0.01
	fit	0.94
Freundlich	Kf	6.09
	n	0.66
	fit	0.13
Temkin	A	34.73
	B	7073.5
	fit	0.15
DR	qo	2822279.36
	β	0.0005
	fit	0.35

Model		
PFO	q	54.049
	K	0.1095
	fit	0.4852
PSO	q	161.29
	K	0.00001
	fit	0.9935
IP	Kp	8.0256
	C	95.885
	fit	0.3308
Elovic h	A	9.57×10^{10}
	B	0.25
	fit	0.3308

Based on the adsorption isotherm model, the maximum adsorption capacity of the electrospun nanomat can be predicted. In this research, the maximum adsorption capacity following the Langmuir model at 20°C was 722.73 Ni²⁺ mg g⁻¹. Compared to previous studies observing maximum adsorption of chitosan-based nanofibers for Ni²⁺ adsorption, the nanomat produced in this research follow the same adsorption isotherm model (Langmuir) [109, 111, 145, 213]. However, the maximum adsorption capacity of PCL/chitosan/PEO nanomat produced in this research was at least two times higher compared to previous studies [109, 111, 145, 213], even at lower adsorption temperature. Compared to chitosan-based nanofibers tested for other metal adsorptions, the adsorption of Ni²⁺ with nanomat produced in this study was also notably higher [214, 215]. The only nanofiber in previous study with higher maximum adsorption capacity for Ni²⁺ was in functionalised electrospun Nylon 66, where q_{max} reached 1269 mg g⁻¹ [216]. However, the electrospinning of Nylon 66 in the study required relatively hazardous solvent (formic acid/chloroform), especially compared to the green electrospinning approach taken in this study, where the solvent was limited to diluted acetic acid. Additionally, the spinning flow rate was lower (0.314 mL h⁻¹, 16 hours electrospinning) compared to the electrospinning of PCL/chitosan/PEO in this study, making the later more favourable in commercial production settings. Therefore, the electrospun nanomat produced in this research display notable advantages compared to most of previous studies due to its high maximum Ni²⁺ adsorption capacity with faster and safer fabrication method.

Appendix-Table 2 Adsorption model and maximum adsorption capacity of previous electrospinning studies involving chitosan and other polymers for Ni²⁺ and other heavy metal adsorptions.

Polymer	Ion	Adsorption condition		Model	q _{max} / mg g ⁻¹	Ref
		Time / min	Temp / °C			
PCL/chitosan/PEO	Ni ²⁺	1440	20	Langmuir	722.73	This study
Chitosan-based nanofibers for Ni ²⁺						
Chitosan/PVA/zeolite	Cr ⁶⁺			Langmuir	8.84	[145]
	Fe ³⁺				6.14	
	Ni ²⁺				1.76	
PEO/chitosan	Ni ²⁺	120	45	Langmuir	357.10	[109]
	Cu ²⁺				310.20	
	Co ²⁺				248.10	
	Pb ²⁺				237.20	
Chitosan/HA	Ni ²⁺		45	Langmuir	180.20	[111]
	Pb ²⁺				296.70	
	Co ²⁺				213.80	
PVA/chitosan/ZnO-NH ₂	Ni ²⁺		45	Langmuir	49.95	[213]
	Cd ²⁺				139.28	
Chitosan-based nanofibers for other metals						
Chitosan (stacking)	Cu ²⁺	1440	25	Langmuir	276.20	[215]
Chitosan/PGMA/PEI	Cr ⁶⁺		25	Langmuir	138.96	[217]
	Cu ²⁺				69.27	
	Co ²⁺				68.31	
Other polymers for Ni ²⁺						
PVA/zeolite	Ni ²⁺	60	45	Langmuir	342.80	[112]
	Cd ²⁺				838.70	
Nylon (functionalised) 66	Ni ²⁺	60		Freundlich	1269.00	[216]
	Cd ²⁺				956.00	
PAN (functionalised)	Ni ²⁺		45	Langmuir	138.70	[206]
	Cd ²⁺				69.50	
	Th ⁴⁺				249.40	
	U ⁶⁺				193.10	
PVA/ZnO	Ni ²⁺	360	45	DR	94.43	[218]

	Cu ²⁺				162.48	
	U ⁶⁺				370.86	

Results – ion exchange resins for Ni²⁺ preconcentration

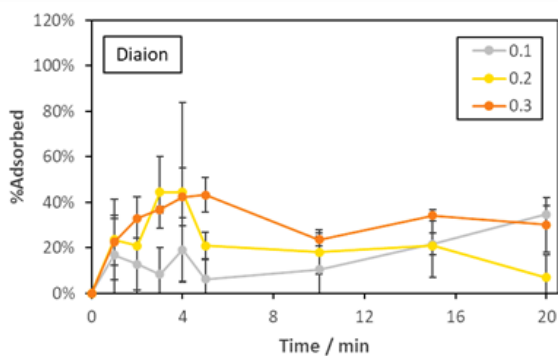
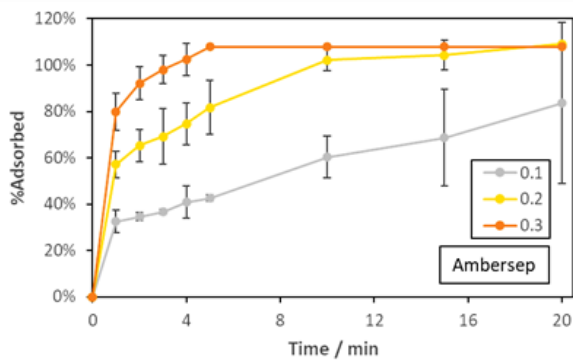
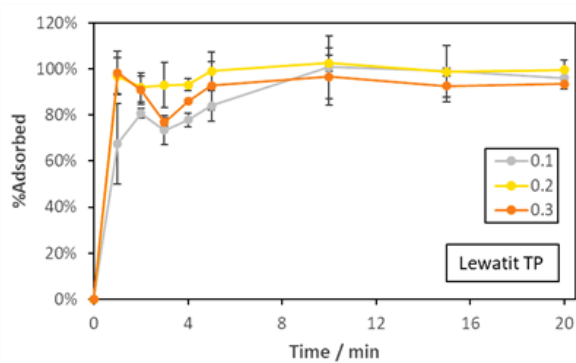
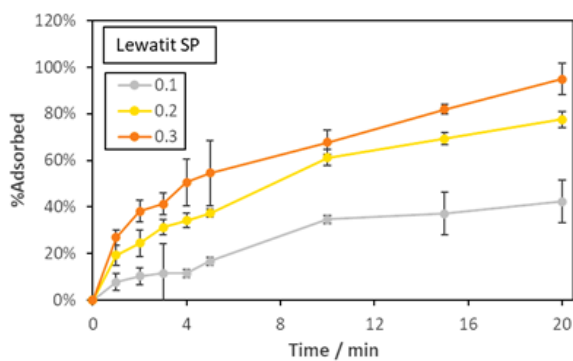
Preliminary observation

In Appendix-Figure 20, the amount of Ni²⁺ adsorbed to the resin is plotted against the mixing time. This was done as preliminary study to observe the adsorption behaviour of the resins. The data in the figures represent the adsorption behaviour of 0.1-0.3 g of respective resins in 50 mL 3 mg L⁻¹ Ni²⁺ solution, stirred at 100 rpm. As can be seen, Lewatit[®] MonoPlus SP 112, or known as Lewatit SP in this research, shows incremental adsorption of Ni²⁺ throughout the mixing duration within the tested mass. The bigger mass of the Lewatit SP resin is correlated to the higher Ni²⁺ adsorption, with error bar in the figure showing the standard deviation between the result of the three repeats. At earlier stage of the mixing, there was less notable difference between the various mass tested, however, after minute 5, more notable difference can be visibly seen. This shows improvement in Ni²⁺ adsorption behaviour of the resin with the increase of mass.

Further, in the same figure (Appendix-Figure 20), the performance of Lewatit[®] TP 207 was also tested with the same experimental conditions. However, evidently, the performance of the chelating resin shows stark difference in trend compared to Lewatit SP. For Lewatit[®] TP 207, also referred to Lewatit TP in this research, more than 50% of Ni²⁺ had been adsorbed in the first 5 min of the mixing in all tested resin mass. The error bar shown in the figure is the standard deviation between the three repeats. This shows that for chelating resin, Ni²⁺ adsorption can be observed immediately in the first minutes of the mixing and stabilise within 10 min. Interestingly, for Ambersep[™] M4195, the Ni²⁺ adsorption trend differs within the tested mass range. For 0.1 g Ambersep[™] M4195, Ni²⁺ adsorption spiked in the first minute, followed by a steady incline in the similar trend to the adsorption character of Lewatit SP. However, at 0.3 g Ambersep[™] M4195, the Ni²⁺ adsorption is more similar to that of Lewatit TP, where adsorption spiked and increased within the first 5 min, followed by stable trend to the end of the observation time. As previous data illustrated in this figure, the error bar represented standard deviation between the three repeats.

Appendix-Figure 20 also presents Diaion[®] HP 20 adsorption of Ni²⁺ within the same range of mass (0.1-0.3 g). However, the Ni²⁺ adsorption performance was notably lower compared to other resins in this research, while also not showing any recognisable trend. Fluctuation within

the duration may be caused by constant adsorption and desorption of the ion from the resin. Error bar in this figure also shows the standard deviation between the three repeats – further showing the non-repetitiveness of the process with this resin.



Appendix-Figure 20 Resin adsorption performance measured by the amount of Ni²⁺ adsorbed throughout the 20 min mixing of 0.1 g Lewatit[®] MonoPlus SP 112, Lewatit[®] TP 207, Ambersep[™] M4195, or Diaion[®] HP 20 in 50 mL Ni²⁺ solution with initial concentration of 3 mg L⁻¹. Error bars illustrating standard deviation between the result of the three repeats (n=3).

Adsorption kinetics

The adsorption kinetics of the ion exchange resins: Lewatit SP, Lewatit TP, and Ambersep was observed using the method described in section 0 Adsorption kinetics. The kinetics models, upon fitting into either PFO, PSO, Elovich, or IP models, for all three tested resins were the same: pseudo-second order. This was also the adsorption kinetics model fitted for the electrospun nanomat discussed earlier in this chapter, showing similar adsorption kinetics character for all tested materials in this research. This model assumes that the rate of reaction would depend on the amount of target ions on the surface of the adsorbent, since the rate is proportional to the number of available active adsorption sites on the adsorbent [209, 210]. For Lewatit SP, this adsorption kinetics model is consistent with findings in previous research [118]. Whereas for Lewatit TP and Ambersep, no prior studies had been published to date on its kinetics for Ni²⁺ adsorption from aqueous solution.

Appendix-Table 3 Ni²⁺ adsorption kinetics data of Lewatit SP, Lewatit TP, and Ambersep resins (T= 20°C, t= 20 min, at 100 rpm).

Model		Resin types		
		Lewatit SP	Lewatit TP	Ambersep
PFO	q	7.26	2.12	20.87
	K	0.24	0.20	0.21
	fit	0.938	0.962	0.245
PSO	q	0.22	0.70	0.37
	K	2.45	0.52	0.87
	fit	0.996	0.990	0.999
Elovich	A	1052.15	350.82	128.37
	B	135.14	41.84	108.70
	fit	0.560	0.642	0.264
IP	Kp	0.09	0.23	0.24
	C	0.01	0.05	0.02
	fit	0.560	0.642	0.264

Adsorption isotherm

The adsorption isotherm of the resins was modelled and observed in similar manner as for electrospun nanomat. The only difference is that for the resins, the mass of resin added to the solution was 0.1 g. Rather than using a similar mass as electrospun nanomat, adsorption observation for the resins used 0.1 g to ease and ensure accuracy in resin weighing process.

Appendix-Table 4 shows the comparison between the different resins and adsorption isotherm models. The table shows that different resins observed in this research showed different fit to the tested adsorption isotherm models. Lewatit SP showed best fit to the semi-empirical DR adsorption model, which is based on Polanyi's adsorption theory [212]. This also implies that the adsorption process would depend on temperature [219]. Through similar method of calculation, the adsorption isotherm model for Lewatit TP was best fit with Freundlich model. This adsorption model is often used to describe multi-layer adsorption on heterogenous surfaces [212]. However, through this linearised calculation, the n for Lewatit TP was determined to be 0.77. This indicates potentially irreversible adsorption, since $1/n > 1$ [219]. Lastly, the best fit for Ambersep data was calculated and found to be Langmuir isotherm. Langmuir isotherm is one of the most common model used in describing adsorption phenomenon, where it assumes monolayer adsorption process that occur at identical and equivalent local sites [219].

Appendix-Table 4 Ni²⁺ adsorption isotherm data of Lewatit SP, Lewatit TP, and Ambersep resins (T= 20°C, t= 24h, at 100 rpm).

Model		Resin types		
		Lewatit SP	Lewatit TP	Ambersep
Henry	K	2.12	2.01	4.33
	D	8.31	5.54	125.93
	fit	0.806	0.748	0.345
Langmuir	qm	12.42	8.42	7.41
	K	1.33	0.05	0.02
	fit	0.797	0.958	0.997
Freundlich	Kf	12.19	1.71	3078.93
	n	1.70	0.77	0.32
	fit	0.864	0.964	0.608
Temkin	A	13.41	2.31	28.83
	B	15.30	29.86	167.01
	fit	0.722	0.598	0.320
DR	qo	86.89	71.29	60.35
	β	0.00	0.00	0.00
	fit	0.917	0.898	0.591

Comparing the adsorption isotherm data to previous studies, the adsorption model for Lewatit MonoPlus SP 112 in this research unconventionally fits DR instead of Langmuir or Freundlich. However, the calculated maximum adsorption capacity using the fitted model is comparable to previous studies, as shown in

[Appendix-Table 5](#). On the other hand, the adsorption isotherm models for the chelating resins (Lewatit TP and Ambersep) in this research agrees with previous studies using similar resins (shown in

[Appendix-Table 5](#)

[Appendix-Table 5](#)). However, the calculated maximum adsorption capacity using the fitted models are notably lower than previous studies. This notably lower values might be due to difference in mixing temperature, pH, or other experimental setup for the adsorption isotherm experiment.

Whereas compared to the electrospun PCL/chitosan/PEO, the calculated maximum adsorption capacity of the tested resins was far lower. For electrospun nanomat developed in this research, the maximum adsorption capacity was determined to be 722.73 mg g⁻¹ (see Chapter 3 - 0 Adsorption isotherm of electrospun composite). Even compared to the maximum adsorption capacity of Lewatit® MonoPlus SP 112 resins, which was the highest amongst the tested resins, the adsorption capacity of the nanomat was still around 8 times higher.

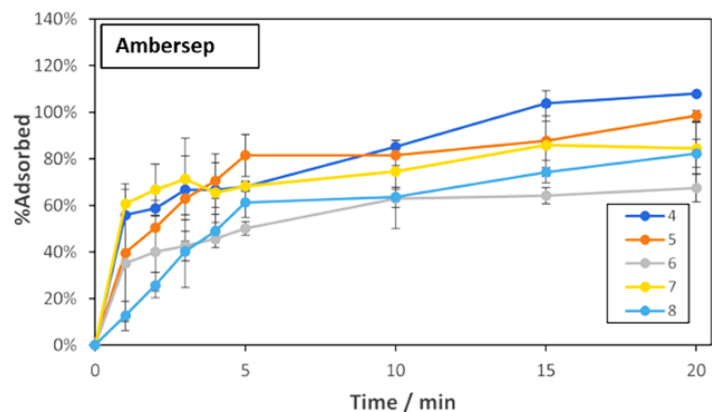
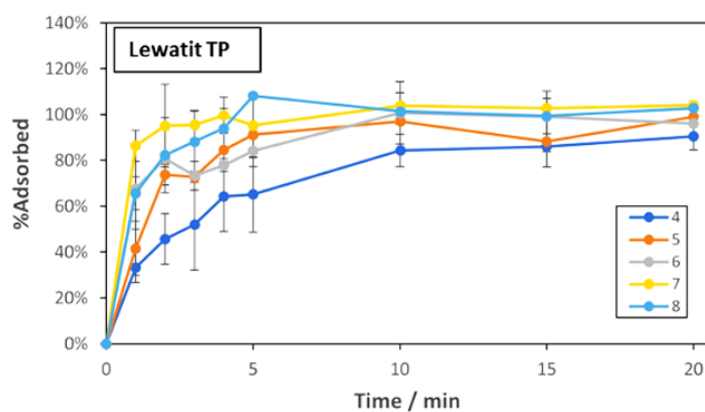
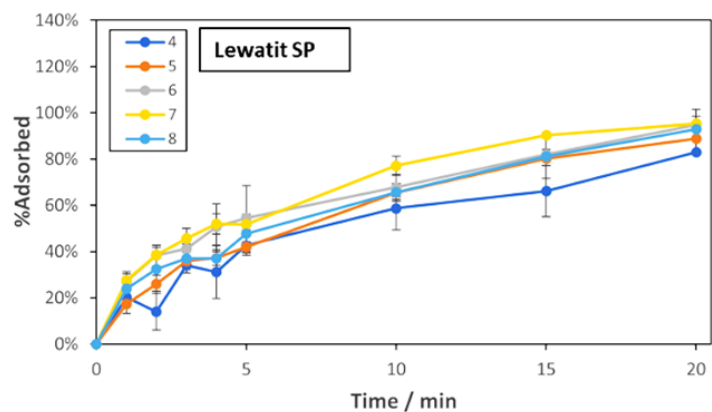
Appendix-Table 5 Comparison of calculated maximum adsorption capacity (or K_f and n , for Freundlich) between the results of this research and previous studies using similar resins.

Resin	Ion	Adsorption condition		Model	$q_{\max} / \text{mg g}^{-1}$	Ref
		Time /min	Temp /°C			
Lewatit MonoPlus SP 112	Ni^{2+}	1440	20	DR	86.89	This work
Lewatit TP 207	Ni^{2+}	1440	20	Freundlich	$K_f = 1.71$ $n = 0.77$	This work
Ambersep M4195	Ni^{2+}	1440	20	Langmuir	7.41	This work
Strongly acidic cation exchange resins for Ni^{2+} adsorption (Lewatit SP)						
Lewatit MonoPlus SP 112	Ni^{2+}	1440	25	Langmuir	170.94	[118]
Dowex HCR S/S	Ni^{2+}		23	Langmuir	156.25	[122]
Dowex HCR-S	Ni^{2+}		20	Sips	87.81	[120]
Amberlite IR 120H	Ni^{2+}	150	25	Langmuir	27.87	[121]
IRN77	Ni^{2+}		25	Freundlich	$K_f = 81.82$ $n = 5.91$	[220]
Chelating cation exchange resins for Ni^{2+} adsorption (Lewatit TP)						
Lewatit TP 207	Ni^{2+}			Langmuir	28.99	[124]
Purolite S930	Ni^{2+}			Freundlich	$K_f = 0.10$ $n = 1.6$	[221]
Amberlite IRC 748	Ni^{2+}	4	25	Langmuir	117.39	[222]
Ionac SR-5	Ni^{2+}	4	25	Langmuir	79.24	
Chelating anion exchange resins for Ni^{2+} adsorption (Ambersep)						
Dowex M4195	Ni^{2+}	4	25	Langmuir	95.38	[222]
Dow M4195	Ni^{2+}	1440		Langmuir	22.72	[223]
Lewatit TP 220	Ni^{2+}	1440		Freundlich	$K_f = 2.317$ $n = 1.59$	[224]

Effect of pH to Ni^{2+} adsorption by ion exchange resins

The effect of pH to the performance of the ion exchange resin in Ni^{2+} adsorption was observed with the method described in section 0 [Effect of pH to \$\text{Ni}^{2+}\$ adsorption by ion exchange resin](#)~~Effect of pH to Ni^{2+} adsorption by ion exchange resin~~. Appendix-Figure 21 show the Ni^{2+} adsorption for the resins within the 20 minutes stirring time. For Lewatit SP, the change of pH within the tested value did not notably affect the Ni^{2+} adsorption rate and capacity, especially at

minute 20. However, at earlier time of sampling, especially at minute 5, a slight difference in the average amount of adsorbed Ni^{2+} can be observed. In this case, adsorption is shown to be slightly higher in more neutral pH (6-7). Similarly, with Lewatit TP, the amount of adsorbed Ni^{2+} at minute 20 did not significantly differ within the tested pH range. However, it shows quite vast difference in adsorption rate through the tested pH values. This is strikingly visible at earlier sampling time below minute 5. The rate of adsorption generally increases with the increase of pH value, with highest adsorption achieved at pH 8 and lowest adsorption for pH 4 in minute 5. Another notable aspect is the rate at which the adsorption reach stability for Lewatit TP. Compared to Lewatit SP, where Ni^{2+} adsorption is increasing steadily throughout the time of experiment, in Lewatit TP, the adsorption of Ni^{2+} reached its peak at minute 5 before relatively stabilises until minute 20. Ambersep, on the other hand showed bigger effect of pH on the adsorption of Ni^{2+} , both at minute 5 and 20.



Appendix-Figure 21 Performance of various ion exchange resins for Ni²⁺ adsorption in various pH values ranging from 4-8, within 20 minutes. Ni²⁺ concentration was measured with UV/Vis spectrophotometry. Error bars illustrating standard deviation between the result of the three repeats (*n*=3).

Incorporation of cafetiere-based Ni²⁺ preconcentration workflow into paper-based analytical system

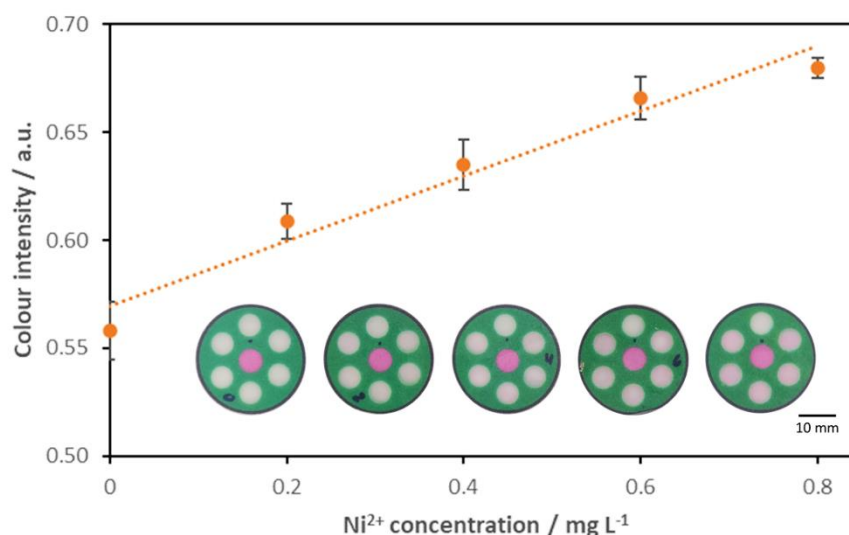
Alternative workflow: 10 mL 5 M NaCl as elution solution, for laboratory-based experiment

In low-cost laboratory settings, adsorption of Ni²⁺ with 2.6 g Lewatit SP can still be achieved with the modified basket with 5 min plunging time followed with 5-10 mL elution with NaCl. This

process would require users to take the resins out of the basket and pour it into the elution solution. Given the complexity of the step, this resin transfer process is not suitable for onsite environmental uses – be it by trained or untrained users. Additionally, the transfer would expose users to higher risk of direct contact with the resin after its metal adsorption process. Which ideally is only done by trained users who understands the risk and mitigation steps required. However, the benefit of this process may overrule this complication in laboratory-based settings. Especially since this process would allow lower volume of elution solution to be used, consequently creating a more effective preconcentration process with high preconcentration factor.

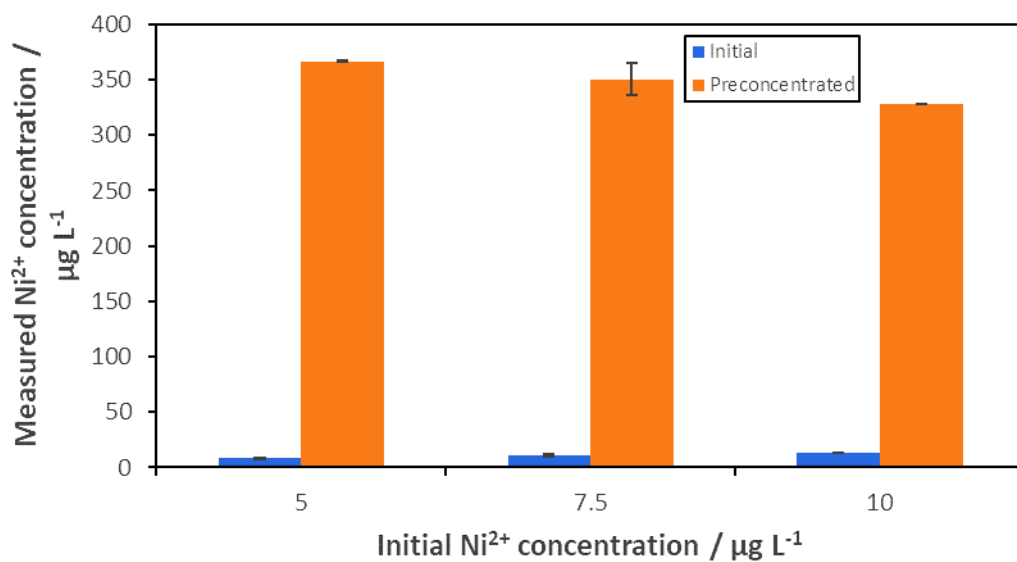
The adsorption part of this workflow remained, where 300 mL of sample solution containing Ni^{2+} was poured into a cafetière with 2.6 g Lewatit SP in its modified basket. The resin was then plunged repeatedly for 5 min. However, in the elution step, the basket was opened and the resins can be transferred into a centrifuge tube containing 10 mL 5 M NaCl. The centrifuge tube containing both resin and elution solution was then mixed vigorously for 1 min, before the entirety of the solution was transferred into a petri dish. The shaking process of the tube can be done manually by hand or by a vortex – both was done to ensure thorough contact between the elution solution with the entire surface area of the resins. This process can enhance the elution process by increasing the ion exchange incidence. A nioxime PAD was then placed on the solution, allowing the solution to enter the reaction wells. After 4 minutes, the reaction wells will reach its peak intensity and picture of the device can be obtained through photography with smartphone camera in a black box setting.

Through this preconcentration method, a factor of 10 can be reached after 6 min of preconcentration process. This is due to the low elution volume, while the elution effectiveness maintained relatively similar. Therefore, higher preconcentration factor was achieved compared to when higher elution volume was used. This process would then allow the nioxime PAD to detect Ni^{2+} at initially lower sample concentration, as shown in Appendix-Figure 22. Combining the preconcentration step with the developed nioxime PAD allowed the PAD to detect down to $0.3 \text{ mg L}^{-1} \text{ Ni}^{2+}$, which is 10 times lower than its detection limit. This concentration of Ni^{2+} is also below the acute limit of Ni^{2+} concentration in the freshwater system according to US EPA (0.47 mg L^{-1}) [34]. Which make it a suitable method of Ni^{2+} detection in low-cost laboratory setting.



Appendix-Figure 22 Colour intensity measured on the sample wells of nioxime μ PAD upon dipping into the 10 mL 5 M NaCl elution solution of 0.2-0.8 mg L⁻¹ Ni²⁺ preconcentration. Error bars illustrating standard deviation between the result of the three repeats (n=3).

The same method of preconcentration with 10 mL 5 M NaCl elution was also tested for environmentally relevant level of Ni²⁺ to observe its preconcentration factor at this level of Ni²⁺. As shown in Appendix-Figure 23, at initial Ni²⁺ concentration of 0.005-0.01 mg L⁻¹ Ni²⁺, the preconcentration method was able to increase the concentration to up to 70 times its initial Ni²⁺ concentration. However, it is also interesting to note that there is a slightly declining trend in the final concentration measured with the increase of initial Ni²⁺ concentration. Despite its effectiveness, the developed nioxime PAD was still not able to detect this level of initial Ni²⁺ concentration in the sample.

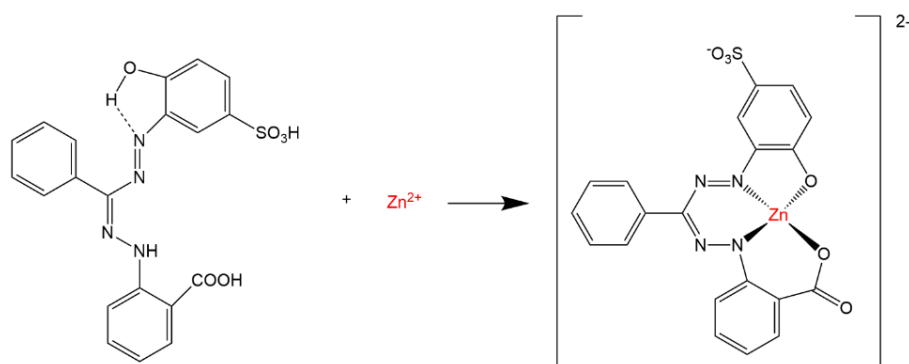


Appendix-Figure 23 ICP result of initial and final Ni²⁺ concentration in pre-concentrated sample with 2.6 g Lewatit SP in 300 mL sample solution and 10 mL 5 M NaCl elution with 1 min mixing time. Error bars illustrating standard deviation between the result of the three repeats (n=3).

Appendix 3 Zn²⁺ detection kit

μPAD for Zn²⁺ detection with Zincon monosodium salt as colorimetric reagent

Zincon monosodium salt has been utilised as zinc colorimetric detection reagent in previous PADs development [12, 83]. The reagent has been proven to show low detection limit and fast reaction time, with limited selectivity. As in previous PAD development in this research, we will start with observation on the reagent properties in aqueous-based reaction measured using UV/Vis spectrophotometry before delve into PAD optimization and development. Theoretically, Zincon monosodium salt creates a ligand-metal complex at 1:1 ligand to metal ratio (Appendix-Figure 24). However, the colorimetric reagent is not zinc-specific, rather, it is commonly used in titration of various other transition metals. Kocłya, *et. al.* [99], demonstrated the metal complex formation properties of the colorimetric reagent with Zn²⁺, Cu²⁺, Ni²⁺, Co²⁺, Pb²⁺, Cd²⁺, and Hg²⁺ measured at pH 9.9 with UV/Vis spectrophotometry wavelength of 615, 599, 664, 657, 551, 598, and 611 nm, respectively. It was also observed that at the change of pH, some of this maximum absorbances would shift, however, this phenomenon had not been observed for zinc.



Appendix-Figure 24 Zincon forming 1:1 ligand to metal complex with zinc ion.

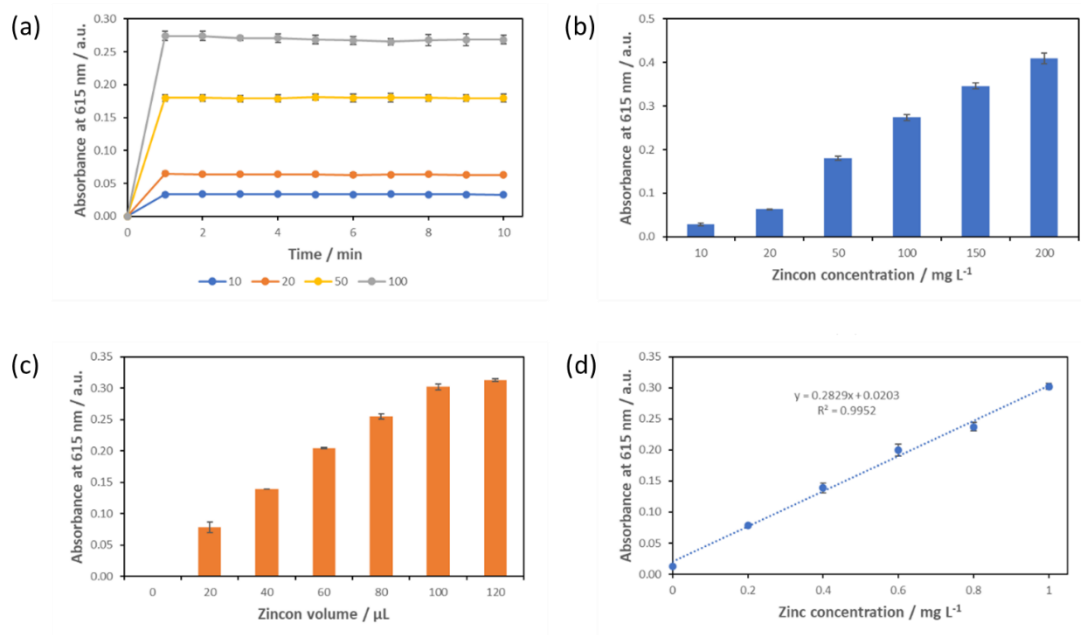
Observation on Zincon monosodium salt as colorimetric reagent in Zn²⁺ detection using UV/Vis spectrophotometry

The reaction time of zincon monosodium salt for Zn²⁺ detection in UV/Vis spectrophotometry followed the method described in section 4.2.3.1 Reaction time. As summarised in Appendix-Figure 25a, Zincon monosodium salt was able to react rapidly with zinc in various Zincon concentration. Between 10, 20, 50, and 100 mg L⁻¹ Zincon concentration tested, all showed immediate increase in the first minute of addition to the zinc sample. Further, the measured absorbance stabilised at this level for all tested Zincon concentration, up to 10 min after the reaction. This implies that the incubation time for this reaction before UV/Vis measurement is as short as 1 min, and measurement can be taken within the 10 min period after reagent

introduction. This approach was therefore applied in further Zn^{2+} measurement with Zincon by UV/Vis method in this research.

The effect of zincon monosodium salt concentration to the reaction was observed using the method described in section 4.2.3.2 Effect of zincon concentration. The result of this analytical measurement is shown in Appendix-Figure 25b, where a gradual increase of absorbance follows the increase of Zincon concentration relatively linearly. The difference in the measured absorbance between each measurement points were significant, showing strong correlation between the increase of Zincon concentration to the blue colour intensity measured at the wavelength. On the other hand, the effect of Zincon volume was observed based on the method described in section 4.2.3.3 Effect of zincon volume. The absorbance measurement was as plotted in Appendix-Figure 25c. It is evident in the illustrated plot that the increase of Zincon volume up to 100 μ L has significant impact on the measured absorbance of the solution. However, between 100 μ L and 120 μ L this significance was no longer observed. This implies that the optimum volume of Zincon to be used in this spectroscopic measurement is 100 μ L.

Lastly, the effect of Zn^{2+} concentration was observed, constructing calibration curve for the Zn^{2+} detection with zincon monosodium salt, with method described in section 4.2.3.4 Effect of Zn^{2+} concentration. In Appendix-Figure 25d, this constructed calibration curve can be seen, showing linear correlation between measured absorbance and the increase of Zn^{2+} concentration. This confirmed the suitability of the optimised spectroscopic method for quantification of Zn^{2+} concentration in an aqueous sample. Further, it shows potential for the reaction to be incorporated to the paper-based platform with similar quantification approach.

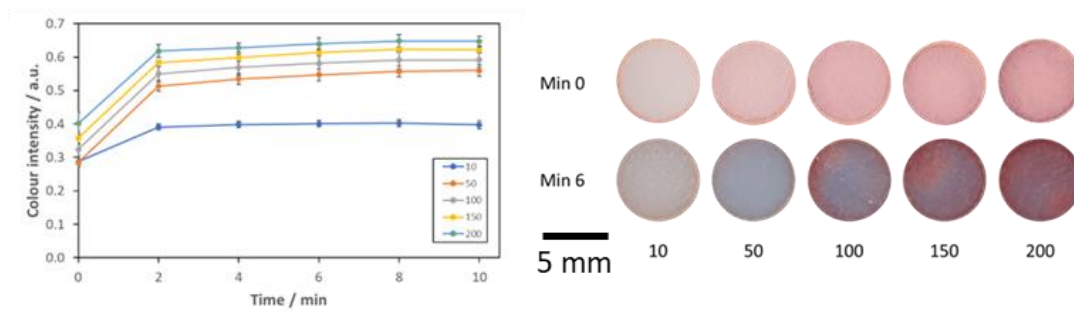


Appendix-Figure 25 Zincon monosodium salt performance as colorimetric reagent for Zn²⁺ detection in UV/Vis spectrophotometry. Observation was done on its (a) reaction time in various Zincon concentration, (b) the effect of Zincon concentration on measured absorbance, (c) the effect of Zincon volume on measured absorbance, and (d) the effect of Zn²⁺ sample concentration on measured absorbance (calibration curve) ($n=3$).

Optimisation of μPAD for Zn²⁺ detection with Zincon monosodium salt as colorimetric reagent

Reaction time

Using this design, the first observation made upon incorporation of the reaction to a μPAD was its reaction time, with method as described in section 4.2.4.4.1 Reaction time. Appendix-Figure 26b shows the measured intensity of Zincon μPAD loaded with a variety of Zincon concentration, dipped into 10 mL 10 mg L⁻¹ Zn²⁺ solution. The measurement is plotted against time, up to 10 mins after initial dipping. Evidently, the colour intensity escalated in the first 2 minutes, with less substantial changes afterwards. This pattern was seen across the Zincon variation and was determined as the optimum reaction time for the Zincon μPAD. Therefore, in further study with the μPAD, measurement would be taken at minute 2 after sample introduction.



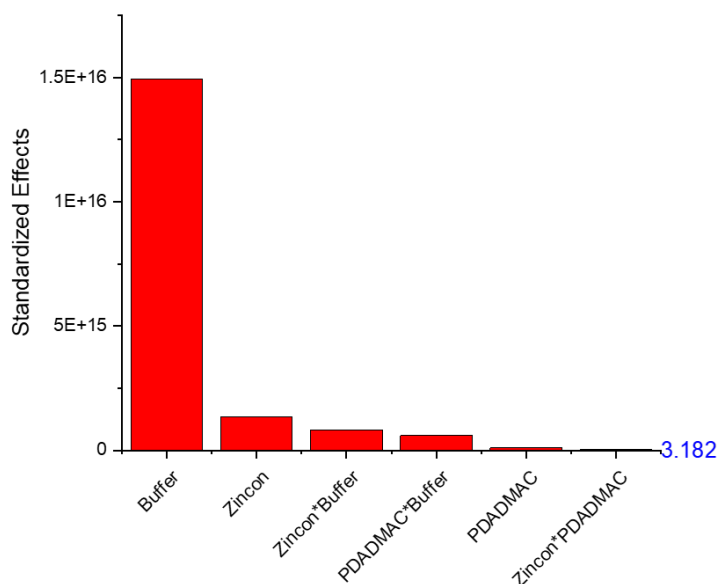
Appendix-Figure 26 Measured colour intensity at red channel of RGB after inversion, taken every 2 minutes after dipping Zincon-loaded μ PAD to 10 mL $10 \text{ mg L}^{-1} \text{ Zn}^{2+}$ solution. Zincon concentration was varied within the range of 10-200 mg L^{-1} ($n=3$).

Optimisation of reagent concentrations using Box-Behnken design of experiment

Standardised effect plot

The standardised effect plot illustrated in Appendix-Figure 27 shows the correlation between the different parameters and interaction between parameters to the magnitude of its effect to the measured colour intensity on the μ PAD. It is plotted as Pareto chart, showing magnitude of the effect of each variable as bar chart and the limit of significance as a blue dashed line. In the figure presented for Zincon optimisation, this dashed line is not clearly visible due to its comparably low value compared to the magnitude of the effect measured. However, a blue-coloured numerical value of this limit can still be observed at the right side of the chart. This shows that most parameters and interaction between parameters would significantly affect the measured colour intensity in this case.

However, as shown in Appendix-Figure 27, the effect of buffer is extremely high compared to other parameters or interaction between parameters. This shows potential that changes in pH value would notably change the measured colour intensity on the μ PAD. Addition of bicarbonate buffer into the reaction, maintained the reaction within more alkaline pH range. Therefore, it confirms the literatures about Zincon as colorimetric reagent for Zn^{2+} detection in the pH-dependency aspect of it [99]. Further, the effect of buffer is notably higher than other parameters and interaction between parameters tested. The most affecting factors by the order of magnitude of standardized effects is buffer concentration \gg Zincon concentration $>$ interaction between Zincon and buffer $>$ interaction between PDADMAC and buffer $>$ PDADMAC concentration $>$ interaction between Zincon and PDADMAC.



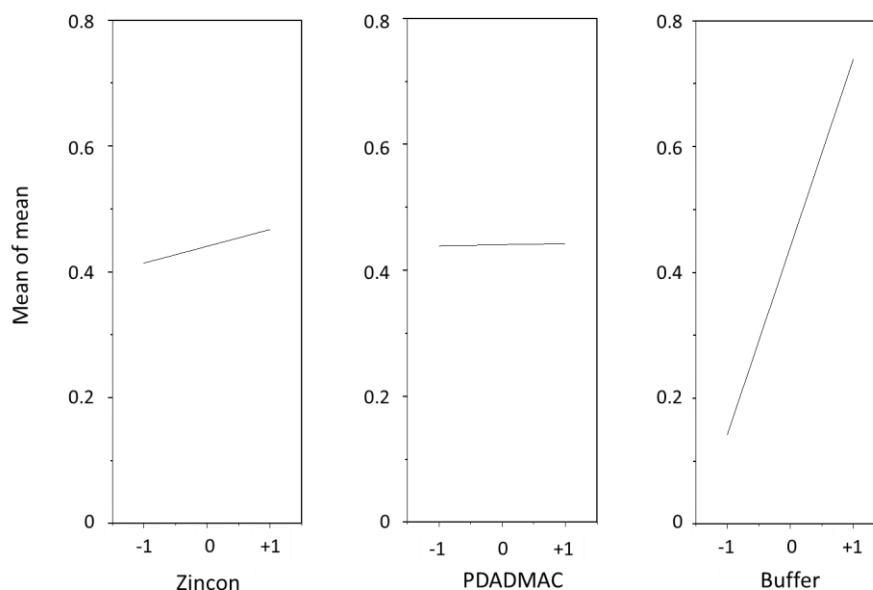
Appendix-Figure 27 Standardised effect Pareto chart showing the effect of various parameters and interaction between parameters to the measured colour intensity on the device after dipping into 10 mL 10 mg L⁻¹ Zn²⁺ solution.

Main effects plot

Whilst knowing the magnitude of effect of a certain parameter can be useful for the optimisation process, the direction of the effect is an equally important information. The main effects plot can help to illustrate in which way the change of concentration of a certain parameter to the measured colour intensity of the μ PAD. Here, the main effects observed were the effects of Zincon, PDADMAC, and buffer concentrations. As illustrated in Appendix-Figure 28, the effect of increasing concentration of each parameter can be correlated to the measured colour intensity. For Zincon, the increase in concentration corresponds to slight increase in measured colour intensity of the μ PAD. Whilst for PDADMAC, the increase in concentration does not notably correspond to the change in measured colour intensity. This agrees with the previous observation with the standardised effect graph. Lastly, the increase of buffer concentration, also following the observation in the standardised effect plot, shows correlation with the increase in measured colour intensity, within the tested range.

In the case of development of Zn²⁺ μ PAD, the optimisation process was done by dipping into 10 mg L⁻¹ Zn²⁺ sample solution. This is a high concentration compared to the target detection range of the μ PAD. Therefore, in this case, optimisation would target a high measured colour intensity of the μ PAD. Since the increase of buffer corresponds to the increase in measured colour intensity in this study, it became almost certain that the buffer concentration that would be

suitable with the target is at the highest buffer concentration tested. Which means the optimum buffer concentration would be 0.1 M bicarbonate buffer.

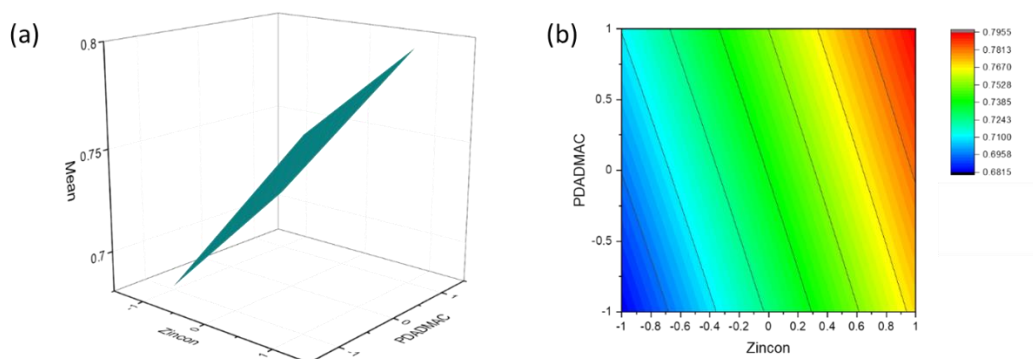


Appendix-Figure 28 Main effect plot showing the magnitude and direction of effect by the three main parameters: Zincon monosodium salt, PDADMAC, and buffer solutions at different concentrations coded to -1 to +1 as minimum to maximum values.

3D and 2D contour plots

Lastly in the optimisation process, 3D and 2D contour plots were constructed as a point of reference for further adjustments down the line. For Zincon μ PAD optimisation, both of these plots were constructed at buffer value coded as 1, which is the maximum tested buffer concentration in the optimisation process corresponding to 0.1 M. In Appendix-Figure 29a, a 3D response surface plot illustrated the correlation between the change in both Zincon and PDADMAC concentration to the modelled colour intensity to be measured on the μ PAD. The plot showed highest point of predicted colour intensity at the highest PDADMAC concentration tested and at the highest Zincon concentration tested. This is supported by the 2D plot in Appendix-Figure 29b, showing the same data. Here, it is easier to see that the highest predicted colour intensity can be achieved at both the highest PDADMAC and Zincon concentration. It is also evident that at highest buffer concentration, lowering the PDADMAC concentration down to the mid-value of the tested range would not cause notable change in colour intensity. This is shown by the red colour smearing down through from the top-right side of the plot down to the middle area of the vertical axis; creating a triangular shape of optimum or desired condition. Therefore, based on the optimisation process, one possible concentration of each reagents

needed to achieve highest colour intensity possible was at 150 mg L⁻¹ Zincon, 6 wt% PDADMAC, and 0.1 M bicarbonate buffer.



Appendix-Figure 29 Response surface plot showing the effect of Zincon monosodium salt and PDADMAC concentration to the measured colour intensity at maximum concentration of buffer (+1), shown as (a) 3D surface plot and (b) contour plot.

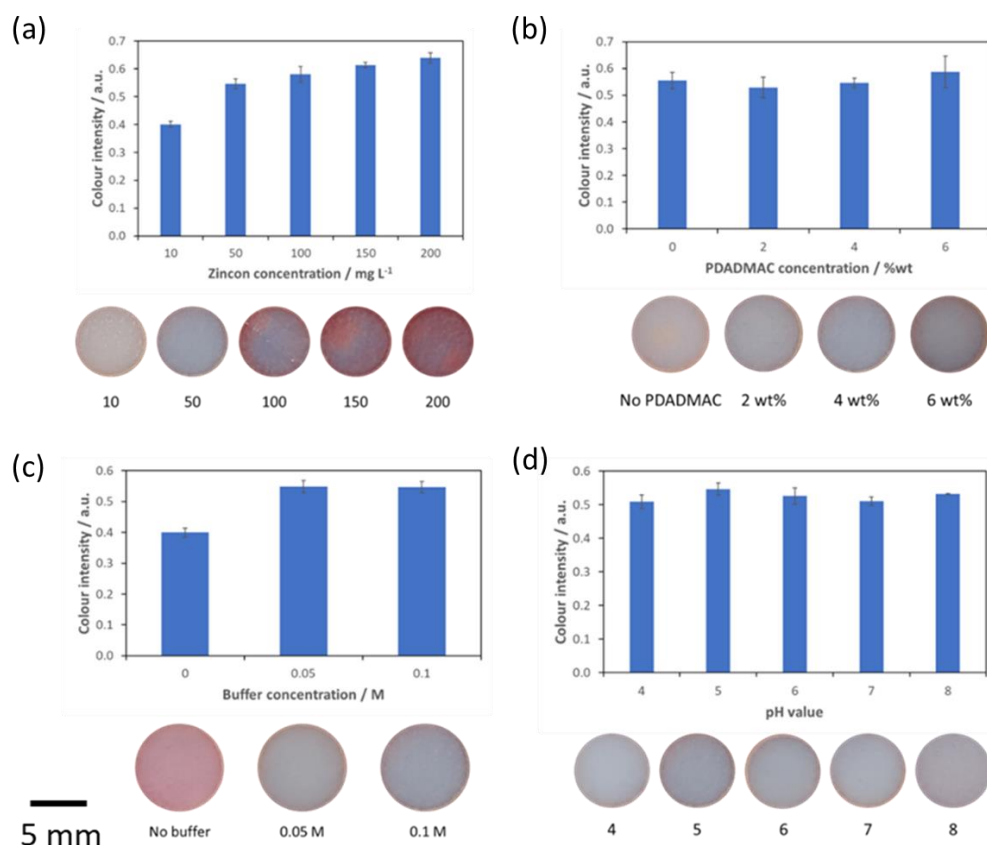
Further observation on Zincon monosodium salt μ PAD characteristics

Further, confirming the observations made through the Box-Behnken design of experiment, observations were also done in tested range of the concentrations. In Appendix-Figure 30a the concentration of Zincon was varied within 10-200 mg L⁻¹ concentration range. The increase of Zincon concentration at the same level of PDADMAC and buffer (4 wt% and 0.1 M, respectively) shows correlation with the increase of measured colour intensity on the μ PAD. However, through this observation, it was found that the difference between measured colour intensity at 100 mg L⁻¹ and 150 mg L⁻¹ Zincon concentration was not notable. Therefore, it is possible to adjust the concentration of Zincon from the suggested value based on the Box-Behnken optimisation process of 150 mg L⁻¹ to 100 mg L⁻¹. This would effectively reduce the amount of Zincon required in the fabrication of μ PAD, cutting down the cost of production in the long run.

Appendix-Figure 30b then showed the correlation between the increase in PDADMAC concentration to the measured colour intensity on the μ PAD containing 100 mg L⁻¹ Zincon and 0.1 M bicarbonate buffer, dipped into 10 mL 10 mg L⁻¹ Zn²⁺. The result of this experiment was also in agreement with the Box Behnken optimisation process, where the change in PDADMAC concentration did not have notable effect on the measured colour intensity on the μ PAD. However, the conclusion from the optimisation process suggested 6 wt% PDADMAC was to be used to achieve highest measured colour intensity. In previous experiments in this study, in the development of μ PADs for Ni²⁺ in water sample, it has been observed that the increase of PDADMAC concentration above 4 wt% would create a coffee-ring effect on the nioxime μ PAD,

as discussed in Chapter 3. This can also be seen in Appendix-Figure 30b, where darker vignette can be seen on the sample well containing 6 wt% PDADMAC. This effect created a darker shade of blue on the edges of the circle, where PDADMAC was deposited upon pipetting. Therefore, with the same reasoning as before, the PDADMAC concentration had to be adjusted to 4 wt%, which had been proven to be suitable for the design of μ PAD used in this study.

In Appendix-Figure 30c, the effect of buffer concentration was correlated to the measured colour intensity of the μ PAD. The buffer used in this study was bicarbonate buffer at pH 9, which allows the reaction to proceed at this alkaline environment. Conversely, the absence of buffer would create uncontrolled environment for the reaction, in terms of acidity. The increase of buffer concentration deposited on the sample well would allow more buffer to be deposited in the well. This would subsequently increase the buffering strength or capacity of the solution, creating pH 9 environment upon introduction of wider variety of acidity. As shown in the figure, however, addition of bicarbonate buffer, be it at 0.05 M or 0.1 M immediately aid in increasing the measured colour intensity. It was also observed that the colour change was more vivid in the presence of buffer at any concentration. This observation underlines further the importance of buffer in the reaction, which agrees with the observation made throughout the Box-Behnken optimisation process. To further investigate the importance of buffer addition to the μ PAD, it was then tested within sample pH range of 4-8. As shown in Appendix-Figure 30d, addition of buffer aided in producing relatively stable colour intensity across the different pH range. This illustrated the ability of the μ PAD to perform the Zn^{2+} detection through the variety of sample pH range, as would be found in environmental water sample.



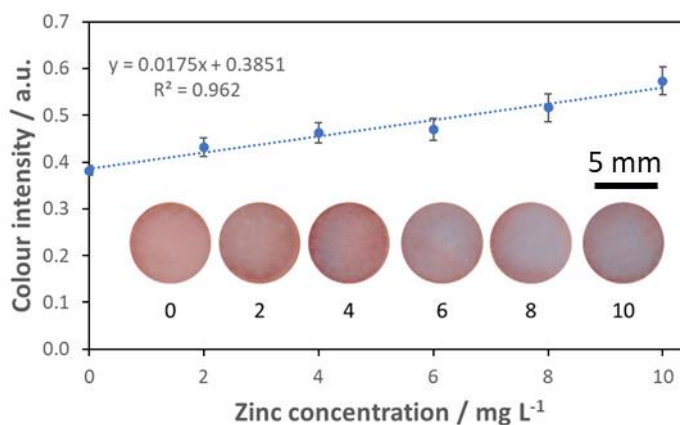
Appendix-Figure 30 The effect of (a) Zincon concentration, (b) PDADMAC concentration, (c) buffer concentration, and (d) sample pH value to the measured colour intensity on the Zincon μ PAD (n=3).

Linearity of Zincon monosodium salt μ PAD for Zn^{2+} detection between 0-10 mg L⁻¹

At this point, the Zincon μ PAD was a two-layered device. The first layer, which was placed closer to the sample entry point, was loaded with 10 μ L 4 wt% PDADMAC and 10 μ L 0.1 M bicarbonate buffer at pH 9. While the second layer was loaded with 10 μ L 100 mg L⁻¹ Zincon as colorimetric reagent. The next step of the process would be to test the performance of the device in a gradient of Zn^{2+} concentration. In this case, it was tested against 0-10 mg L⁻¹ Zn^{2+} concentration.

Appendix-Figure 31 shows the linear correlation between the Zn^{2+} concentration to the measured colour intensity on the Zincon μ PAD. For Zincon μ PAD, the colour intensity was measured in blue channel rather than green one as nioxime μ PAD, as discussed in Chapter 3. The main reason for this change was due to the difference in the colour at the endpoint of the reaction. As seen in the figure, the reaction would change colour from red to blue within the tested concentration range. Therefore, measurement of the inverted image in blue channel would allow for measurement of only blue spots created through the reaction. Through the linear correlation depicted in Appendix-Figure 31, the detection limit can be calculated for the

Zincon μ PAD. The limit of detection (LOD, $3\sigma/m$) was $2 \text{ mg L}^{-1} \text{ Zn}^{2+}$ concentration, while the limit of quantification was $6 \text{ mg L}^{-1} \text{ Zn}^{2+}$ concentration. These are 20 times higher than the US EPA National Recommendation Water Quality Criteria for Aquatic Life, which set the acute and chronic limit of Zn^{2+} at 0.1 mg L^{-1} [34]. This mimics the detection limit of nioxime μ PAD, where the workflow requires an integrated preconcentration workflow.



Appendix-Figure 31 Measured colour intensity on the sample wells of the device containing $10 \mu\text{L}$ Zincon monosodium salt as colorimetric reagent (100 mg L^{-1} zincin monosodium salt, 4 wt% PDADMAC, and 0.1 M bicarbonate buffer pH 9).

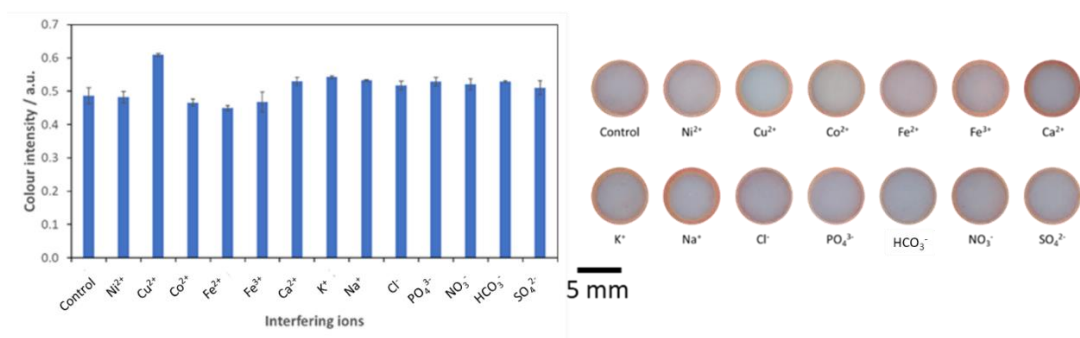
Performance of Zincon monosodium salt μ PAD in the presence of other ions

As per previous devices, the Zincon μ PAD performance was also tested in the presence of various ions commonly present in environmental water samples. Specifically, for Zincon, interference is expected from other metal ions such as Cu^{2+} or Fe^{2+} . However, the observation was still done to determine how many of the tested ions would significantly ($p < 0.05$) interfere with the Zincon- Zn^{2+} reaction. The Zincon μ PAD was tested by dipping into a 10 mL solution containing $10 \text{ mg L}^{-1} \text{ Zn}^{2+}$ and 10 mg L^{-1} of another ion. The tested ion species were: Ni^{2+} , Cu^{2+} , Co^{2+} , Fe^{2+} , Fe^{3+} , Ca^{2+} , K^+ , Na^+ , Cl^- , PO_4^{3-} , NO_3^- , HCO_3^- , and SO_4^{2-} .

Appendix-Figure 32 shows the result of the performance test of Zincon μ PAD in the presence of interfering ions. The control sample is a 10 mL $10 \text{ mg L}^{-1} \text{ Zn}^{2+}$ without addition of other ions. This was used as a basis of comparison to measure the effect of the presence of other ions to the measured colour intensity of the μ PAD. Throughout the tested ion range, Cu^{2+} showed most effect on the reaction, observable both through the colour intensity measurement and naked eyes observation. The presence of Cu^{2+} produced vivid blue colour on the sample well, increasing the measured colour intensity significantly ($p < 0.05$). Conversely, the presence of Co^{2+} , Fe^{2+} , and Fe^{3+} produced significantly lower colour intensity ($p < 0.05$). However, the decrease in the colour intensity might not be as vivid through naked eyes observation. These interferences were

expected, since all ions discussed so far were metals – which Zincon can detect, but has no specificity to. Masking these metals would require different masking reagents, usually through addition of metal complexing reagent that would produce colourless complex. Although masking reagents for metal can sometimes be non-specific, combination of different reagents with high affinity towards the target metals to be masked: Cu^{2+} , Co^{2+} , Fe^{2+} , and Fe^{3+} , can trap these metals before reaching the Zincon layer.

Further testing, however, showed notable difference in measured colour intensity was also observed with the presence of Ca^{2+} , K^+ , and Na^+ . Again, this difference was not visible through naked-eye observation. These cations are commonly found in water samples. Ca^{2+} and Na^{2+} , especially, may exist at higher concentration than tested (10 mg L^{-1}). Therefore, the fact that Zincon-based detection in the μPAD would be affected by the presence of these ions would require an extra-masking step. Due to the number of ions affecting the Zincon μPAD reaction for Zn^{2+} detection, and considering the amount of masking necessary to obtain direct result, the development of Zincon μPAD was paused at this point. This was done in favour of discovery of alternative colorimetric reagent with better specificity for μPAD -based Zn^{2+} detection.



Appendix-Figure 32 Measured colour intensity on the sample well of the Zincon μPAD after dipping into 10 mL solution containing $10 \text{ mg L}^{-1} \text{Zn}^{2+}$ and 10 mg L^{-1} of respective interfering ion ($n=3$).

μPAD for Zn^{2+} detection with 5-Br-PAPs as colorimetric reagent

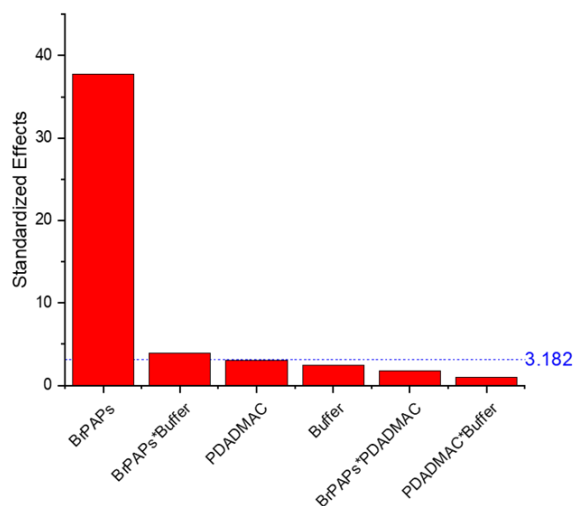
Optimisation of μPAD for Zn^{2+} detection using 5-Br-PAPs as colorimetric reagent

Optimisation of reagent concentrations using Box-Behnken design of experiment

Standardised effects

The standardised effect was plotted after optimisation following the Box-Behnken design of experiment. This again is presented as Pareto chart, showing the magnitude of the effects from each parameter and interaction between parameters as bar chart, while a blue dashed line shows the limit of significance. In Appendix-Figure 33, this blue dashed line is shown clearly. Therefore, the parameters with standardised effects magnitude lower than the line would be

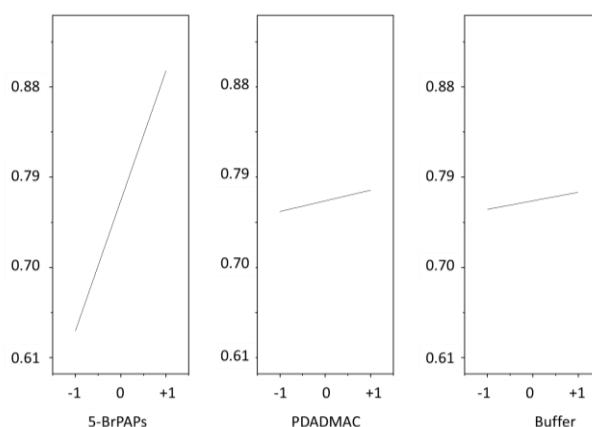
classified as non-significant ($p>0.05$) to the measured colour intensity on the μ PAD, as discussed in Chapter 3. The non-significant parameters for this μ PAD were buffer concentration, 5-Br-PAPs and PDADMAC interaction, and PDADMAC and buffer interaction. Whereas the significant parameters, in ascending order of effect magnitude were PDADMAC concentration, 5-Br-PAPs and buffer interaction, and 5-Br-PAPs concentration. However, the 5-Br-PAPs concentration showed comparatively biggest effect on the measured colour intensity on the μ PAD.



Appendix-Figure 33 Standardised effect Pareto chart showing the effect of various parameters and interaction between parameters to the measured colour intensity on the 5-Br-PAPs μ PAD after dipping into 10 mL 10 mg L⁻¹ Zn²⁺ sample solution, where blue dotted line indicate the “significance line”.

Main effects plot

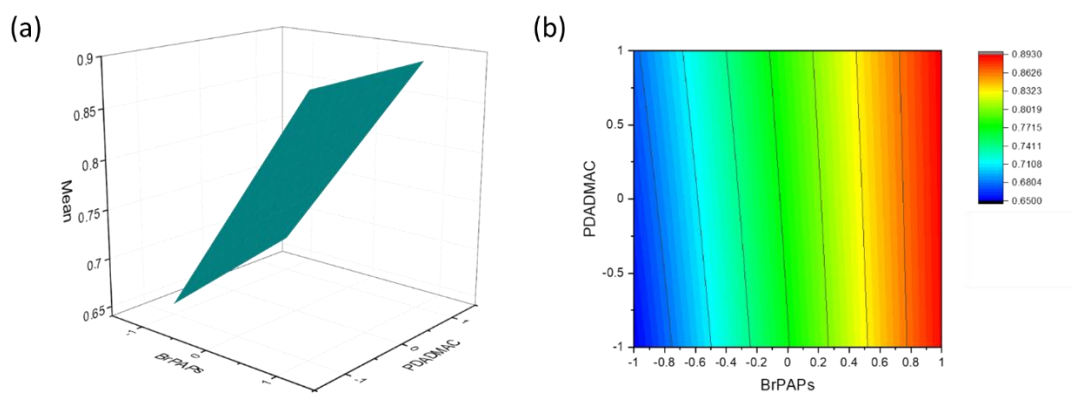
Similar to the previous studies in development of μ PAD, the main effects plot analysis was used to observe the direction of the effect, used in tandem with the standardised effects plot. Appendix-Figure 34 shows the direction of the effect upon variation in 5-Br-PAPs, PDADMAC, and PBS buffer concentration, separately. Evidently, the increase in 5-Br-PAPs concentration within the tested range can be correlated to the increase in measured colour intensity on the μ PAD. As shown in the figure, this linear increase in colour intensity was notably drastic; which agrees with the conclusion from the standardised effects plot. Whereas the increase in PDADMAC and PBS buffer concentrations, although can also be correlated to an increase in measured colour intensity, was not affecting the intensity as notably as 5-Br-PAPs.



Appendix-Figure 34 Main effect plots illustrating the magnitude and direction of the effect of the three main effects: 5-Br-PAPs, PDADMAC, and buffer concentrations.

3D surface and 2D contour plots

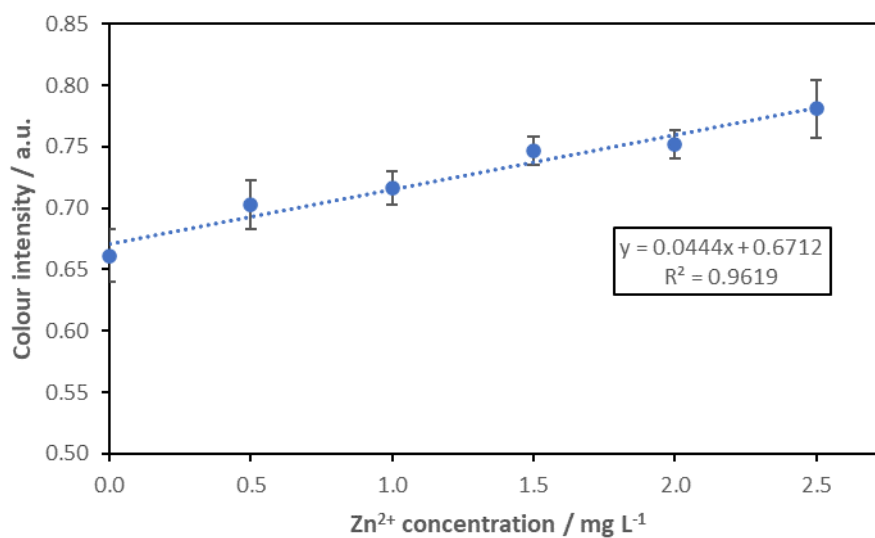
Lastly, a 3D response surface plot, as well as a 2D contour plot were constructed to be used as a point of reference for further optimisation process. Similar to previous optimisation process in Chapter 3, these plots were constructed at the held condition of maximum buffer concentration of 0.01 M PBS buffer. This was done to ensure that the buffer would be able to aid in the robustness of the developed μ PAD, upon introduction of environmental water sample, which would have a variety in pH value and acidity. Appendix-Figure 35a shows the 3D surface plot, which shows the correlation between the 5-Br-PAPs concentration and the PDADMAC concentration, to the modelled colour intensity based on the optimisation data. Through this plot, it is evident that the highest colour intensity can be achieved by loading the μ PAD with the highest concentration of 5-Br-PAPs, while the PDADMAC concentration may vary within the tested range. The same conclusion can be drawn from the 2D contour plot in Appendix-Figure 35b, where red area indicating the high colour intensity can be seen throughout the right-most side of the plot. This shows that at the highest tested concentration of PBS buffer, highest colour intensity can be measured at the highest 5-Br-PAPs concentration within the range of the PDADMAC concentration tested. Therefore, for 5-Br-PAPs μ PAD, the concentration of reagents used were 100 mg L^{-1} 5-Br-PAPs, 4 wt% PDADMAC, and 0.01 M PBS buffer. The decision on the PDADMAC concentration was based on previous observation in nioxime μ PAD development, as discussed in Chapter 3.



Appendix-Figure 35 Response surface plot showing the correlation between 5-Br-PAPs and PDADMAC concentration to the measured colour intensity on the developed device, at maximum concentration of buffer, after dipping into 10 mL 10 mg L⁻¹ Zn²⁺ solution. Correlations were presented as (a) 3D plot and (b) contour plot.

Appendix 4 User experience evaluation

Zn²⁺ calibration curve for μ PAD measurement



Appendix-Figure 36 Zn²⁺ calibration curve used for μ PAD-based measurements in volunteer activity.

Volunteer's technical specification

Appendix-Table 6 Smartphone camera specification of the participants of this study

Number	Width / px	Height / px	Resolution / dpi	F-stop	Exposure time/ 1/x s	ISO speed	Focal length/ mm	Flash	Brightness	White balance	Zoom
101	1557	1516	72	1/1.8	1/17	ISO-403	5	No	1.60	Auto	100.0
102	1988	1975	72	1/1.8	1/252	ISO-40	5	Yes	6.06	Auto	
103	1702	1634	72	1/1.7	1/17	ISO-6400	4	No	3.00	Auto	
104	811	743	72	1/1.9	1/100	ISO-103	5	Yes	3.18	Auto	
105	744	992	72	1/1.8	1/17	ISO-1250	5	No		Auto	1.0
106	2161	2372	72	1/1.8	1/11	ISO-3200	5	No	1.80	Auto	3.4
201	1993	2156	72	1/1.8	1/20	ISO-1250	5	Yes	1.20	Auto	3.4
202	516	590	96	1/1.7	1/189	ISO-55	4	Yes	5.01	Auto	0.0
203	763	686	72								
204	223	219	96								
205	747	800	72	1/2.2	1/492	ISO-100	3	Yes	0.01	Auto	
206	661	826	72								
301	884	700	72								
302	663	733	72	1/1.8	1/50	ISO-200	5	Yes	0.30	Auto	1.0
303	825	731	72								
304	709	733	72								
305	605	805	72								
306	581	556	72	1/2.0	1/429	ISO-107	3			Auto	1.0
401	726	758	72								
402	1377	1313	72	1/1.5	1/1290	ISO-50	4	Yes	7.59	Auto	
403	343	362	96	1/1.6	1/22	ISO-1000	5	Yes	6.39E-05	Auto	
404	801	664	72	1/1.7	1/10	ISO-800	4	No	0.01	Auto	
405	717	757	72								
406	647	875	72	1/1.5	1/4	ISO-1250	4	No	0.01	Auto	
501	2748	2748	72								
502	1548	1529	72								
503	696	741	72	1/1.5	1/10	ISO-1250	4	No		Auto	1.0
504	1144	1119	72	1/1.8	1/100	ISO-32	5	Yes	0.60	Auto	1.7
505	681	710	72								
506	1700	1771	72	1/1.8	1/17	ISO-1250	5	Yes	0.01	Auto	
601	766	730	72	1/0.5	1/3676	ISO-50	4	Yes	9.09	Auto	

Letter of ethics approval for the research



Mila Sari
Chemistry

Date: 01/03/2022

Our Ref: FEC_2022_38

Dear Mila

ETHICAL APPROVAL OF RESEARCH

Following consideration of an application submitted by you for:

FEC_2022_38 – Citizen science activity for testing heavy metal detection workflow

I am pleased to confirm that your ethics was approved by Chair's Action on behalf of the Faculty of Science and Engineering Ethics Committee.

This approval will be reported at the next Faculty Ethics Committee meeting.

This ethics approval is conditional on you ensuring that you are compliant with the University of Hull General Data Protection Regulations.

Yours sincerely

pp T. Turner

Dr Thomas Breithaupt
Co-Chair of the Faculty Ethics Committee
Faculty of Science and Engineering

Dr T Breithaupt
Co-Chair of Faculty Ethics Committee
Faculty of Science and Engineering
01482 465377

Appendix-Figure 37 Letter of ethics approval of research by University of Hull

Ethics application as submitted to the committee

RESEARCH ETHICS COMMITTEE
FORM A – New Application
(Involving human participants, subjects or material)

It is essential that you are familiar with the University Code of Good Research Practice, Research Ethics Policy and the Procedures for Granting Ethical Approval before you complete this form that can be found [here](#). Please confirm that you have read and understood these documents:

Yes

No

Please read each question carefully, taking note of instructions and completing all parts. If a question is not applicable please indicate so. Where a question asks for information which you have previously provided in answer to another question, please refer to your earlier answer rather than repeating information.

Ethics reference number (for office use):	FEC_2022_38
WorkTribe project URL	

PART A: SUMMARY

A.1 Title of the research	
Mapping heavy metal pollution in river water with paper-based devices through citizen science	
A.2 Principal investigator's contact details	
Name (<i>Title, first name, surname</i>)	Professor Mark Lorch
Position	Head of department, Professor in Science Communication
Faculty/School	Faculty of Science and Engineering Department of Chemistry and Biochemistry
Telephone number	
University of Hull email address	M.Lorch@hull.ac.uk
A.3 To be completed by students only	
Qualification working towards (e.g. Masters, PhD, ClinPsyD)	PhD
Student number	201940464
Supervisor's name (<i>Title, first name, surname</i>)	Mila Sari
Faculty/ School	Faculty of Science and Engineering Department of Chemistry and Biochemistry
Supervisor's telephone number	University of Hull
Supervisor's email address	m.sari-2019@hull.ac.uk

A.4 Other relevant members of the research team (e.g. co-investigators, co-supervisors)	
Name (Title, first name, surname)	Professor Nicole Pamme
Position	Visiting professor
Faculty/ School	Faculty of Science and Engineering Department of Chemistry and Biochemistry
Telephone number	
Institution	
Email address	nicole.pamme@mmk.su.se

Name (Title, first name, surname)	Dr Will Mayes
Position	Lecturer in Environmental Science
Faculty/ School	Faculty of Science and Engineering Department of Geography, Geology and Environment
Telephone number	
Email address	W.Mayes@hull.ac.uk

A.5 Select from the list below to describe your research: (Select all that apply)

- Research on or with human participants
- Research working with data of human participants
 - New data collected by qualitative methods
 - New data collected by quantitative methods
 - New data collected from observing individuals or populations
 - Routinely collected data or secondary data
 - Research working with aggregated or population data
 - Research using already published data or data in the public domain
 - Research taking direct measurements from individuals e.g. physiology
- Research working with human tissue samples
- Research involving any invasive techniques including administering substances, food (other than refreshments), vitamins or supplements.
- Research involving discussion of sensitive topics or topics that could be considered sensitive
- Research involving discussion of culturally sensitive issues
- Prolonged or frequent participant involvement
- Research involving members of the public in a research capacity (participant research)
- Research conducted outside the UK
- Research involving accessing social media sites
- Research involving accessing or encountering security sensitive material
- Research involving accessing websites or material associated with extreme or terrorist communities
- Research involving storing or transmitting any material that could be interpreted as sympathetic, endorsing or promoting terrorist acts

--

- Research involving financial inducements for participants (other than reasonable expenses and compensation for time)

PART B: THE RESEARCH

B.1 Give a short summary of the research (max 300 words)

*This section must be completed in **language comprehensible to the lay person**. Your answers should be easily understood by someone who is not experienced in the field you are researching, (eg a member of the public) - otherwise it may be returned to you. Where technical terms are used they should be explained. Any acronyms not generally known should be described in full. Do not simply reproduce or refer to the research method or protocol, although these can also be submitted to provide any technical information that you think the ethics committee may require. This section should cover the main parts of the proposal.*

In plain English provide a brief summary of the aims and objectives of the research.

- The summary should briefly describe the background to the research and why it is important,
- the questions it will answer and potential benefits,
- the study design and what is involved for participants.

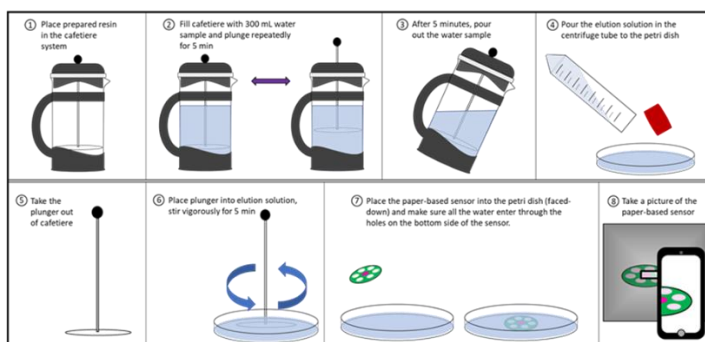
Monitoring of heavy metal level in the river water is an important step in managing potentially hazardous pollutants. With the currently available technology, this process can be costly and time-consuming, requiring experts to collect the data. In this research, we are developing a simple workflow involving paper-based sensor with preconcentration using a cafetiere. This developed workflow would allow involvement of citizen scientists in rapid, in-situ heavy metal detection in the environment in a safe manner.

In order to ensure that the developed workflow is suitable for the end-user and to obtain feedback on the usability of the developed device/workflow, we will work with small focus groups asking them to trial the prototype system that has been developed in the laboratory as part of the applicant's PhD research.

These focus groups will consist of University of Hull students from various faculties and level of study (further referred to as participants). Participants will be briefed on the workflow and safety procedures before the activity. **Participants will be asked to test the sample preconcentration method** involving repeated plunging in an adapted cafetiere filled with freshwater sample, followed by placing developed paper-based sensor into the preconcentrated sample. The freshwater sample will be provided by the researcher and/or obtainable for the participants from the University premises. **Participants will then be asked to take a picture of the device** with the developed picture-taking workflow (by placing the device in a black cardboard box with a slit on it, to act as light-controlling environment), as well as **completing an online anonymous questionnaire** (20 questions in total) to evaluate the usability of the developed workflow in general public's perspective. Throughout the activity, researchers will be present to supervise the participants and aid in case of spillage or exposure, however, researchers will not instruct or guide the procedure as it is part of evaluated aspect of the activity.

Experimental workflow that will be done by the volunteers (also available in Appendix):

HOW TO USE HEAVY METAL DETECTION KIT



The main aims of the activity are to gather end-user perspective on the developed workflow and to assess aspects of the workflow that will improve the robustness of the workflow (image quality using the developed workflow).

B.2 Proposed study dates and duration

Research start date (DD/MM/YY): Sep 2019 Research end date (DD/MM/YY): Sep 2022

Fieldwork start date (DD/MM/YY): _Mar 2022_____ Fieldwork end date (DD/MM/YY):
_Sep 2022_____

B.3 Where will the research be undertaken? (i.e. in the street, on University of Hull premises, in schools, on-line etc.)

University of Hull premises, within teaching laboratories or other University-owned premise (e.g. outside on campus water features, e.g. SuDS)

Do you have permission to conduct the research on the premises?

Yes No

If no, please describe how this will be addressed.

B.4 Does the research involve any risks to the researchers themselves, or people not directly involved in the research? E.g. lone working

Yes No

If yes, please describe and say how these will be addressed (include reference to relevant lone working policies):

Activity may include working with environmental samples of water containing dilute concentrations of metals (e.g. zinc and nickel) at environmentally relevant levels (300 mL). Appropriate COSHH form and risk assessment will be filled and signed off before any activity is undertaken (see attached). Safety precautions in working with possible environmental samples will be in place, where participants will be given personal protective equipment (e.g. gloves, glasses. Aside from water samples, all chemicals involved in the activity will be stored in small volumes under standard laboratory procedures.

If yes, please include a copy of **your complete risk assessment form with your application.**

NB: If you are unsure whether a risk assessment is required visit the Health and Safety SharePoint site. Risk assessments are required for all fieldwork taking place off campus.

B.5 What are the main ethical issues with the research and how will these be addressed?

Indicate any issues on which you would welcome advice from the ethics committee

Add some text here:

In recruitment process, participants will be required to send an email expressing interest in participating in the study to the researcher's University email address. Participants are also encouraged to use the official University of Hull email address for this purpose. Email address will be used to set up a meeting time for the study where participants are expected to attend

to test the workflow and fill in the questionnaires. Email addresses will not be recorded and will not be maintained after participant's attendance to the study.

Participants will complete a task in a focus group of 1-5 participants. This condition will be made clear in the registration process.

Participants will not be required to submit any personal information in the questionnaire, which will be handed separately from the registration form or consent form. The questionnaire will be anonymised without any identifying data of participants filling it. Consequently, participants cannot withdraw their participation after the submission of the questionnaire as at that point, there will be no identifier to withdraw a specific questionnaire from the data pool.

Participants will be asked to upload a picture taken from their smartphone devices into a Box folder through their university email address. This step is optional, as a smartphone will be provided for the participant in case they are not willing to use their own devices. This upload procedure will use the 'File Request Form' feature in Box, without requiring participants to log in to their Box folder. The upload link will be provided to the participants through email or questionnaire.

Collection of personal data: participants' email address might be required for communication purposes, such as: briefing and kit collection, sharing link of data (image) collection Box folder, and questionnaire dissemination. All email-correspondence and asked email address will be done through University email address/system and will be strictly related to the research project. Email correspondence will be done through university-approved digital platform and emails will only be retained until the end of volunteer-based activity (at the end of voluntary activity by participants, all email address of attendees of the day will be removed).

Participants also will be asked to fill in a physical consent form before testing activity. The collected consent form will be stored in the university premise and will be made accessible only to researchers involved in the study, if deemed necessary. Consent form will also be scanned for digital storage. Physical consent form will be shredded upon completion of volunteer-based activity.

B.6 Does the research involve an international collaborator or research conducted overseas:

Yes No

If yes, describe any ethical review procedures that you will need to comply with in that country:

Describe the measures you have taken to comply with these:

Include copies of any ethical approval letters/ certificates with your application.

PART C: HUMAN PARTICIPANTS AND SUBJECTS

C.1 Are the participants expected to be from any of the following groups? (Tick as appropriate)

- Children under 16 years old. *Specify age group:* _____
- Adults with learning disabilities
- Adults with other forms of mental incapacity or mental illness
- Adults in emergency situations
- Prisoners or young offenders
- Those who could be considered to have a particularly dependent relationship with the investigator, e.g. members of staff, students
- Other vulnerable groups
- No participants from any of the above groups

Include in Section D5 details of extra steps taken to assure their protection.

Does your research require you to have a DBS check Yes No

It is the researcher's responsibility to check whether a DBS check (or equivalent) is required and to obtain one if it is needed. See also <http://www.homeoffice.gov.uk/agencies-public-bodies/dbs>

C.2 What are the potential benefits and/ or risks for research participants in both the short and medium-term?

Risks may include health and safety, physical harm and emotional well-being

Participant will be asked to complete an experimental workflow involving environmental water sample which may contain low (<1 mg L⁻¹) level of heavy metals. **The health and safety risk are low.**

Upon mishandling and contact with the water sample, participant risks: itchiness on the skin or rashes. To prevent this, participant will be provided with nitrile gloves and will be advised about the potential risk of mishandling. Researcher will also supervise the process, equipped with first-aid kit. Other risks correlated to handling of solutions that is involved in this workflow is as presented in the Risk Assessment form (Appendix).

By participating in the research, participants will gain insight on research activity on campus and the research methods. This is a form of informal education that will benefit participants, especially those who are interested in research or in continuing their study. Participants will also be briefed on a currently developing technology for environmental monitoring and in doing so, gain awareness in current and emerging environmental problems.

Involvement in this research will not impact participants' academic assessments.

C.3 Is there a potential for criminal or other disclosures to the researcher requiring action to take place during the research? (e.g. during interviews/group discussions, or use of screen tests for drugs?)

Yes No

If yes, please describe and say how these will be addressed:

C.4 What will participants be asked to do in the study? (e.g. number of visits, time involved, travel required, interviews)

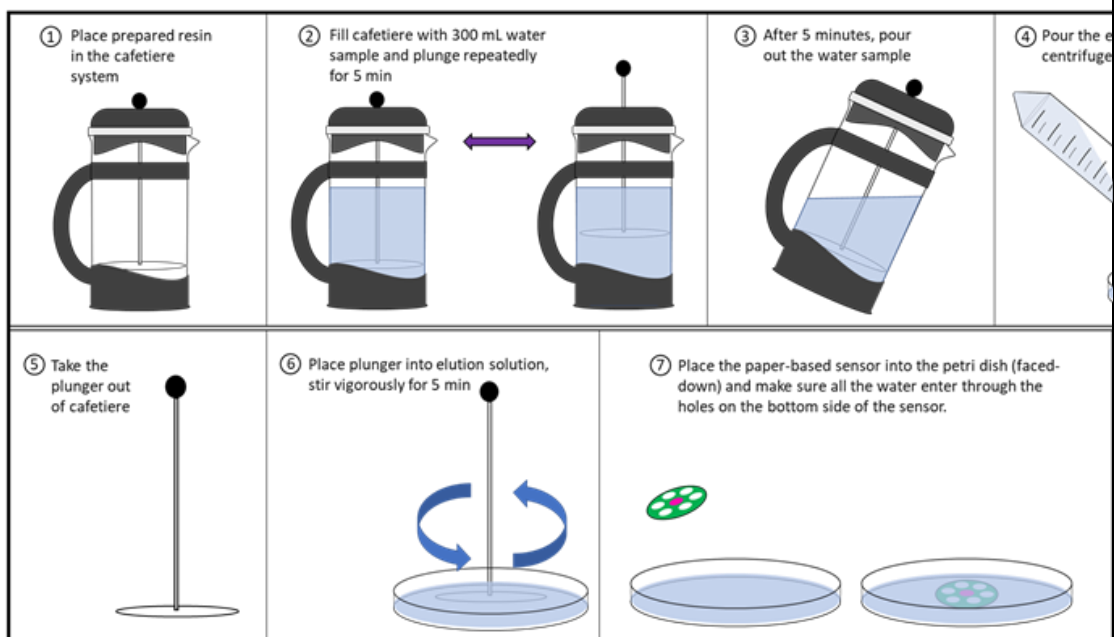
Participants will be asked to collect the heavy metal detection kit comprising of: a cafetiere loaded with ion exchange resin, paper-based sensor, and preconcentration reagent. Participants will then conduct the heavy metal detection in assigned the laboratory or assigned SuDSlab monitoring points. The heavy metal detection workflow is as follows:

1. 300 mL water sample is placed in the cafetiere
2. Resin is plunged in the water sample repeatedly for 5 minutes to extract metals for analysis
3. Resin is rinsed with preconcentration reagent
4. Paper-based sensor is placed in the preconcentrated sample
5. After 5 minutes, a picture of the sensor was taken and uploaded in a shared Box folder.

After the metal detection activity, **participants will be asked to complete an anonymous survey/questionnaire** to evaluate the developed workflow. The survey will mainly focus on the evaluation of the workflow they just tried, with around 20 questions, 15 consisting of rating a statement (agree-disagree) and 5 short answers. Participants will be asked to do this survey immediately after the activity, as they are returning the detection kit. The survey will be online and anonymous, not requiring any personal information.

Experimental workflow:

HOW TO USE HEAVY METAL DETECTION KIT



PART D: RECRUITMENT & CONSENT PROCESSES

How participants are recruited is important to ensure that they are not induced or coerced into participation. The way participants are identified may have a bearing on whether the results can be generalised. Explain each point and give details for subgroups separately if appropriate. Also say who will identify, approach and recruit participants. Remember to include all advertising material (posters, emails etc) as part of your application.

D.1 Describe how potential participants in the study be identified, approached and recruited and who will do this:

Recruitment will be done by sending out recruitment emails via the faculties/University email system (e.g. doctoral college/postgrad hub) with registration link in it, additional approach to encourage participation might be done through student societies (e.g. international student societies) or other communities. Recruitment will specify requirement for **participants with and without background in practical laboratory-works**, focusing on obtaining a pool of participants **with mixed level of laboratory experience** related to the device. **The recruitment will be open to all students at the University of Hull.**

D.2 Will you be excluding any groups of people, and if so what is the rationale for that?

Excluding certain groups of people, intentionally or unintentionally may be unethical in some circumstances. It may be wholly appropriate to exclude groups of people in other cases

No intentional exclusion or discrimination against particular groups of people will be done, however, due to the nature of the activity, which will require certain level of physical activity and perceptive capability (i.e. observing colour change on the device), certain disabilities (e.g. blindness) may exclude some participants. An overview of the tasks will be included in recruitment process, at which participant can decide to partake at their own risk or by notifying the researchers in advance.

Should participant need further advice or accommodation to participate in the research, they are encouraged to contact the researchers in advance.

D.3 How many participants will be recruited and how was the number decided upon?

It is important to ensure that enough participants are recruited to be able to answer the aims of the research. The number of participants should be sufficient to achieve worthwhile results but should not be so high as to involve unnecessary recruitment and burdens for participants. This is especially pertinent in research which involves an element of risk. Describe here how many participants will be recruited, and whether this will be enough to answer the research question.

30 participants will be separated into 5-people groups. At this step, the involvement of volunteers will be for preliminary research on the workflow feasibility and therefore this number of participants is regarded enough to fulfil the aim. The number of participants in a group (5-people) is limited to the number of kits (cafetiere) available and to ensure manageability. The groups will be based on participants' availability.

D.4 Will the research involve any element of deception?

Yes No

If yes, please describe why this is necessary and whether participants will be informed at the end of the study.

D.5 Will informed consent be obtained from the research participants?

Yes No

If yes, give details of how it will be done. Give details of any particular steps to provide information (in addition to a written information sheet) e.g. videos, interactive material. If you are not going to be obtaining informed consent you will need to justify this.

Yes, an informed consent form (*Appendix 2*) will be filled by means of physical/paper form. This will be given out along with all written information and other explanatory materials upon briefing. Any copy of the paper consent form will be stored in the University of Hull premise until the end of works involving volunteers.

Further, at the beginning of the questionnaire, another consent form will be provided (online), with 'click to proceed' system to maintain anonymity.

If participants are to be recruited from any of potentially vulnerable groups, give details of extra steps taken to assure their protection. Describe any arrangements to be made for obtaining consent from a legal representative.

Copies of any written consent form, written information and all other explanatory material should accompany this application.

D.6 Describe whether participants will be able to withdraw from the study, and up to what point (e.g. if data is to be anonymised). If withdrawal is not possible, explain why not.

Any limits to withdrawal, e.g. once the results have been written up or published, should be made clear to participants in advance, preferably by specifying a date after which withdrawal would not be possible. Make sure that the information provided to participants (e.g. information sheets, consent forms) is consistent with the answer to C12.

Participants are allowed to withdraw from the study at any point before anonymous questionnaire (Appendix 4) submission (end step of the activity), however they will be required to return the provided detection kit (cafetière, paper sensor, etc.; Appendix 1) to researchers before withdrawal. This information will be supplied in the information sheets and consent form.

D.7 How long will the participant have to decide whether to take part in the research?

It may be appropriate to recruit participants on the spot for low risk research; however consideration is usually necessary for riskier projects.

Participants will be recruited by dissemination of recruitment email. In the email, participant will be asked to email the researcher to show interest. Participant will be given up to 3 weeks to decide on their participation.

The recruitment email may be disseminated multiple times throughout the project period.

D.8 What arrangements have been made for participants who might have difficulties understanding verbal explanations or written information, or who have particular communication needs that should be taken into account to facilitate their involvement in the research? Different populations will have different information needs, different communication abilities and different levels of understanding of the research topic.

Reasonable efforts should be made to include potential participants who could otherwise be prevented from participating due to disabilities or language barriers.

Participants will be provided with instruction in written (*Appendix 3*) and video form in order to ensure accessibility. Participants can then access this instruction throughout their volunteering period as many times as necessary. Participants are also allowed to ask questions to the guiding researcher about the activity at any point during the briefing (before activity).

D.9 Will individual or group interviews/ questionnaires discuss any topics or issues that might be sensitive, embarrassing or upsetting, or is it possible that criminal or other disclosures requiring action could take place during the study (e.g. during interviews or group discussions)? *The information sheet should explain under what circumstances action may be taken.*

Yes No

If yes, give details of procedures in place to deal with these issues.

D.10 Will individual research participants receive any payments, fees, reimbursement of expenses or any other incentives or benefits for taking part in this research?

Yes No

If Yes, please describe the amount, number and size of incentives and on what basis this was decided.

PART E: RESEARCH INVOLVING HUMAN TISSUES OR MATERIAL

E.1 Will the research involve the use of any of the following? (Select as appropriate)

- Foetal material
- The recently deceased
- Cadavers
- Human bodily fluid
- Human tissue
- Human organs
- Human gametes

Go to Section F if the research does not involve any of the above material.

E.2 Will the material be accessed be collected as part of this study or 3rd party accessed (E.g. material collected as part of another study or purchased)?

If yes to 3rd party access, please provide details on appropriate consent for this use.

E.3 What type of tissue or material will be collected?
E.4 How will the tissue or material be collected and who will do this?
E.5 How many samples will be collected?
E.6 How long will samples be stored?
E.7 Do you require a regulatory licence to use or store this material? <input type="radio"/> Yes <input checked="" type="radio"/> No <i>All material is expected to be stored in line with the Human Tissue Authority storage expectations.</i>

E.8 Do you have the appropriate Health and Safety procedures in place for the researchers to handle the samples?

Yes No

PART F: RESEARCH DATA

F.1 Explain what measures will be put in place to protect personal data. E.g. anonymisation procedures and coding of data. Any potential for re-identification should be made clear to participants in advance.

Personal data required for the project will be:

- Email address. This will be made clear upon recruitment, volunteer registration, and briefing/kit collection. Email address will be used for communications on kit collection, briefing, and questionnaires dissemination. After the volunteer activity, this personal data will be deleted.

F2. What security measures are place to ensure secure storage of data at any stage of the research?

Provide details on where personal data will be stored, any of the following: (Select all that apply)

University approved cloud computing services

UOH Server, consent forms and any data on paper copies will be scanned for storage. Physical copy will be stored in the university premises.

- Other cloud computing services
- Manual files
- Private company computers
- Portable devices
- Home or other personal computers (not recommended; data should be stored on a University of Hull server such as your G,T, X or Z: drive where it is secure and backed up regularly)

Please attach the data management plan in the appendices; for further information visit <http://libguides.hull.ac.uk/researchdata>

F.3 Who will have access to participant's personal data during the study?

PhD student (Mila) will have access to participant's email address for communication purposes. However, this information will not be stored pass the volunteering activity.

F.4 Where will the data generated by the research be analysed and by whom?

The data generated by the research will be in the form of image (.jpg/.png file) of the paper-based sensor. This will be stored in a Box folder shared with PI and participating researchers in this project. The quality of collected images will be analysed by the PhD student (Mila) using image processing software.

The data generated from the distributed questionnaire will be in an online form (Microsoft Forms) that will be stored in the researchers' account with university email. The data from the form will be exported and stored in a shared Box folder along with other data related to the research. No personal information will be asked through this form, and therefore no personal information will be shared.

The consent form will be gathered in paper/physical form and scanned for storage in a separate Box folder. The physical form will be stored in the University premises (Ferens building) and shredded at the end of volunteering activity, after questionnaire submission.

F.5 Who will have access and act as long term custodian for the research data generated by the study?

The PI and project supervisors will have access to the research data generated by the study.

F.6 Have all researchers that have access to the personal data that will be collected as part of the research study, completed the University (or equivalent) data protection training?

Yes No

Yes, as part of the Modern Researcher training.

It is mandatory that all researchers accessing personal data have completed data protection training prior to commencing the research.

F.7 Will the research involve any of the following activities at any stage (including identification of potential research participants)? (Select all that apply)

Examination of personal records by those who would not normally have access

- Access to research data on individuals by people from outside the research team
- Electronic surveys, please specify survey tool: Microsoft Forms (included in the University ICT platforms)
- Other electronic transfer of data
- Use of personal addresses, postcodes, faxes, e-mails or telephone numbers
- Use of audio/ visual recording devices (NB this should usually be mentioned in the information for participants)
(1) Participants will be asked to take a picture of the device as part of the workflow. The use of personal device is optional

F.8 Are there any reasons to prevent or delay the publication of this research? E.g. Commercial embargoes, sensitive material.

Yes No

If yes, provide details:

F.9 If there are restrictions on where this research should be published or reported, where will the results of this study be disseminated? (Select all that apply)

- Conference presentation
- Peer reviewed journals
- Publication as an eThesis in the Institutional repository HYDRA

- Publication on website
- Other publication or report, please state: _____
- Submission to regulatory authorities
- Other, please state: _____.
- No plans to report or disseminate the results

F.10 How long will research data from the study be stored?

years

F.11 When will the personal data collected during the study be destroyed and how?

Participant's email address, collected upon registration, will be stored in an Excel form throughout the study and destroyed upon completion of volunteer activity.

Researchers must comply with the General Data Protection Regulations that are live from May 2018.

PART G: CONFLICTS OF INTEREST

G.1 Will any of the researchers or their institutions receive any other benefits or incentives for taking part in this research over and above normal salary or the costs of undertaking the research?

Yes No

If yes, indicate how much and on what basis this has been decided

G.2 Is there scope for any other conflict of interest? For example, could the research findings affect any ongoing relationship between any of the individuals or organisations involved and the researcher(s)? Will the research funder have control of publication of research findings?

Yes No

If so, please describe this potential conflict of interest, and outline what measures will be taken to address any ethical issues that might arise from the research.

G.3 Does the research involve external funding? (Tick as appropriate)

Yes No

If yes, what is the source of this funding? _____

PART H: TRAINING

PART I: DECLARATIONS

Declaration by Principal Investigator

1. The information in this form is accurate to the best of my knowledge and belief.
2. I take full responsibility for the information I have supplied in this document.
3. I undertake to abide by the University's ethical and health and safety guidelines, and the ethical principles underlying good practice guidelines appropriate to my discipline.
4. I will seek the relevant School Risk assessment/COSHH approval if required.
5. If the research is approved, I undertake to adhere to the project protocol, the terms of this application and any conditions set out by the Faculty Research Ethics Committee.
6. Before implementing substantial amendments to the protocol, I will submit an amendment request to the Faculty Research Ethics Committee seeking approval.
7. If requested, I will submit progress reports.
8. I am aware of my responsibility to be up to date and comply with the requirements of the law and relevant guidelines relating to security and confidentiality of participants or other personal data, including the need to register when necessary with the appropriate Data Protection Officer.
9. I understand that research records/data may be subject to inspection for audit purposes if required in future.
10. I take full responsibility for the actions of the research team and individuals supporting this study, thus all those involved will be given training relevant to their role in the study.
11. By signing the validation I agree that the Faculty Research Ethics Committee, on behalf of the University of Hull, will hold personal data in this application and this will be managed according to the principles established in the Data protection Act (1998).

Sharing information for training purposes: Optional – please tick as appropriate:

- I would be content for members of other Research Ethics Committees to have access to the information in the application in confidence for training purposes. All personal identifiers and references to researchers, funders and research units would be removed.


Principal Investigator

Signature of Principal Investigator: 

(This needs to be an actual signature rather than just typed. Electronic signatures are acceptable)

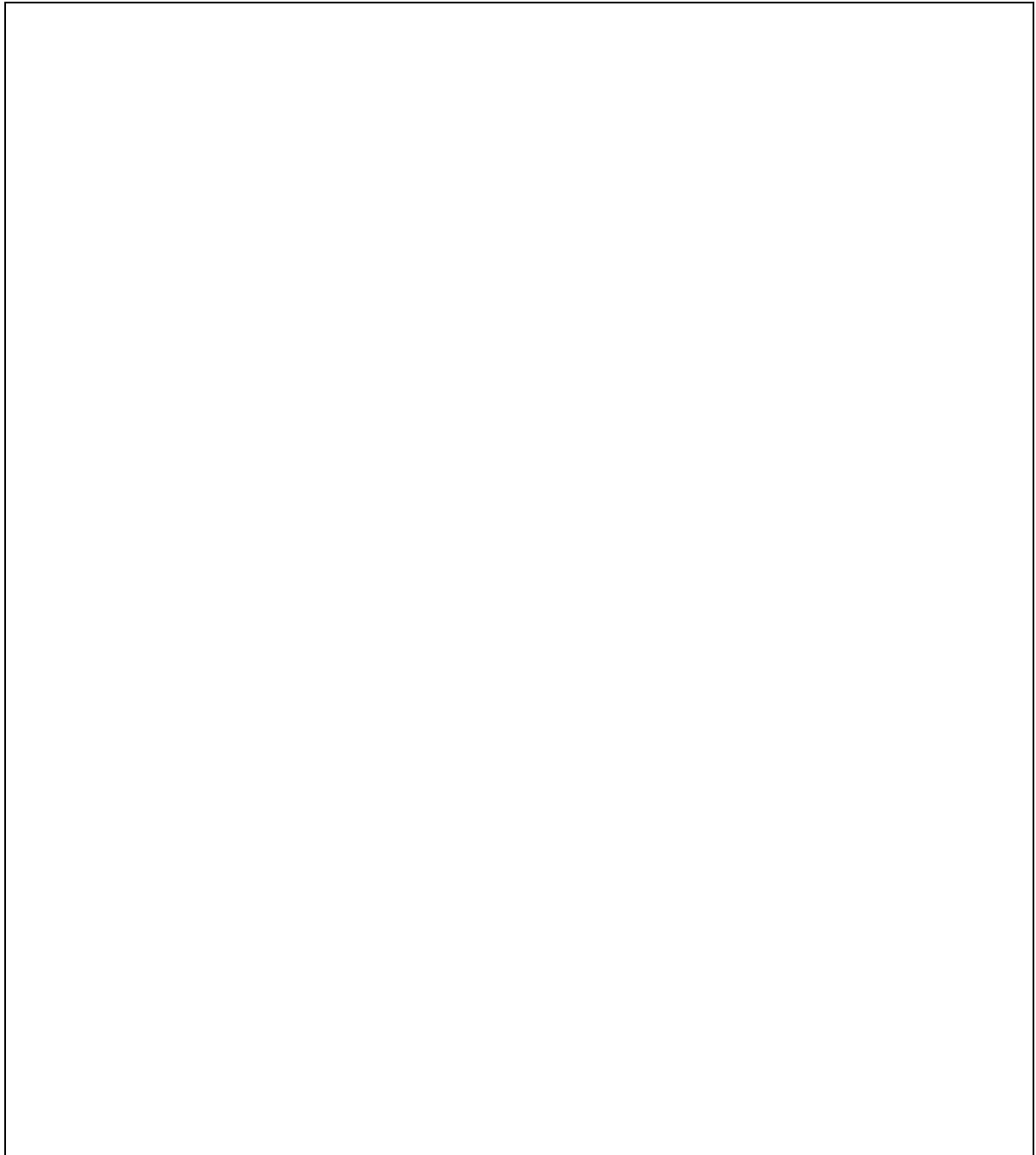
Print name:.....Mark Lorch..... Date: ..13/12/2021.....

Supervisor of student research: I have read, edited and agree with the form above.

Supervisor's signature:..... 

(This needs to be an actual signature rather than just typed. Electronic signatures are acceptable)

Print name:Mila Sari Date: (01/02/2022).....






Remember to include any supporting material such as your participant information sheet, consent form, interview questions and recruitment material with your application. Version control should be adopted to include the version number and date on relevant documents in the appendices.

These should be pasted as Appendices to this form.

Multiple documents will not be accepted.

Please submit your form **by email** to your Faculty Ethics Office

PROCEDURAL RISK ASSESSMENT AND COSHH FORM			Page 1
ref:	Date:	Group: Pamme research group	Overall Risk Level: LOW

PROCEDURE TITLE:	Heavy metal detection in freshwater environment with paper-based analytical device (PADs)		
Ethics Approval <input type="checkbox"/> YES <input type="checkbox"/> NO	Home Office Licence <input type="checkbox"/> YES <input type="checkbox"/> NO		
Reference No:	Home Office No:	Other:	
Further information must be provided in the appropriate section within the BioCOSH H part of this form.			
Name and status of assessor: Mila Sari / PhD student	I consider that all precautions listed are adequate and reduce risks to an acceptable level Date: 29/11/2021 Signature: 		
Head of Group (Authorisation): Mark Lorch	I am satisfied that the risk assessment completed is suitable and sufficient Review Date: 30/11/21 Signature: 		
<input checked="" type="checkbox"/> School/Departmental Safety Officer <input type="checkbox"/> University Biological Hazards Officer	I have reviewed this assessment DR ROB LEWIS Date: 06/12/2021 Countersignature: 		

Location(s): University of Hull premises (laboratory,...)

PROCEDURAL RISK ASSESSMENT AND COSHH FORM			Page 2
ref:	Date:	Group: Pamme research group	Overall Risk Level: LOW

Who might be affected:

Staff Undergraduate Students Postgraduate Students Cleaners Maintenance Contractors Visitors General Public

Young Persons (<18 yrs) Elderly New and expectant mothers Immune-compromised Persons

Other:

Risk to pregnancy: <input checked="" type="checkbox"/> Yes <input type="checkbox"/> No	Lone Working permitted: <input type="checkbox"/> Yes <input checked="" type="checkbox"/> No	Out of hours permitted: <input type="checkbox"/> Yes <input checked="" type="checkbox"/> No
---	--	--

PROCEDURE DESCRIPTION	
Technical Summary outlining the Procedure being followed	
Corresponding Detailed Protocol/SOP Reference No:	(Where currently not available must be provided within <u>3 months</u> of the approved date)
<p>Water sampling and heavy metal detection by volunteers.</p> <p>Volunteers will be asked to collect water sample (300 mL) from designated premise and place it into a container (an adapted cafetière) to be mixed with cation exchange resin for a short period of time (5 min). This mixing process will allow heavy metal content in the water sample to be adsorbed into the resin.</p> <p>After 5 min of mixing, water sample will be disposed of and resin will be rinsed with provided elution solution (<10 mL) for 1 min. The elution solution will then be placed into a small container and analysed using a paper analytical device. The device will be dipped into the elution solution. Chemical reaction will occur on the device within 5 min, yielding colour change proportional to the amount of analyte present in the sample. A picture of the device will be recorded using a smartphone camera.</p> <p>Device and cafetière will be returned back to the researchers for disposal and cleaning.</p>	

PROCEDURAL RISK ASSESSMENT AND COSHH FORM			Page 3
ref:	Date:	Group: Pamme research group	Overall Risk Level: LOW

RISK RATING					
L = Likelihood of event occurring	Rare = 1	Unlikely = 2	Possible = 3	Likely = 4	Almost certain = 5
C = Consequences of event occurring	Insignificant = 1	Minor = 2	Moderate = 3	Major = 4	Catastrophic = 5

EQUIPMENT				
Equipment used	How might someone be harmed?	RISK (L X C)	Control Measures	Residual RISK (L X C)
French press cafetière	<ul style="list-style-type: none"> • Cafetière glass may be cracked or leaking the sample solution contained • Cafetière body is made out of glass and might be mishandled and break 	1*4 = 4	<ul style="list-style-type: none"> • Cafetiere will be inspected prior to use by volunteers. • In cases where leaks is suspected or cafetière glass is broken, do not use cafetière 	1*1 = 1
Working in laboratory	<ul style="list-style-type: none"> • Chemical spillage • Unintended exposure to the chemicals involved in the activity 	2*4 = 8	<ul style="list-style-type: none"> • Volunteer activity in the laboratory will be supervised by researchers • Spill kit is readily available • All personnel involved will be equipped with adequate personal protective equipment • Work in the laboratory will be contained to the fume hood area 	1*1 = 1

PROCEDURAL RISK ASSESSMENT AND COSHH FORM

ref:

Date:

Group: Pamme research group

**Overall Risk Level:
LOW**

CHEMICAL SUBSTANCES

Take note of Concentration and Volumes of Chemicals Used e.g. stock versus working diluted concentrations

Substance Name	Quantity Used	WEL Value	Hazardous Properties (Incl. form/route of entry)	Risk (L x C)	Control Measures	Residual Risk (L x C)	Waste Disposal	Emergency Action in the Event of Spillage/Exposure
Nickel (II) sulfate hexahydrate Ni detection	Spiked sample solution, < 1 mg L ⁻¹ , 300 mL		H302 + H332: Harmful if swallowed or inhaled H315: Causes skin irritation H317 : May cause an allergic skin reaction H334: May cause allergy or asthma symptoms or breathing difficulties if inhaled H341: Suspected of causing genetic defects H350: May cause cancer H360D: May damage the unborn child	2*4 = 8	<ul style="list-style-type: none"> In the event of known/suspected high concentration (>0.03 mg L⁻¹) of nickel in the water sample, volunteers will be asked to work in a fume hood in the laboratory. Researcher will be present to guide and supervise. Use of proper personal protective equipment throughout activity. Volunteers will be informed on the risks of exposure. Voluntary activity will be a one-time event (eliminating repeated exposure), and work involving sample concluded within 20 minutes (eliminating prolonged exposure). 	1*4 = 4	Water sample containing high concentration of nickel (>0.03 mg L ⁻¹) will be handled by the researcher and disposed safely through toxic waste disposal procedure.	<ul style="list-style-type: none"> Spill kit is available in the premise In the event of spillage, volunteers will be evacuated out of the premise (fume hood/laboratory) and asked to report any contact with spillage If inhaled: fresh air. Contact physician Skin contact: take off

PROCEDURAL RISK ASSESSMENT AND COSHH FORM

ref:

Date:

Group: Pamme research group

**Overall Risk Level:
LOW**

			<p>H372: Causes damage to organs (respiratory tract) through prolonged or repeated exposure if inhaled</p> <p>H410: Very toxic to aquatic life with long lasting effects</p>					<p>contaminated clothing, rinse skin thoroughly with running water, contact physician.</p> <ul style="list-style-type: none"> • Eye contact: rinse with running water, call ophthalmologist, remove contact lenses • Swallowed: drink 2 glasses of water, consult physician
--	--	--	--	--	--	--	--	---

PROCEDURAL RISK ASSESSMENT AND COSHH FORM

ref:

Date:

Group: Pamme research group

**Overall Risk Level:
LOW**

Zinc (II) sulfate heptahydrate	Spiked sample solution, <math><1 \text{ mg L}^{-1}</math>, 300 mL	H302: Harmful if swallowed H318: Causes serious eye damage H410: Very toxic to aquatic	2*2 = 4	<ul style="list-style-type: none"> In the event of known/suspected high concentration (>5 mg L⁻¹) of zinc in the water sample, volunteers will be asked to work in a fume hood in the laboratory. 	1*2 = 2	Water sample containing high concentration of zinc (>5 mg L ⁻¹) will be handled by the researcher and disposed safely	<ul style="list-style-type: none"> Spill kit is available in the premise In the event of spillage,
Zn detection							

PROCEDURAL RISK ASSESSMENT AND COSHH FORM

ref:

Date:

Group: Pamme research group

**Overall Risk Level:
LOW**

			life with long lasting effects		<p>Researcher will be present to guide and supervise.</p> <ul style="list-style-type: none"> • Use of proper personal protective equipment throughout activity. • Volunteers will be informed on the risks of exposure. • Voluntary activity will be a one-time event (eliminating repeated exposure), and work involving sample concluded within 20 minutes (eliminating prolonged exposure). 		through toxic waste disposal procedure.	<p>volunteers will be evacuated out of the premise (fume hood/labo ratory) and asked to report any contact with spillage</p> <ul style="list-style-type: none"> • If inhaled: fresh air • Skin contact: take off contaminated clothing, rinse skin thoroughly with running water • Eye contact: rinse with running water, call ophtalmol ogist,
--	--	--	--------------------------------	--	---	--	---	--

PROCEDURAL RISK ASSESSMENT AND COSHH FORM

ref:

Date:

Group: Pamme research group

**Overall Risk Level:
LOW**

								remove contact lenses • Swallowed: drink 2 glasses of water, consult physician
1,2-Cyclohexanedione dioxime Ni detection	Colourimetric detection of Ni, 1400 mg L ⁻¹ 10 µL * 5 zones = 50 µL	N/A	Non hazardous	1*1	Devices are laminated after production so that the reagents are stored within the device.	1*1	Devices will be returned to the researchers after use for disposal.	N/A
2-(5-Bromo-2-pyridylazo)-5-[N-propyl-N-(3-sulfopropyl)amino]phenol disodium salt dihydrate Zn detection	Colourimetric detection of Zn, 100 mg L ⁻¹ 10 µL * 5 zones = 50 µL	N/A	Non hazardous	1*1	Devices are laminated after production so that the reagents are stored within the device.	1*1	Devices will be returned to the researchers after use for disposal.	N/A
Phosphate buffered saline Ni and Zn detection	Colourimetric detection of Ni and Zn, 10 mM 10 µL	N/A	Non hazardous	1*1	Devices are laminated after production so that the reagents are stored within the device.	1*1	Devices will be returned to the researchers after use for disposal.	N/A

PROCEDURAL RISK ASSESSMENT AND COSHH FORM

ref:

Date:

Group: Pamme research group

**Overall Risk Level:
LOW**

	* 5 zones = 50 µL							
Polydiallyldimethylammonium chloride (polymer) Ni and Zn detection	Colourimetric detection of Ni and Zn, 4 % wt. 10 µL * 5 zones = 50 µL	N/A	Non hazardous	1*1	Devices are laminated after production so that the reagents are stored within the device.	1*1	Devices will be returned to the researchers after use for disposal.	N/A
Sodium thiosulfate Ni and Zn detection	Colourimetric detection of Ni and Zn, 0.1 M 10 µL * 5 zones = 50 µL	N/A	Non hazardous	1*1	Devices are laminated after production so that the reagents are stored within the device.	1*1	Devices will be returned to the researchers after use for disposal.	N/A
Sodium fluoride Ni detection	Colourimetric detection of Ni, 0.1 M 10 µL * 5 zones = 50 µL	TWA: 2.5 mg m ⁻³	H301: Toxic if swallowed	1*4	<ul style="list-style-type: none"> • Low volume of chemicals will be used in the device. • Devices are laminated after production so that the reagents are stored within the device. 	1*1	Devices will be returned to the researchers after use for disposal.	N/A
Meso-2,3-Dimercaptosuccinic acid Zn detection	Colourimetric detection of Zn, 300 mg L ⁻¹ 10 µL * 5	N/A	Non hazardous	1*1	Devices are laminated after production so that the reagents are stored within the device.	1*1	Devices will be returned to the researchers after use for disposal.	N/A

PROCEDURAL RISK ASSESSMENT AND COSHH FORM

ref:

Date:

Group: Pamme research group

**Overall Risk Level:
LOW**

	zones = 50 µL							
Lewatit MonoPlus SP 112 Na ⁺ form Ni and Zn detection	Preconcentration of Ni and Zn, 2.6 g	N/A	Non hazardous	1*1	Resin will be placed in a cartridge. Volunteers will be briefed on the procedure as to not mishandle the resin.	1*1	Returned to the researchers along with devices.	N/A
Sodium bicarbonate Ni and Zn detection	Preconcentration of Ni and Zn, elution solution, 1 M 5 mL	N/A	Non hazardous	1*1	Volunteers will be briefed on the procedure as to not mishandle the chemicals.	1*1	Returned to the researchers along with devices.	N/A
Sodium chloride Ni and Zn detection	Preconcentration of Ni and Zn, elution solution, 5 M 5 mL	N/A	Non hazardous	1*1	Volunteers will be briefed on the procedure as to not mishandle the chemicals.	1*1	Returned to the researchers along with devices.	N/A

Add more lines if required

PROCEDURAL RISK ASSESSMENT AND COSHH FORM

ref:

Date:

Group: Pamme research group

**Overall Risk Level:
LOW**

BIOLOGICAL SUBSTANCES

NO Biological Substances Used

Biological Agents or Hazards	Human	Animal	Microorganism	Other
	<input type="checkbox"/> Cells <input type="checkbox"/> Tissue/body parts <input type="checkbox"/> Primary cell culture <input type="checkbox"/> Continuous cell culture <input type="checkbox"/> Blood <input type="checkbox"/> Human excretions/fluids <input type="checkbox"/> Patient contact	<input type="checkbox"/> Cells <input type="checkbox"/> Tissue/body parts <input type="checkbox"/> Primary cell culture <input type="checkbox"/> Continuous cell culture <input type="checkbox"/> Blood <input type="checkbox"/> Animal excretions/fluids <input type="checkbox"/> Animal contact	Pathogens listed by ACDP/DEFRA as <input type="checkbox"/> Hazard Group 1 <input type="checkbox"/> Hazard Group 2 <input type="checkbox"/> Hazard Group 3 <input type="checkbox"/> Not Listed by ACDP/DEFRA <input type="checkbox"/> Unknown	<input type="checkbox"/> Plants <input type="checkbox"/> Soil <input type="checkbox"/> Toxins <input type="checkbox"/> Carcinogens <input type="checkbox"/> Allergen <input type="checkbox"/> DNA <input type="checkbox"/> Other:
	<input type="checkbox"/> Genetic Modified Organism <input type="checkbox"/> Lentiviral Transfection		<input type="checkbox"/> Genetic Modified Microorganism	<input type="checkbox"/> Unknown Biological Hazards <input checked="" type="checkbox"/> No known Biological Hazards
Description, include species, cell line or technical name	Aquatic microorganisms			
Source	<input type="checkbox"/> Unknown <input type="checkbox"/> Isolated in own Laboratory <input type="checkbox"/> Provided by: <input type="checkbox"/> Purchased from: <input type="checkbox"/> Collection Site:			
Quantity/Scale	<input type="checkbox"/> Small <input type="checkbox"/> Medium <input type="checkbox"/> Large	Risk if maximum quantity used	<input type="checkbox"/> Negligible <input type="checkbox"/> Low <input type="checkbox"/> Medium <input type="checkbox"/> High	
Exposure Route	<input type="checkbox"/> Inhalation (Airborn) <input type="checkbox"/> Ingestion <input type="checkbox"/> Splash in eyes or mouth <input type="checkbox"/> Percutaneous (Skin) <input type="checkbox"/> Animal bite or scratch <input type="checkbox"/> Other:			
Exposure frequency	<input type="checkbox"/> Daily <input type="checkbox"/> Weekly <input type="checkbox"/> Monthly <input type="checkbox"/> Other:	Potential of exposure	<input type="checkbox"/> Negligible <input type="checkbox"/> Low <input type="checkbox"/> Medium <input type="checkbox"/> High	

PROCEDURAL RISK ASSESSMENT AND COSHH FORM			Page 11
ref:	Date:	Group: Pamme research group	Overall Risk Level: LOW

Risk of Aerosol or Airborne Particle formation	<input type="checkbox"/> Negligible <input type="checkbox"/> Low <input type="checkbox"/> Medium <input type="checkbox"/> High
---	--

PROCEDURAL RISK ASSESSMENT AND COSHH FORM			Page 12
ref:	Date:	Group: Pamme research group	Overall Risk Level: LOW

Risk to Human Health	<input type="checkbox"/> Effectively Zero <input type="checkbox"/> Low <input type="checkbox"/> Medium <input type="checkbox"/> High Disease or Condition that might be caused upon exposure (specify):
Health Surveillance	<input type="checkbox"/> Not required <input type="checkbox"/> Only required upon exposure to risk (incident/accident) <input type="checkbox"/> Required
Effective Treatment	<input type="checkbox"/> Do not know if available <input type="checkbox"/> Not available <input type="checkbox"/> Available (specify):
Immunisation and Prophylaxis	<input type="checkbox"/> Not available <input type="checkbox"/> Not required <input type="checkbox"/> Optional <input type="checkbox"/> Essential <input type="checkbox"/> Other:
Risk to Animal Health	<input type="checkbox"/> Effectively Zero <input type="checkbox"/> Low <input type="checkbox"/> Medium <input type="checkbox"/> High Disease or Condition that might be caused upon exposure (describe if applicable): Effective treatment available: <input type="checkbox"/> No <input type="checkbox"/> Yes (specify):
Risk to the Environment	<input type="checkbox"/> Effectively Zero <input type="checkbox"/> Low <input type="checkbox"/> Medium/Low <input type="checkbox"/> Medium <input type="checkbox"/> High Possible hazards/risks/damage to the Environment (describe if applicable): Effective remediation available? <input type="checkbox"/> No <input type="checkbox"/> Yes (specify): Not applicable
Facility	<input type="checkbox"/> Laboratory <input type="checkbox"/> Animal Facility <input type="checkbox"/> Plant Facility <input type="checkbox"/> Microbiological Containment Facility <input type="checkbox"/> Other:
Containment Level	<input type="checkbox"/> No containment required <input type="checkbox"/> Containment Level 1 (CL1) <input type="checkbox"/> Containment Level 2 (CL2) <input type="checkbox"/> Containment Level 3 (CL3)
Biosafety Cabinet	<input type="checkbox"/> No biosafety cabinet required <input type="checkbox"/> Class 1 <input type="checkbox"/> Class 2 <input type="checkbox"/> Class 3

PROCEDURAL RISK ASSESSMENT AND COSHH FORM

ref:

Date:

Group: Pamme research group

**Overall Risk Level:
LOW**

Other Controls	<input type="checkbox"/> Spill tray <input type="checkbox"/> Physical barrier to contain splashing <input type="checkbox"/> Tubes secured with cap to contain aerosols <input type="checkbox"/> Secondary containment <input type="checkbox"/> Sharps not permitted <input type="checkbox"/> Other (specify): non required	
Long-Term Storage (>24 hours)	<input type="checkbox"/> No storage required <input type="checkbox"/> Locked Storage <input type="checkbox"/> Cupboard <input type="checkbox"/> Refrigerator <input type="checkbox"/> -20°C Freezer <input type="checkbox"/> -80°C Freezer <input type="checkbox"/> Liquid Nitrogen <input type="checkbox"/> Incubator <input type="checkbox"/> Other:	
Transport	<input type="checkbox"/> Allowed, if <u>appropriate containment</u> is used to avoid accidental release during transport Specify containment: Sealed plastic sleeves/ containers to return used devices in. <input type="checkbox"/> Transport according to Dangerous Goods Classification: <input type="checkbox"/> Transport only allowed with HSE consent/Environmental Agency/DEFRA license License Number or Consent Letter (specify): <input type="checkbox"/> Other:	
Inactivation	<input type="checkbox"/> Chemical inactivation <input type="checkbox"/> Autoclaving (heat inactivation) <input type="checkbox"/> Incineration (heat inactivation) <input type="checkbox"/> Fumigation	
Disinfection	Surfaces	<input type="checkbox"/> 70% Ethanol <input type="checkbox"/> 1% (w/v) Virkon solution <input type="checkbox"/> 10% (v/v) Trigene/Distel solution <input type="checkbox"/> Clinell sanitising wipes <input type="checkbox"/> Other: Not applicable
	Hand wash	<input type="checkbox"/> Lab Guard microbial soap <input type="checkbox"/> Other: Soap and water
	Spills	<input type="checkbox"/> Virkon powder <input type="checkbox"/> Other: Not applicable
	Water bath	<input type="checkbox"/> Aquarest <input type="checkbox"/> Other: Not applicable
Waste Disposal	<input type="checkbox"/> Clinical waste <input type="checkbox"/> Autoclaved waste <input type="checkbox"/> Landfill waste <input type="checkbox"/> Sink Disposal <u>after</u> effective inactivation <input type="checkbox"/> Other:	
Instruction, Training and Supervision	<input type="checkbox"/> Appropriate Instruction required regarding Biological Safety, including appropriate Standard Operating Procedures (SOP) <input type="checkbox"/> Basic training required <input type="checkbox"/> Specialist training required <input type="checkbox"/> Constant supervision required	

PROCEDURAL RISK ASSESSMENT AND COSHH FORM			Page 14
ref:	Date:	Group: Pamme research group	Overall Risk Level: LOW

	Add details: Volunteers will attend briefing before sampling activity
--	---

PROCEDURAL RISK ASSESSMENT AND COSHH FORM			Page 15
ref:	Date:	Group: Pamme research group	Overall Risk Level: LOW

Consent or License from DEFRA, EA, DEFRA, HSE or Home Office	<input type="checkbox"/> Not required <input type="checkbox"/> Required/obligatory, provide HSE consent/DEFRA license number and details:
Emergency Procedure(s)	<input type="checkbox"/> No special requirements for the used biological substances <input type="checkbox"/> Required (describe):

	PROCEDURAL RISK ASSESSMENT AND COSHH FORM			Page 16
	ref:	Date:	Group: Pamme research group	Overall Risk Level: LOW

SAFE WORKING PROCEDURE
<ul style="list-style-type: none">• Wear suitable protective clothing, laboratory coat, gloves and eye protection where required• Strictly follow procedure protocol

PROCEDURAL RISK ASSESSMENT AND COSHH FORM			Page 17
ref:	Date:	Group: Pamme research group	Overall Risk Level: LOW

FIRST AID
Basic First Aid
<p>In case of inhalation, seek for fresh air If skin contact occurs, wash off in running cold water for 10 minutes If chemical ingested, rinse out mouth with cold water and spit out If eye contact occurs, irrigate with cold water for 10 minutes In case of continued symptoms, contact a University first aider</p>
Specific First Aid (if different from above as a result of the risk assessment & COSHH requirements)

PROCEDURAL RISK ASSESSMENT AND COSHH FORM			Page 18
ref:	Date:	Group: Pamme research group	Overall Risk Level: LOW

EMERGENCY CONTACTS			
Please use emergency contacts in the order shown below. If you are unable to reach the first person on the list, contact the next person, etcetera.			
Role	Name	Telephone Numbers	
Supervisor			
Departmental/School Safety Officer	Jennie Brigham (SBBES)	5519	
	Sian Leech (HYMS)	6761	
	Laura Sadofsky (Daisy)	(9) 461876	
	Steve Archibald (PET)	5488	
	Barry Penrose (BMS)	3217	
University Chemical Hazards Officer	Rob McDonald	6407	
University Biological Hazards Officer	Frank Voncken	5280	
University Laser Hazards Officer	Howard Snelling	5690	
University Radiation Hazards Officer	Tim Coldwell	6992	
Health and Safety Service	Secretary	5165	
	Alan Hewett	6571	
	Tim Coldwell	6992	
	Jonathan Grainger	5785	
University Hull Campus	Emergency Call Centre	5555	Castle Hill/Daisy Emergency Call Centre is 4444

University of Hull

Data Management Plan

(NB: This form should be completed at the start of all projects where data management is not dealt with otherwise). Shaded areas are considered essential, particularly when a data management plan is required for a grant application.

Date	<u>21/01/2022</u>
Researcher(s)	<u>Prof. Mark Lorch</u> <u>Prof. Nicole Pamme</u> <u>Dr Will Mayes</u> <u>Mila Sari (PhD student)</u>
Project title	<u>Mapping heavy metal pollution in river water with paper-based devices through citizen science.</u>
Brief description	

	A part of Sensing and Safeguarding Water Environment PhD project cluster, this project will focus on developing paper-microfluidics device with preconcentration workflow to be utilised in a citizen science activity
--	--

For detailed, updated explanations of the various parts of the document that require completion, please refer to the accompanying Appendices.

This University of Hull History Data Management Plan (HDMP) applies the DCC Checklist for Data Management (v3.0 17 March 2011).

Contents

Section 1: Project Information	3
Section 2: Data, Materials, Resource Collection Information	4
Section 3: Ethics, Intellectual Property, Citation	5
Section 4: Access and Use of Information	6
Section 5: Storage and Backup of Data	7
Section 6: Archiving and Future Proofing of Information.....	8
Section 7: Resourcing of Data Management	9
Section 8: Review of Data Management process	10
Section 9: Statements and Personnel Details	11
9.1 Statement of Agreement	11
9.2 Expertise of Researchers	13
Section 10: Appendices.....	15
10.1 Specific Help with completing the Plan	15
10.2 Notes.....	16
10.3 Relevant Contacts	22

Section 1: Project Information

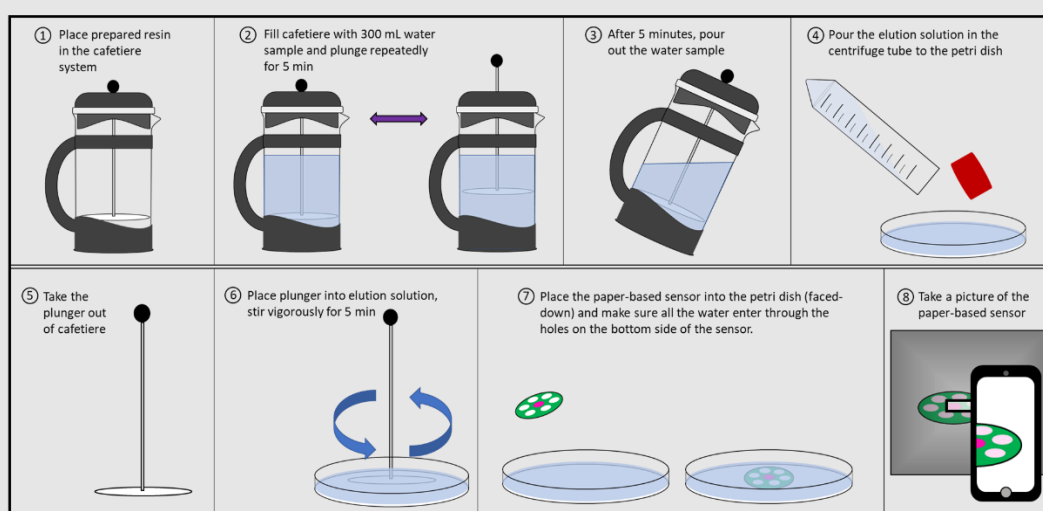
A summary of the project details and associated data management requirements

1.1 Project title: Mapping heavy metal pollution in river water with paper-based devices through citizen science
1.2 Project duration (aa/bb/cc-xx/yy/zz) November 2019-September 2022
1.3 Partners (if applicable) Sensing and Safeguarding the Water Environment, PhD cluster (2019 – 2022)
1.4 Brief description <p>Monitoring of heavy metal level in the river water is an important step in managing potentially hazardous pollutants. With the currently available technology, this process can be costly and time-consuming, requiring experts to collect the data. In this research, we are developing a simple workflow involving paper-based sensor with preconcentration using a cafetiere. This developed workflow would allow involvement of citizen scientists in rapid, in-situ heavy metal detection in the environment in a safe manner.</p> <p>In order to ensure that the developed workflow is suitable for the end-user and to obtain feedback on the usability of the developed device/workflow, we will work with small focus groups asking them to trial the prototype system that has been developed in the laboratory as part of the applicant's PhD research.</p> <p>These focus groups will consist of University of Hull students from various faculties and level of study (further referred to as participants). Participants will be briefed on the workflow and safety procedures before the activity. Participants will be asked to test the sample preconcentration method involving repeated plunging in an adapted cafetiere filled with freshwater sample, followed by placing developed paper-based sensor into the preconcentrated sample. The freshwater sample will be provided by the researcher and/or obtainable for the participants from the University premises. Participants will then be asked to take a picture of the device with the developed picture-taking</p>

workflow (by placing the device in a black cardboard box with a slit on it, to act as light-controlling environment), as well as completing an online anonymous questionnaire (20 questions in total) to evaluate the usability of the developed workflow in general public's perspective. Throughout the activity, researchers will be present to supervise the participants and aid in case of spillage or exposure, however, researchers will not instruct or guide the procedure as it is part of evaluated aspect of the activity.

Experimental workflow that will be done by the volunteers:

HOW TO USE HEAVY METAL DETECTION KIT



1.5 Faculty or University requirements for data management

The University requirements for data management is as stated in the University of Hull Data Protection Guidelines, the University of Hull data protection policy,

1.6 Funding body(ies)

The University of Hull.

1.6 Budget (estimate if necessary)

GBP 3,000 per annum from The University of Hull scholarship

1.7 Funding body requirements for data management

The University of Hull requirements (see 1.5).

Section 2: Data, Materials, Resource Collection Information

This section is used to more fully describe the data

2.1 Brief description of data being created or compiled

In order to assess the feasibility of the developed workflow, volunteers will be recruited to perform the workflow and will be asked to fill an anonymous questionnaire to evaluate and give feedback on the workflow.

Participants will be recruited through email and approaches through student communities or other university infrastructure (e.g. doctoral college). To register, participants will be required to provide their university email address for communication purposes.

At the beginning of the volunteer activity, participants will be asked to fill a physical consent form. This physical consent form will be stored in the university premises until the end of the volunteer-based activity. It will also be scanned for storage.

Participants will then be asked to go through the workflow. At the end of the workflow, participant will be asked to take a picture of the device and upload the file anonymously in the anonymous questionnaire (later in the step). The use of personal device is optional. Participants will be given a smartphone to complete this step if they are not consenting for the use of their personal device.

After the experimental step, participants will be asked to fill an anonymous online questionnaire form to evaluate and give feedback related to the workflow. Upon the completion of this questionnaire, participant will not be able to retract or withdraw their

participation due to the anonymity. The picture of the device will be uploaded in a segment in this questionnaire.

2.2 Data collection process

Participant email address: collected upon registration for communication purposes. Stored until the end of the volunteer activity (after participants attend the test, their email address will no longer be stored)

Picture of the device, taken with a smartphone: whether by participant's personal device or provided smartphone. Collected as part of the workflow. Stored digitally in a shared Box folder for up to 5 years.

Questionnaire: completed anonymously. Result will be stored digitally for up to 5 years

2.3 Are there existing forms of the data that will be used within this research project, or which will be used as the basis for the research? If so, provide a brief description and citation

No.

2.3 Will data be available in electronic format (if so then state format(s))?

Yes, email address, consent form (scanned), pictures, and questionnaire result will be available in digital format. This will only be accessible to researchers, PI, and supervisors.

2.4 Will the data be available in non-digital form (if so then state format(s))?

Yes, a consent form will be available in paper form. This will be stored until the end of the volunteer-based activity in the university premises, that is not accessible by the general public.

2.5 Will the data stand alone and be comprehensible to a third party or be accompanied by explanatory documentation (e.g., a data dictionary)?

No, data would not be comprehensible to parties not involved in the research without further explanatory documentation.

2.6 Describe the quality assurance process for data management

Non-digital data would be stored in the research building and/or will be under constant supervision of the researchers involved. Digital data and digital rendition of the data would be uploaded to Box shared folder which can only be accessed by the researchers involved.

Section 3: Ethics, Intellectual Property

This section is used to address issues surrounding relevant ethical and intellectual property issues the research will encounter

3.1 How will the ethical aspects of data storage and subsequent access be addressed?

The personal information (email address) collected from the volunteers will be collected only for communication purposes. This will be made clear to the volunteers during recruitment process. Participants email address will not be stored beyond participant's attendance on the study.

Physical consent form will be collected from participants during the activity, no personal information will be collected. Physical form will be stored until the end of the volunteer-based activity and will be scanned for storage in University shared Box folder. Physical form will be stored in the university premises and shredded upon completion of the volunteer-based activity.

The cloud data storage used is a service provided by the University of Hull and therefore has been trusted with its security. The cloud storage can also be accessed by all researchers involved in the project, therefore minimizing the need of data transfer through other means (e.g. hard drive or email).

The data storage and subsequent access of the data generated in this project will be under the surveillance and review by the researchers involved in the project.

3.2 Will the data comply with relevant legislation such as Data Protection Act, Copyright, Design and Patents Act, Freedom of Information Act, etc.?

Yes.

3.3 If several partners are involved how will compliance with 3.1 and 3.2 be assured?

No external partners will be involved.

Section 4: Access and Use of Information

This section is used to consider if and how you will share the data once it has been created/compiled

4.1 Are you required, or do you intend, to share the data, and with whom? If so, when?

The data would be made available to the researchers (supervisors, PhD students, PDRAs) involved in the project. The digital rendition of the data would be available through shared Box folder which can be accessed anytime.

4.2 If 'yes' to 4.1, in what format will data be shared?

The digital and digital rendition of the data would be shared through Box folder. The non-digital data is made available if seen necessary in the discussion regarding the project.

4.3 Will the data have to be stored and/or made accessible for a specific period (if so, how long)?

In compliance to the University of Hull recommendation, the data will be stored for 5 years.

4.4 Who may need or wish to have access to the data?

The researchers involved in the project including the PhD student(s) and supervisors.

4.5 How do you anticipate the data being used subsequent to the project?

The data might be required for review purposes should the project continue.

Section 5: Storage and Backup of Data

This section is used to clarify details of how the data will be stored

5.1 Where and how will the data be stored during the lifespan of the project?

The digital and digital rendition of the data will be stored in Box shared folder which can be accessed by supervisors and researchers involved in the project.

5.2 Where and how will the data be stored on completion of the project?

On completion of the project, the data stored in the Box shared folder would be available to be accessed by the supervisors who still participate in the continuation of the project.

5.3 What provision is being made for backup of the data?

The back up for non-digital data would be made by converting them to digital format, which will be stored in the shared Box folder.

5.4 Will different versions of the data be stored? If so, what frequency of versioning will be appropriate?

Versioning will be done as required.



Section 6: Archiving and Future Proofing of Information

This section is used to describe long-term, post-project aspects of managing the data

6.1 What is the long-term strategy for future proofing of the data?

After the end of the project lifespan, data would be stored and be made available through the University of Hull repository service (WorkTribe) as a mean of future proofing. Data would also be available in the Box folder for designated amount of time should it be required for the continuation of the research.

No personal data will be stored in this repository.

6.2 How will the data be managed after the life of the project, for how long and in what format (NB this section refers to the detail of preservation and archiving actions, not just how it will be stored – this is addressed in section 5.2)?

The data will be stored in the University of Hull repository service (WorkTribe) after the completion of the project as the mean of archiving.

No personal data will be stored in this repository.

6.3 If the data include confidential or sensitive information, how will these data be managed to prevent possible future breaches?

The personal information (email address) collected was solely for communication purposes and consent and will not be stored further after the completion of the voluntary activities. Therefore, the personal information collected will not be published or included in the analysis.

6.4 If metadata or explanatory information is to be archived, how will this be linked to the data?

Should it be required, the data would be stored along with the rest of the digital rendition of the data in the University of Hull repository service (WorkTribe).

No personal data will be stored in this repository.

6.5 How will the data be cited?

Part of publications in scientific journals, also available through WorkTribe repository.

No personal information will be disclosed during citation.

Section 7: Resourcing of Data Management

This section is used to outline the staffing and financial details of the data management

7.1 List the specific staff who will have access to the data and denote who will have the responsibility for data management.

Mila Sari (PhD student) – responsible for data management.

Prof. Mark Lorch – principal investigator.

Prof. Nicole Pamme – project supervisor.

Dr. Will Mayes – project co-supervisor.

7.2 How will the data management described in this document be funded?

The data will be managed by the researchers and supervisors involved in the project using the free services provided by the University of Hull throughout the lifespan of the project.

7.3 How will data storage be funded?

The data storage throughout the lifespan of the project is stored in the free service provided by the University of Hull.



Section 8: Review of Data Management process

This section is used to clarify how data management will be an embedded part of the research project

8.1 How will the data management plan be adhered to?

The data management plan will be used as a guidance throughout the project data processing and will be the point of reference should there be any confusion on data processing in the lifespan of the project. It will be the responsibility of the researchers (PhD student) involved in the project, and the adherence to it will be supervised by the supervisors involved in the project.

8.2 Who will review the data management plan? What is the schedule for this review?

The data management plan will be reviewed by all researchers and supervisors involved in the project and be evaluated annually. Should any problems arise within the lifespan of the project regarding data management, assistance from the data management experts/professional in the University of Hull will be requested.

Section 9: Statements and Personnel Details

9.1 Statement of agreement

I/we agree to the specific elements of the plan as outlined:

Principal investigator or PhD supervisor

Title	Principal Investigator
Designation	Principal Investigator
Name	Professor Mark Lorch
Date	
Signature	

Researcher


Title	Project supervisor
Designation	Project supervisor
Name	Professor Nicole Pamme
Date	
Signature	

Researcher

Title	Project co-supervisor
Designation	Project co-supervisor
Name	Professor Will Mayes
Date	
Signature	

Researcher

Title	PhD student
Designation	PhD student

Name	Mila Sari
Date	01/02/2022
Signature	

9.2 Expertise of Researchers

Title	Principal Investigator
Name	Mark Lorch
Contact Details	m.lorch@hull.ac.uk
Expertise	

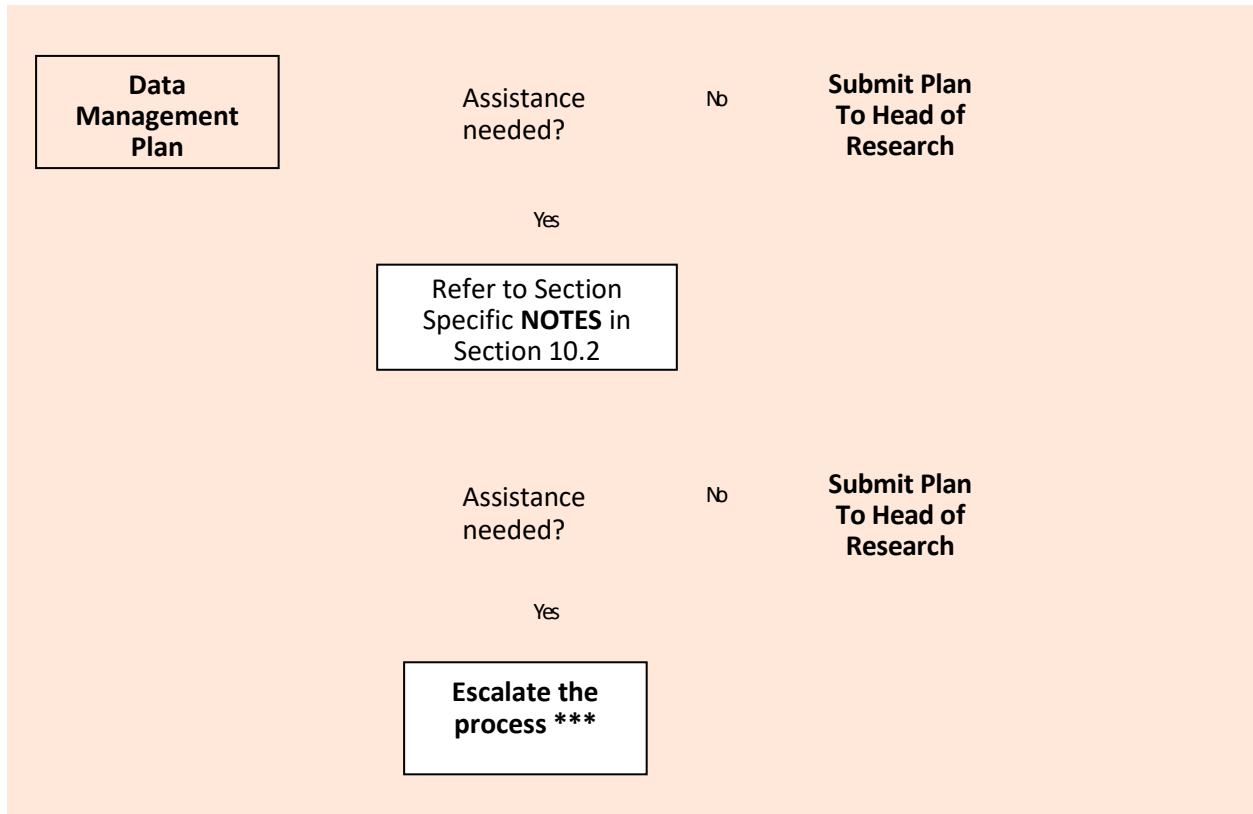
Title	Project co-supervisor
Name	Nicole Pamme
Contact Details	nicole.pamme@mmk.su.se
Expertise	

Title	Project co-supervisor
Name	Will Mayes
Contact Details	W.Mayes@hull.ac.uk
Expertise	

Title	PhD student
Name	Mila Sari
Contact Details	M.Sari-2019@hull.ac.uk
Expertise	

Section 10: Appendices

10.1 *Specific Help with completing the Plan*



In certain instances, specific guidance may be required in order to complete this Data Management Plan. Assistance should be sought by following the flow chart below:

Escalate the process by requesting assistance from the Departmental Head of Research. Typically this will entail contacting Departmental or Faculty data managers and/or Library and Learning Innovation and ICTD. Specific assistance may be available through the Research Funding Office as well, particularly in relation to funder requirements for data management.

10.2 Notes

These notes refer to the specified sections and subsections in this document. Any areas not addressed may be referred to the project lead, supervisor, or the Head of Research. Technical issues may be addressed to the HDMP development team in the first instance.

Front Cover

Details are required to ensure the correct future referencing, storage and archiving of the Data Management Plan. There will be strict adherence to applicable law, including the Data Protection Act; this information will not be made available outside of the specific remit of the Faculty of Health and Social Care of the University of Hull.

Section 1: Project Information

- 1.1 No specific guidance available
- 1.2 No specific guidance available
- 1.3 Required for funded projects – this refers to organisations other than the University of Hull
- 1.4 If necessary, further information may be provided on an attached, clearly labelled **typed** or **printed** sheet. For online forms, the space will automatically be increased to accommodate extra text.
- 1.5 State what local requirements are in place – details from Head of Research
- 1.6 Details may be requested from the project Supervisor, or the Head of Research.
- 1.7 Applies specifically to funded projects. If necessary, further information may be provided on an attached, clearly labelled **typed** or **printed** sheet. For online forms, the space will automatically be increased to accommodate extra text.
- 1.8 Applies specifically to funded projects. If necessary, further information may be provided on an attached, clearly labelled **typed** or **printed** sheet. For online forms, the space will automatically be increased to accommodate extra text. Details may be requested from the project Supervisor, or the Head of Research.

Section 2: Data, Materials, Resource Collection Information

- 2.1 If necessary, further information may be provided on an attached, clearly labelled **typed** or **printed** sheet. For online forms, the space will automatically be increased to accommodate extra text. NOTE: details may change as the project evolves; provide a best estimate.
- 2.2 If necessary, further information may be provided on an attached, clearly labelled **typed** or **printed** sheet. For online forms, the space will automatically be increased to accommodate extra text.

- 2.3 It is vital that there is a clear understanding of exactly which data types are being discussed in order to plan for future storage, accessibility and integrity. Example data types and formats are available at http://en.wikipedia.org/wiki/List_of_file_formats.
- 2.4 A great deal of non-digital data may need to be stored securely and/or archived. Various examples of this type of data are:
- Documents: Printed digital, Original artefact, , etc.
 - Images: Photographs (size, print type, age), posters, etc.
 - Artefacts: Physical model (scale/non-scale, size, availability), archaeological, etc.
 - Film: 8/16/32mm, Video, microfilm, negative, etc.
 - Other: Live performance, logical model, etc.
- 2.5 “Standalone” implies a provided information resource that requires no further explanation and may be used “as is” without additional resource. Accompanied implies information that is informed by accompanying documentation or resource(s) which help to understand the resource. For example, a database may need to be accompanied by a “metadata” informative document which explains the purpose, use of specific fields, and instructions for utilisation. Details may be requested from the project Supervisor, or the Head of Research.
- 2.6 Quality Assurance/Management in this context refers to the concise provision of a breakdown of what will be done to ensure that the project’s progress will be monitored for accuracy, quality of work or research, and timely delivery at regular intervals. Typically, this would be the remit of the Research Supervisor, the Project Lead, or the Head of Department. Details may be requested from the project Supervisor, or the Head of Research.

Section 3: Ethics, Intellectual Property, Citation

- 3.1 If your research has an impact on the welfare, confidentiality or economic status of any individual or corporate group, this should be clearly stated. If necessary, further information may be provided on an attached, clearly labelled **typed** or **printed** sheet. For online forms, the space will automatically be increased to accommodate extra text. **NOTE:** details may change as the project evolves; provide a best estimate.
- 3.2 It is vital to comply with applicable law. Provide a brief outline of how relevant legislation and regulations will be complied with where appropriate. Where there is any doubt, the first line of contact is the project Supervisor, or the Head of Research.
- 3.3 See note 3.2 above. Partners in the project must be held to the same legal and regulatory standards. Partners are also protected by applicable law and may avail themselves of the prospect of legal recourse in the event of any perceived illegality or infringement by any party. This applies to all participants effecting or affected by the research project. Where there is any doubt, the first line of contact is the project Supervisor, or the Head of Research.

Section 4: Access and Use of Information

- 4.1 Sharing data, i.e. making it publically available, may be a requirement of a funding bid, or of a University research project (e.g. Doctoral thesis or research project). Details may be requested from the project Supervisor, or the Head of Research.
- 4.2 Provide details of how you intend to share your data (if relevant). This may include several options, such as an online accessible dataset or database, or online images. It could also be in the form of a paper based document or set of documents. If you are uncertain, or wish to explore this avenue further, the first line of contact is the project Supervisor, or the Head of Research.
- 4.3 If your data are sensitive (e.g. not suitable for general access until you have completed, or contains personal data or information) you may need to keep the data secure until you are ready to publish – if at all. Similarly, if the project funder requires “mile-stone” releases, this should be indicated. If in doubt, check this with the project Supervisor, or the Head of Research.
- 4.4 It is vital that you have a clear perspective of who the outcome of your research is intended to reach. Funding bodies may stipulate specific outcomes – e.g. public access, etc.
- 4.5 Funding bodies will typically require an explanation of the usefulness of your research once completed, and you should be able to provide a clear idea of what will be done with your data once published or released. Certain obvious options should not be overlooked, such as: paper presented at conference for history community, or book chapter published for community and public research/interest, etc.

Section 5: Storage and Backup of Data

- 5.1 It is vital that the research materials and data are kept *safely at every stage* of the research process lifespan. There may be help available from IT Services, the Library or the Department. If you are uncertain, or wish to explore this avenue further, the first line of contact is the project Supervisor, or the Head of Research.
- 5.2 As for 5.1 above, it is vital that you have a clear understanding of how, where and when the research materials and data will be maintained after research process lifespan. This is particularly true where funding bodies have specific outcome criteria (e.g. making a public website available, etc.). There may be help available from IT Services, the Library or the Department. If you are uncertain, or wish to explore this avenue further, the first line of contact is the project Supervisor, or the Head of Research.
- 5.3 Similarly to 5.1 and 5.2 above, it is vital that you have a clear understanding of how, where and when the research materials and data will be backed up and kept safely, both during and after the after the research process lifespan. This is particularly true where funding bodies have specific outcome criteria (e.g. ensuring that online datasets are maintained for a specific period after the end of a project, etc.). There may be help available from IT Services, the Library or the Department. If you are uncertain, or wish to explore this avenue further, the first line of contact is the project Supervisor, or the Head of Research.
- 5.4 Very often work is added to, revised or altered and older versions are either overwritten, left as they were, or deleted. It may be wise to maintain a clearly labelled and

stored set of older versions of current work in order to backtrack if necessary. It is imperative that a logical and sequenced filing system is used. On computer systems this may be attained by uniquely numbering each version. A useful means of achieving this is by using the current date and time as the unique numbering reference – e.g. “yyyymmdd FHSC Data Management Plan”.

Section 6: Archiving and Future Proofing of Information

- 6.1 Provide information about how you intend for the project outcome(s) or deliverable(s) to be maintained after the end of the project. For example, a dataset may be perpetually maintained by the University’s online provision. However, this will need to be confirmed. There may be help available from IT Services, the Library or the Department. If you are uncertain, or wish to explore this avenue further, the first line of contact is the project Supervisor, or the Head of Research.
- 6.2 Any information that is kept after the lifespan of a project will still need to be stored safely, maintained and be provided in a useable format. If specific file formats are used, they may become unusable after a few years as new software replaces the old. Also, media such as DVDs, CDs and diskettes may become unusable after a while. There may be help available from IT Services, the Library or the Department. If you are uncertain, or wish to explore this avenue further, the first line of contact is the project Supervisor, or the Head of Research.
- 6.3 It is vital that any confidential data (e.g. personal information about any individual who is protected under the terms of the Data Protection Act, or information that may infringe copyright if released, etc.) must be kept and maintained in a secure environment. All reasonable steps should be taken to ensure the safety of such information. This applies to any information that is kept after the lifespan of a project as well. If you are uncertain, or wish to explore this avenue further, the first line of contact is the project Supervisor, or the Head of Research.
- 6.4 Datasets, databases, standalone documents, and even artefacts may prove useless without explanatory notes (metadata) accompanying them. These materials need to be clearly linked to the materials so that they can adequately inform any future user about the material. For example, a published dataset will typically be accompanied by a metadata document that explains the various fields, their usefulness and summarises the purpose of the dataset in general. These documents will be stored along with the dataset and are accessible in the same manner as the dataset (e.g. online, or download). Examples of such accompanying documentation are available for download. If you wish to explore this avenue further, the first line of contact is the project Supervisor, or the Head of Research.
- 6.5 Typically, any stored data, materials, artefacts, etc. will need to be cited when accessed and referenced by other researchers. It is useful to provide clear and concise citation information for researchers to access. This can be done via the accompanying documentation (metadata) indicated in 6.4 above. If you wish to explore this avenue further, the first line of contact is the project Supervisor, or the Head of Research.

Section 7: Resourcing of Data Management

- 7.1 In the event that this is an individual project or piece of research, your own name should be listed. Include any other staff or assistants are to be involved in the project as well. It may be necessary to include staff from other departments of the University. If you are uncertain, or wish to explore this avenue further, the first line of contact is the project Supervisor, or the Head of Research.
- 7.2 Funding strategies are often outlined by funders and will include a data management aspect. The costs of any materials, equipment and specialist knowledge will need to be factored to arrive at a reasonable estimate. Include any materials or equipment that will be funded by the University and/or you. If you are uncertain, or wish to explore this avenue further, the first line of contact is the project Supervisor, or the Head of Research.
- 7.3 As in 7.2 above, funding strategies are often outlined by funders and will include a data management aspect. Typically the University will support on-going research projects, and assist in facilitating post project maintenance and/or presence of outputs. However, this needs to be confirmed to ensure that the service will be available in the form that is required. If you are uncertain, or wish to explore this avenue further, the first line of contact is the project Supervisor, or the Head of Research.

Section 8: Review of Data Management process

- 8.1 Funders will need to be informed about how the data management process will be implemented. Provide specific information about how you intend to follow through with the commitments and processes that have been discussed in the rest of this document. Typically, regular reviews, reports and assessments of progress will suffice, but some funders may require specific means of identifying adherence to the plan. If you are uncertain, or wish to explore this avenue further, the first line of contact is the project Supervisor, or the Head of Research.
- 8.2 Based on 8.1 above, list those who will be carrying out the reviews and subsequent reports or processes necessary to ensure the successful implementation and completion of the data management plan. Typically, in the event of smaller research projects or individual research, the project Supervisor will fill this role. In the event of PhD research, this role will be carried out by the PhD Supervisor(s). If you are uncertain, or wish to explore this avenue further, the first line of contact is the project Supervisor, or the Head of Research.

Section 9: Statements and Personnel Details

- 9.1 The Statement of Agreement is necessary to clarify the areas of responsibility and work that will be carried out by the various researchers engaged in the project. This information is vital for funding bodies that will require these details.
- 9.2 As in 9.1 above, the Expertise of Researchers is necessary to clarify the areas of responsibility and work that will be carried out by the various researchers engaged in the

project. This information is vital for funding bodies that will require these details in the form of a brief résumé for each researcher.

Section 10: Appendices

10.1 Assistance with completing the Plan; follow the instructions to obtain help specific to each section.

10.2 Follow the guidance for each specific section as necessary.

10.3 This list of Relevant Contacts will be reviewed and altered regularly.

10.3 Relevant Contacts

The following list of contacts should be regularly revised as appropriate for the purposes of your research:

Head of Research	Prof Mark Lorch Principal Investigator Email: M.Lorch@hull.ac.uk
Library and Learning Innovation	Chris Awre Head of Information Management Phone: +44 (0) 1482 465441 Email: c.awre@hull.ac.uk
ICT Directorate	IT Helpdesk Phone: +44 (0)1482 462010 E-mail: help@hull.ac.uk
Head of Department	
Document Author	Chris Awre Details as above

Volunteer consent form

Heavy metal detection in freshwater environment - Volunteer Consent Form (Experiment)

By placing the volunteer activity date and checking the boxes in this form, you are registering as a volunteer for the heavy metal detection in freshwater environment project.

Date:

	Yes
I have read and understood what the research is about, and the risks involved with it.	
I confirm that my participation in this research is voluntary, without any payment/remuneration, and I understand that <u>it will have no impact on my academic outcomes.</u>	
I understand that my email address will only be stored (in line with GDPR requirements) until the completion of today's volunteer activity, and this information is only accessible to the researchers involved in this study	
I understand I can withdraw from the project at any time <u>before the anonymous questionnaire submission</u> , without any penalty	
I understand that the project has been reviewed and passed by the University of Hull research ethics committee	
I understand that if I have any concerns or complaints, I can raise them by contacting the named researchers at the University of Hull	
I understand that these results will be published by the University of Hull and will not contain any of my personal data	
I understand that as a part of this project, I will be required to take pictures of the experiments I perform and upload them through the given link, where they will be stored for further analysis by the University of Hull	
I understand that the data collected through this study is only accessible to researchers involved in this study and will be processed for further scientific analysis by the researchers. This scientific data processing will not include my email address.	
I consent to use my personal device to take the picture of the device as informed above (optional , please leave the box blank if you wish to opt out. We will provide you with another smartphone to complete the activity)	

If you have any further question, queries, and concern related to this study, please contact:

Mila Sari – m.sari-2019@hull.ac.uk

Prof. Mark Lorch – m.lorch@hull.ac.uk

FOSE ethics - fose-ethics@hull.ac.uk

Online questionnaire filled by the participants

Heavy metal detection in freshwater environment questionnaire

* Required

Heavy metal detection in freshwater environment

Introduction

This study is a part of a PhD research project “Mapping heavy metal pollution in river water with paper-based analytical device through citizen science” conducted by Mila Sari, 3rd year PhD researcher in Department of Chemistry, Faculty of Science and Engineering, University of Hull, UK. The project is supervised by Professor Mark Lorch, Professor Nicole Pamme, and Professor Will Mayes, based in the University of Hull.

We are developing a simple and rapid method to detect pollutants in the water through paper devices. This process includes a water-treatment step to ensure pollutants can easily be detected by the device. This system is developed to be used by scientists and non-scientists alike, ensuring that everyone can have access and contribute to monitoring the water environment.

Purpose

In this study, we want your feedback and input from you about the process we have developed. Your feedback will be used to improve the user-friendliness of the process.

What happens to the information in this project?

At this point of the study, we expect you to have completed the experiment as part of the study. Before completing/submitted this questionnaire, this information will be required to be anonymous, no personal information will be asked. Due to this, you will not be able to retract the result of the

If you have any further question, queries, and concern related to this study, please contact:
Mila Sari - m.sari2019@hull.ac.uk

Prof. Mark Lorch – m.lorch@hull.ac.uk

FOSE ethics - fose-ethics@hull.ac.uk

1. By ticking the following box, you agree to all the following statements:

a.) I have read and understood what the research is about, and the risks involved with it.

b.) I confirm that my participation in this research is voluntary, without any payment/ remuneration, and I understand it will have no impact on my academic outcomes.

c.) I understand that the researchers will not identify me by email address in any reports using information captured throughout the study; and this personal information is handled in line with University of Hull regulations and GDPR.

d.) I understand that upon completion of this anonymous questionnaire, I will not be able to withdraw my participation or retract my answers. *

I agree to all statements above

Evaluating the workflow

2. Is the provided instruction sheet clear and helpful? *

- Yes
- No
- N/A

Preconcentration

<input type="radio"/>	<input type="radio"/>	<input type="radio"/>	<input type="radio"/>
-----------------------	-----------------------	-----------------------	-----------------------

3. Workflow duration *

Too short Just right Too long N/A

PAD

<input type="radio"/>	<input type="radio"/>	<input type="radio"/>	<input type="radio"/>
-----------------------	-----------------------	-----------------------	-----------------------

Overall

<input type="radio"/>	<input type="radio"/>	<input type="radio"/>	<input type="radio"/>
-----------------------	-----------------------	-----------------------	-----------------------

4. Simplicity of the workflow *

	Too easy	Just right	Too difficult	N/A
Preconcentration	<input type="radio"/>	<input type="radio"/>	<input type="radio"/>	<input type="radio"/>
Picture-taking step PAD	<input type="radio"/>	<input type="radio"/>	<input type="radio"/>	<input type="radio"/>
Overall	<input type="radio"/>	<input type="radio"/>	<input type="radio"/>	<input type="radio"/>

5. How easy do you think it will be to complete the entire workflow in a riverbank setting? *

- Extremely easy
- Somewhat easy
- Neutral
- Somewhat not easy
- Extremely not easy

6. What do you think is the most important aspect in improving the developed workflow (overall)? *

Please drag the options to rank the aspects according to your opinion

Duration of workflow

Simplicity of the workflow

Accuracy of the result

Affordability of the kit

Visual (design)

Ability to detect very low concentration of contaminant

7. If you have any feedback on the preconcentration workflow, please write your feedback here

8. If you have any feedback on the PAD workflow, please write your feedback here

9. If you have any feedback on the overall workflow, please write your feedback here

10. Please select one option *

- I use my own smartphone to take device pictures
- I use provided smartphone to take device pictures

11. Please upload the picture of the PAD in this section *

 **Upload file**

File number limit: 1 Single file size limit: 1GB Allowed file types: Image, Video

12. Please select your current level of study

- Undergraduate
- Postgraduate taught
- Postgraduate research
- Other

13. Which of the following best describes your laboratory experience? *

- I have never worked in chemistry laboratory settings
- I only have ever worked in a chemistry laboratory as part of a coursework
- I am currently regularly working in a chemistry laboratory setting
- Other

14. How interested are you in on-going environmental problems?

- Extremely interested
- Somewhat interested
- Neutral
- Somewhat not interested
- Extremely not interested

15. Prior to this activity, have you ever heard of 'microfluidics' before?

Yes

No

16. To what extent have you ever heard of/involved with microfluidics?

I have heard of microfluidics

I learn about microfluidics in my class(es)

I have used microfluidics device before

I regularly use microfluidics device

I am (or was) a researcher on microfluidics

Other

17. Prior to this activity, have you ever heard of 'citizen science' before?

Yes

No

18. To what extent have you ever heard of/involved with citizen science activities?

- I have heard of citizen science activity
- I have participated in a citizen science activity
- I am studying/researching on the topic of citizen science
- Other

19. If this device (or similar type) is publicly available, would you be interested in participating in citizen science activity related to monitoring water environment with it?

Yes

No

This content is neither created nor endorsed by Microsoft. The data you submit will be sent to the form

owner.

 Microsoft Forms

Participant information sheet

Heavy metal detection in freshwater environment – Participant Information Sheet

Study: Heavy metal detection in freshwater environment

Highlights:

- This study is a part of PhD research project. PhD researcher: Mila Sari (M.Sari-2019@hull.ac.uk).
- We are developing a way to detect pollutants in the water through paper device, this device is developed to be used by non-scientists.
- We need your voluntary input on the process and the device we have developed.
- We invite you to participate in testing the process and filling feedback questionnaire.
- We will ask you to email us (M.Sari-2019@hull.ac.uk) if you are interested and we will arrange a group (up to 5 people) meeting to test the device.
- After registration, you are allowed to withdraw participation before questionnaire submission.
- **Participation in this study is voluntary and will not affect your academic assessments**

Introduction

This study is a part of a PhD research project “Mapping heavy metal pollution in river water with paper-based analytical device through citizen science” conducted by Mila Sari, 3rd year PhD researcher in Department of Chemistry, Faculty of Science and Engineering, University of Hull, UK. The project is supervised by Professor Mark Lorch, Professor Nicole Pamme, and Professor Will Mayes, based in the University of Hull.

We are developing a simple and rapid method to detect pollutants in the water through paper devices. This process includes a water-treatment step to ensure pollutants can easily be detected by the device. This system is developed to be used by scientists and non-scientists alike, ensuring that everyone can have access and contribute to monitoring the water environment.

Purpose

In this study, we want your feedback and input about the process we have developed. Your feedback will be used to improve the user-friendliness of the process.

Do you have to take part?

Your involvement in this study is voluntary and will not affect your university studies/academic outcomes. You will have the opportunity to withdraw your participation before the anonymous questionnaire submission, at which you and your feedback will no longer be identifiable.

What will you do in the project?

In this study, you will be asked to test the water treatment and paper device we are developing. This activity might be done in a group of up to 5 people. Afterwards, you will be asked to complete an anonymous online questionnaire where you will be able to provide feedback on the process you just tested. This questionnaire is anonymous, and therefore you will not be able to withdraw your participation upon submission of this step.

The water treatment involves pouring a water sample (300 mL) into a cafetiere and plunging it repeatedly with modified plunger for 5 minutes. You will then be asked to remove the plunger from the cafetiere and place it in a different liquid for 1 minute. You can then put in the paper device and observe the colour change on the device. You will be asked to take a picture of the device. We appreciate if you can do this with your phone, but otherwise, we have a smartphone to help you complete this step. The picture of the device will be uploaded along with the anonymous questionnaire, which you will complete as soon as you are done with the experiment.

If you think you will need additional precautions to participate in this study, please contact the researcher: M.Sari-2019@hull.ac.uk.

Why have you been invited to take part?

You are invited because you are a student in the University of Hull. Currently, we will need feedback from anyone, with or without previous laboratory-experience to ensure that the process we are developing is user-friendly. However, your participation in this research is voluntary and will not affect your study or assessments.

What are the potential risks to you in taking part?

You will be given 300 mL of environmental water sample to handle in the testing process. This water sample may contain low-level of various pollutants, which may give you itch or rash upon

contact with your skin. We will give you appropriate personal-protective-equipment (PPE) to avoid this, and a researcher will be present in case of spillage or mishandling.

If you think you will need additional precautions to participate in this study, please contact the researcher: M.Sari-2019@hull.ac.uk.

What happens to data collected in this project?

The data collected in this research will be processed according to the University of Hull regulation following the GDPR.

Your university email address will only be used to communicate the testing date. **After your attendance, completion of the test and the questionnaire, we will not store your email address.**

During the study, we will ask you to take a picture of the device as part of the process, which will be uploaded anonymously through the questionnaire. However, if you don't want to use your own smartphone for this, we will provide you with a device to complete this step.

After going through the testing, you will be asked to fill an anonymous questionnaire to record your experience and feedback on the workflow. This questionnaire will be anonymous, no personal information will be asked. Due to this, you will not be able to retract the result of the questionnaire once it is submitted. The result of the questionnaire will be analysed to assess the user experience and to further improve the workflow design.

All data submitted and gathered throughout this study is accessible to the researchers involved in the study, principal investigator, and supervisors. All scientific data submitted and gathered will be processed and stored following the University of Hull regulations in line with GDPR, which require 5 years storage of the data.

If you have any further question, queries, and concern related to this study, please contact:

Mila Sari – m.sari-2019@hull.ac.uk

Prof. Mark Lorch – m.lorch@hull.ac.uk

FOSE ethics - fose-ethics@hull.ac.uk